NASA CR-134800
BCAC D6-42440-4

PHASE II PROGRAM ON GROUND TEST OF REFANNED JT8D TURBOFAN ENGINES AND NACELLES FOR THE 727 AIRPLANE

FINAL REPORT

VOLUME IV
AIRPLANE EVALUATION AND ANALYSIS

December 1975

Boeing Commercial Airplane Company
Seattle, Washington 98124

prepared for

NATIONAL AERONAUTICS AND SPACE ADMINISTRATION

NASA Lewis Research Center
Contract NAS3-17842

1. Report No.	2. Government Accession No.	3. Recipient's Catalog No.
NASA CR-134800		

4. Title and Subtitle	5. Report Date
Phase II Program on Ground Test of Refanned JT8D Turbofan Engines and Nacelles for the 727 Airplane–Final Report–Volume IV, Airplane Evaluation and Analysis	December 1975
	6. Performing Organization Code
7. Author(s)	8. Performing Organization Report No. D6-42440-4
	10. Work Unit No.
9. Performing Organization Name and Address Boeing Commercial Airplane Company P.O. Box 3707 Seattle, Washington 98124	11. Contract or Grant No. NAS3-17842
	13. Type of Report and Period Covered Contractor Report
12. Sponsoring Agency Name and Address National Aeronautics and Space Administration Washington, D.C. 20546	14. Sponsoring Agency Code

15. Supplementary Notes

V/STOL and Noise Division Chief, R.W. Schroeder
NASA Lewis Research Center, Cleveland, Ohio 44135

16. Abstract

The objective of Phase II of the NASA-sponsored Refan Program was to evaluate the retrofit of JT8D-109 (refan) engines on a 727-200 airplane in terms of airworthiness, performance, and noise. The program included the design of certifiable hardware, manufacture and ground testing of the essential nacelle components, and analysis of the certifiable airplane design to ensure airworthiness compliance and to predict the in-flight performance and noise characteristics of the modified airplane. This report documents the analyses and evaluation of the 727 refan airplane.

Airplane performance estimates include range at maximum gross weight, field lengths, takeoff profiles, block fuel, and descent profile limitations. Extensive acoustic analyses are presented, emphasizing the improvements relative to the 727-200 (baseline) airplane. Propulsion system performance of the refan engine is compared with that of the baseline engine. Inlet and exhaust system performance is compared with predictions. Thrust-reverser performance is compared with requirements. Further analyses included nacelle subsystems; flight and ground idle power settings; refan engine stability characteristics; detailed structural analyses; airplane weight and balance; longitudinal and lateral directional stability and control characteristics; and ice protection, air-conditioning, and brake systems.

The analyses confirm that the 727 refan airplane is certifiable. The refan airplane range would be 15% less that of the baseline airplane and block fuel would be increased by 1.5% to 3%. However, with this particular 727-200 model, with a brake release gross weight of 172 500 lb (78 245 kg), it is possible to operate the airplane (with minor structural modifications) at higher gross weights and increase the range up to 15% over the 727-200 (baseline) airplane. The refan airplane FAR Part 36 noise levels would be 6 to 8 EPNdB (effective perceived noise in decibels) below the baseline. Noise footprint studies showed that approach noise contour areas are small compared to takeoff areas. The 727 refan realizes a 68% to 83% reduction in annoyance-weighted area when compared to the 727-200 over a range of gross weights and operational procedures.

17. Key Words (Suggested by Author(s))		18. Distribution Statement
FAR 36 noise	Structural analysis	Unclassified -- unlimited
Acoustic lining	Weight and balance	
Refan engine	Mission performance	
Inlet	Propulsion	
Nozzle		

19. Security Classif. (of this report)	20. Security Classif. (of this page)	21. No. of Pages	22. Price*
Unclassified	Unclassified	310	

* For sale by the National Technical Information Service, Springfield, Virginia 22151

PHASE II PROGRAM ON GROUND TEST
OF REFANNED JT8D TURBOFAN ENGINES AND NACELLES
FOR THE 727 AIRPLANE

FINAL REPORT

OVERALL REPORT ORGANIZATION

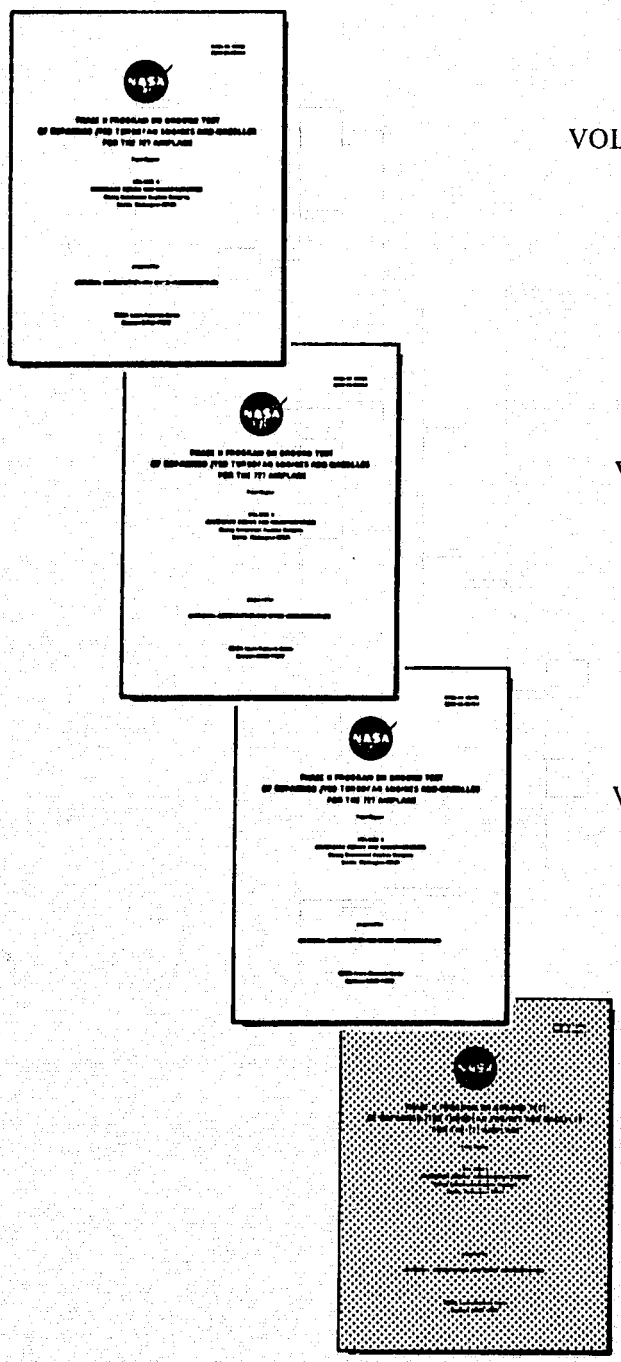

VOLUME I -SUMMARY (NASA CR-134797)

VOLUME II–HARDWARE DESIGN AND
MANUFACTURING
(NASA CR-134798)

VOLUME III–GROUND TESTS
(NASA CR-134799)

VOLUME IV–AIRPLANE EVALUATION
AND ANALYSIS
(NASA CR-134800)

CONTENTS

CONTENTS (Concluded)

FIGURES

FIGURES (Continued)

FIGURES (Continued)

FIGURES (Continued)

FIGURES (Continued)

FIGURES (Concluded)

TABLES

TABLES (Concluded)

1.0 SUMMARY

The objective of Phase II of the NASA-sponsored Refan Program was to evaluate the retrofit of JT8D-109 (refan) engines on a 727-200 airplane in terms of airworthiness, performance, and noise. The program included the design of certifiable hardware, manufacture and ground testing of the essential nacelle components, and analysis of the certifiable airplane design to ensure airworthiness and to predict the in-flight performance and noise characteristics of the modified airplane. The retrofit design objectives were to significantly reduce community noise, while preserving airplane performance and the reliability and maintainability of the 727 at minimum retrofit cost. The manufacturing objective was to demonstrate the producibility of the design, and the test objective was to determine the performance and noise increments between a production JT8D and the refan version of the same engine, and to verify key nacelle structural design assumptions. This report documents the analyses and evaluation of the 727 refan airplane.

Study results (table 1) indicate that the 727 refan range performance is approximately 15% less than the 727-200 at a brake release gross weight (BRGW) of 172 500 lb (78 245 kg). The block fuel requirements for the refan airplane would be 1.5% to 3% greater than the unmodified airplane.

One option that is available with this specific model of 727-200 is a structural modification to the airplane to allow a 10 000-lb (4536-kg) increase in BRGW, which could be accomplished in association with the engine retrofit. Taking advantage of this option, the higher BRGW refan airplane could provide a 15% *increase* in range relative to the 727-200 at a BRGW of 172 500 lb (78 245 kg). A takeoff field length improvement would be accomplished along with the increased range because of the substantial takeoff thrust increase of the refan engine. These benefits, however, are not available to certain other versions of the 727-200 because of other structural limitations.

The thrust specific fuel consumption (SFC) performance of the JT8D-109 engine is summarized in table 1. The installed takeoff side- and center-engine thrust is greatly improved on the 727 refan airplane. For both sea level and 5000 ft (1524 m) at standard and 84°F (302 K) day conditions, the JT8D-109 side- and center-engines would produce approximately 14% and 10% more thrust statically and at 100 knots (51.4 m/s), respectively, than the JT8D-9 engine. JT8D-109 cruise performance was compared to the JT8D-9 engine at Mach 0.84, 30 000-ft (9144-m) altitude conditions. The average JT8D-109 SFC for two side engines and the center engine was approximately 0.6% higher than the JT8D-9 SFC at an average midcruise thrust of 4050 lb (18 015 N).

The acoustic characteristics of the 727-200 and 727 refan airplanes were analyzed with a method which combined JT8D-15 (baseline) and JT8D-115 (refan) ground test data with existing 727-200/JT8D-9 certification flight test data. The keynote of the analysis method was the emphasis on major engine noise components.

Table 1 presents a summary of the Federal Aviation Regulation (FAR) Part 36 community noise levels predicted for the 727 refan. These are seen to be 6 to 8 EPNdB lower than for the 727-200 airplane. At cutback and sideline conditions the refan airplane would be

Table 1.—727-200/727 Refan Noise/Performance Summary

	FAR 36 limits	727-200	727 Refan	
			Increments from -200	
NOISE[a]				
FAR 36 EPNL, EPNdB				
Approach at 40° flaps	104.4	109.5	-6.8	102.7
Approach at 30° flaps	104.4	108.2	-7.5	100.7
Takeoff/cutback at 5° flaps	99.0	100.0	-6.3	93.7
Full-power takeoff at 5° flaps	99.0	107.4	-7.7	99.7
Sideline at 5° flaps	104.4	99.9	-6.4	93.5
Percent reduction in annoyance weighted area			68% to -83%	
			Increments from -200	
PERFORMANCE				
Uninstalled SL static thrust, lb (N)		14 500 (64 499)	+14.5%	
Takeoff thrust at 100 kn (51.4 m/s), 84°F (302 K), lb (N)		12 700 (56 492)	+9.1%	
Maximum cruise thrust, lb (N) engine[b]		4 325 (19 239)	+6.0%	
Cruise SFC, lb/hr/lb (kg/hr/daN)[c]		0.833 (0.849)	+0.6%	
Range, nmi (km)[a]		1 405 (2 602)	-205 (-380)	
Takeoff field length, SL, 84°F (302 K), ft (m)[a]		8 370 (2 551)	-1450 (-442)	
Range from 6900-ft (2103-m) field, nmi (km)[d]		1 000 (1 852)	+180 (+334)	
WEIGHT				
Maximum brake release gross weight, lb (kg)		172 500 (78 245)		
Maximum landing weight (30° flaps), lb (kg)		150 000 (68 040)		
Maximum landing weight (40° flaps), lb (kg)		142 500 (64 638)		
			Increments from -200	
Operational empty weight, lb (kg)		99 000 (44 906)	+3839 (+1741)	
Nacelle and structure, lb (kg)		15 760 (7 149)	+2849 (+1292)	
Ballast, lb (kg)		0	+990 (+449)	

[a] Brake release gross weight = 172 500 lb (78 245 kg)

[b] Std day, 30 000 ft (9144 m), $M_\infty = 0.84$

[c] Std day, 30 000 ft (9144 m), $M_\infty = 0.84$, midcruise weight = 155 000 lb (70 307 kg)

[d] SL, 84°F (302 K) takeoff, $M_\infty = 0.84$ at 30 000-ft (9144-m) cruise, std day, zero wind, payload of 134 passengers at 205 lb (93 kg)/passenger = 27 470 lb (12 460 kg)

significantly below FAR Part 36. The 727 refan would nominally meet the FAR Part 36 certification requirements without resorting to thrust cutback on takeoff.

Level flyby noise characteristics were predicted as a function of corrected net thrust and altitude. Figure 1 shows typical comparisons at altitudes of 400 ft (122 m) and 2000 ft (610 m). At high power settings, the 727 refan jet noise reduction due to the engine cycle change results in a significant noise improvement, as seen by comparing the 727-200 and 727 refan with a hardwall nacelle. At the lower power settings, other noise sources dominate the total, and the noise reduction is primarily due to the effectiveness of the acoustic linings, as seen from the comparison of the 727 refan with hardwall and treated nacelles. Over the complete matrix of thrusts and altitudes, the combined noise reduction would be 3 to 9 EPNdB (while at FAR Part 36 conditions it is 6 to 8 EPNdB).

A footprint contour area study considered the community noise exposure of both the 727-200 and 727 refan airplanes for a variety of takeoff and landing gross weights and operational procedures. Approach contour areas were found to have little impact on total community noise exposure when compared to the takeoff contour areas. A comparison of different takeoff profile results for the 727-200 and 727 refan airplanes (fig. 2) showed a weighted total area reduction of 68% to 83%, depending on gross weight and flight operations.

A target-type thrust reverser was selected for evaluation on the 727 refan airplane. With this reverser configuration, performance estimates showed that the refan thrust reverser could provide stopping capability equivalent to that of the 727-200 airplane. Since the refan thrust reverser was not evaluated in full-scale ground tests, further development work would be required to finalize the design and performance characteristics.

Separate ground and flight idle power settings would be required with the JT8D refan engine. The flight idle power setting would be established so that the certification engine acceleration time requirements for a refused landing could be met; the flight idle thrust would be increased over that of the JT8D engine. The refan engine in-flight idle thrust increase would result in the loss of the refan airplane capability to fly a 6°/3° multigradient approach condition for noise abatement procedures. Normal 3° approaches would be attainable. The ground idle power setting would provide adequate engine speed characteristics to satisfy 727-200 generator load requirements and low enough thrust for satisfactory 727 refan ground-handling characteristics.

The airplane weight and balance analysis showed a 2849-lb (1292-kg) weight increase and a 6% mean aerodynamic chord (MAC) aft center-of-gravity (c.g.) shift for the 727 refan at a BRGW of 172 500 lb (78 245 kg). This aft c.g. shift would be unacceptable. One solution is the addition of 990 lb (449 kg) of ballast, bringing the total weight increase to 3839 lb (1741 kg). (See table 1.) By adding 990 lb (449 kg) of ballast to the nose radome bulkhead, the "as delivered fleet average" refan airplane operating empty weight c.g. would shift forward to a recommended 42% MAC limit. For ground handling, additional temporary ballast would be required to prevent tipping.

The structural modifications were designed to meet the program design objectives for flightworthy and certifiable hardware, and analysis showed that all requirements were met. Positive margins of safety were calculated in all areas where the design was finalized, and analyses

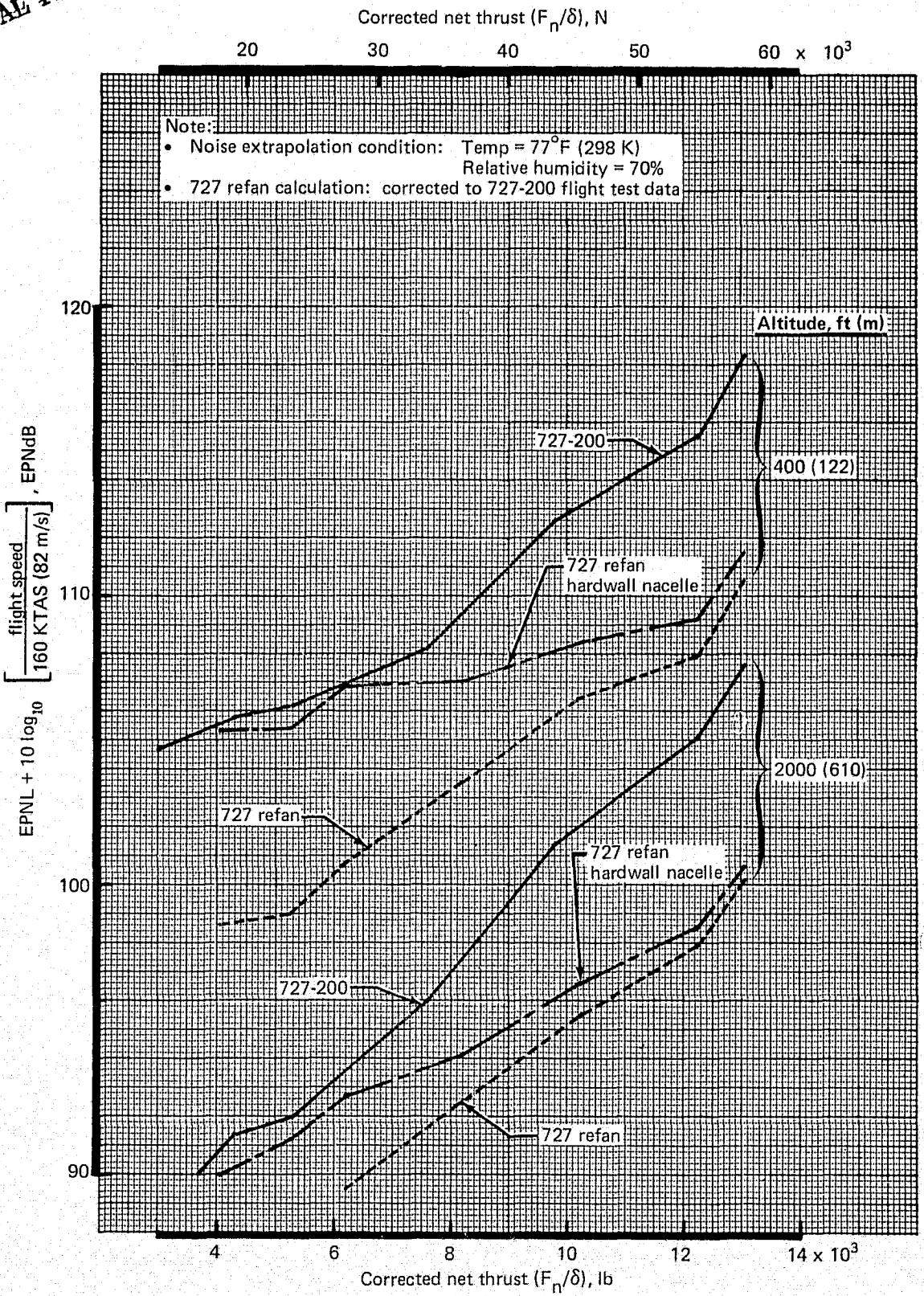

Figure 1.—Summary of the Refan Concept Effectiveness

Note:

- Airplane: 727-200/727 refan
- Takeoff condition: Flap position = 5°
- Approach condition: LGW = 150 000 lb (68 039 kg) or 126 700 lb (57 470 kg)
  Conventional 3° approach
  Flap position = 30°
- Noise extrapolation condition: Temp = 77°F (298 K)
  Relative humidity = 70%
- EPNL calculation: Corrected to 727-200 flight test data
  +5 EPNdB limit on duration correction

Legend:

Takeoff profile designations

- MFPOP
- FAR
- ATA
- CI 1000
- CI 500
- ALPA

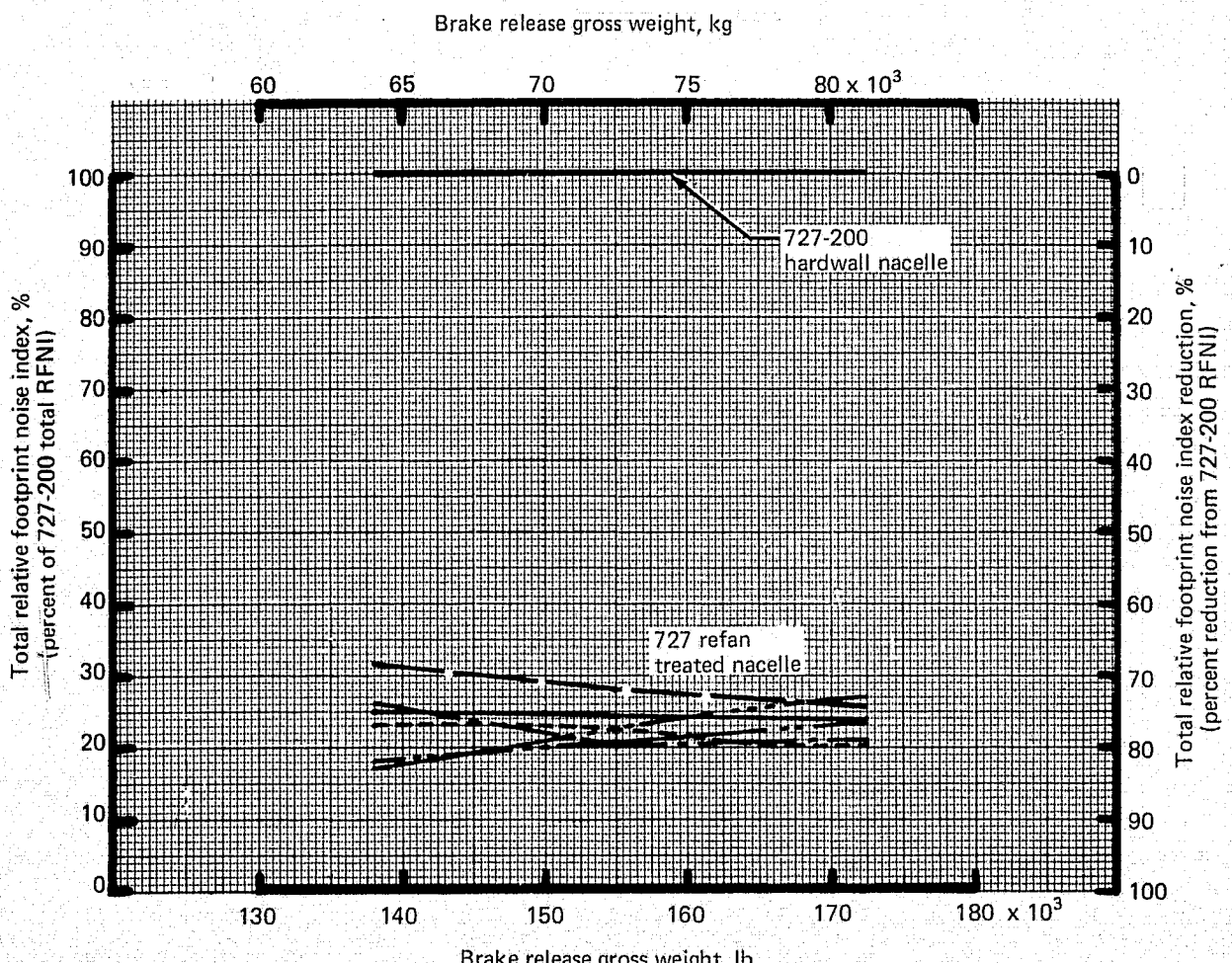

Figure 2.—Summary of 727-200/727 Refan Total Relative Noise Footprint Index (RFNI) Reduction

using definitive loads were completed. A detailed fatigue durability analysis was not attempted, but the fatigue objectives were met by maintaining low stress levels. Where the designs were not finalized, the structural modifications were reviewed only for feasibility, and further structural and fatigue analyses would be required.

Other analyses performed to verify the certifiability of the airplane included a variety of stability and control characteristics, ice protection, cabin environment, brake performance, fire safety, and engine stability with flight inlets.

Further analyses in the structures area included center-engine inlet duct stress, deflection, and dynamic response to surge; exhaust duct thermal stress analysis; and exhaust duct flange and thrust-reverser rail design criteria.

Maximum 727 commonality was assured by analyses verifying the appropriateness of minimum change to engine accessories, airplane and nacelle mechanical and electrical systems, and air-conditioning systems.

2.0 INTRODUCTION

The NASA-sponsored Refan Program was established in mid-1972 with the objective of developing and evaluating JT3D and JT8D refan engine retrofit installations on 707, DC-8, 727, 737, and DC-9 airplanes to reduce aircraft noise with minimum total cost. Participants in the program were the Boeing Commercial Airplane Company, Douglas Aircraft Company, Pratt & Whitney Aircraft, United Air Lines, and American Airlines.

The Boeing Phase I program (Contract NAS3-16815) was undertaken in August 1972 with the initial objective of identifying changes in the existing Boeing airplane fleet to retrofit the refan engine. The Phase I work, reported in reference 1, documents studies relating to the model 707, 727, and 737 airplanes. It describes proposed retrofit configurations, projected performance, and estimated economic aspects of each. Those preliminary design studies led to the conclusion that the JT8D refan engine with its increased bypass ratio could be installed with appropriate inlet and exhaust acoustic treatment on the existing 727-200 airplane to provide substantial reduction in community noise.

In Phase II of the NASA-sponsored Refan Program (Contract NAS3-17842), the Contractor's main tasks were to define the propulsion installation hardware and aircraft modifications required to install the JT8D refan engine in the 727-200 airplane. Flightworthy hardware was designed, manufactured, and ground tested, and the resulting test data were used in performance and noise predictions of the 727-200 retrofitted with JT8D refan engines.

The 727 airplane has been manufactured in two series (-100 and -200) having maximum brake release gross weights (BRGW) from 139 500 lb (63 276 kg) to 207 500 lb (94 120 kg). These airplanes have been equipped with five different JT8D engine models having thrust ratings consistent with the requirements of the particular airplane model.

This volume of the Contractor's Final Report, "Airplane Evaluation and Analysis," presents the analysis of one model of the 727-200 airplane (at a 172 500-lb (78 245-kg) BRGW) as modified by the installation of P&WA JT8D-109 (refan) engines. The engine installation configuration selected for analysis included a treated inlet with ring, treated exhaust duct, and treated fan/primary flow divider (splitter). A sketch of the nacelle configuration is shown in figure 3. The inlet with ring provides forward noise attenuation equivalent to that of a longer inlet without ring and is compatible with aft galley service door access. The selection of a short inlet with a ring, as opposed to a short inlet without a ring, reflects the expressed desires of the NASA to analyze the configuration which yielded the largest noise suppression of those tested during the program; this choice does not necessarily reflect the views of the Contractor.

Most of the hardware tested in the full-scale ground test program was designed and manufactured as certifiable hardware. Extensive structural analyses were conducted for this hardware and are described in this volume. However, additional hardware, which would be required for airplane certification, was only analyzed to assure feasibility.

The performance and noise results presented in this document are not specifications, commitments, or guarantees and are intended only to portray engineering estimates commensurate with program development status.

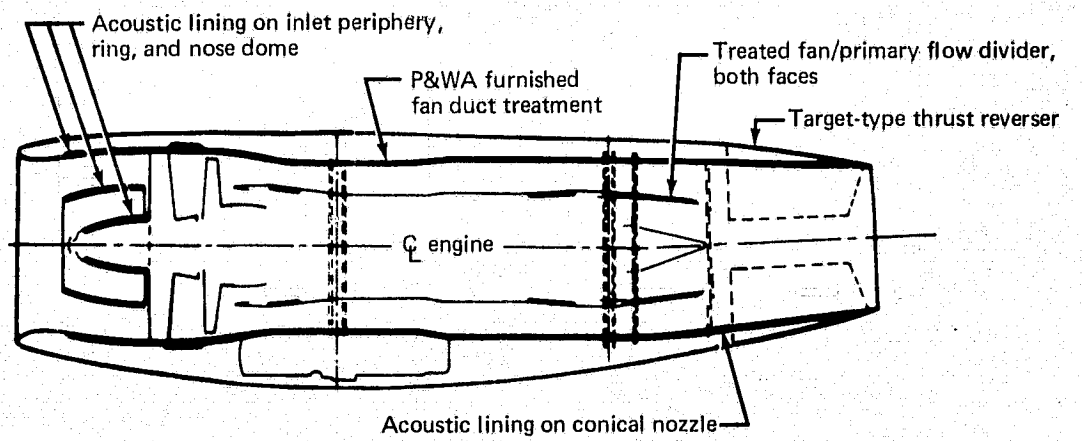

Figure 3.—JT8D Refan Nacelle Configuration for the 727-200 Refan Airplane

The Phase II program used the English system of measurements, with conversion to the International System of Units (SI) (ref. 2) for this report where applicable. The SI units will be found in parentheses following the English units, in additional columns, or as secondary scales where appropriate.

3.0 DISCUSSION

The analyses required to support design studies and predict the JT8D refan noise characteristics and performance on the 727-200 airplane included the following technical disciplines:

- Aerodynamics
- Acoustics
- Propulsion
- Structures
- Weight and balance
- Airplane stability and control
- Electrical and mechanical systems

Discussions and results of these analyses are presented in the following subsections.

3.1 AIRPLANE PERFORMANCE

The airplane performance characteristics that directly affect operational capability are described in this section. The baseline airplane, selected as being typical of the 727-200 fleet, has a maximum BRGW of 172 500 lb (78 245 kg); but is capable of operation at a BRGW of 182 500 lb (82 781 kg) following some minor structural changes resulting in an operational empty weight (OEW) increase of 160 lb (72.6 kg). The higher gross weight is more consistent with the increased thrust capability of the JT8D refan engine. For this reason, performance is shown and discussed in this section for the 172 500-lb (78 245-kg) BRGW baseline airplane, the 727 refan with a maximum BRGW of 172 500 lb (78 245 kg), and the 727 refan with a maximum BRGW of 182 500 lb (82 781 kg)—designated the 727 refan growth option.

The physical characteristics of these airplanes are shown in table 2.

3.1.1 TAKEOFF FIELD LENGTH

The calculated Civil Air Regulation (CAR) takeoff field length comparison between the 727-200 and the 727 refan is shown in figure 4. The takeoff field length is shown as a function of BRGW for sea level and 5000-ft (1524-m) pressure altitude at a temperature of 84°F (302 K). The 727 refan center-engine installation reduces the available rotation angle by approximately 0.4°. This does not affect the takeoff performance with 25° or 15° flaps. For the 5° flap position, the takeoff speed would have to be increased to maintain a minimum ground clearance angle comparable to the 727-200. This effect has been included in the takeoff performance.

The minimum control speeds do not limit the takeoff performance for the 727 refan airplane.

Table 2.—Airplane Characteristics

	727-200 (baseline)	727 refan	727 refan growth option
Maximum taxi weight, lb (kg)	173 000 (78 471)	173 000 (78 471)	183 000 (83 008)
Maximum brake release gross weight, lb (kg)	172 500 (78 245)	172 500 (78 245)	182 500 (82 781)
Maximum landing weight, lb (kg)			
30° flaps	150 000 (68 040)	150 000 (68 040)	154 500 (70 081)
40° flaps	142 500 (64 638)	142 500 (64 638)	142 500 (64 638)
Maximum zero fuel weight, lb (kg)	136 000 (61 689)	136 000 (61 689)	138 000 (62 596)
Passenger seating capacity	134 passengers (20 FC/114 TC)	134 passengers (20 FC/114 TC)	134 passengers (20 FC/114 TC)
Fuel capacity, gal (m^3)	7 680 (29.071)	7 680 (29.071)	7 780 (29.449)
Interior	2-class seating, typical galley and furnishings arrangement	2-class seating, typical galley and furnishings arrangement	2-class seating, typical galley and furnishings arrangement
Engine	JT8D-9	JT8D-109	JT8D-109
Operating empty weight, lb (kg)	99 000 (44 906)	102 840 (46 647)	103 000 (46 720)
C.G. (at operating empty weight)	40%	42%	42%

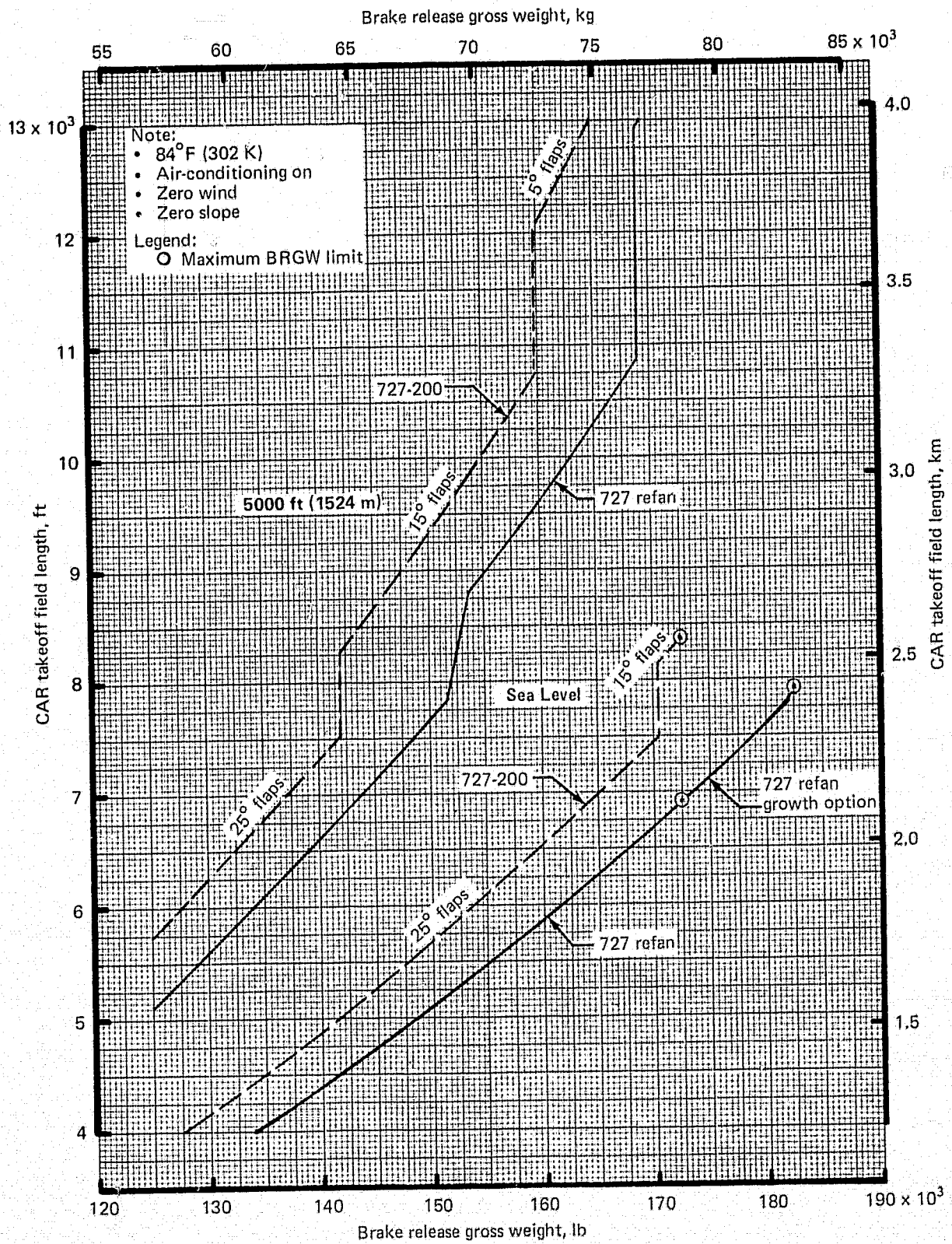

Figure 4.—727-200/727 Refan Performance Comparison—Takeoff Field Length

3.1.2 TAKEOFF FLIGHTPATH

The all-engine takeoff and climb comparison is presented in terms of airplane height above the runway, as a function of distance from brake release. Figure 5 compares the takeoff flightpaths between the 727-200 and the 727 refan at 172 500-lb (78 245-kg) BRGW. These data are used in conjunction with the Federal Aviation Regulation (FAR) Part 36 noise analyses.

Flightpaths are shown with and without thrust cutback. In the cutback case, the thrust is reduced to an engine thrust setting that provides level flight capability with one engine inoperative. The thrust cutback is initiated 3.2 nmi (5.9 km) from brake release. The takeoff flap setting (5°) and a flight speed equal to V_2 + 10 kn (V_2 + 5.1 m/s) are maintained during the climbout.

From the figure, it can be seen that the 727 refan is 210 ft (64.0 m) higher than the 727-200 at the noise measuring point, 3.5 nmi (6.5 km) from brake release. This contributes to the reduction in the takeoff noise levels discussed in section 3.2.

3.1.3 INITIAL CRUISE ALTITUDE CAPABILITY

In general the 727 refan has reasonable altitude capability, although a small cruise thrust increase for altitudes below 35 000 ft (10 668 m) would make it more attractive, particularly for the growth option operating at its maximum BRGW of 182 500 lb (82 781 kg). The initial cruise altitude capability of the 727 refan at the range recovery weight of 177 200 lb (80 377 kg) (see discussion in section 3.1.6) is slightly less (≃1000 ft (≃305 m)) than that of the 727-200 at maximum BRGW using M_∞ = 0.80 on an ISA + 18°F (10 K) day as the criterion. These are the conditions at which some airplane/engine combinations have altitude capability deficiencies that are bothersome to the airlines. Considering the 727-200 and the 727 refan at the same BRGW, 172 500 lb (78 245 kg), the altitude capability of the 727 refan is slightly better (≃500 ft (≃152 m)) than that of the 727-200.

3.1.4 PAYLOAD RANGE

A comparison of the payload range characteristics of the 727-200 airplane with the 727 refan is shown in figure 6. The cruise conditions, weights, and mission ground rules are identified in the figure. At the same BRGW of 172 500 lb (78 245 kg), the 727 refan loses 205 nmi (380 km) of range relative to the 727-200. By taking advantage of the growth option, the 727 refan range is much more attractive. (See table 3.) Because of the substantial takeoff thrust increase for the JT8D-109 engine, the weight growth can be accommodated with no loss in takeoff field performance.

Takeoff field length-versus-range comparisons are shown in figures 7 and 8 for full passenger payload and 55% load factor conditions, respectively. The 727 refan offers significant range improvement from the same takeoff field length. The data shown in these figures are for the 727 refan growth option airplane with an OEW of 103 000 lb (46 720 kg). The corresponding information for the 102 840-lb (46 647-kg) OEW 727 refan would show a 7-nmi (12.96-km) range increase at a given field length, but would show a 30-nmi (55.56-km) lower fuel-capacity-limited range.

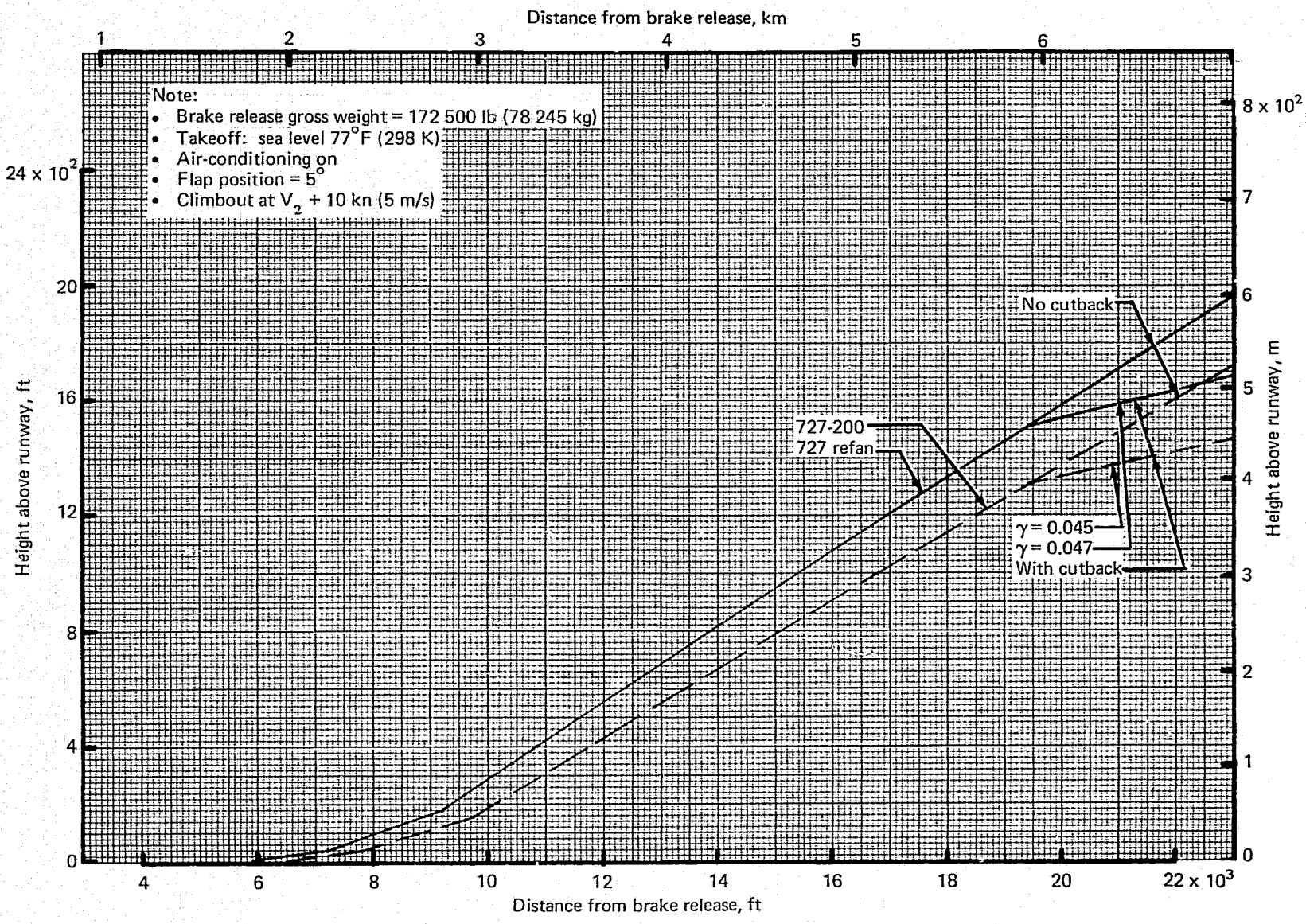

Figure 5.—727-200/727 Refan Performance Comparison—Takeoff Flightpath

Note:
M_∞ = 0.84 at 30 000 ft (9144 m)
ATA domestic reserves
Standard day
No wind

Airplane	Engine	Max BRGW, lb (kg)	Fuel capacity, U.S. gal (m^3)	OEW, lb (kg)
727-200	JT8D-9	172 500 (78 245)	7680 (29.071)	99 000 (44 906)
727 refan	JT8D-109	172 500 (78 245)	7680 (29.071)	102 840 (46 647)
727 refan growth option	JT8D-109	182 500 (82 781)	7780 (29.450)	103 000 (46 720)

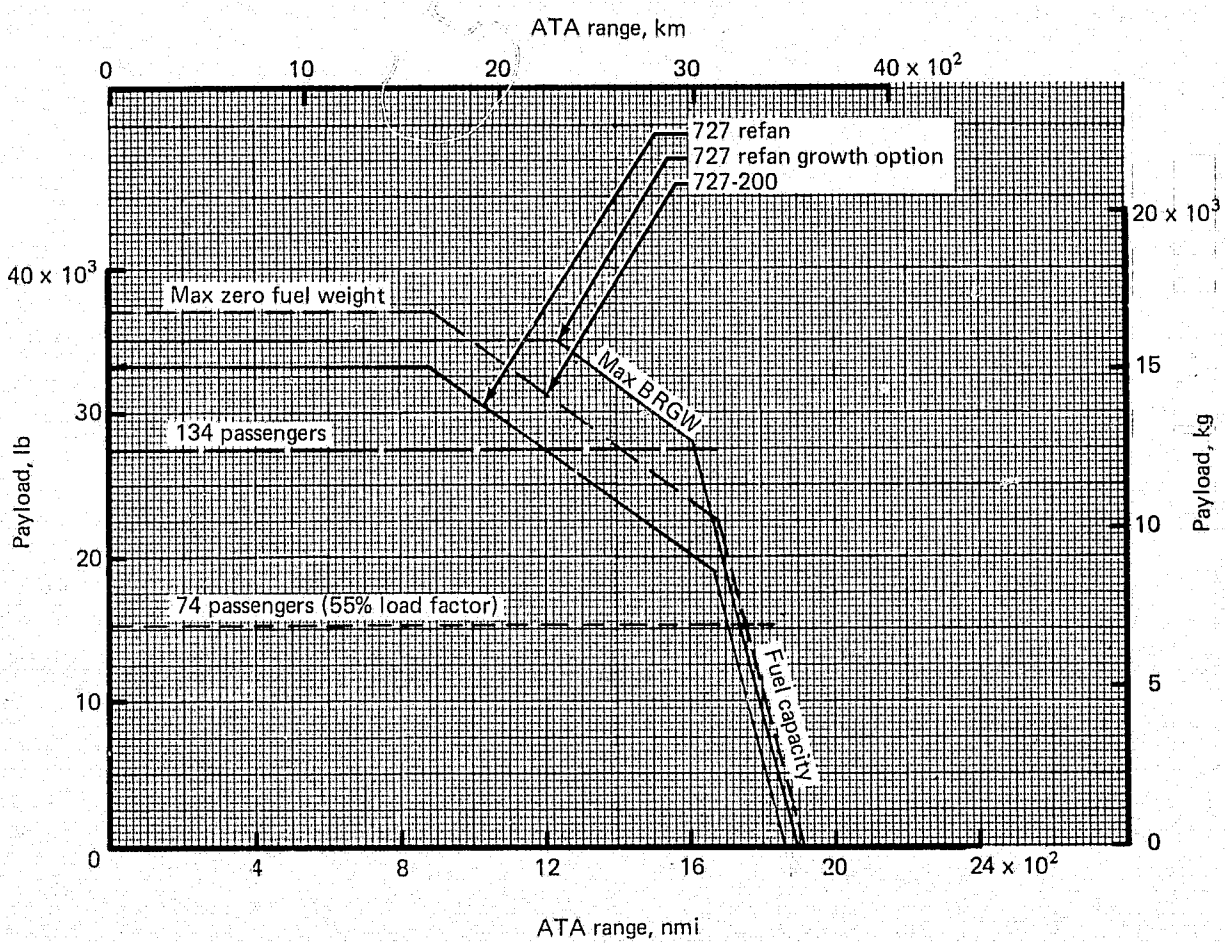

Figure 6.—727-200/727 Refan Performance Comparison—Payload Versus Range

Table 3.—Full Passenger Payload Range Comparison

Airplane	BRGW, lb (kg)	OEW, lb (kg)	Range, nmi (km)	Δ Range, nmi (km)	Takeoff field length, ft (m)
727-200	172 500 (78 245)	99 000 (44 906)	1405 (2602)	0 (0)	8370 (2551)
727 refan	172 500 (78 245)	102 840 (46 647)	1200 (2222)	-205 (-380)	6920 (2109)
727 refan growth option	182 180 (82 635)	103 000 (46 720)	1615 (2991)	+210 (+389)	7860 (2396)

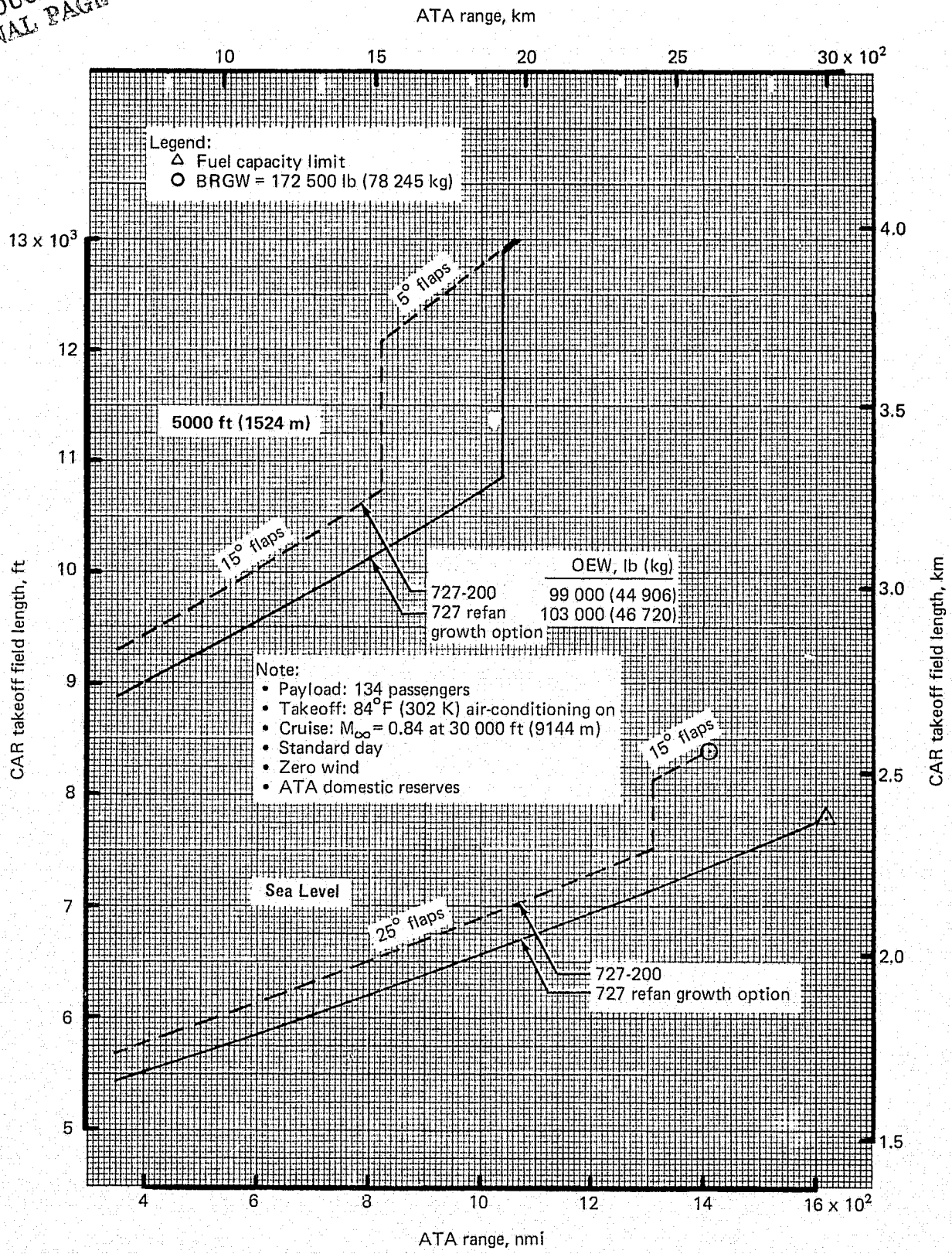

Figure 7.—727-200/727 Refan Performance Comparison—Field Length Versus Range for Full Passenger Payload

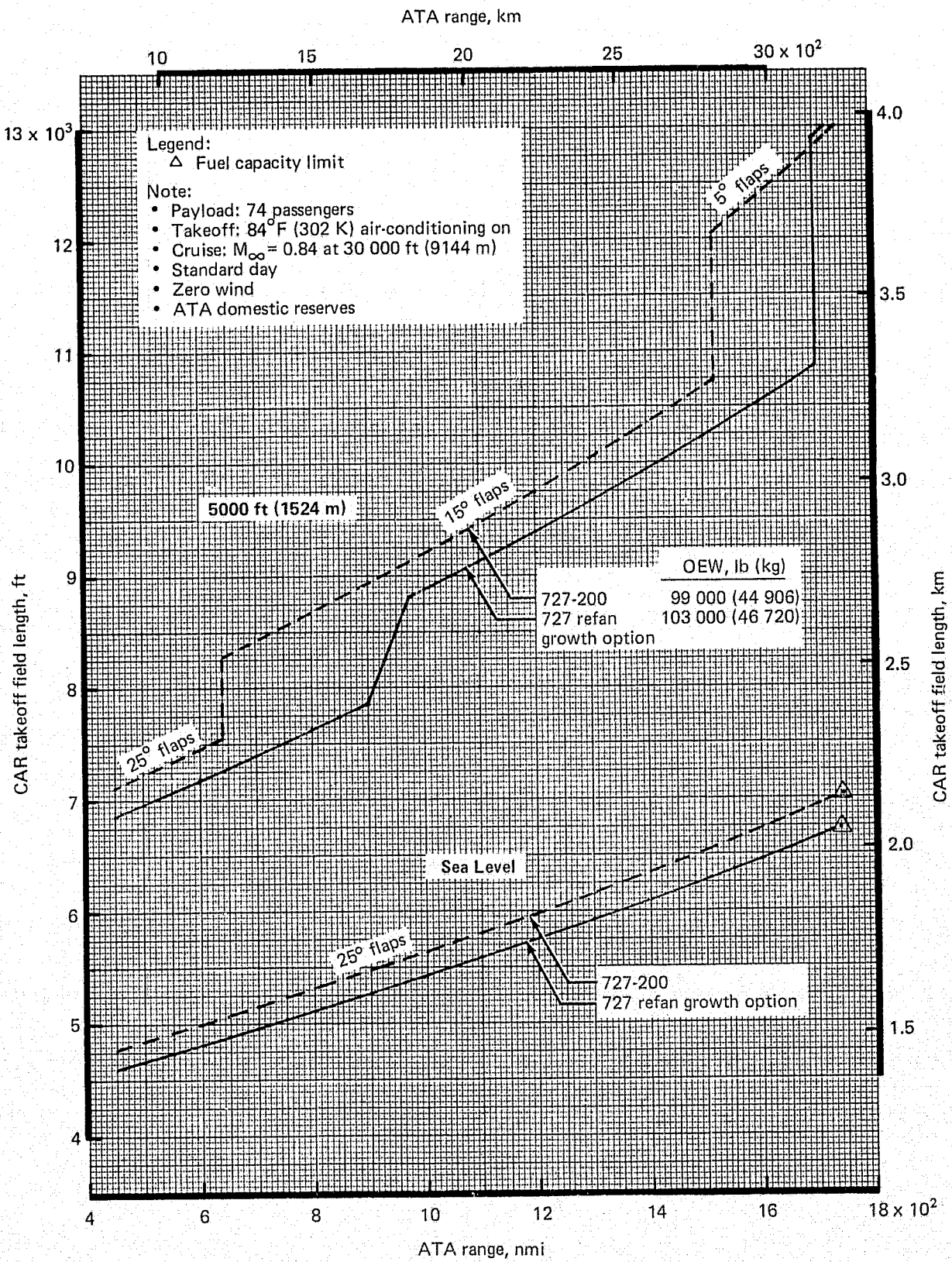

Figure 8.—727-200/727 Refan Performance Comparison—Field Length Versus Range for 55% Load Factor

3.1.5 BLOCK FUEL

A comparison of the block fuel used by the 727-200 airplane with that of the 727 refan is shown in figures 9 and 10 for full passenger payload and 55% load factor missions, respectively. The block fuel is shown as a function of range. The cruise conditions, weights, and mission ground rules are identified in the figures. It can be seen that for both full and 55% load factor payloads, the 727 refan block fuel is approximately 1.5% to 3% greater than the 727-200 for all ranges.

3.1.6 PERFORMANCE OPTIONS

There are a number of ways of comparing the performance of the 727 refan with the 727-200 and a number of ways in which the airlines could operate the 727 refan. Four performance options will be discussed in terms of their major performance changes relative to the 727-200 (with full passenger payload):

- *OPTION 1: Constant maximum BRGW equal to that of the 727-200 (172 500 lb (78 245 kg)).*—At the same BRGW of 172 500 lb (78 245 kg), the 727 refan loses 205 nmi (380 km) of range relative to the 727-200 while offering a 1450-ft (442-m) reduction in CAR takeoff field length.

- *OPTION 2: Takeoff field length equal to that of the 727-200 (8370 ft (2551 m)).*—For a takeoff field length of 8370 ft (2551 m), the 727 refan could take off with 183 800 lb (83 370 kg) if it were neither structurally nor fuel-capacity-limited to a lesser BRGW. However, for a full passenger payload and full fuel tanks, the airplane weighs 182 180 lb (82 635 kg) at brake release. Even with this fuel capacity weight restriction, this growth option 727 refan offers a 210-nmi (389-km) increase in range while also requiring 510 ft (155 m) less takeoff field length.

- *OPTION 3: Range equal to that of the 727-200 (1405 nmi (2602 km)).*—If it were required to match the 727-200 range of 1405 nmi (2602 km) with the 727 refan, a growth in BRGW to 177 200 lb (80 377 kg) would accomplish this while providing a decrease of 1000 ft (305 m) in takeoff field length and a 1.5% increase in block fuel.

- *OPTION 4: Practical weight growth with minor structural changes (182 500 lb (82 781 kg)).*—A practical maximum BRGW limit (minor structural changes) for many of the 727-200's is 182 500 lb (82 781 kg). Growth above that weight requires more extensive structural changes and is more costly in terms of increased operating empty weight, airplane modification time, and actual cost. From a performance standpoint, growth from 172 500 lb (78 245 kg) to 182 500 lb (82 781 kg) requires only 160-lb (72.6-kg) OEW increase. To take advantage of the performance benefits of this growth, airlines could carry more than a full passenger payload (i.e., possibly 4230 lb (1919 kg) of cargo) and still match the 727-200 range of 1405 nmi (2602 km). For just the full passenger payload, this growth is restricted by fuel capacity as discussed in the equal takeoff field length option.

Table 4 summarizes the incremental performance of these options.

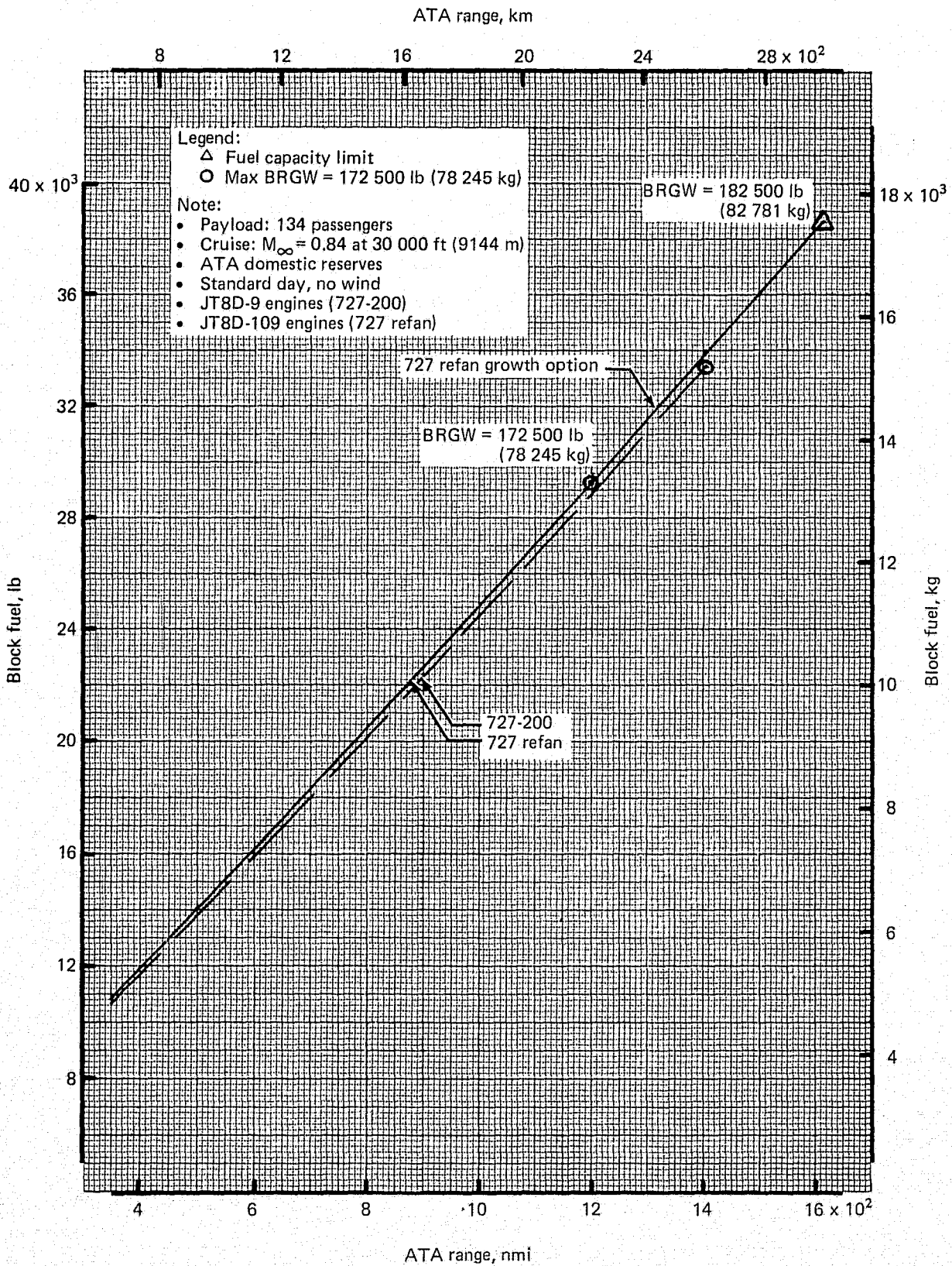

Figure 9.—727-200/727 Refan Performance Comparison—Block Fuel for Full Passenger Payload

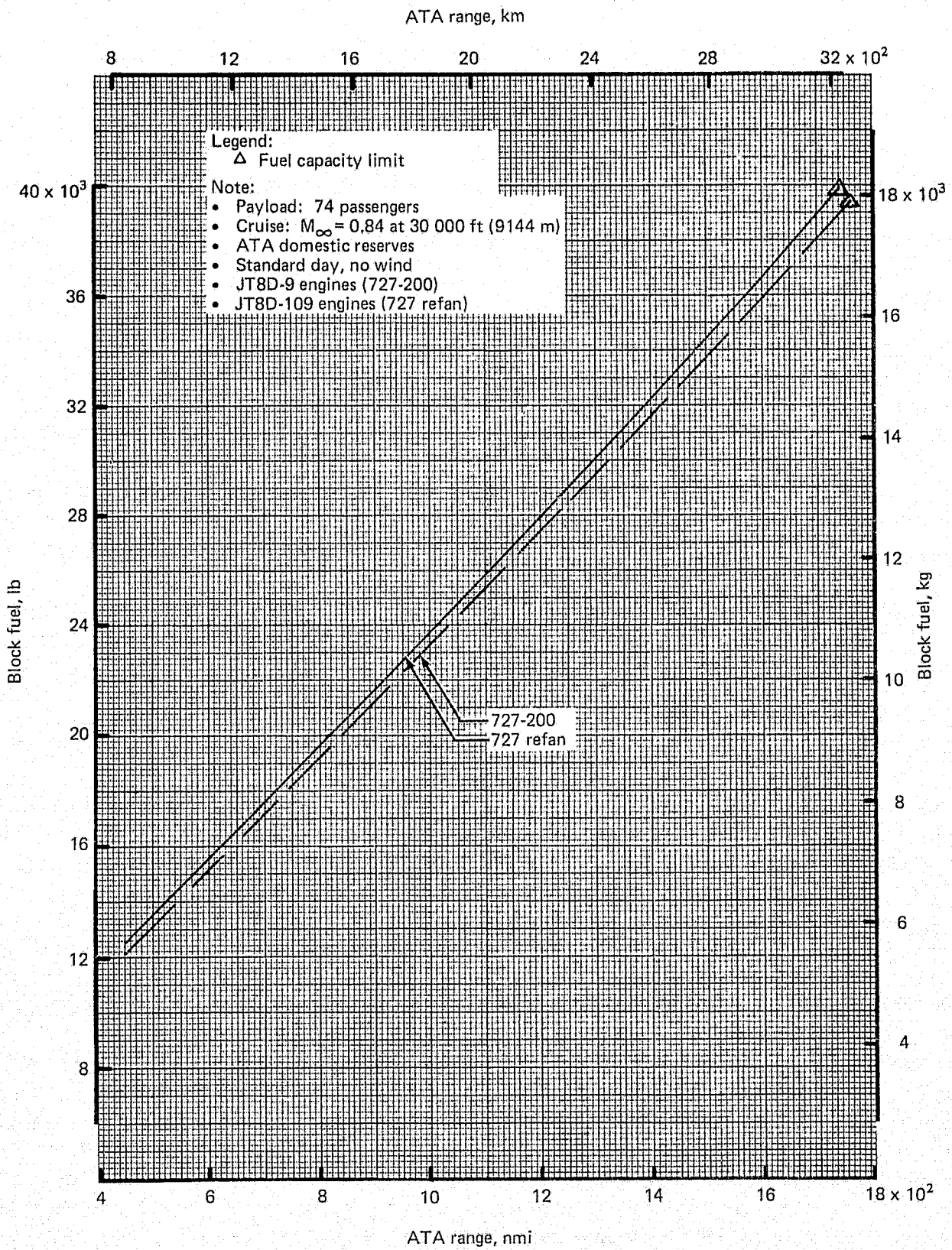

Figure 10.—727-200/727 Refan Performance Comparison—Block Fuel for 55% Payload

Table 4.—727 Refan Performance Options

Option	Airplane	Performance basis	ΔBRGW, lb (kg)	ΔOEW, lb (kg)	ΔRange, nmi (km)	Δ T/O field length, ft (m)
1	727 refan	Brake release gross weight = 172 500 lb (78 245 kg)	0 (0)	+3840 (+1742)	-205 (-380)	-1450 (-442)
2	[a]727 refan growth option	Takeoff field length = 8370 ft (2551 m)	[b]+9680 (+4391)	+4000 (+1814)	+210 (+389)	-510 (-155)
3	[a]727 refan growth option	Range = 1405 nmi (2602 km)	+4700 (+2132)	+4000 (+1814)	0 (0)	-1000 (-305)
4	[a]727 refan growth option	Practical growth limit = 182 500 lb (82 781 kg)	[b]+9680 (+4391)	+4000 (+1814)	+210 (+389)	-510 (-155)

727-200 airplane:
Max taxi wt. = 173 000 lb (78 471 kg)
Max BRGW = 172 500 lb (78 245 kg)
OEW = 99 000 lb (44 906 kg)
Max fuel capacity = 7680 U.S. gal (29.071 m^3)

Baseline performance:
ATA range = 1405 nmi (2602 km)
T/O field length = 8370 ft (2551 m)

Takeoff conditions:
Sea level; 84°F (302 K)
Air-conditioning on

Cruise conditions:
M_∞ = 0.84 at 30 000 ft (9144 m)
Standard day
Payload = 134 passengers 27 470 lb (12 460 kg)
Zero wind
ATA domestic reserves

[a] Fuel capacity of growth options is increased to 7780 U.S. gal (29.450 m^3)

[b] Fuel capacity limits gross weight to 182 180 lb (82 635 kg) for the 134-passenger payload.

3.1.7 DESCENT AND LANDING PERFORMANCE

The JT8D refan engine requires higher flight idle thrust than the JT8D engine to attain the 8-sec acceleration for landing go-around. This increased thrust would cause the 727 refan to descend more slowly than the 727-200. Consequently, the fuel burned, the time to descend, and the distance to descend from a given altitude would all increase. Figures 11 and 12 show the descent comparison. From an airline operational standpoint, the result of this would be to increase the block times for the 727 refan missions by up to 1 minute compared to the 727-200. This increase would have a small detrimental effect on direct operating cost. Although the fuel required to descend from any altitude increases for the 727 refan, the overall effect on mission block fuel of the higher idle thrust is insignificant since the 727 refan starts its descent farther from the destination airport, thereby decreasing the fuel burned during cruise.

The high flight idle thrust of the JT8D-109 would also restrict the operational flexibility of the airplane relative to that of the 727-200. For noise purposes, some airlines have flown dual segment glide slope approaches (i.e., 6°/3°) with the 727-200. The 6° glide slope requires the 727 refan to have the capability to descend at a 7.2° glide slope in order to maintain glide slope control in the case of a tailwind or gust. Figure 13 shows that the idle thrust level of the JT8D refan engine would be too high to allow the 727 refan to descend on a 6° slope. It could, however, descend at the normal operational 3° glide slope for all gross weights.

There would be no changes in the landing performance of the 727 refan relative to the 727-200.

The data in figures 11, 12, and 13 apply to both the 727 refan and the growth option 727 refan.

3.2 AIRPLANE COMMUNITY NOISE

This section presents the community noise predictions for the 727 refan airplane powered by JT8D-109 engines installed in the refan nacelle. The refan nacelle designates a nacelle with peripheral treatment (wall treatment in the center duct, side inlet, and exhaust duct) plus a single, treated, inlet ring and treated exhaust splitter for each side engine. This nacelle configuration is matched to a JT8D-109 engine with fan case and fan duct wall treatment. A detailed discussion of the engine/nacelle acoustic design is presented in section 3.2.3 of reference 3.

This section begins with an explanation (section 3.2.1) of the method of application of the ground static test data of reference 3 to the 727-200 and 727 refan airplanes. The FAR Part 36 noise performance, representative tone-corrected perceived noise level (PNLT) time histories, and component-noise sensitivity studies are the subjects of section 3.2.2. Generalized noise-thrust-altitude (NTA) curves, including component noise versus net thrust, are shown in section 3.2.3. Single-event effective perceived noise level (EPNL) footprint contours and single-number relative footprint noise index (RFNI) are shown for a variety of gross weights and flight profiles in section 3.2.4.

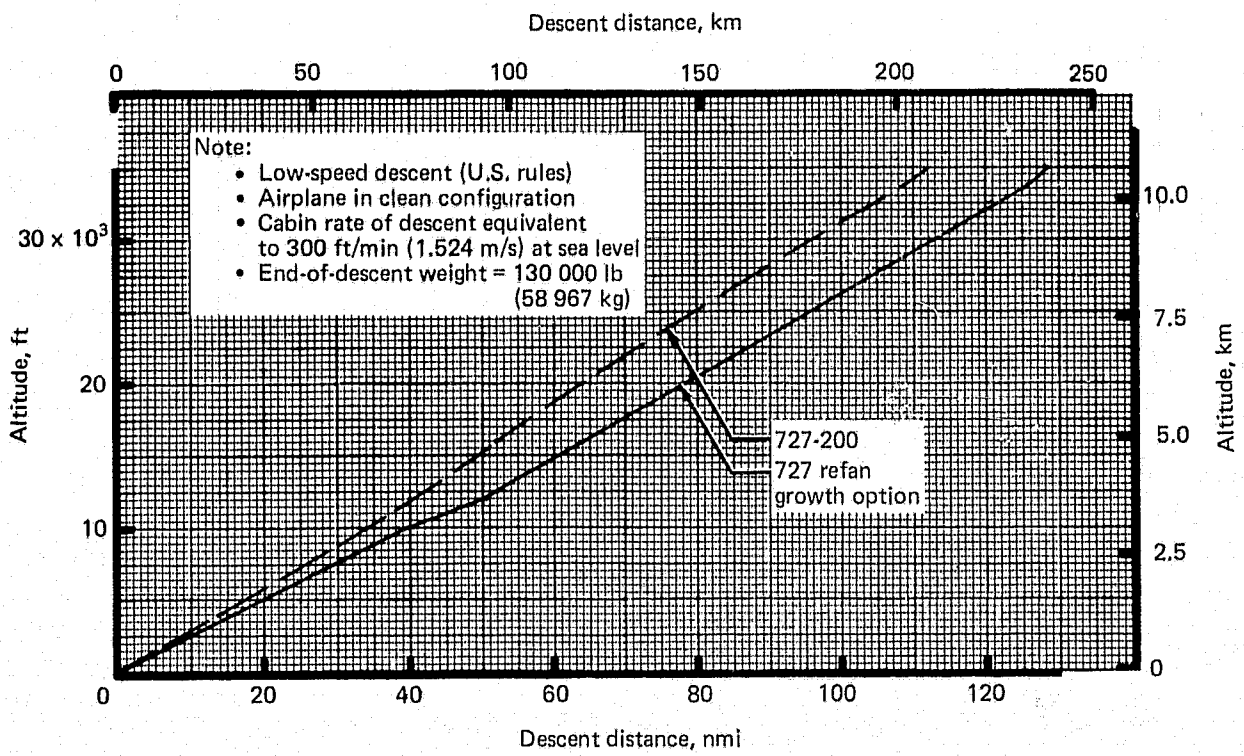

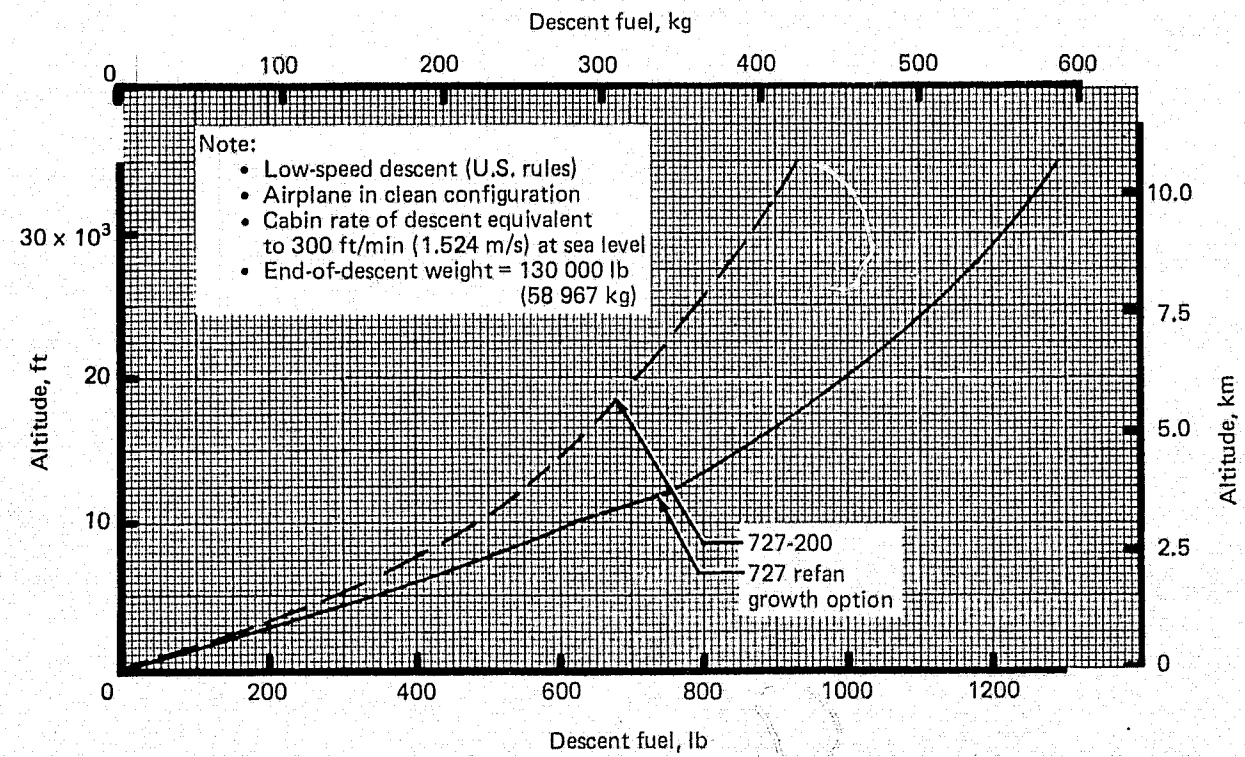

Figure 11.—727-200/727 Refan Performance Comparison—Descent Fuel and Distance

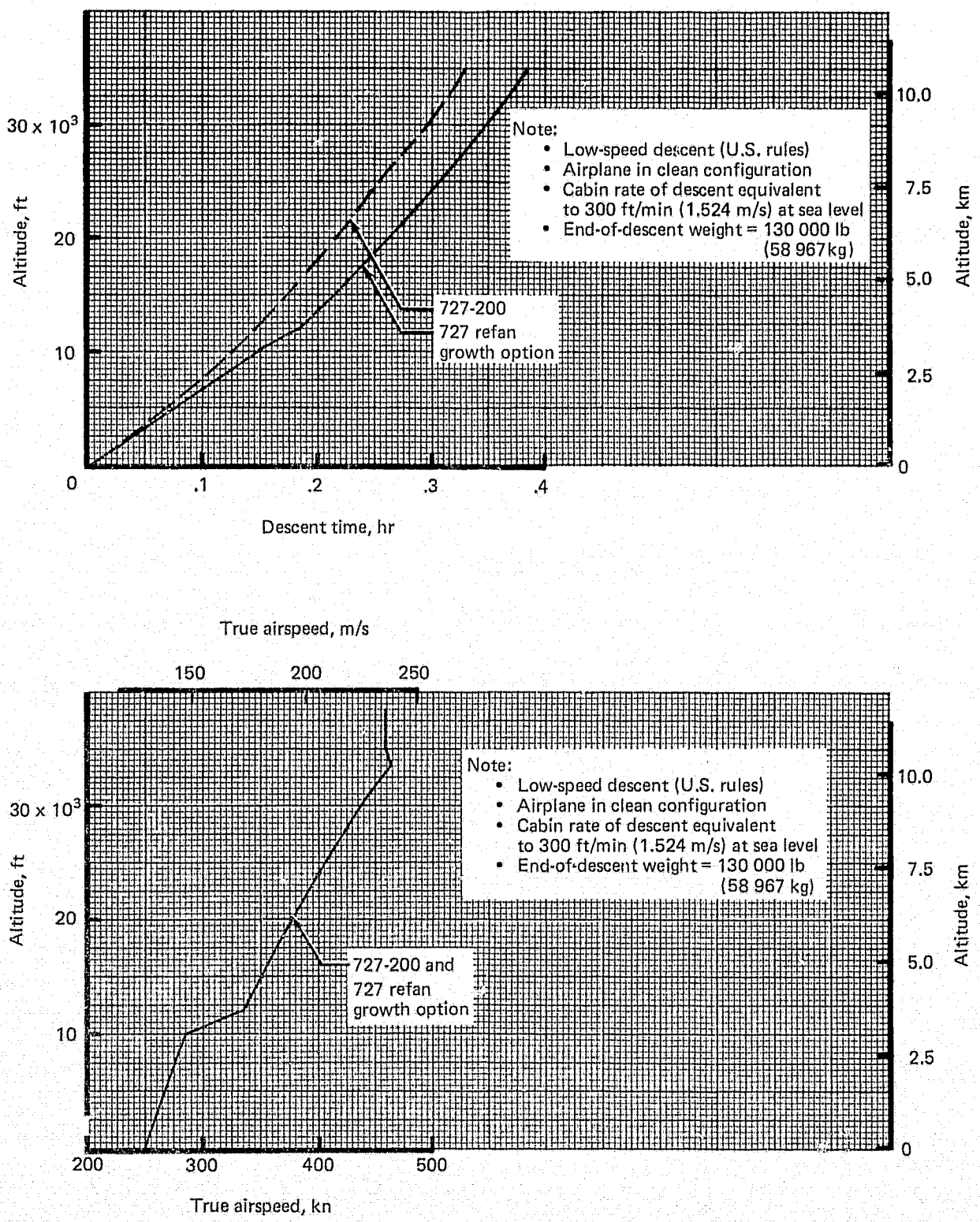

Figure 12.—727-200/727 Refan Performance Comparison—Descent Time and Speed

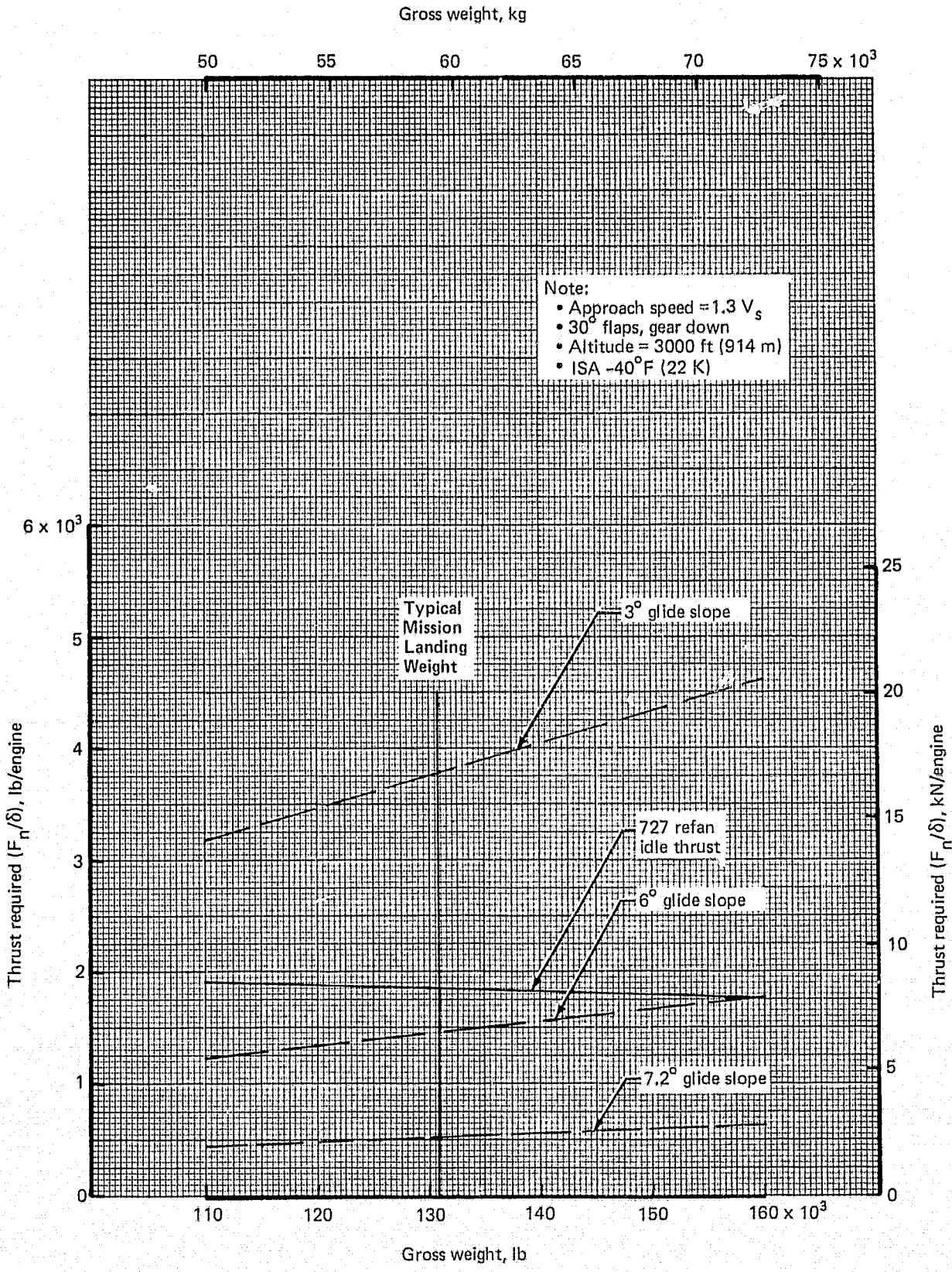

Figure 13.—727-200/727 Refan Performance—Glide Slope Capability

3.2.1 727-200 AND 727 REFAN FLYOVER NOISE PREDICTION METHOD

Acoustic characteristics of the 727-200 airplane, both with JT8D-9 (baseline) and with JT8D-109 (refan) engines, were evaluated using a Contractor-developed flyover noise prediction method. This method used engine performance parameters (e.g., corrected rpm and jet velocity) and airplane performance parameters (e.g., speed, altitude, and corrected thrust) as basic inputs. Sound pressure levels (SPL) for the various noise components and a logarithmic total were predicted for 17 radiation angles and twenty-four 1/3-octave bandwidth center frequencies. Also predicted were perceived noise levels (PNL), PNLT, and EPNL.

The logic of the prediction method is illustrated in detail in figure 14. The method combines JT8D-15 (baseline) and JT8D-115 (refan) ground test noise and propulsion cycle data with existing 727-200 JT8D-9 propulsion performance and noise flight test data, and leads to the prediction of flyover component and total noise of the JT8D-9 powered 727-200 airplane and the JT8D-109 powered 727 refan airplane.

The keynote of the analysis method is the emphasis on five major engine noise components:

- Inlet fan noise, including buzzsaw, emitted from the inlet duct (and designated inlet radiated fan noise in ref. 3)
- Aft fan noise emitted from the fan discharge duct (and designated discharge radiated fan noise in ref. 3)
- Low-frequency core noise, internally generated in the burner and emitted from the primary duct
- Turbine noise emitted from the primary duct
- Jet exhaust noise, including exhaust duct flow noise as described in reference 3

Estimates of each noise source were based on semiempirical prediction models.

The first step in the prediction analysis is the establishment of ground-to-flight corrections for the various noise components. This process is indicated by the solid lines in the upper left-hand part of figure 14. Component source noise for the JT8D-15 engine (block 1) and airframe noise for the 727-200 (block 2) were extrapolated to 727-200 JT8D-9 flight conditions including number of engines, atmospheric attenuation, Doppler shift, spherical divergence, and extra ground attenuation. The spectral content and directional properties of the logarithmic sum of the extrapolated component source noises (block 3) were then compared with those of the existing 727-200 JT8D-9 flight test data (block 2); this comparison yielded the desired component ground-to-flight corrections linking the existing 727-200 flight test data and the Boardman JT8D-15 ground test data.

The values of the component noise ground-to-flight corrections (block 3) are presented in table 5. The ground-to-flight increments for all components are assumed to be independent of power setting, with the exception of jet noise which includes the relative jet velocity

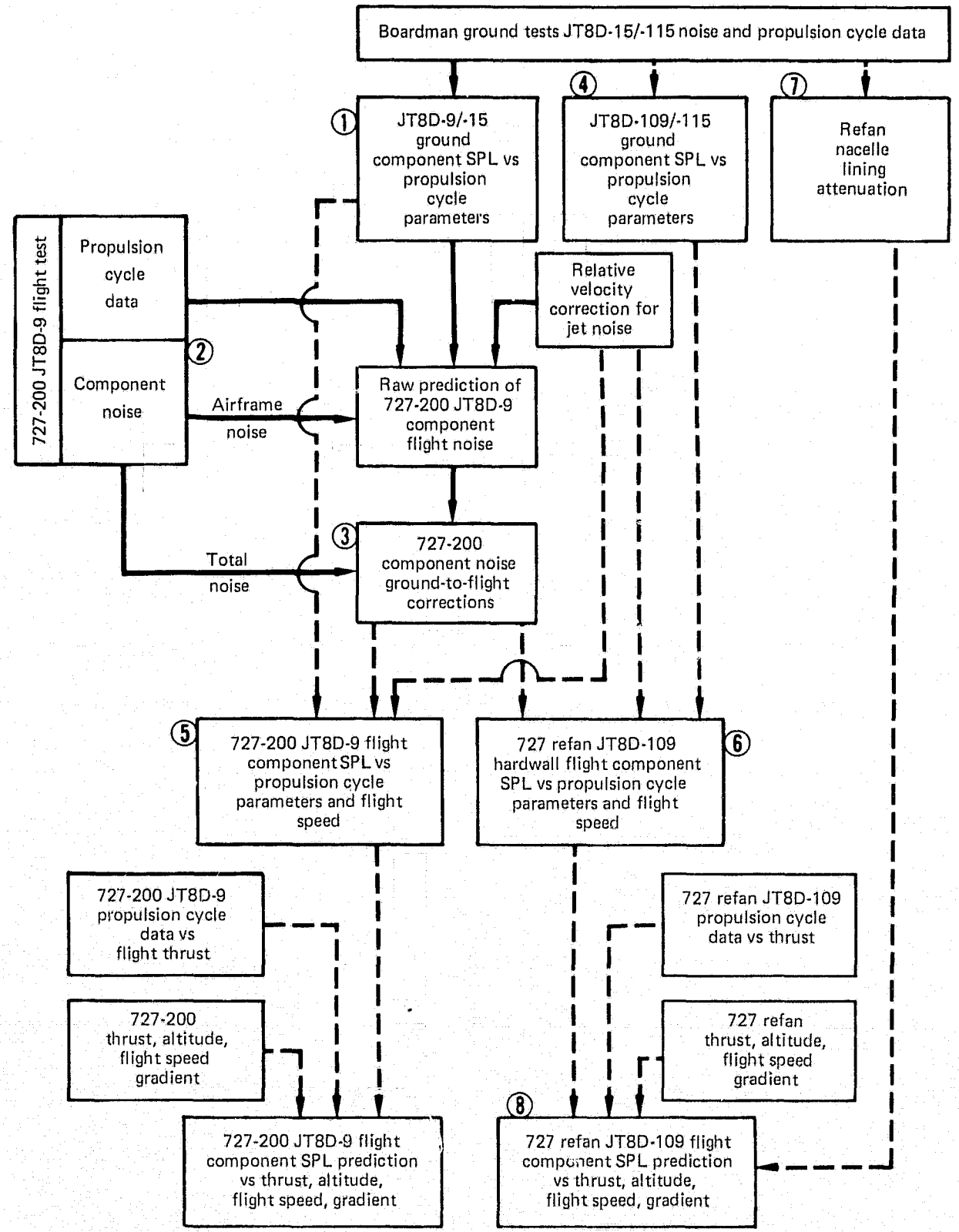

Figure 14.—Flyover Noise Prediction Method

Table 5.—Ground-to-Flight Corrections Based on JT8D-15 Ground Test and JT8D-9 Flight Test Data

(Tabulated values are ΔSPL in dB to be applied to tone frequencies for discrete tone sources and to all frequencies for broadband sources)

Component	Directivity angle, deg										
	10 to 65	70	80	90	100	110	120	130	140	150	160
Inlet fan											
Fundamental	-0.8	-0.8	-0.8	-0.8	-0.8	-0.8	-0.8	-0.8	-0.8	-0.8	-0.8
Harmonics	2.2	2.2	2.2	2.2	2.2	2.2	2.2	2.2	2.2	2.2	2.2
Broadband	2.2	2.2	2.2	2.2	2.2	2.2	2.2	2.2	2.2	2.2	2.2
Buzzsaw	-3.0	-3.0	-3.0	-3.0	-3.0	-3.0	-3.0	-3.0	-3.0	-3.0	-3.0
Aft fan											
Fundamental	-2.5	-2.5	-2.5	-2.5	-2.5	-2.5	-3.5	-5.0	-5.0	-5.0	-5.0
Harmonics	1.5	1.5	1.5	1.5	1.5	1.5	0.5	-1.0	-1.0	-1.0	-1.0
Broadband	-2.0	-2.0	-2.0	-2.0	-2.0	-2.0	-3.0	-4.5	-4.5	-4.5	-4.5
Turbine	-2.0	-2.0	-2.0	-2.0	-2.0	-3.0	-4.0	-4.0	-4.0	-4.0	-4.0
Core	0.0	0.0	0.0	0.0	0.0	0.0	0.0	0.0	0.0	0.0	0.0
Jet[a]	2.6	2.4	2.3	2.1	1.8	1.6	1.6	1.6	1.1	-0.6	-2.2

[a]The jet component ground-to-flight increment includes the additional correction:

$$60 \log_{10} \frac{V_{pri} - V_{\infty}}{V_{pri}}$$

correction: $60 \log_{10}[(V_{pri} - V_{\infty})/V_{pri}]$. This correction is based on wind tunnel model tests and free jet experiments, as well as from observations of flight test data.

These ground-to-flight corrections account for airplane installation effects such as wing and body shielding of inlet noise, inlet turbulence effects on inlet noise, and interaction of clustered exhausts. They are assumed to be also applicable to the 727 refan airplane.

The dashed lines of figure 14 show how these ground-to-flight corrections are used together with the component noise predictions obtained from the Boardman JT8D-15 ground test data (block 1) and JT8D-115 ground test data (block 4), to predict component flyover SPL's for both the 727-200 airplane (block 5) and the 727 refan airplane (block 6).

A key element of this procedure is the use of flight propulsion cycle data for the JT8D-9 and -109 engines in order to properly relate the component noise to thrust, altitude, and airplane speed. Installed propulsion system performance data were calculated by the Contractor for both the JT8D-9 and -109 engines. The engine cycle data for the noise analysis were representative of three side engines at flight conditions on an ISA + 18°F (10 K) day. The Contractor's engine simulation computer program incorporated the latest JT8D-9 and -109 computer decks received from P&WA.

Lining attenuation estimates, based on measured attenuation of the refan nacelle, were used to describe the acoustic performance of the linings designed for the nacelle and are described in section 4.2.4 of reference 3. The lining attenuation spectra for each noise component were calculated for each power setting at a 90° radiation angle. The attenuation spectra were expanded over 17 radiation angles to account for directivity effects (block 7) and were subtracted from the hardwall SPL's to obtain the treated SPL's (block 8).

For the inlet noise, the JT8D-9 hardwall noise levels assumed equal contributions from the three 727-200 engines. The treated JT8D-109 inlet noise was calculated by applying the side-engine inlet and center-engine inlet duct attenuation separately to the appropriate engines, then logarithmically summing the noise of the three suppressed engines.

Airframe noise was recognized as one of the contributors to the total far-field noise. An estimate of the airframe noise was included in this study and was based on data available from flight tests of the 747 and 727 airplanes. It was assumed that airframe noise was predominantly generated by turbulent flow at the edges of airfoils, cavities, and landing gear and varied with wing area, drag coefficients, flap setting, gear position, and flight speed.

In summary, the ground-to-flight corrections force basic component agreement of the prediction method with existing 727-200 JT8D-9 flight test data; and the component noise improvements of the treated JT8D refan engine and nacelle demonstrated by the Boardman ground testing are appropriately recognized in the flight situation.

The prediction method was used to calculate FAR Part 36 noise levels (section 3.2.2) using the appropriate takeoff climb gradients and landing glide slopes. It was also used to calculate level-flyover NTA data (section 3.2.3) for use in footprint calculations (section 3.2.4).

3.2.2 FAR PART 36 ESTIMATES, FLYOVER TIME HISTORIES, AND COMPONENT-NOISE SENSITIVITY STUDIES

The acoustic signatures of the source noise components were predicted for the FAR Part 36 measuring stations and used to calculate:

1. Total and component EPNL noise levels at the FAR Part 36 conditions

2. Flyover time histories of PNLT versus time

3. The relative impact of changes in the component noise levels (inlet and aft fan, jet, low-frequency core, turbine, and airframe) on the total noise level at each FAR Part 36 condition

3.2.2.1 Total and Component EPNL at FAR Part 36 Conditions

Airplane performance data, calculated for 727-200 and 727 refan airplanes for a sea level airport at ISA + 18°F (10 K), are shown in table 6. The FAR Part 36 component and total noise levels are given in table 7. The FAR Part 36 noise levels of the 172 500-lb (78 245-kg) BRGW 727-200 were obtained through flight test and FAA-approved analysis procedures. Those for the 172 500-lb (78 245-kg) and 182 500-lb (82 781-kg) BRGW 727 refan were calculated by a two-step process: (1) the flyover prediction method described in section 3.2.1 was applied to the 727-200 and 727 refan airplanes, using the appropriate thrust, altitude, flight speeds, climb gradients, and landing glide slopes of each airplane; (2) the resulting 727-200/727 refan EPNL increments were applied to the 727-200 flight test FAR Part 36 levels. In this manner, the absolute values of the 727 refan noise levels were anchored to existing flight test data while maintaining the predicted analytical increments for the 727 refan. The 177 200-lb (80 377-kg) equal-range 727 refan FAR Part 36 levels were calculated by interpolating on gross weight.

The 727 refan shows a significant improvement in terms of FAR Part 36 noise levels as compared to the 727-200. As shown by the ΔEPNL in table 7, the FAR Part 36 noise levels are 6 to 8 EPNdB lower than the 727-200 for the 172 500-lb (78 245-kg) 727 refan, 4 to 8 EPNdB for the 182 500-lb (82 781-kg) growth option 727 refan, and 5 to 8 EPNdB for the equal-range 727 refan. At all three BRGW's, the 727 refan is significantly below FAR Part 36 at the cutback and sideline conditions and nominally meets the FAR Part 36 three-point requirement without the use of thrust cutback (i.e., with trades).

The goal of the JT8D refan program was to reduce the noise levels from those of the 727-200 by 10 EPNdB or more for the 172 500-lb (78 245-kg) BRGW model and by 9 EPNdB or more for the 182 500-lb (82 781-kg) growth BRGW. These goals were not met according to this analysis, partly because exhaust duct flow noise was not known to exist, and core noise was of unknown significance at the start of the program. An exhaust mixer would have satisfied the program goals at full-power takeoff and sideline.

The relative impact of the source noise components on the total EPNL far-field noise at each FAR Part 36 measuring location is presented in table 8 and indicates that for the 727-200:

Table 6.—727 JT8D Flight Engine Cycle Parameters at FAR Part 36 Measuring Stations, Sea Level Airport at ISA + 18°F (10 K)

(a) 727-200/JT8D-9 Hardwall Nacelle (Baseline)

	Approach 1 nmi (1.85 km)		Takeoff (with cutback) 3.5 nmi (6.58 km)	Takeoff (without cutback) 3.5 nmi (6.48 km)	Sideline 0.25 nmi (0.46 km)
BRGW, lb (kg)	--	--	172 500 (78 245)	172 500 (78 245)	172 500 (78 245)
LGW, lb (kg)	150 000 (68 039)	142 500 (64 637)	--	--	--
Flaps, deg	30	40	5	5	5
Altitude, ft (m)	370 (113)	370 (113)	1390 (423.7)	1520 (463.3)	800 (244)
Sideline distance, ft (m)	--	--	--	--	1520 (463.3)
F_n/δ, lb (N)	4570 (20 327)	6300 (28 022)	8060 (35 851)	12 420 (55 244)	12 310 (54 755)
Flight speed, KTAS (m/s)	146.1 (75.2)	139.1 (71.6)	177.5 (91.3)	177.9 (91.5)	176.0 (90.5)
FPR	1.400	1.529	1.667	1.950	1.943
N_1, rpm	5950	6578	7120	8164	8154
$N_1/\sqrt{\theta_{t2}}$, rpm	--	--	--	--	--
A_{pri}, $ft^2(m^2)$	2.315 (0.215)	2.398 (0.223)	2.481 (0.230)	2.707 (0.251)	2.701 (0.251)
W_{pri}, lb/s (kg/s)	89.9 (40.78)	106.0 (48.08)	119.8 (54.34)	152.0 (68.95)	154.7 (70.17)
V_{pri}, ft/s (m/s)	1083 (330)	1265 (386)	1477 (450)	1847 (563)	1839 (561)
A_{sec}, ft^2 (m^2)	2.212 (0.206)	2.177 (0.202)	2.141 (0.199)	1.971 (0.183)	1.976 (0.184)
W_{sec}, lb/s (kg/s)	127.3 (57.74)	140.3 (63.64)	150.2 (68.13)	158.7 (71.99)	162.2 (73.57)
V_{sec}, ft/s (m/s)	810 (247)	913 (278)	1028 (313)	1203 (367)	1201 (366)
RTS	0.879	0.978	1.067	1.242	1.238
T_{t5}, °R (K)	1756 (976)	1884 (1047)	2025 (1125)	2311 (1284)	2311 (1284)
T_{t8e}, °R (K)	1184 (658)	1244 (691)	1320 (733)	1490 (828)	1491 (828)
WHP, lb/s (kg/s)	22.61 (10.26)	22.57 (10.24)	22.54 (10.22)	22.49 (10.20)	22.49 (10.20)
TPR	5.451	6.064	6.539	7.166	7.154
CORGE	--	--	--	--	--
V_{rel4}, ft/s (m/s)	651 (198)	720 (219)	779 (237)	893 (272)	892 (272)
V_{son}, ft/s (m/s)	1685 (514)	1728 (527)	1781 (543)	1890 (576)	1890 (576)

Table 6.—(Continued)

(b) 727 Refan/JT8D-109

	Approach 1 nmi (1.85 km)		Takeoff (with cutback) 3.5 nmi (6.58 km)	Takeoff (without cutback) 3.5 nmi (6.48 km)	Sideline 0.25 nmi (0.46 km)
BRGW, lb (kg)	--	--	172 500 (78 245)	172 500 (78 245)	172 500 (78 245)
LGW, lb (kg)	150 000 (68 039)	142 500 (64 637)	--	--	--
Flaps, deg	30	40	5	5	5
Altitude, ft (m)	370 (113)	370 (113)	1600 (487.7)	1745 (531.9)	800 (244)
Sideline distance, ft (m)	--	--	--	--	1520 (463.3)
F_n/δ, lb (N)	4570 (20 327)	6300 (28 022)	8220 (36 563)	13 190 (58 669)	13 050 (58 046)
Flight speed, KTAS (m/s)	146.1 (75.2)	139.1 (71.6)	179.9 (92.5)	180.3 (92.7)	177.8 (91.5)
FPR	1.247	1.320	1.422	1.629	1.623
N_1, rpm	5237	5738	6338	7405	7387
$N_1/\sqrt{\theta_{t2}}$, rpm	5131	5624	6220	7271	7231
A_{pri}, ft^2 (m^2)	2.755 (0.256)	2.790 (0.259)	2.824 (0.262)	3.055 (0.284)	3.049 (0.283)
W_{pri}, lb/s (kg/s)	84.4 (38.28)	96.9 (43.95)	111.0 (50.35)	143.3 (65.00)	146.6 (66.50)
V_{pri}, ft/s (m/s)	879 (268)	1028 (313)	1253 (305)	1608 (490)	1599 (487)
A_{sec}, ft^2 (m^2)	4.814 (0.447)	4.792 (0.445)	4.742 (0.441)	4.555 (0.423)	4.560 (0.424)
W_{sec}, lb/s (kg/s)	222.6 (100.97	246.7 (111.4)	270.3 (122.6)	304.9 (138.3)	313.1 (142.02)
V_{sec}, ft/s (m/s)	650 (198)	724 (221)	839 (256)	998 (304)	995 (303)
RTS	1.003	1.106	1.236	1.474	1.465
T_{t5}, °R (K)	1756 (976)	1882 (1046)	2036 (1131)	2328 (1293)	2331 (1295)
T_{t8e}, °R (K)	1183 (657)	1240 (689)	1313 (729)	1470 (817)	1473 (818)
WHP, lb/s (kg/s)	22.19 (10.07)	22.13 (10.04)	22.09 (10.02)	22.05 (10.00)	22.05 (10.00)
TPR	5.724	6.383	7.100	8.117	8.089
CORGE	4.425	4.546	4.670	4.892	4.906
V_{rel4}, ft/s (m/s)	606 (185)	677 (206)	760 (232)	888 (271)	887 (270)
V_{son}, ft/s (m/s)	1675 (511)	1717 (523)	1769 (539)	1874 (571)	1876 (572)

Table 6.—(Concluded)

(c) 727 Refan Growth Option/JT8D-109

		Approach 1 nmi (1.85 km)	Takeoff (with cutback) 3.5 nmi (6.48 km	Takeoff (without cutback) 3.5 nmi (6.48 km)	Sideline 0.25 nmi (0.46 km)
BRGW, lb (kg)	--	--	182 500 (87 781)	182 500 (82 781)	182 500 (82 781)
LGW, lb (kg)	154 500 (70 080)	142 500 (64 637)	--	--	--
Flaps, deg	30	40	5	5	5
Altitude, ft (m)	370 (113)	370 (113)	1340 (408.4)	1465 (446.5)	800 (244)
Sideline distance, ft (m)	--	--	--	--	1520 (463.3)
F_n/δ, lb (N)	4710 (20 950)	6300 (28 022)	8630 (38 386)	13 100 (58 269)	13 000 (57 824)
Flight speed, KTAS (m/s)	148.4 (76.3)	139.1 (71.6)	183.5 (94.4)	183.8 (94.5)	182.0 (93.6)
FPR	1.253	1.320	1.441	1.721	1.713
N_1, rpm	5301	5738	6452	7402	7388
$N_1/\sqrt{\theta_{t2}}$, rpm	5192	5624	6324	7258	7230
A_{pri}, ft^2 (m^2)	2.761 (0.257)	2.790 (0.259)	2.839 (0.264)	3.053 (0.284)	3.049 (0.283)
W_{pri}, lb/s (kg/s)	85.9 (38.96)	96.9 (43.95)	115.4 (52.35)	144.5 (65.55)	146.8 (66.59)
V_{pri}, ft/s (m/s)	895 (273)	1028 (313)	1291 (393)	1607 (490)	1601 (488)
A_{sec}, ft^2 (m^2)	4.812 (0.447)	4.792 (0.445)	4.726 (0.439)	4.558 (0.423)	4.561 (0.424)
W_{sec}, lb/s (kg/s)	225.5 (102.3)	245.7 (111.4)	277.5 (125.9)	308.0 (139.7)	313.8 (142.34)
V_{sec}, ft/s (m/s)	659 (201)	724 (221)	858 (262)	999 (304)	997 (304)
RTS	1.015	1.106	1.259	1.471	1.465
T_{t5}, °R (K)	1770 (983)	1882 (1046)	2066 (1148)	2329 (1294)	2331 (1295)
T_{t8e}, °R (K)	1188 (660)	1240 (689)	1328 (738)	1471 (817)	1473 (818)
WHP, lb/s (kg/s)	22.19 (10.07)	22.13 (10.04)	22.09 (10.02)	22.05 (10.00)	22.05 (10.00)
TPR	5.806	6.383	7.215	8.110	8.090
CORGE	4.439	4.546	4.701	4.897	4.907
V_{rel4}, ft/s (m/s)	615 (187)	677 (206)	774.7 (236)	888.2 (271)	887.0 (270)
V_{son}, ft/s (m/s)	1679 (512)	1717 (523)	1779 (522)	1874 (571)	1876 (572)

Table 7.—727-200/JT8D Noise Comparisons at FAR Part 36 Measuring Stations, Sea Level Airport at ISA + 18°F (10 K)

Nacelle Configuration	Condition	Approach 1 nmi (1,85 km)		Takeoff (with cutback) 3,5 nmi (6.48 km)	Takeoff (full-power) 3.5 nmi (6.48 km)	Sideline 0,25 nmi (0.46 km)
JT8D-9 hardwall (baseline)	BRGW, lb (kg)	--	--	172 500 (78 245)	172 500 (78 245)	172 500 (78 245)
	LGW, lb (kg)	150 000 (68 039)	142 500 (64 637)	--	--	--
	Flaps, deg	30	40	5	5	5
	Altitude, ft (m)	370 (113)	370 (113)	1390 (423.7)	1520 (463.3)	800 (244)
	Sideline distance, ft (m)	--	--	--	--	1520 (463.3)
	F_n/δ, lb (N)	4570 (20 327)	6300 (28 022)	8060 (35 851)	12 420 (55 244)	12 310 (54 755)
	Flight speed, KTAS (m/s)	146.1 (75.2)	139.1 (71.6)	177.5 (91.3)	177.9 (91.5)	176.0 (90.5)
	EPNL, EPNdB	108.2	109.5	100.0	107.4	99.9
	FAR 36 limit, EPNdB	104.4	104.4	99.0	99.0	104.4
JT8D-109 (refan)	BRGW, lb (kg)	--	--	172 500 (78 245)	172 500 (78 245)	172 500 (78 245)
	LGW, lb (kg)	150 000 (68 039)	142 500 (64 637)	--	--	--
	Flaps, deg	30	40	5	5	5
	Altitude, ft (m)	370 (113)	370 (113)	1600 (487.7)	1745 (531.9)	800 (244)
	Sideline distance, ft (m)	--	--	--	--	1520 (463.3)
	F_n/δ, lb (N)	4570 (20 327)	6300 (28 022)	8220 (36 563)	13 190 (58 669)	13 050 (58 046
	Flight speed, KTAS (m/s)	146.1 (75.2)	139.1 (71.6)	179.9 (92.5)	180.3 (92.7)	177.8 (91.5)
	ΔEPNL, EPNdB[a]	*-7.5*	*-6.8*	*-6.3*	*-7.7*	*-6.4*
	EPNL, EPNdB	100.7	102.7	93.7	99.7	93.5
	FAR 36 limit, EPNdB	104.4	104.4	99.0	99.0	104.4
JT8D-109 (refan) growth option airplane	BRGW, lb (kg)	--	--	182 500 (82 781)	182 500 (82 781)	182 500 (82 781)
	LGW, lb (kg)	154 500 (70 080)	142 500 (64 637)	--	--	--
	Flaps, deg	30	40	5	5	5
	Altitude, ft (m)	370 (113)	370 (113)	1340 (408.4)	1465 (446.5)	800 (244)
	Sideline distance, ft (m)	--	--	--	--	1520 (463.3)
	F_n/δ, lb (N)	4710 (20 950)	6300 (28 022)	8630 (38 386)	13 100 (58 269)	13 000 (57 824)
	Flight speed, KTAS (m/s)	148.4 (76.3)	139.1 (71.6)	183.5 (94.4)	183.8 (94.5)	182.0 (93.6)
	ΔEPNL, EPNdB[a]	*-7.2*	*-6.8*	*-4.3*	*-6.6*	*-6.6*
	EPNL, EPNdB	101.0	102.7	95.7	100.8	93.3
	FAR 36 limit, EPNdB	104.6	104.6	99.4	99.4	104.6
JT8D-109 (refan) equal-range airplane	BRGW, lb (kg)	--	--	177 200 (80 377)	177 200 (80 377)	177 200 (80 377)
	LGW, lb (kg)	154 500 (70 080)	142 500 (64 637)	--	--	--
	Flaps, deg	30	40	5	5	5
	Sideline distance, ft (m)	--	--	--	--	1520 (463.3)
	ΔEPNL, EPNdB[a]	*-7.2*	*-6.8*	*-5.4*	*-7.2*	*-6.5*
	EPNL, EPNdB	101.0	102.7	94.6	100.2	93.4
	FAR 36 limit, EPNdB	104.5	104.5	99.2	99.2	104.5

[a]Noise reduction relative to JT8D-9 hardwall (baseline)

Table 8.—727/JT8D Noise Comparisons at FAR Part 36 Measuring Stations, Sea Level Airport at ISA + 18° F (10 K)

Configuration and noise component	Component EPNL at indicated FAR Part 36 measuring station, EPNdB				
	Approach		Takeoff		
	Flap 30°	Flap 40°	Cutback	No cutback	Sideline
JT8D-9 hardwall (baseline)					
Inlet fan	(104.3)	(105.2)	84.0	79.9	72.5
Aft fan	(102.6)	(102.1)	(91.0)	90.3	82.0
Jet	96.7	(102.5)	(98.4)	(107.2)	(99.6)
Low freq core	89.9	90.6	83.7	84.6	77.2
Turbine	92.4	92.5	80.2	80.0	71.8
Subtotal	107.7	109.2	99.9	107.4	99.9
Airframe	93.9	93.8	82.4	80.9	73.4
Total	108.2	109.5	100.0	107.4	99.9
JT8D-109 (refan)					
Inlet fan	(95.5)	(97.1)	78.7	79.1	73.6
Aft fan	88.0	89.9	78.0	80.8	74.2
Jet	(90.5)	(96.0)	(91.0)	(98.4)	(92.1)
Low freq core	(91.6)	(93.2)	(86.7)	(91.3)	(85.3)
Turbine	83.9	82.2	Negligible	Negligible	Negligible
Subtotal	99.7	102.0	93.3	99.6	93.4
Airframe	(93.9)	(93.8)	81.3	79.8	73.6
Total	100.7	102.7	93.7	99.7	93.5
JT8D-109 (refan) growth option airplane					
Inlet fan	(95.4)	(97.1)	81.4	81.4	73.5
Aft fan	88.1	89.9	80.5	82.9	74.0
Jet	(90.9)	(96.0)	(92.8)	(99.3)	(91.9)
Low freq core	(91.7)	(93.2)	(88.6)	(92.6)	(85.2)
Turbine	83.7	82.2	Negligible	Negligible	Negligible
Subtotal	99.8	102.0	95.3	100.7	93.2
Airframe	(94.2)	(93.8)	83.4	81.9	74.1
Total	101.0	102.7	95.7	100.8	93.3

Note: Circled numbers designate the major source noise contributors to the total far-field noise.

1. Inlet fan, aft fan, and jet noise are major contributors at the approach conditions.

2. Aft fan and jet noise are significant contributors at the cutback condition.

3. Jet noise controls at the full-power takeoff and sideline conditions.

The results in table 8 also indicate that for the 727 refan:

1. Inlet fan, jet, low-frequency core, and airframe noise are major contributors at the approach conditions.

2. Jet and low-frequency core are major contributors at the cutback, full-power takeoff, and sideline conditions.

The component data in table 8 were obtained from flyover time histories of PNLT versus time which were calculated by direct use of the prediction procedure and then adjusted so that the total EPNL's would agree precisely with those shown in table 7. In this manner, the relative levels of the components were preserved, and the total EPNL's are consistent with the existing flight data base.

3.2.2.2 FAR Part 36 Flyover Time Histories

The flyover PNLT time histories for the FAR Part 36 are shown in figures 15 through 26 for 30° and 40° flaps approach, cutback, and takeoff conditions. Plots are shown for the 727-200 and both the hardwall nacelle and treated nacelle 727 refan at 150 000-lb (68 039-kg) and 142 500-lb (64 637-kg) landing gross weight (LGW) and 172 500-lb (78 245-kg) BRGW. The time histories were calculated by direct use of the prediction procedure and did not include a final EPNL flight data correction. Consequently, the significance of these plots is restricted to the relative levels (as opposed to absolute levels) of the components and the shape of the time histories.

A comparison of the predicted 30° flaps *approach* (150 000-lb (68 039-kg) LGW) time histories shows that for the 727-200 (fig. 15), there is a dominance of fan noise. For the hardwall nacelle 727 refan (fig. 16), there is a significant decrease in jet noise and a decrease in total noise, which is now dominated by inlet fan noise. The low aft fan level, relative to inlet level, is due to fan case and fan duct treatment. For the treated nacelle 727 refan (fig. 17), there is a dominance of fan, low-frequency core noise, and airframe noise.

A comparison of the predicted 40° flaps *approach* (142 500-lb (64 637-kg) LGW) time histories (figs. 18, 19, and 20) shows results similar to the 30° flaps case, with jet noise playing a more significant role for the 727-200 and 727 refan.

A comparison of the predicted *cutback* time histories indicates that for the 727-200 (fig. 21) there is a dominance of jet and aft fan noise. For the hardwall nacelle 727 refan (fig. 22), there is a significant decrease in jet noise and emergence of inlet fan and low-frequency core noise as major sources. For the treated nacelle 727 refan (fig. 23), there is a suppression of the inlet fan noise so that the jet and low-frequency core components remain as the major noise sources.

Note:

- Flight condition: F_n/δ = 4570 lb (20 327 N)
  Altitude = 370 ft (113 m)
  Flight speed = 146.1 KTAS (75.2 m/s)
  LGW = 150 000 lb (68 039 kg)
  Flap position = 30°
- Engine cycle condition: Exact flight conditions
  Temp = std day + 18°F (10 K)
- Noise extrapolation condition: Temp = 77°F (298 K)
  Relative humidity = 70%
- EPNL (corrected to 727-200 flight data) = 108.2 EPNdB
- Not anchored to 727-200 flight data base;
  do not use as absolute values for flight.

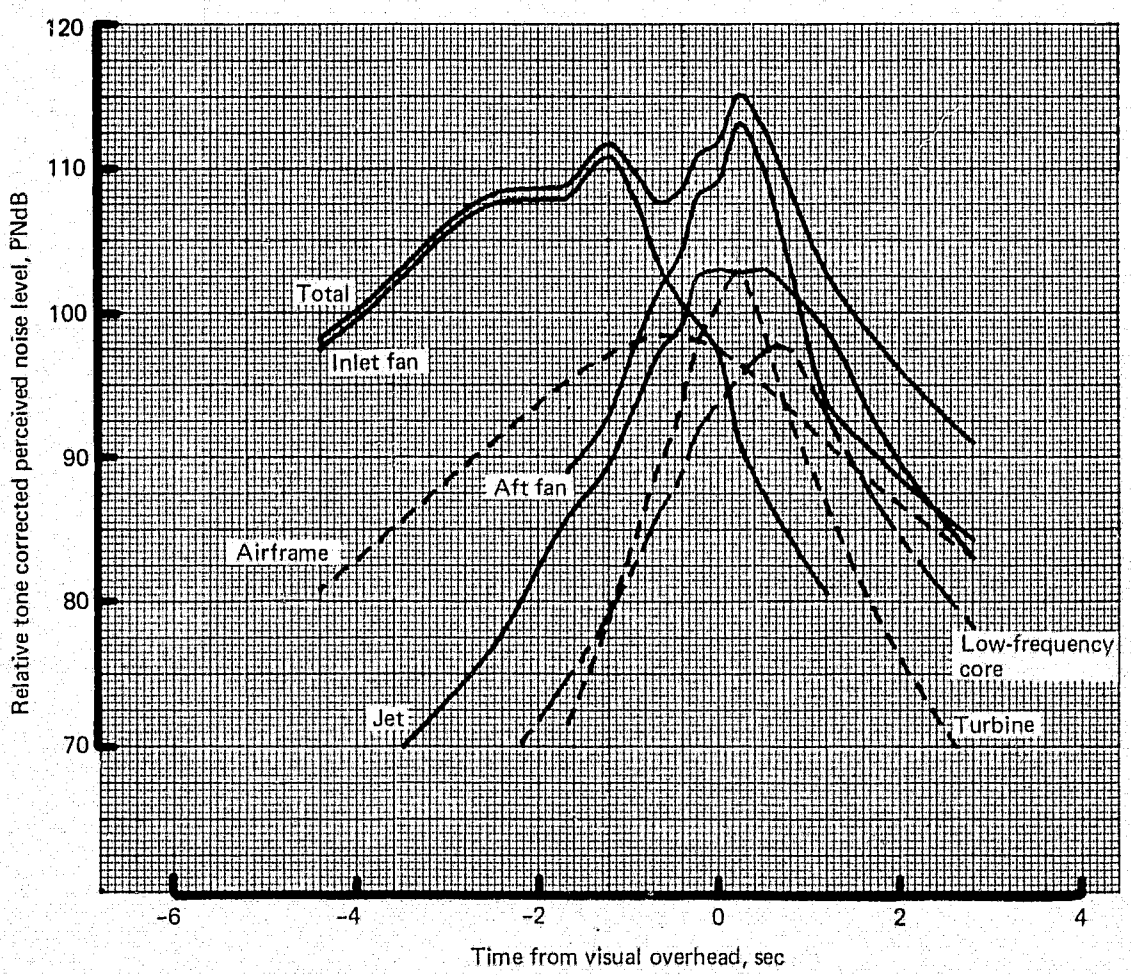

Figure 15.—727-200 Hardwall Nacelle, Component Flyover Time History, 30° Flaps Approach

Note:

- Flight condition: F_n/δ = 4570 lb (20 327 N)
  Altitude = 370 ft (113 m)
  Flight speed = 146.1 KTAS (75.2 m/s)
  LGW = 150 000 lb (68 039 kg)
  Flap position = 30°
- Engine cycle condition: Exact flight conditions
  Temp = std day + 18°F (10 K)
- Noise extrapolation condition: Temp = 77°F (298 K)
  Relative humidity = 70%
- EPNL (corrected to 727-200 flight data) = 107.8 EPNdB
- Not anchored to 727-200 flight data base; do not use as absolute values for flight.

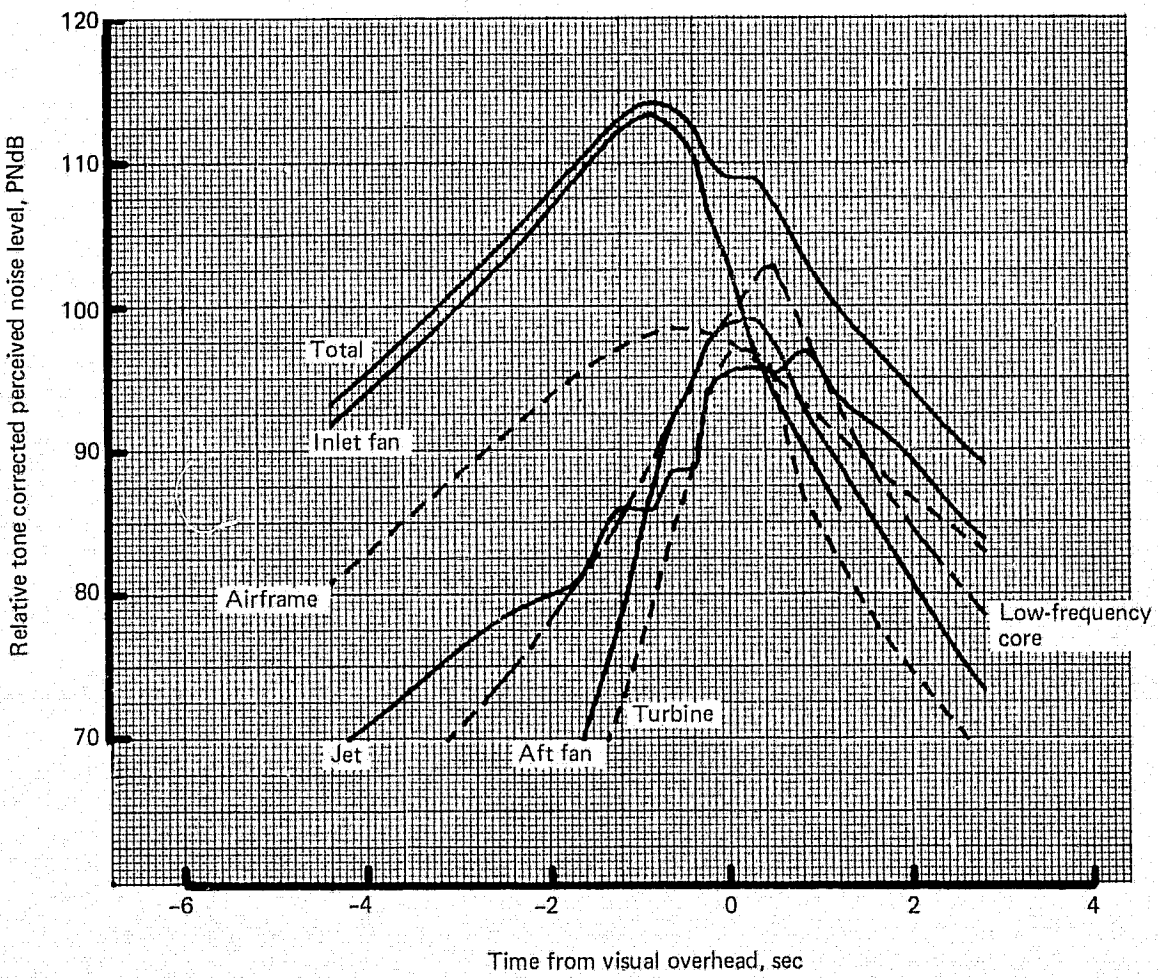

Figure 16.—727 Refan Hardwall Nacelle, Component Flyover Time History, 30° Flaps Approach

Note:

- Flight condition: F_n/δ = 4570 lb (20 327 N)
  Altitude = 370 ft (113 m)
  Flight speed = 146.1 KTAS (75.2 m/s)
  LGW = 150 000 lb (68 039 kg)
  Flap position = 30°
- Engine cycle condition: Exact flight conditions
  Temp = std day + 18°F (10 K)
- Noise extrapolation condition: Temp = 77°F (298 K)
  Relative humidity = 70%
- EPNL (corrected to 727-200 flight data) = 100.7 EPNdB
- Not anchored to 727-200 flight data base; do not use as absolute values for flight.

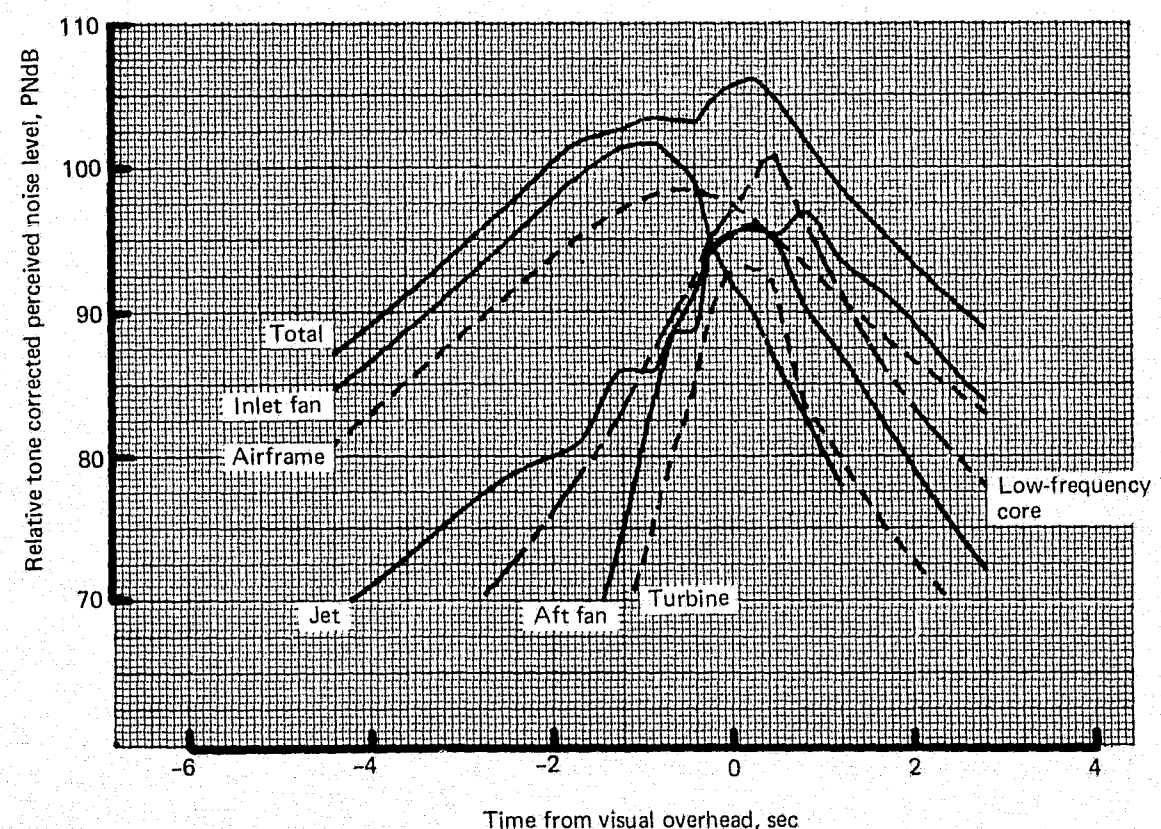

Figure 17.—727 Refan Treated Nacelle, Component Flyover Time History, 30° Flaps Approach

Note:

- Flight condition: F_n/δ = 6300 lb (28 022 N)
  Altitude = 370 ft (113 m)
  Flight speed = 139.1 KTAS (71.6 m/s)
  LGW = 142 500 lb (64 637 kg)
  Flap position = 40°
- Engine cycle condition: Exact flight conditions
  Temp = std day + 18°F (10 K)
- Noise extrapolation condition: Temp = 77°F (298 K)
  Relative humidity = 70%
- EPNL (corrected to 727-200 flight data) = 109.5 EPNdB
- Not anchored to 727-200 flight data base; do not use as absolute values for flight.

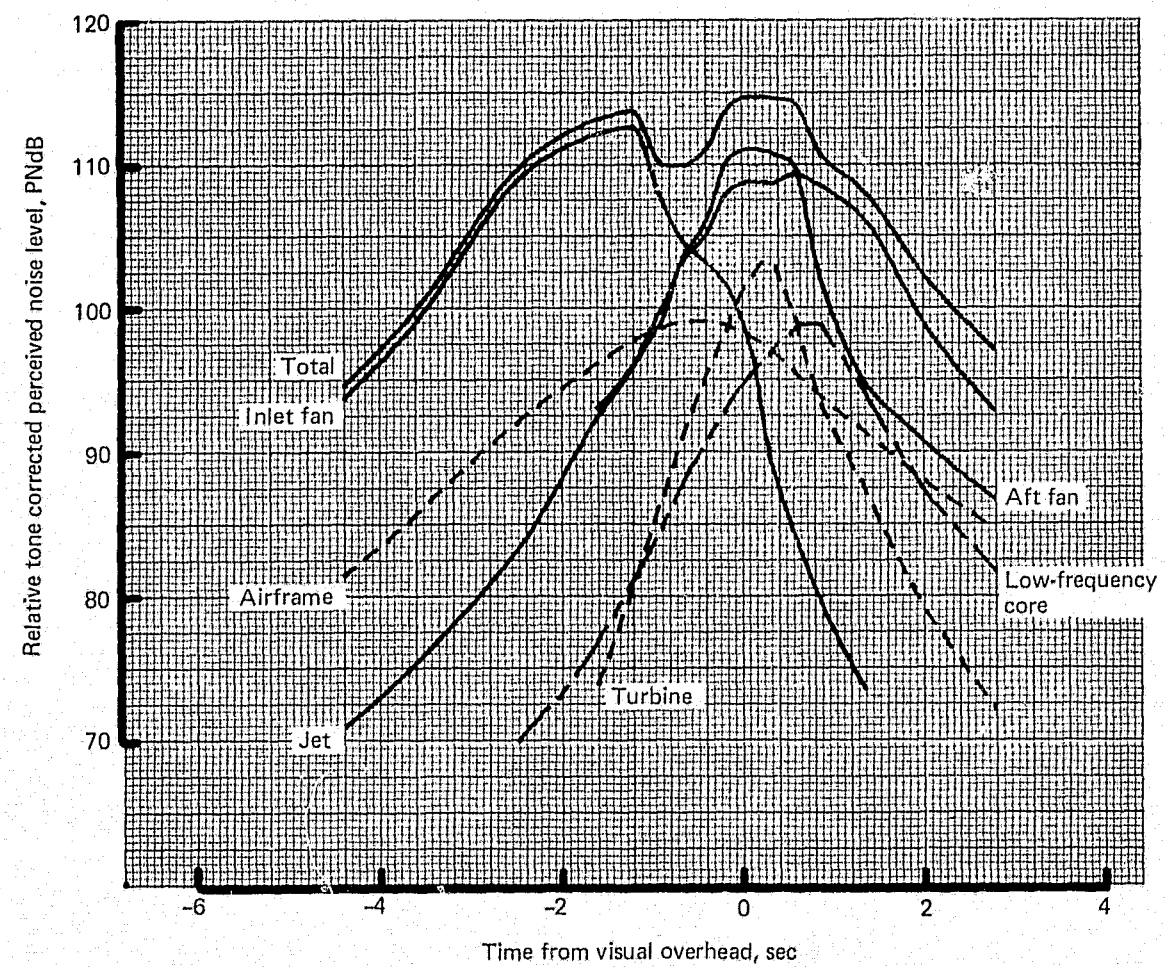

Figure 18.—727-200 Hardwall Nacelle, Component Flyover Time History, 40° Flaps Approach

Note:

- Flight condition: F_n/δ = 6300 lb (28 022 N)
  Altitude = 370 ft (113 m)
  Flight speed = 139.1 KTAS (71.6 m/s)
  LGW = 142 500 lb (64 637 kg)
  Flap position = 40°
- Engine cycle condition: Exact flight conditions
  Temp = std day + 18°F (10 K)
- Noise extrapolation condition: Temp = 77°F (298 K)
  Relative humidity = 70%
- EPNL (corrected to 727-200 flight data) = 109.3 EPNdB
- Not anchored to 727-200 flight data base; do not use as absolute values for flight.

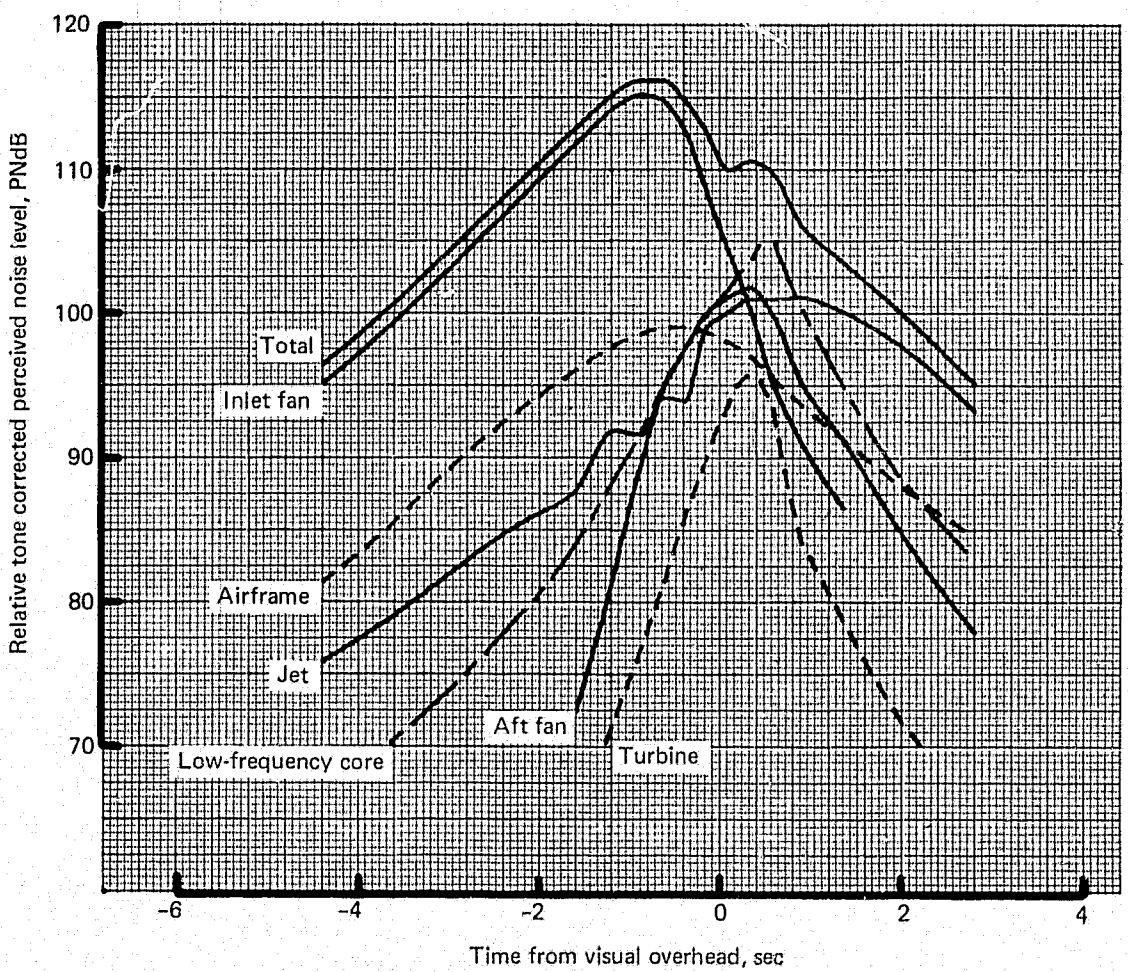

Figure 19.—727 Refan Hardwall Nacelle, Component Flyover Time History, 40° Flaps Approach

Note:

- Flight condition: F_n/δ = 6300 lb (28 022 N)
  Altitude = 370 ft (113 m)
  Flight speed = 139.1 KTAS (71.6 m/s)
  LGW = 142 500 lb (64 637 kg)
  Flap position = 40°
- Engine cycle condition: Exact flight conditions
  Temp = std day + 18°F (10 K)
- Noise extrapolation condition: Temp = 77°F (298 K)
  Relative humidity = 70%
- EPNL (corrected to 727-200 flight data) = 102.7 EPNdB
- Not anchored to 727-200 flight data base; do not use as absolute values for flight.

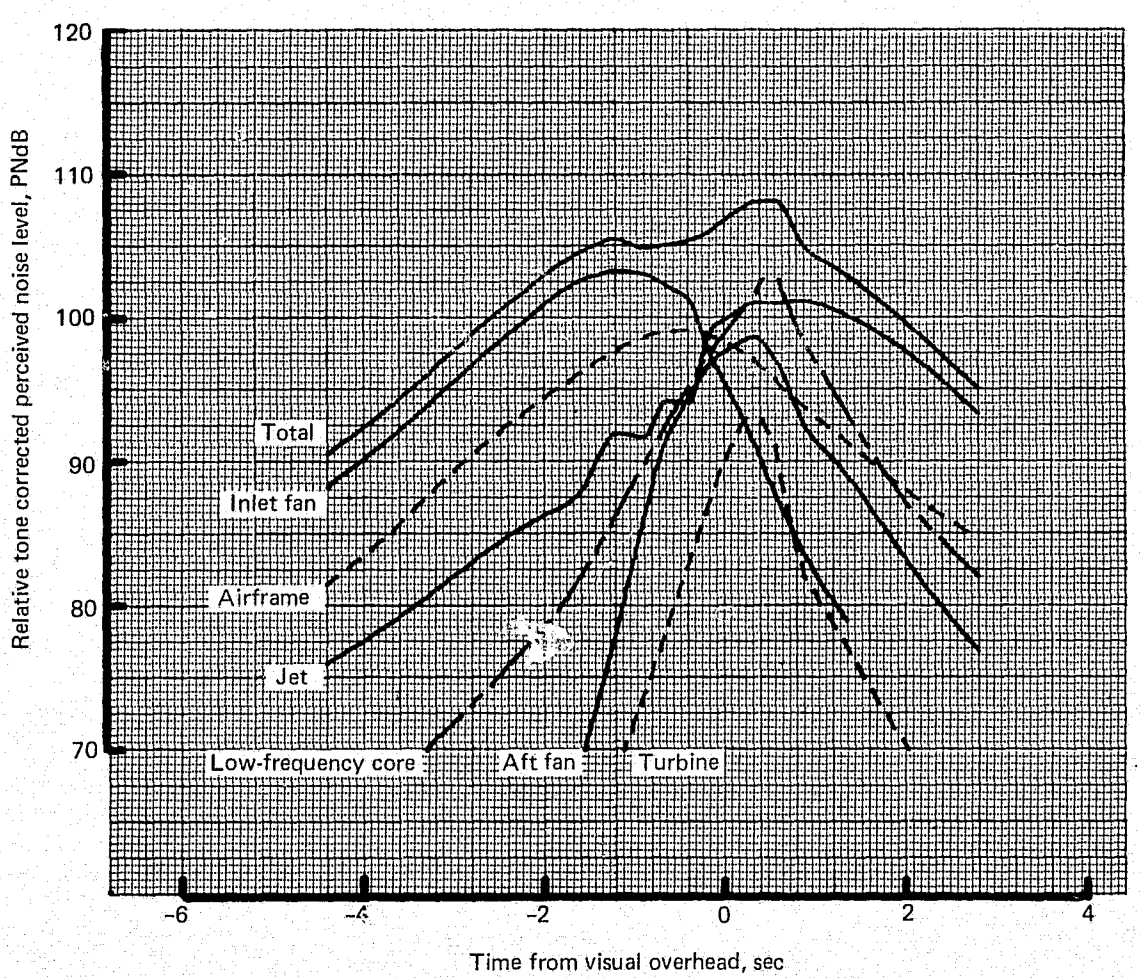

Figure 20.—727 Refan Treated Nacelle, Component Flyover Time History, 40° Flaps Approach

Note:

- Flight condition: F_n/δ = 8060 lb (35 851 N)
  Altitude = 1390 ft (423.7 m)
  Flight speed = 177.5 KTAS (91.3 m/s)
  BRGW = 172 500 lb (78 245 kg)
  Flap position = 5°
- Engine cycle condition: Exact flight conditions
  Temp = std day + 18°F (10 K)
- Noise extrapolation condition: Temp = 77°F (298 K)
  Relative humidity = 70%
- EPNL (corrected to 727-200 flight data) = 100.0 EPNdB
- Not anchored to 727-200 flight data base; do not use as absolute values for flight.

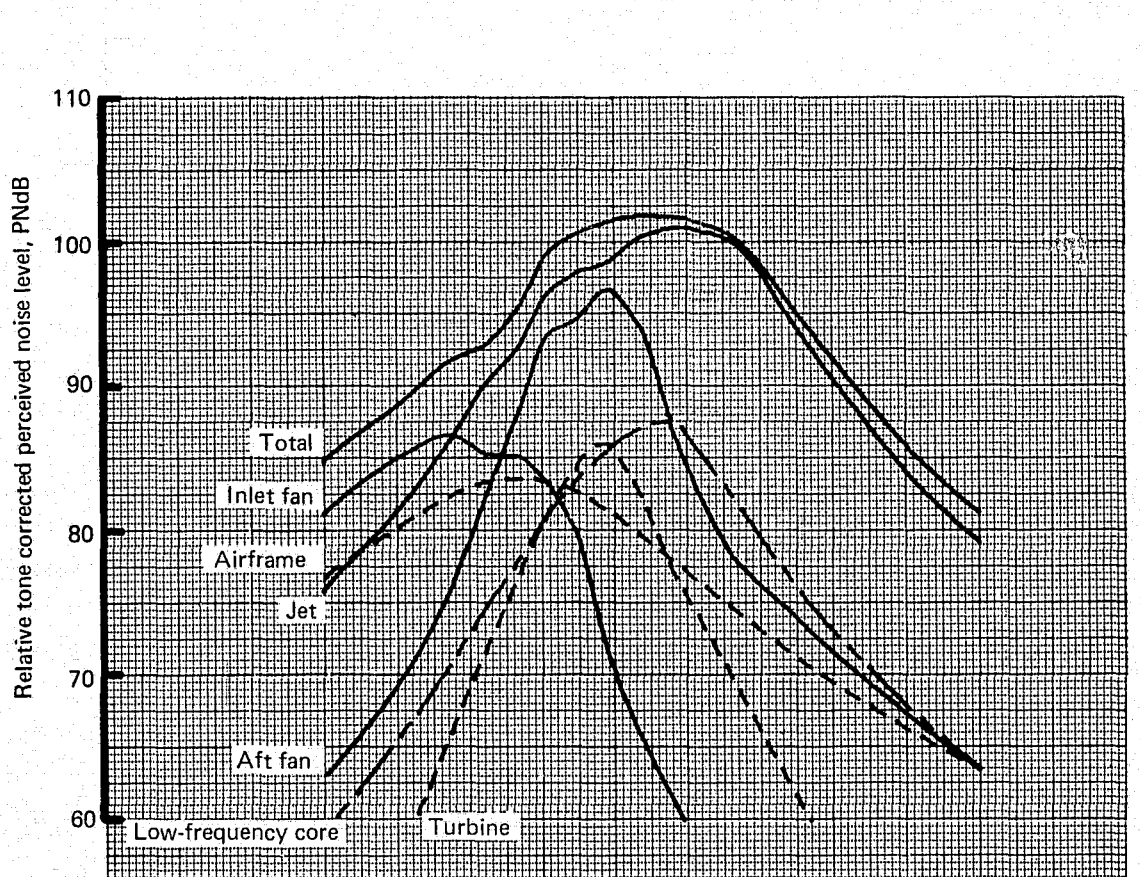

Figure 21.—727-200 Hardwall Nacelle, Component Flyover Time History, Cutback

Note:

- Flight condition: F_n/δ = 8220 lb (36 563 N)
  Altitude = 1600 ft (487.7 m)
  Flight speed = 179,9 KTAS (92,5 m/s)
  BRGW = 172 500 lb (78 245 kg)
  Flap position = 5°
- Engine cycle condition: Exact flight conditions
  Temp = std day + 18°F (10 K)
- Noise extrapolation condition: Temp = 77°F (298 K)
  Relative humidity = 70%
- EPNL (corrected to 727-200 flight data) = 95.2 EPNdB
- Not anchored to 727-200 flight data base;
  do not use as absolute values for flight.

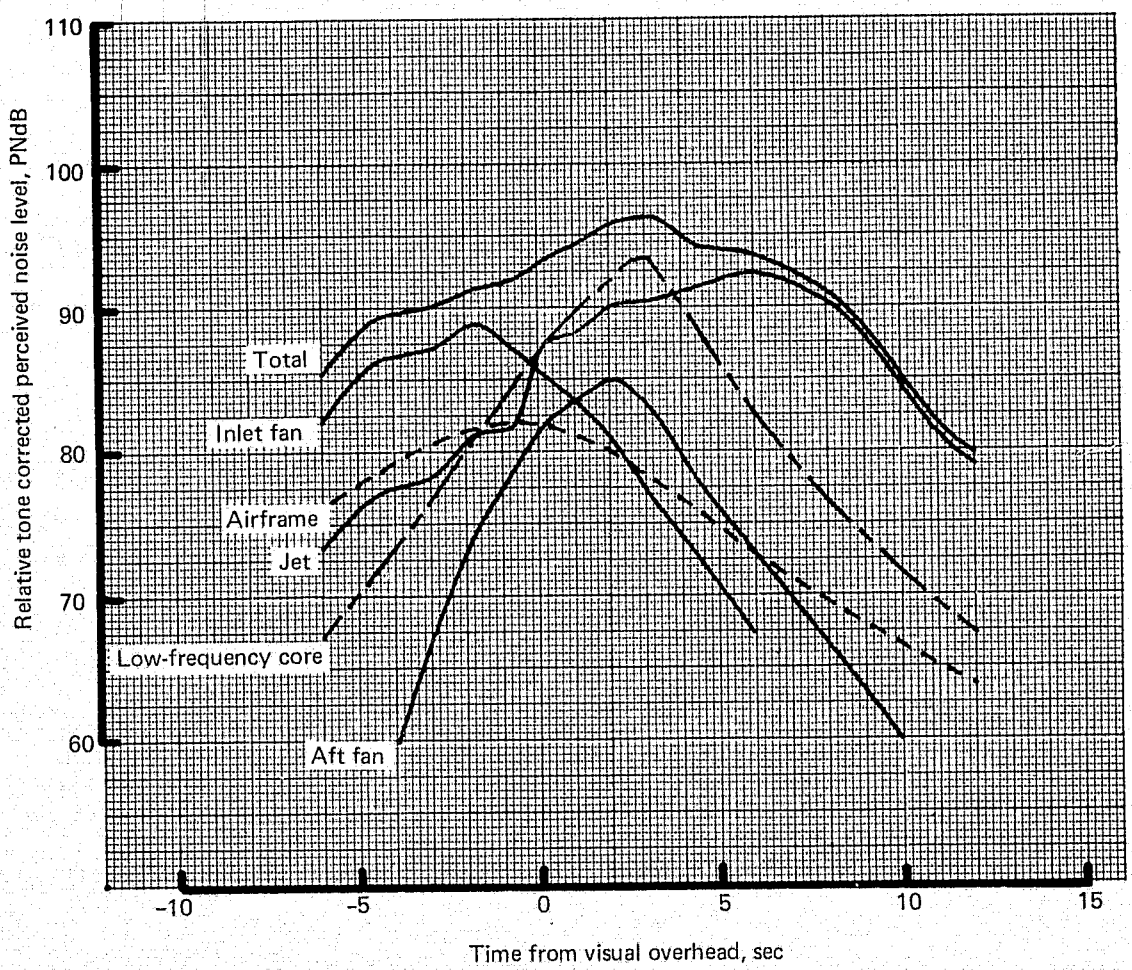

Figure 22.—727 Refan Hardwall Nacelle, Component Flyover Time History, Cutback

Note:

- Flight condition: F_n/δ = 8220 lb (36 563 N)
  Altitude = 1600 ft (487.7 m)
  Flight speed = 179.9 KTAS (92.5 m/s)
  BRGW = 172 500 lb (78 245 kg)
  Flap position = 5°
- Engine cycle condition: Exact flight conditions
  Temp = std day + 18°F (10 K)
- Noise extrapolation condition: Temp = 77°F (298 K)
  Relative humidity = 70%
- EPNL (corrected to 727-200 flight data) = 93.7 EPNdB
- Not anchored to 727-200 flight data base;
  do not use as absolute values for flight.

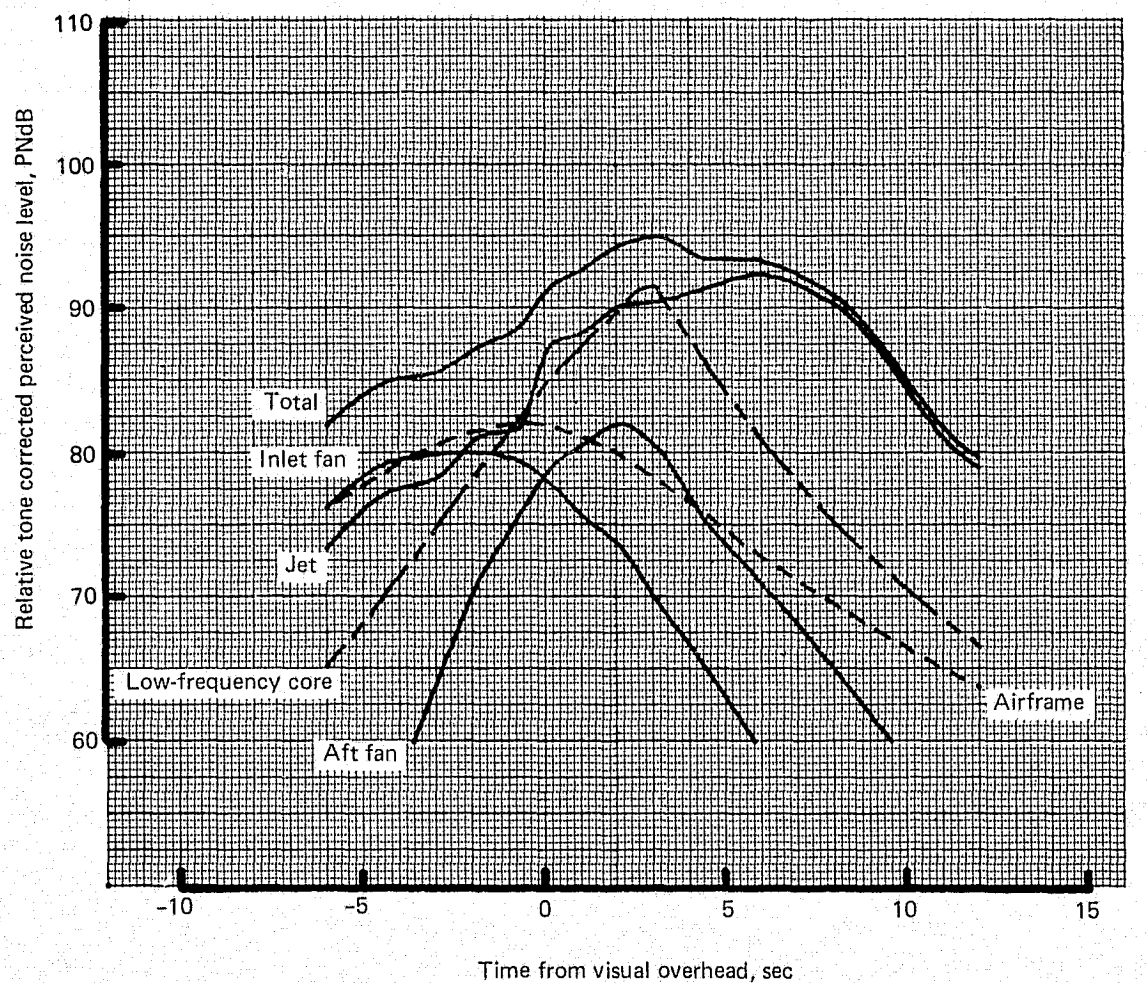

Figure 23.—727 Refan Treated Nacelle, Component Flyover Time History, Cutback

A comparison of the predicted *full-power takeoff* time histories shows dominance of jet noise for each configuration and indicates the sole dominance of the jet component for the 727-200 (fig. 24). For the hardwall nacelle 727 refan (fig. 25) and particularly the treated nacelle 727 refan (fig. 26), there is significant contribution from the jet and low-frequency core components.

Sideline time histories showed relative component contributions similar to those at full-power takeoff.

3.2.2.3 FAR Part 36 Sensitivity Studies

The purpose of the component noise sensitivity study for the 727-200 and 727 refan was to determine the relative impact of changes in different noise components (low-frequency core, inlet and aft fan, jet, turbine, and airframe) on the total noise level at each FAR Part 36 condition. The SPL of each noise component was varied analytically by applying positive and negative SPL increments to that component (independent of frequency and directivity angle). The change in total EPNL was then determined for each SPL increment while holding the other noise components at a fixed level.

The sensitivity of FAR Part 36 EPNL to changes to individual noise components (jet, low-frequency core, inlet and aft fan, turbine, and airframe) is presented in figures 27 through 36. These results support the earlier discussion in this section which identifies the importance of each noise component and its contribution to the total far-field noise.

The results confirm that the slope of the noise component sensitivity curves varies from zero, at large negative ΔSPL values (where that noise component is reduced to an insignificant level), to unity at large positive ΔSPL values (where that noise component is increased until it completely controls the total airplane noise level). For each FAR Part 36 condition, the approximate slope of each noise component at the reference condition is tabulated on each figure to indicate the leverage of each component on the total EPNL

An alternate way of looking at the component noise impact is summarized in table 9, which shows the airplane noise reduction obtainable by completely eliminating each noise source while not changing the other noise components.

3.2.3 LEVEL-FLYOVER COMPONENT NOISE AND AIRPLANE EPNL ESTIMATES

Level flyby noise characteristics were predicted as a function of corrected net thrust (4050 lb (18 014 N) to 13 050 lb (58 046 N)) and altitude (200 ft (61 m) to 15 000 ft (4572 m)) at 160 KTAS (82 m/s) for the 727-200 and the 727 refan airplanes. These calculations were made using the prediction method described in section 3.2.1.

3.2.3.1 Component Noise Versus Thrust

Detailed acoustic trends in the total far-field level flyby noise due to the contribution of each source noise component were studied using the peak PNLT and EPNL noise parameters predicted at 400 ft (122 m) and a flight speed of 160 KTAS (82 m/s). These parameters were plotted versus corrected net thrust. The significance of these plots was limited to the relative levels of the components because the absolute levels do not include a correction to the 727-200 flight data base.

Note:

- Flight condition: F_n/δ = 12 420 lb (55 244 N)
  Altitude = 1520 ft (463.3 m)
  Flight speed = 177.9 KTAS (91.5 m/s)
  BRGW = 172 500 lb (78 245 kg)
  Flap position = 5°
- Engine cycle condition: Exact flight conditions
  Temp = std day + 18°F (10 K)
- Noise extrapolation condition: Temp = 77°F (298 K)
  Relative humidity = 70%
- EPNL (corrected to 727-200 flight data) = 107.4 EPNdB
- Not anchored to 727-200 flight data base; do not use as absolute values for flight.

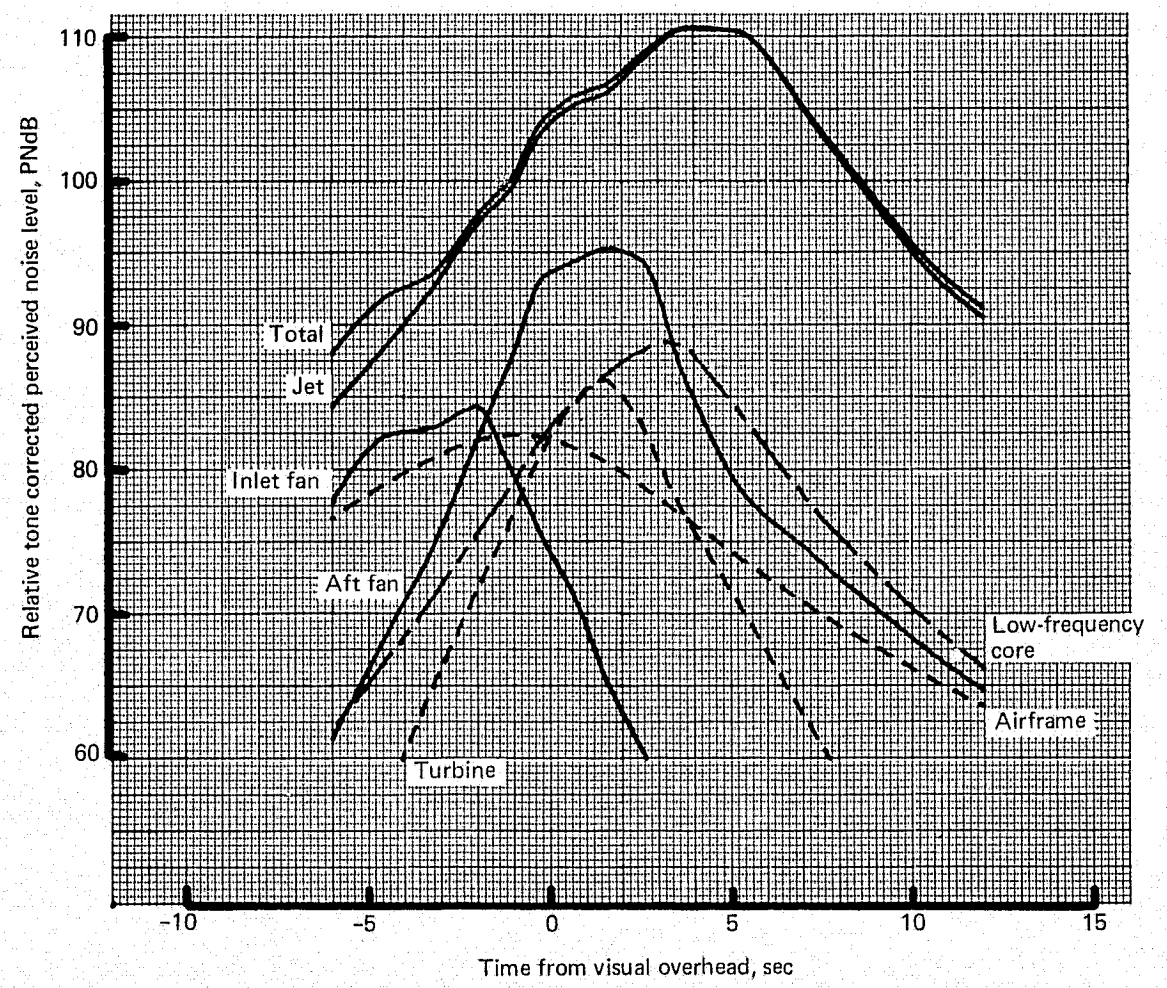

Figure 24.—727-200 Hardwall Nacelle, Component Flyover Time History, Takeoff

Note:
- Flight condition: F_n/δ = 13 190 lb (58 669 N)
  Altitude = 1745 ft (531.9 m)
  Flight speed = 180.3 KTAS (92.7 m/s)
  BRGW = 172 500 lb (78 245 kg)
  Flap position = 5°
- Engine cycle condition: Exact flight conditions
  Temp = std day + 18°F (10 K)
- Noise extrapolation condition: Temp = 77°F (298 K)
  Relative humidity = 70%
- EPNL (corrected to 727-200 flight data) = 100.1 EPNdB
- Not anchored to 727-200 flight data base; do not use as absolute values for flight.

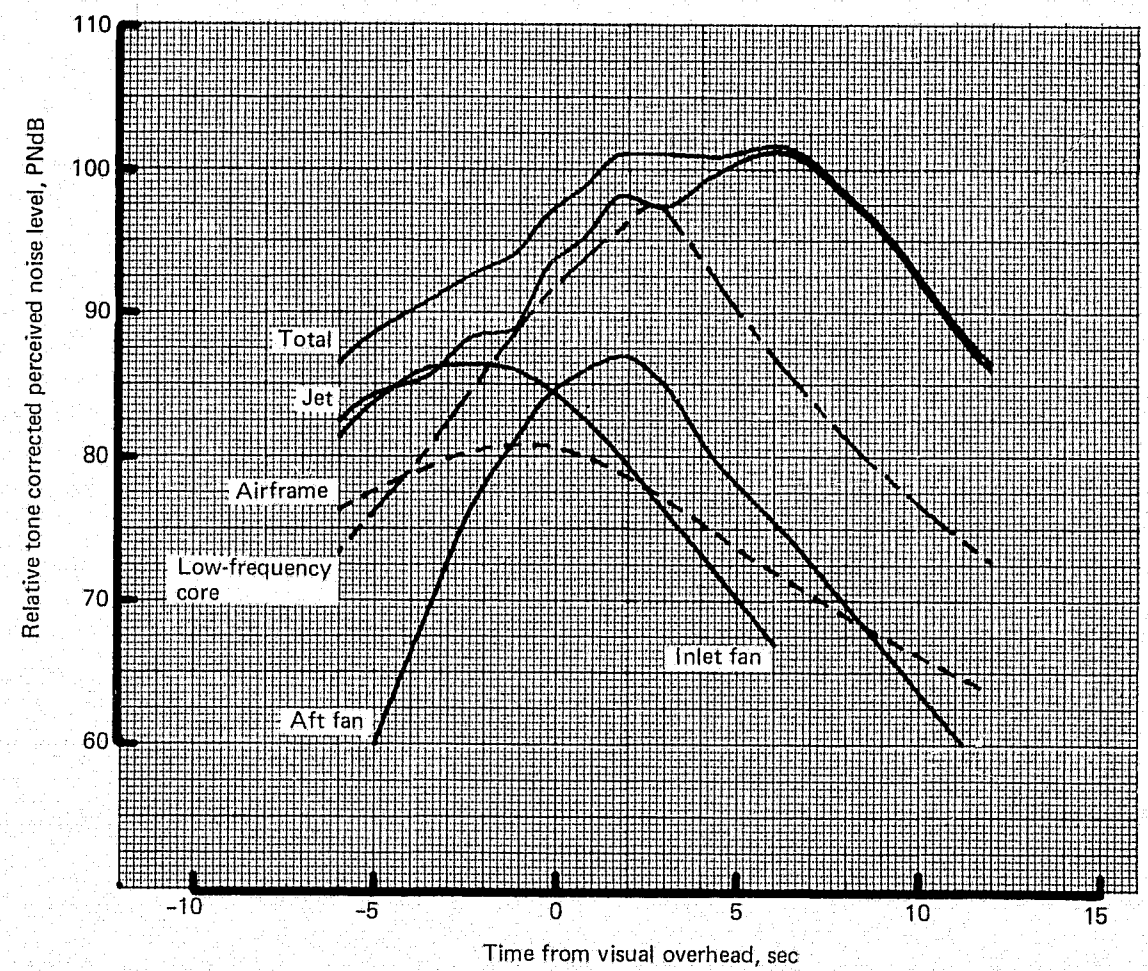

Figure 25.—727 Refan Hardwall Nacelle, Component Flyover Time History, Takeoff

Note:

- Flight condition: F_n/δ = 13 190 lb (58 669 N)
  Altitude = 1745 ft (531.9 m)
  Flight speed = 180.3 KTAS (92.7 m/s)
  BRGW = 172 500 lb (78 245 kg)
  Flap position = 5°
- Engine cycle condition: Exact flight conditions
  Temp = std day + 18°F (10 K)
- Noise extrapolation condition: Temp = 77°F (298 K)
  Relative humidity = 70%
- EPNL (corrected to 727-200 flight data) = 99.7 EPNdB
- Not anchored to 727-200 flight data base; do not use as absolute values for flight.

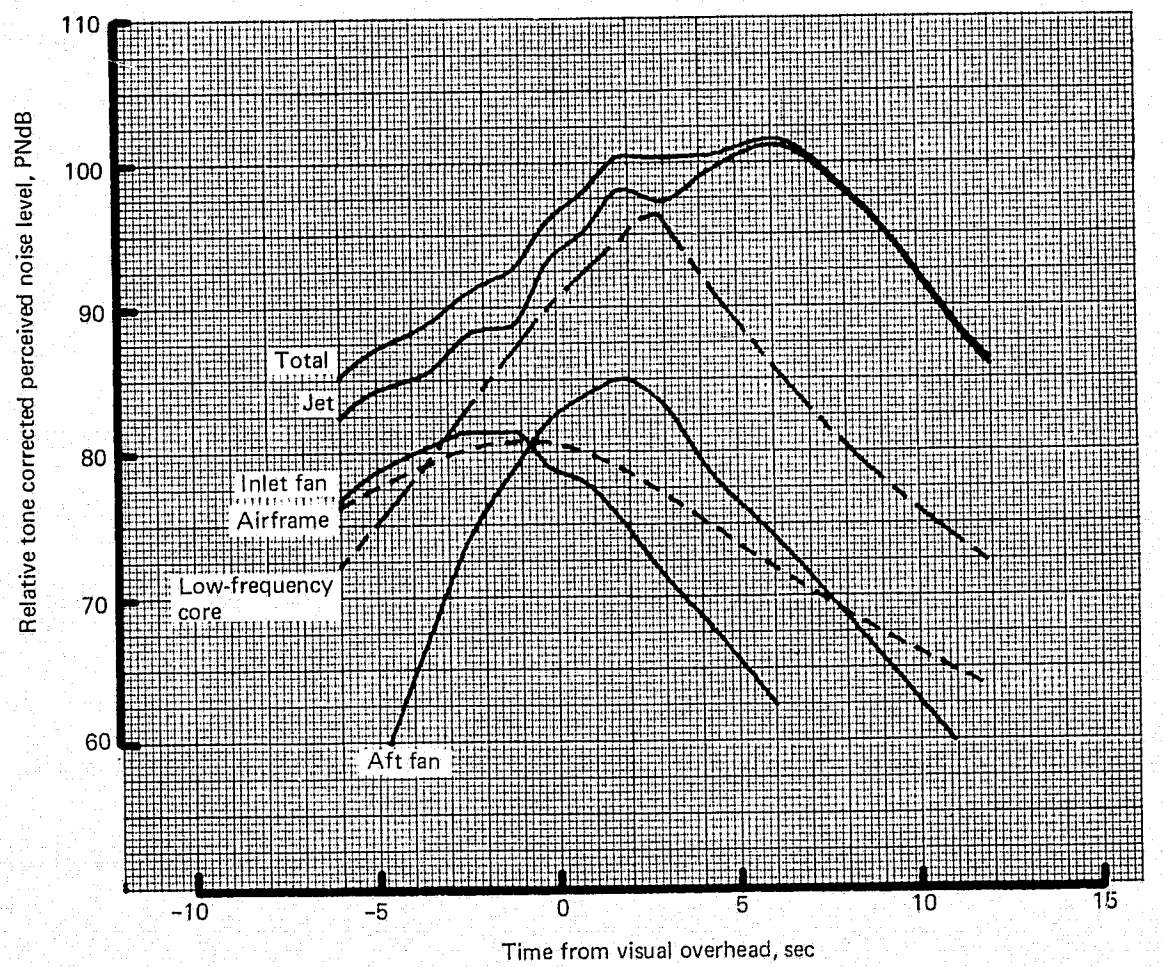

Figure 26.—727 Refan Treated Nacelle, Component Flyover Time History, Takeoff

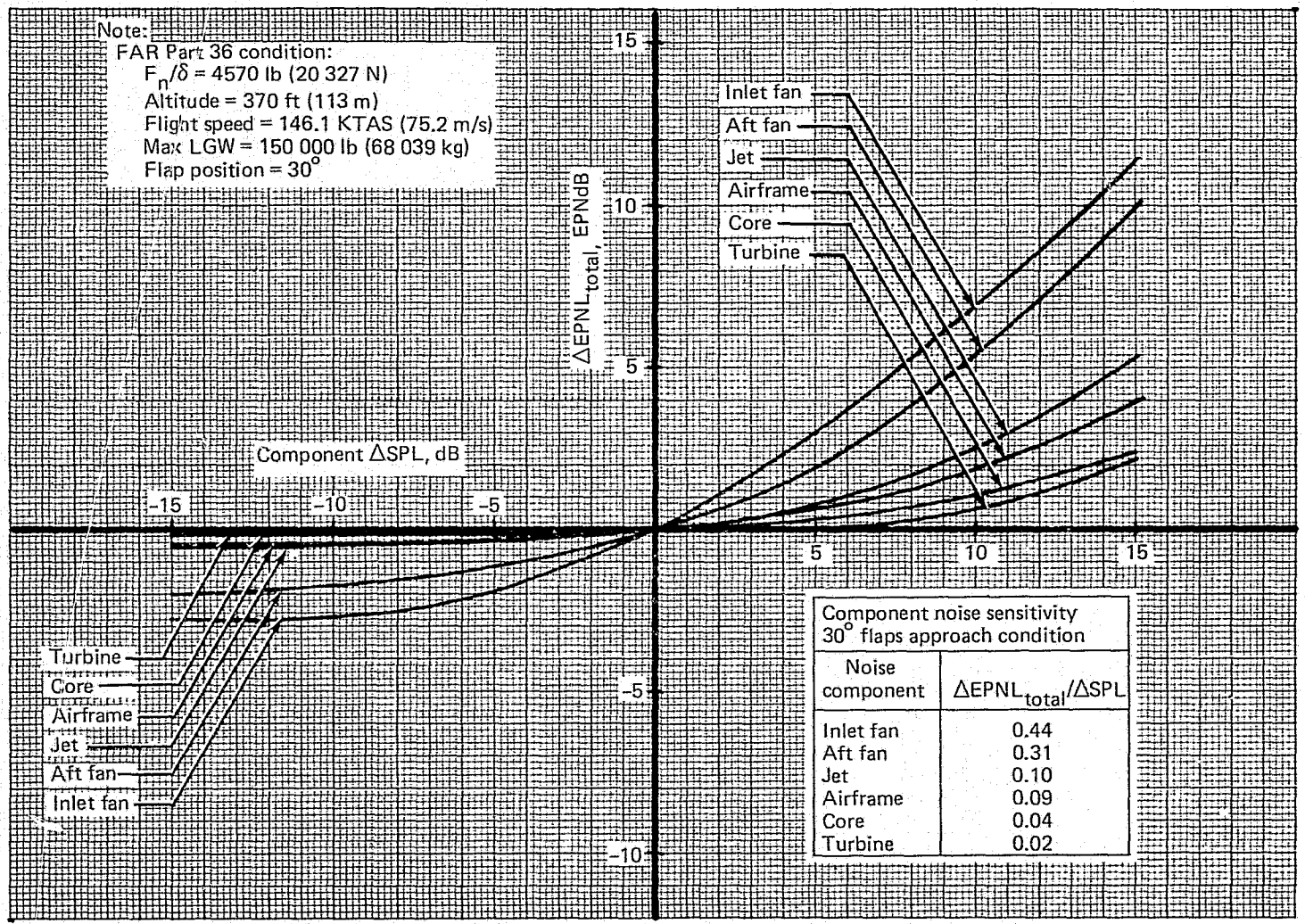

Figure 27.—727-200 Hardwall Nacelle, Component Noise Sensitivity Curves, 30° Flaps Approach

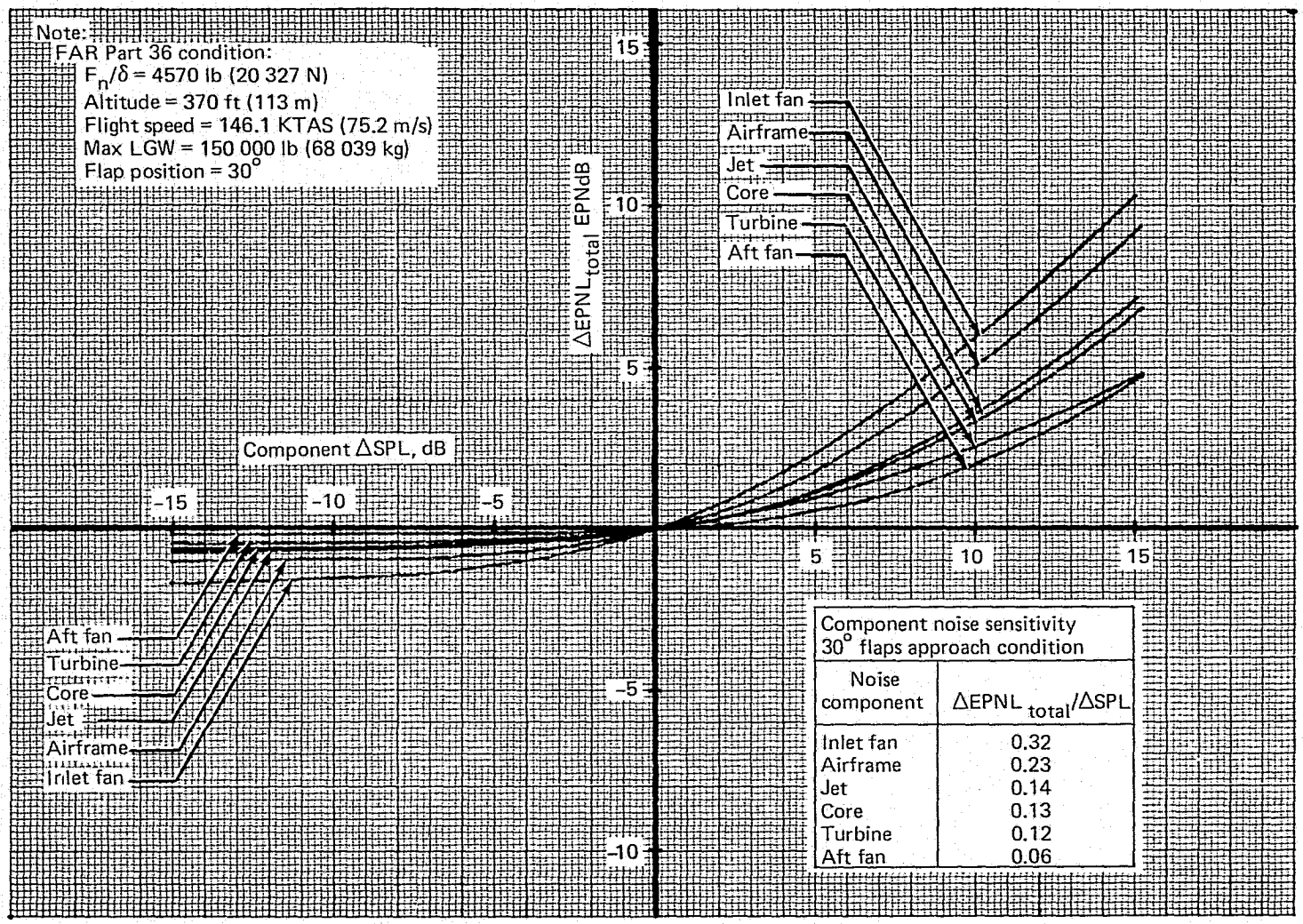

Figure 28.—727 Refan Treated Nacelle, Component Noise Sensitivity Curves, 30° Flaps Approach

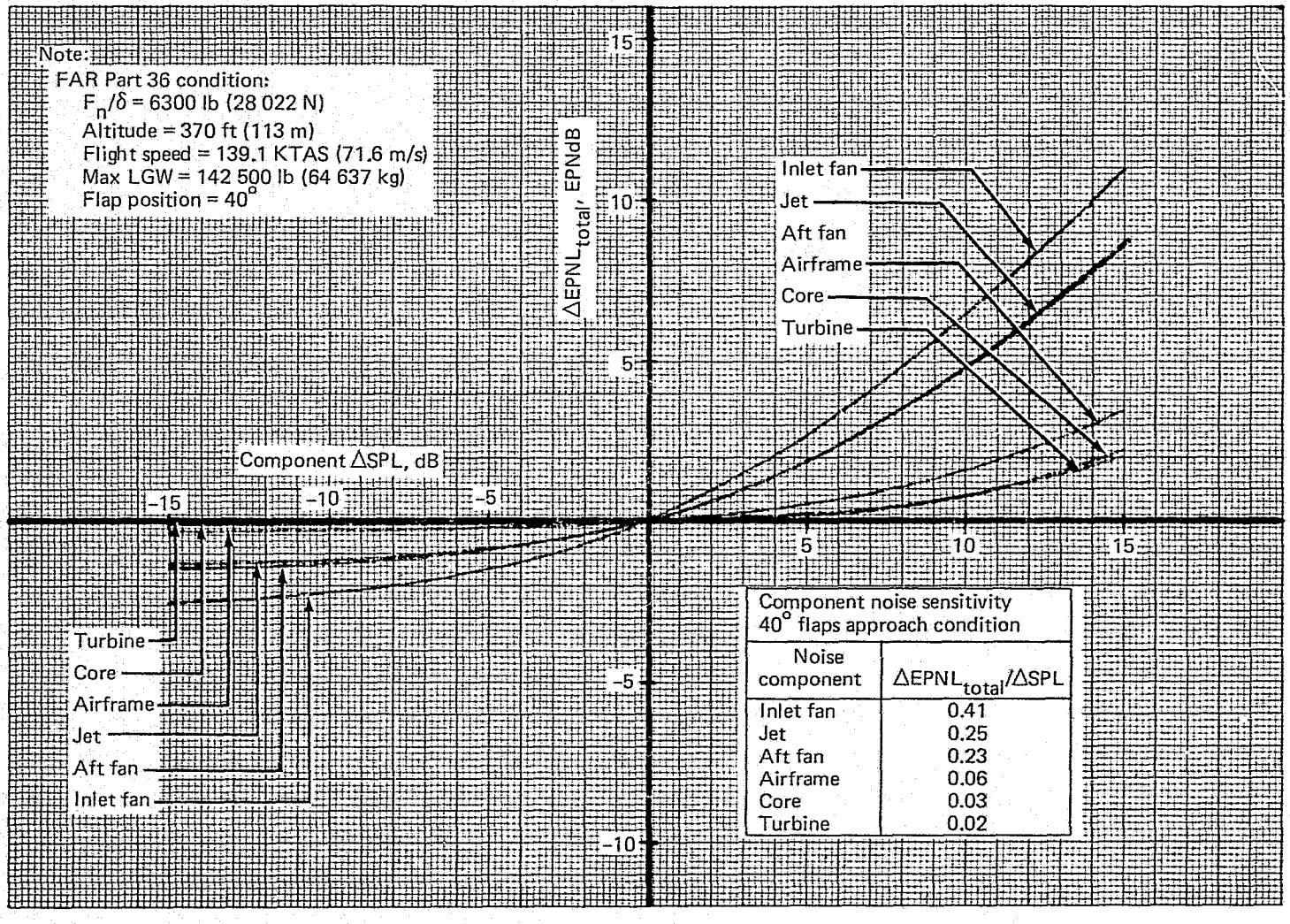

Figure 29.—727-200 Hardwall Nacelle, Component Noise Sensitivity Curves, 40° Flaps Approach

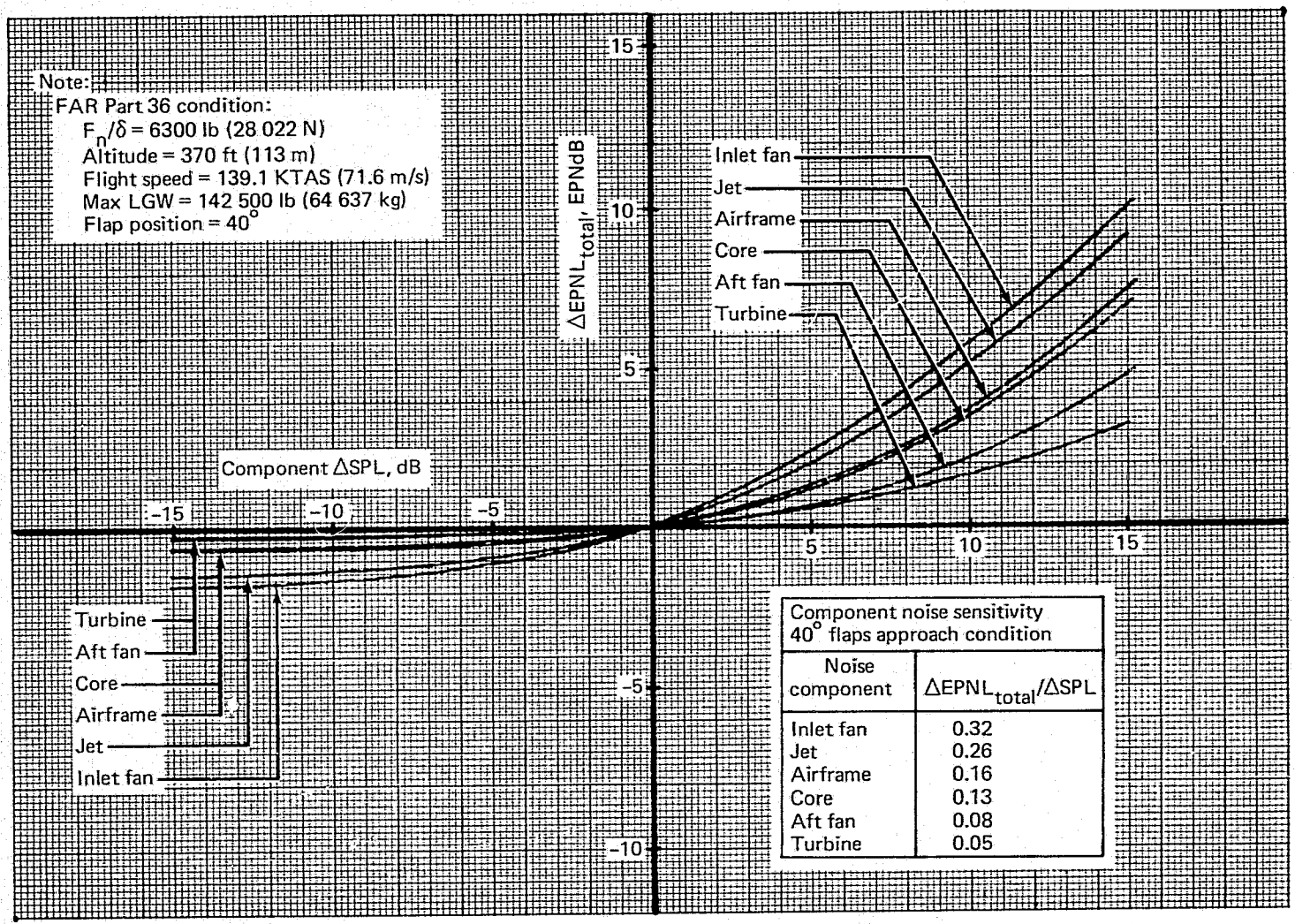

Figure 30.—727 Refan Treated Nacelle, Component Noise Sensitivity Curves, 40° Flaps Approach

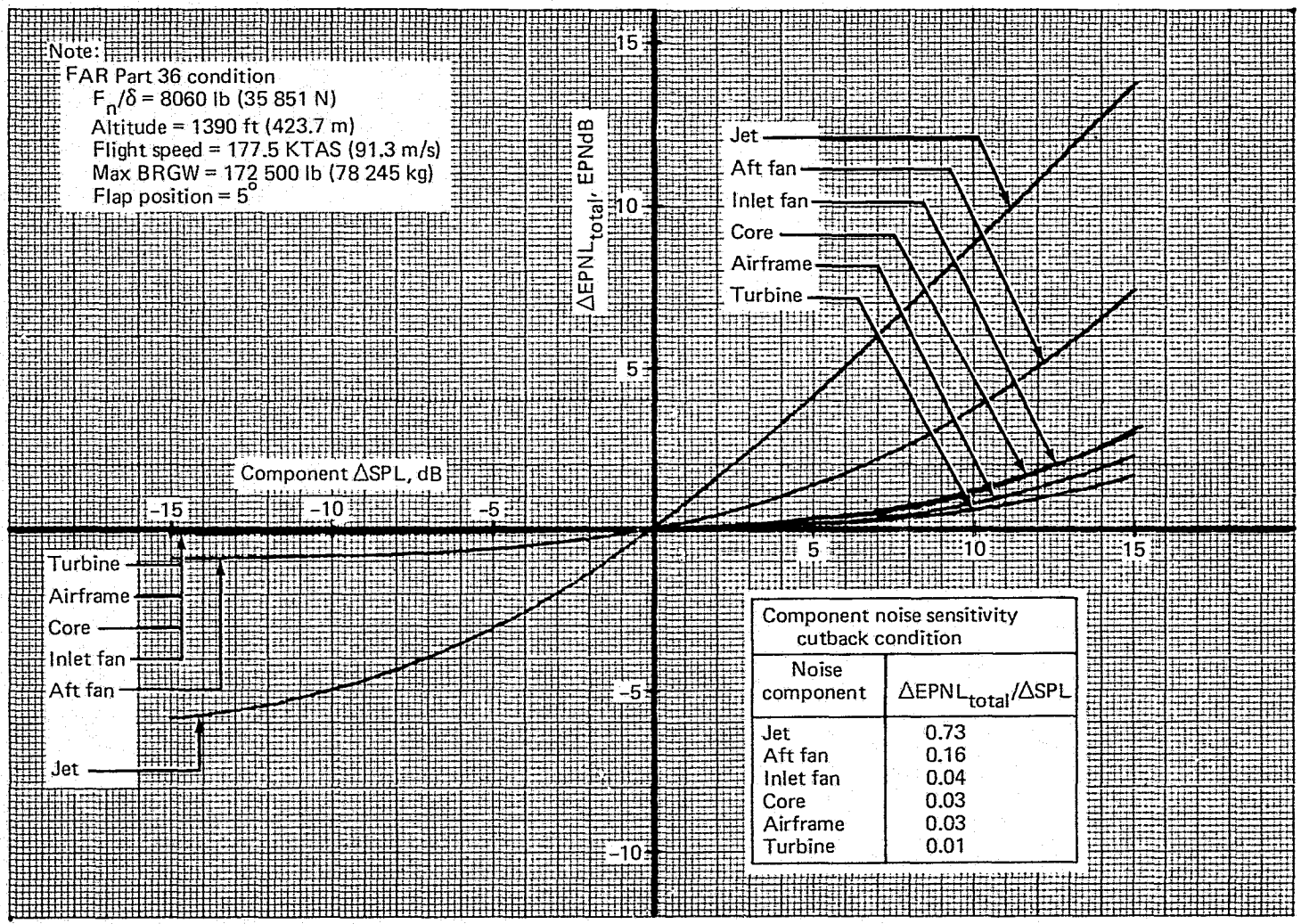

Component noise sensitivity cutback condition	
Noise component	$\Delta EPNL_{total}/\Delta SPL$
Jet	0.73
Aft fan	0.16
Inlet fan	0.04
Core	0.03
Airframe	0.03
Turbine	0.01

Figure 31.—727-200 Hardwall Nacelle, Component Noise Sensitivity Curves, Cutback

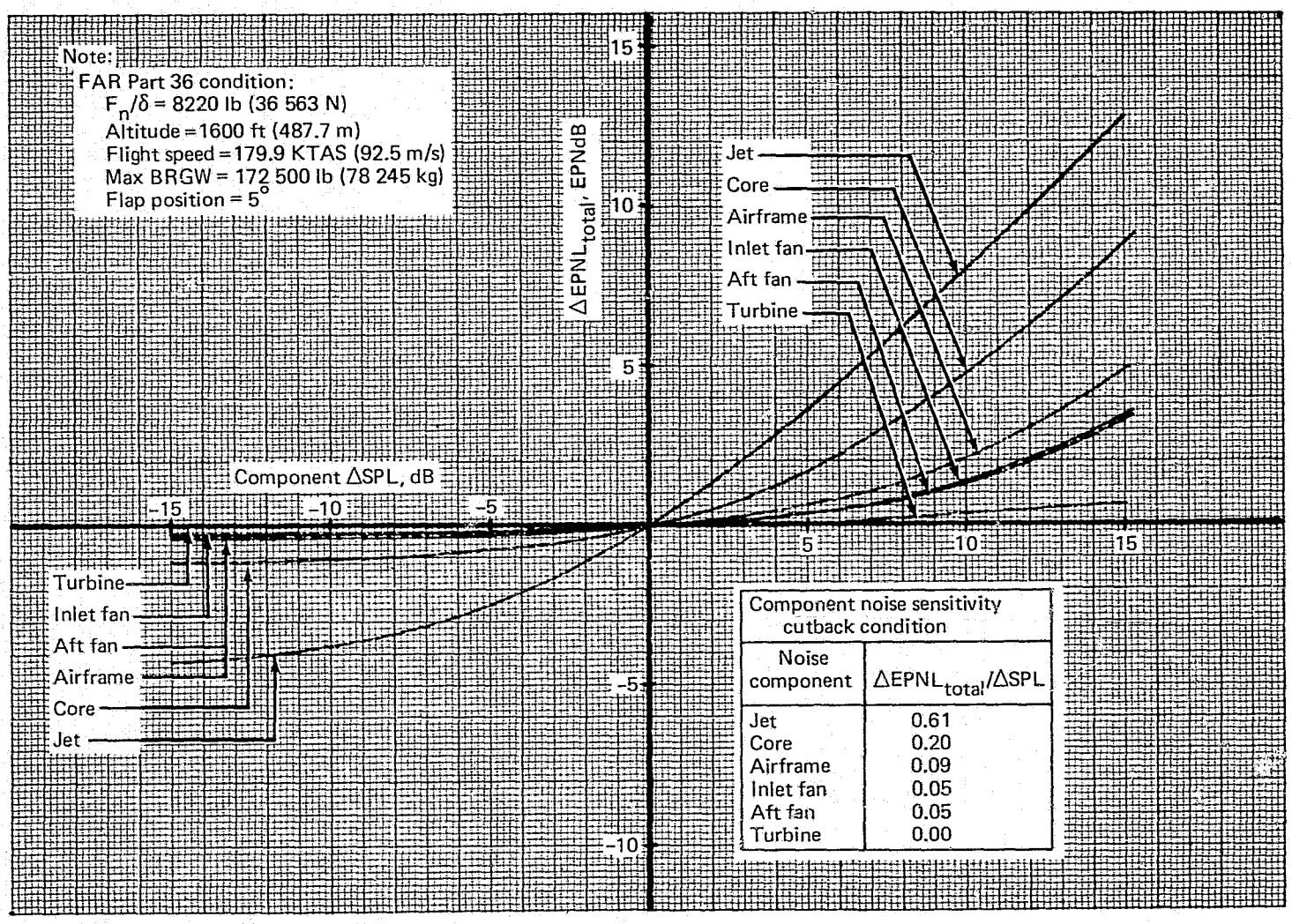

Figure 32.—727 Refan Treated Nacelle, Component Noise Sensitivity Curves, Cutback

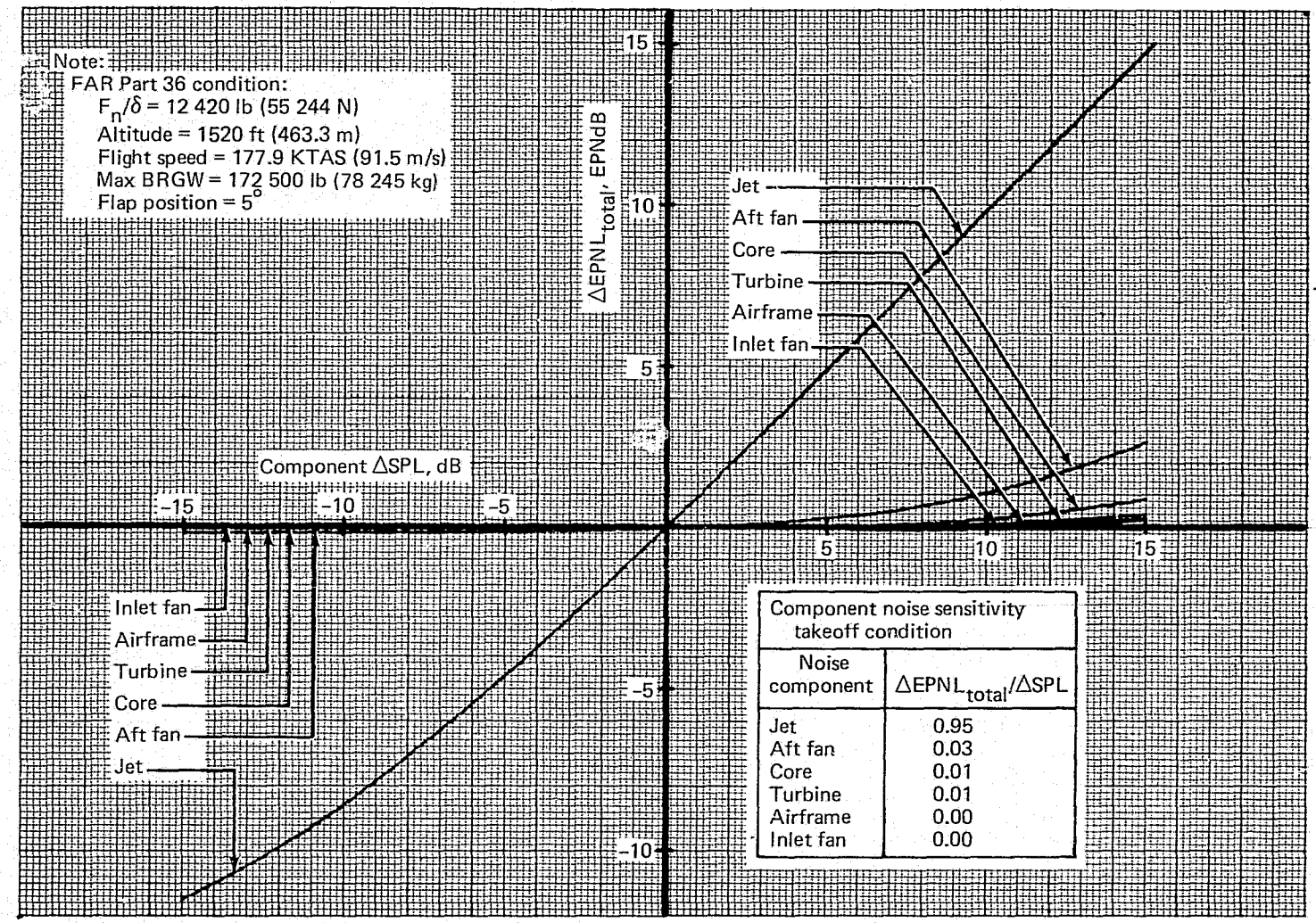

Figure 33.—727-200 Hardwall Nacelle, Component Noise Sensitivity Curves, Takeoff

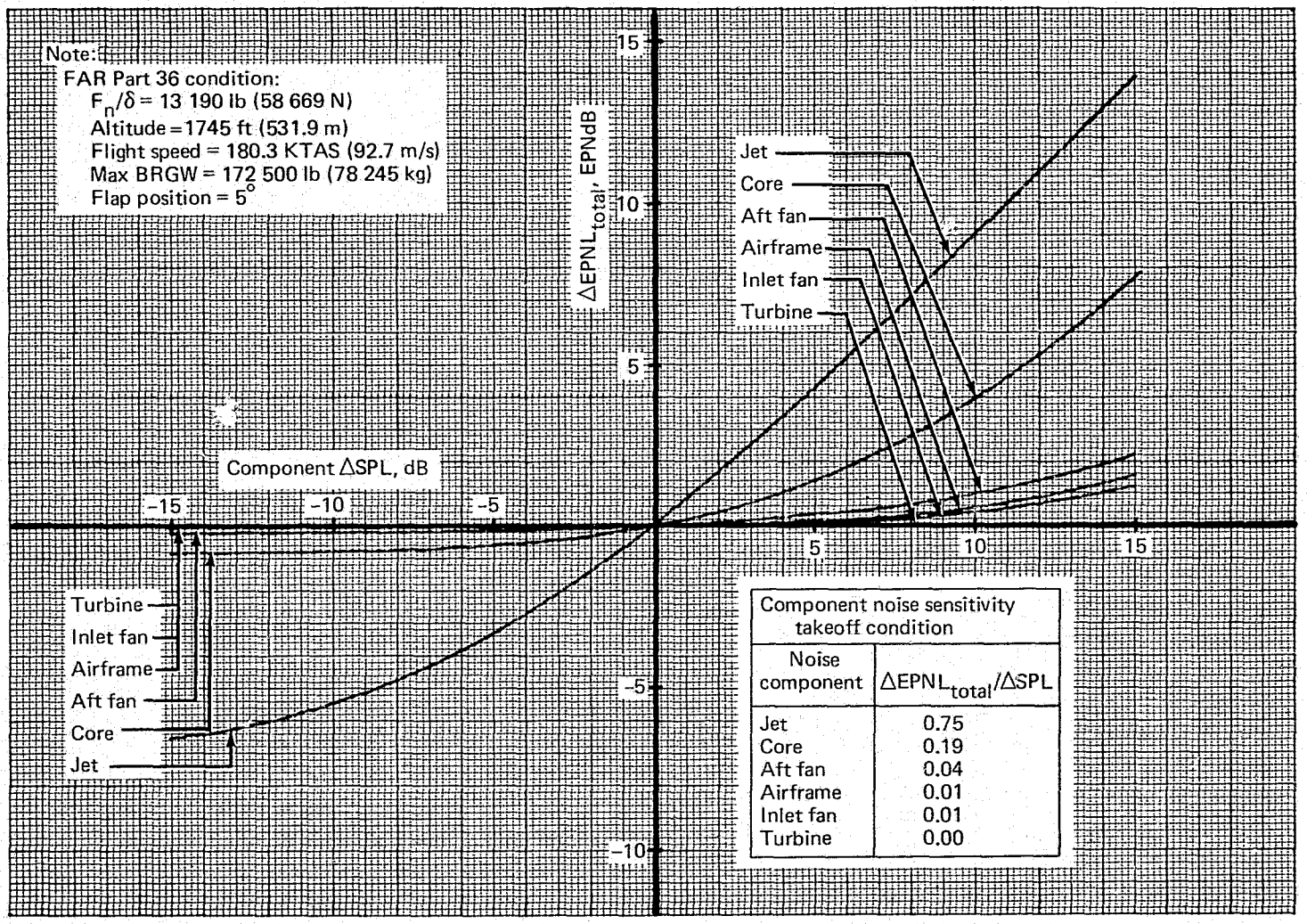

Figure 34.—727 Refan Treated Nacelle, Component Noise Sensitivity Curves, Takeoff

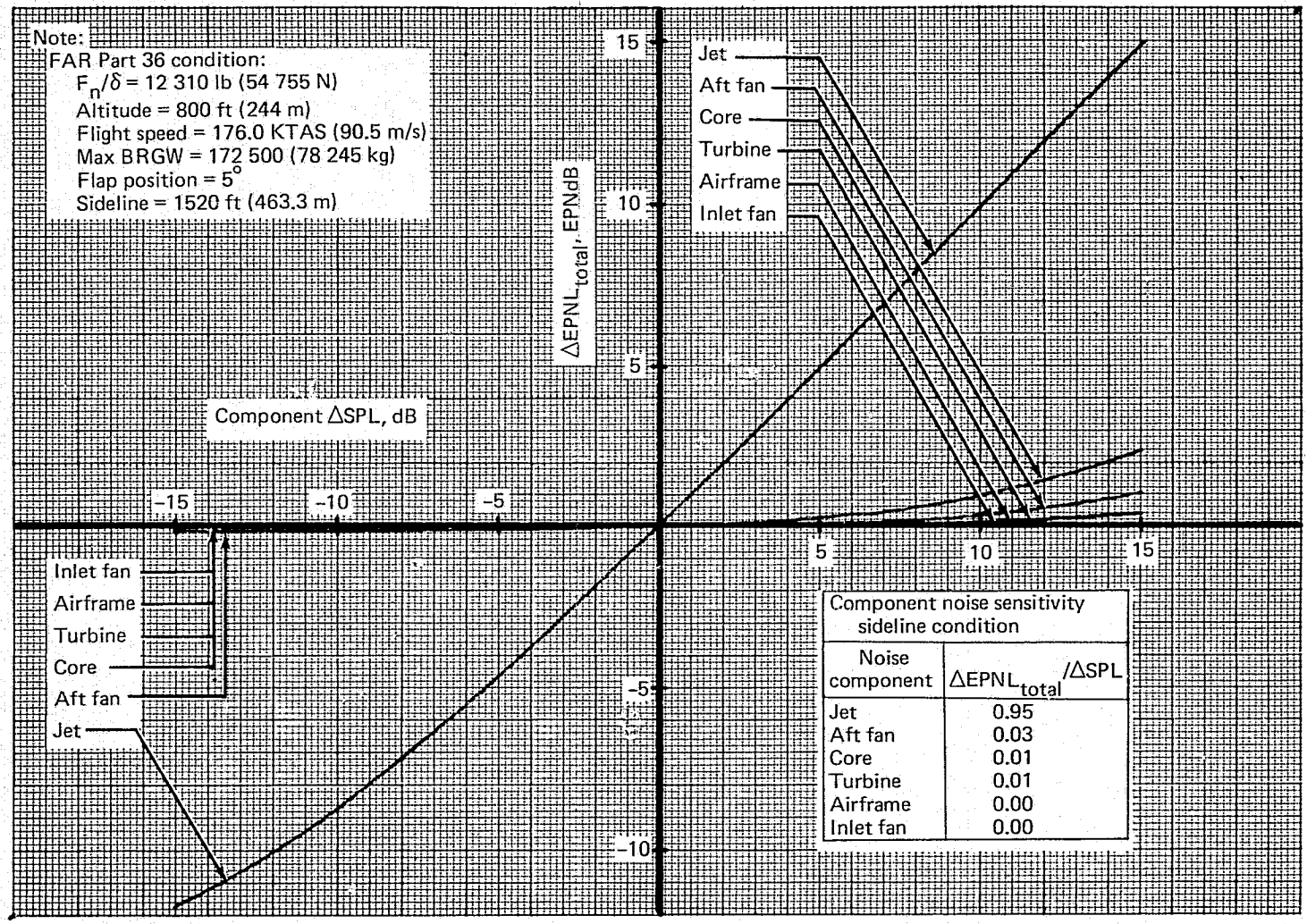

Figure 35.—727-200 Hardwall Nacelle, Component Noise Sensitivity Curves, Sideline

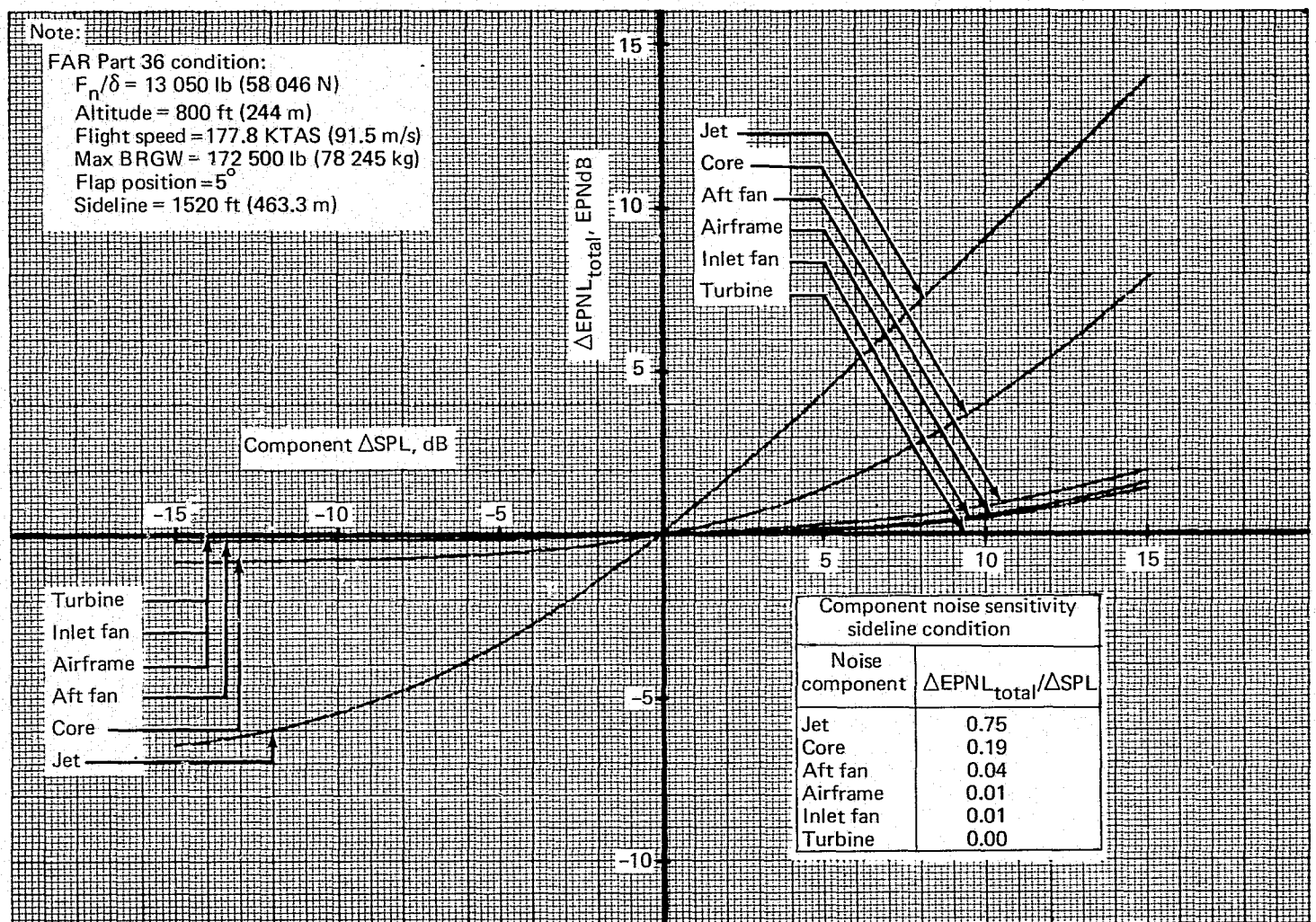

Figure 36.—727 Refan Treated Nacelle, Component Noise Sensitivity Curves, Sideline

Table 9.—Maximum Potential 727-200 Airplane Noise Level Reduction Corresponding to Elimination of Individual Noise Components

Configuration and noise component eliminated	Noise reduction at indicated FAR Part 36 measuring station $\Delta EPNL_{total}$, EPNdB				
	Approach		Takeoff		Sideline
	Flap 30°	Flap 40°	Cutback	No cutback	
JT8D-9 hardwall (baseline)					
Inlet fan	(-2.8)	(-2.6)	-0.1	0	0
Aft fan	-1.8	-1.3	-0.9	-0.2	-0.2
Jet	-0.5	-1.4	(-6.3)	(-14.3)	(-14.7)
Low freq core	-0.2	-0.1	-0.1	0	-0.1
Turbine	-0.1	-0.1	-0.1	0	0
Airframe	-0.4	-0.3	-0.1	0	0
JT8D-109 (refan)					
Inlet fan	(-1.8)	(-1.9)	-0.2	-0.1	-0.1
Aft fan	-0.1	-0.3	-0.3	-0.3	-0.2
Jet	-0.7	-1.6	(-4.5)	(-7.2)	(-7.0)
Low freq core	-0.6	-0.7	-1.1	-0.9	-0.9
Turbine	-0.4	-0.3	0	0	0
Airframe	-1.0	-0.7	-0.4	-0.1	-0.1

Note: Circled increments designate the major source noise contributor to the total far-field noise.

Component noise versus thrust curves at an altitude of 400 ft (122 m) and a flight speed of 160 KTAS (82 m/s) are presented in figures 37 through 39 for PNLT and in figures 40 through 42 for EPNL. These curves are not anchored to the 727-200 flight test EPNL values and therefore should not be used for absolute levels.

The 727-200 data (figs. 37 and 40) indicate a dominance of jet noise at the higher power settings and a dominance of fan noise at the lower power settings. Low-frequency core, turbine, and airframe components are minor contributors to the total. There is a significant difference in level between the inlet and aft fan source noise at high power settings, which diminishes and reverses the difference as the power setting decreases.

The effect of the engine cycle change is apparent when comparing the 727-200 (figs. 37 and 40) and the hardwall nacelle 727 refan (figs. 38 and 41). The jet noise contributes less to the total noise which is now inlet fan dominated except at the highest power settings; and even though the low-frequency core noise increases, it remains a minor contributor. The low aft fan noise is due to acoustic treatment in the fan duct as delivered by P&WA.

The contributions of the components again change when comparing the hardwall nacelle 727 refan (figs. 38 and 41) and treated nacelle 727 refan (figs. 39 and 42). The turbine noise and aft fan noise remain minor contributors as does airframe noise at higher power settings. Airframe noise is a major contributor at the lower power settings. The inlet fan component is suppressed; however, it remains a significant noise source at lower power settings. Jet exhaust noise is the most significant component except at the lowest power settings. Low-frequency core noise is a significant contributor at all power settings.

3.2.3.2 Total Airplane Noise-Thrust-Altitude Curves

Total airplane level-flyover EPNL for the 727-200 was obtained through flight test. The corresponding information for the 727 refan was calculated by a two-step process, analogous to the method used for FAR Part 36 levels: (1) the flyover prediction method described in section 3.2.1 was applied to the 727-200 and 727 refan airplanes, assuming level flyovers at a matrix of thrusts and altitudes and an airspeed of 160 KTAS (82 m/s) (2) the resulting 727-200/727 refan EPNL increments were applied to the 727-200 flight data base. In this manner, as for the FAR Part 36 levels, the absolute EPNL values of the 727 refan were anchored to existing flight test data while maintaining the analytically predicted increments for the refan.

In the calculation of EPNL, the time duration correction was limited to +5 EPNdB; this restriction had an effect only at heights of 6000 ft (1829 m) or more above the runway.

NTA plots are shown in figures 43 through 47. The NTA curves show the acoustic trends for the 727-200, 727 refan hardwall nacelle, and 727 refan treated nacelle; the 727-200 and 727 refan were used for the estimation of EPNL contours.

Generalized trends in the effectiveness of the refan noise reduction concept are seen from the NTA curves (figs. 45 through 47) and are summarized in figure 48 at altitudes of 400 ft (122 m) and 2000 ft (610 m). Large reductions in jet noise between the 727-200 (fig. 45)

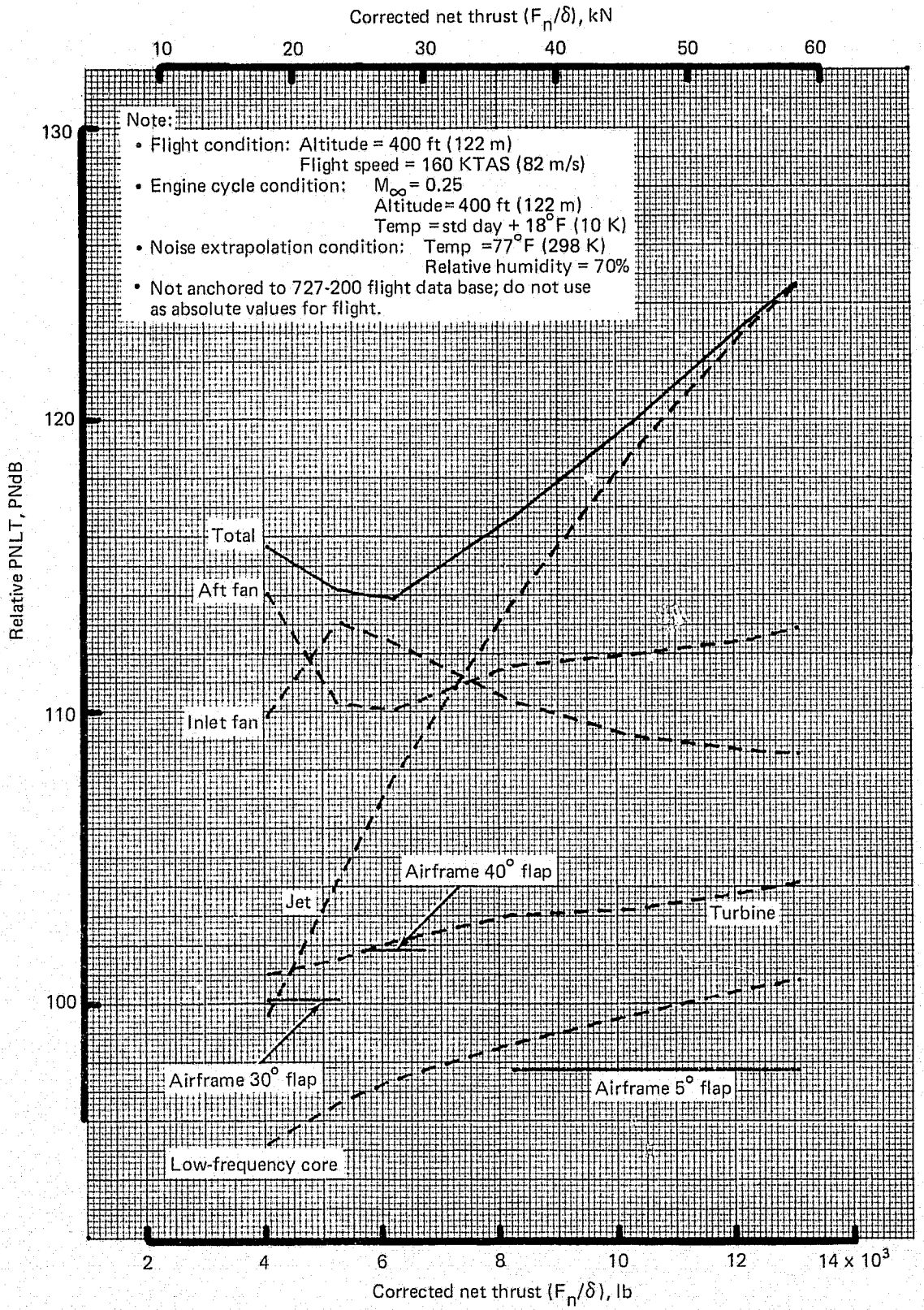

Figure 37.—727-200 Hardwall Nacelle, Component PNLT Versus Corrected Net Thrust

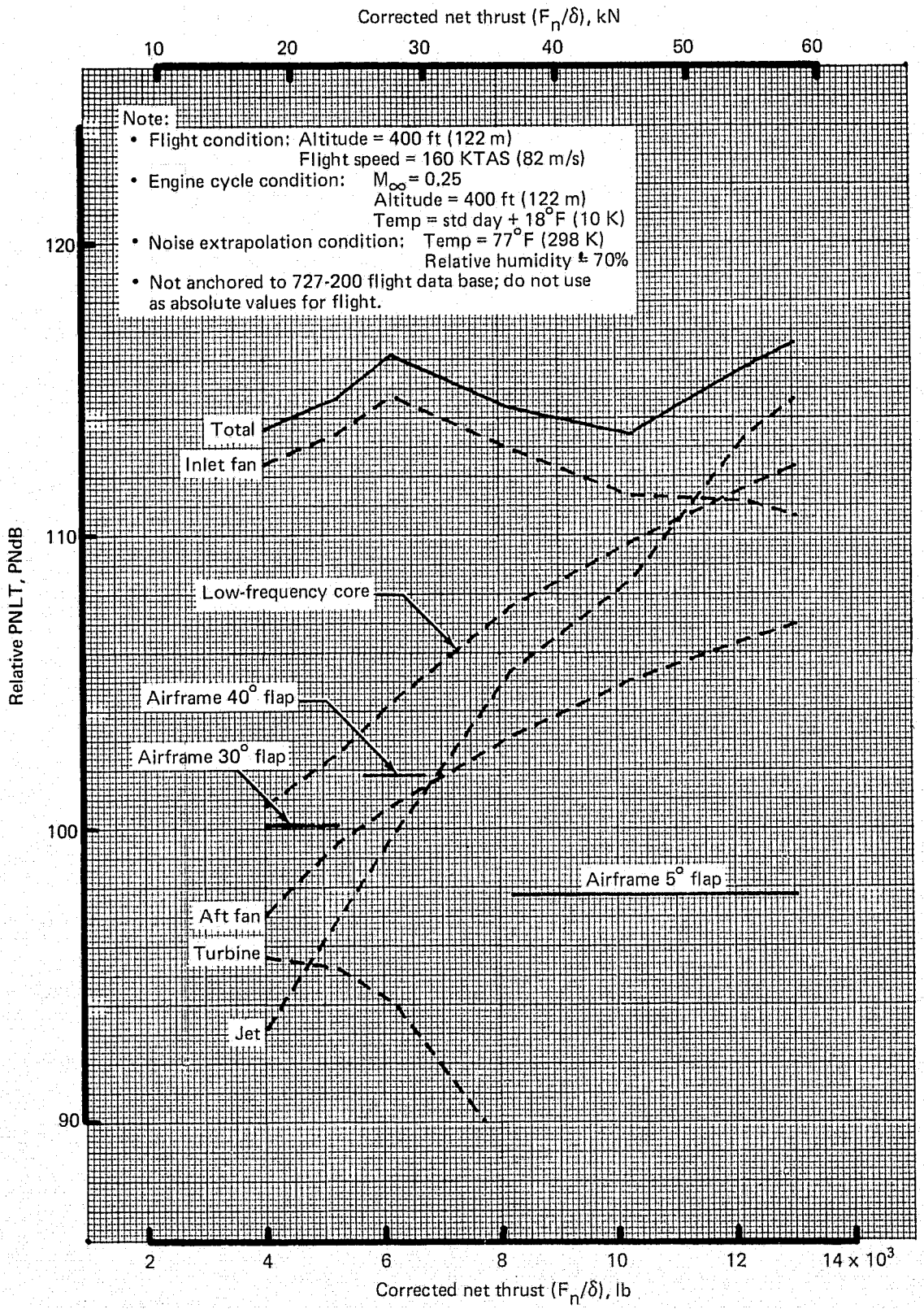

Figure 38.—727 Refan Hardwall Nacelle, Component PNLT Versus Corrected Net Thrust

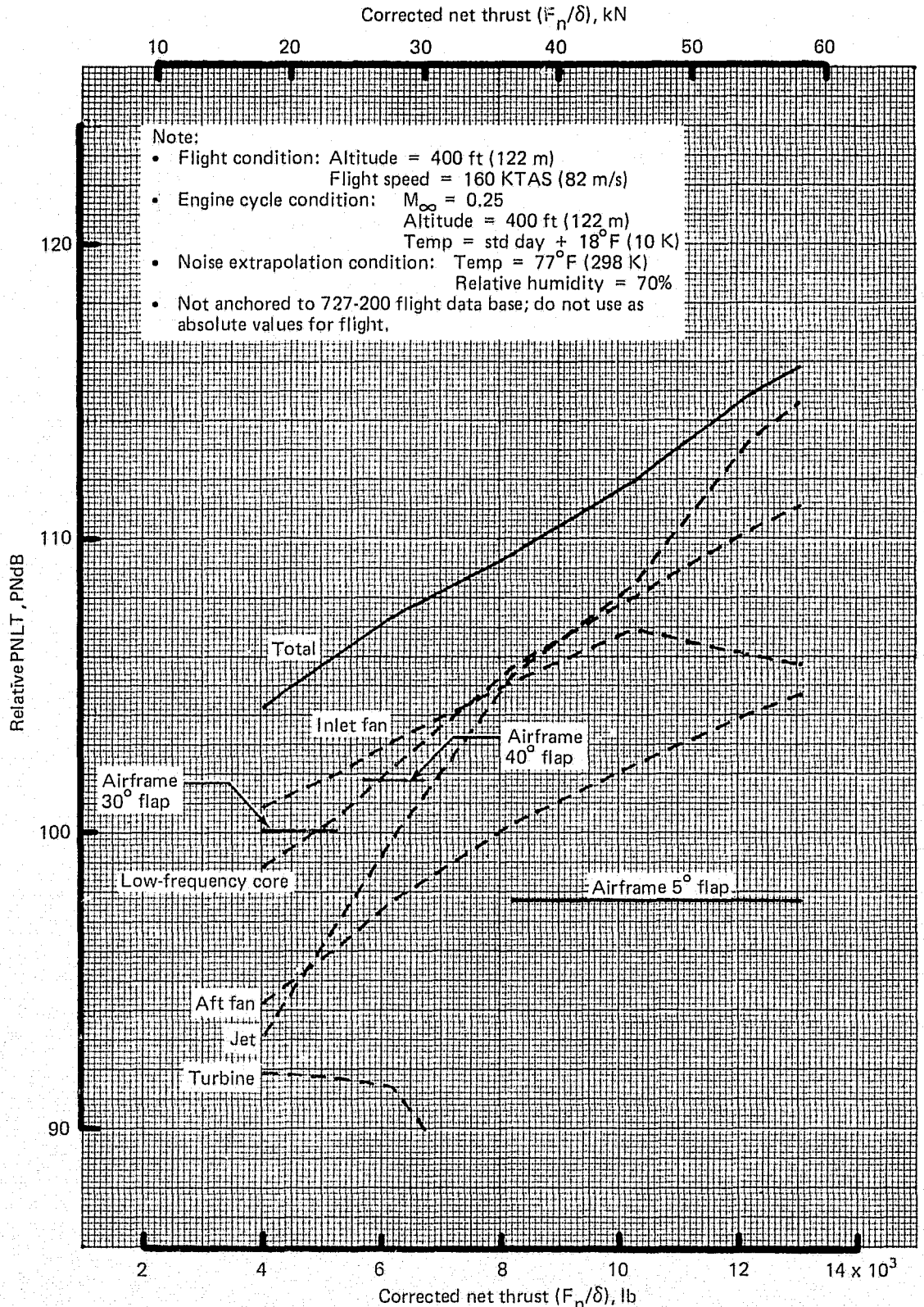

Figure 39.—727 Refan Treated Nacelle, Component PNLT Versus Corrected Net Thrust

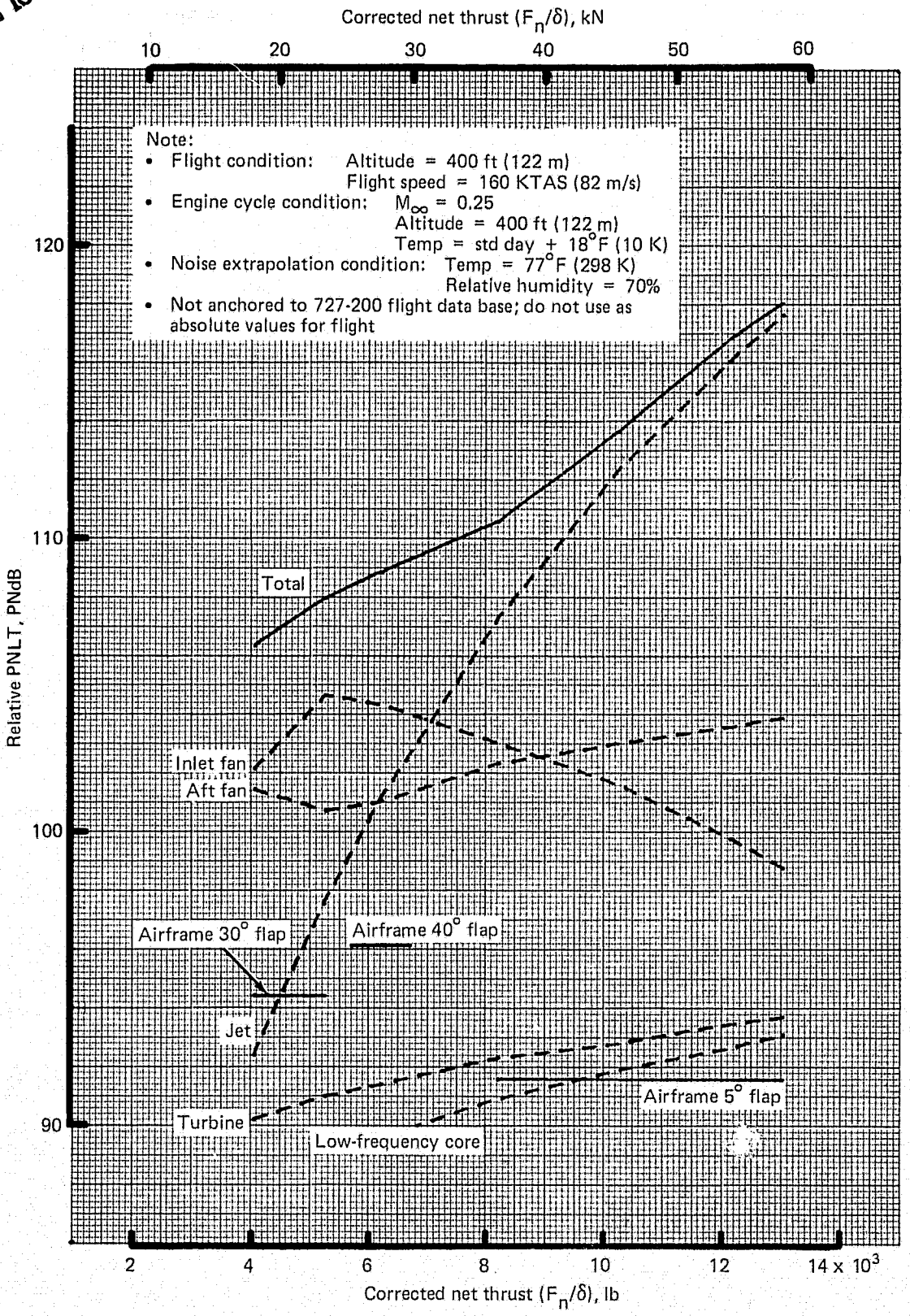

Figure 40.—727-200 Hardwall Nacelle, Component EPNL Versus Corrected Net Thrust

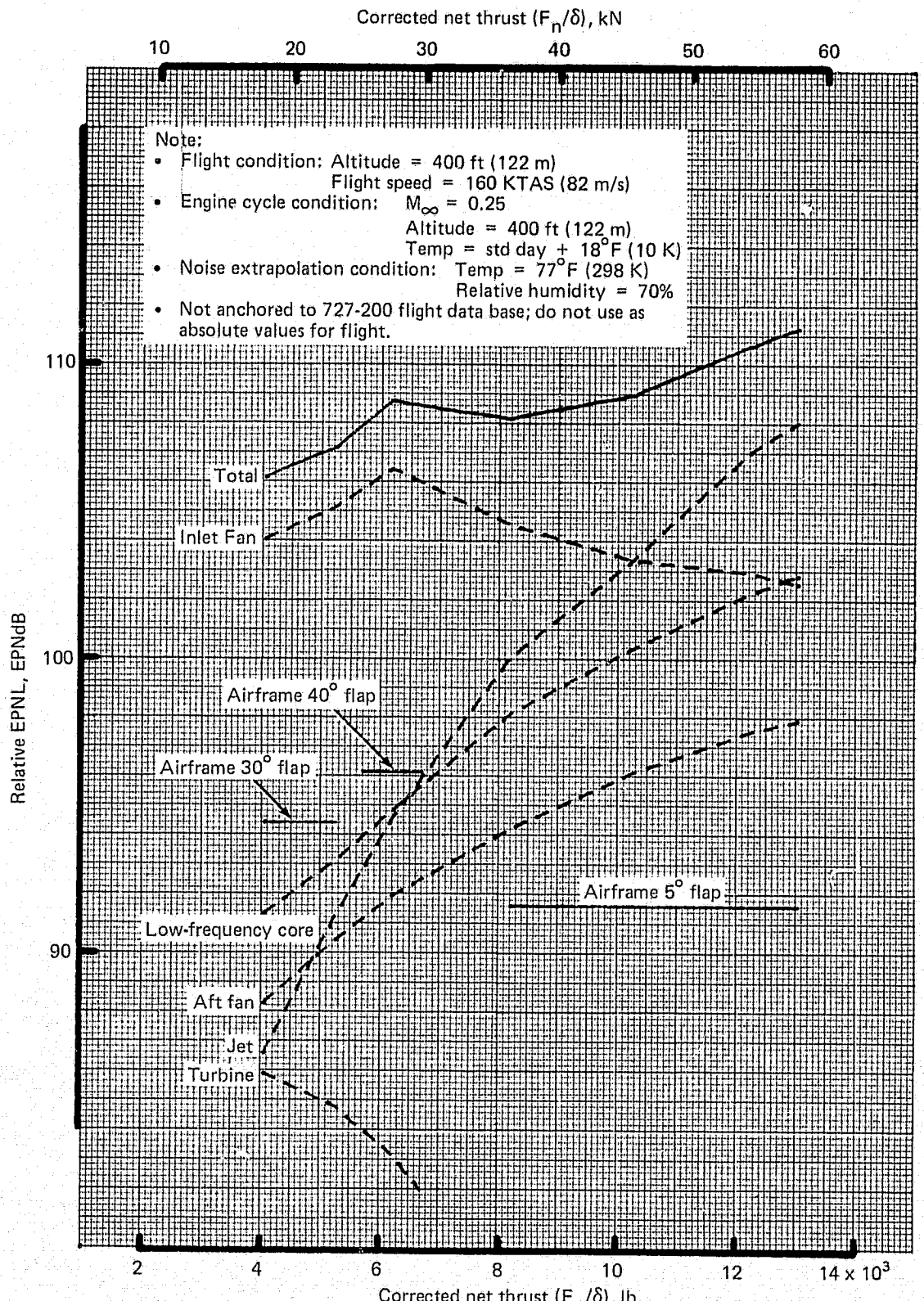

Figure 41.—727 Refan Hardwall Nacelle, Component EPNL Versus Corrected Net Thrust

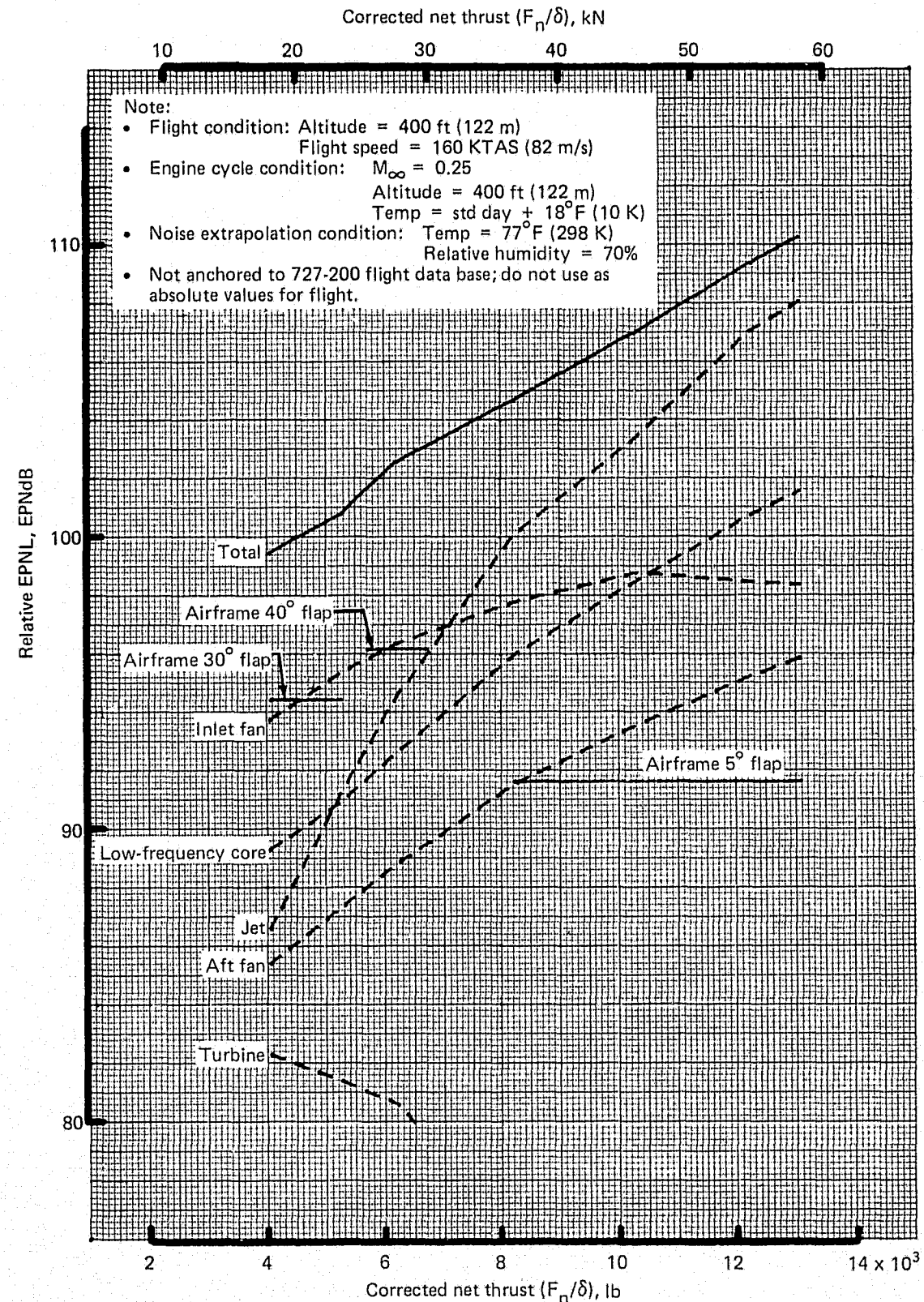

Figure 42.—727 Refan Treated Nacelle, Component Noise Corrected Net Thrust

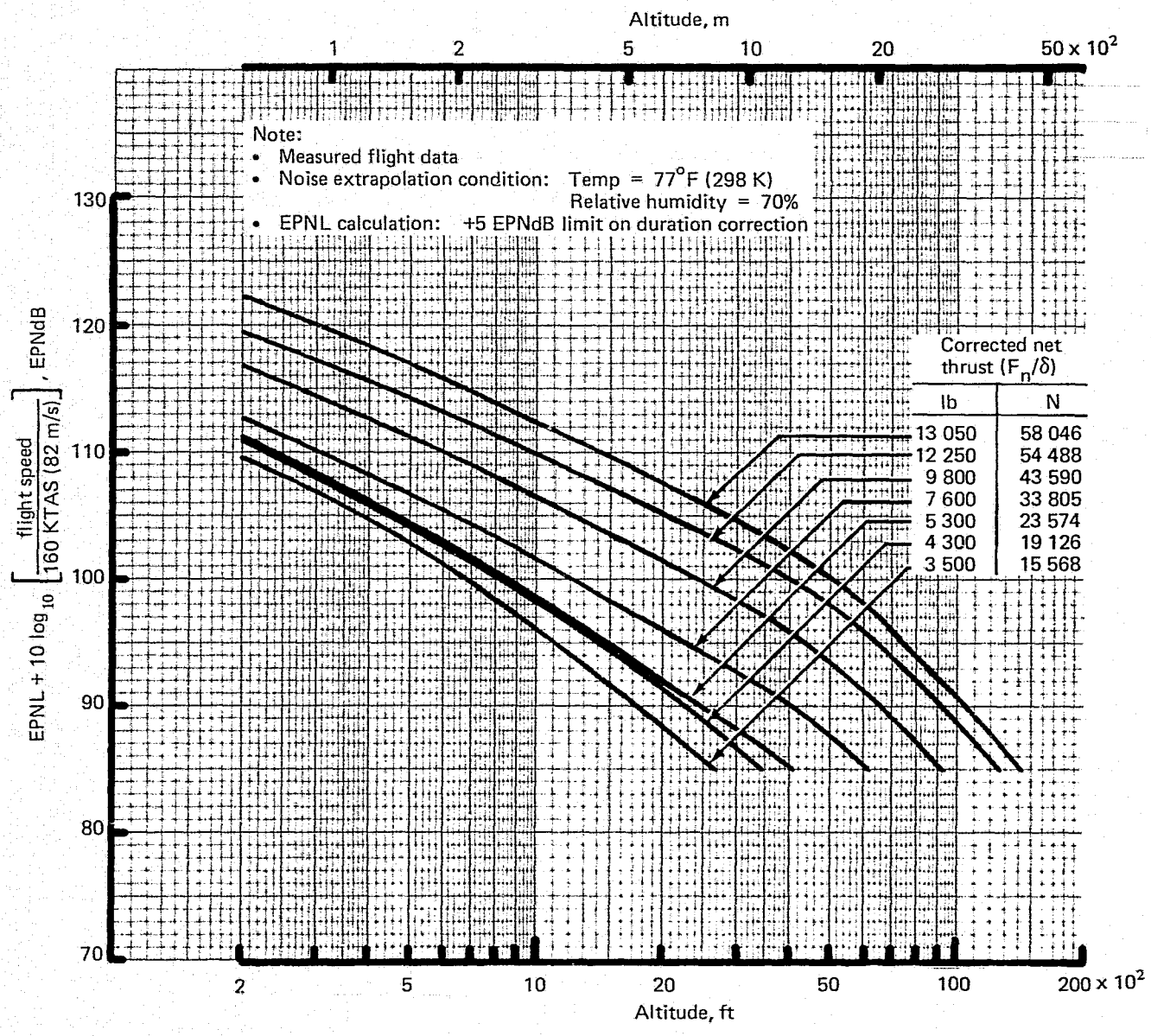

Figure 43.—727-200 Hardwall Nacelle, Noise Versus Altitude With Varying Thrust

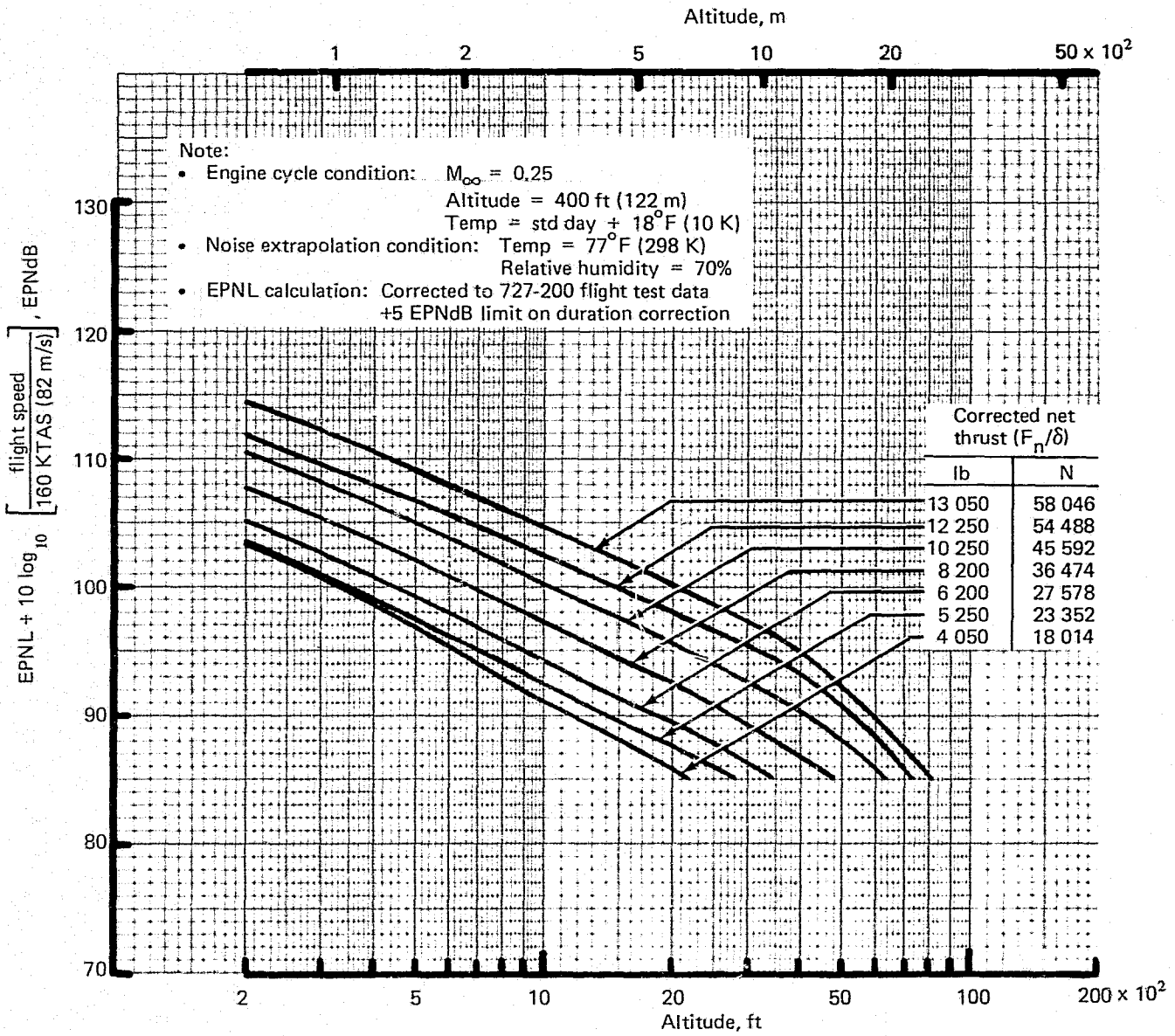

Figure 44.—727 Refan Treated Nacelle, Noise Versus Altitude With Varying Thrust

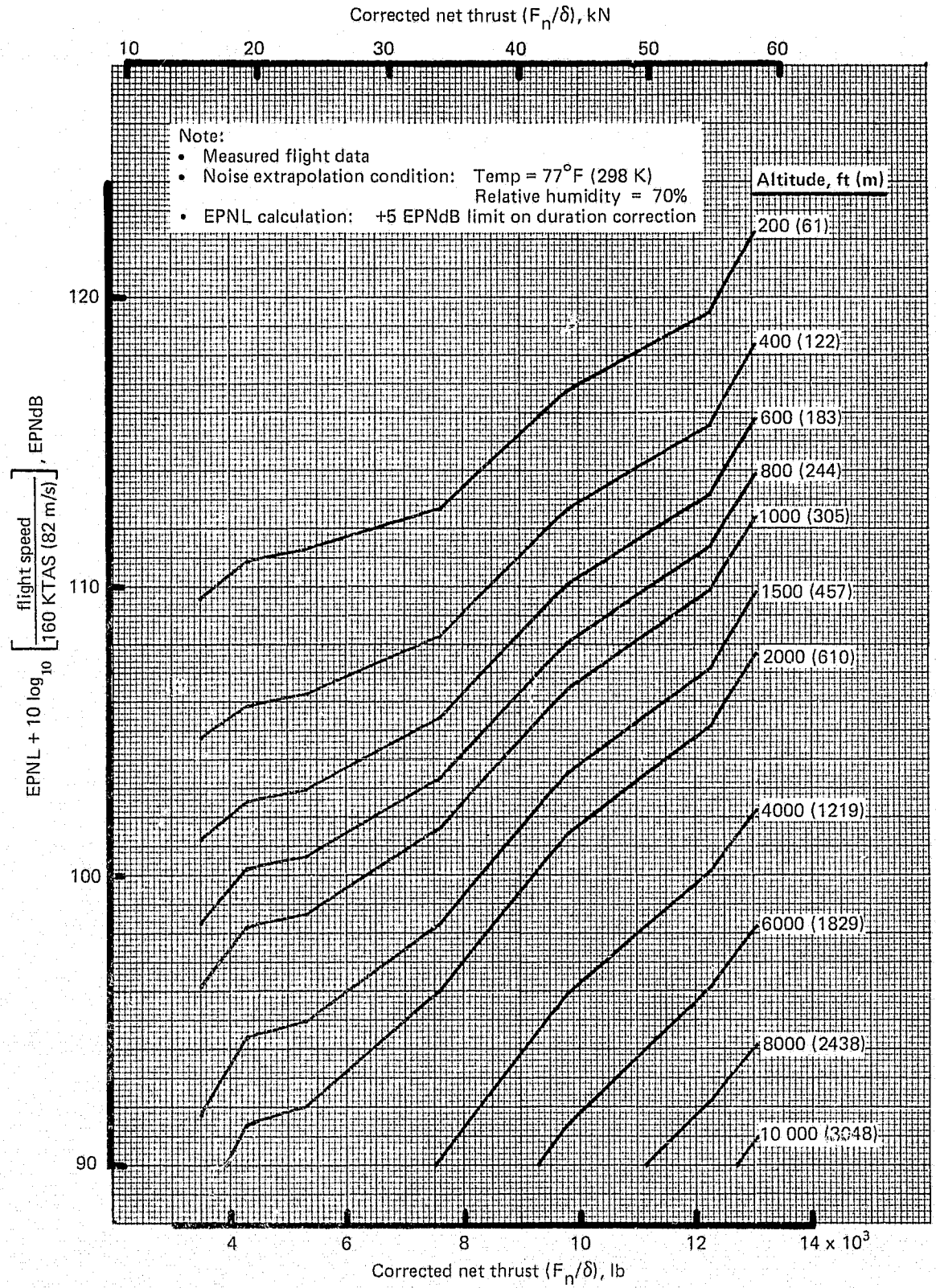

Figure 45.—727-200 Hardwall Nacelle, Noise Versus Thrust With Varying Altitude

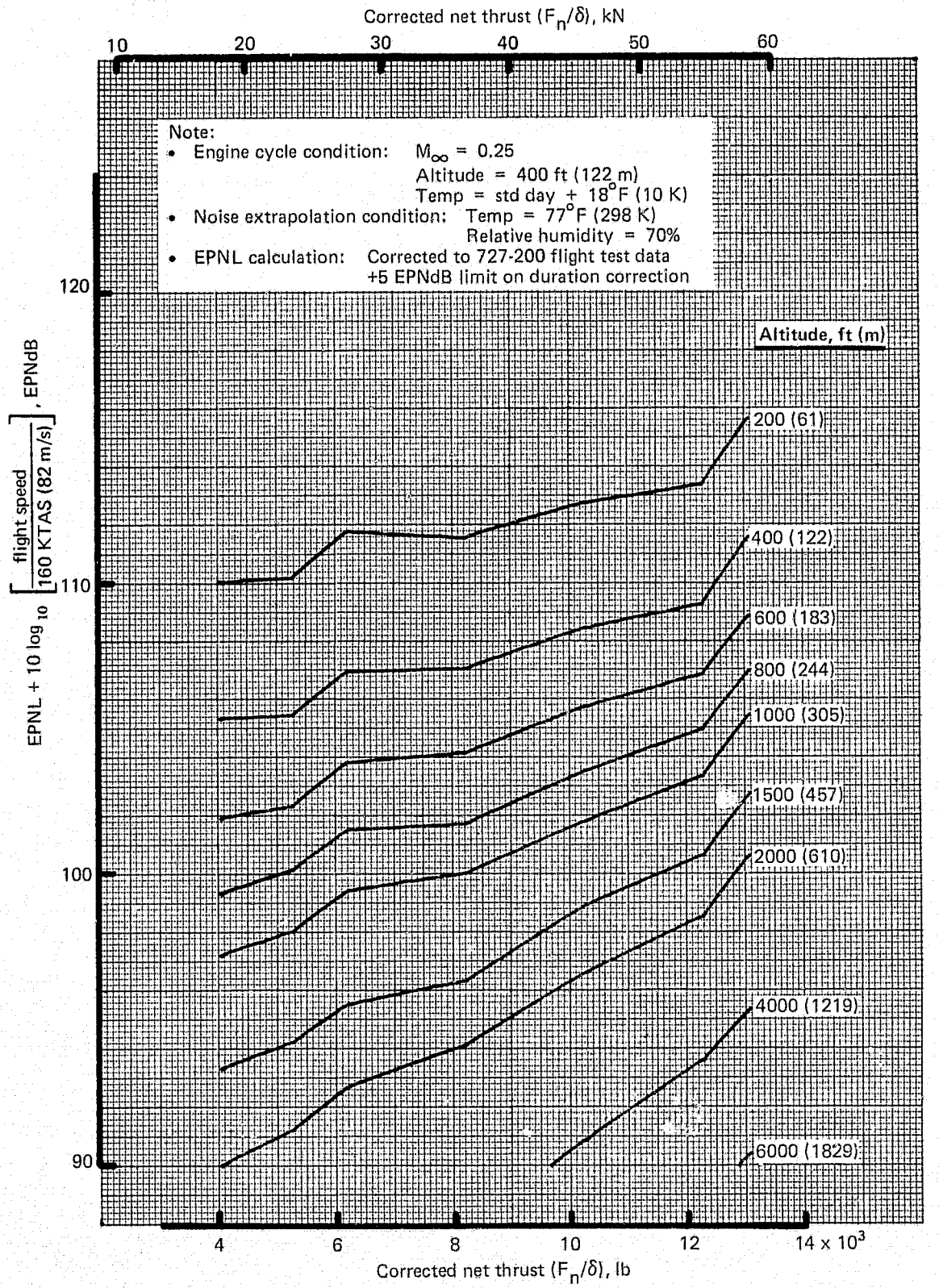

Figure 46.—727 Refan Hardwall Nacelle, Noise Versus Thrust With Varying Altitude

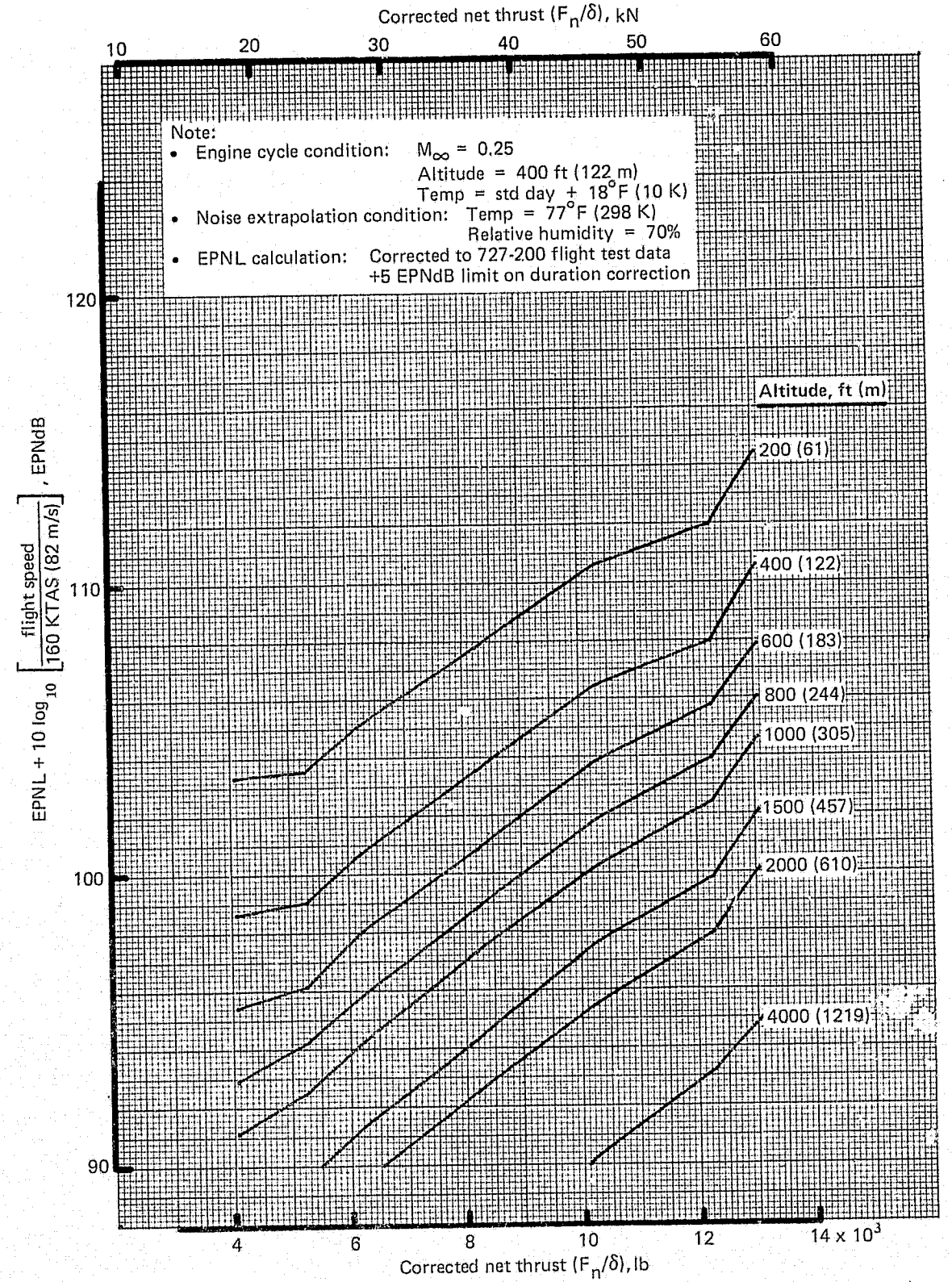

Figure 47.—727 Refan Treated Nacelle, Noise Versus Thrust With Varying Altitude

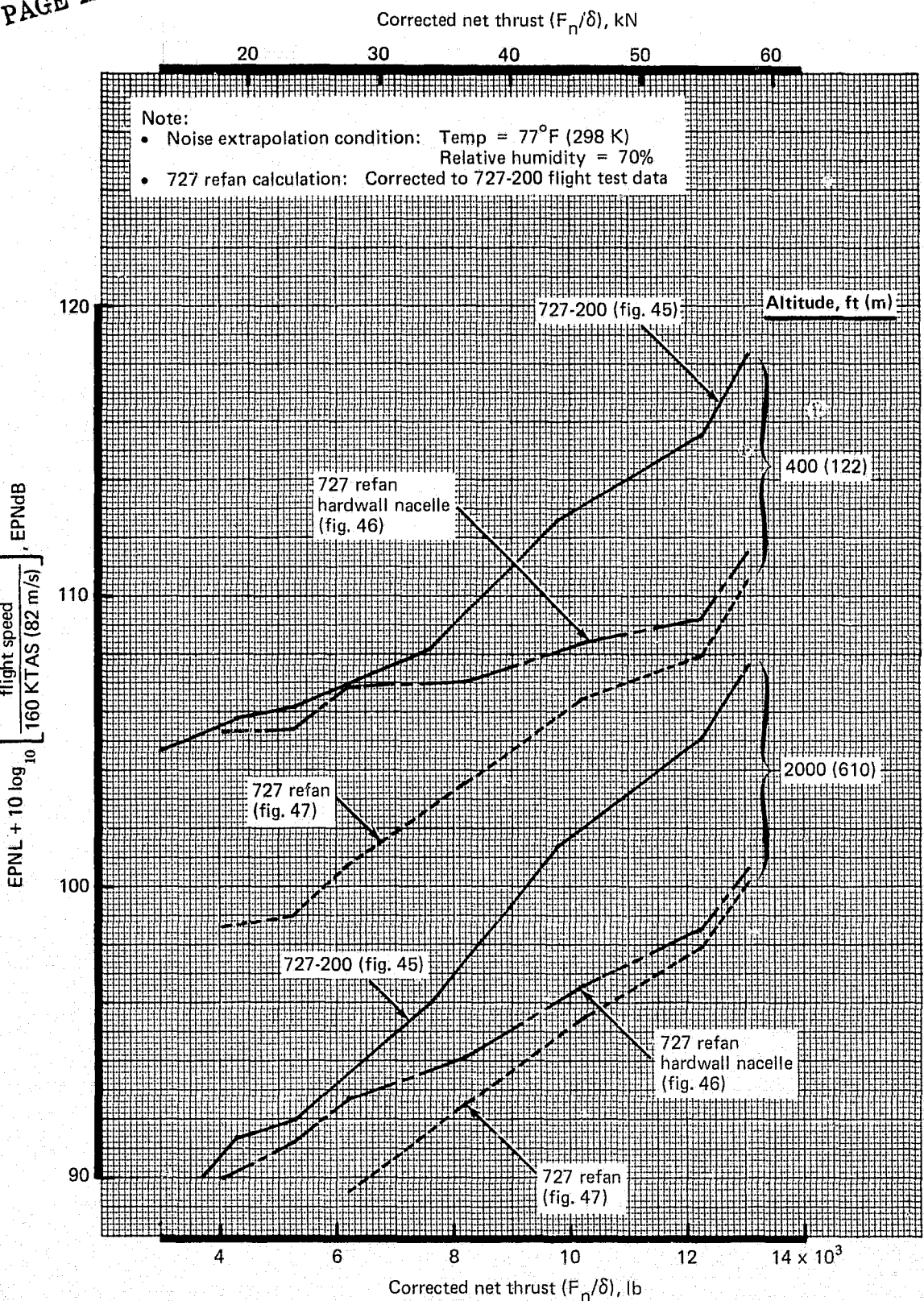

Figure 48.—Effectiveness of the Refan Concept

and the hardwall nacelle 727 refan (fig. 46) are evident at the higher power settings at all altitudes. At the lower power settings, other source noises dominate the total; consequently, there is no significant noise reduction. Additional noise reduction is shown between the 727 refan hardwall nacelle (fig. 46) and 727 refan treated nacelle (fig. 47) at all power settings at all altitudes. This reduction resulted from the effectiveness of the acoustic linings in suppressing the inlet fan noise. Acoustic linings were predicted to be most effective at low power settings and low altitudes (where high-frequency noise dominates) and less effective as the power setting or altitude increases (where there is increased dominance of low-frequency noise). The combined effect of the cycle modification and acoustic treatment is a 3.2- to 9.0-EPNdB reduction for the 727 refan relative to the 727-200 at a given net thrust and altitude.

These NTA curves were used for footprint calculations, as described in section 3.2.4.

3.2.4 EPNL FOOTPRINT CONTOURS AND FLIGHT PROFILE OPTIMIZATION

The EPNL contour area information, which provides an indication of airport community exposure and the noise reduction benefit of the JT8D refan engine, is presented in four forms:

1. Noise directly under the flightpath

2. Normalized footprint contour areas for different EPNL levels

3. Percent area reductions referenced to the 727-200

4. A single-number relative footprint noise index

These comparisons are made specifically for the 727-200 airplane and similar comparisons for other airplane types may show significantly different trends.

3.2.4.1 Flight Profiles and Gross Weights

The takeoff and landing profile noise reduction trade study completed for the 727-200 and 727 refan airplanes included six takeoff profile and two landing profile types. The six takeoff profiles studied were:

- Modified full power operational profile (MFPOP)
- Air Transport Association profile (ATA)
- Airline Pilots Association profile (ALPA)
- FAR Part 36 cutback profile (FAR)
- Community interface–1000-ft/min (5.08-m/s) climb (CI 1000)
- Community interface–500-ft/min (2.54-m/s) climb (CI 500)

A recommendation as to which takeoff or approach profile should be flown in commercial service is beyond the scope of this study. That choice must include airline assessment of the safety and economic aspects of each flight profile, as well as the community noise impact.

Descriptions of the profiles are presented in table 10. The aircraft performance data for the flight profiles studied (tables 11 through 24) were representative of a sea level airport at ISA + 18°F (10 K).

Each takeoff profile was studied at 138 000 lb (62 596 kg), which is a typical mission and noise average gross weight for the 727-200; 155 000 lb (70 307 kg), which is an intermediate weight; and 172 500 lb (78 245 kg), which is the maximum BRGW for the 727-200. In addition, the 727 refan takeoff profiles were studied at 182 500-lb (82 781-kg) BRGW, which is the practical refan airplane growth limit.

Footprints for the 172 500-lb (78 245-kg) airplanes were combined with those for 150 000-lb (68 039-kg) landing weight, using a conventional 3° approach with glide slope intercept at 3000-ft (914.4-m) altitude. The intermediate weight (155 000 lb (70 307 kg)) airplane's takeoff profiles were compared using 126 700-lb (57 470-kg) typical mission (55% payload) landing weights with a conventional 3° approach. The 138 000-lb (62 596-kg) typical mission takeoff weight airplanes were combined with 126 700-lb (57 470-kg) typical mission landing weights using both conventional 3° approaches and dual slope approaches. Both dual slope approaches had a level flight intercept at 5000-ft (1524-m) altitude. The dual slope approach for the 727-200 had 6°/3° glide slopes and for the 727 refan had 4.2°/3° glide slopes. The 4.2° glide slope is the maximum approach slope that can be used by the 126 700-lb (57 470-kg) landing weight 727 refan because of the higher flight idle setting of the refan engine and the requirement to be able to approach at 1.2° greater than the prescribed glide slope to allow for flightpath adjustments during descent. The glide slope limitation corresponding to a very low landing weight for the 727 refan is actually 3° to 4°, which, from a practical standpoint, negates any benefits obtainable from a dual glide slope. The 727-200 has a low enough idle thrust to allow it to descend on a 6° glide slope. The applicability of any dual glide slope procedure can be severely constrained by atmospheric conditions such as air turbulence, tailwinds, and icing conditions.

3.2.4.2 Noise Under the Flightpath

Plots of noise under the takeoff flightpath and height above runway versus distance from brake release for the 727-200 airplane at 172 500-lb (78 245-kg), 155 000-lb (70 307-kg), and 138 000-lb (62 596-kg) BRGW's are shown in figures 49 through 51. Those for the 727 refan airplane at 182 500-lb (82 781-kg), 172 500-lb (78 245-kg), 155 000-lb (70 307-kg), and 138 000-lb (62 596-kg) BRGW's are shown in figures 52 through 55.

These results show that no one profile is clearly superior to the others for either airplane at any gross weight. The choice of profile has an impact of 0 to 15 EPNdB on the noise level at a given distance from brake release.

Figure 56 shows the approach profiles and the associated noise under the landing flightpath for both the 727-200 and 727 refan. The two-segment approach is seen to have a benefit of 0 to 12 EPNdB for the 727-200 and 0 to 2 EPNdB for the 126 700-lb (57 470-kg) LGW 727 refan when the 4.2° glide slope limit is recognized.

Table 10.—727-200/727 Refan—Trade Study Takeoff Profiles

Takeoff profile	Thrust	Flight altitude	Flight speed	Flaps, deg
MFPOP	Takeoff	Climb to 1500 ft (457 m)	V_2 + 10 kn (5.144 m/s)	5
	Max climb	1500 ft (457 m)	Accelerate to 250 KEAS (128.6 m/s)	Cleanup
ATA	Takeoff	Climb to 1500 ft (457 m)	V_2 + 10 kn (5.144 m/s)	5
	Max climb	Climb to 3000 ft (914 m)	V_2 + 10 kn (5.144 m/s)	5
	Max climb	300-ft/min (1.52-m/s) climb	Accelerate to 250 KEAS (128.6 m/s)	Cleanup
FAR	Takeoff	Climb until 19 443 ft (5926 m) from brake release	V_2 + 10 kn (5.144 m/s)	5
	FAR gradient cutback	FAR gradient climb until 50 000 ft (15 240 m) from brake release	V_2 + 10 kn (5.144 m/s)	5
	Max climb	Constant altitude	Accelerate to 250 KEAS (128.6 m/s)	Cleanup
CI	Takeoff	Climb until 12 000 ft (3658 m) from brake release	V_2 + 10 kn (5.144 m/s)	5
	Climb gradient cutback	Climb at 500 or 1000 ft/min (2.54 or 5.08 m/s) until 50 000 ft (15 240 m) from brake release	V_2 + 10 kn (5.144 m/s)	5
	Max climb	Constant altitude	Accelerate to 250 KEAS (128.6 m/s)	Cleanup
ALPA	Takeoff	Climb to 800 ft (244 m)	V_2 + 10 kn (5.144 m/s)	5
	Takeoff	200-ft/min (1.02-m/s) climb until cleaned up	Accelerate to 250 KEAS (128.6 m/s)	Cleanup
	Takeoff	Climb to 1500 ft (457 m) minimum altitude	Maintain 250 KEAS (128.6 m/s)	0
	Climb gradient cutback	Climb at 1000 ft/min (5.08 m/s) until 4000 ft (1219 m) altitude	Maintain 250 KEAS (128.6 m/s)	0

Note: All profiles begin with a ground roll at takeoff thrust and climb until landing gear is retracted while accelerating to V_2 + 10 kn (5.144 m/s)

All profiles conclude with en route climb at 250 KEAS (128.6 m/s) with maximum climb thrust.

Table 11.—727-200: Modified Full-Power Operational Profiles

Takeoff Profiles for EPNL Footprints

Brake release gross weight, lb (kg)	Airplane Position at Start of Segment		Segment Average		Flap position, deg	Gear position
	Distance from brake release, ft (m)	Altitude, ft (m)	Power setting (F_n/δ), lb (N)	Flight speed, KTAS (m/s)		
172 500 (78 245)	0 (0)	0 (0)	12 230 (54 399)	117.5 (60.4)	5	Down
	7 810 (2 380)	0 (0)	12 240 (54 444)	171.4 (88.2)	5	Retract
	11 740 (3 578)	400 (122)	12 280 (54 621)	175.5 (90.3)	5	Up
	15 100 (4 602)	800 (244)	12 360 (54 977)	176.9 (91.0)	5	Up
	21 110 (6 434)	1 500 (457)	9 820 (43 679)	189.0 (97.2)	Cleanup	Up
	25 880 (7 888)	1 500 (457)	9 570 (42 567)	230.1 (118.4)	0	Up
	38 890 (11 829)	1 500 (457)	9 440 (41 989)	261.8 (134.7)	0	Up
	49 340 (15 039)	2 400 (732)	9 520 (42 345)	265.1 (136.4)	0	Up
	59 090 (18 011)	3 200 (975)	9 600 (42 701)	268.4 (138.1)	0	Up
	69 200 (21 092)	4 000 (1219)	9 710 (43 190)	272.5 (140.2)	0	Up
	85 100 (25 938)	5 200 (1585)	9 830 (41 500)	276.6 (142.3)	0	Up
	96 210 (29 325)	6 000 (1829)	9 950 (44 258)	280.9 (144.5)	0	Up
	113 690 (34 653)	7 200 (2195)	10 070 (44 791)	285.3 (146.8)	0	Up
	125 940 (38 386)	8 000 (2438)	10 190 (45 325)	289.8 (144.5)	0	Up
	145 280 (44 281)	9 200 (2804)	10 310 (45 859)	294.4 (151.4)	0	Up
	158 900 (48 433)	10 000 (3048)	10 510 (46 748)	301.0 (154.8)	0	Up
	195 570 (59 610)	12 000 (3658)	10 800 (48 038)	310.9 (159.9)	0	Up
	236 570 (72 107)	14 000 (4267)	11 080 (49 284)	321.2 (165.2)	0	Up
	282 890 (86 225)	16 000 (4877)	11 460 (50 974)	332.0 (170.8)	0	Up
	335 010 (102 111)	18 000 (5486)	11 840 (52 664)	343.4 (176.6)	0	Up
	394 370 (120 204)	20 000 (6096)				
155 000 (70 307)	0 (0)	0 (0)	12 290 (54 666)	112.3 (57.8)	5	Down
	6 190 (1 887)	0 (0)	12 300 (54 710)	163.9 (84.3)	5	Retract
	9 520 (2 902)	400 (122)	12 330 (54 844)	167.8 (86.3)	5	Up
	12 290 (3 746)	800 (244)	12 420 (55 244)	169.2 (87.0)	5	Up
	17 250 (5 258)	1 500 (457)	9 840 (43 768)	186.5 (95.9)	Cleanup	Up
	22 890 (6 977)	1 500 (457)	9 560 (42 523)	231.5 (119.1)	0	Up
	33 310 (10 153)	1 500 (457)	9 440 (41 989)	261.8 (134.7)	0	Up
	42 260 (12 881)	2 400 (732)	9 520 (42 345)	265.1 (136.4)	0	Up
	50 510 (15 395)	3 200 (975)	9 600 (42 701)	268.4 (138.1)	0	Up
	59 070 (18 005)	4 000 (1219)	9 710 (43 190)	272.5 (140.2)	0	Up
	72 490 (22 095)	5 200 (1585)	9 710 (43 724)	276.6 (142.3)	0	Up
	81 840 (24 945)	6 000 (1829)	9 950 (44 258)	280.9 (144.5)	0	Up
	96 520 (29 419)	7 200 (2195)	10 070 (44 791)	285.3 (146.8)	0	Up
	106 770 (32 543)	8 000 (2438)	10 190 (45 325)	289.8 (149.1)	0	Up
	122 920 (37 466)	9 200 (2804)	10 310 (45 859)	294.4 (151.4)	0	Up
	134 240 (40 916)	10 000 (3048)	10 510 (46 848)	301.0 (154.8)	0	Up
	164 590 (50 167)	12 000 (3658)	10 800 (48 038)	310.9 (159.9)	0	Up
	198 240 (60 424)	14 000 (4267)	10 080 (49 284)	321.2 (165.2)	0	Up
	235 890 (71 899)	16 000 (4877)	11 460 (50 974)	332.0 (170.8)	0	Up
	277 820 (84 680)	18 000 (5486)	11 840 (52 664)	343.4 (176.6)	0	Up
	324 980 (99 054)	20 000 (6096)				
138 000 (62 596)	0 (0)	0 (0)	12 340 (54 888)	107.2 (55.1)	5	Down
	4 810 (1 466)	0 (0)	12 350 (54 933)	156.3 (80.4)	5	Retract
	7 640 (2 329)	400 (122)	12 390 (55 111)	159.9 (82.3)	5	Up
	9 920 (3 024)	800 (244)	12 480 (55 511)	161.3 (83.0)	5	Up
	13 990 (4 264)	1 500 (457)	9 870 (43 902)	184.1 (94.7)	Cleanup	Up
	20 100 (6 126)	1 500 (457)	9 550 (42 478)	233.0 (119.9)	0	Up
	28 540 (8 699)	1 500 (457)	9 440 (41 989)	261.8 (134.7)	0	Up
	36 130 (11 012)	2 400 (732)	9 520 (42 345)	265.1 (136.4)	0	Up
	43 130 (13 146)	3 200 (975)	9 600 (42 701)	268.4 (138.1)	0	Up
	50 370 (15 353)	4 000 (1219)	9 710 (43 190)	272.5 (140.2)	0	Up
	61 710 (18 809)	5 200 (1585)	9 830 (43 724)	276.6 (142.3)	0	Up
	69 600 (21 214)	6 000 (1829)	9 950 (44 258)	280.9 (144.5)	0	Up
	81 950 (24 978)	7 200 (2195)	10 070 (44 791)	285.3 (146.8)	0	Up
	90 570 (27 606)	8 000 (2438)	10 190 (45 325)	289.8 (149.1)	0	Up
	104 100 (31 730)	9 200 (2804)	10 310 (45 859)	294.4 (151.4)	0	Up
	113 570 (34 616)	10 000 (3048)	10 510 (46 748)	301.0 (154.8)	0	Up
	138 840 (42 318)	12 000 (3658)	10 800 (48 038)	310.9 (159.9)	0	Up
	166 720 (50 816)	14 000 (4267)	11 080 (49 284)	321.2 (165.2)	0	Up
	197 690 (60 256)	16 000 (4877)	11 460 (50 974)	332.0 (170.8)	0	Up
	231 940 (70 695)	18 000 (5486)	11 840 (52 664)	343.4 (176.6)	0	Up
	270 130 (82 336)	20 000 (6096)				

Table 12.—727-200: Air Transportation Association Profiles

Takeoff Profiles for EPNL Footprints

Brake release gross weight, lb (kg)	Airplane Position at Start of Segment		Segment Average		Flap position, deg	Gear position
	Distance from brake release, ft (m)	Altitude, ft (m)	Power setting (F_n/δ), lb (N)	Flight speed, KTAS (m/s)		
172 500 (78 245)	0 (0)	0 (0)	12 230 (54 399)	117.5 (60.4)	5	Down
	7 810 (2 380)	0 (0)	12 240 (54 444)	171.4 (88.2)	5	Retract
	11 740 (3 578)	400 (122)	12 280 (54 621)	175.5 (90.3)	5	Up
	15 100 (4 602)	800 (244)	12 360 (54 977)	176.9 (91.0)	5	Up
	21 110 (6 434)	1 500 (457)	9 930 (44 169)	178.5 (91.8)	5	Up
	27 920 (8 510)	2 000 (610)	9 990 (44 436)	180.0 (92.6)	5	Up
	36 350 (11 079)	2 600 (792)	10 040 (44 658)	181.4 (93.3)	5	Up
	42 140 (12 844)	3 000 (914)	9 810 (43 635)	224.6 (115.5)	Cleanup	Up
	66 200 (20 178)	3 320 (1012)	9 610 (42 745)	268.6 (138.2)	0	Up
	74 760 (22 787)	4 000 (1219)	9 710 (43 190)	272.5 (140.2)	0	Up
	90 640 (27 627)	5 200 (1585)	9 830 (43 724)	276.6 (142.3)	0	Up
	101 730 (31 007)	6 000 (1829)	9 950 (44 258)	280.9 (144.5)	0	Up
	119 180 (36 326)	7 200 (2195)	10 070 (44 791)	285.3 (146.8)	0	Up
	131 410 (40 054)	8 000 (2438)	10 190 (45 325)	289.8 (149.1)	0	Up
	150 720 (45 939)	9 200 (2804)	10 310 (45 859)	294.4 (151.4)	0	Up
	164 310 (50 082)	10 000 (3048)	10 510 (46 748)	301.1 (154.9)	0	Up
	200 910 (61 237)	12 000 (3658)	10 800 (48 038)	310.9 (159.9)	0	Up
	241 840 (73 713)	14 000 (4267)	11 080 (49 284)	321.2 (165.2)	0	Up
	288 060 (87 801)	16 000 (4877)	11 460 (50 974)	332.1 (170.8)	0	Up
	340 070 (103 653)	18 000 (5486)	11 840 (52 664)	343.4 (176.6)	0	Up
	399 310 (121 771)	20 000 (6096)				
155 000 (70 307)	0 (0)	0 (0)	12 290 (54 666)	112.3 (57.8)	5	Down
	6 190 (1 887)	0 (0)	12 300 (54 710)	163.9 (84.3)	5	Retract
	9 520 (2 902)	400 (122)	12 330 (54 844)	167.8 (86.3)	5	Up
	12 290 (3 746)	800 (244)	12 410 (55 200)	169.2 (87.0)	5	Up
	17 250 (5 258)	1 500 (457)	9 990 (44 436)	170.7 (87.8)	5	Up
	22 630 (6 898)	2 000 (610)	10 050 (44 702)	172.1 (88.5)	5	Up
	29 270 (8 921)	2 600 (792)	10 100 (44 925)	173.4 (89.2)	5	Up
	33 820 (10 308)	3 000 (914)	9 840 (43 768)	220.5 (113.4)	Cleanup	Up
	54 820 (16 709)	3 290 (1003)	9 610 (42 745)	268.6 (138.2)	0	Up
	62 450 (19 035)	4 000 (1219)	9 710 (43 190)	272.5 (140.2)	0	Up
	75 850 (23 119)	5 200 (1585)	9 830 (43 724)	276.6 (142.3)	0	Up
	85 190 (25 966)	6 000 (1829)	9 950 (44 258)	280.9 (144.5)	0	Up
	99 850 (30 434)	7 200 (2195)	10 020 (45 569)	285.3 (146.8)	0	Up
	110 080 (33 552)	8 000 (2438)	10 190 (45 325)	289.8 (149.1)	0	Up
	126 210 (38 469)	9 200 (2804)	10 310 (45 859)	294.4 (151.4)	0	Up
	137 520 (41 916)	10 000 (3048)	10 510 (46 748)	301.0 (154.8)	0	Up
	167 810 (51 148)	12 000 (3658)	10 800 (48 038)	310.9 (159.9)	0	Up
	201 420 (61 393)	14 000 (4267)	11 080 (49 284)	321.2 (165.2)	0	Up
	239 010 (72 850)	16 000 (4877)	11 460 (50 974)	332.0 (170.8)	0	Up
	280 870 (85 609)	18 000 (5486)	11 840 (52 664)	343.4 (176.6)	0	Up
	327 950 (99 959)	20 000 (6096)				
138 000 (62 596)	0 (0)	0 (0)	12 340 (54 888)	107.2 (55.1)	5	Down
	4 810 (1 466)	0 (0)	12 350 (54 933)	156.3 (80.4)	5	Retract
	7 640 (2 329)	400 (122)	12 390 (55 111)	159.9 (82.3)	5	Up
	9 920 (3 024)	800 (244)	12 480 (55 511)	161.3 (83.0)	5	Up
	13 990 (4 264)	1 500 (457)	10 060 (44 747)	162.7 (83.7)	5	Up
	18 280 (5 572)	2 000 (610)	10 110 (44 969)	164.1 (84.4)	5	Up
	23 550 (7 178)	2 600 (792)	10 160 (45 192)	164.6 (84.7)	5	Up
	27 150 (8 275)	3 000 (914)	9 870 (43 902)	216.4 (111.3)	Cleanup	Up
	45 600 (13 899)	3 260 (994)	9 610 (42 745)	268.6 (138.2)	0	Up
	52 330 (15 950)	4 000 (1219)	9 710 (43 190)	272.5 (140.2)	0	Up
	63 660 (19 404)	5 200 (1585)	9 830 (43 724)	276.6 (142.3)	0	Up
	71 540 (21 804)	6 000 (1829)	9 950 (44 258)	280.9 (144.5)	0	Up
	83 880 (25 567)	7 200 (2195)	10 070 (44 791)	285.3 (146.8)	0	Up
	92 480 (28 188)	8 000 (2438)	10 190 (45 325)	289.8 (149.1)	0	Up
	106 000 (32 309)	9 200 (2804)	10 310 (45 859)	294.4 (151.4)	0	Up
	115 460 (35 192)	10 000 (3048)	10 510 (46 748)	301.1 (154.8)	0	Up
	140 710 (42 888)	12 000 (3658)	10 800 (48 038)	310.9 (159.9)	0	Up
	168 560 (51 377)	14 000 (4267)	11 080 (49 284)	321.2 (165.2)	0	Up
	199 490 (60 805)	16 000 (4877)	11 460 (50 974)	332.0 (170.8)	0	Up
	233 690 (71 229)	18 000 (5486)	11 840 (52 664)	343.4 (176.6)	0	Up
	271 830 (82 854)	20 000 (6096)				

Table 13.—727-200: Airline Pilots' Association Profiles

Takeoff Profiles for EPNL Footprints

Brake release gross weight, lb (kg)	Airplane Position at Start of Segment		Segment Average		Flap position, deg	Gear position
	Distance from brake release, ft (m)	Altitude, ft (m)	Power setting (F_n/δ), lb (N)	Flight speed, KTAS (m/s)		
172 500 (78 245)	0 (0)	0 (0)	12 230 (54 399)	117.5 (60.4)	5	Down
	7 810 (2 380)	0 (0)	12 240 (54 440)	171.4 (88.2)	5	Retract
	11 740 (3 578)	400 (122)	12 280 (54 621)	175.5 (90.3)	5	Up
	15 100 (4 602)	800 (244)	12 070 (53 687)	216.9 (111.6)	Cleanup	Up
	27 710 (8 446)	920 (280)	11 880 (52 842)	258.9 (133.2)	0	Up
	32 280 (9 839)	1 500 (457)	6 250 (27 800)	261.1 (134.3)	0	Up
	47 200 (14 387)	2 070 (631)	6 360 (28 289)	263.4 (135.5)	0	Up
	62 200 (18 959)	2 630 (802)	6 470 (28 779)	265.6 (136.6)	0	Up
	77 200 (23 531)	3 190 (972)	6 610 (29 401)	268.4 (138.1)	0	Up
	99 270 (30 257)	4 000 (1219)	9 710 (43 190)	272.5 (140.2)	0	Up
	115 150 (35 098)	5 200 (1585)	9 830 (43 724)	276.6 (142.3)	0	Up
	126 250 (38 481)	6 000 (1829)	9 950 (44 258)	280.9 (144.5)	0	Up
	143 710 (43 803)	7 200 (2195)	10 070 (44 791)	285.3 (146.8)	0	Up
	155 940 (47 531)	8 000 (2438)	10 190 (45 325)	289.8 (149.1)	0	Up
	175 270 (53 422)	9 200 (2804)	10 310 (45 859)	294.4 (151.4)	0	Up
	188 870 (57 568)	10 000 (3048)	10 510 (46 748)	301.0 (154.8)	0	Up
	225 490 (68 729)	12 000 (3658)	10 800 (48 038)	310.9 (159.9)	0	Up
	266 450 (81 214)	14 000 (4267)	11 080 (49 234)	321.2 (165.2)	0	Up
	312 700 (95 311)	16 000 (4877)	11 460 (50 974)	332.0 (170.8)	0	Up
	364 750 (111 176)	18 000 (5486)	11 840 (52 664)	343.4 (176.6)	0	Up
	424 030 (129 244)	20 000 (6096)				
155 000 (70 307)	0 (0)	0 (0)	12 290 (54 666)	112.3 (57.8)	5	Down
	6 190 (1 887)	0 (0)	12 300 (54 710)	163.9 (84.3)	5	Retract
	9 520 (2 902)	400 (122)	12 330 (54 844)	167.8 (86.3)	5	Up
	12 290 (3 746)	800 (244)	12 100 (53 821)	213.1 (109.6)	Cleanup	Up
	23 870 (7 276)	910 (277)	11 880 (52 842)	258.3 (132.9)	0	Up
	27 860 (8 492)	1 500 (457)	5 670 (25 220)	261.1 (134.3)	0	Up
	42 800 (13 045)	2 070 (631)	5 780 (25 709)	263.4 (135.5)	0	Up
	57 800 (17 617)	2 630 (802)	5 880 (26 154)	265.6 (136.6)	0	Up
	72 800 (22 189)	3 190 (972)	6 000 (26 688)	268.4 (138.1)	0	Up
	94 850 (28 910)	4 000 (1219)	9 710 (43 190)	272.5 (140.2)	0	Up
	108 260 (32 998)	5 200 (1585)	9 830 (43 724)	276.6 (142.3)	0	Up
	117 590 (35 841)	6 000 (1829)	9 950 (44 258)	280.9 (144.5)	0	Up
	132 250 (40 310)	7 200 (2195)	10 070 (44 791)	285.3 (146.8)	0	Up
	142 490 (43 431)	8 000 (2438)	10 190 (45 325)	289.8 (149.1)	0	Up
	158 610 (48 431)	9 200 (2804)	10 310 (45 859)	294.4 (151.4)	0	Up
	169 920 (51 792)	10 000 (3048)	10 510 (46 748)	301 0 (154.8)	0	Up
	200 220 (61 027)	12 000 (3658)	10 800 (48 038)	310.9 (159.9)	0	Up
	233 820 (71 268)	14 000 (4267)	11 080 (49 284)	321.2 (165.2)	0	Up
	271 410 (82 726)	16 000 (4877)	11 460 (50 974)	332.0 (170.8)	0	Up
	313 270 (95 485)	18 000 (5486)	11 840 (52 664)	343.4 (176.6)	0	Up
	360 350 (109 835)	20 000 (6096)				
138 000 (62 596)	0 (0)	0 (0)	12 340 (54 888)	107.2 (55.1)	5	Down
	4 810 (1 466)	0 (0)	12 350 (54 933)	156.3 (80.4)	5	Retract
	7 640 (2 329)	400 (122)	12 390 (55 111)	159.9 (82.3)	5	Up
	9 920 (3 024)	800 (244)	12 130 (53 954)	209.1 (107.6)	Cleanup	Up
	20 480 (6 242)	900 (274)	11 880 (52 842)	258.9 (133.2)	0	Up
	23 960 (7 303)	1 500 (457)	5 150 (22 907)	261.1 (134.3)	0	Up
	38 900 (11 857)	2 070 (631)	5 240 (23 308)	263.4 (135.5)	0	Up
	53 900 (16 429)	2 630 (802)	5 330 (23 708)	265.6 (136.6)	0	Up
	68 900 (21 001)	3 190 (972)	5 440 (24 197)	268.4 (138.1)	0	Up
	90 950 (27 722)	4 000 (1219)	9 710 (43 190)	272.5 (140.2)	0	Up
	102 270 (31 172	5 200 (1585)	9 830 (43 724)	276.6 (142.3)	0	Up
	110 150 (33 574)	6 000 (1829)	9 950 (44 258)	280.9 (144.5)	0	Up
	122 480 (37 332)	7 200 (2195)	10 070 (44 791)	285.3 (146.8)	0	Up
	131 080 (39 953)	8 000 (2438)	10 190 (45 325)	289.8 (149.1)	0	Up
	144 590 (44 071)	9 200 (2804)	10 310 (45 859)	294.4 (151.4)	0	Up
	154 040 (46 951)	10 000 (3048)	10 510 (46 748)	301.0 (154.8)	0	Up
	179 270 (54 641)	12 000 (3658)	10 800 (48 038)	310.9 (159.9)	0	Up
	207 100 (63 124)	14 000 (4267)	11 080 (49 284)	321.2 (165.2)	0	Up
	238 010 (72 545)	16 000 (4877)	11 460 (50 974)	332.0 (170.8)	0	Up
	272 190 (82 964)	18 000 (5486)	11 840 (52 664)	343.4 (176.6)	0	Up
	310 310 (94 582)	20 000 (6096)				

Table 14.—727-200: FAR Part 36 Cutback Profiles

Takeoff Profiles for EPNL Footprints

Brake release gross weight, lb (kg)	Airplane Position at Start of Segment		Segment Average		Flap position, deg	Gear position
	Distance from brake release, ft (m)	Altitude, ft (m)	Power setting (F_n/δ), lb (N)	Flight speed, KTAS (m/s)		
172 500 (78 245)	0 (0)	0 (0)	12 230 (54 399)	117.5 (60.4)	5	Down
	7 810 (2 380)	0 (0)	12 290 (54 666)	172.2 (88.6)	5	Retract
	16 800 (5 121)	1 000 (305)	12 360 (54 977)	176.9 (91.0)	5	Up
	19 440 (5 925)	1 310 (399)	8 100 (36 029)	177.9 (91.5)	5	Up
	29 400 (8 961)	1 760 (536)	8 230 (36 607)	179.2 (92.2)	5	Up
	39 400 (12 009)	2 210 (674)	8 370 (37 230)	180.5 (92.8)	5	Up
	50 000 (15 240)	2 690 (820)	9 910 (44 080)	197.3 (101.5)	Cleanup	Up
	57 510 (17 529)	2 690 (820)	9 660 (42 968)	239.1 (123.0)	0	Up
	69 290 (21 120)	2 690 (820)	9 580 (42 612)	267.4 (133.6)	0	Up
	85 570 (26 082)	4 000 (1219)	9 710 (43 190)	272.5 (140.2)	0	Up
	101 440 (30 919)	5 200 (1585)	9 830 (43 724)	276.6 (142.3)	0	Up
	112 530 (34 299)	6 000 (1829)	9 950 (44 258)	280.9 (144.9)	0	Up
	129 960 (39 612)	7 200 (2195)	10 070 (44 791)	285.3 (146.8)	0	Up
	142 180 (43 336)	8 000 (2438)	10 190 (45 325)	289.8 (149.1)	0	Up
	161 480 (49 219)	9 200 (2804)	10 310 (45 859)	294.4 (151.4)	0	Up
	175 061 (53 359)	10 000 (3048)	10 510 (46 748)	301.0 (154.8)	0	Up
	211 630 (64 505)	12 000 (3658)	10 800 (48 038)	310.9 (159.9)	0	Up
	252 530 (76 971)	14 000 (4267)	11 080 (49 284)	321.2 (165.2)	0	Up
	298 710 (91 047)	16 000 (4877)	11 460 (50 974)	332.0 (170.8)	0	Up
	350 670 (106 884)	18 000 (5486)	11 840 (52 664)	343.4 (176.6)	0	Up
	409 850 (124 922)	20 000 (6096)				
155 000 (70 307)	0 (0)	0 (0)	12 290 (54 666)	112.3 (57.8)	5	Down
	6 180 (1 884)	0 (0)	12 360 (54 977)	164.9 (84.8)	5	Retract
	15 110 (4 606)	1 200 (366)	12 470 (55 467)	170.5 (87.7)	5	Up
	19 440 (5 925)	1 800 (549)	7 380 (32 826)	171.4 (88.2)	5	Up
	29 400 (8 961)	2 250 (686)	7 500 (33 360)	172.6 (88.8)	5	Up
	39 400 (12 009)	2 700 (823)	7 620 (33 894)	173.8 (89.4)	5	Up
	50 000 (15 240)	3 190 (972)	9 980 (44 391)	196.9 (101.3)	Cleanup	Up
	58 650 (17 877)	3 190 (972)	9 690 (43 101)	243.0 (125.0)	0	Up
	68 080 (20 751)	3 190 (972)	9 600 (42 701)	268.4 (138.1)	0	Up
	76 750 (23 393)	4 000 (1219)	9 710 (43 190)	272.5 (140.2)	0	Up
	90 130 (27 472)	5 200 (1585)	9 830 (43 724)	276.6 (142.3)	0	Up
	99 460 (30 315)	6 000 (1829)	9 950 (44 258)	280.9 (144.9)	0	Up
	114 100 (34 778)	7 200 (2195)	10 070 (44 791)	285.3 (146.8)	0	Up
	124 320 (37 893)	8 000 (2438)	10 190 (45 325)	289.8 (149.1)	0	Up
	140 420 (42 800)	9 200 (2804)	10 310 (45 859)	294.4 (151.4)	0	Up
	151 720 (46 244)	10 000 (3048)	10 510 (46 748)	301.0 (154.8)	0	Up
	181 970 (55 464)	12 000 (3658)	10 800 (48 038)	310.9 (159.9)	0	Up
	215 530 (65 694)	14 000 (4267)	11 080 (49 284)	321.2 (165.2)	0	Up
	253 060 (77 133)	16 000 (4877)	11 460 (50 974)	332.0 (170.8)	0	Up
	294 850 (89 870)	18 000 (5486)	11 840 (52 664)	343.4 (176.6)	0	Up
	341 850 (104 196)	20 000 (6096)				
138 000 (62 596)	0 (0)	0 (0)	12 340 (54 888)	107.2 (55.1)	5	Down
	4 810 (1 466)	0 (0)	12 400 (55 155)	157.0 (80.8)	5	Retract
	11 070 (3 374)	1 000 (305)	12 560 (55 867)	162.6 (83.6)	5	Up
	19 440 (5 925)	2 410 (735)	6 690 (29 757)	164.9 (84.8)	5	Up
	29 400 (8 961)	2 860 (872)	6 800 (30 246)	166.0 (85.4)	5	Up
	39 400 (12 009)	3 310 (1009)	6 910 (30 736)	167.1 (86.0)	5	Up
	50 000 (15 240)	3 790 (1155)	10 060 (44 746)	196.7 (101.2)	Cleanup	Up
	59 420 (18 111)	3 790 (1155)	9 740 (43 324)	247.4 (127.3)	0	Up
	67 010 (20 425)	3 790 (1155)	9 630 (42 834)	269.6 (138.7)	0	Up
	68 930 (21 010)	4 000 (1219)	9 710 (43 190)	272.5 (140.2)	0	Up
	80 240 (24 457)	5 200 (1585)	9 830 (43 724)	276.6 (142.3)	0	Up
	88 100 (26 853)	6 000 (1829)	9 950 (44 258)	280.9 (144.9)	0	Up
	100 420 (30 608)	7 200 (2195)	10 070 (44 791)	285.3 (146.8)	0	Up
	109 010 (33 226)	8 000 (2438)	10 190 (45 325)	289.8 (149.1)	0	Up
	122 500 (37 338)	9 200 (2804)	10 310 (45 859)	294.4 (151.4)	0	Up
	131 940 (40 215)	10 000 (3048)	10 510 (46 748)	301.0 (154.8)	0	Up
	157 140 (47 896)	12 000 (3658)	10 800 (48 038)	310.9 (159.9)	0	Up
	184 930 (56 367)	14 000 (4267)	11 080 (49 284)	321.2 (165.2)	0	Up
	215 800 (65 776)	16 000 (4877)	11 460 (50 974)	332.0 (170.8)	0	Up
	249 930 (76 179)	18 000 (5486)	11 840 (52 664)	343.4 (176.6)	0	Up
	287 980 (87 776)	20 000 (6096)				

Table 15.—727-200: Community Interface Profiles—1000-ft/min (5.08-m/s) Climb

Takeoff Profiles for EPNL Footprints

Brake release gross weight, lb (kg)	Airplane Position at Start of Segment		Segment Average		Flap position, deg	Gear position
	Distance from brake release, ft (m)	Altitude, ft (m)	Power setting (F_n/δ), lb (N)	Flight speed, KTAS (m/s)		
172 500 (78 245)	0 (0)	0 (0)	12 230 (54 399)	117.5 (60.4)	5	Down
	7 810 (2 380)	0 (0)	12 240 (54 444)	171.5 (88.2)	5	Retract
	12 000 (3 658)	430 (131)	8 540 (37 986)	175.8 (90.4)	5	Up
	22 000 (6 706)	990 (302)	8 690 (38 653)	177.3 (91.2)	5	Up
	32 000 (9 754)	1 550 (472)	8 830 (39 276)	178.8 (92.0)	5	Up
	42 000 (12 802)	2 110 (643)	8 950 (39 810)	180.1 (92.6)	5	Up
	50 000 (15 240)	2 550 (777)	9 900 (44 035)	197.0 (101.3)	Cleanup	Up
	57 480 (17 520)	2 550 (777)	9 640 (42 879)	238.7 (122.8)	0	Up
	69 070 (21 053)	2 550 (777)	9 570 (42 567)	267.1 (137.4)	0	Up
	87 150 (26 563)	4 000 (1219)	9 710 (43 190)	272.5 (140.2)	0	Up
	103 020 (31 400)	5 200 (1585)	9 830 (43 724)	276.6 (142.3)	0	Up
	114 100 (34 778)	6 000 (1829)	9 950 (44 258)	280.9 (144.9)	0	Up
	131 540 (40 093)	7 200 (2195)	10 070 (44 791)	285.3 (146.8)	0	Up
	143 750 (43 815)	8 000 (2438)	10 190 (45 325)	289.8 (149.1)	0	Up
	163 050 (49 698)	9 200 (2804)	10 310 (45 859)	294.4 (151.4)	0	Up
	176 630 (53 837)	10 000 (3048)	10 510 (46 748)	301.0 (154.8)	0	Up
	213 200 (64 983)	12 000 (3658)	10 800 (48 038)	310.9 (159.9)	0	Up
	254 100 (77 450)	14 000 (4267)	11 080 (49 284)	321.2 (165.2)	0	Up
	300 280 (91 525)	16 000 (4877)	11 460 (50 974)	332.0 (170.8)	0	Up
	352 240 (107 363)	18 000 (5486)	11 840 (52 664)	343.4 (176.6)	0	Up
	411 410 (125 398)	20 000 (6096)				
155 000 (70 307)	0 (0)	0 (0)	12 290 (54 665)	112.3 (57.8)	5	Down
	6 180 (1 884)	0 (0)	12 320 (54 799)	164.3 (84.5)	5	Retract
	12 000 (3 658)	760 (232)	7 870 (35 006)	168.9 (86.9)	5	Up
	22 000 (6 706)	1 340 (408)	8 010 (35 628)	170.4 (87.7)	5	Up
	32 000 (9 754)	1 930 (588)	8 150 (36 251)	171.9 (88.4)	5	Up
	42 000 (12 802)	2 500 (762)	8 260 (36 740)	173.2 (89.1)	5	Up
	50 000 (15 240)	2 960 (902)	9 960 (44 302)	196.4 (101.0)	Cleanup	Up
	58 570 (17 852)	2 960 (902)	9 670 (43 012)	242.4 (124.7)	0	Up
	67 780 (20 659)	2 960 (902)	9 590 (42 656)	267.9 (137.8)	0	Up
	78 050 (24 033)	4 000 (1219)	9 710 (43 190)	272.5 (140.2)	0	Up
	92 230 (28 112)	5 200 (1585)	9 830 (43 724)	276.6 (142.3)	0	Up
	101 560 (30 955)	6 000 (1829)	9 950 (44 258)	280.9 (144.9)	0	Up
	116 200 (35 418)	7 200 (2195)	10 070 (44 791)	285.3 (146.8)	0	Up
	126 420 (38 533)	8 000 (2438)	10 190 (45 325)	289.8 (149.1)	0	Up
	142 520 (43 440)	9 200 (2804)	10 310 (45 859)	294.4 (151.4)	0	Up
	153 810 (46 881)	10 000 (3048)	10 510 (46 748)	301.0 (154.8)	0	Up
	184 070 (56 105)	12 000 (3658)	10 800 (48 038)	310.9 (159.9)	0	Up
	217 620 (66 331)	14 000 (4267)	11 080 (49 284)	321.2 (165.2)	0	Up
	255 150 (77 770)	16 000 (4877)	11 460 (50 974)	332.0 (170.8)	0	Up
	296 940 (90 507)	18 000 (5486)	11 840 (52 664)	343.4 (176.6)	0	Up
	343 940 (104 833)	20 000 (6096)				
138 000 (62 596)	0 (0)	0 (0)	12 340 (54 888)	107.2 (55.1)	5	Down
	4 810 (1 466)	0 (0)	12 410 (55 200)	157.2 (80.9)	5	Retract
	12 000 (3 658)	1 160 (354)	7 210 (32 070)	162.0 (83.3)	5	Up
	22 000 (6 706)	1 770 (539)	7 350 (32 693)	163.5 (84.1)	5	Up
	32 000 (9 754)	2 380 (725)	7 480 (33 271)	165.0 (84.9)	5	Up
	42 000 (12 802)	2 980 (908)	7 590 (33 760)	166.3 (85.5)	5	Up
	50 000 (15 240)	3 450 (1052)	10 030 (44 613)	196.0 (100.8)	Cleanup	Up
	59 290 (18 072)	3 450 (1052)	9 710 (43 190)	246.4 (126.7)	0	Up
	66 600 (20 300)	3 450 (1052)	9 620 (42 790)	268.9 (138.3)	0	Up
	71 580 (21 818)	4 000 (1219)	9 710 (43 190)	272.5 (140.2)	0	Up
	82 890 (25 265)	5 200 (1585)	9 830 (43 724)	276.6 (142.3)	0	Up
	90 760 (27 664)	6 000 (1829)	9 950 (44 258)	280.9 (144.9)	0	Up
	103 080 (31 419)	7 200 (2195)	10 070 (44 791)	285.3 (146.8)	0	Up
	111 660 (34 034)	8 000 (2438)	10 190 (45 325)	289.8 (149.1)	0	Up
	125 160 (38 149)	9 200 (2804)	10 310 (45 859)	294.4 (151.4)	0	Up
	134 600 (41 026)	10 000 (3048)	10 510 (46 748)	301.0 (154.8)	0	Up
	159 800 (48 707)	12 000 (3658)	10 800 (48 038)	310.9 (159.9)	0	Up
	187 590 (57 177)	14 000 (4267)	11 080 (49 284)	321.2 (165.2)	0	Up
	218 450 (66 584)	16 000 (4877)	11 460 (50 974)	332.0 (170.8)	0	Up
	252 580 (76 986)	18 000 (5486)	11 840 (52 664)	343.4 (176.6)	0	Up
	290 640 (88 587)	20 000 (6096)				

Table 16.—727-200: Community Interface Profiles—500-ft/min (2.54-m/s) Climb

Takeoff Profiles for EPNL Footprints

Brake release gross weight, lb (kg)	Airplane Position at Start of Segment		Segment Average		Flap position, deg	Gear position
	Distance from brake release, ft (m)	Altitude, ft (m)	Power setting (F_n/δ), lb (N)	Flight speed, KTAS (m/s)		
172 500 (78 245)	0 (0)	0 (0)	12 230 (54 399)	117.5 (60.4)	5	Down
	7 810 (2 380)	0 (0)	12 240 (54 444)	171.5 (88.2)	5	Retract
	12 000 (3 658)	430 (131)	6 780 (30 157)	175.5 (90.3)	5	Up
	22 000 (6 706)	710 (216)	6 840 (30 424)	176.2 (90.6)	5	Up
	32 000 (9 754)	990 (302)	6 900 (30 691)	176.9 (91.0)	5	Up
	42 000 (12 802)	1 270 (387)	6 950 (30 914)	177.6 (91.4)	5	Up
	50 000 (15 240)	1 500 (457)	9 790 (43 546)	194.7 (100.2)	Cleanup	Up
	57 230 (17 444)	1 500 (457)	9 530 (42 389)	235.8 (121.3)	0	Up
	67 640 (20 617)	1 500 (457)	9 520 (42 345)	265.0 (136.3)	0	Up
	98 010 (29 873)	4 000 (1219)	9 710 (43 190)	272.5 (140.2)	0	Up
	113 870 (34 708)	5 200 (1585)	9 830 (43 724)	276.6 (142.3)	0	Up
	124 950 (38 085)	6 000 (1829)	9 950 (44 258)	280.9 (144.9)	0	Up
	142 380 (43 397)	7 200 (2195)	10 070 (44 791)	285.3 (146.8)	0	Up
	154 590 (47 119)	8 000 (2438)	10 190 (45 325)	289.8 (149.1)	0	Up
	173 880 (52 999)	9 200 (2804)	10 310 (45 859)	294.4 (151.4)	0	Up
	187 460 (57 138)	10 000 (3048)	10 510 (46 748)	301.0 (154.8)	0	Up
	224 020 (68 281)	12 000 (3658)	10 800 (48 038)	310.9 (159.9)	0	Up
	264 900 (80 742)	14 000 (4267)	11 080 (49 284)	321.2 (165.2)	0	Up
	311 060 (94 811)	16 000 (4877)	11 460 (50 974)	332.0 (170.8)	0	Up
	363 000 (110 642)	18 000 (5486)	11 840 (52 664)	343.4 (176.6)	0	Up
	422 150 (128 671)	20 000 (6096)				
155 000 (70 307)	0 (0)	0 (0)	12 290 (54 666)	112.3 (57.8)	5	Down
	6 180 (1 884)	0 (0)	12 320 (54 799)	164.3 (84.5)	5	Retract
	12 000 (3 658)	760 (232)	6 210 (27 622)	168.6 (86.7)	5	Up
	22 000 (6 706)	1 050 (320)	6 270 (27 889)	169.3 (87.1)	5	Up
	32 000 (9 754)	1 340 (148)	6 320 (28 111)	170.0 (87.4)	5	Up
	42 000 (12 802)	1 630 (497)	6 370 (28 334)	170.7 (87.8)	5	Up
	50 000 (15 240)	1 870 (570)	9 840 (43 768)	194.2 (99.9)	Cleanup	Up
	58 240 (17 752)	1 870 (570)	9 560 (42 523)	239.4 (123.1)	0	Up
	66 440 (20 251)	1 870 (570)	9 540 (42 434)	265.7 (136.7)	0	Up
	88 540 (26 987)	4 000 (1219)	9 710 (43 190)	272.5 (140.2)	0	Up
	101 920 (31 065)	5 200 (1585)	9 830 (43 724)	276.6 (142.3)	0	Up
	111 250 (33 909)	6 000 (1829)	9 950 (44 258)	280.9 (144.9)	0	Up
	125 880 (38 368)	7 200 (2195)	10 070 (44 791)	285.3 (146.8)	0	Up
	136 100 (41 483)	8 000 (2438)	10 190 (45 325)	289.8 (149.1)	0	Up
	152 200 (46 391)	9 200 (2804)	10 310 (45 859)	294.4 (151.4)	0	Up
	163 490 (49 832)	10 000 (3048)	10 510 (46 748)	301.0 (154.8)	0	Up
	193 730 (59 049)	12 000 (3658)	10 800 (48 038)	310.9 (159.9)	0	Up
	227 280 (69 275)	14 000 (4267)	11 080 (49 284)	321.2 (165.2)	0	Up
	264 800 (80 711)	16 000 (4877)	11 460 (50 974)	332.0 (170.8)	0	Up
	306 580 (93 446)	18 000 (5486)	11 840 (52 664)	343.4 (176.6)	0	Up
	353 560 (107 765)	20 000 (6096)				
138 000 (62 596)	0 (0)	0 (0)	12 340 (54 888)	107.2 (55.1)	5	Down
	4 810 (1 466)	0 (0)	12 410 (55 200)	157.2 (80.9)	5	Retract
	12 000 (3 658)	1 160 (354)	5 660 (25 176)	161.7 (83.2)	5	Up
	22 000 (6 706)	1 470 (448)	5 710 (25 398)	162.4 (83.5)	5	Up
	32 000 (9 754)	1 780 (543)	5 760 (25 620)	163.1 (83.9)	5	Up
	42 000 (12 802)	2 070 (631)	5 810 (25 843)	163.8 (84.3)	5	Up
	50 000 (15 240)	2 310 (704)	9 910 (44 080)	193.9 (99.7)	Cleanup	Up
	58 910 (17 956)	2 310 (704)	9 590 (42 656)	243.4 (125.2)	0	Up
	65 330 (19 913)	2 310 (704)	9 560 (42 523)	266.6 (137.1)	0	Up
	80 260 (24 463)	4 000 (1219)	9 710 (43 191)	272.5 (140.2)	0	Up
	91 570 (27 911)	5 200 (1585)	9 830 (43 724)	276.6 (142.3)	0	Up
	99 440 (30 309)	6 000 (1829)	9 950 (44 258)	280.9 (144.5)	0	Up
	111 750 (34 061)	7 200 (2195)	10 070 (44 791)	285.3 (146.8)	0	Up
	120 340 (36 680)	8 000 (2438)	10 190 (45 325)	289.8 (149.1)	0	Up
	133 830 (40 791)	9 200 (2804)	10 310 (45 859)	294.4 (151.4)	0	Up
	143 270 (43 669)	10 000 (3048)	10 510 (46 748)	304.0 (154.8)	0	Up
	168 460 (51 347)	12 000 (3658)	10 800 (48 083)	310.9 (159.9)	0	Up
	196 240 (59 814)	14 000 (4267)	11 080 (49 284)	321.2 (165.2)	0	Up
	227 100 (69 220)	16 000 (4877)	11 460 (50 974)	332.0 (170.8)	0	Up
	261 230 (79 623)	18 000 (5486)	11 840 (52 664)	343.4 (176.6)	0	Up
	299 270 (91 217)	20 000 (6096)				

Table 17.—727 Refan: Modified Full-Power Operational Takeoff Profiles

Takeoff Profiles for EPNL Footprints

Brake release gross weight, lb (kg)	Airplane Position at Start of Segment		Segment Average		Flap position, deg	Gear position
	Distance from brake release, ft (m)	Altitude, ft (m)	Power setting (F_n/δ), lb (N)	Flight speed, KTAS (m/s)		
182 500 (82 781)	0 (0)	0 (0)	12 960 (57 646)	121.7 (62.6)	5	Down
	8 160 (2 487)	0 (0)	12 950 (57 602)	177.5 (91.3)	5	Retract
	12 160 (3 706)	400 (122)	12 970 (57 691)	181.5 (93.4)	5	Up
	15 530 (4 734)	800 (244)	13 050 (58 046)	183.0 (94.1)	5	Up
	21 670 (6 575)	1 500 (457)	10 040 (44 658)	191.5 (98.5)	Cleanup	Up
	25 140 (7 663)	1 500 (457)	9 650 (42 923)	229.6 (118.1)	0	Up
	39 460 (12 027)	1 500 (457)	9 450 (42 034)	261.8 (134.7)	0	Up
	50 960 (15 533)	2 400 (732)	9 640 (42 879)	265.1 (136.4)	0	Up
	61 410 (18 718)	3 200 (975)	9 820 (43 079)	268.4 (138.1)	0	Up
	72 070 (21 967)	4 000 (1219)	10 050 (44 702)	272.5 (140.2)	0	Up
	88 510 (26 978)	5 200 (1585)	10 270 (45 681)	276.6 (142.3)	0	Up
	99 800 (30 419)	6 000 (1829)	10 490 (46 660)	280.9 (144.5)	0	Up
	117 270 (35 744)	7 200 (2195)	10 710 (47 638)	285.3 (146.8)	0	Up
	129 310 (39 414)	8 000 (2438)	10 940 (48 661)	289.8 (149.1)	0	Up
	148 030 (45 120)	9 200 (2804)	11 160 (49 640)	294.4 (151.4)	0	Up
	160 970 (49 064)	10 000 (3048)	11 470 (51 019)	301.0 (154.8)	0	Up
	195 190 (59 494)	12 000 (3658)	11 920 (53 020)	310.9 (159.9)	0	Up
	232 460 (70 854)	14 000 (4267)	12 360 (54 977)	321.2 (165.2)	0	Up
	273 460 (83 351)	16 000 (4877)	12 800 (56 934)	332.0 (170.8)	0	Up
	319 000 (97 231)	18 000 (5486)	13 290 (59 114)	343.4 (176.6)	0	Up
	369 820 (112 721)	20 000 (6096)				
172 500 (78 245)	0 (0)	0 (0)	13 010 (57 868)	118.9 (61.2)	5	Down
	7 200 (2 195)	0 (0)	13 000 (57 824)	173.3 (89.1)	5	Retract
	10 860 (3 310)	400 (122)	13 020 (57 913)	177.3 (91.2)	5	Up
	13 890 (4 234)	800 (244)	13 100 (58 269)	178.7 (91.9)	5	Up
	19 330 (5 892)	1 500 (457)	10 050 (44 702)	190.2 (97.8)	Cleanup	Up
	23 660 (7 212)	1 500 (457)	9 640 (42 879)	230.4 (118.5)	0	Up
	36 290 (11 061)	1 500 (457)	9 450 (42 034)	261.8 (134.7)	0	Up
	46 810 (14 268)	2 400 (732)	9 640 (42 879)	265.1 (136.4)	0	Up
	56 350 (17 175)	3 200 (975)	9 820 (43 679)	268.4 (138.1)	0	Up
	66 080 (20 141)	4 000 (1219)	10 050 (44 702)	272.5 (140.2)	0	Up
	81 080 (24 713)	5 200 (1585)	10 270 (45 681)	276.6 (142.3)	0	Up
	91 370 (27 850)	6 000 (1829)	10 490 (46 660)	280.9 (144.5)	0	Up
	107 280 (32 699)	7 200 (2195)	10 710 (47 638)	285.3 (146.8)	0	Up
	118 240 (36 040)	8 000 (2438)	10 940 (48 661)	289.8 (149.1)	0	Up
	135 250 (41 224)	9 200 (2804)	11 160 (49 640)	294.4 (151.4)	0	Up
	147 000 (44 806)	10 000 (3048)	11 470 (51 019)	301.0 (154.8)	0	Up
	178 000 (54 254)	12 000 (3658)	11 920 (53 020)	310.9 (159.9)	0	Up
	211 670 (64 517)	14 000 (4267)	12 360 (54 977)	321.2 (165.2)	0	Up
	248 570 (75 764)	16 000 (4877)	12 800 (56 934)	332.0 (170.8)	0	Up
	289 360 (88 197)	18 000 (5486)	13 290 (59 114)	343.4 (176.6)	0	Up
	334 650 (102 001)	20 000 (6096)				
155 000 (70 307)	0 (0)	0 (0)	13 100 (58 269)	113.8 (58.5)	5	Down
	5 690 (1 734)	0 (0)	13 090 (58 224)	166.8 (85.3)	5	Retract
	8 820 (2 688)	400 (122)	13 110 (58 313)	169.5 (87.2)	5	Up
	11 340 (3 456)	800 (244)	13 190 (58 669)	170.9 (87.9)	5	Up
	15 830 (4 825)	1 500 (457)	10 080 (44 836)	187.8 (96.6)	Cleanup	Up
	21 070 (6 422)	1 500 (457)	9 630 (42 834)	231.9 (119.3)	0	Up
	31 260 (9 528)	1 500 (457)	9 450 (42 034)	261.8 (134.7)	0	Up
	40 190 (12 250)	2 400 (732)	9 640 (42 879)	265.1 (136.4)	0	Up
	48 280 (14 716)	3 200 (975)	9 820 (43 079)	268.4 (138.1)	0	Up
	56 540 (17 233)	4 000 (1219)	10 050 (44 702)	272.5 (140.2)	0	Up
	69 240 (21 104)	5 200 (1585)	10 270 (45 681)	276.6 (142.3)	0	Up
	77 940 (23 756)	6 000 (1829)	10 490 (46 660)	280.9 (144.5)	0	Up
	91 370 (27 850)	7 200 (2195)	10 710 (47 638)	285.3 (146.8)	0	Up
	100 610 (30 666)	8 000 (2438)	10 940 (48 661)	289.8 (149.1)	0	Up
	114 920 (35 028)	9 200 (2804)	11 160 (49 640)	294.4 (151.4)	0	Up
	124 800 (38 039)	10 000 (3048)	11 470 (51 019)	301.0 (154.8)	0	Up
	150 760 (45 952)	12 000 (3658)	11 920 (53 020)	310.9 (159.9)	0	Up
	178 810 (54 501)	14 000 (4267)	12 360 (54 977)	321.2 (165.2)	0	Up
	209 390 (63 822)	16 000 (4877)	12 800 (56 934)	332.0 (170.8)	0	Up
	242 960 (74 054)	18 000 (5486)	13 290 (59 114)	343.4 (176.6)	0	Up
	279 930 (85 323)	20 000 (6096)				
138 000 (62 596)	0 (0)	0 (0)	13 190 (58 669)	108.7 (55.9)	5	Down
	4 410 (1 344)	0 (0)	13 180 (58 625)	158.3 (81.4)	5	Retract
	7 090 (2 161)	400 (122)	13 210 (58 758)	161.7 (83.2)	5	Up
	9 160 (2 792)	800 (244)	13 290 (59 114)	163.1 (83.9)	5	Up
	12 860 (3 920)	1 500 (457)	10 120 (45 014)	185.4 (95.4)	Cleanup	Up
	18 610 (5 672)	1 500 (457)	9 610 (42 745)	233.5 (120.1)	0	Up
	26 840 (9 181)	1 500 (457)	9 450 (42 034)	261.8 (134.7)	0	Up
	34 420 (10 491)	2 400 (732)	9 640 (42 879)	265.1 (136.4)	0	Up
	41 290 (12 585)	3 200 (975)	9 820 (43 679)	268.4 (138.1)	0	Up
	48 290 (14 719)	4 000 (1219)	10 050 (44 702)	272.5 (140.2)	0	Up
	59 050 (17 998)	5 200 (1585)	10 270 (45 681)	276.6 (142.3)	0	Up
	68 410 (20 242)	6 000 (1829)	10 490 (46 660)	280.9 (144.5)	0	Up
	77 770 (23 704)	7 200 (2195)	10 710 (47 638)	285.3 (146.8)	0	Up
	85 570 (26 082)	8 000 (2438)	10 940 (48 661)	289.8 (149.1)	0	Up
	97 640 (29 761)	9 200 (2804)	11 160 (49 640)	294.4 (151.4)	0	Up
	105 950 (32 294)	10 000 (3048)	11 470 (51 019)	301.0 (154.8)	0	Up
	127 770 (38 944)	12 000 (3658)	11 920 (53 020)	310.9 (159.9)	0	Up
	151 270 (46 107)	14 000 (4267)	12 360 (54 977)	321.2 (165.2)	0	Up
	176 770 (53 879)	16 000 (4877)	12 800 (56 934)	332.0 (170.8)	0	Up
	204 630 (62 371)	18 000 (5486)	13 290 (59 114)	343.4 (176.6)	0	Up
	235 150 (71 674)	20 000 (6096)				

Table 18.—727 Refan: Air Transportation Association Takeoff Profiles

Takeoff Profiles for EPNL Footprints

Brake release gross weight, lb (kg)	Airplane Position at Start of Segment		Segment Average		Flap position, deg	Gear position
	Distance from brake release, ft (m)	Altitude, ft (m)	Power setting (F_n/δ), lb (N)	Flight speed, KTAS (m/s)		
182 500 (82 781)	0 (0)	0 (0)	12 960 (57 646)	121.7 (62.6)	5	Down
	8 160 (2 487)	0 (0)	12 950 (57 602)	177.5 (91.3)	5	Retract
	12 160 (3 706)	400 (122)	12 970 (57 691)	181.5 (93.4)	5	Up
	15 530 (4 734)	800 (244)	13 050 (58 046)	183.0 (94.1)	5	Up
	21 570 (6 575)	1 500 (457)	10 180 (45 281)	184.6 (95.0)	5	Up
	28 870 (8 800)	2 000 (610)	10 310 (45 859)	186.2 (95.8)	5	Up
	37 770 (11 512)	2 600 (792)	10 430 (46 393)	187.6 (96.5)	5	Up
	43 790 (13 347)	3 000 (914)	10 110 (44 969)	227.7 (117.1)	Cleanup	Up
	67 330 (20 522)	3 310 (1009)	9 830 (43 724)	268.6 (138.2)	0	Up
	76 530 (23 326)	4 000 (1219)	10 050 (44 702)	272.5 (140.2)	0	Up
	92 940 (28 328)	5 200 (1585)	10 270 (45 681)	276.6 (142.3)	0	Up
	104 210 (31 763)	6 000 (1829)	10 490 (46 660)	280.9 (144.5)	0	Up
	121 660 (37 082)	7 200 (2195)	10 710 (47 638)	285.3 (146.8)	0	Up
	133 690 (40 749)	8 000 (2438)	10 940 (48 661)	289.8 (149.1)	0	Up
	152 370 (46 442)	9 200 (2804)	11 160 (49 640)	294.4 (151.4)	0	Up
	165 300 (50 383)	10 000 (3048)	11 470 (51 019)	301.0 (154.8)	0	Up
	199 470 (60 798)	12 000 (3658)	11 920 (53 020)	310.9 (159.9)	0	Up
	236 680 (72 140)	14 000 (4267)	12 360 (54 977)	321.2 (165.2)	0	Up
	277 620 (84 619)	16 000 (4877)	12 800 (56 934)	332.0 (170.8)	0	Up
	323 080 (98 475)	18 000 (5486)	13 290 (59 114)	343.4 (176.6)	0	Up
	373 810 (113 937)	20 000 (6096)				
172 500 (78 245)	0 (0)	0 (0)	13 010 (57 868)	118.9 (61.2)	5	Down
	7 200 (2 195)	0 (0)	13 000 (57 824)	173.3 (89.1)	5	Retract
	10 860 (3 310)	400 (122)	13 020 (57 913)	177.3 (91.2)	5	Up
	13 890 (4 234)	800 (244)	13 100 (58 269)	178.7 (91.9)	5	Up
	19 330 (5 892)	1 500 (457)	10 240 (45 548)	180.3 (92.7)	5	Up
	25 700 (7 833)	2 000 (610)	10 360 (46 081)	181.8 (93.5)	5	Up
	33 470 (10 202)	2 600 (792)	10 480 (46 615)	183.2 (94.2)	5	Up
	32 730 (9 976)	3 000 (914)	10 140 (45 103)	225.4 (115.9)	Cleanup	Up
	60 540 (18 453)	3 290 (1003)	9 830 (41 055)	268.6 (138.2)	0	Up
	69 180 (21 086)	4 000 (1219)	10 050 (44 702)	272.5 (140.2)	0	Up
	84 160 (25 652)	5 200 (1585)	10 270 (45 681)	276.6 (142.3)	0	Up
	94 430 (28 782)	6 000 (1829)	10 490 (46 660)	280.9 (144.5)	0	Up
	110 330 (33 629)	7 200 (2195)	10 710 (47 638)	285.3 (146.8)	0	Up
	121 270 (36 963)	8 000 (2438)	10 940 (48 661)	289.8 (149.1)	0	Up
	138 260 (42 142)	9 200 (2804)	11 160 (49 640)	294.4 (151.4)	0	Up
	150 000 (45 720)	10 000 (3048)	11 470 (51 019)	301.0 (154.8)	0	Up
	180 960 (55 157)	12 000 (3658)	11 920 (53 020)	310.9 (159.9)	0	Up
	214 580 (65 404)	14 000 (4267)	12 360 (54 977)	321.2 (165.2)	0	Up
	251 420 (76 633)	16 000 (4877)	12 800 (56 934)	332.0 (170.8)	0	Up
	292 160 (89 050)	18 000 (5486)	13 290 (59 114)	343.4 (176.6)	0	Up
	337 380 (102 833)	20 000 (6096)				
155 000 (70 307)	0 (0)	0 (0)	13 100 (58 269)	113.8 (58.5)	5	Down
	5 690 (1 734)	0 (0)	13 090 (58 224)	165.8 (85.3)	5	Retract
	8 820 (2 688)	400 (122)	13 110 (58 313)	169.5 (87.2)	5	Up
	11 340 (3 456)	800 (244)	13 190 (58 669)	170.9 (87.9)	5	Up
	15 830 (4 825)	1 500 (457)	10 330 (45 948)	172.5 (88.7)	5	Up
	20 880 (6 364)	2 000 (610)	10 460 (46 526)	173.9 (89.5)	5	Up
	27 030 (8 239)	2 600 (792)	10 580 (47 060)	175.2 (90.1)	5	Up
	31 170 (9 501)	3 000 (914)	10 180 (45 281)	221.4 (113.9)	Cleanup	Up
	50 430 (15 371)	3 260 (994)	9 830 (43 724)	268.5 (138.1)	0	Up
	58 050 (17 694)	4 000 (1219)	10 050 (44 702)	272.5 (140.2)	0	Up
	70 740 (21 562)	5 200 (1585)	10 270 (45 681)	276.6 (142.3)	0	Up
	79 430 (24 210)	6 000 (1829)	10 490 (46 660)	280.9 (144.5)	0	Up
	92 850 (28 301)	7 200 (2195)	10 710 (47 638)	285.3 (146.8)	0	Up
	102 080 (31 114)	8 000 (2438)	10 940 (48 661)	289.8 (149.1)	0	Up
	116 380 (35 473)	9 200 (2804)	11 160 (49 640)	294.4 (151.4)	0	Up
	126 240 (38 478)	10 000 (3048)	11 470 (51 019)	301.0 (154.8)	0	Up
	152 170 (46 381)	12 000 (3658)	11 920 (53 020)	310.9 (159.9)	0	Up
	180 200 (54 925)	14 000 (4267)	12 360 (54 977)	321.2 (165.2)	0	Up
	210 740 (64 234)	16 000 (4877)	12 800 (56 934)	332.0 (170.8)	0	Up
	244 270 (74 453)	18 000 (5486)	13 290 (59 114)	343.4 (176.6)	0	Up
	281 200 (85 710)	20 000 (6096)				
138 000 (62 596)	0 (0)	0 (0)	13 190 (58 669)	108.7 (55.9)	5	Down
	4 410 (1 344)	0 (0)	13 180 (58 625)	158.2 (81.4)	5	Retract
	7 090 (2 161)	400 (122)	13 210 (58 758)	161.7 (83.2)	5	Up
	9 160 (2 792)	800 (244)	13 290 (59 114)	163.1 (83.9)	5	Up
	12 860 (3 920)	1 500 (457)	10 420 (46 348)	164.5 (84.6)	5	Up
	16 880 (5 145)	2 000 (610)	10 560 (46 971)	165.9 (85.3)	5	Up
	21 770 (6 635)	2 600 (792)	10 680 (47 505)	167.1 (86.0)	5	Up
	25 060 (7 638)	3 000 (914)	10 230 (45 503)	217.3 (111.8)	Cleanup	Up
	42 080 (12 826)	3 240 (988)	9 820 (43 679)	268.5 (138.1)	0	Up
	48 770 (14 865)	4 000 (1219)	10 050 (44 702)	272.5 (140.2)	0	Up
	59 520 (18 142)	5 200 (1585)	10 270 (45 681)	276.6 (142.3)	0	Up
	66 880 (20 385)	6 000 (1829)	10 490 (46 660)	280.9 (144.5)	0	Up
	78 230 (23 845)	7 200 (2195)	10 710 (47 638)	285.3 (146.8)	0	Up
	86 020 (26 219)	8 000 (2438)	10 940 (48 661)	289.8 (149.1)	0	Up
	98 080 (29 895)	9 200 (2804)	11 160 (49 640)	294.4 (151.4)	0	Up
	106 390 (32 428)	10 000 (3048)	11 430 (50 841)	301.0 (154.8)	0	Up
	128 190 (39 072)	12 000 (3658)	11 920 (53 020)	310.9 (159.9)	0	Up
	151 670 (46 229)	14 000 (4267)	12 360 (54 977)	321.2 (165.2)	0	Up
	177 150 (53 995)	16 000 (4877)	12 800 (56 934)	332.0 (170.8)	0	Up
	204 990 (62 481)	18 000 (5486)	13 290 (59 114)	343.4 (176.6)	0	Up
	235 480 (71 774)	20 000 (6096)				

Table 19.—727 Refan: Airline Pilots' Association Takeoff Profiles

Takeoff Profiles for EPNL Footprints

Brake release gross weight, lb (kg)	Airplane Position at Start of Segment		Segment Average		Flap position, deg	Gear position
	Distance from brake release, ft (m)	Altitude, ft (m)	Power setting (F_n/δ), lb (N)	Flight speed, KTAS (m/s)		
182 500 (82 781)	0 (0)	0 (0)	12 960 (57 646)	121,7 (62,6)	5	Down
	8 160 (2 487)	0 (0)	12 950 (57 602)	177,5 (91,3)	5	Retract
	12 160 (3 706)	400 (122)	12 970 (57 691)	181,5 (93,4)	5	Up
	15 530 (4 734)	800 (244)	12 590 (56 000)	219,9 (113,1)	Cleanup	Up
	27 530 (8 391)	910 (277)	12 230 (54 399)	258,9 (133,2)	0	Up
	32 330 (9 854)	1 500 (457)	6 580 (29 268)	261,1 (134,3)	0	Up
	47 300 (14 417)	2 070 (631)	6 700 (29 802)	263,4 (135,5)	0	Up
	62 300 (18 989)	2 630 (802)	6 820 (30 335)	265,6 (136,6)	0	Up
	77 300 (23 561)	3 190 (972)	6 960 (30 958)	268,4 (138,1)	0	Up
	99 320 (30 273)	4 000 (1219)	10 050 (44 702)	272,5 (140,2)	0	Up
	115 740 (35 278)	5 200 (1585)	10 270 (45 681)	276,6 (142,3)	0	Up
	127 020 (38 716)	6 000 (1829)	10 490 (46 660)	280,9 (144,5)	0	Up
	144 470 (44 034)	7 200 (2195)	10 710 (47 638)	285,3 (146,8)	0	Up
	156 600 (47 701)	8 000 (2438)	10 940 (48 661)	289,8 (149,1)	0	Up
	175 190 (53 398)	9 200 (2804)	11 160 (49 640)	294,4 (151,4)	0	Up
	188 130 (57 342)	10 000 (3048)	11 470 (51 019)	301,0 (154,8)	0	Up
	222 300 (67 757)	12 000 (3658)	11 920 (53 020)	310,9 (159,9)	0	Up
	259 530 (79 105)	14 000 (4267)	12 360 (54 977)	321,2 (165,2)	0	Up
	300 480 (91 586)	16 000 (4877)	12 800 (56 934)	332,0 (170,8)	0	Up
	345 960 (105 449)	18 000 (5486)	13 290 (59 114)	343,4 (176,6)	0	Up
	396 710 (120 917)	20 000 (6096)				
172 500 (78 245)	0 (0)	0 (0)	13 010 (57 868)	118,9 (61,2)	5	Down
	7 200 (2 195)	0 (0)	13 000 (57 824)	173,3 (89,1)	5	Retract
	10 860 (3 310)	400 (122)	13 020 (57 913)	177,3 (91,2)	5	Up
	13 890 (4 234)	800 (244)	12 620 (56 134)	217,8 (112,0)	Cleanup	Up
	25 380 (7 736)	910 (277)	12 230 (54 399)	258,9 (133,2)	0	Up
	29 840 (9 095)	1 500 (457)	6 250 (27 800)	261,1 (134,3)	0	Up
	44 800 (13 655)	2 070 (631)	6 360 (28 289)	263,4 (135,5)	0	Up
	59 800 (18 227)	2 630 (802)	6 480 (28 823)	265,6 (136,6)	0	Up
	74 800 (22 799)	3 190 (972)	6 610 (29 401)	268,4 (138,1)	0	Up
	96 830 (29 514)	4 000 (1219)	10 050 (44 702)	272,5 (140,2)	0	Up
	111 810 (34 080)	5 200 (1585)	10 270 (45 681)	276,6 (142,3)	0	Up
	122 090 (37 213)	6 000 (1829)	10 490 (46 660)	280,9 (144,5)	0	Up
	137 980 (42 056)	7 200 (2195)	10 710 (47 638)	285,3 (146,8)	0	Up
	148 920 (45 391)	8 000 (2438)	10 940 (48 661)	289,8 (149,1)	0	Up
	165 910 (50 569)	9 200 (2804)	11 160 (49 640)	294,4 (151,4)	0	Up
	177 650 (54 148)	10 000 (3048)	11 470 (51 019)	301,0 (154,8)	0	Up
	208 600 (63 581)	12 000 (3658)	11 920 (53 020)	310,9 (159,9)	0	Up
	242 220 (73 829)	14 000 (4267)	12 360 (54 977)	321,2 (165,2)	0	Up
	279 070 (85 061)	16 000 (4877)	12 800 (56 934)	332,0 (170,8)	0	Up
	319 800 (97 475)	18 000 (5486)	13 290 (59 114)	343,4 (176,6)	0	Up
	365 020 (111 258)	20 000 (6096)				
155 000 (70 307)	0 (0)	0 (0)	13 100 (58 269)	113,8 (58,5)	5	Down
	5 690 (1 734)	0 (0)	13 090 (58 224)	165,8 (85,3)	5	Retract
	8 820 (2 688)	400 (122)	13 110 (58 313)	169,5 (87,2)	5	Up
	11 340 (3 456)	800 (244)	12 660 (56 312)	213,9 (110,0)	Cleanup	Up
	21 920 (6 681)	890 (271)	12 230 (54 399)	258,9 (133,2)	0	Up
	25 820 (7 870)	1 500 (457)	5 670 (25 220)	261,1 (134,3)	0	Up
	40 800 (12 436)	2 070 (631)	5 780 (25 709)	263,4 (135,5)	0	Up
	55 800 (17 008)	2 630 (802)	5 880 (26 154)	265,6 (136,6)	0	Up
	70 800 (21 580)	3 190 (972)	6 000 (26 688)	268,4 (138,1)	0	Up
	92 800 (28 285)	4 000 (1219)	10 050 (44 702)	272,5 (140,2)	0	Up
	105 490 (32 153)	5 200 (1585)	10 270 (45 681)	276,6 (142,3)	0	Up
	114 170 (34 799)	6 000 (1829)	10 490 (46 660)	280,9 (144,5)	0	Up
	127 590 (38 889)	7 200 (2195)	10 710 (47 638)	285,3 (146,8)	0	Up
	136 810 (41 700)	8 000 (2438)	10 940 (48 661)	289,8 (149,1)	0	Up
	151 100 (46 052)	9 200 (2804)	11 160 (49 640)	294,4 (151,4)	0	Up
	160 960 (49 061)	10 000 (3048)	11 470 (51 019)	301,0 (154,8)	0	Up
	186 880 (56 967)	12 000 (3658)	11 920 (53 020)	310,9 (159,9)	0	Up
	214 090 (65 498)	14 000 (4267)	12 360 (54 977)	321,2 (165,2)	0	Up
	245 410 (74 801)	16 000 (4877)	12 800 (56 934)	332,0 (170,8)	0	Up
	278 910 (85 012)	18 000 (5486)	13 290 (59 114)	343,4 (176,6)	0	Up
	315 820 (96 262)	20 000 (6096)				
138 000 (62 596)	0 (0)	0 (0)	13 190 (58 669)	108,7 (55,9)	5	Down
	4 410 (1 344)	0 (0)	13 180 (58 625)	158,3 (81,4)	5	Retract
	7 090 (2 161)	400 (122)	13 210 (58 758)	161,7 (83,2)	5	Up
	9 160 (2 792)	800 (244)	12 710 (56 534)	210,0 (108,0)	Cleanup	Up
	18 840 (5 742)	890 (271)	12 230 (54 399)	258,9 (133,2)	0	Up
	22 240 (6 779)	1 500 (457)	5 150 (22 907)	261,1 (134,3)	0	Up
	37 200 (11 339)	2 070 (631)	5 240 (23 308)	263,4 (135,5)	0	Up
	52 200 (15 911)	2 630 (802)	5 330 (23 708)	265,6 (136,6)	0	Up
	67 200 (20 483)	3 190 (972)	5 450 (24 242)	268,4 (138,1)	0	Up
	89 230 (27 197)	4 000 (1219)	10 050 (44 702)	272,5 (140,2)	0	Up
	99 960 (30 468)	5 200 (1585)	10 270 (45 681)	276,6 (142,3)	0	Up
	107 310 (32 708)	6 000 (1829)	10 490 (46 660)	280,9 (144,5)	0	Up
	118 650 (36 165)	7 200 (2195)	10 710 (47 638)	285,3 (146,8)	0	Up
	126 440 (38 539)	8 000 (2438)	10 940 (48 661)	289,8 (149,1)	0	Up
	138 490 (42 212)	9 200 (2804)	11 160 (49 640)	294,4 (151,4)	0	Up
	146 790 (44 742)	10 000 (3048)	11 470 (51 019)	301,0 (154,8)	0	Up
	168 570 (51 380)	12 000 (3658)	11 920 (53 020)	310,9 (159,9)	0	Up
	192 020 (58 528)	14 000 (4267)	12 360 (54 977)	321,2 (165,2)	0	Up
	217 470 (66 285)	16 000 (4877)	12 800 (56 934)	332,0 (170,8)	0	Up
	245 280 (74 761)	18 000 (5486)	13 290 (59 114)	343,4 (176,6)	0	Up
	275 740 (84 046)	20 000 (6096)				

Table 20.—727 Refan: FAR Part 36 Cutback Profiles

Takeoff Profiles for EPNL Footprints

Brake release gross weight, lb (kg)	Airplane Position at Start of Segment		Segment Average		Flap position, deg	Gear position
	Distance from brake release, ft (m)	Altitude, ft (m)	Power setting (F_n/δ), lb (N)	Flight speed, KTAS (m/s)		
182 500 (82 781)	0 (0)	0 (0)	12 960 (57 646)	121.7 (62.6)	5	Down
	8 160 (2 487)	0 (0)	12 970 (57 691)	177.7 (91.4)	5	Retract
	13 840 (4 218)	600 (183)	13 020 (57 913)	182.4 (93.8)	5	Up
	19 440 (5 925)	1 260 (384)	8 670 (38 564)	184.0 (94.6)	5	Up
	29 400 (8 961)	1 730 (527)	8 820 (39 231)	185.3 (95.3)	5	Up
	39 400 (12 009)	2 200 (671)	8 970 (39 899)	186.6 (96.0)	5	Up
	50 000 (15 240)	2 700 (823)	10 270 (45 681)	199.9 (102.8)	Cleanup	Up
	56 150 (17 115)	2 700 (823)	9 870 (43 902)	238.6 (122.7)	0	Up
	69 000 (21 031)	2 700 (823)	9 770 (43 457)	267.4 (137.6)	0	Up
	86 220 (26 280)	4 000 (1219)	10 050 (44 702)	272.5 (140.2)	0	Up
	102 630 (31 282)	5 200 (1585)	10 270 (45 681)	276.6 (142.3)	0	Up
	113 890 (34 714)	6 000 (1829)	10 490 (46 660)	280.9 (144.5)	0	Up
	131 330 (40 029)	7 200 (2195)	10 710 (47 638)	285.3 (146.8)	0	Up
	143 340 (43 690)	8 000 (2438)	10 940 (48 661)	289.8 (149.1)	0	Up
	162 020 (49 384)	9 200 (2804)	11 160 (49 640)	294.4 (151.4)	0	Up
	174 940 (53 322)	10 000 (3048)	11 470 (51 019)	301.0 (154.8)	0	Up
	209 080 (63 728)	12 000 (3658)	11 920 (53 020)	310.9 (159.9)	0	Up
	246 270 (75 063)	14 000 (4267)	12 360 (54 977)	321.2 (165.2)	0	Up
	287 180 (87 532)	16 000 (4877)	12 800 (56 934)	332.0 (170.8)	0	Up
	332 610 (101 380)	18 000 (5486)	13 290 (59 114)	343.4 (176.6)	0	Up
	383 300 (116 830)	20 000 (6096)				
172 500 (78 245)	0 (0)	0 (0)	13 010 (57 868)	118.9 (61.2)	5	Down
	7 200 (2 195)	0 (0)	13 030 (57 957)	173.8 (89.4)	5	Retract
	13 890 (4 234)	800 (244)	13 100 (58 269)	178.8 (92.0)	5	Up
	19 440 (5 925)	1 510 (460)	8 270 (36 785)	180.3 (92.7)	5	Up
	29 400 (8 961)	1 980 (604)	8 410 (37 408)	181.6 (93.4)	5	Up
	39 400 (12 009)	2 460 (750)	8 550 (38 030)	182.9 (94.1)	5	Up
	50 000 (15 240)	2 960 (902)	10 340 (45 992)	199.8 (102.8)	Cleanup	Up
	57 030 (17 383)	2 960 (902)	9 920 (44 124)	240.9 (123.9)	0	Up
	68 240 (20 800)	2 960 (902)	9 790 (43 546)	267.9 (137.8)	0	Up
	80 870 (24 649)	4 000 (1219)	10 050 (44 702)	272.5 (140.2)	0	Up
	95 840 (29 212)	5 200 (1585)	10 270 (45 681)	276.6 (142.3)	0	Up
	106 100 (32 339)	6 000 (1829)	10 490 (46 660)	280.9 (144.5)	0	Up
	121 980 (37 180)	7 200 (2195)	10 710 (47 638)	285.3 (146.8)	0	Up
	132 910 (40 511)	8 000 (2438)	10 940 (48 661)	289.8 (149.1)	0	Up
	149 890 (45 686)	9 200 (2804)	11 160 (49 640)	294.4 (151.4)	0	Up
	161 610 (49 259)	10 000 (3048)	11 470 (51 019)	301.0 (154.8)	0	Up
	192 540 (58 686)	12 000 (3658)	11 920 (53 020)	310.9 (159.9)	0	Up
	226 130 (68 924)	14 000 (4267)	12 360 (54 977)	321.2 (165.2)	0	Up
	262 940 (80 144)	16 000 (4877)	12 800 (56 934)	332.0 (170.8)	0	Up
	303 630 (92 546)	18 000 (5486)	13 290 (59 114)	343.4 (176.6)	0	Up
	348 800 (106 314)	20 000 (6096)				
155 000 (70 307)	0 (0)	0 (0)	13 100 (58 269)	113.8 (58.5)	5	Down
	5 690 (1 734)	0 (0)	13 140 (58 447)	166.6 (85.7)	5	Retract
	12 610 (3 844)	1 000 (305)	13 250 (58 936)	171.9 (88.4)	5	Up
	19 440 (5 925)	2 050 (625)	7 560 (33 627)	173.8 (89.4)	5	Up
	29 400 (8 961)	2 520 (768)	7 680 (34 161)	175.1 (90.1)	5	Up
	39 400 (12 009)	2 990 (911)	7 820 (34 783)	176.4 (90.7)	5	Up
	50 000 (15 240)	3 490 (1064)	10 490 (46 660)	199.7 (102.7)	Cleanup	Up
	58 170 (17 730)	3 490 (1064)	10 020 (44 560)	245.1 (126.1)	0	Up
	67 030 (20 431)	3 490 (1064)	9 850 (43 813)	269.0 (138.4)	0	Up
	72 250 (22 022)	4 000 (1219)	10 050 (44 702)	272.5 (140.2)	0	Up
	84 920 (25 884)	5 200 (1585)	10 270 (45 681)	276.6 (142.3)	0	Up
	93 600 (28 529)	6 000 (1829)	10 490 (46 660)	280.9 (144.5)	0	Up
	107 000 (32 614)	7 200 (2195)	10 710 (47 638)	285.3 (146.8)	0	Up
	116 210 (35 421)	8 000 (2438)	10 940 (48 661)	289.8 (149.1)	0	Up
	130 490 (39 773)	9 200 (2804)	11 160 (49 640)	294.4 (151.4)	0	Up
	140 340 (42 776)	10 000 (3048)	11 470 (51 019)	301.0 (154.8)	0	Up
	166 230 (50 667)	12 000 (3658)	11 920 (53 020)	310.9 (159.9)	0	Up
	194 220 (59 198)	14 000 (4267)	12 360 (54 977)	321.2 (165.2)	0	Up
	224 710 (68 492)	16 000 (4877)	12 800 (56 934)	332.0 (170.8)	0	Up
	258 180 (78 693)	18 000 (5486)	13 290 (59 114)	343.4 (176.6)	0	Up
	295 050 (89 931)	20 000 (6096)				
138 000 (62 596)	0 (0)	0 (0)	13 190 (58 669)	108.7 (55.9)	5	Down
	4 410 (1 344)	0 (0)	13 240 (58 892)	159.3 (81.9)	5	Retract
	11 260 (3 432)	1 200 (366)	13 400 (59 603)	165.1 (84.9)	5	Up
	19 440 (5 925)	2 700 (823)	6 870 (30 558)	167.5 (86.2)	5	Up
	29 400 (8 961)	3 170 (966)	6 990 (31 092)	168.7 (86.8)	5	Up
	39 400 (12 009)	3 650 (1113)	7 110 (31 625)	169.9 (87.4)	5	Up
	50 000 (15 240)	4 150 (1265)	10 670 (47 460)	199.9 (102.8)	Cleanup	Up
	58 930 (17 962)	4 150 (1265)	10 150 (45 147)	250.0 (128.6)	0	Up
	65 920 (20 092)	4 150 (1265)	9 970 (44 347)	271.1 (139.5)	0	Up
	68 150 (20 772)	4 400 (1341)	10 090 (44 880)	273.3 (140.6)	0	Up
	76 340 (22 964)	5 200 (1585)	10 270 (45 681)	276.6 (142.3)	0	Up
	82 680 (25 201)	6 000 (1829)	10 490 (46 660)	280.9 (144.5)	0	Up
	94 010 (28 654)	7 200 (2195)	10 710 (47 638)	285.3 (146.8)	0	Up
	101 790 (31 026)	8 000 (2438)	10 940 (48 661)	289.8 (149.1)	0	Up
	113 830 (34 695)	9 200 (2804)	11 160 (49 640)	294.4 (151.4)	0	Up
	122 120 (37 222)	10 000 (3048)	11 470 (51 019)	301.0 (154.8)	0	Up
	143 880 (43 855)	12 000 (3658)	11 920 (53 020)	310.9 (159.9)	0	Up
	167 310 (50 996)	14 000 (4267)	12 360 (54 977)	321.2 (165.2)	0	Up
	192 740 (58 747)	16 000 (4877)	12 800 (56 934)	332.0 (170.8)	0	Up
	220 520 (67 214)	18 000 (5486)	13 290 (59 114)	343.4 (176.6)	0	Up
	250 950 (76 490)	20 000 (6096)				

Table 21.—727 Refan: Community Interface Takeoff Profiles—1000-ft/min (5.08-m/s) Climb Rate

Takeoff Profiles for EPNL Footprints

Brake release gross weight, lb (kg)	Airplane Position at Start of Segment		Segment Average		Flap position, deg	Gear position
	Distance from brake release, ft (m)	Altitude, ft (m)	Power setting (F_n/δ), lb (N)	Flight speed, KTAS (m/s)		
182 500 (82 781)	0 (0)	0 (0)	12 960 (57 646)	121.7 (62.6)	5	Down
	8 160 (2 487)	0 (0)	12 950 (57 602)	177.4 (91.3)	5	Retract
	12 000 (3 658)	380 (116)	8 890 (39 543)	181.7 (93.5)	5	Up
	22 000 (6 706)	930 (283)	9 040 (40 210)	183.1 (94.2)	5	Up
	32 000 (9 754)	1 470 (448)	9 190 (40 877)	184.6 (95.0)	5	Up
	42 000 (12 802)	2 000 (610)	9 310 (41 411)	185.9 (95.6)	5	Up
	50 000 (15 240)	2 430 (741)	10 200 (45 370)	199.2 (102.5)	Cleanup	Up
	56 120 (17 105)	2 430 (741)	9 810 (43 635)	237.7 (122.3)	0	Up
	68 730 (20 949)	2 430 (741)	9 740 (43 324)	266.8 (137.2)	0	Up
	89 450 (27 264)	4 000 (1219)	10 050 (44 702)	272.5 (140.2)	0	Up
	105 850 (32 263)	5 200 (1585)	10 270 (45 681)	276.6 (142.3)	0	Up
	117 110 (35 695)	6 000 (1829)	10 490 (46 660)	280.9 (144.5)	0	Up
	134 550 (41 011)	7 200 (2195)	10 710 (47 638)	285.3 (146.8)	0	Up
	146 570 (44 675)	8 000 (2438)	10 940 (48 661)	289.8 (149.1)	0	Up
	165 240 (50 365)	9 200 (2804)	11 160 (49 640)	294.4 (151.4)	0	Up
	178 160 (54 303)	10 000 (3048)	11 470 (51 019)	301.0 (154.8)	0	Up
	212 300 (64 709)	12 000 (3658)	11 920 (53 020)	310.9 (159.9)	0	Up
	249 490 (76 045)	14 000 (4267)	12 360 (54 977)	321.2 (165.2)	0	Up
	290 400 (88 514)	16 000 (4877)	12 800 (56 934)	332.0 (170.8)	0	Up
	335 830 (102 361)	18 000 (5486)	13 290 (59 114)	343.4 (176.6)	0	Up
	386 520 (117 811)	20 000 (6096)				
172 500 (78 245)	0 (0)	0 (0)	13 010 (57 868)	118.9 (61.2)	5	Down
	7 200 (2 195)	0 (0)	13 010 (57 868)	173.5 (89.2)	5	Retract
	12 000 (3 658)	550 (168)	8 520 (37 897)	177.9 (91.5)	5	Up
	22 000 (6 706)	1 110 (338)	8 670 (38 564)	179.3 (92.2)	5	Up
	32 000 (9 754)	1 660 (506)	8 810 (39 187)	180.8 (93.0)	5	Up
	42 000 (12 802)	2 210 (674)	8 920 (39 676)	182.1 (93.7)	5	Up
	50 000 (15 240)	2 640 (805)	10 270 (45 681)	199.0 (102.4)	Cleanup	Up
	56 980 (17 368)	2 640 (805)	9 850 (43 813)	239.9 (123.4)	0	Up
	67 940 (20 708)	2 640 (805)	9 760 (43 412)	267.3 (137.5)	0	Up
	84 330 (25 704)	4 000 (1219)	10 050 (44 702)	272.5 (140.2)	0	Up
	99 300 (30 267)	5 200 (1585)	10 270 (45 681)	276.6 (142.3)	0	Up
	109 560 (33 394)	6 000 (1829)	10 490 (46 660)	280.9 (144.5)	0	Up
	125 440 (38 234)	7 200 (2195)	10 710 (47 638)	285.3 (146.8)	0	Up
	136 370 (41 566)	8 000 (2438)	10 940 (48 661)	289.8 (149.1)	0	Up
	153 350 (46 741)	9 200 (2804)	11 160 (49 640)	294.4 (151.4)	0	Up
	165 070 (50 313)	10 000 (3048)	11 470 (51 019)	301.0 (154.8)	0	Up
	196 000 (59 741)	12 000 (3658)	11 920 (53 020)	310.9 (159.9)	0	Up
	229 580 (69 976)	14 000 (4267)	12 360 (54 977)	321.2 (165.2)	0	Up
	266 390 (81 196)	16 000 (4877)	12 800 (56 934)	332.0 (170.8)	0	Up
	307 080 (93 598)	18 000 (5486)	13 290 (59 114)	343.4 (176.6)	0	Up
	352 250 (107 366)	20 000 (6096)				
155 000 (70 307)	0 (0)	0 (0)	13 100 (58 269)	113.8 (58.5)	5	Down
	5 690 (1 734)	0 (0)	13 130 (58 402)	166.5 (85.6)	5	Retract
	12 000 (3 658)	900 (274)	7 860 (34 961)	171.1 (88.0)	5	Up
	22 000 (6 706)	1 480 (451)	8 000 (35 584)	172.5 (88.7)	5	Up
	32 000 (9 754)	2 060 (628)	8 130 (36 162)	174.0 (89.5)	5	Up
	42 000 (12 802)	2 630 (802)	8 240 (36 652)	175.3 (90.2)	5	Up
	50 000 (15 240)	3 080 (939)	10 390 (46 215)	198.7 (102.2)	Cleanup	Up
	58 080 (17 703)	3 080 (939)	9 920 (44 124)	243.8 (125.4)	0	Up
	66 660 (20 318)	3 080 (939)	9 810 (43 635)	268.1 (137.9)	0	Up
	76 150 (23 211)	4 000 (1219)	10 050 (44 702)	272.5 (140.2)	0	Up
	88 820 (27 072)	5 200 (1585)	10 270 (45 681)	276.6 (142.3)	0	Up
	97 500 (29 718)	6 000 (1829)	10 490 (46 660)	280.9 (144.5)	0	Up
	110 900 (33 802)	7 200 (2195)	10 710 (47 638)	285.3 (146.8)	0	Up
	120 110 (36 610)	8 000 (2438)	10 940 (48 661)	289.8 (149.1)	0	Up
	134 390 (40 962)	9 200 (2804)	11 160 (49 640)	294.4 (151.4)	0	Up
	144 240 (43 964)	10 000 (3048)	11 470 (51 019)	301.0 (154.8)	0	Up
	170 130 (51 856)	12 000 (3658)	11 920 (53 020)	310.9 (159.9)	0	Up
	198 110 (60 384)	14 000 (4267)	12 360 (54 977)	321.2 (165.2)	0	Up
	228 600 (69 677)	16 000 (4877)	12 800 (56 934)	332.0 (170.8)	0	Up
	262 080 (79 882)	18 000 (5486)	13 290 (59 114)	343.4 (176.6)	0	Up
	298 940 (91 117)	20 000 (6096)				
138 000 (62 596)	0 (0)	0 (0)	13 190 (58 669)	108.7 (55.9)	5	Down
	4 410 (1 344)	0 (0)	13 250 (58 936)	159.4 (82.0)	5	Retract
	12 000 (3 658)	1 340 (408)	7 200 (32 026)	164.3 (84.5)	5	Up
	22 000 (6 706)	1 940 (591)	7 340 (32 648)	165.7 (85.2)	5	Up
	32 000 (9 754)	2 540 (774)	7 470 (33 227)	167.2 (86.0)	5	Up
	42 000 (12 802)	3 130 (954)	7 580 (33 716)	168.5 (86.7)	5	Up
	50 000 (15 240)	3 600 (1097)	10 540 (46 882)	198.7 (102.2)	Cleanup	Up
	58 790 (17 919)	3 600 (1097)	10 020 (44 569)	248.3 (127.7)	0	Up
	65 470 (19 955)	3 600 (1097)	9 870 (43 902)	269.2 (138.5)	0	Up
	68 980 (21 025)	4 000 (1219)	10 050 (44 702)	272.5 (140.2)	0	Up
	79 710 (24 296)	5 200 (1585)	10 270 (45 681)	276.6 (142.3)	0	Up
	87 050 (26 533)	6 000 (1829)	10 490 (46 660)	280.9 (144.5)	0	Up
	98 380 (29 986)	7 200 (2195)	10 710 (47 638)	285.3 (146.8)	0	Up
	106 160 (32 358)	8 000 (2438)	10 940 (48 661)	289.8 (149.1)	0	Up
	118 200 (36 027)	9 200 (2804)	11 160 (49 640)	294.4 (151.4)	0	Up
	126 490 (38 554)	10 000 (3048)	11 470 (51 019)	301.0 (154.8)	0	Up
	148 240 (45 184)	12 000 (3658)	11 920 (53 020)	310.9 (159.9)	0	Up
	171 670 (52 325)	14 000 (4267)	12 360 (54 977)	321.2 (165.2)	0	Up
	197 100 (60 076)	16 000 (4877)	12 800 (56 934)	332.0 (170.8)	0	Up
	224 870 (68 540)	18 000 (5486)	13 290 (59 114)	343.4 (176.7)	0	Up
	255 300 (77 815)	20 000 (6096)				

Table 22.—727 Refan: Community Interface Takeoff Profiles— 500-ft/min (2.54-m/s) Climb Rate

Takeoff Profiles for EPNL Footprints

Brake release gross weight, lb (kg)	Airplane Position at Start of Segment: Distance from brake release, ft (m)	Airplane Position at Start of Segment: Altitude, ft (m)	Segment Average: Power setting (F_n/δ), lb (N)	Segment Average: Flight speed, KTAS (m/s)	Flap position, deg	Gear position
182 500 (82 781)	0 (0)	0 (0)	12 960 (57 646)	121.7 (62.6)	5	Down
	8 160 (2 487)	0 (0)	12 950 (57 602)	177.4 (91.3)	5	Retract
	12 000 (3 658)	380 (116)	7 100 (31 581)	181.3 (93.3)	5	Up
	22 000 (6 706)	660 (198)	7 160 (31 848)	182.0 (93.6)	5	Up
	32 000 (9 754)	930 (283)	7 220 (32 115)	182.8 (94.0)	5	Up
	42 000 (12 802)	1 200 (366)	7 270 (32 337)	183.4 (94.3)	5	Up
	50 000 (15 240)	1 410 (430)	9 960 (44 302)	196.7 (101.2)	Cleanup	Up
	56 010 (17 072)	1 410 (430)	9 580 (42 612)	234.7 (120.7)	0	Up
	67 760 (20 653)	1 410 (430)	9 620 (42 790)	264.9 (136.3)	0	Up
	101 420 (30 913)	4 000 (1219)	10 050 (44 702)	272.5 (140.2)	0	Up
	117 820 (35 912)	5 200 (1585)	10 270 (45 681)	276.6 (142.3)	0	Up
	129 070 (39 341)	6 000 (1829)	10 490 (46 660)	280.9 (144.5)	0	Up
	146 500 (44 653)	7 200 (2195)	10 710 (47 638)	285.3 (146.8)	0	Up
	158 510 (48 314)	8 000 (2438)	10 940 (48 661)	289.8 (149.1)	0	Up
	177 180 (54 004)	9 200 (2804)	11 160 (49 640)	294.4 (151.4)	0	Up
	190 100 (57 942)	10 000 (3048)	11 470 (51 019)	301.0 (154.8)	0	Up
	224 220 (68 342)	12 000 (3658)	11 920 (53 020)	310.9 (159.9)	0	Up
	261 390 (79 672)	14 000 (4267)	12 360 (54 977)	321.2 (165.2)	0	Up
	302 280 (92 135)	16 000 (4877)	12 800 (56 934)	332.0 (170.8)	0	Up
	347 690 (105 976)	18 000 (5486)	13 290 (59 114)	343.4 (176.6)	0	Up
	398 350 (121 417)	20 000 (6096)				
172 500 (78 245)	0 (0)	0 (0)	13 010 (57 868)	118.9 (61.2)	5	Down
	7 200 (2 195)	0 (0)	13 010 (57 868)	173.5 (89.2)	5	Retract
	12 000 (3 658)	550 (168)	6 770 (30 113)	177.5 (91.3)	5	Up
	22 000 (6 706)	830 (253)	6 830 (30 390)	178.2 (91.7)	5	Up
	32 000 (9 754)	1 110 (338)	6 890 (30 647)	179.0 (92.1)	5	Up
	42 000 (12 802)	1 380 (421)	6 940 (30 869)	179.6 (92.4)	5	Up
	50 000 (15 240)	1 600 (488)	10 020 (44 569)	196.4 (101.0)	Cleanup	Up
	56 820 (17 319)	1 600 (488)	9 610 (42 745)	236.7 (121.8)	0	Up
	67 010 (20 425)	1 600 (488)	9 640 (42 879)	265.2 (136.4)	0	Up
	95 530 (29 118)	4 000 (1219)	10 050 (44 702)	272.5 (140.2)	0	Up
	110 490 (33 677)	5 200 (1585)	10 270 (45 681)	276.6 (142.3)	0	Up
	120 750 (36 805)	6 000 (1829)	10 490 (46 660)	280.9 (144.5)	0	Up
	136 630 (41 645)	7 200 (2195)	10 710 (47 638)	285.3 (146.8)	0	Up
	147 560 (44 976)	8 000 (2438)	10 940 (48 661)	289.8 (149.1)	0	Up
	164 520 (50 146)	9 200 (2804)	11 160 (49 640)	294.4 (151.4)	0	Up
	176 240 (53 718)	10 000 (3048)	11 470 (51 019)	301.0 (154.8)	0	Up
	207 160 (63 142)	12 000 (3658)	11 920 (53 020)	310.9 (159.9)	0	Up
	240 730 (73 375)	14 000 (4267)	12 360 (54 977)	321.2 (165.2)	0	Up
	277 520 (84 588)	16 000 (4877)	12 800 (56 934)	332.0 (170.8)	0	Up
	318 190 (96 984)	18 000 (5486)	13 290 (59 114)	343.4 (176.6)	0	Up
	363 340 (110 746)	20 000 (6096)				
155 000 (70 307)	0 (0)	0 (0)	13 100 (58 269)	113.8 (58.5)	5	Down
	5 690 (1 734)	0 (0)	13 130 (58 402)	166.5 (85.6)	5	Retract
	12 000 (3 658)	900 (274)	6 220 (27 667)	170.7 (87.8)	5	Up
	22 000 (6 706)	1 190 (363)	6 270 (27 889)	171.4 (88.2)	5	Up
	32 000 (9 754)	1 480 (451)	6 320 (28 111)	172.2 (88.6)	5	Up
	42 000 (12 802)	1 770 (539)	6 370 (28 334)	172.8 (88.9)	5	Up
	50 000 (15 240)	2 000 (610)	10 130 (45 058)	196.1 (100.9)	Cleanup	Up
	57 850 (17 633)	2 000 (610)	9 670 (43 012)	240.6 (123.8)	0	Up
	65 770 (20 047)	2 000 (610)	9 690 (43 101)	266.0 (136.8)	0	Up
	86 070 (26 234)	4 000 (1219)	10 050 (44 702)	272.5 (140.2)	0	Up
	98 730 (30 093)	5 200 (1585)	10 270 (45 681)	276.6 (142.3)	0	Up
	107 410 (32 739)	6 000 (1829)	10 490 (46 660)	280.9 (144.5)	0	Up
	120 810 (36 823)	7 200 (2195)	10 710 (47 638)	285.3 (146.8)	0	Up
	130 020 (39 630)	8 000 (2438)	10 940 (48 661)	289.8 (149.1)	0	Up
	144 290 (43 980)	9 200 (2804)	11 160 (49 640)	294.4 (151.4)	0	Up
	154 140 (46 982)	10 000 (3048)	11 470 (51 019)	301.0 (154.8)	0	Up
	180 020 (54 870)	12 000 (3658)	11 920 (53 020)	310.9 (159.9)	0	Up
	207 990 (63 395)	14 000 (4267)	12 360 (54 977)	321.2 (165.2)	0	Up
	238 470 (72 686)	16 000 (4877)	12 800 (56 934)	332.0 (170.8)	0	Up
	271 930 (82 884)	18 000 (5486)	13 290 (59 114)	343.4 (176.6)	0	Up
	308 790 (94 119)	20 000 (6096)				
138 000 (62 596)	0 (0)	0 (0)	13 190 (58 689)	108.7 (55.9)	5	Down
	4 410 (1 344)	0 (0)	13 250 (58 936)	159.4 (82.0)	5	Retract
	12 000 (3 658)	1 340 (408)	5 660 (25 176)	163.9 (84.3)	5	Up
	22 000 (6 706)	1 640 (500)	5 710 (25 398)	164.6 (84.7)	5	Up
	32 000 (9 754)	1 940 (591)	5 760 (25 620)	165.4 (85.1)	5	Up
	42 000 (12 802)	2 240 (683)	5 810 (25 843)	166.0 (85.4)	5	Up
	50 000 (15 240)	2 480 (756)	10 270 (45 681)	196.1 (100.9)	Cleanup	Up
	58 530 (17 840)	2 480 (756)	9 760 (43 412)	244.9 (126.0)	0	Up
	64 620 (19 696)	2 480 (756)	9 740 (43 324)	266.9 (137.3)	0	Up
	77 790 (23 710)	4 000 (1219)	10 050 (44 702)	272.5 (140.2)	0	Up
	88 510 (26 978)	5 200 (1585)	10 270 (45 681)	276.6 (142.3)	0	Up
	95 850 (29 215)	6 000 (1829)	10 490 (46 660)	280.9 (144.5)	0	Up
	107 180 (32 668)	7 200 (2195)	10 710 (47 638)	285.3 (146.8)	0	Up
	114 960 (35 040)	8 000 (2438)	10 940 (48 661)	289.8 (149.1)	0	Up
	126 990 (38 707)	9 200 (2804)	11 160 (49 640)	294.4 (151.4)	0	Up
	135 280 (41 233)	10 000 (3048)	11 470 (51 019)	301.0 (154.8)	0	Up
	157 040 (47 868)	12 000 (3658)	11 920 (53 020)	310.9 (159.9)	0	Up
	180 460 (55 004)	14 000 (4267)	12 360 (54 977)	321.2 (165.2)	0	Up
	205 880 (62 752)	16 000 (4877)	12 800 (56 934)	332.0 (170.8)	0	Up
	233 650 (71 217)	18 000 (5486)	13 290 (59 114)	343.4 (176.6)	0	Up
	264 070 (80 489)	20 000 (6096)				

Table 23.—727-200/727 Refan: 3° Approach Profiles

Approach Profiles for EPNL Footprints

Airplane configuration	Landing gross weight, lb (kg)	Airplane position at start of segment		Segment average		Flap position, deg	Gear position
		Distance from threshold, ft (m)	Altitude, ft (m)	Power setting (F_n/δ), lb (N)	Flight speed, KTAS (m/s)		
All	150 000 (68 039)	-100 000 (-30 480)	3000 (914)	5340 (23 752)	152.0 (78.2)	15	Up
		-78 000 (-23 744)	3000 (914)	5340 (23 752)	152.0 (78.2)	15	Up
		-56 290 (-17 157)	3000 (914)	5175 (23 018)	151.9 (78.1)	30	Down
		-55 010 (-16 767)	2935 (895)	4955 (22 040)	151.2 (77.8)	30	Down
		-44 000 (-13 411)	2355 (718)	4850 (21 573)	149.8 (77.1)	30	Down
		-32 000 (-9 754)	1725 (526)	4760 (21 172)	148.7 (76.5)	30	Down
		-24 000 (-7 315)	1310 (399)	4690 (20 861)	147.7 (76.0)	30	Down
		-16 000 (-4 877)	890 (271)	4620 (20 550)	146.8 (75.5)	30	Down
		-8 000 (-2 438)	470 (143)	4550 (20 238)	145.9 (75.1)	30	Down
		0 (0)	50 (15)				
727 refan	154 500 (70 080)	-100 000 (-30 480)	3000 (914)	5500 (24 464)	154.4 (79.4)	15	Up
		-78 000 (-23 774)	3000 (914)	5500 (24 464)	154.4 (79.4)	15	Up
		-56 290 (-17 157)	3000 (914)	5330 (23 708)	154.3 (79.4)	30	Down
		-54 990 (-16 761)	2930 (893)	5110 (22 729)	153.6 (79.0)	30	Down
		-44 000 (-13 411)	2355 (718)	5000 (22 240)	152.2 (78.3)	30	Down
		-32 000 (-9 754)	1725 (526)	4905 (21 817)	151.0 (77.7)	30	Down
		-24 000 (-7 315)	1310 (399)	4830 (21 484)	150.1 (77.2)	30	Down
		-16 000 (-4 877)	890 (271)	4760 (21 172)	149.1 (76.7)	30	Down
		-8 000 (-2 438)	470 (143)	4690 (20 861)	148.2 (76.2)	30	Down
		0 (0)	50 (15)				

Table 24.—727-200/727 Refan 126 700-lb (57 470-kg) Landing Weight Approach Profiles

Approach Profiles for EPNL Footprints

Landing glide slope, deg	Airplane position at start of segment		Segment average		Flap position, deg	Gear position
	Distance from threshold, ft (m)	Altitude, ft (m)	Power setting (F_n/δ), lb (N)	Flight speed, KTAS (m/s)		
0	-100 000 (-30 480)	3000 (914)	4520 (20 105)	139.2 (71.6)	15	Up
0	-78 000 (-23 774)	3000 (914)	4520 (20 105)	139.2 (71.6)	15	Up
3	-56 290 (-17 157)	3000 (914)	4375 (19 460)	139.2 (71.6)	30	Down
3	-55 120 (-16 801)	2940 (896)	4185 (18 615)	138.5 (71.2)	30	Down
3	-44 000 (-13 411)	2355 (718)	4095 (18 215)	137.2 (70.6)	30	Down
3	-32 000 (-9 754)	1725 (526)	4015 (17 859)	136.1 (70.0)	30	Down
3	-24 000 (-7 315)	1310 (399)	3955 (17 592)	135.3 (69.6)	30	Down
3	-16 000 (-4 877)	890 (271)	3895 (17 325)	134.5 (69.2)	30	Down
3	-8 000 (-2 438)	470 (143)	3840 (17 080)	133.6 (68.7)	30	Down
	0 (0)	50 (15)				
0	-100 000 (-30 480)	5000 (1524)	4750 (21 128)	149.0 (76.6)	15	Up
0	-76 000 (-23 165)	5000 (1524)	4750 (21 128)	149.0 (76.6)	15	Up
6	-53 220 (-16 221)	5000 (1524)	3230 (14 367)	143.2 (73.7)	30	Down
6	-50 850 (-15 499)	4750 (1448)	1680 (7 473)	136.6 (70.3)	30	Down
6	-42 000 (-12 802)	3820 (1164)	1620 (7 206)	134.3 (69.1)	30	Down
6	-30 000 (-9 144)	2560 (780)	1560 (6 939)	132.2 (68.0)	30	Down
6	-22 000 (-6 706)	1720 (524)	1515 (6 739)	130.3 (67.0)	30	Down
3	-12 210 (-3 722)	690 (210)	3780 (16 813)	129.1 (66.4)	30	Down
3	-8 000 (-2 438)	470 (143)	3735 (16 613)	128.5 (66.1)	30	Down
	0 (0)	50 (15)				
0	-100 000 (-30 480)	5000 (1524)	4750 (21 128)	149.0 (76.6)	15	Up
0	-88 000 (-26 822)	5000 (1524)	4750 (21 128)	149.0 (76.6)	15	Up
4.2	-76 860 (-23 427)	5000 (1524)	3940 (17 525)	141.6 (72.8)	30	Down
4.2	-51 660 (-15 746)	3150 (960)	3090 (13 744)	133.5 (68.7)	30	Down
4.2	-42 000 (-12 802)	2440 (744)	3020 (13 433)	132.1 (68.0)	30	Down
4.2	-33 030 (-10 068)	1780 (543)	3910 (17 392)	131.0 (67.4)	30	Down
3	-24 000 (-7 315)	1310 (399)	3850 (17 125)	130.1 (66.9)	30	Down
3	-16 000 (-4 877)	890 (271)	3790 (16 858)	129.3 (66.5)	30	Down
3	-8 000 (-2 438)	470 (143)	3735 (16 613)	128.5 (66.1)	30	Down
	0 (0)	50 (15)				

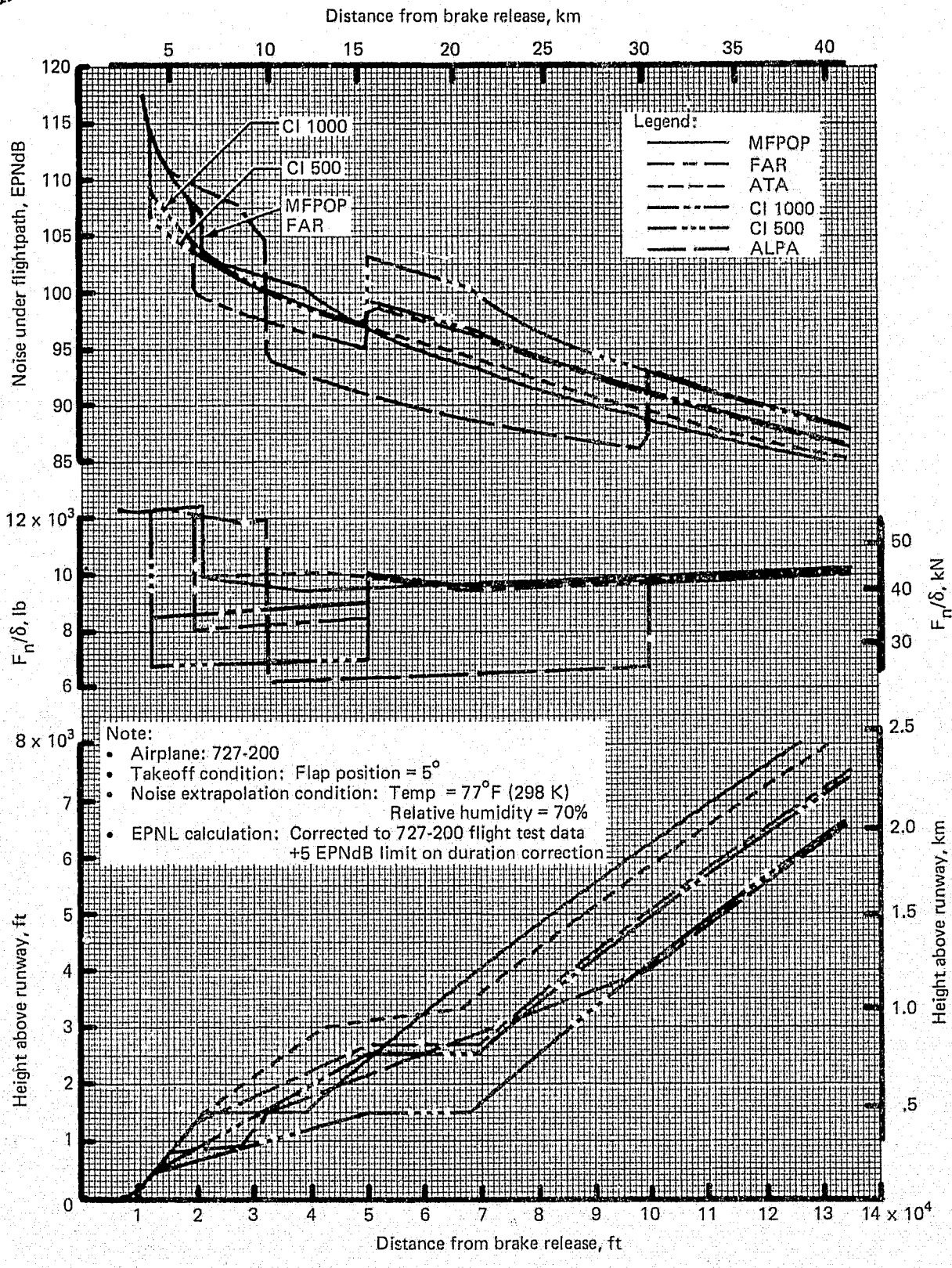

Figure 49.—727-200 Hardwall Nacelle, 172 500-lb (78 245-kg) BRGW Takeoff Flight Profiles and Noise Under Flightpath

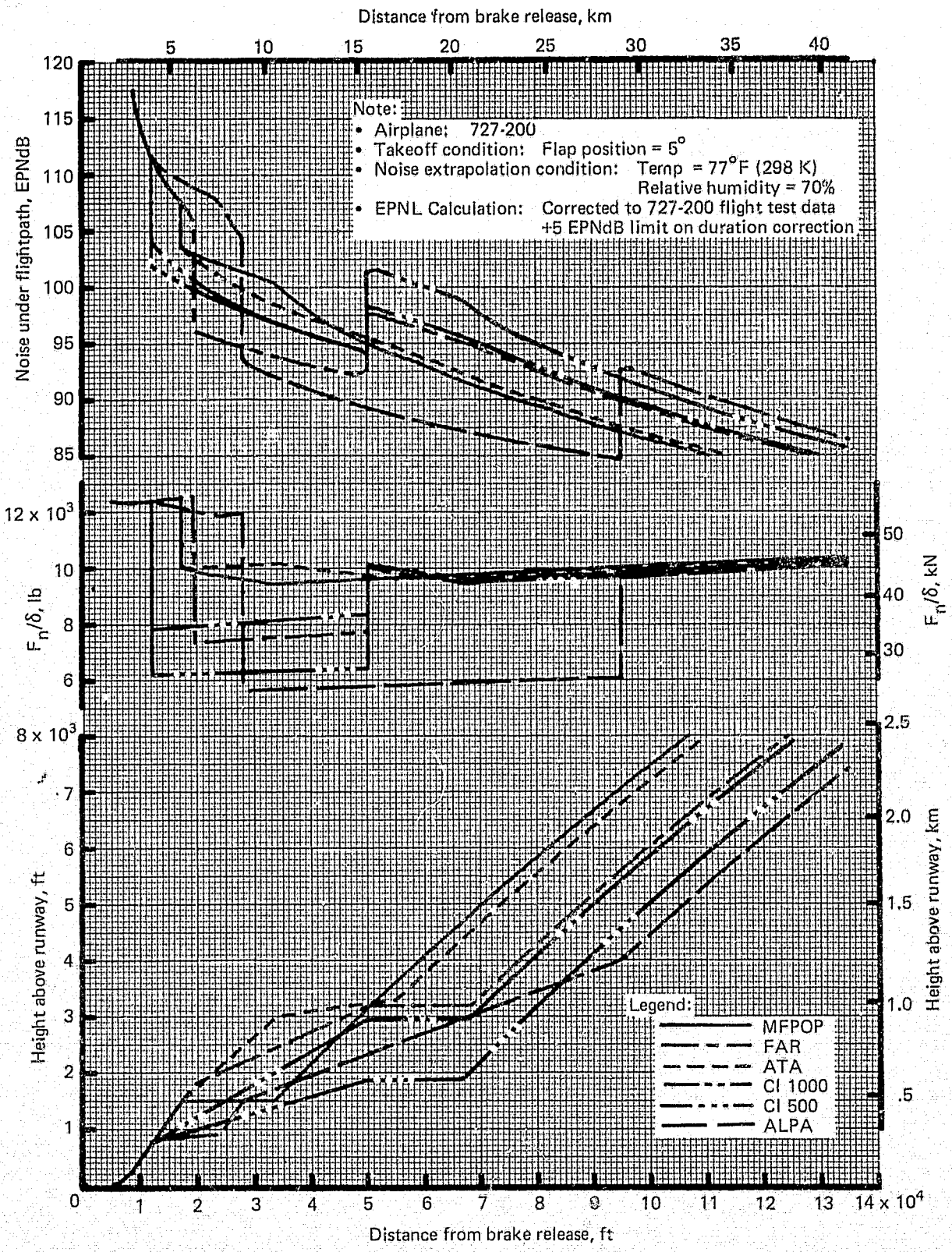

Figure 50.—727-200 Hardwall Nacelle, 155 000-lb (70 307-kg) BRGW Takeoff Flight Profiles and Noise Under Flightpath

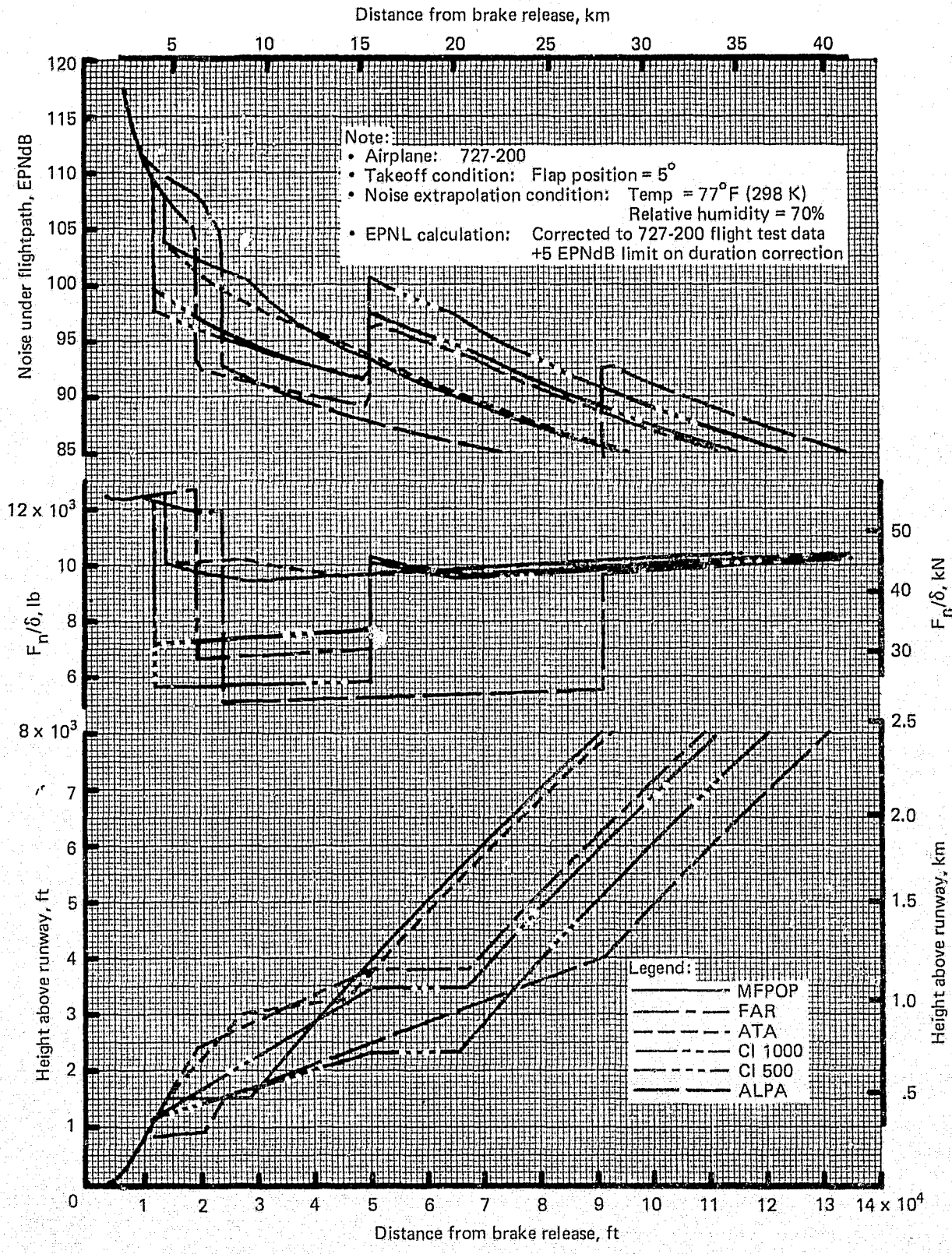

Figure 51.—727-200 Hardwall Nacelle, 138 000-lb (62 596-kg) BRGW Takeoff Flight Profiles and Noise Under Flightpath

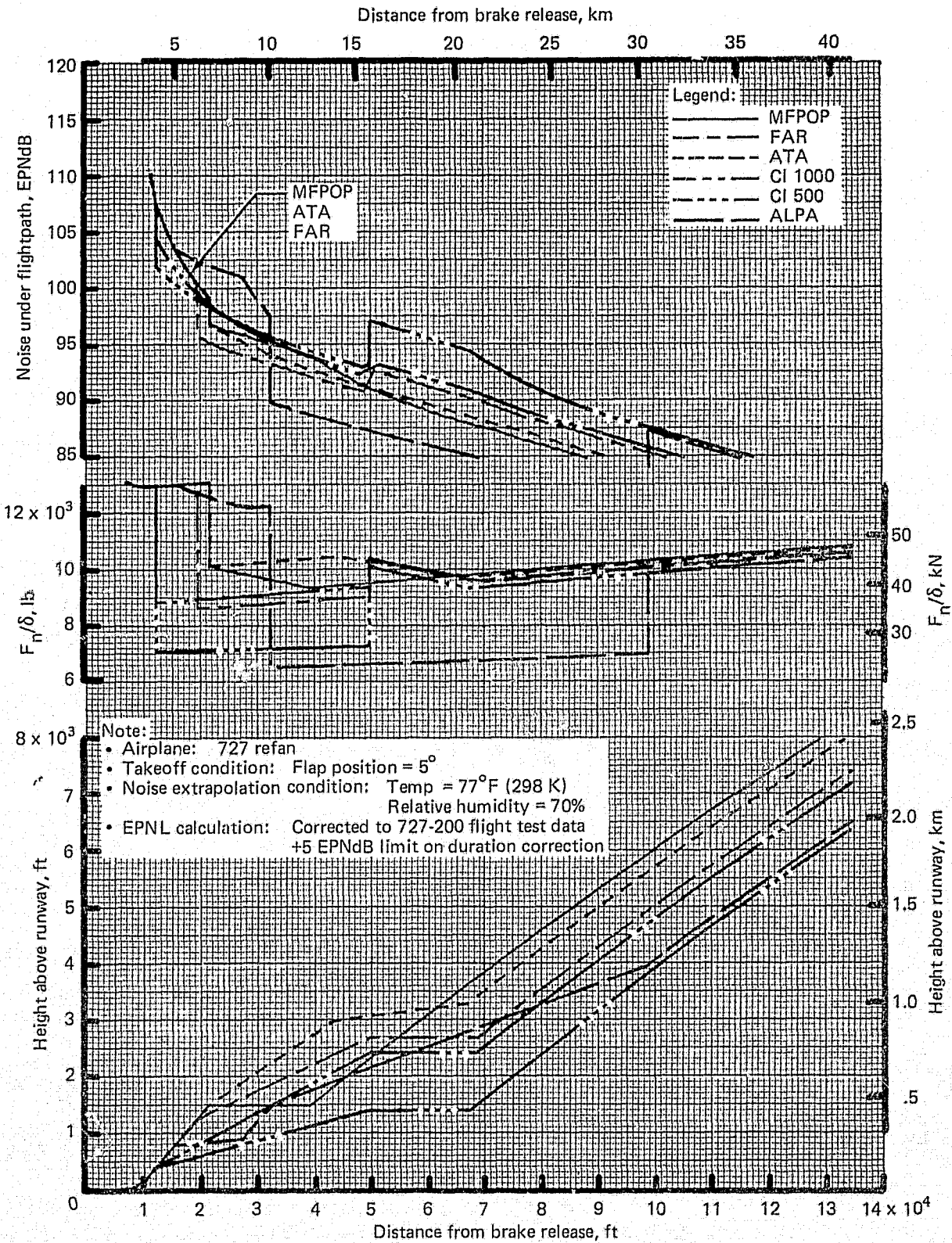

Figure 52.—727 Refan Treated Nacelle, 182 500-lb (82 781-kg) BRGW Takeoff Flight Profiles and Noise Under Flightpath

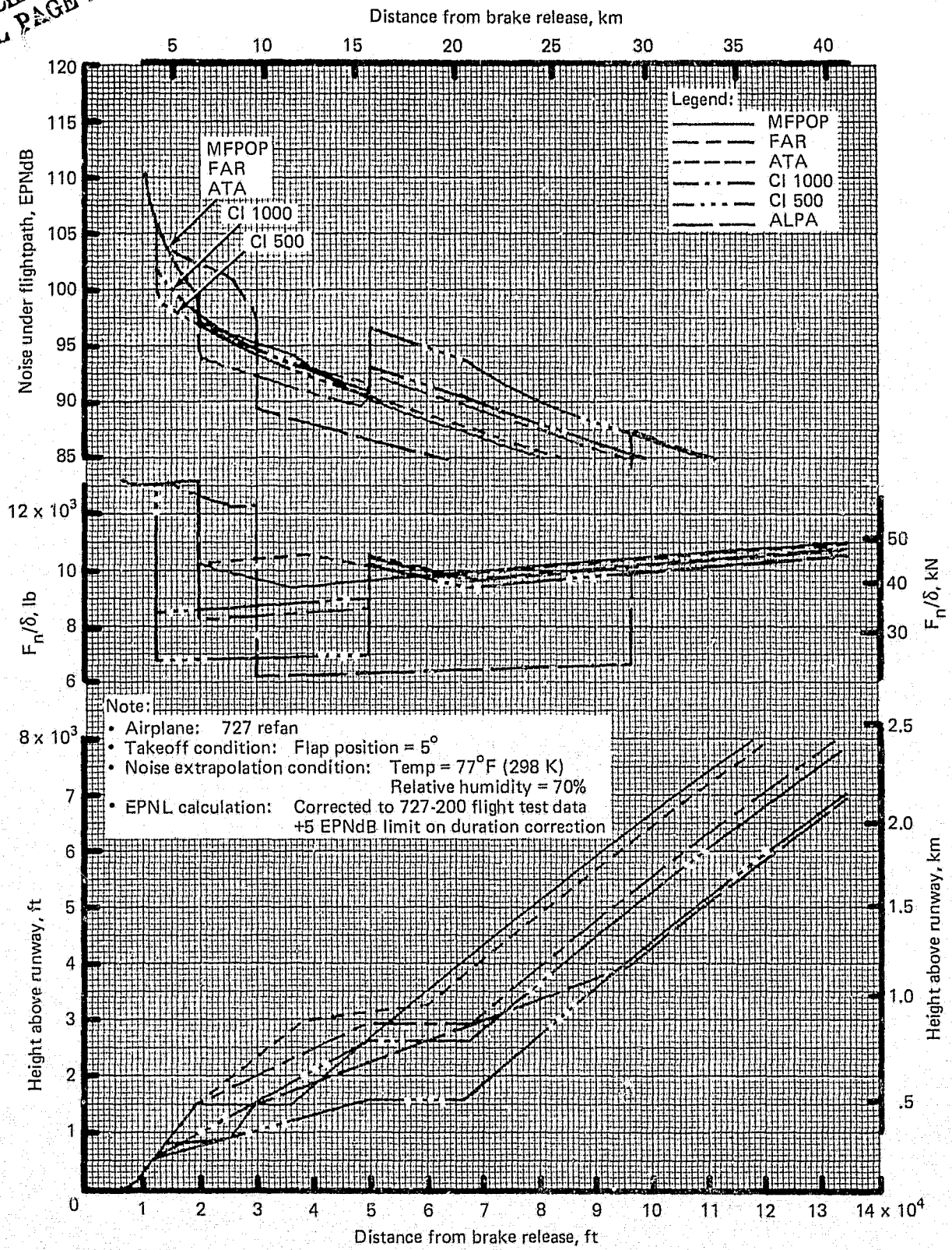

Figure 53.—727 Refan Treated Nacelle, 172 500-lb (78 245-kg) BRGW Takeoff Flight Profiles and Noise Under Flightpath

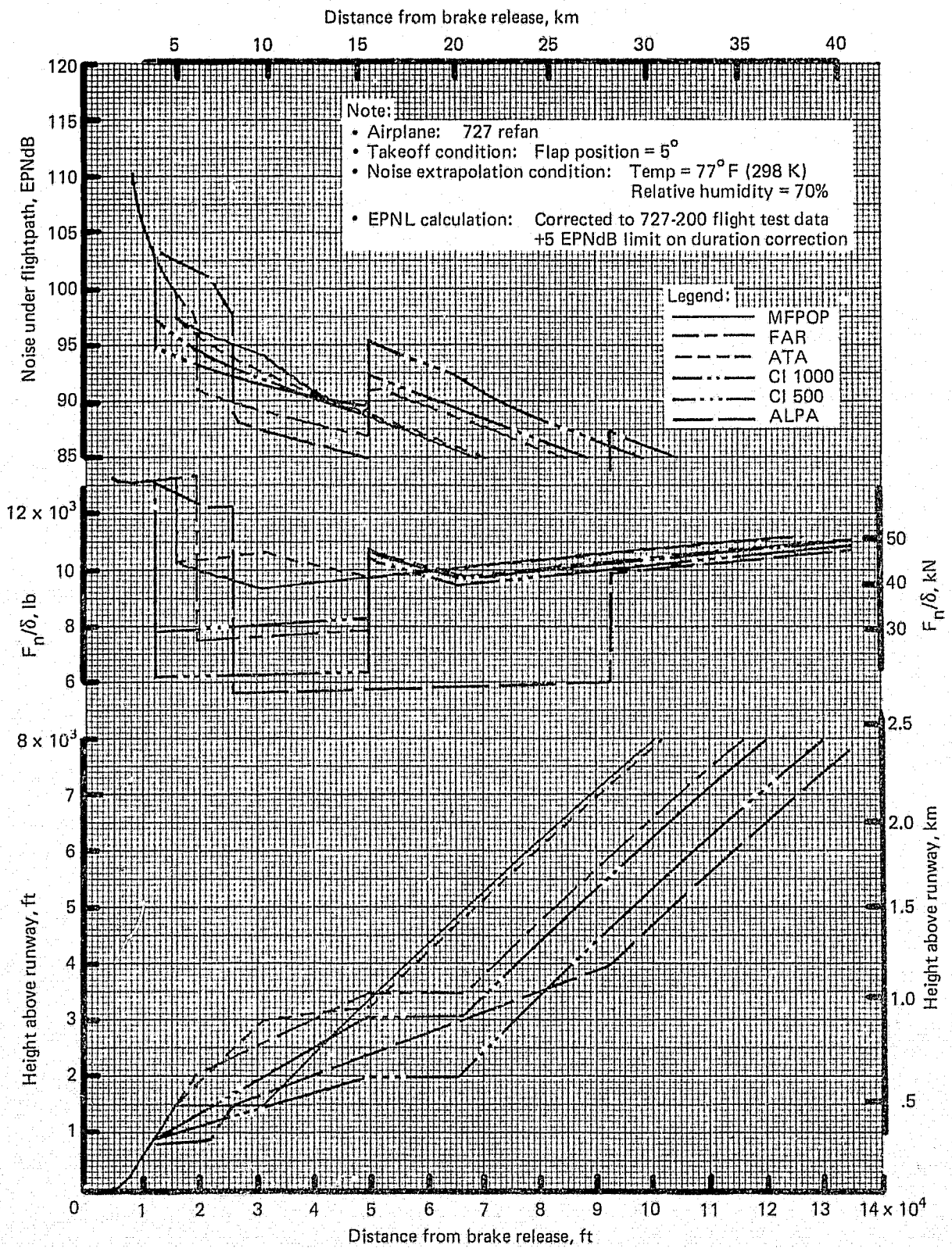

Figure 54.—727 Refan Treated Nacelle, 155 000-lb (70 307-kg) BRGW Takeoff Flight Profiles and Noise Under Flightpath

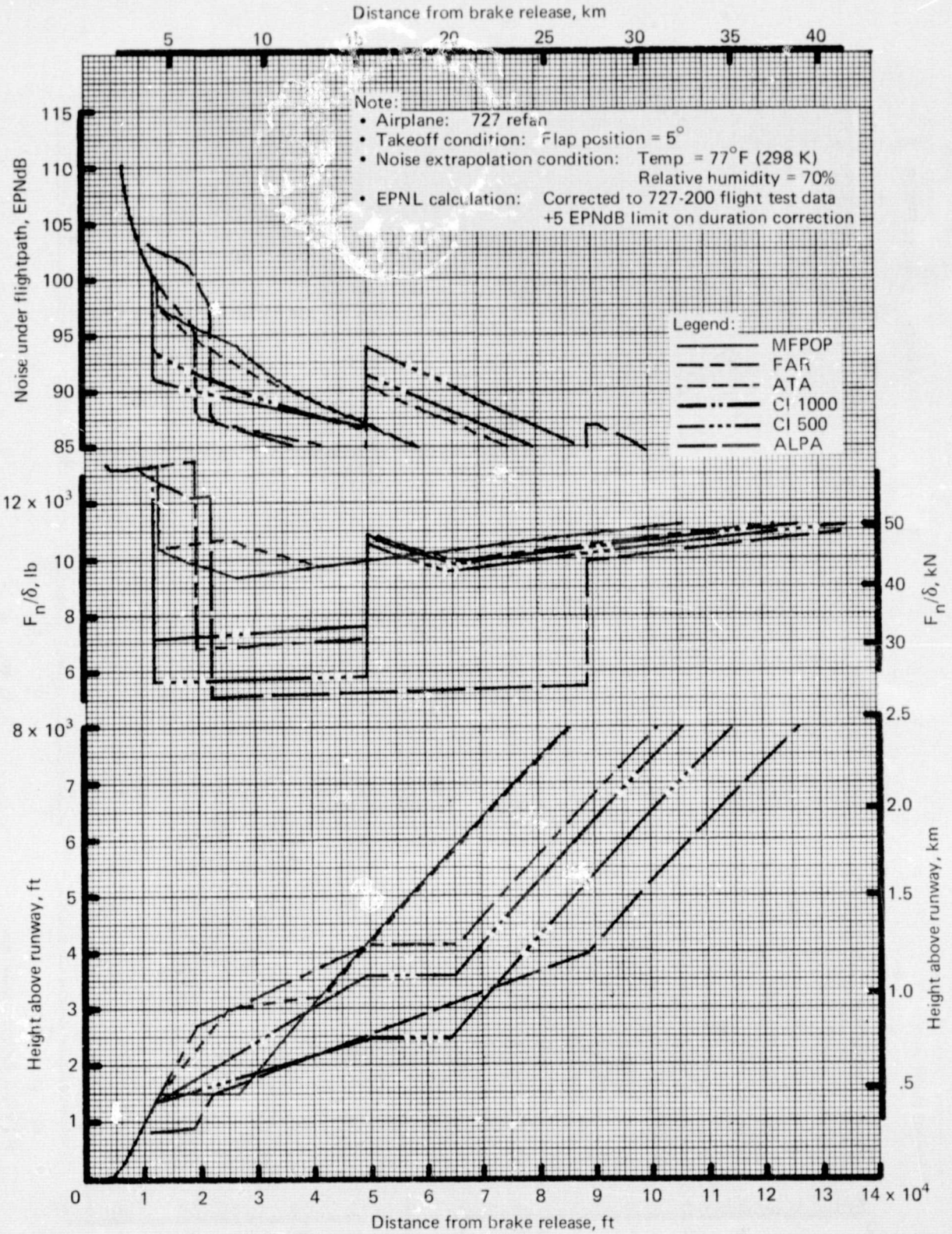

Figure 55.—727 Refan Treated Nacelle, 138 000-lb (62 596-kg) BRGW Takeoff Flight Profiles and Noise Under Flightpath

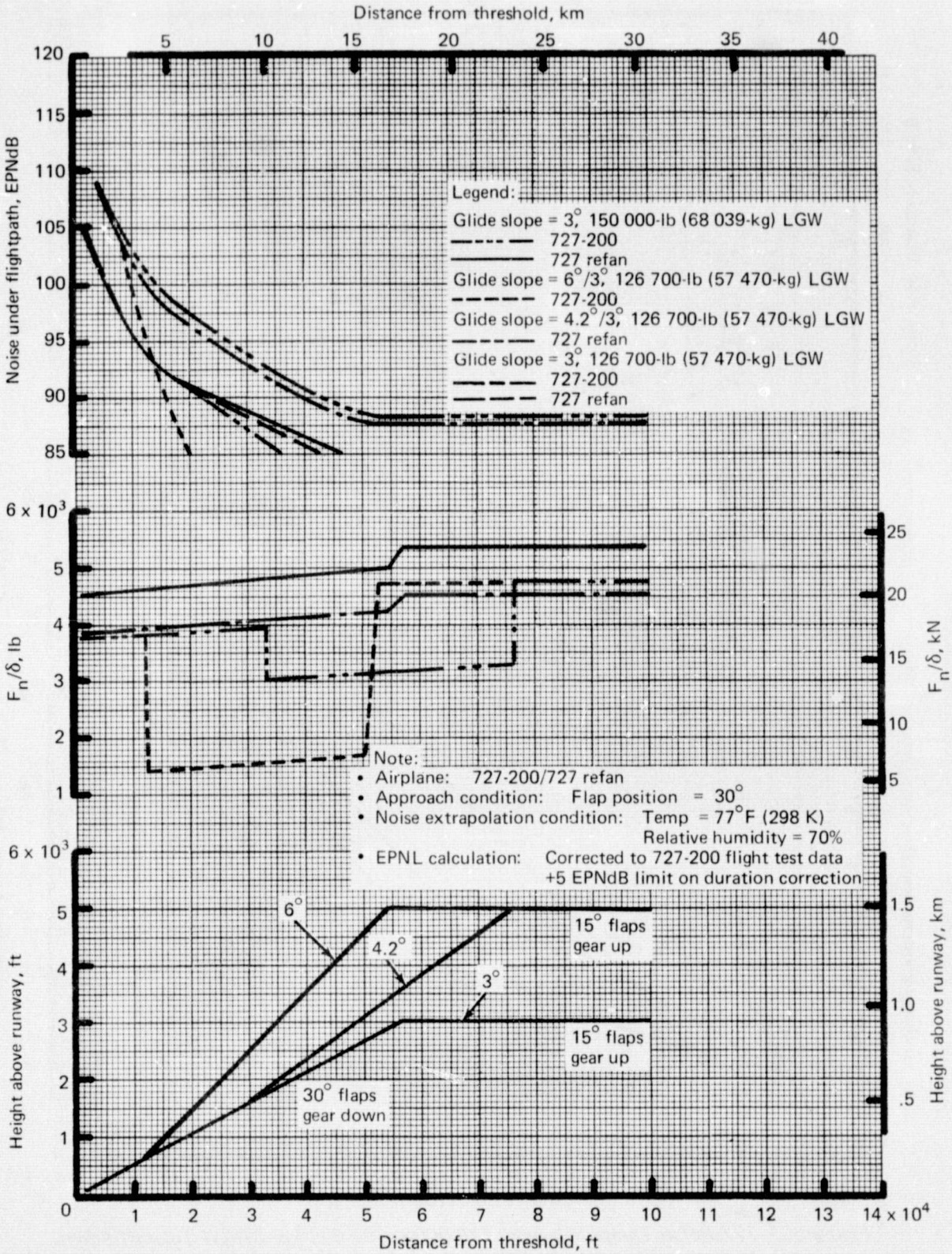

Figure 56.—727-200/727 Refan Approach Flight Profiles and Noise Under Flightpath

3.2.4.3 Footprint Calculations

Airplane noise level contours (footprints) were estimated by using airplane performance and NTA data (section 3.2.3) to calculate ground plane coordinates of equal EPNL, and the area enclosed within each contour. When the airplane location, power setting, and flight speed were known, simple geometric considerations were coupled with the NTA curves to determine the noise at intersections of a ground-plane grid surrounding the runway. At each intersection, noise from the various segments of the flightpath was estimated from the NTA data using the shortest slant distance between the grid point and the appropriate flightpath segment, and the power setting for that flightpath segment. The EPNL value was then corrected for appropriate additional ground attenuation, aircraft noise shielding, and flight speed duration. The noise values during landing and takeoff were calculated at each grid point, and contours for prescribed noise levels were determined by interpolation within the grid. The area within each contour was calculated and then normalized to the 90-EPNdB area of the 727-200 airplane.

Footprint contour areas were calculated for three cases: takeoff profiles alone, approach profiles alone, and total composite areas representing a takeoff and landing in the same direction. Figure 57 shows how these areas were calculated. The total area corresponding to a given noise level was calculated by considering the greater of the approach and takeoff EPNL's at each point, drawing the family of equal-EPNL contours, then subtracting 1.0 mile^2 (2.6 km^2), to represent the approximate area inside a small airport boundary. The composite area, prior to subtraction of the 1.0 mile^2 (2.6 km^2) was broken up into a takeoff and approach area by a line which was perpendicular to the runway centerline and intersected the composite contour at the points of equal takeoff and approach noise. The approximations introduced by this somewhat arbitrary delineation were small.

Tables 25 and 26 contain the normalized takeoff footprint areas, table 27 contains the normalized landing footprint areas, and tables 28 and 29 contain the normalized total footprint areas for the 727-200 and 727 refan airplanes. All of the areas are normalized to the total 90-EPNdB area (minus 1.0 mile^2 (2.6 km^2)) of the 727-200 airplane with the 172 500-lb (78 245-kg) BRGW and 150 000-lb (68 039-kg) LGW, utilizing an MFPOP takeoff profile and a conventional 3° approach profile. Plots of the normalized takeoff footprint areas for the 172 500-lb (78 245-kg) and 138 000-lb (62 596-kg) BRGW are shown in figures 58 and 59. Normalized landing footprint areas for the 150 000-lb (68 039-kg) and 126 700-lb (57 470-kg) LGW are shown in figures 60 and 61; and normalized total footprint areas are shown in figures 62 and 63 for 172 500-lb (78 245-kg) and 138 000-lb (62 596-kg) BRGW.

A comparison of figures 60 and 61 with figures 58 and 59 shows that the approach areas are small compared to the takeoff and total areas.

Because the total footprint areas are dominated by takeoff areas and nearly independent of the approach profile used, all normalized total areas plotted use the same conventional 3° approach profile and the results are very similar to those obtained from the takeoff area comparison.

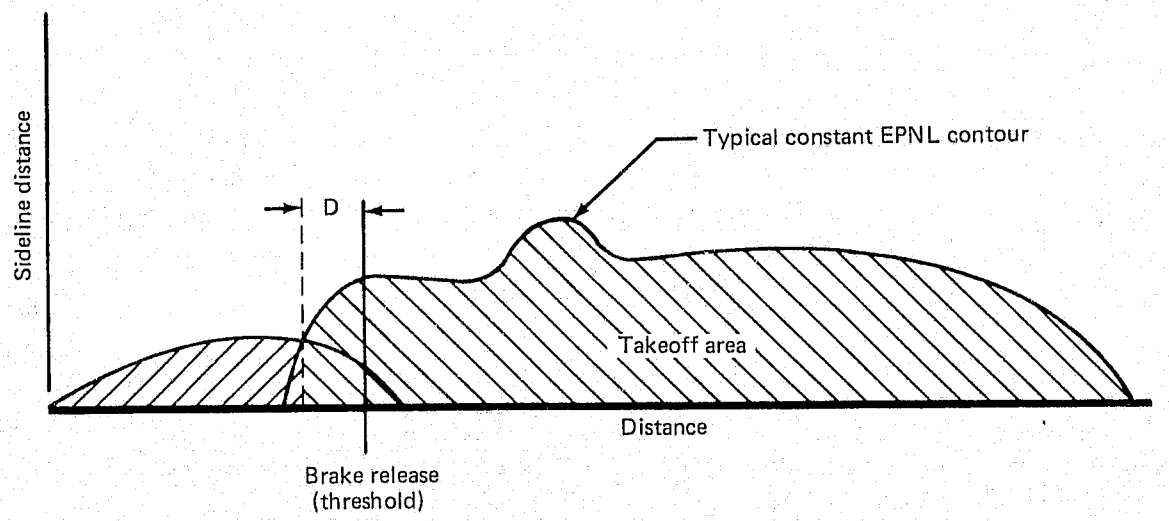

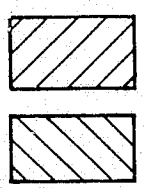

Total area = takeoff area + approach area −1.0 mile^2 (2.59 km^2)
D = 3000 ft (914 m) for 727-200
D = 1000 ft (305 m) for 727 refan

Figure 57.—Composite Footprint Contour Areas

Table 25.—727-200 Normalized Takeoff Footprint Area and Relative Footprint Noise Index (RFNI)

BRGW, lb (kg)	EPNL, EPNdB / T/O profile	Normalized takeoff footprint area[a]										
		85	87.5	90	92.5	95	97.5	100	105	110	115	RFNI[b]
172 500 (78 245)	MFPOP	1.792	1.247	0.836	0.551	0.353	0.223	0.135	0.051	0.017	0.002	1.000 (ref)[b]
	FAR	2.007	1.409	0.934	0.585	0.310	0.135	0.086	0.044	0.017	0.001	1.045
	ATA	1.974	1.390	0.943	0.623	0.379	0.206	0.121	0.051	0.017	0.002	1.113
	CI 1000	2.017	1.421	0.960	0.620	0.379	0.181	0.098	0.039	0.015	0.001	1.108
	CI 500	2.011	1.423	0.973	0.645	0.414	0.222	0.105	0.034	0.014	0.001	1.146
	ALPA	1.827	1.065	0.582	0.356	0.269	0.198	0.140	0.067	0.017	0.002	0.700
155 000 (70 307)	MFPOP	1.532	1.070	0.717	0.470	0.302	0.190	0.113	0.042	0.013	0.0	0.835
	FAR	1.762	1.217	0.773	0.412	0.189	0.116	0.084	0.041	0.013	0.0	0.822
	ATA	1.659	1.168	0.790	0.518	0.312	0.172	0.101	0.042	0.013	0.0	0.908
	CI 1000	1.778	1.250	0.828	0.514	0.254	0.119	0.071	0.033	0.011	0.0	0.904
	CI 500	1.819	1.291	0.871	0.559	0.309	0.147	0.066	0.032	0.010	0.0	0.973
	ALPA	1.547	0.878	0.480	0.300	0.228	0.168	0.120	0.057	0.014	0.0	0.558
138 000 (62 596)	MFPOP	1.295	0.902	0.604	0.397	0.254	0.160	0.095	0.034	0.014	0.002	0.682
	FAR	1.518	1.007	0.542	0.284	0.164	0.115	0.083	0.040	0.014	0.002	0.565
	ATA	1.405	0.989	0.669	0.442	0.270	0.140	0.080	0.034	0.014	0.002	0.748
	CI 1000	1.556	1.078	0.680	0.351	0.156	0.088	0.060	0.032	0.014	0.002	0.696
	CI 500	1.621	1.136	0.735	0.400	0.197	0.096	0.059	0.032	0.014	0.002	0.771
	ALPA	1.168	0.655	0.359	0.244	0.187	0.137	0.098	0.050	0.013	0.002	0.398

[a] Normalized to 727-200, 172 500-lb (78 245-kg) BRGW MFPOP takeoff flight profile, 150 000-lb (68 039-kg) LGW conventional 3° approach flight profile, 90 EPNdB total footprint area

[b] Referenced to 172 500-lb (78 245-kg) BRGW MFPOP takeoff flight profile RFNI for 727-200

Table 26.—727 Refan Normalized Takeoff Footprint Area and Relative Footprint Noise Index (RFNI)

BRGW, lb (kg)	EPNL, EPNdB / T/O profile	Normalized takeoff footprint area[a]										RFNI[b]
		85	87.5	90	92.5	95	97.5	100	105	110	115	
182 500 (82 781)	MFPOP	0.723	0.457	0.285	0.173	0.095	0.064	0.043	0.014	0.001	0.0	0.255
	FAR	0.854	0.531	0.295	0.135	0.081	0.059	0.042	0.014	0.001	0.0	0.254
	ATA	0.812	0.505	0.281	0.158	0.092	0.064	0.043	0.014	0.001	0.0	0.247
	CI 1000	0.856	0.543	0.327	0.160	0.087	0.051	0.032	0.011	0.001	0.0	0.290
	CI 500	0.903	0.596	0.382	0.210	0.091	0.047	0.030	0.011	0.001	0.0	0.354
	ALPA	0.580	0.334	0.226	0.163	0.115	0.080	0.052	0.014	0.001	0.0	0.203
172 500 (78 245)	MFPOP	0.668	0.424	0.266	0.162	0.089	0.060	0.041	0.013	0.001	0.0	0.232
	FAR	0.803	0.489	0.242	0.120	0.083	0.059	0.041	0.013	0.001	0.0	0.199
	ATA	0.722	0.448	0.245	0.147	0.087	0.060	0.041	0.013	0.001	0.0	0.208
	CI 1000	0.811	0.511	0.293	0.136	0.074	0.046	0.031	0.013	0.001	0.0	0.249
	CI 500	0.867	0.566	0.352	0.168	0.070	0.040	0.030	0.013	0.001	0.0	0.312
	ALPA	0.526	0.300	0.209	0.152	0.107	0.075	0.049	0.013	0.001	0.0	0.181
155 000 (70 307)	MFPOP	0.578	0.368	0.233	0.143	0.079	0.050	0.035	0.013	0.002	0.0	0.192
	FAR	0.697	0.371	0.179	0.122	0.089	0.060	0.038	0.013	0.001	0.0	0.139
	ATA	0.639	0.404	0.233	0.130	0.078	0.054	0.036	0.013	0.002	0.0	0.190
	CI 1000	0.731	0.445	0.217	0.101	0.059	0.042	0.031	0.013	0.001	0.0	0.165
	CI 500	0.795	0.502	0.255	0.104	0.056	0.041	0.031	0.013	0.001	0.0	0.203
	ALPA	0.424	0.249	0.187	0.136	0.096	0.067	0.044	0.013	0.002	0.0	0.153
138 000 (62 596)	MFPOP	0.504	0.324	0.208	0.128	0.073	0.046	0.032	0.011	0.001	0.0	0.163
	FAR	0.510	0.269	0.177	0.129	0.092	0.056	0.033	0.010	0.001	0.0	0.138
	ATA	0.547	0.351	0.206	0.114	0.068	0.046	0.032	0.011	0.001	0.0	0.159
	CI 1000	0.636	0.333	0.155	0.083	0.060	0.043	0.031	0.010	0.001	0.0	0.102
	CI 500	0.692	0.363	0.158	0.087	0.060	0.043	0.031	0.010	0.001	0.0	0.106
	ALPA	0.341	0.223	0.171	0.124	0.087	0.060	0.040	0.011	0.001	0.0	0.131

[a] Normalized to 727-200, 172 500-lb (78 245-kg) BRGW MFPOP takeoff flight profile, 150 000-lb (68 039-kg) LGW conventional 3° approach flight profile, 90 EPNdB total footprint area

[b] Referenced to 172 500-lb (78 245-kg) BRGW MFPOP takeoff flight profile RFNI for 727-200

Table 27.—727-200/727 Refan Normalized Landing Footprint Area

Airplane configuration	Landing gross weight, lb (kg)	EPNL, EPNdB / Landing glide slope, deg	Normalized landing footprint area[a]									RFNI[b]
			85	87.5	90	92.5	95	97.5	100	105	110	
727-200 hardwall nacelle	150 000 (68 039)	3	0.975	0.563	0.221	0.130	0.071	0.034	0.014	0.001	0.0	1.000
	126 700 (57 470)	3	0.805	0.318	0.182	0.104	0.055	0.027	0.013	0.001	0.0	0.821
		6/3	0.084	0.064	0.048	0.035	0.026	0.018	0.011	0.001	0.0	0.258
727 refan treated nacelle	154 500 (70 080)	3	0.275	0.143	0.065	0.032	0.016	0.007	0.003	0.0	0.0	0.284
	150 000 (68 039)	3	0.263	0.137	0.065	0.031	0.015	0.007	0.003	0.0	0.0	0.278
	126 700 (57 470)	3	0.217	0.117	0.057	0.029	0.015	0.007	0.003	0.0	0.0	0.248
		4.2/3	0.188	0.117	0.057	0.029	0.015	0.008	0.003	0.0	0.0	0.249

[a] Normalized to 1.000 for 727-200 total footprint area using 172 500-lb (78 245-kg) BRGW MFPOP takeoff flight profile and 150 000-lb (68 039-kg) LGW conventional 3° approach flight profile

[b] Relative to 727-200, 150 000-lb (68 039-kg) LGW conventional 3° approach flight profile

Table 28.—727-200 Hardwall Nacelle, Normalized Total Footprint Area and Relative Footprint Noise Index (RFNI)

BRGW, lb (kg)	Landing glide slope, deg	Landing gross weight, lb (kg)	EPNL, EPNdB / T/O profile	Normalized total footprint area[a]									RFNI[b]
				85	87.5	90	92.5	95	97.5	100	105	110	
172 500 (78 245)	3	150 000 (68 030)	MFPOP	2.710	1.754	1.008	0.624	0.367	0.201	0.092	0.0	0.0	1.000 (ref)[b]
			FAR	2.925	1.916	1.098	0.658	0.324	0.112	0.043	0.0	0.0	1.036
			ATA	2.892	1.896	1.107	0.696	0.392	0.184	0.079	0.0	0.0	1.088
			CI 1000	2.935	1.927	1.124	0.693	0.392	0.158	0.056	0.0	0.0	1.087
			CI 500	2.929	1.929	1.137	0.718	0.428	0.200	0.063	0.0	0.0	1.118
			ALPA	2.745	1.457	0.746	0.429	0.283	0.176	0.098	0.011	0.0	0.766
155 000 (70 307)	3	126 700 (57 470)	MFPOP	2.281	1.331	0.843	0.518	0.300	0.161	0.068	0.0	0.0	0.835
			FAR	2.510	1.478	0.899	0.460	0.187	0.087	0.040	0.0	0.0	0.823
			ATA	2.407	1.429	0.916	0.566	0.310	0.143	0.057	0.0	0.0	0.891
			CI 1000	2.526	1.511	0.953	0.562	0.252	0.089	0.026	0.0	0.0	0.887
			CI 500	2.567	1.552	0.997	0.607	0.307	0.117	0.022	0.0	0.0	0.940
			ALPA	2.295	1.139	0.605	0.348	0.226	0.138	0.075	0.001	0.0	0.613
138 000 (62 596)	3	126 700 (57 470)	MFPOP	2.043	1.163	0.730	0.445	0.252	0.130	0.050	0.0	0.0	0.715
			FAR	2.266	1.268	0.667	0.332	0.162	0.086	0.039	0.0	0.0	0.622
			ATA	2.153	1.250	0.795	0.490	0.268	0.111	0.035	0.0	0.0	0.765
			CI 1000	2.304	1.339	0.805	0.399	0.154	0.058	0.016	0.0	0.0	0.722
			CI 500	2.369	1.397	0.861	0.448	0.195	0.066	0.015	0.0	0.0	0.780
			ALPA	1.916	0.916	0.485	0.292	0.185	0.107	0.054	0.0	0.0	0.490
138 000 (62 596)	6/3	126 700 (57 470)	MFPOP	1.323	0.909	0.595	0.375	0.223	0.121	0.049	0.0	0.0	0.595
			FAR	1.545	1.014	0.532	0.262	0.133	0.076	0.038	0.0	0.0	0.501
			ATA	1.432	0.995	0.660	0.421	0.239	0.101	0.034	0.0	0.0	0.644
			CI 1000	1.584	1.084	0.670	0.330	0.125	0.049	0.015	0.0	0.0	0.601
			CI 500	1.649	1.143	0.726	0.379	0.166	0.057	0.014	0.0	0.0	0.659
			ALPA	1.195	0.661	0.350	0.222	0.156	0.098	0.052	0.0	0.0	0.369

[a] Normalized to 172 500-lb (78 245-kg) BRGW MFPOP takeoff flight profile, 150 000-lb (68 039-kg) LGW conventional 3° approach flight profile for 727-200 90-EPNdB total footprint area

[b] Referenced to 727-200, 172 500-lb (78 245-kg) BRGW MFPOP takeoff flight profile, 150 000-lb (68 039-kg) LGW conventional 3° approach profile RFNI (ref)

Table 29.—727 Refan Treated Nacelle, Normalized Total Footprint Area and Relative Footprint Noise Index (RFNI)

BRGW, lb (kg)	Landing glide slope, deg	Landing gross weight, lb (kg)	EPNL, EPNdB / T/O profile	Normalized total footprint area[a]									RFNI[b]
				85	87.5	90	92.5	95	97.5	100	105	110	
182 500 (82 781)	3	154 500 (70 080)	MFPOP	0.942	0.543	0.294	0.148	0.065	0.014	0.0	0.0	0.0	0.260
			FAR	1.070	0.617	0.304	0.109	0.040	0.009	0.0	0.0	0.0	0.259
			ATA	1.031	0.591	0.290	0.133	0.051	0.014	0.0	0.0	0.0	0.254
			CI 1000	1.080	0.628	0.336	0.135	0.046	0.001	0.0	0.0	0.0	0.286
			CI 500	1.122	0.682	0.391	0.185	0.050	0.0	0.0	0.0	0.0	0.336
			ALPA	0.799	0.420	0.235	0.138	0.074	0.030	0.0	0.0	0.0	0.220
172 500 (78 245)	3	150 000 (68 039)	MFPOP	0.875	0.504	0.274	0.136	0.047	0.010	0.0	0.0	0.0	0.240
			FAR	1.009	0.569	0.250	0.094	0.041	0.009	0.0	0.0	0.0	0.215
			ATA	0.928	0.528	0.253	0.121	0.044	0.010	0.0	0.0	0.0	0.222
			CI 1000	1.017	0.591	0.301	0.109	0.032	0.0	0.0	0.0	0.0	0.253
			CI 500	1.073	0.645	0.360	0.141	0.027	0.0	0.0	0.0	0.0	0.302
			ALPA	0.732	0.380	0.217	0.125	0.065	0.025	0.0	0.0	0.0	0.201
155 000 (70 307)	3	126 700 (57 470)	MFPOP	0.738	0.429	0.233	0.114	0.036	0.0	0.0	0.0	0.0	0.202
			FAR	0.856	0.431	0.179	0.094	0.047	0.010	0.0	0.0	0.0	0.161
			ATA	0.798	0.464	0.233	0.101	0.035	0.003	0.0	0.0	0.0	0.200
			CI 1000	0.891	0.505	0.217	0.073	0.017	0.0	0.0	0.0	0.0	0.180
			CI 500	0.949	0.562	0.255	0.075	0.014	0.0	0.0	0.0	0.0	0.210
			ALPA	0.584	0.309	0.187	0.107	0.054	0.017	0.0	0.0	0.0	0.172
138 000 (62 596)	3	126 700 (57 470)	MFPOP	0.664	0.384	0.208	0.099	0.031	0.0	0.0	0.0	0.0	0.179
			FAR	0.669	0.330	0.177	0.100	0.050	0.006	0.0	0.0	0.0	0.160
			ATA	0.707	0.412	0.206	0.086	0.026	0.0	0.0	0.0	0.0	0.176
			CI 1000	0.796	0.393	0.155	0.055	0.018	0.0	0.0	0.0	0.0	0.130
			CI 500	0.852	0.423	0.158	0.058	0.018	0.0	0.0	0.0	0.0	0.133
			ALPA	0.501	0.284	0.171	0.096	0.044	0.010	0.0	0.0	0.0	0.155
138 000 (62 596)	4.2/3	126 700 (57 470)	MFPOP	0.635	0.384	0.208	0.099	0.031	0.0	0.0	0.0	0.0	0.179
			FAR	0.641	0.330	0.177	0.100	0.050	0.007	0.0	0.0	0.0	0.161
			ATA	0.678	0.412	0.206	0.086	0.026	0.0	0.0	0.0	0.0	0.176
			CI 1000	0.767	0.393	0.155	0.055	0.018	0.0	0.0	0.0	0.0	0.130
			CI 500	0.823	0.423	0.158	0.058	0.018	0.0	0.0	0.0	0.0	0.133
			ALPA	0.472	0.284	0.171	0.096	0.044	0.011	0.0	0.0	0.0	0.155

[a] Normalized to 727-200, 172 500-lb (78 245-kg) BRGW MFPOP takeoff flight profile, 150 000-lb (68 039-kg) LGW conventional 3° approach flight profile total 90-EPNdB footprint area

[b] Referenced to 727-200, 172 500-lb (78 245-kg) BRGW MFPOP takeoff flight profile, 150 000-lb (68 039-kg) LGW conventional 3° approach flight profile total RFNI

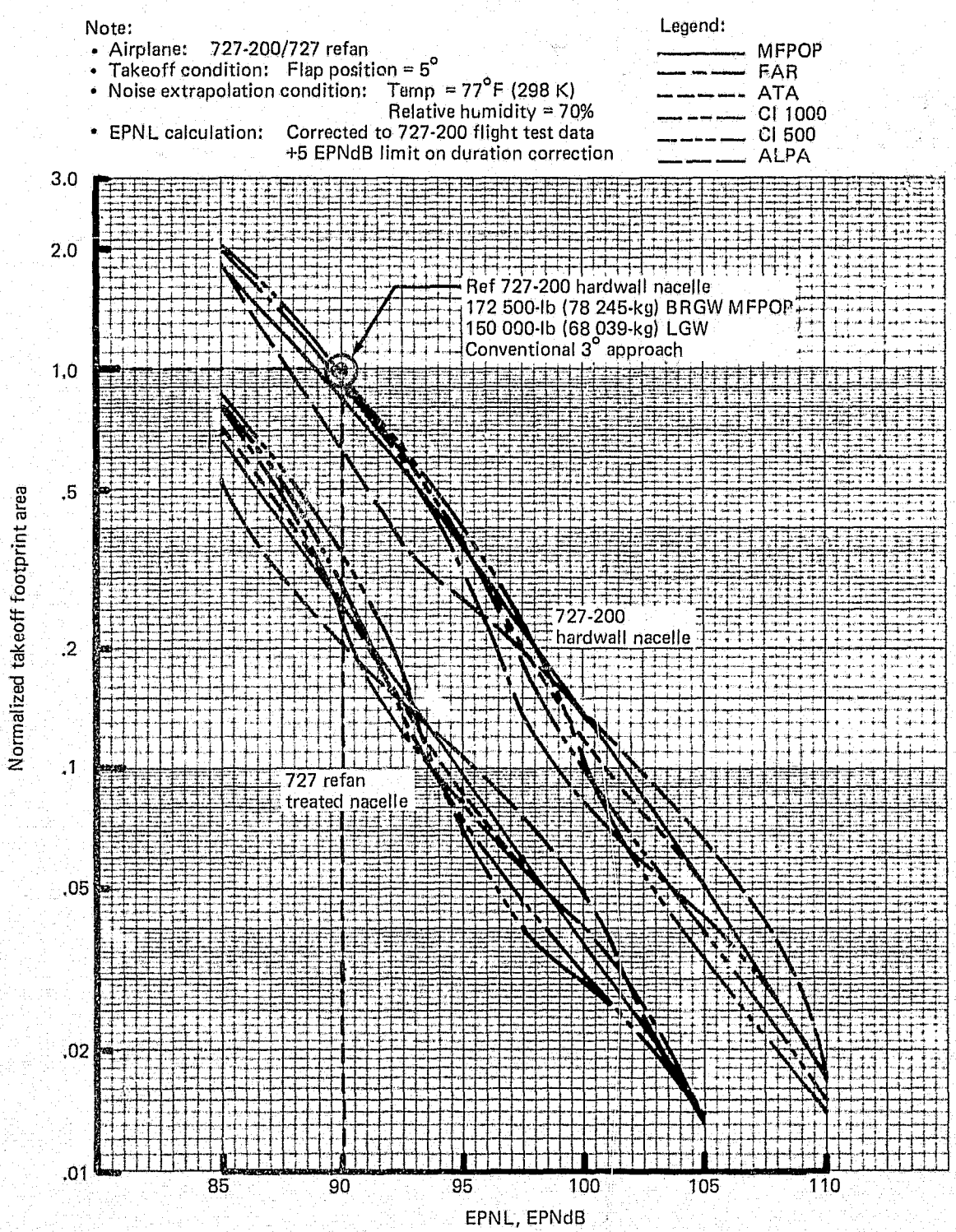

Figure 58.—727-200/727 Refan 172 500-lb (78 245-kg) BRGW Normalized Takeoff Footprint Area

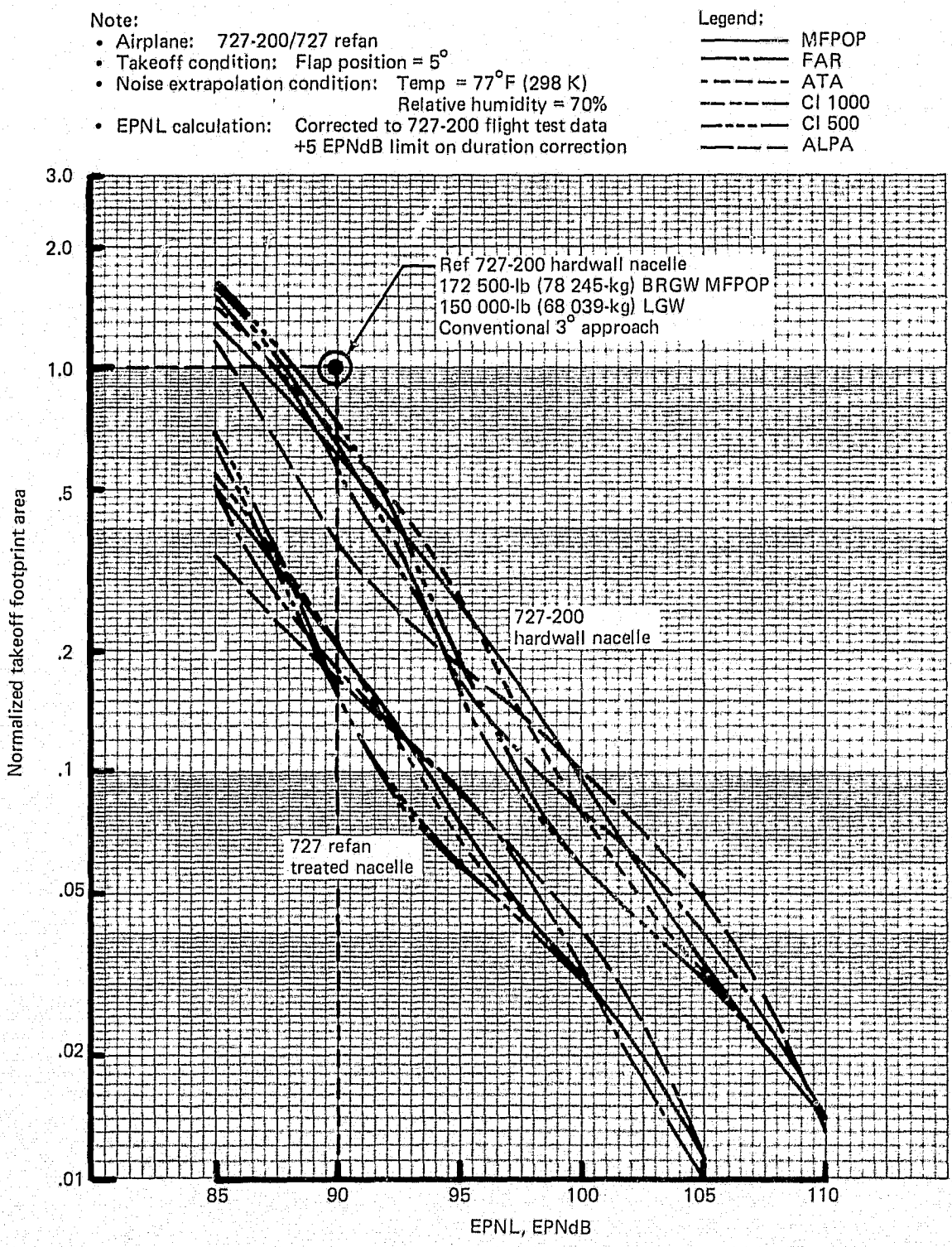

Figure 59.—727-200/727 Refan 138 000-lb (62 596-kg) BRGW Normalized Takeoff Footprint Area

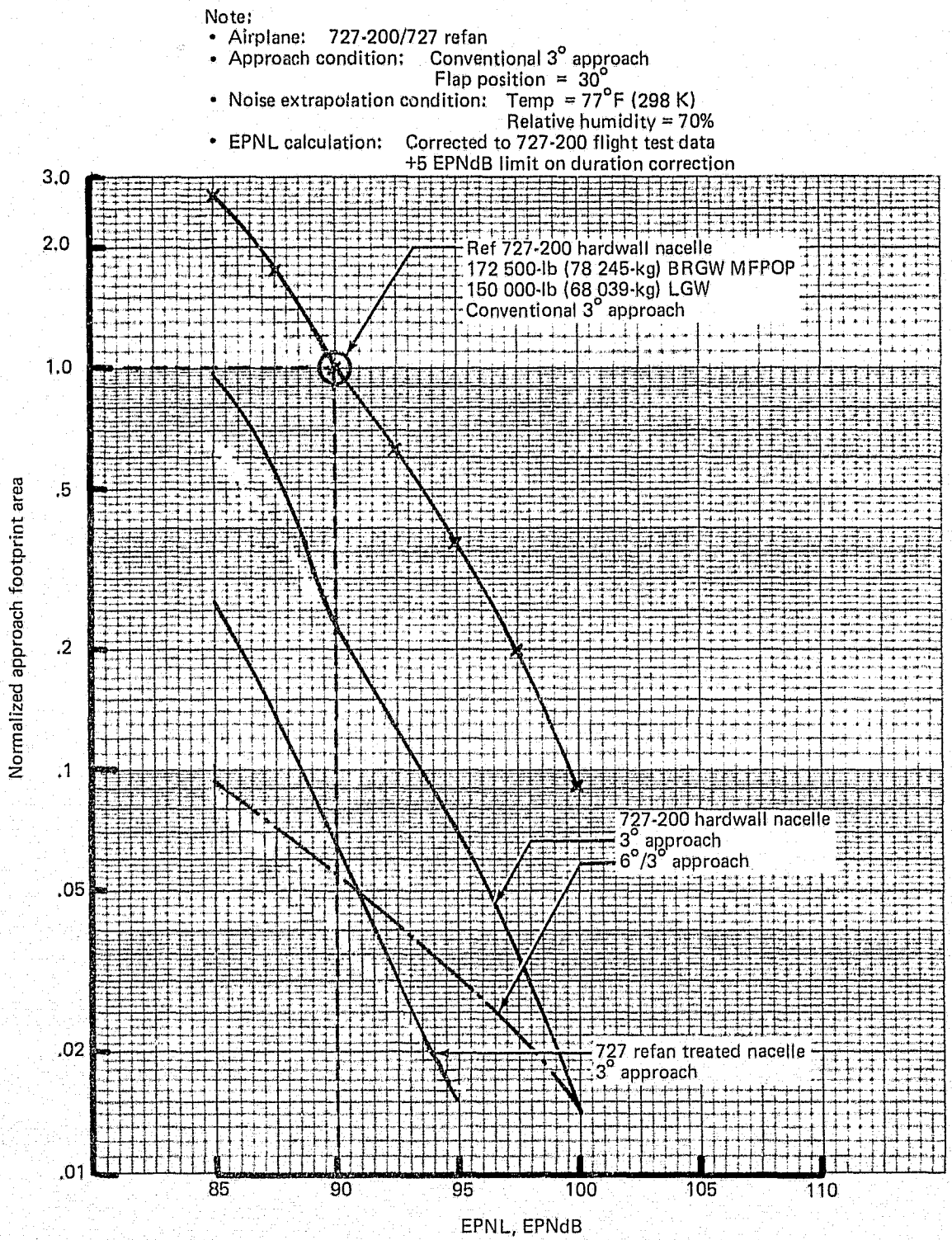

Figure 60.—727-200/727 Refan 150 000-lb (68 039-kg) LGW Normalized Approach Footprint Area

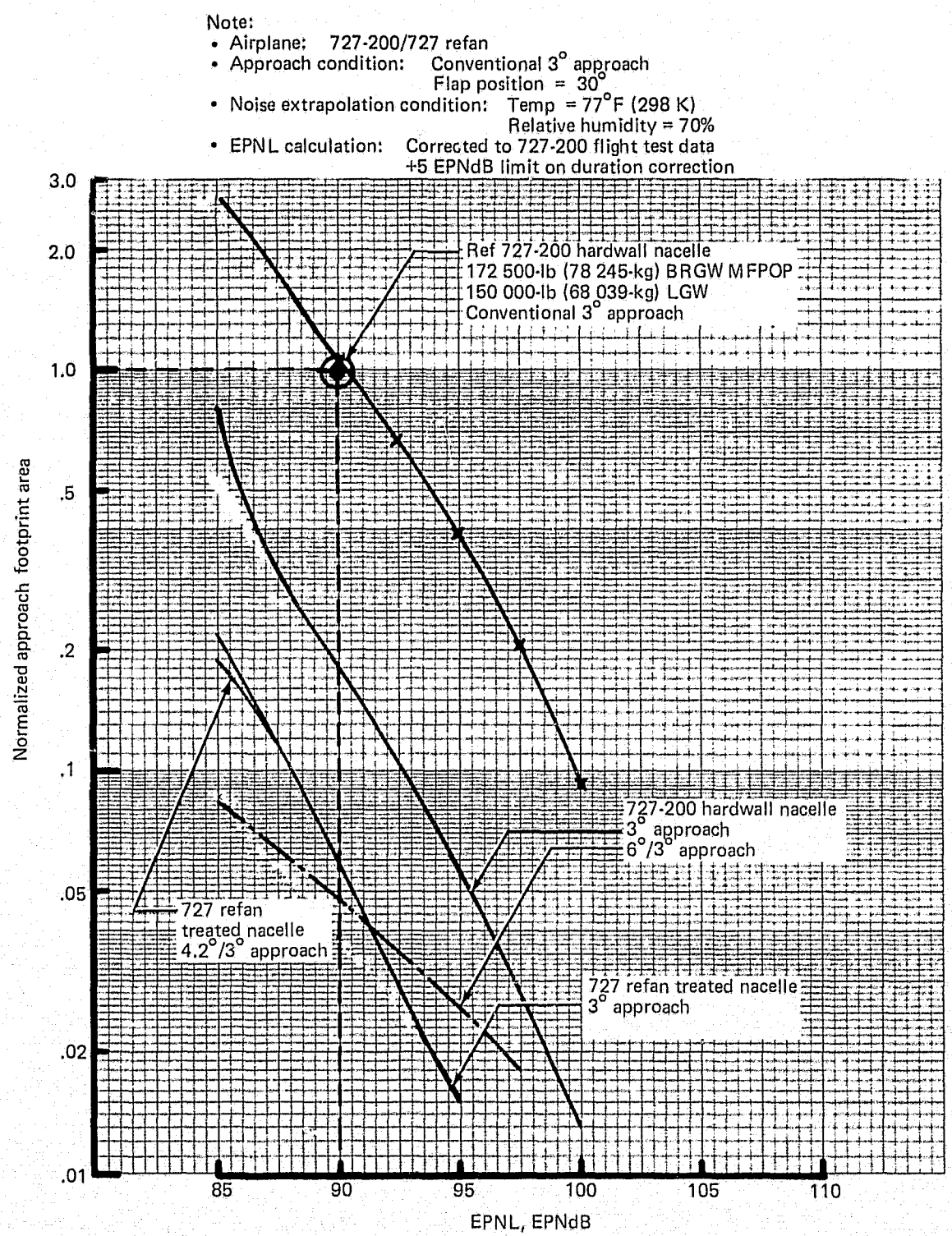

Figure 61.—727-200/727 Refan 126 700-lb (57 470-kg) LGW Normalized Approach Footprint Area

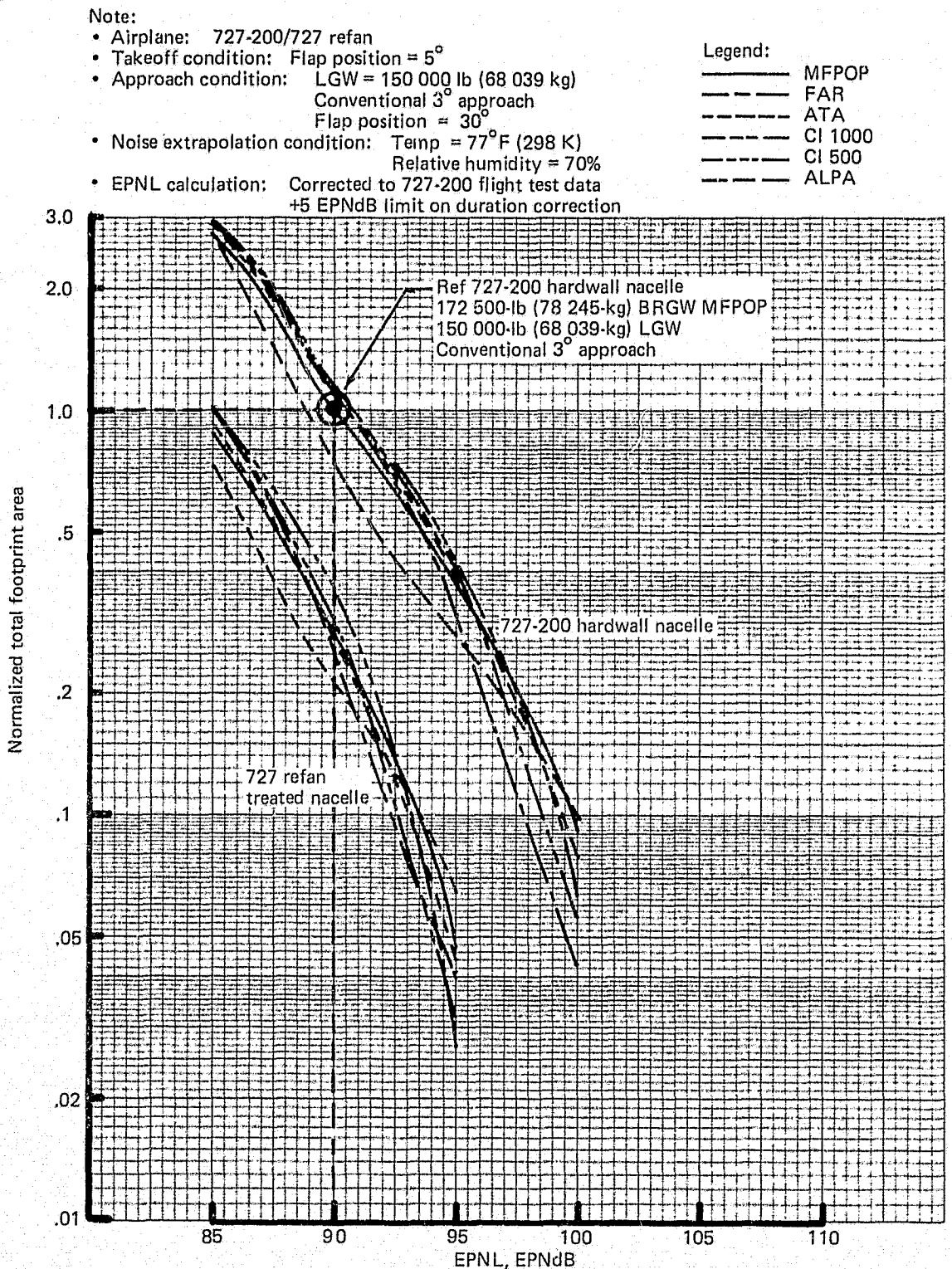

Figure 62.—727-200/727 Refan 172 500-lb (78 245-kg) BRGW Normalized Total Footprint Area

Note:
- Airplane: 727-200/727 refan
- Takeoff condition: Flap position = 5°
- Approach condition: LGW = 126 700 lb (57 470 kg)
  Conventional 3° approach
  Flap position = 30°
- Noise extrapolation condition: Temp = 77°F (298 K)
  Relative humidity = 70%
- EPNL calculation: Corrected to 727-200 flight test data
  +5 EPNdB limit on duration correction

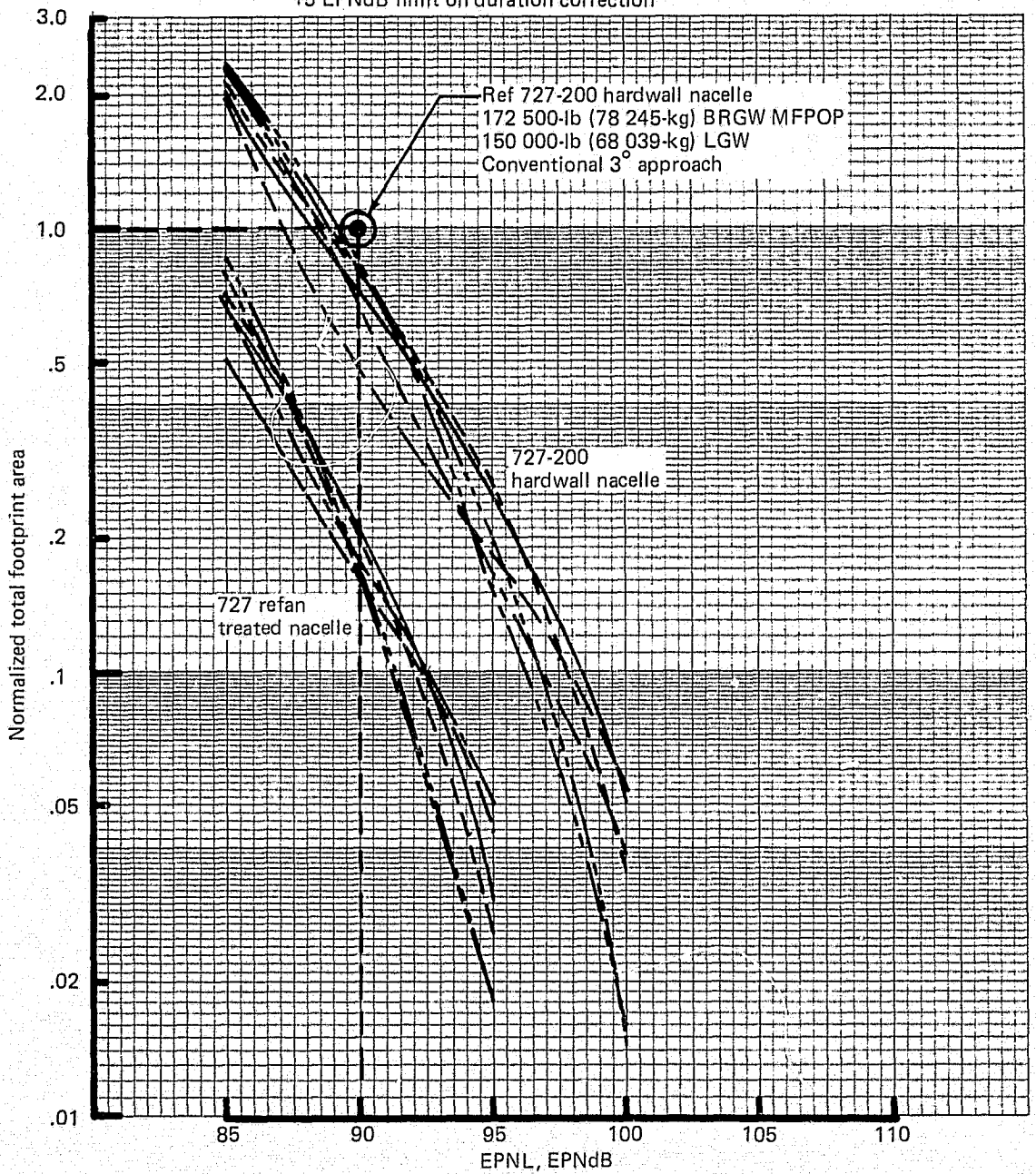

Figure 63.—727-200/727 Refan 138 000-lb (62 596-kg) BRGW Normalized Total Footprint Area

3.2.4.4 Percent Area Reductions for the 727 Refan

Figure 64 shows the percent EPNL total area reductions of the 172 500-lb (78 245-kg) BRGW 727 refan referenced to the 172 500-lb (78 245-kg) BRGW 727-200 for different EPNL levels. Figure 65 gives the corresponding percent reductions for the 138 000-lb (62 596-kg) BRGW airplanes. For both gross weights, the 727 refan is referenced to the 727-200 for a comparable type of takeoff profile (e.g., an ATA 727 refan is compared to an ATA 727-200) and a 3° approach profile. Percent area reduction is at best an approximate method of representing the number of people exposed to specific noise levels for different airplanes and/or flight profiles. However, a precise comparison would require an airport population density analysis which is beyond the scope of this study. For every profile type, BRGW, or EPNL, the 727 refan area reduction benefit is at least 63%. The individual noise reduction benefits depend more strongly on profile type than on BRGW. Percent area reduction increases with EPNL as the 727 refan areas approach 1.0 mile^2 (2.6 km^2).

3.2.4.5 Relative Footprint Noise Index

A relative footprint noise index (RFNI) was developed to aid in assessing the degree of benefit achieved by altering an aircraft's community noise exposure. The RFNI unit allowed direct comparisons of single numbers, each of which represents the relative community annoyance produced by an aircraft.

The RFNI evaluation was based on an annoyance area integral, in which the weighting factor is doubled with each 10-EPNdB increase in noise. The area of integration on the EPNL contour map extended from the 90-EPNdB contour to the constant noise contour of 1.0 mile^2 (2.6 km^2) in area, which approximates a minimum area contour completely contained within a small airport boundary. RFNI was thus, defined as:

$$\text{RFNI} = \frac{\displaystyle\int_{1.0\ \text{mile}^2\ (2.6\ \text{km}^2)}^{A_{90\ \text{EPNdB}}} 2^{\left(\frac{\text{EPNL} - 90\ \text{EPNdB}}{10}\right)}\, dA}{\left[\displaystyle\int_{1.0\ \text{mile}^2\ (2.6\ \text{km}^2)}^{A_{90\ \text{EPNdB}}} 2^{\left(\frac{\text{EPNL} - 90\ \text{EPNdB}}{10}\right)}\, dA\right]_{727\text{-}200}}$$

As an approximation of these integrals, the EPNL contour areas were calculated in 5-EPNdB increments over the range of 90 EPNdB to that noise level which had a contour area of 1.0 mile^2 (2.6 km^2) and the weighting factor was evaluated at the midpoint of each increment.

This unit was referenced to the noise exposure of the 727-200. Therefore, the 727-200 has an RFNI value of 1.0, while an RFNI value of 0.0 corresponds to a reduction of the 90-EPNdB contour to an area of 1.0 mile^2 (2.6 km^2).

Note:
- Airplane: 727-200/727 refan
- Takeoff condition: Flap position = 5°
- Approach condition: LGW = 150 000 lb (68 039 kg)
  Conventional 3° approach
  Flap position = 30°
- Noise extrapolation condition: Temp = 77°F (298 K)
  Relative humidity = 70%
- EPNL calculation: Corrected to 727-200 flight test data
  +5 EPNdB limit on duration correction

Legend:
- MFPOP
- FAR
- ATA
- CI 1000
- CI 500
- ALPA

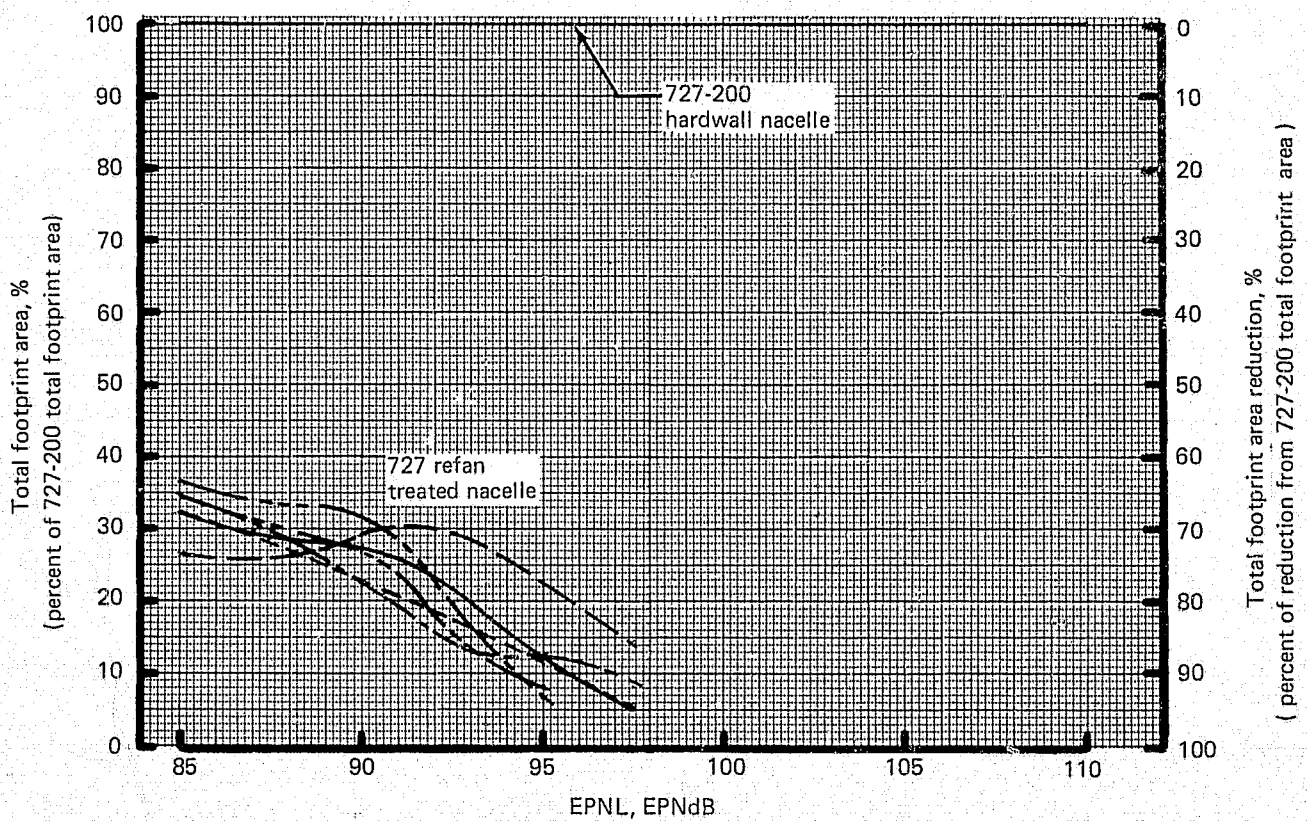

Figure 64.—727-200/727 Refan 172 500-lb (78 245-kg) BRGW Total Footprint Area Reduction

Note:

- Airplane: 727-200/727 refan
- Takeoff condition: Flap position = 5°
- Approach condition: LGW = 126 700 lb (57 470 kg)
  Conventional 3° approach
  Flap position = 30°
- Noise extrapolation condition: Temp = 77°F (298 K)
  Relative humidity = 70%
- EPNL calculation: Corrected to 727-200 flight test data
  +5 EPNdB limit on duration correction

Legend:

- MFPOP
- FAR
- ATA
- CI 1000
- CI 500
- ALPA

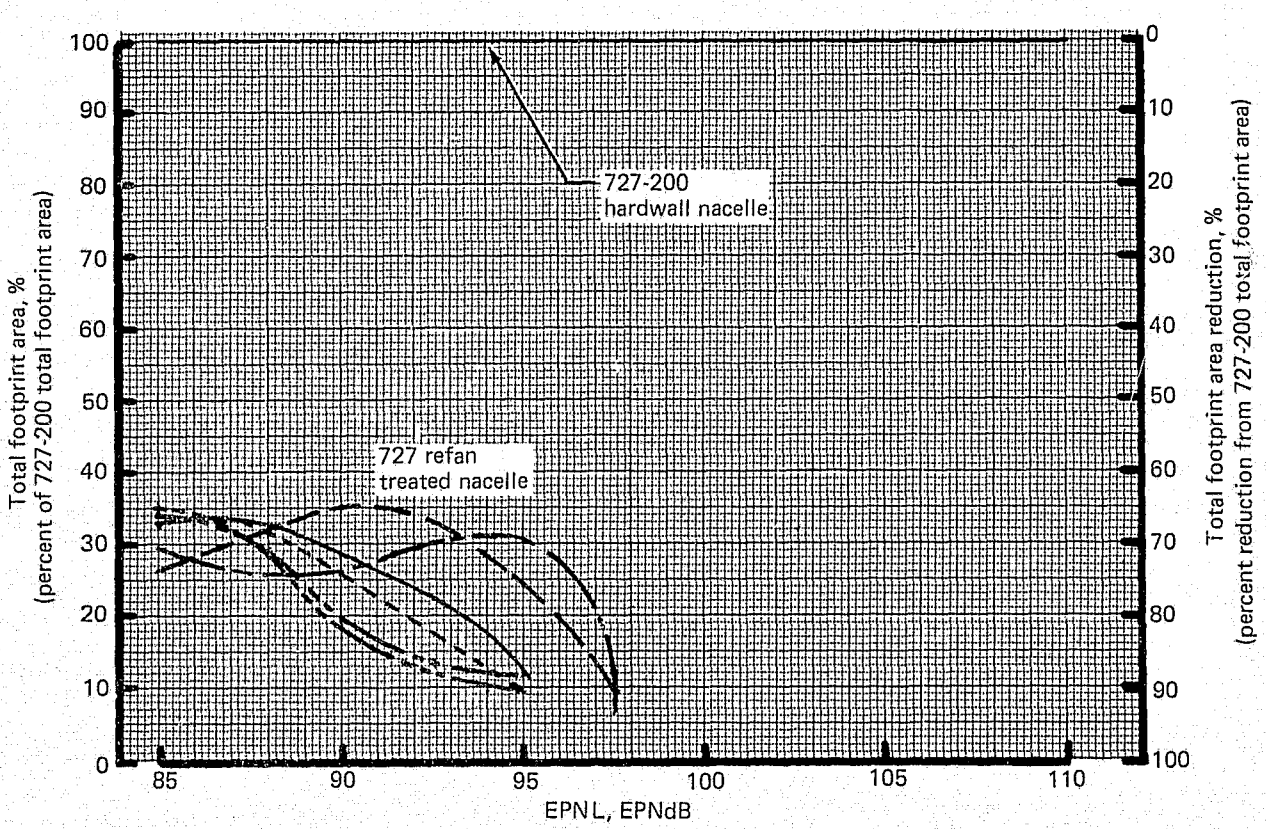

Figure 65.—727-200/727 Refan 138 000-lb (62 596-kg) BRGW Total Footprint Area Reduction

Takeoff RFNI is plotted against takeoff gross weight for different takeoff profiles for both the 727-200 and 727 refan in figure 66. The RFNI values are normalized on the weighted takeoff area of the 172 500-lb (78 245-kg) BRGW 727-200 with the modified full power operational profile. With each percent increase in BRGW, the takeoff RFNI's are seen to increase 2% to 3%.

Approach RFNI is plotted in figure 67 against landing gross weight for conventional and two-segment approaches. The RFNI values are normalized on the weighted approach area for the 150 000-lb (60 039-kg) LGW 727-200 with a conventional 3° approach. With each percent increase in LGW, the approach RFNI's are seen to increase approximately 1%. The two-segment approach has significant advantages for the 727-200; however, for the 727 refan, the benefits are minimal, particularly when the 4.2° idle thrust limit is recognized.

Total RFNI is dominated by takeoff RFNI, as shown in section 3.2.4.3. Therefore, total RFNI is plotted against BRGW in figure 68 where each situation was coupled with a 3° approach glide slope. The RFNI values are normalized on the weighted total area for the 172 500-lb (78 245-kg) BRGW 727-200 using the modified full power operational profile and 150 000-lb (68 039-kg) LGW with the 3° approach glide slope.

As seen in section 3.2.4.4, the benefits of the 727 refan depend on the takeoff profile selected. A comparison of the minimum RFNI for the 727 refan with that of the 727-200 would indicate an advantage to fly a different profile at different gross weights (for minimum noise), a situation unacceptable for normal airline operation. The final result, and the one considered most representative of the benefits of the 727 refan, is a comparison of percentage reduction in total area (takeoff and approach composite areas) for the respective takeoff profiles. The result (fig. 69) is dominated by the takeoff areas and shows a 68% to 83% reduction in RFNI. A comparison at equal-range and unlimited-field length would result in 1% to 2% less benefit.

3.3 PROPULSION SYSTEM

Uninstalled engine performance is quoted by the engine manufacturer for a low-loss bell-mouth inlet and reference exhaust nozzle hardware mounted on the engine without any airbleed or mechanical power extractions. The airframe manufacturer must adjust this uninstalled engine performance for his specific hardware, with the airbleed and mechanical power extractions required for the particular airplane application. In order to assess the performance of the refanned JT8D engine on the 727-200 airplane, the performance increments for the following hardware differences from the engine manufacturer must be considered: (1) side-engine inlet, (2) center-engine inlet and duct, (3) exhaust system, (4) thrust reverser, (5) nacelle subsystems, and (6) airplane systems requiring engine airbleed. In addition to the installed performance considerations, the airframe manufacturer must demonstrate by test and/or analyses that the engine installation, including nacelle subsystems, does not jeopardize the airplane operational safety and fire integrity. These items are discussed in the subsequent sections.

Note:

- Airplane: 727-200/727 refan
- Takeoff condition: Flap position = 5°
- Noise extrapolation condition: Temp = 77°F (298 K)
  Relative humidity = 70%
- EPNL calculation: Corrected to 727-200 flight test data
  +5 EPNdB limit on duration correction

Legend:

- MFPOP
- FAR
- ATA
- CI 1000
- CI 500
- ALPA

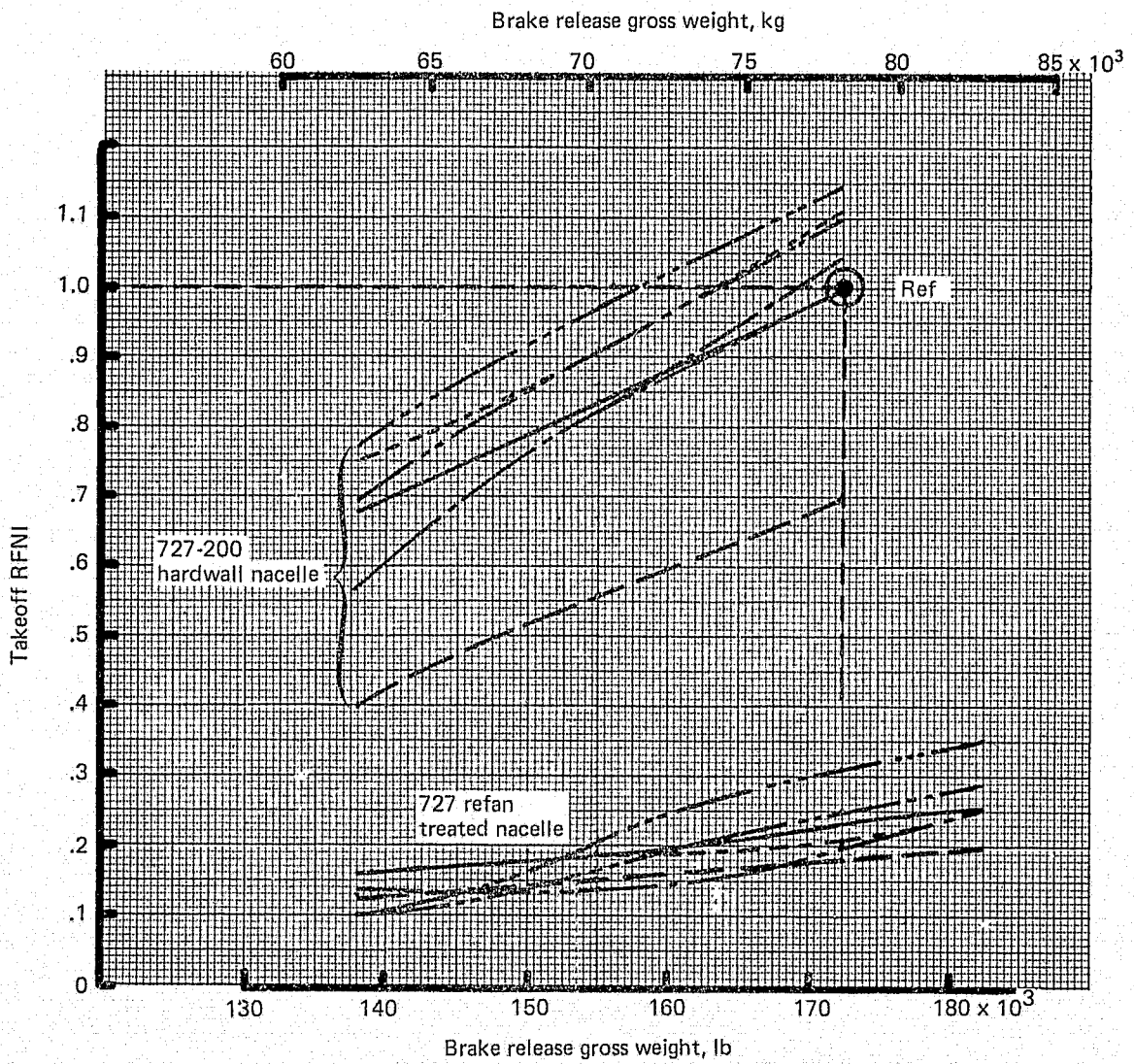

Figure 66.—727-200/727 Refan Takeoff RFNI

Note:

- Airplane: 727-200/727 refan
- Approach condition: Flap position = 30°
- Noise extrapolation condition: Temp = 77°F (298 K)
  Relative humidity = 70%
- EPNL calculation: Corrected to 727-200 flight test data
  +5 EPNdB limit on duration correction

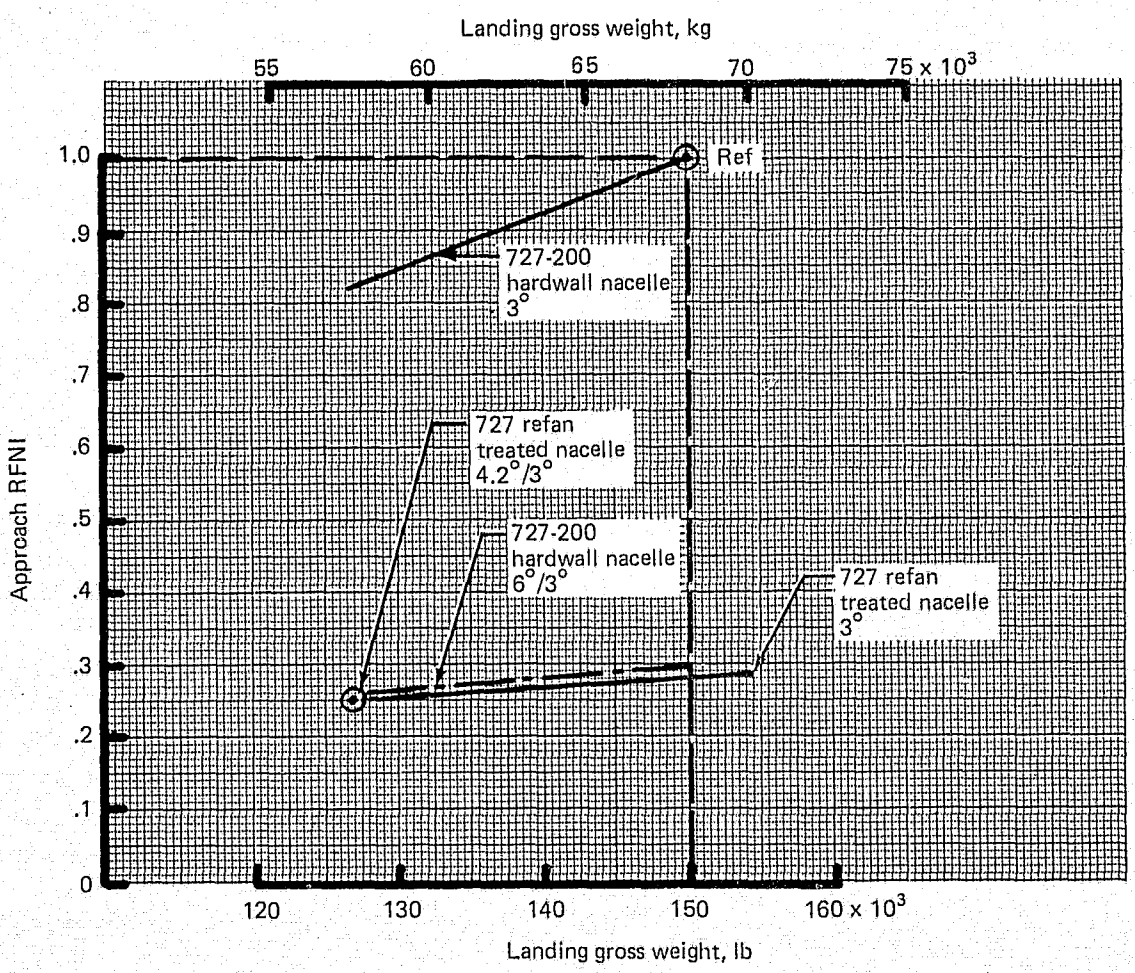

Figure 67.—727-200/727 Refan Approach RFNI

Note:

- Airplane: 727-200/727 refan
- Takeoff condition: Flap position = 5°
- Approach condition: Conventional 3° approach
  Flap position = 30°
- Noise extrapolation condition: Temp = 77°F (298 K)
  Relative humidity = 70%
- EPNL calculation: Corrected to 727-200 flight test data
  +5 EPNdB limit on duration correction

Legend:

- MFPOP
- FAR
- ATA
- CI 1000
- CI 500
- ALPA

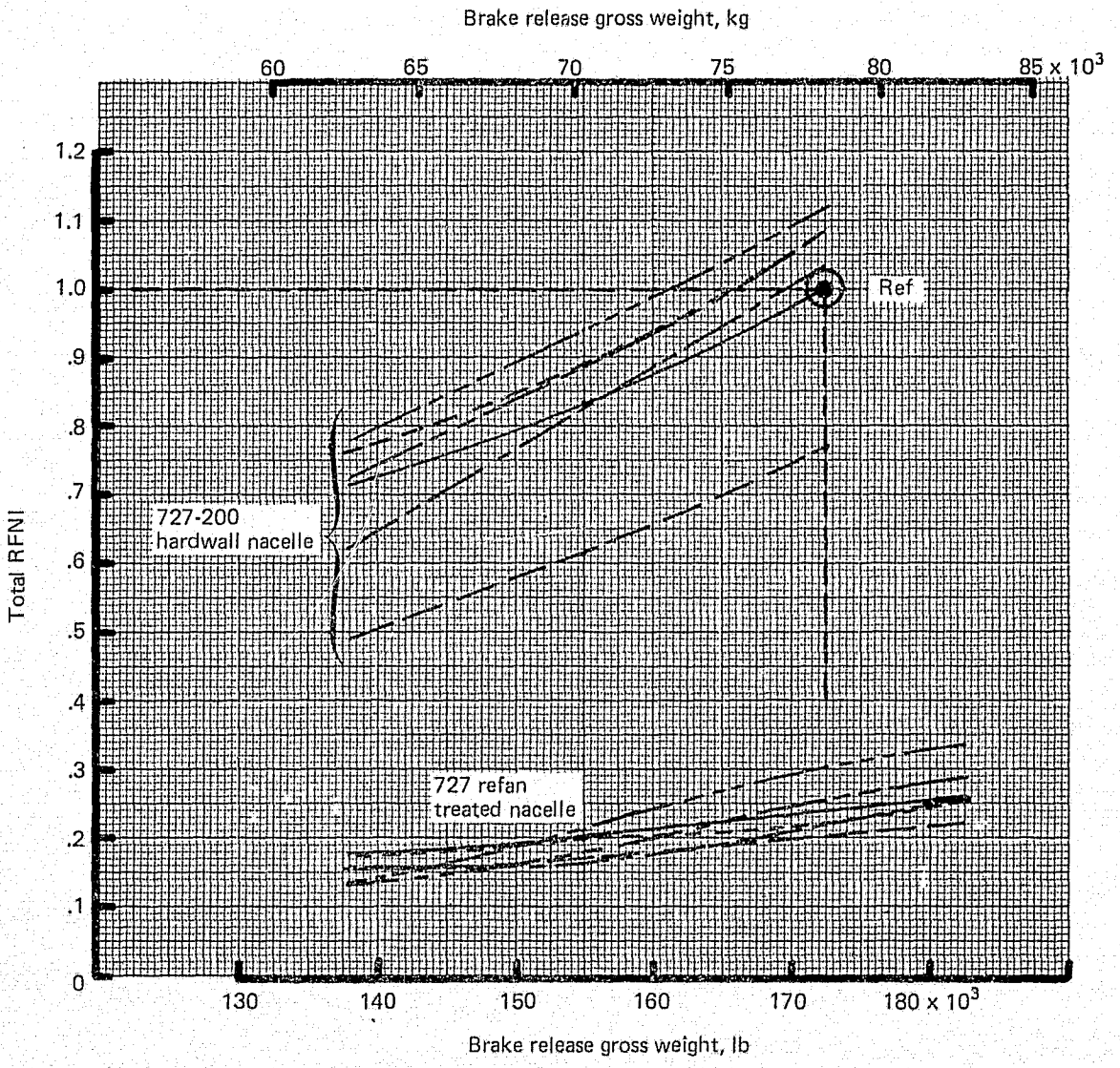

Figure 68.—727-200/727 Refan Total RFNI

Note:

- Airplane: 727-200 refan
- Takeoff condition: Flap position = 5°
- Approach condition: LGW = 150 000 lb (68 039 kg)
  or 126 700 lb (57 470 kg)
  Conventional 3° approach
  Flap position = 30°
- Noise extrapolation condition: Temp = 77°F (298 K)
  Relative humidity = 70%
- EPNL calculation: Corrected to 727-200 flight test data
  +5 EPNdB limit on duration correction

Legend:

- MFPOP
- FAR
- ATA
- CI 1000
- CI 500
- ALPA

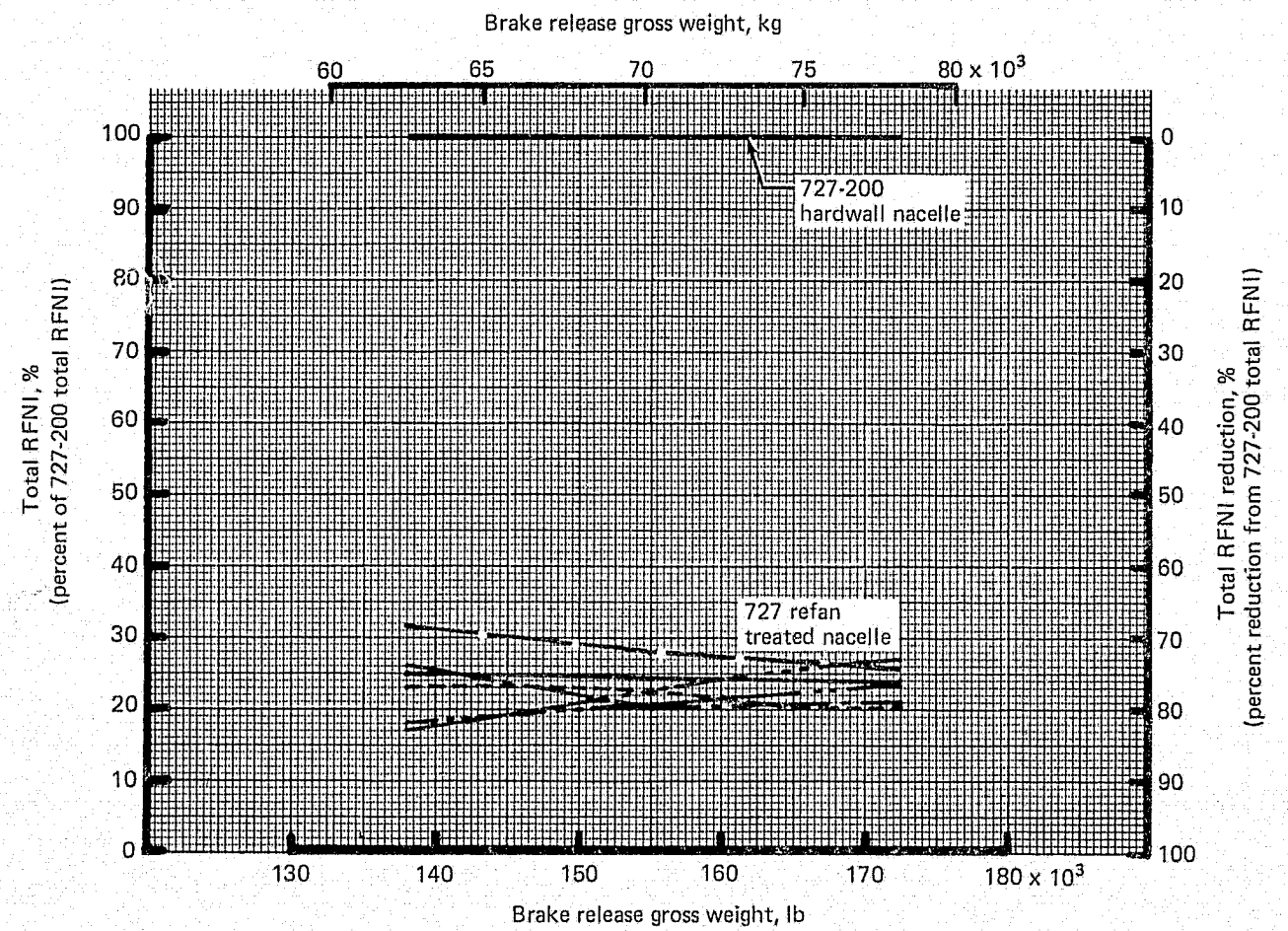

Figure 69.—727-200/727 Refan Total RFNI Reduction

3.3.1 UNINSTALLED PERFORMANCE

Uninstalled engine performance was obtained directly from customer computer decks provided by P&WA. Uninstalled JT8D-9 (baseline) performance was obtained from P&WA customer deck number CCD-219-01.1 and uninstalled performance JT8D-109 (refan) was obtained from P&WA customer deck number CCD-287-0.0. The JT8D-109 engine deck includes P&WA ground test data and NASA LeRC altitude chamber data to arrive at the engine specific fuel consumption (SFC) characteristics. Both the JT8D-9 and -109 engine decks provide minimum thrust estimates. The JT8D-9 engine deck provides estimated average fuel flow. The JT8D-109 engine fuel flow is representative of that obtained from P&WA ground tests and estimated altitude performance; however, the JT8D-9 and -109 SFC characteristics discussed are considered nominal for the purposes of this report.

The JT8D-9 engine deck performance characteristics were based on a large number of engines built over a long time period and therefore represent a mature engine. The JT8D-109 engine deck is based on test results from ground rig component tests and one engine tested at sea level and altitude. It therefore does not represent the same level of maturity as the JT8D-9 with respect to SFC. Both engine decks use fuel with a heating value of 18 400 Btu/lb (42.82×10^6 J/kg). A comparison of the uninstalled takeoff thrust lapse rate and typical cruise SFC characteristics is shown in figure 70.

The takeoff thrust lapse rate comparison shown at the top of figure 70 illustrates the uninstalled takeoff thrust benefit the JT8D-109 has over the JT8D-9 as a function of takeoff airspeed for a sea level, standard day, 59°F (288 K). At the static conditions, the JT8D-109 thrust benefit amounts to 14.5%. At 110 kn (56.6 m/s) the JT8D-109 thrust benefit has decreased to 9% and at 250 kn (128.6 m/s) the thrust benefit has further decreased to 3.7%. The decrease in JT8D-109 takeoff thrust benefit relative to the JT8D-9 as airspeed increases is due to the higher bypass ratio of the JT8D-109 engine. In general, increases in engine bypass ratio cause the slope of thrust lapse rate curves to become steeper.

The uninstalled cruise SFC performance comparison at $M_\infty = 0.84$ and 30 000 ft (9144 m), standard day, is shown in the lower portion of figure 70. Two levels of performance are shown for the JT8D-9 engine. One represents nominal (average) thrust SFC and the other represents specification levels of SFC. The JT8D-109 SFC is shown only for a nominal engine since specification performance estimates do not exist. Comparisons between the nominal JT8D-9 and -109 SFC characteristics show that at an uninstalled, approximate midcruise net thrust of 4150 lb (18 460 N), the SFC's of the two engines are the same.

3.3.2 SIDE-ENGINE INLET

The 727 refan side-engine inlet was designed so that it could be operated with an acoustic splitter ring. The inlet diameter was increased over that used in the existing 727-200 side-engine inlet to accommodate the increased refan airflow. Figure 71 shows the details of the refan side-engine inlet. Reference 4 (section 3.1.1) describes the design and manufacturing details of the side-engine inlet. Reference 5 describes the aerodynamic analysis of the design and the 3/10 scale model test results of the hardwall side-engine inlet configuration. Reference 3 (section 4.1.2.4) describes the Contractor full-scale ground test results for the refan side-engine inlet.

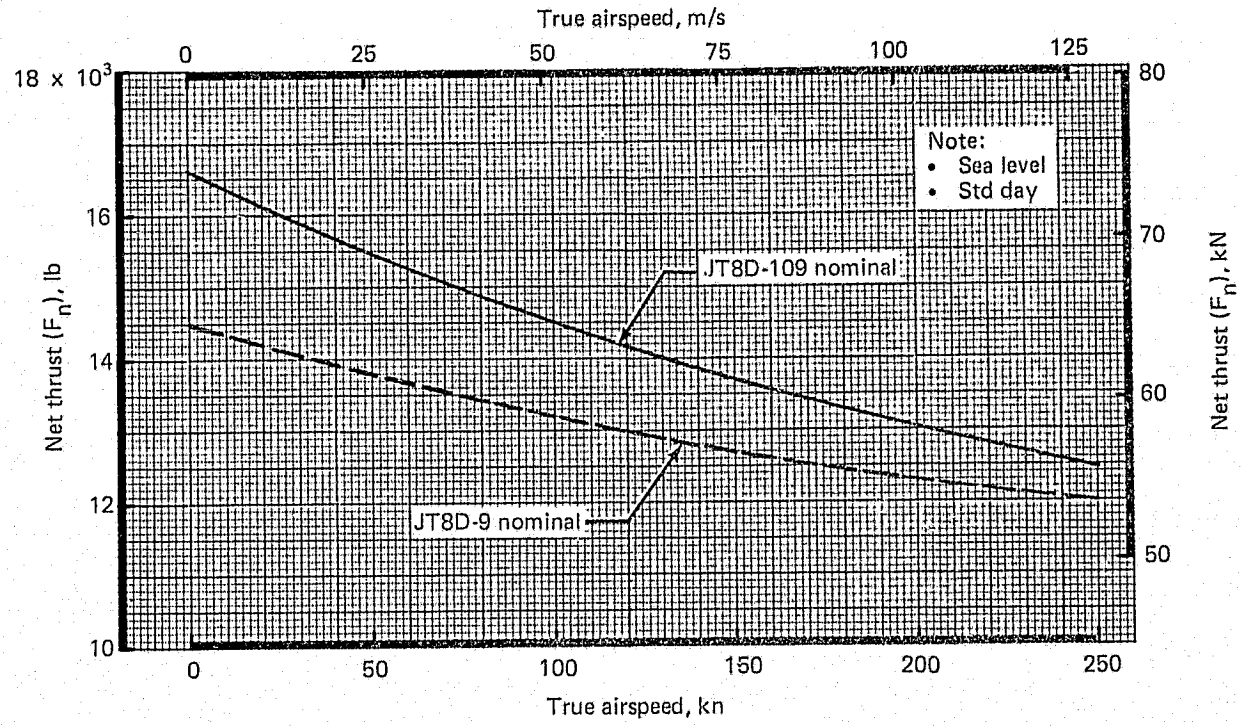

(a) Uninstalled Takeoff Lapse Rate Comparison

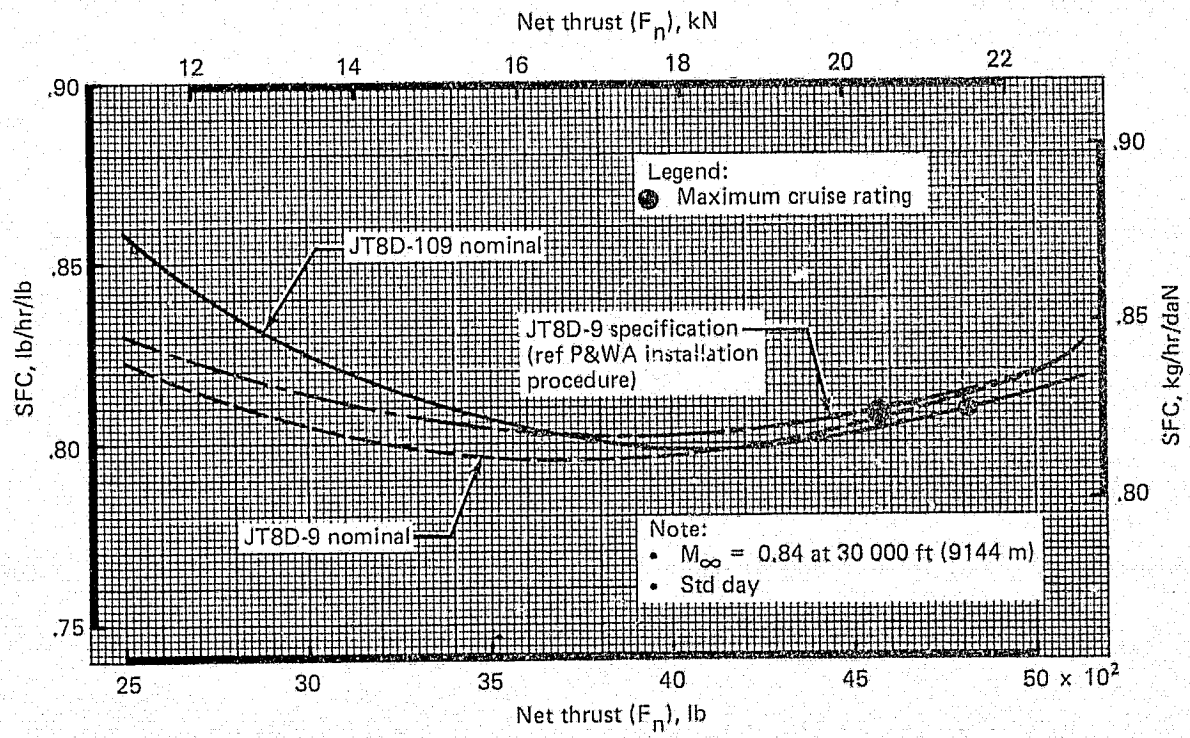

(b) Uninstalled Cruise Performance Comparison

Figure 70.—Uninstalled Engine Performance Comparisons

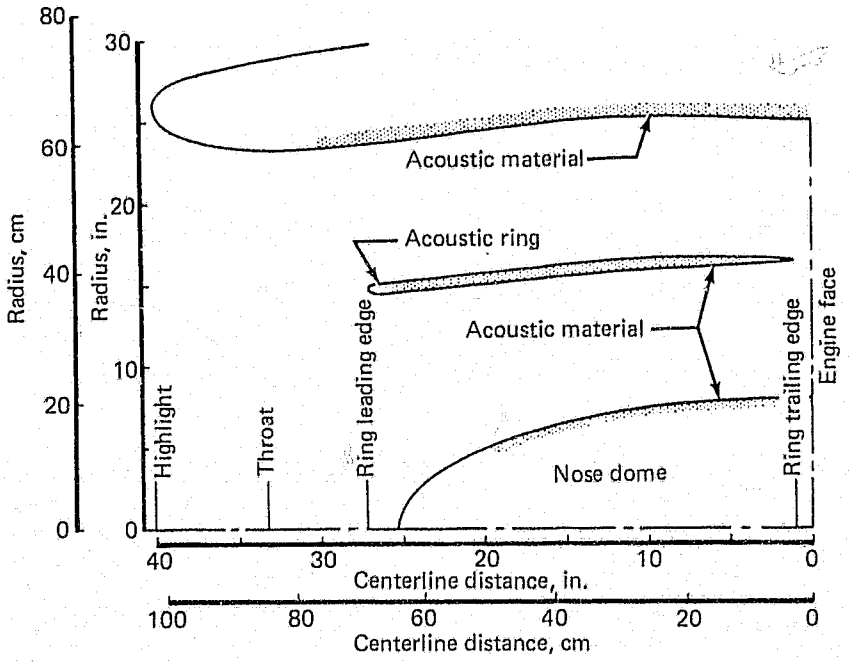

Throat diameter	46.7 in. (118.62 cm)
Throat area	1712.9 in.^{2} (11 051 cm^2)
Contraction ratio (highlight area/throat area)	1.25
Engine face diameter	50.1 in. (127.25 cm)
Nose dome diameter	16.0 in. (40.64 cm)
Engine face area	1770.3 in.^{2} (11 421 cm^2)
Engine face area/throat area	1.034
Nose dome length	25.2 in. (64.01 cm)
Inlet length/engine face diameter	0.8
Splitter ring diameter at trailing edge	32.9 in. (83.57 cm)
Ring length (℄)	26.2 in. (66.55 cm)
Distance ring leading edge to throat	6 in. (15.24 cm)

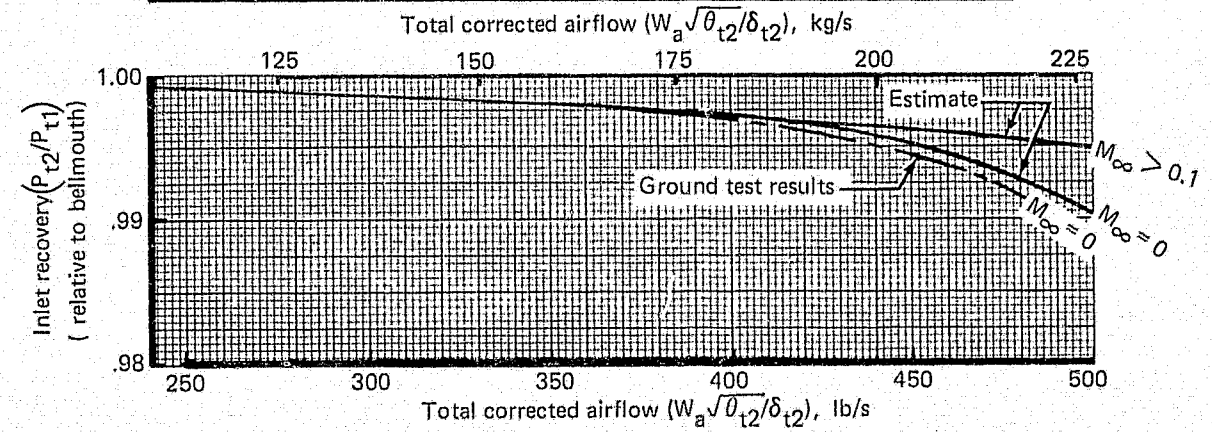

Figure 71.—727 Refan Side-Engine Inlet

The side-engine inlet full-scale total pressure recovery (including acoustic lining losses) was estimated, based on analysis and the model-scale hardwall data prior to the full-scale ground test. Both the estimate and the ground test total pressure recoveries are shown in figure 71. Since the original estimate and the ground test recovery levels were equal within 0.1%, the estimated recovery values were used in the 727 refan performance evaluation for purposes of convenience.

3.3.3 CENTER-ENGINE INLET AND DUCT

The 727 refan center-engine inlet and duct were designed with a minimum of modifications for the existing 727 airplane, but with an increased duct area to meet the increased refan airflow requirement. The JT8D-109 engine requires approximately 45% more airflow at cruise then the existing JT8D-9 engine. Figure 72 shows the 727 refan center-engine inlet and duct. Reference 4 (section 3.1.5) describes the design and manufacturing details of the center-engine inlet installation. Reference 6 describes the aerodynamic analysis of the design and the 3/10 scale model test results of the hardwall configuration. Reference 3 (section 4.1.2.4) describes the Contractor's full-scale ground test results for the center-engine inlet.

The center-engine inlet duct full-scale total pressure recovery (including acoustic lining losses) was estimated, based on analysis and the model-scale hardwall data prior to the full-scale ground test. Both the estimate and the ground test total pressure recoveries are shown in figure 72. Since the original estimate and the ground test recovery levels were equal within 0.2%, the estimated recovery values were used in the 727 refan performance evaluation for purposes of convenience.

3.3.4 EXHAUST SYSTEM

Reference 4 describes the materials, fabrication, and mechanical design of the 727 refan flight exhaust system and associated thrust reverser. This section describes the aerodynamic considerations that resulted in the selected exhaust system geometry.

3.3.4.1 Nozzle Aerodynamic Design

The following are the major factors that influenced the final geometry:

- Commonality to the maximum extent possible between the flight configuration and the reference hardware
- Engine match, which depends on mixing plane and nozzle exit geometry
- Commonality of outer exhaust duct (wedge duct and nozzle) wall for all JT8D-100 series engines (JT8D-109, -115, -117)
- Length of the exhaust duct, which was a compromise between rotation restraints, mixing length requirements, and the dimensional requirements of the target-type thrust reverser

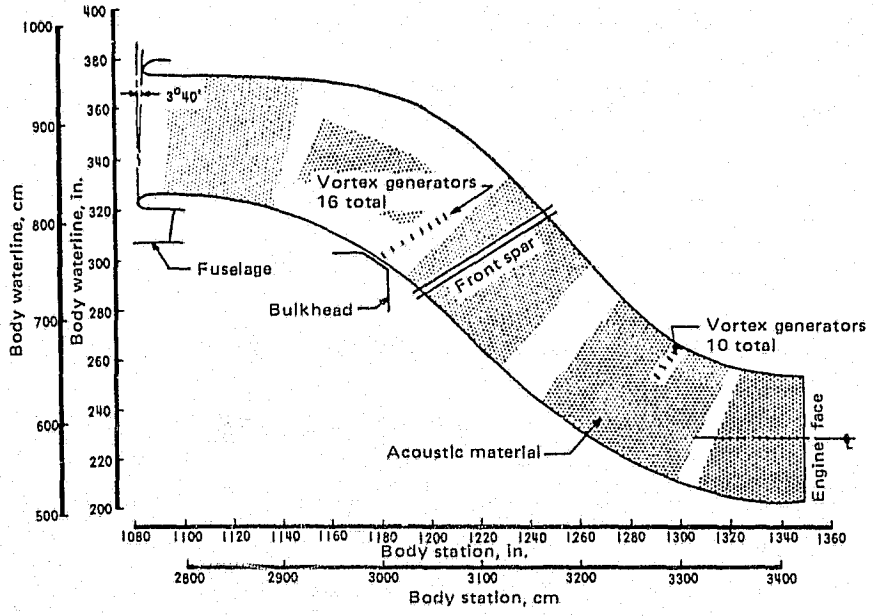

Throat diameter	47.8 in. (121.4 cm)
Throat area	1794.5 in.^{2} (4558 cm^2)
Contraction ratio (highlight area/throat area)	1.30
Engine face diameter	50.1 in. (127.25 cm)
Nose dome diameter	16.0 in. (40.64 cm)
Engine face area	1770.3 in.^{2} (11 421 cm^2)
Engine face area/throat area	0.99
Nose dome length	25.2 in. (64.01 cm)
Offset ratio (inlet length/inlet height)	2.1

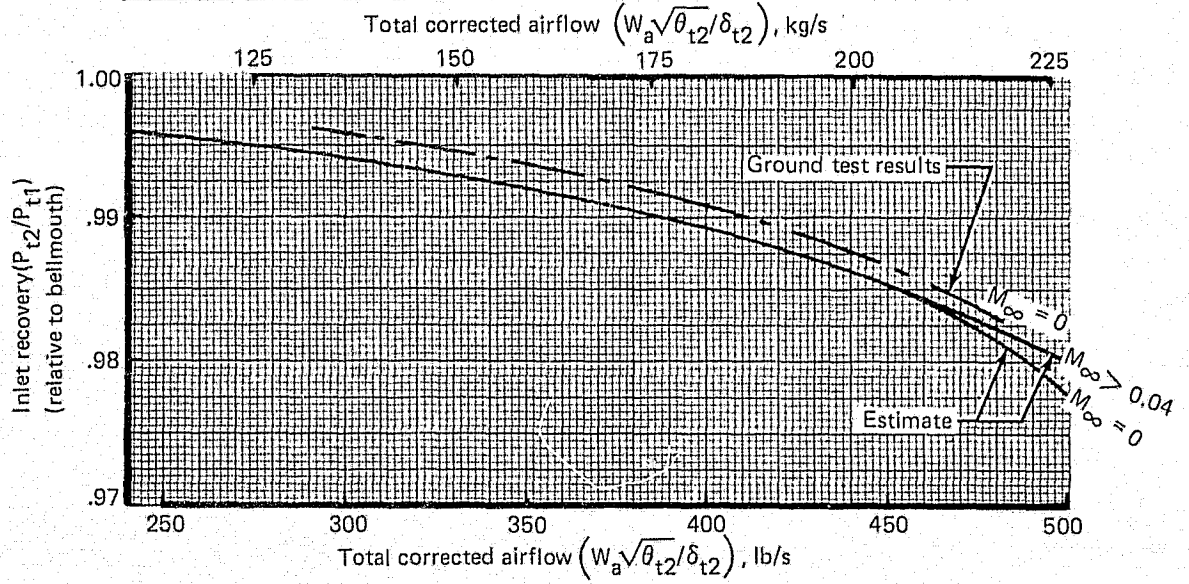

Figure 72.—727 Refan Center-Engine Inlet and Duct

All these factors are interrelated. P&WA and the Contractor agreed to have commonality of the outer nozzle wall to a location 21 in. (53.3 cm) downstream of the engine rear flange. The flight exhaust duct was manufactured with a slight taper downstream of this location, as compared to the parallel walls of the reference nozzle, to accommodate the thrust-reverser design. The flight exhaust duct length was restricted by the rotation restraints to 66 in. (167.6 cm) as opposed to the reference exhaust duct which was 70 in. (177.8 cm) long. Both exhaust systems have convergent conical nozzles.

The mixing-plane and nozzle-exit geometries providing proper match of the engine were based on inputs from P&WA and results of the Contractor's model nozzle tests (ref. 7).

The concepts adopted for accommodating the different geometric requirements of the different models of the JT8D-100 series engines were as follows:

- Variation of the mixing plane area split required to match the various refan engine models was accomplished by varying the primary/secondary flow divider (splitter) radial position while maintaining a common plug. To facilitate the thrust-reverser design, which was to be common for all engine models, it was decided to maintain a constant nozzle half angle. The nozzle length was varied to accommodate the nozzle-exit area changes required to match the different engine models.

- Outer nozzle wall cone angle was selected with two requirements in mind. One was to have adequate area change available to satisfy the area match requirements of the various JT8D-100 series engines as noted above. The other was to depress the engine idle thrust as much as possible by tailoring the exhaust system geometry, since the -100 series engines tend to produce more idle thrust than the corresponding basic JT8D models. The differences in exhaust system geometry (splitter length, mixing plane total area, nozzle half angle, and mixing length) between the reference and flight configurations led to a corresponding difference in discharge coefficients.

A trade study was accomplished to determine the exhaust duct length. This trade study considered airplane performance and noise characteristics as influenced by the exhaust duct length. Those features influencing airplane performance were exhaust system performance (C_V), weight, and airplane rotational capability. The acoustic considerations related primarily to the treatment area available. The mixing length available downstream of the splitter was a consideration from the standpoint of both the exhaust system performance and the acoustic performance. The resultant exhaust duct length was 66 in. (167.6 cm). In addition, the nozzles were canted upward 3°30' relative to the engine centerline. For the center-engine installation, this cant enhanced the airplane rotational capability at the expense of a small cosine thrust loss. For the side-engine installations, this cant directs the exhaust flow parallel to the airplane centerline.

3.3.4.2 Nozzle Performance

Model and full-scale tests conducted by the Contractor (refs. 7 and 3, respectively) demonstrated that the performance, in terms of velocity coefficient (C_V), is identical for the reference and flight configurations. The discharge coefficient of the flight nozzle was different from that of the reference nozzle with the differences depending on the engine model (-109, -115, or -117). The differences were partly due to internal aerodynamics of the long flow

divider relative to the short divider and partly due to the nozzle cone angles as discussed previously. The differences between the reference and flight nozzle discharge coefficients were accounted for in the flight nozzle geometric areas required to provide the same nozzle effective areas. As a consequence, the installed engine performance calculated in section 3.3.11 for the flight exhaust nozzle configuration shows no thrust penalty relative to the reference exhaust system, while accommodating the aircraft design requirements.

3.3.5 THRUST REVERSER

A target-type thrust reverser was selected for use on the 727 refan to replace the clamshell/deflector door thrust reverser currently used on the 727-200. This choice was made in the interest of weight, reliability, clean internal nozzle contours, and the absence of reverser installation losses relative to the exhaust nozzle. The mechanical design and features of the target-type thrust reverser are described in reference 4.

3.3.5.1 Thrust-Reverser Efficiency and Match

Static model tests were conducted to develop suitable configurations which would provide adequate reverse thrust efficiency and satisfy the requirements of reverse thrust match. These tests are reported in reference 8 and resulted in candidate configurations for the low-speed wind tunnel test.

The candidate configurations proposed for wind tunnel test were all of fixed lip height (the variable lip height having demonstrated no advantage in the static tests) and with fences tapered to zero height from the maximum lip height.

Constant lip heights of 3.5 in. (8.9 cm) and 1.5 in. (3.8 cm) were chosen to be candidate configurations with recommended setback ratios (ratio of distance from nozzle exit to the doors in the deployed position, to the nozzle exit diameter) of unity. These configurations, tested with a door length exhaust nozzle diameter ratio of 1.05, resulted in reverse thrusts of 46.5% and 38% of forward thrust, respectively, at takeoff nozzle pressure ratio.

All three configurations exhibited match acceptable to the Engine Contractor (see ref. 8).

Static pressure surveys on the door internal surface were made on selected configurations during the static test. These data were used to obtain door loads for use in the structural design of the thrust reverser/exhaust duct system.

Tests with no lips on the doors showed that the reverse thrust was only about 15% of forward thrust. Since this was a possible solution to hot-gas ingestion problems of the side engines, if used in combination with a high-performance configuration on the center engine, it was also a candidate configuration.

3.3.5.2 Ingestion Speed and Aircraft Interference Effects

Low-speed wind tunnel model tests were conducted to determine the thrust-reverser configuration most compatible to the 727 refan airplane. This test was reported in reference 9. The main aspects of the investigation concerned hot-gas ingestion, effects on airplane controllability, interference between the reversed gas flows and the airplane aerodynamics, and hot-gas impingement on the airplane structure. Variables investigated included the thrust-reverser geometry as described in section 3.3.5.1, the side-engine thrust-reverser clock angle relative to the vertical, the wing trailing-edge flap angle, and the engine thrust level in terms of engine pressure ratio (EPR). The criterion for thrust-reverser compatibility with the 727 refan was the capability to stop the refan airplane in a ground roll distance equal to or less than that available with the 727-200. The best reverser capability was primarily associated with the lowest tunnel velocity at which inlet ingestion of exhaust gases occurred; other factors were the changes to airplane lift, drag, and directional control.

Significant test results that would influence the 727 refan stopping distance included:

- *Thrust-Reverser Lip Height.*—In general, the 1.5-in. (3.8-cm) lip fence gave the lowest full-power ingestion speeds, 92 kn (47.3 m/s), while retaining reverse thrust efficiency comparable to the 727-200 configuration. The 3.5-in. (8.9-cm) lip provided an ingestion speed at full power approximately 10 kn (5.1 m/s) higher than the 1.5-in. (3.8-cm) lip.

- *Clock Angle.*—As the top reverser doors were rotated toward the vertical tail, ingestion speeds tended to decrease, thus allowing longer reverser operation. Rotation of the top reverser door from the vertical to 20° inboard decreased the ingestion speed by approximately 25 kn (12.8 m/s).

- *Airplane Interference Effects.*—For the combination of lip heights and clock angles investigated, thrust-reverser operation tended to reduce airplane drag, increase lift, and decrease pitching moment. These changes in airplane characteristics tend to increase landing roll distances.

    - *Exhaust gas impingement on airplane structure.*—No hot-gas impingement problems would exist on the airplane structure (based on the thermocouple coverage of the airplane model) for a thrust-reverser orientation range of 0° to -20°. In general, the highest measured temperatures occur on the lower portion of the airplane fuselage.

    - *Airplane controllability.*—Airplane controllability may be reduced as the thrust-reverser doors are tilted toward the rudder. This was indicated by measuring the tunnel dynamic pressure in the vicinity of the rudder. No dynamic pressure loss occurred with the thrust-reverser doors in the vertical position. As the reverser clock angle approached -20°, significant dynamic pressure loss was apparent.

3.3.5.3 Landing Roll Analysis

The 727 refan stopping characteristics with thrust reversers only were determined using information discussed in sections 3.3.5.1 and 3.3.5.2 in a landing roll evaluation. The thrust-reverser variables selected as most likely to provide 727 refan landing distances comparable to the 727-200, using comparable operational procedures, included:

- 1.5-in. (3.8-cm) lip height on all thrust-reverser doors
- Setting the side-engine reverser clock angles at -20°

This evaluation made use of an analysis that accounts for the influence of aerodynamic lift and drag, reverse thrust, and aircraft brake application. The effects of delay times for pilot operation of wing spoilers, wheel brakes, reverser actuation, engine spin-up time in reverse, and modulation of the engine power at lower airplane speeds are included. Since the reduction in ground roll distance when using the thrust reversers is small compared with that using even moderate wheel braking, the landing roll studies were performed using no wheel braking, but the studies did account for rolling resistance. This was considered to provide a better basis for comparison of reverser stopping capability and to determine the ground roll distance for a no-brakes landing. Landing on an icy runway would approach this condition since the influence of the reversers in stopping the airplane is considerably more important. The calculations were performed using the same delay times, touchdown speeds, and operational procedures for both the 727 refan and 727-200 airplanes where appropriate. Engine power is assumed to be reduced from the maximum available during the ground roll to prevent exhaust gas ingestion into the inlet and provide longer reverser operation time. The major input differences to the analysis relative to the 727-200 airplane were the engine spin-up times, thrust-reverser performance, and aerodynamic interference effects.

Figure 73 compares the spin-up characteristics of the JT8D-9 and -109 engines. The estimated spin-up time of the larger fan engine is approximately 30% longer than for the JT8D-9 engine. The slower spin-up time results in reduction of the time available at the maximum permitted reverse thrust EPR, before the airplane speed drops to 70 kn (36 m/s) where the throttle is retarded as shown in table 30.

Figure 74 shows the comparable EPR schedule for given JT8D-9 and -109 thrust-reverser characteristics as a function of airplane speed. The schedule for the JT8D-109 is identical to the procedure currently employed on the 727-200 airplane, thereby introducing no new pilot operational procedure. The schedule is shown in relationship with the maximum permissible EPR to prevent ingestion with -20° clocking of the reversers.

Figure 75 shows a comparison between the JT8D-9 and -109 effective reverse thrust per engine available as a function of airplane speed. The data include the loss of airplane drag due to aerodynamic interference. The engine spin-up schedule is not shown since this will depend upon the speed at which reversers are applied.

Figure 76 shows the no-brake application, wet runway, landing distance for the 727-200 airplane compared to the predicted 727 refan, using reversers and spoilers only, for various airplane landing weights at 40° flaps. The landing distance is made up of the ground roll distance plus the air distance from the runway threshold altitude (50 ft (15.2 m)).

The stopping capability of the target-type thrust reverser on the 727 refan airplane is estimated to be slightly better than the current clamshell/deflector door installation. This is achieved without changing the pilots' procedure for operating the thrust reversers. The higher reverser performance from the target-type thrust reverser compensates for the slower spin-up time of the JT8D-109 engine. The JT8D-109 engine ingestion characteristics are

Table 30.—JT8D-9 and -109 Spin-Up Characteristics During Reverse Thrust Operation

Landing weight, lb (kg)	Airplane touchdown speed – flaps 40°, kn (m/s)	Time in seconds at maximum permitted reverse thrust EPR[a]	
		JT8D-9 EPR = 1.745	JT8D-109 EPR = 1.5
110 000 (49 895)	106 (54.5)	2.4	None
120 000 (54 431)	111 (57.1)	3.8	1.3
130 000 (58 967)	117 (60.2)	5.3	2.8
142 500 (64 637)	124 (63.8)	7.5	4.4

[a] Assuming acceleration schedules as in fig. 73

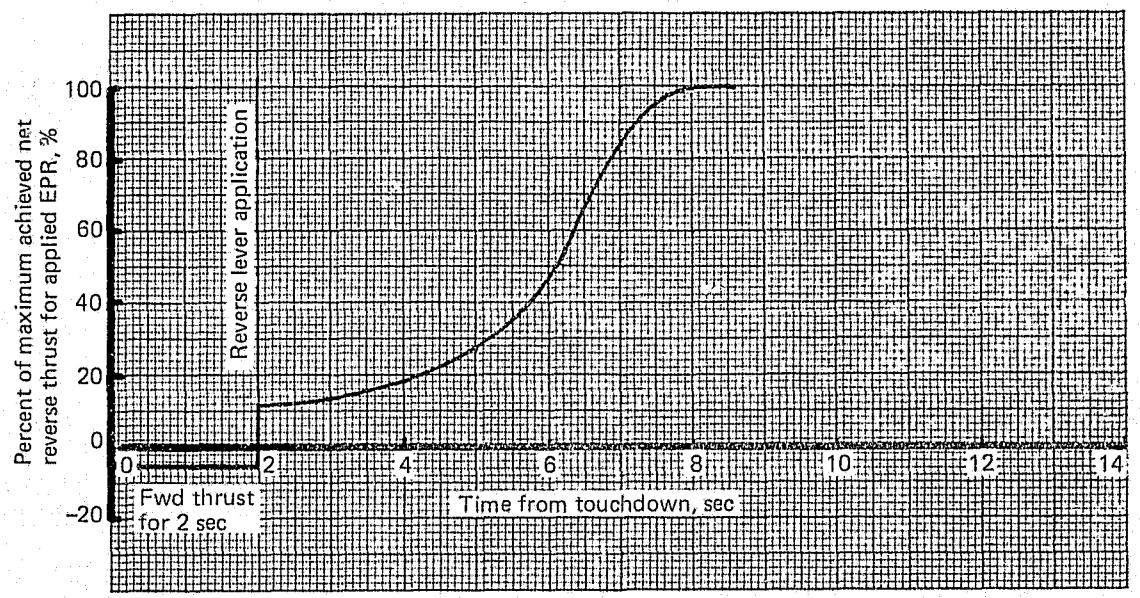

(a) JT8D-9 Engine

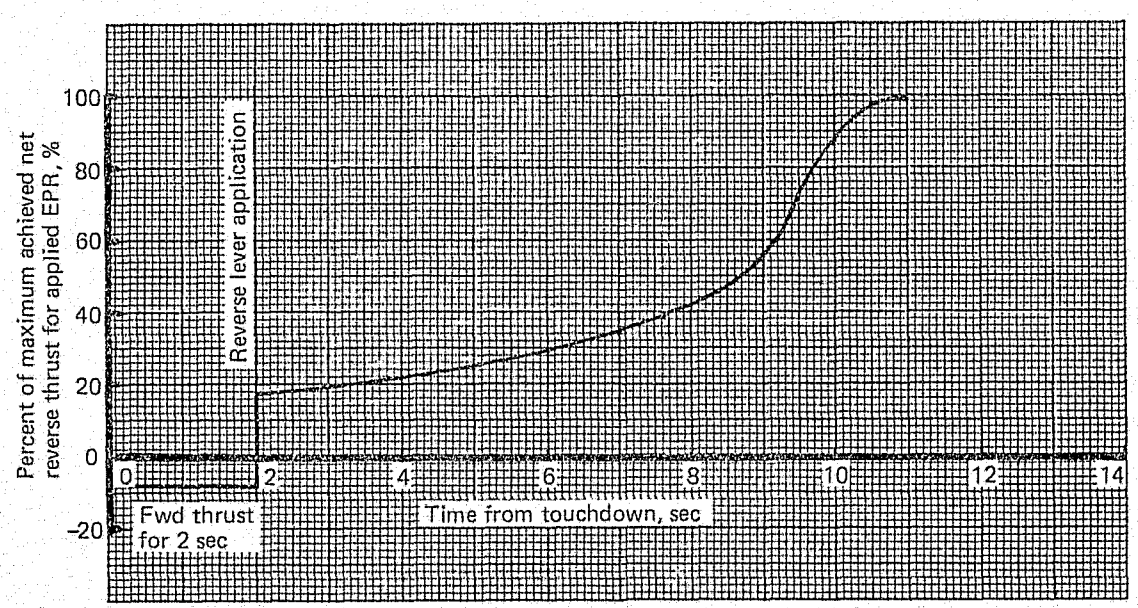

(b) JT8D-109 Engine

Figure 73.—JT8D-9 and -109 Engine Estimated Reverse Thrust Spin-Up Schedule

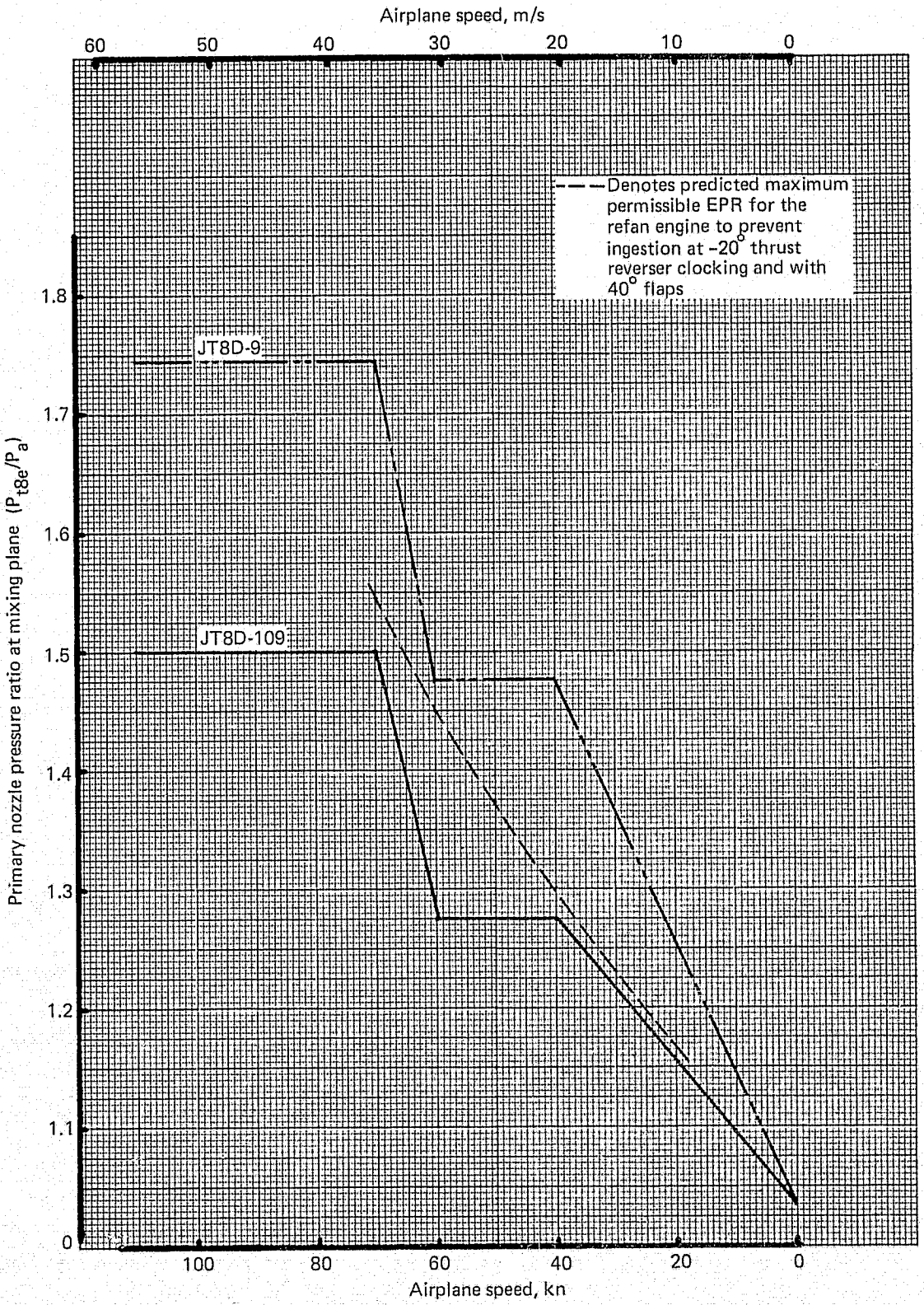

Figure 74.—Reverse Thrust Engine Pressure Ratio Schedule Versus Airplane Speed

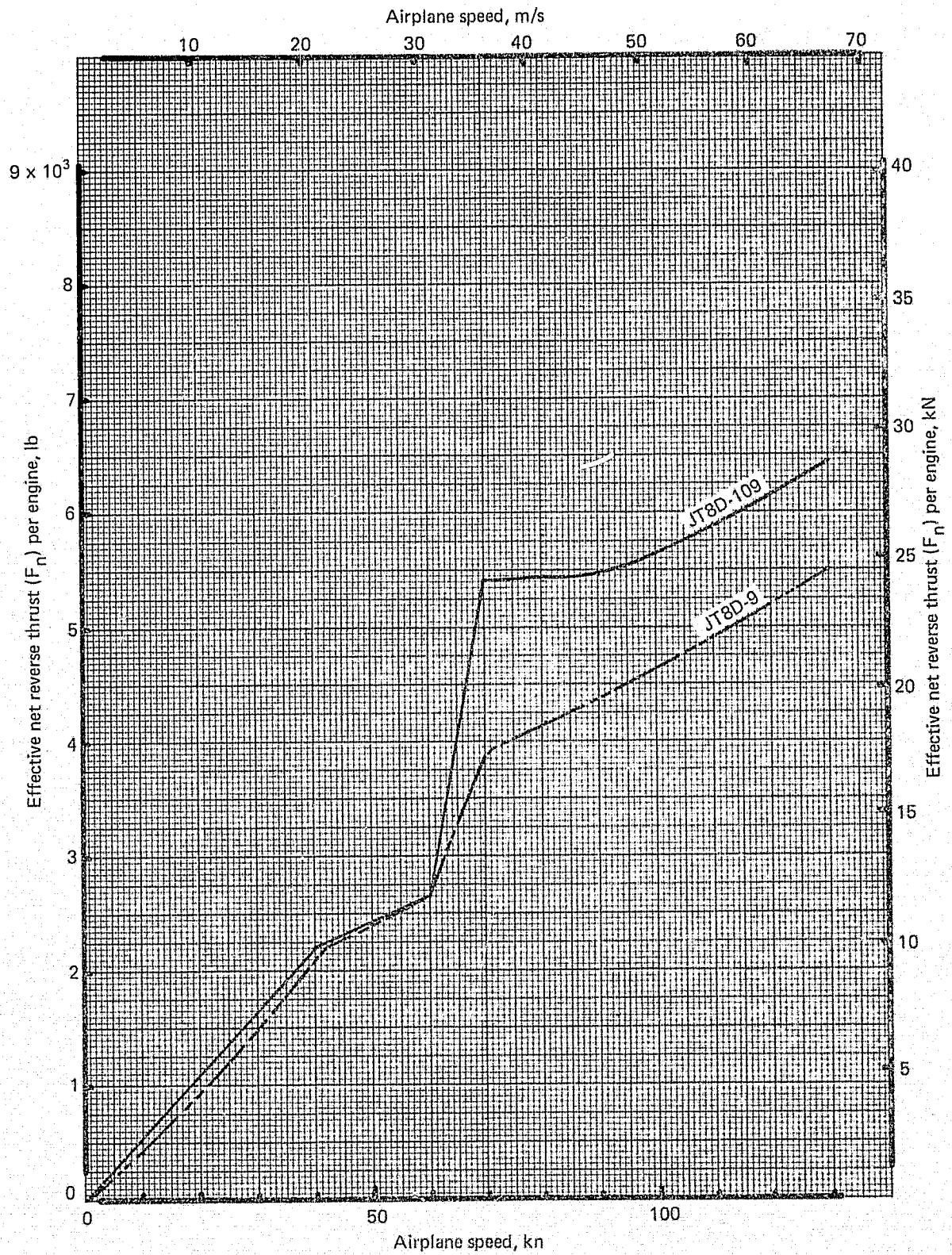

Figure 75.—Effective Net Reverse Thrust Per Engine for JT8D-9 and JT8D-109

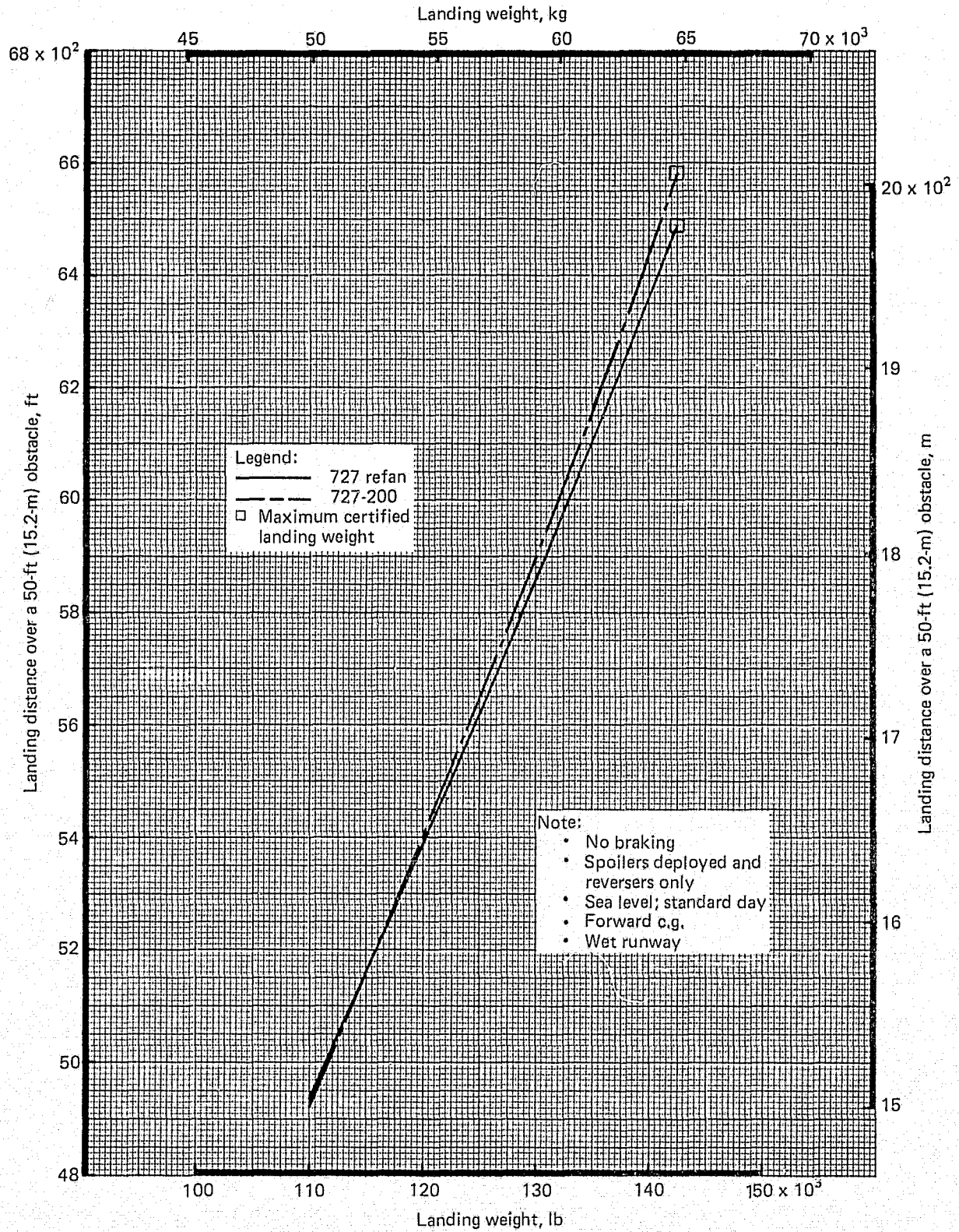

Figure 76.—Comparison of 727-200 and 727 Refan Landing Distance—40° Flaps, -20° Thrust-Reverser Clocking

based on estimates of the tolerance of the engine to hot-gas ingestion and do not account for possible inlet pressure distortion. The exact operational procedure and final 727 refan airplane configuration effects can only be determined from full-scale taxi tests.

3.3.6 NACELLE INSTALLATION SUBSYSTEMS

The nacelle subsystems (such as cowls, starters, generators, etc.) installed on the JT8D-109 engine were designed and selected to minimize the cost of retrofit. Nacelle subsystems were therefore changed only for the following reasons: maximum engine diameter increase, engine performance differences, or the subsystem environment changes. Reference 4 discusses the required hardware changes.

3.3.6.1 Nacelle Design Maximum Operating Temperatures

Table 31 lists the maximum operating temperatures for which the JT8D refan engine hardware was designed. These temperatures are based on a hot day takeoff power setting of a JT8D-117 engine rather than for the JT8D-109. The JT8D-117 engine would be the the highest thrust rated engine in the JT8D-100 series and would be a refan derivative of the production JT8D-17 engine. Thus the hardware designed would be compatible with the more severe temperature environment of the -117 engine. The higher temperatures were estimated using a computer simulation of the JT8D-117.

3.3.6.2 Cowl Panel Fire Test Results

The cowl panel fiberglass/honeycomb construction for the JT8D refan engine installation was adopted to reduce the number of detailed parts and labor involved in fabrication of a typical riveted sheet metal cowling. A description of the cowl panels and their construction was reported in reference 4. Because the accessory compartment (i.e., the space between the engine case and cowl) is considered a fire zone, the cowl panels must be able to withstand a 2000°F (1366 K) temperature flame for 15 minutes to obtain FAA certification. Cowl panel fire tests of six types of honeycomb construction were conducted, which resulted in the selection of the following cowl panel construction because it was the only one to endure the 2000°F (1366 K) temperature for 15 minutes:

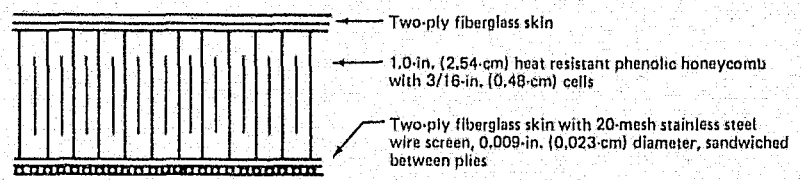

A 3-ft by 4-ft (0.9-m by 1.2-m) panel of this construction, with edges simulating the proposed cowl mating edges, was exposed to a 2000°F (1366 K) flame. A sketch and a photograph of the test setup are shown in figures 77 and 78. The panel was tested in a manner similar to that used for the certification fire tests of the existing 727 cowl panels, including the provision for blowing

Table 31.—JT8D-117 Engine Nacelle Design Maximum Operating Temperatures

Nacelle hardware	JT8D-117 Engine nacelle design maximum operating temperatures,[a] °F (K)
Nose cowl inner surface	[b]400 (478)
Inlet ring	[b]550 (561)
Nose dome	[b]290 (416)
Nose dome (internal)	[b]310 (428)
Outer fan duct wall	245 (392)
Inner fan duct wall (near turbine section)	1300 (978)
Fan/primary flow divider	1200 (922)
Exhaust plug	1200 (922)
Exhaust duct	245 (392)

[a] Based on sea level; 120°F (322 K) day; 380-kn (195-m/s) speed; takeoff power condition of the JT8D-117 engine

[b] Anti-icing condition

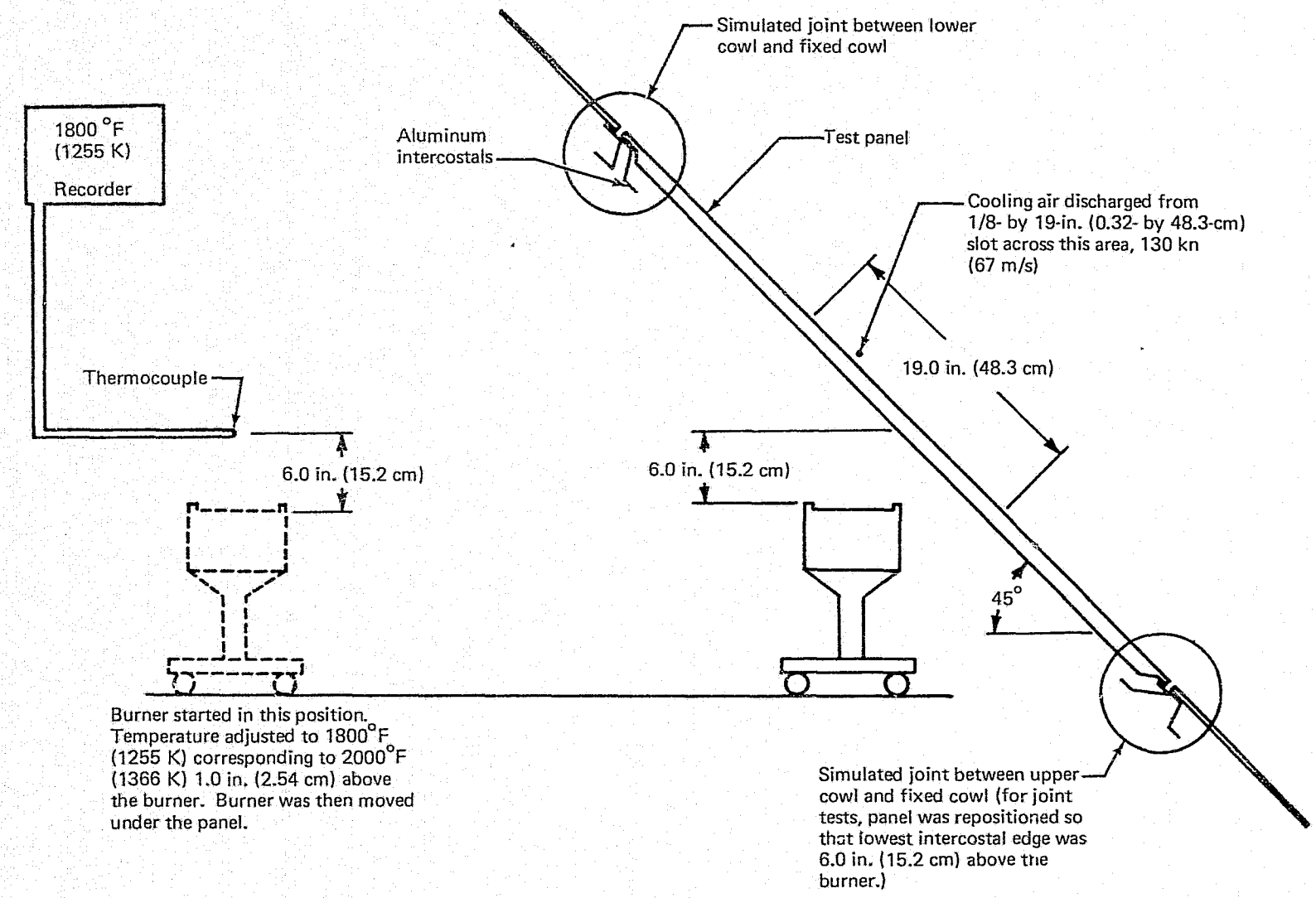

Figure 77.—Cowl Panel Fire Test Setup

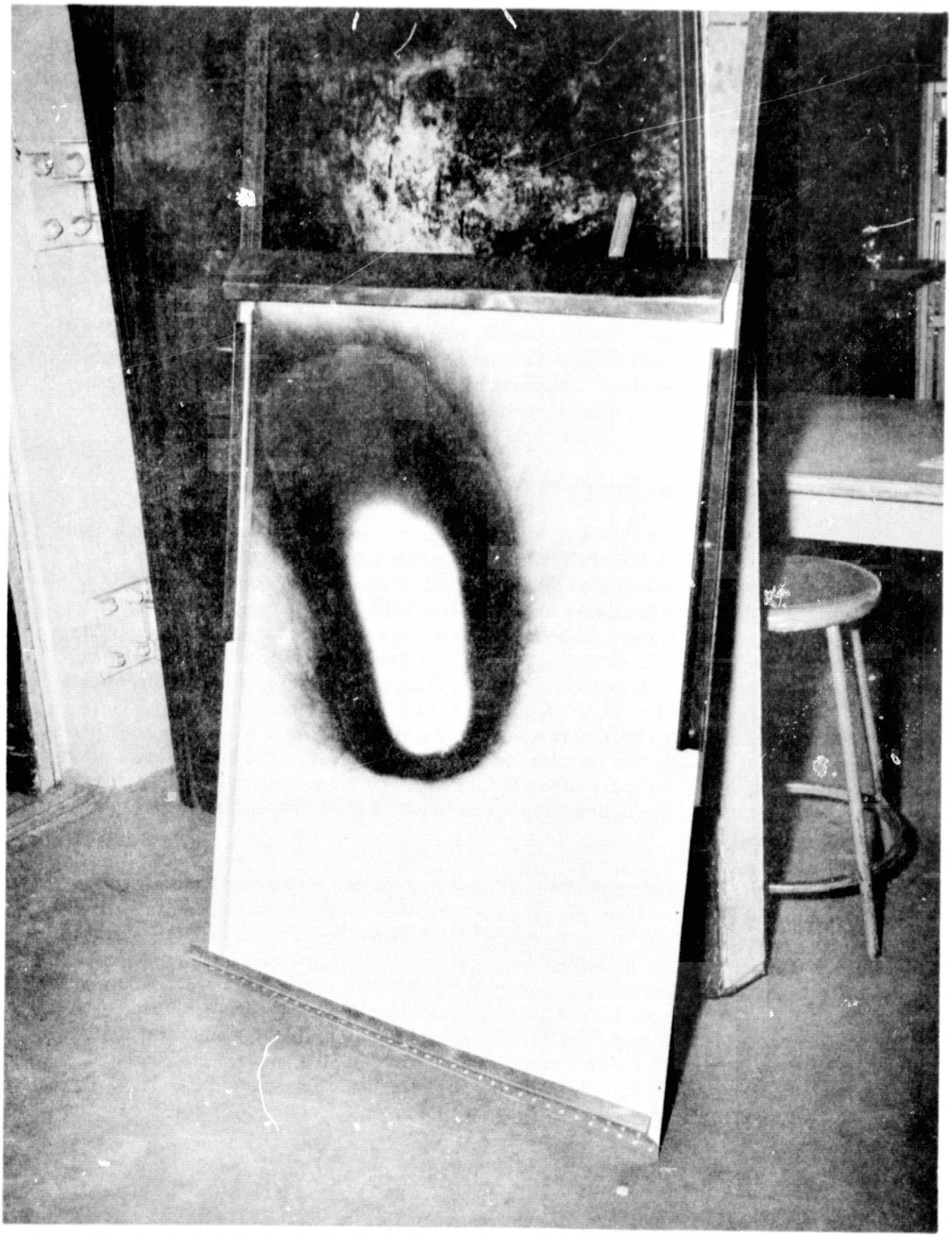

Figure 78.—Photograph of Cowl Panel Fire Test Setup

air over the external surface. During the previous 727 cowl fire tests, the thermocouple which measured 2000°F (1366 K) was mounted 1.0 in. to 2.0 in. (2.5 cm to 5.1 cm) above the burner. For the current test, the thermocouple was 6.0 in. (15.2 cm) above the burner, to match the distance from the burner to test panel. A calibration of the burner indicated that 1800°F (1255 K) at 6.0 in. (15.2 cm) corresponds to 2000°F (1366 K), 1.0 in. (2.5 cm) above the burner.

Test results are summarized in table 32. The cowl panel, plus the simulated cowling joints between the fixed cowl and removable cowls, passed the 15-minute fire test without burn-through. (See fig. 79.) The backside of all the hardware showed only scant evidence of even having been heated. Another objective was to investigate the problem of venting the gas that was generated during the first few seconds after heat was applied. The test showed that the panel quite easily *vented* the gases through the honeycomb structure in the region where the heat was applied. Additional tests would be required, however, to determine whether special venting provisions would be required to preclude burn-through or the possibility of explosion.

3.3.6.3 Cowl Temperatures Near Bleed Ducts

On the 727-200 airplane, the bleed ducts do not create a cowl heating problem because the thin aluminum skin is a good heat conductor and is adequately cooled by freestream air. The fiberglass/honeycomb side cowl panels designed for the refan installation are good insulators. Because of the proximity of the hot 8th- and 13th-stage compressor bleed ducts to the nacelle cowls, there was a problem of conducting away the energy radiated from the ducts to the cowling without exceeding the 350°F (450 K) temperature limit of the honeycomb panel. An analysis was performed which indicated that the expected 13th-stage bleed duct temperature of 681°F (634 K) produced a cowl inner wall temperature of 615°F (597 K); this occurred on a 50°F (283 K) day with icing conditions at sea level takeoff power setting. Subsequent engine data revealed the maximum 13th-stage bleed duct temperatures to be 732°F (662 K) for a hot day with a failed anti-icing valve at sea level takeoff power. The maximum 8th-stage bleed duct temperature of 545°F (558 K) would occur on a hot day takeoff condition.

To investigate the cowl heating problem, a test was conducted simulating the cowl panel and bleed duct as shown in figure 80. Temperatures were measured on the simulated bleed duct wall and on the metal wire screen sandwiched between the two inner plies of fiberglass at the center of the 14.0-in. by 36.0-in. (35.6-cm by 91.4-cm) cowl panel section. Figure 81 shows a sketch of the seven configurations tested. In addition, some of the configurations were tested after the bleed duct had been blackened by a kerosene flame. The temperatures recorded are shown in figures 82 and 83. These results indicate that the only configuration which adequately protects the cowl panel from the 350°F (450 K) limit at the bleed duct maximum temperature was with 0.4-in. (1.02-cm) insulation on the bleed duct. The design of the cowls did provide clearance for bleed duct insulation.

3.3.6.4 Cowl Internal Pressure Blowout Protection

In the event of a 13th-stage bleed duct failure, the cowl panels are protected from overpressurization by a pressure relief door. This door is retained in the cowl panel by shear pins until the pressure on the door is sufficient to shear the pins. A nacelle pressure relief analysis was conducted of the peak pressures inside the nacelle due to a 13th-stage bleed duct failure.

Table 32.—Cowl Panel Fire Test Observations

Run no.	Region of fire test	Observations
1	Center of panel	Flame applied for 15 minutes—no burn-through. No apparent problem from liberated gas. Laminate on flame side blistered and all the gas generated was librated through the heated area. At end of test there was no damage to back side—flame side was blistered but intact.
2	Joint between upper cowl and fixed cowl	Flame applied for 15 minutes—no burn-through. Intercostal nearest flame began glowing red shortly after application of heat. Condition appeared stabilized after about 1 minute. After the run, the aluminum intercostals were distorted but the outside of the panel was in good condition. Warping caused joint to open up slightly.
3	Joint between upper cowl and fixed cowl	Following run no. 2 it was discovered that the back side airflow was set at an excessively high velocity [approximately 245 kn (126 m/s)]. Airflow was reset to the desired cooling air velocity of 130 kn (67 m/s), the same as used on the 727 fire tests, and run no. 2 was repeated on the same portion of the panel. Flame was applied for 15 minutes—no burn-through. A small piece of the nearest aluminum intercostal burned off after 38 seconds; then the condition stabilized with about an 8.0-in. (20.3-cm) wide section of the aluminum glowing red during the entire period. Reduction in air velocity did not seem to affect outcome of this test.
4	Joint between lower cowl and fixed cowl	Flame applied for 15 minutes—no burn-through. A portion of intercostal nearest burner began melting after 1 minute. Condition stabilized after 2 minutes. There was more distortion and intercostal damage on this joint than the upper joint but there was no evidence of burn through.

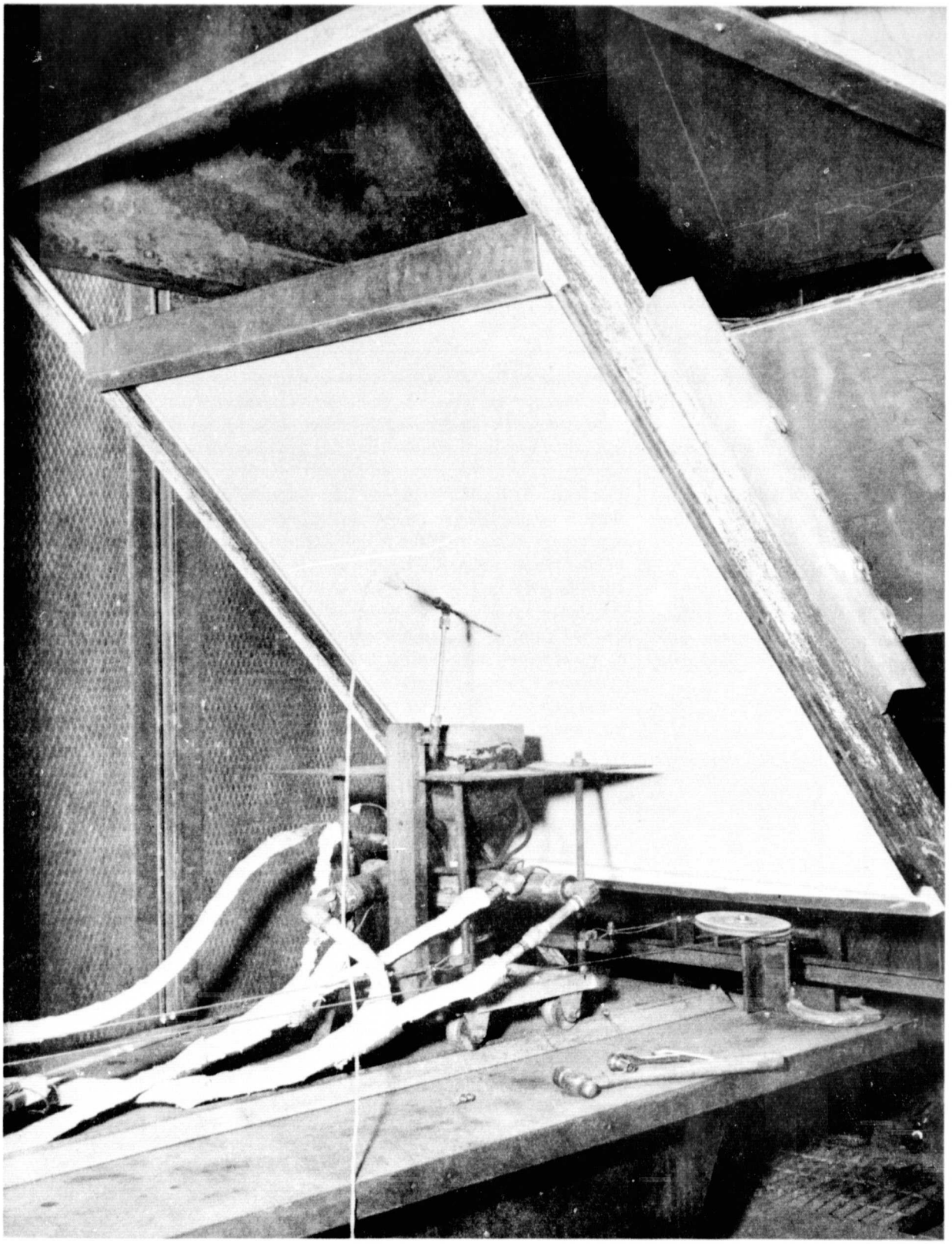

Figure 79.—Photograph of Cowl Panel Fire Test Results

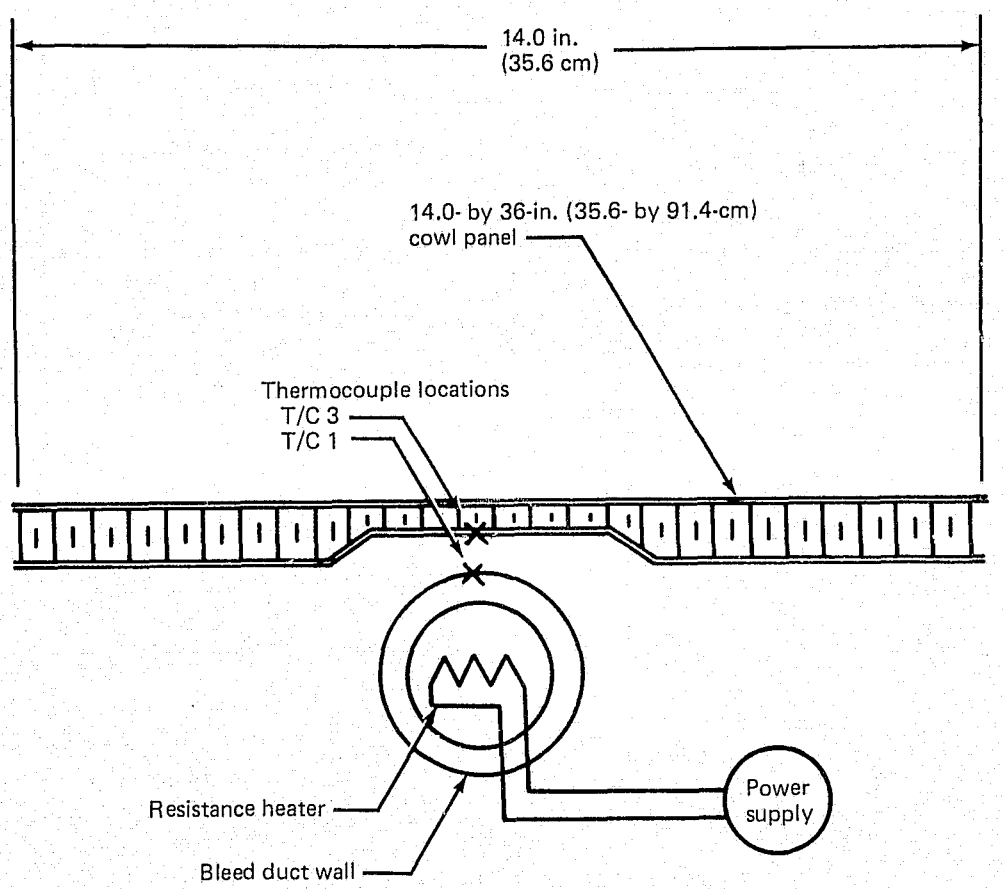

Figure 80.—Cowl/Bleed Duct Temperature Test Setup

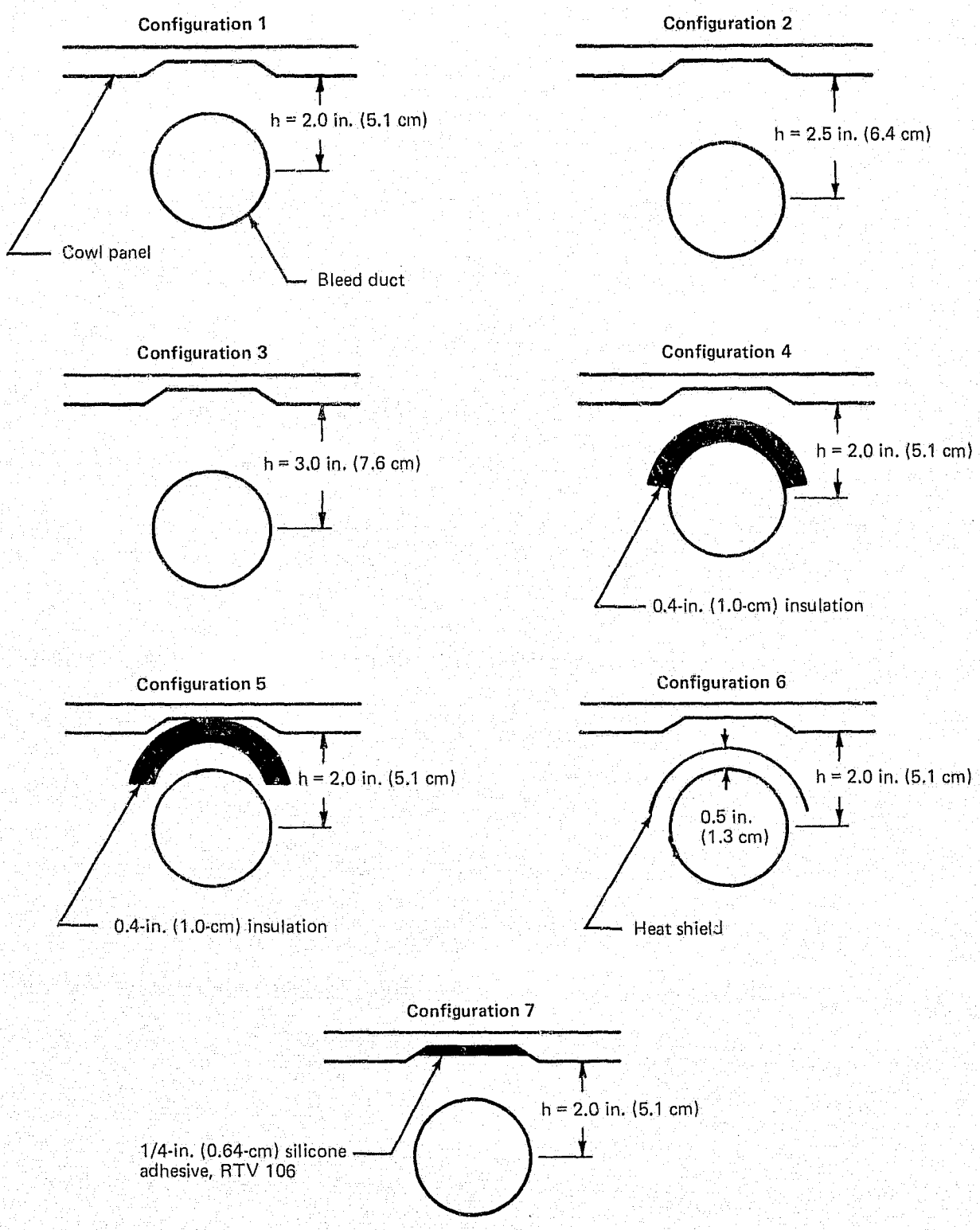

Figure 81.—Cowl/Bleed Duct Temperature Test Configurations

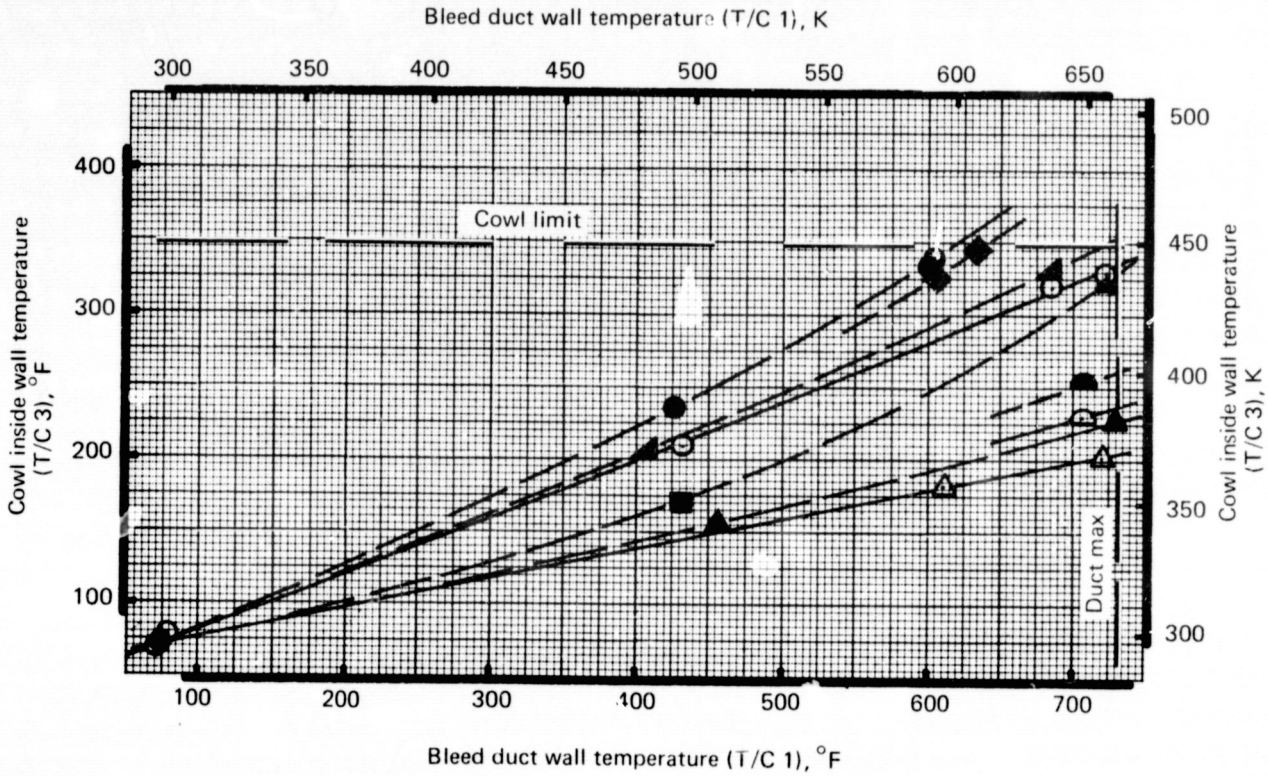

Symbol	Configuration number	Description
○	1	Shiny duct
●	1	Black duct
◆	1	Black duct; 6 kn (3 m/s) cooling air on cowl outer wall
△	4	Shiny duct; insulation on duct
▲	4	Black duct; black insulation on duct
◘	5	Shiny duct; insulation touching cowl
◓	5	Black duct; black insulation touching cowl
■	6	Black duct; heat shield
◢	7	Black duct; black RTV 106 on cowl

Figure 82.—Cowl/Bleed Duct Temperature Test Results

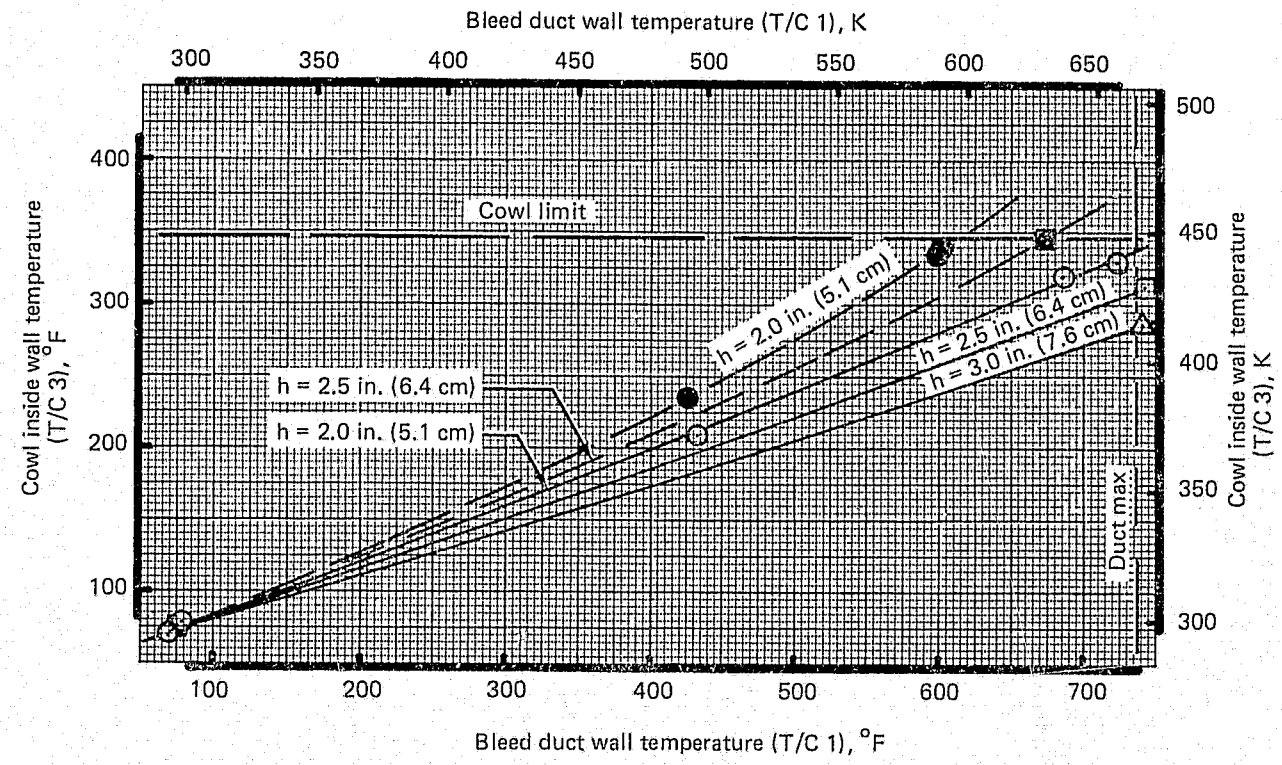

Symbol	Configuration number	Description
○	1	Shiny duct; h = 2.0 in. (5.1 cm)
□	2	Shiny duct; h = 2.5 in. (6.4 cm)
△	3	Shiny duct; h = 3.0 in. (7.6 cm)
●	1	Black duct; h = 2.0 in. (5.1 cm)
■	2	Black duct; h = 2.5 in. (6.4 cm)

Figure 83.—Effect of Bleed Duct Spacing on Cowl Wall Temperature

Figure 84 shows the resulting nacelle peak pressure versus the relief door opening pressure for the JT8D-109 cowl door design. The JT8D-109 cowl relief door is designed to open at 1.48-psi (1.02-N/cm^2) pressure. At this door opening pressure, the peak pressure inside the cowl panel was 2.49 psi (1.72 N/cm^2) which is below the 3.36-psi (2.32-N/cm^2) ultimate design pressure for the cowl panel structure, assuring adequate blowout protection.

3.3.6.5 Gearcase Breather

The bearing compartments and the oil tank are vented to the gearbox. A rotor separator in the gearbox separates the oil particles from the air. These oil particles collect in the gearbox and are returned to the oil tank by the gearbox scavenge pump. The relatively oil-free breather air is then discharged overboard. The Engine Contractor has stated that the breather air temperatures of the JT8D refan are expected to be similar to those of the basic JT8D engine because of the similarity of the oil system. The maximum expected air temperature on a high service engine is 375°F (464 K). This means that the breather duct exhaust has to be insulated from the honeycomb cowl panel because these panels have a 350°F (450 K) maximum temperature limit.

3.3.6.6 Generator Cooling

An analysis was performed to determine the adequacy of generator air cooling for the JT8D refan installation. Reference 4 describes the generator cooling system. The most critical generator cooling conditions occur at hot day, 8000-ft (2438-m) idle power, and 42 000-ft (12 802-m) low flight speed idle descent. Both conditions were examined for the JT8D refan installation and the analysis showed: (1) the generator exhaust duct had to be enlarged to 3.5 in.^{2} (22.6 cm^2) compared to the 2.65 in.^{2} (17.1 cm^2) for the basic JT8D installation; (2) generator air cooling is adequate for the hot day, 42 000-ft (12 802-m) idle descent condition; and (3) for the hot day, 8000-ft (2438-m) ground idle condition, the generator cooling is slightly deficient. Since the estimated ground idle data were uncertain at the time, further analyses and possibly a test would be necessary to substantiate the adequacy of the generator cooling.

3.3.6.7 Constant-Speed Drive (CSD) Oil Cooler Installation

Reference 4 discussed the installation of the CSD oil cooler in the fan duct similar to that on the production 737 airplane. No performance penalty has been assessed to the CSD oil cooler because previous 737 ground tests could not discern a difference with the oil cooler installed. This test would have to be repeated during refan certification tests.

3.3.6.8 Starting Characteristics

Since the engine mass moment of inertia at the starter is the same for the JT8D refan and the basic JT8D engines, there are no starting problems anticipated.

3.3.6.9 Nacelle Fire Detection and Extinguishing Systems

Reference 4 describes the fire protection systems for the current 727-200 airplane. The JT8D refan engine installation retains the existing 727-200 airplane fire protection system with only minor wiring and bracket relocations.

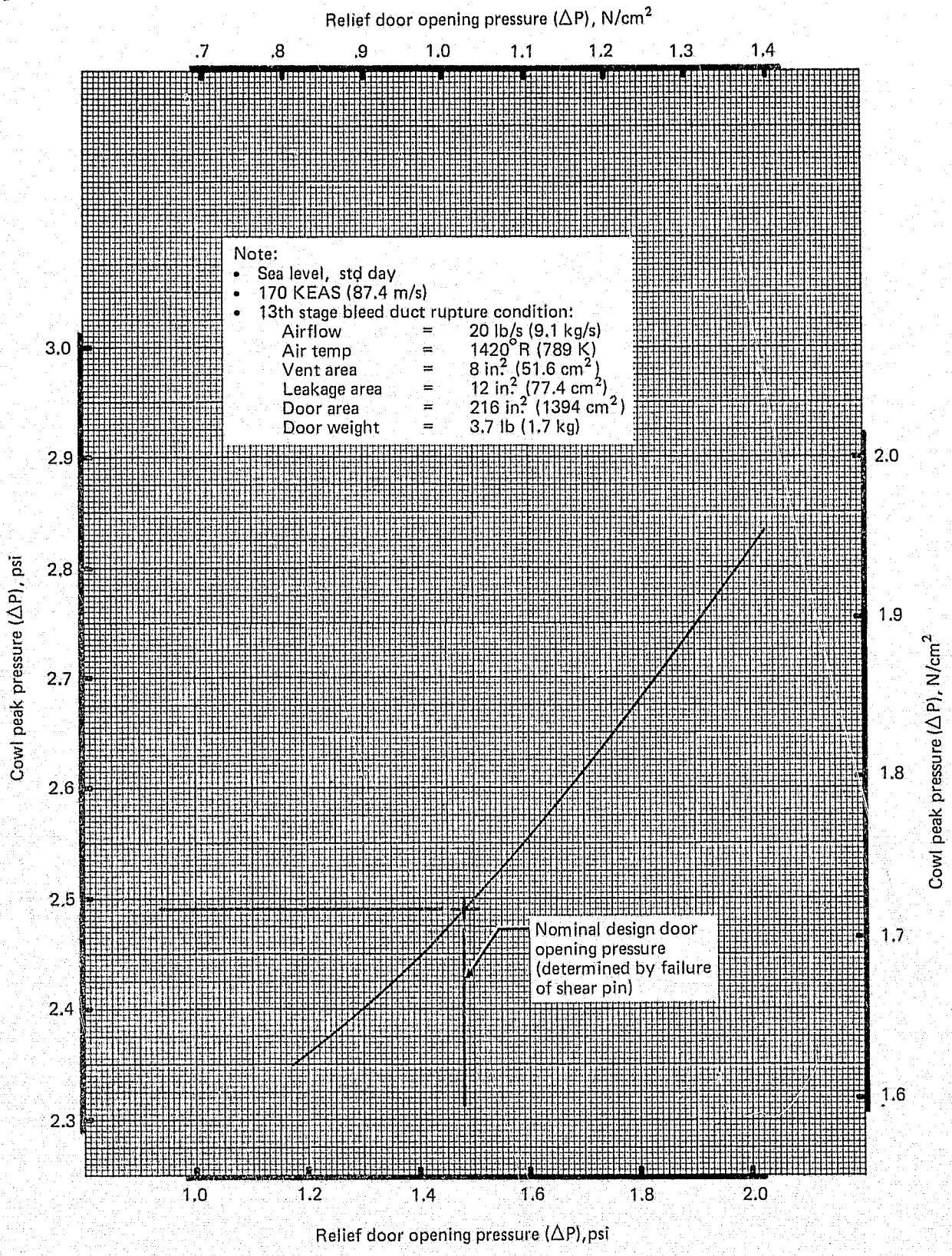

Figure 84.—Cowl Peak Pressure Versus Door Opening Pressure

3.3.7 ENGINE BLEED AIR AND HORSEPOWER EXTRACTION

3.3.7.1 Engine Bleed Air

The engines on the 727-200 are used as a source of pressurized air to support airplane air-conditioning, inlet and wing anti-icing (ice protection), generator cooling, fuel heating, and thrust-reverser pneumatic actuation systems. The JT8D-109 provides engine bleed air for the same systems with the one exception of the 727 refan thrust reverser, which was designed for hydraulic actuation.

The bleed air requirements for the 727 refan air-conditioning system are unchanged from those used for the 727-200. Figure 85 shows the takeoff and normal bleed airflow requirements. At takeoff and most altitudes, the airflow requirements shown in the figure along with attendant pressures and temperatures are met by using 8th-stage compressor airbleed. For some high-altitude, hot day conditions, 8th-stage airbleed is insufficient to meet air-conditioning requirements and a switch ("crossover") is made to 13th-stage compressor airbleed. Airflow and pressure for 13th-stage airbleed were determined to be adequate for the flight envelope.

Fan airbleed is used for the air-conditioning precooler. The airconditioning precooler (i.e., cross-flow heat exchanger) uses engine fan air extracted from the fan duct to cool compressor bleed air prior to entry into the air-conditioning packs. After going through the precooler, the fan bleed air is then exhausted outside the airplane.

Sixth-stage compressor airbleed is used for wing and inlet ice protection. The bleed air requirements for the 727 refan are the same as for the 727-200. Section 3.7 describes the refan ice protection system.

727 refan engine airbleed for generator cooling and fuel heating is also the same as that required for the 727-200.

3.3.7.2 Power Extraction

Power is extracted through the engine-driven CSD from the JT8D-9 and -109 engines to drive generators, power pumps, motors, etc., as required to support aircraft systems. Figure 86 shows the power extraction schedule for the 727-200 and 727 refan airplanes at takeoff, climb, and cruise. These schedules were used in installed engine performance calculations for the JT8D-9 and -109 engines.

3.3.8 INSTALLED ENGINE PERFORMANCE CALCULATION PROCEDURE

The 727-200 airplane performance used as the baseline for comparisons to the 727 refan airplane included:

1. Installed JT8D-9 engine performance that represents minimum thrust and maximum SFC values that are consistent with P&WA's calculation procedures

2. Contractor specification airplane performance

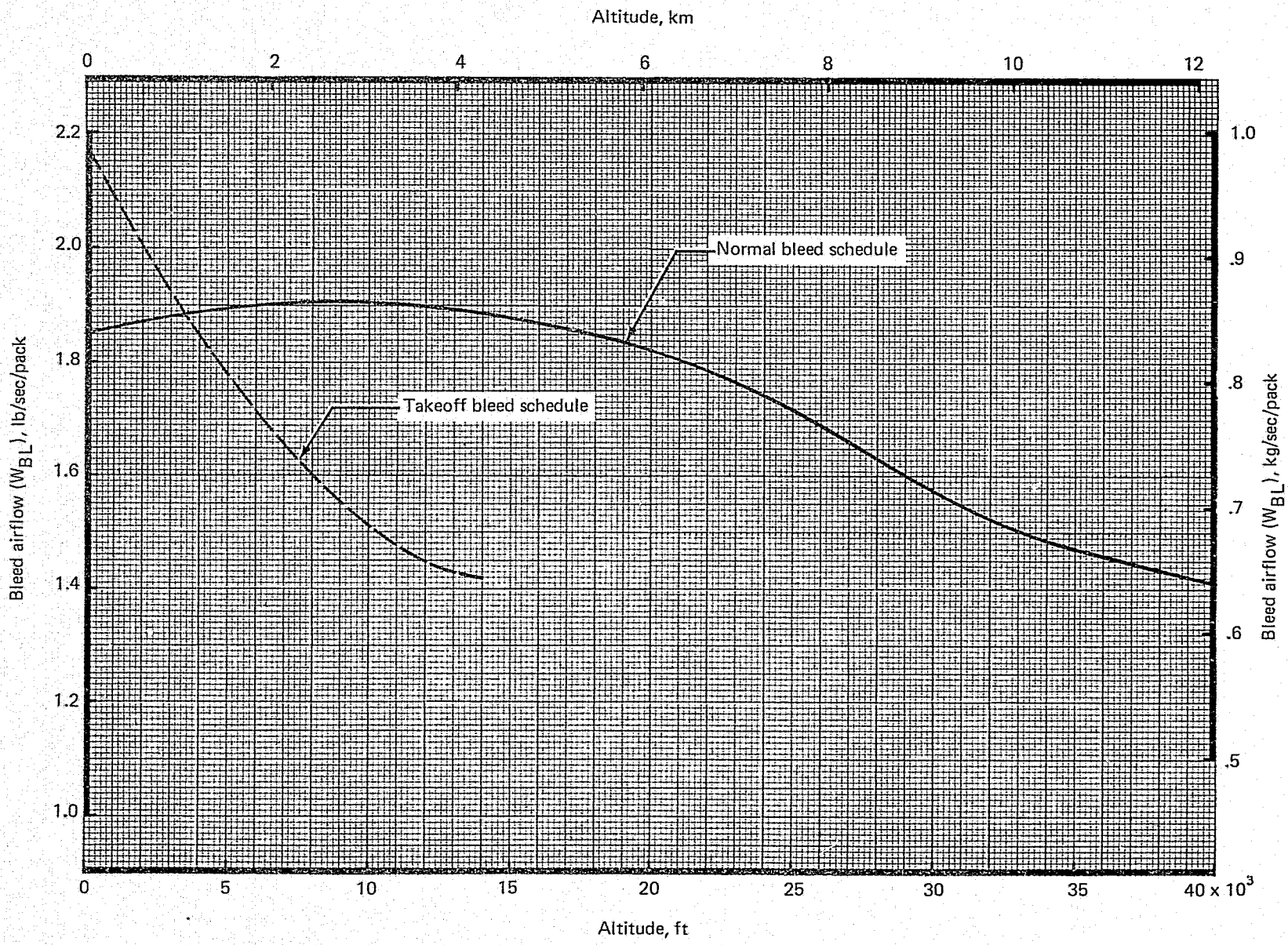

Figure 85.—727 Refan Cabin Air-Conditioning Bleed Schedule

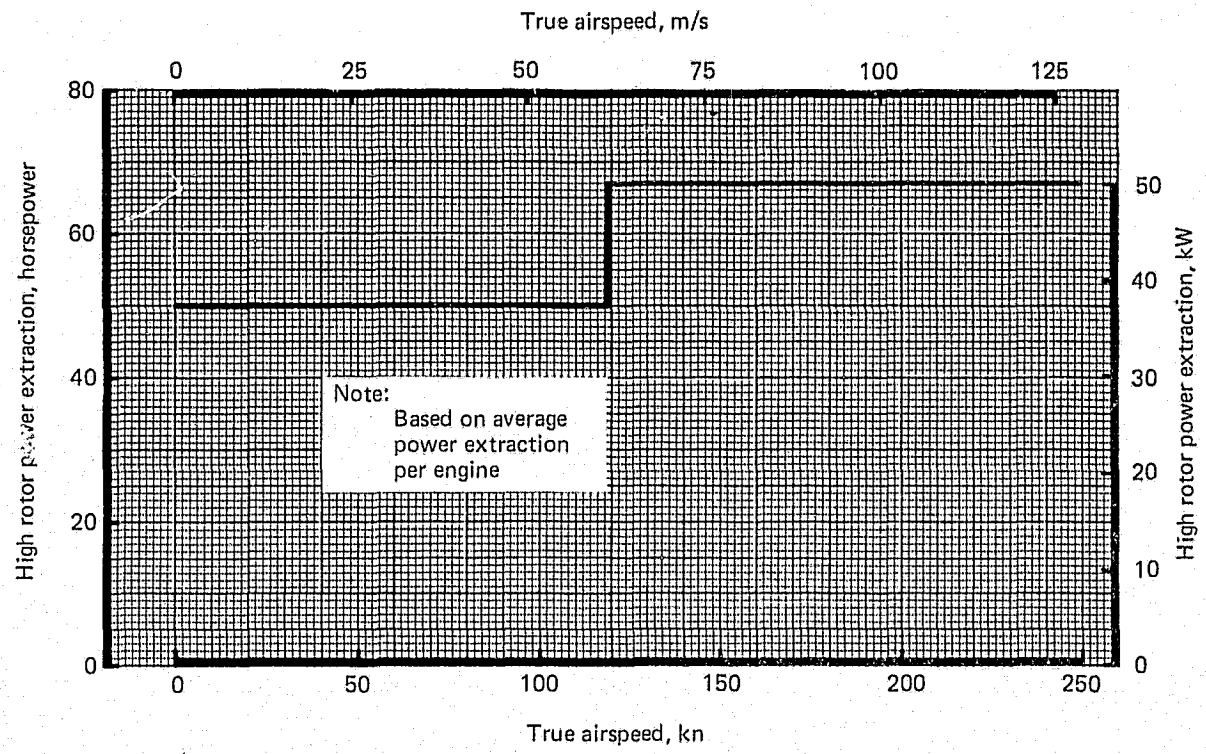

(a) Power Extraction at Takeoff Power

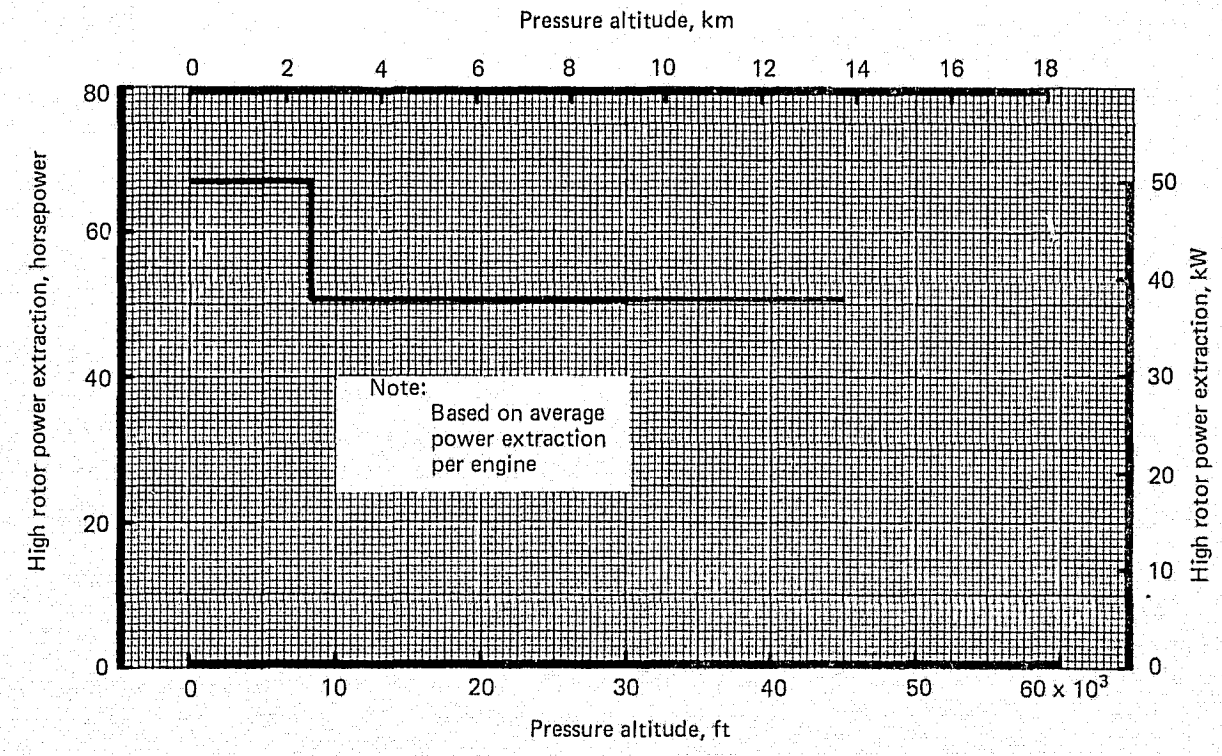

(b) Power Extraction at Climb and Cruise

Figure 86.—727-200 and 727 Refan Power Extraction Schedule

Thus the 727-200 airplane represents specification performance levels.

Installed engine performance for the 727 refan analyses was prepared using JT8D-9 and -109 nominal engine decks provided by P&WA. The changes to uninstalled thrust, SFC, and other engine characteristics that result from installation of an inlet, exhaust system, and nacelle subsystems, as well as the capability to bleed pressurized compressor air were included by the Contractor in both the JT8D-9 and -109 engine decks. The installed engine performance prepared with these decks provided *minimum* installed thrust and *nominal* installed SFC.

In order to provide a consistent comparison between the 727-200 and 727 refan airplane installed SFC performance, the ratio of JT8D-9 installed SFC performance (obtained through established P&WA procedures) and installed JT8D-9 nominal deck SFC's was applied to the installed SFC values obtained from the JT8D-109 performance deck.

3.3.9 INSTALLED TAKEOFF PERFORMANCE

Estimated installed takeoff thrust was generated for normal 727 refan takeoff operation as described in section 3.3.8. The takeoff thrust was generated for the center and side engines for a standard and 84°F (302 K) day at sea level and for a 84°F (302 K) day at 5000-ft (1524-m) altitude.

Installation penalties for the center and side engines are described in sections 3.3.2 through 3.3.7. Cabin air-conditioning bleed air is taken only from the side engines, whereas power extraction via the CSD is taken from all three engines. Thrust penalties for inlet and wing anti-icing were not evaluated since anti-icing is not required on hot days when takeoff thrust is critical. Installed JT8D-9 performance was based on P&WA JT8D-9 installation procedures with adjustments for installation penalties.

Figure 87 shows the sea level standard day installed takeoff lapse rate comparison between the JT8D-9 and -109 center and side engines. At static (airspeed = 0) conditions, the JT8D-109 center and side engines show a 14.8% and 13% thrust increase relative to the JT8D-9 engines. At 100 kn (51.4 m/s), the JT8D-109 center and side engines show a 10.8% and 10.2% increase in takeoff thrust whereas at 250 kn (128.6 m/s), the refan thrust advantage has dwindled to 3.4% and 2.8%, respectively. The greater lapse rate of the JT8D-109 relative to the JT8D-9 is due to the higher bypass ratio of the JT8D-109 engine.

Figure 88 shows the JT8D-9 and -109 engine installed takeoff lapse rate comparison at sea level and 5000 ft (1524 m) for an 84°F (302 K) day. At static, 100-kn (51.4-m/s), and 250-kn (128.6-m/s) conditions, the JT8D-109 shows the same percent thrust advantage at sea level and 5000 ft (1524 m) over the JT8D-9, on a standard day.

3.3.10 INSTALLED CRUISE PERFORMANCE

The installed JT8D-109 side- and center-engine cruise performance was prepared as described in section 3.3.8. The installed JT8D-9 engine performance was obtained from P&WA JT8D-9 installation procedures with adjustments for installation penalties. Figure 89 shows the JT8D-9 and -109 side- and center-engine performance comparison in terms of installed net thrust versus thrust SFC at the 727-200 minimum cost cruise condition ($M_\infty = 0.84$ and 30 000 ft (9144 m)). The cruise thrust required for both the 727-200 and 727 refan varies

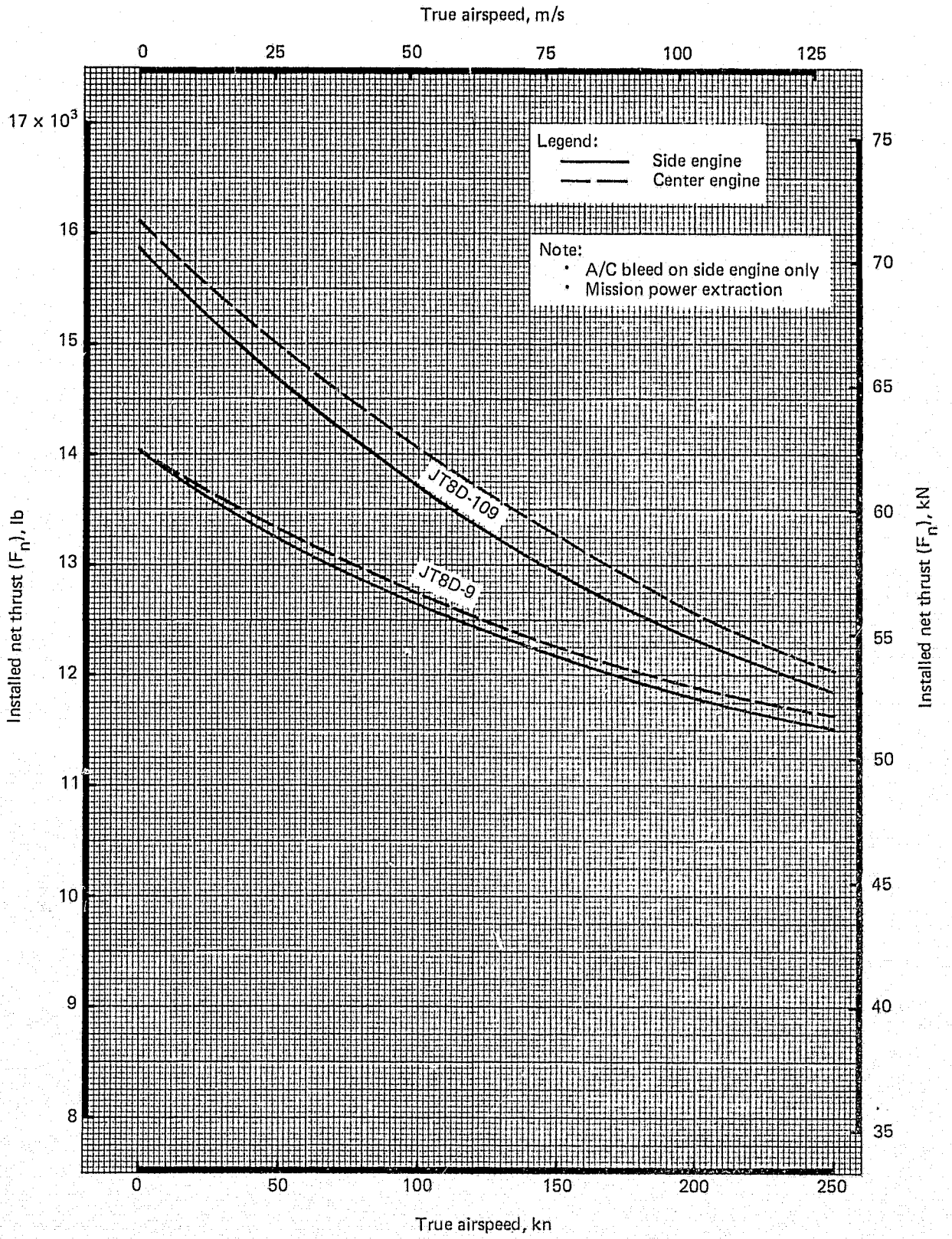

Figure 87.—JT8D-9 and -109 Installed Takeoff Lapse Rate Comparison—Sea Level; Standard Day—727-200 Airplane

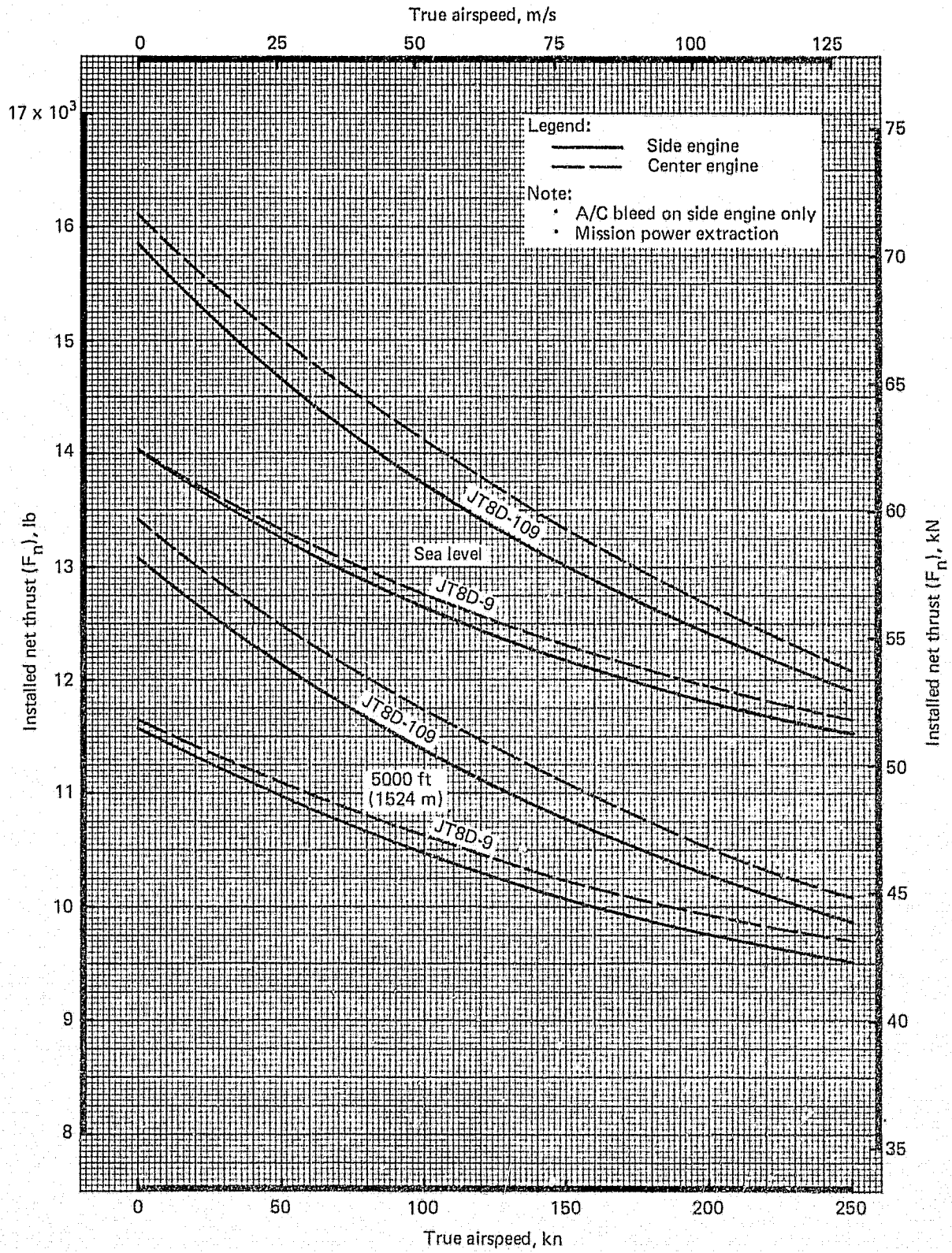

Figure 88.—JT8D-9 and -109 Installed Takeoff Lapse Rate Comparison—84° F (302 K) Day—727-200 Airplane

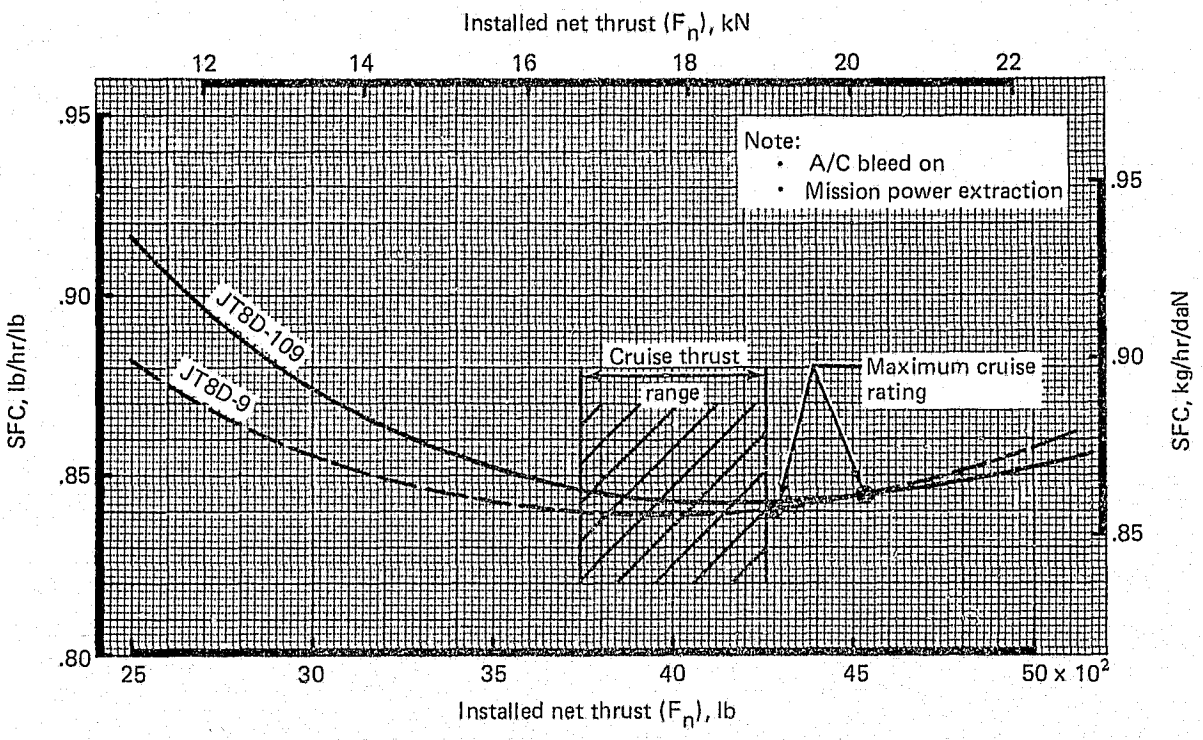

(a) Side-Engine Installation

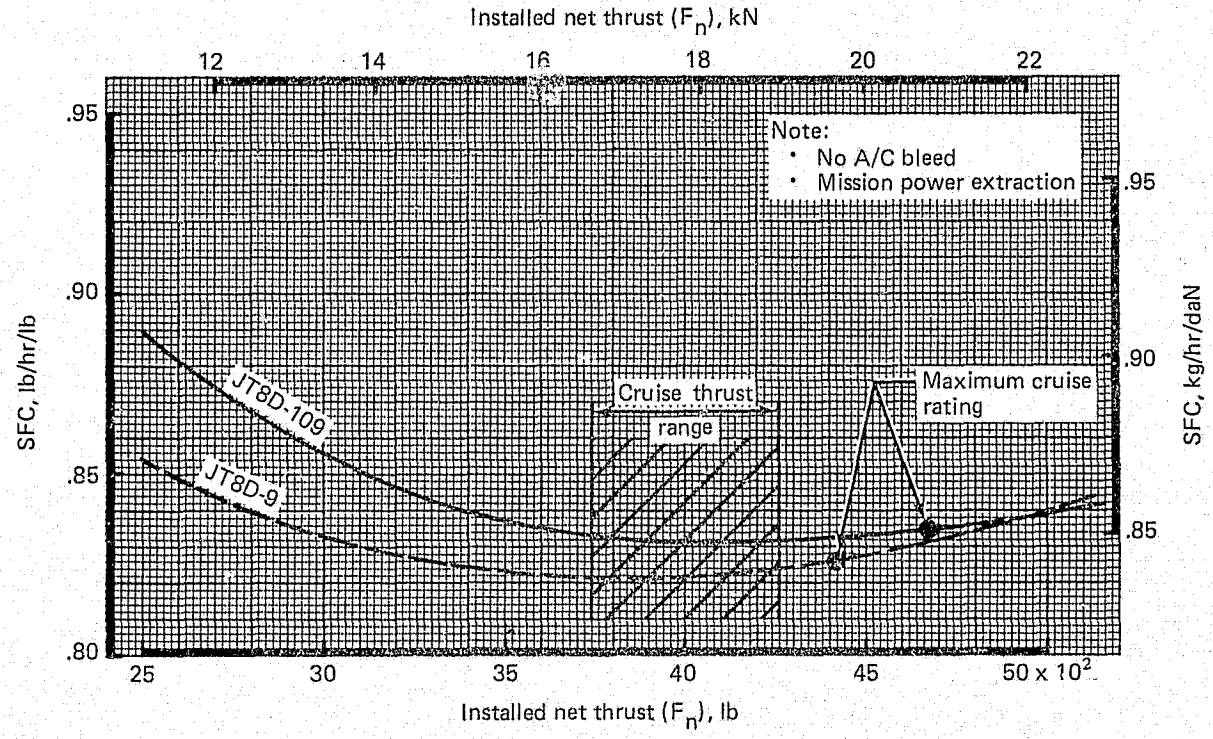

(b) Center-Engine Installation

Figure 89.—JT8D-9 and -109 Installed Cruise Performance Comparison—M_∞ = 0.84 at 30 000 ft (9144 m); Standard Day—727-200 Airplane

between 4260 lb (18 949 N) at the beginning of cruise and 3740 lb (16 636 N) near the end of cruise at a constant altitude of 30 000 ft (9144 m). This variation in required thrust is due to the decrease of the airplane gross weight as fuel is burned. Performance comparisons between the JT8D-9 and -109 engines were made at an approximate midcruise thrust of 4050 lb (18 015 N). Figure 89 shows the JT8D-109 installed SFC to be higher than the JT8D-9 on the center and side engines at 4050-lb (18 015-N) net thrust. The JT8D-109 side-engine SFC is up 0.4% compared to a JT8D-9 side engine, and the JT8D-109 center engine is up 1.1% relative to the JT8D-9. Combining one JT8D-109 center engine with two -109 side engines shows the refan average SFC to be 0.6% above that of the JT8D-9 installation.

3.3.11 INSTALLED PERFORMANCE SENSITIVITIES TO INSTALLATION LOSSES

Installed engine performance sensitivities to various installation penalties for the JT8D-9 and -109 engines were calculated to indicate the individual contribution of the various installation losses to the total. The sensitivity evaluations were conducted at takeoff and cruise conditions for the 727-200 and 727 refan airplane side and center engines. Engine performance penalties were calculated using the P&WA JT8D-9 and -109 nominal engine computer decks in conjunction with the nominal to installed performance ratioing procedure described in section 3.3.8.

Installed takeoff performance thrust penalties were calculated at sea level, static, standard day conditions. A constant burner exit total temperature (T_{t5}) at the uninstalled takeoff thrust rating was used to maintain a takeoff rating during the sensitivity study. The comparison of the takeoff penalties began with the uninstalled takeoff net thrust levels shown in figure 70 and decreased to the installed takeoff net thrust levels shown in figure 87.

Figure 90 shows the comparison of JT8D-9 and -109 *side-engine* takeoff performance sensitivities. The major portion of *side-engine* installation loss is due to engine airbleed for cabin air-conditioning and pressurization. The greater airbleed loss for the JT8D-109 is characteristic of a higher bypass ratio engine. The inlet ring causes the inlet recovery loss for the JT8D-109 to be greater than for the JT8D-9. No nozzle velocity coefficient loss was incorporated in the JT8D-109 because the flight and reference nozzle velocity coefficients were the same.

Figure 91 shows JT8D-9 and -109 *center-engine* takeoff sensitivity study results. The predominant loss for both engines is center-engine inlet duct recovery. The percent of uninstalled thrust decrease for the total installation effects was greater for the JT8D-9 engine than the JT8D-109 due to the omission of nozzle velocity loss in the refan engine.

Installed cruise performance sensitivities were calculated at 30 000 ft (9144 m), $M_\infty = 0.84$, standard day conditions. A constant midcruise net thrust of 4050 lb (18 015 N) was maintained to establish the fuel flow penalty for the individual installation items. The cruise study began with the uninstalled nominal SFC levels shown in figure 70 and increased to the installed SFC levels shown in figure 89.

Figure 92 shows the JT8D-9 and -109 *side-engine* cruise sensitivity study results. Again, engine airbleed loss is the predominant installation effect on both engines. Inlet recovery

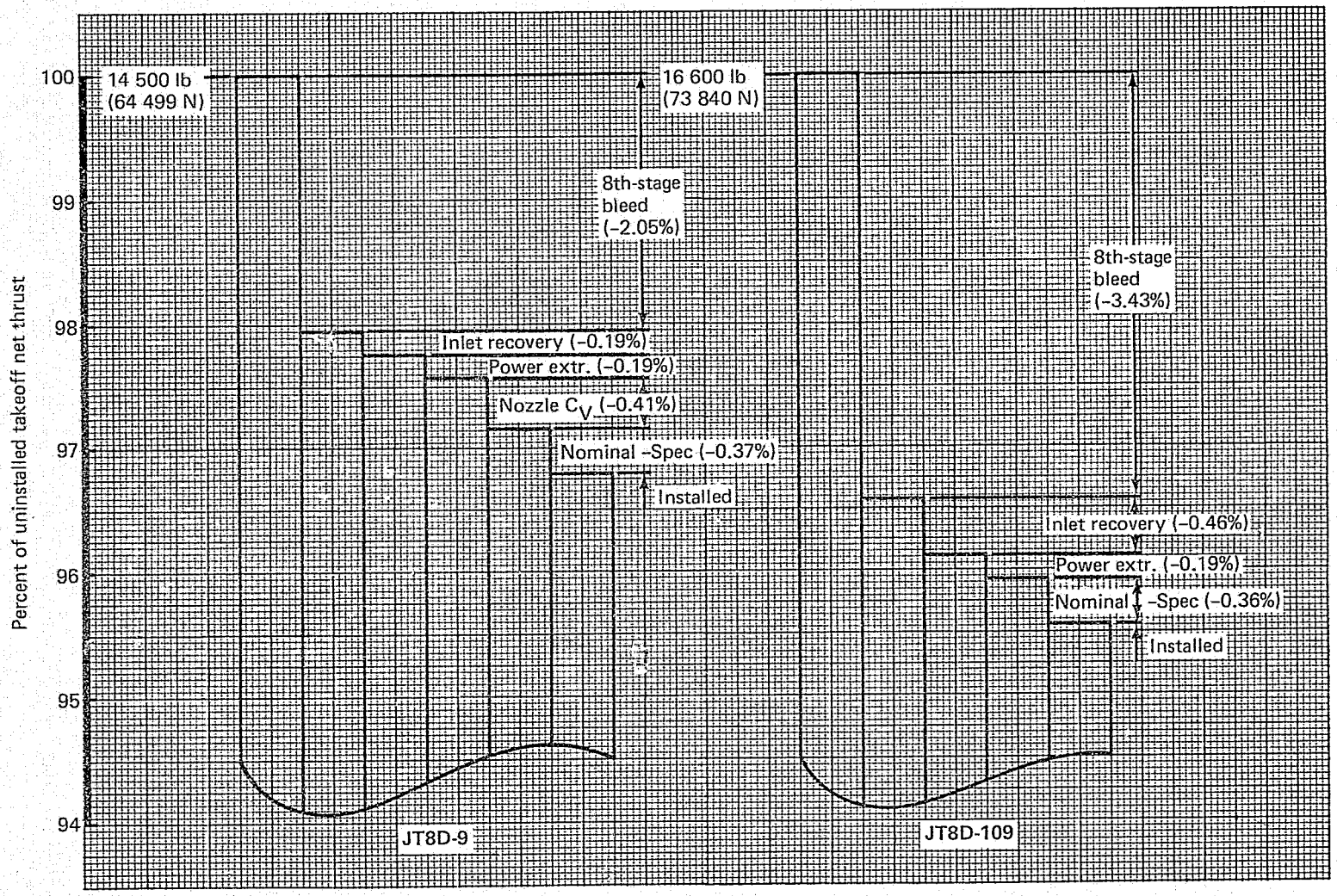

Figure 90.—JT8D-9 and -109 Side-Engine Takeoff Sensitivity Comparison—Installation Effects—Sea Level Static, Standard Day

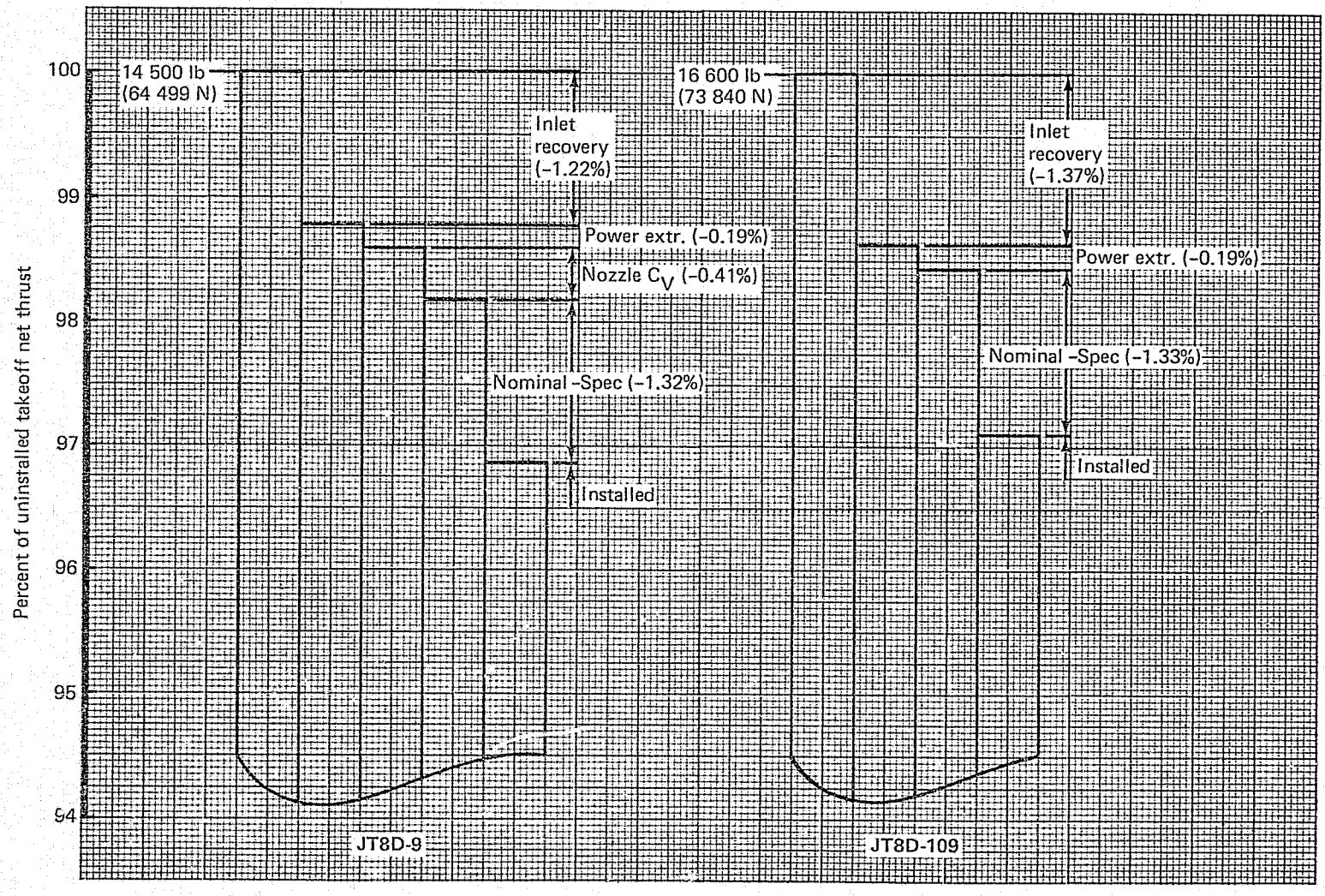

Figure 91.—JT8D-9 and -109 Center-Engine Takeoff Sensitivity Comparison—Installation Effects—Sea Level Static, Standard Day

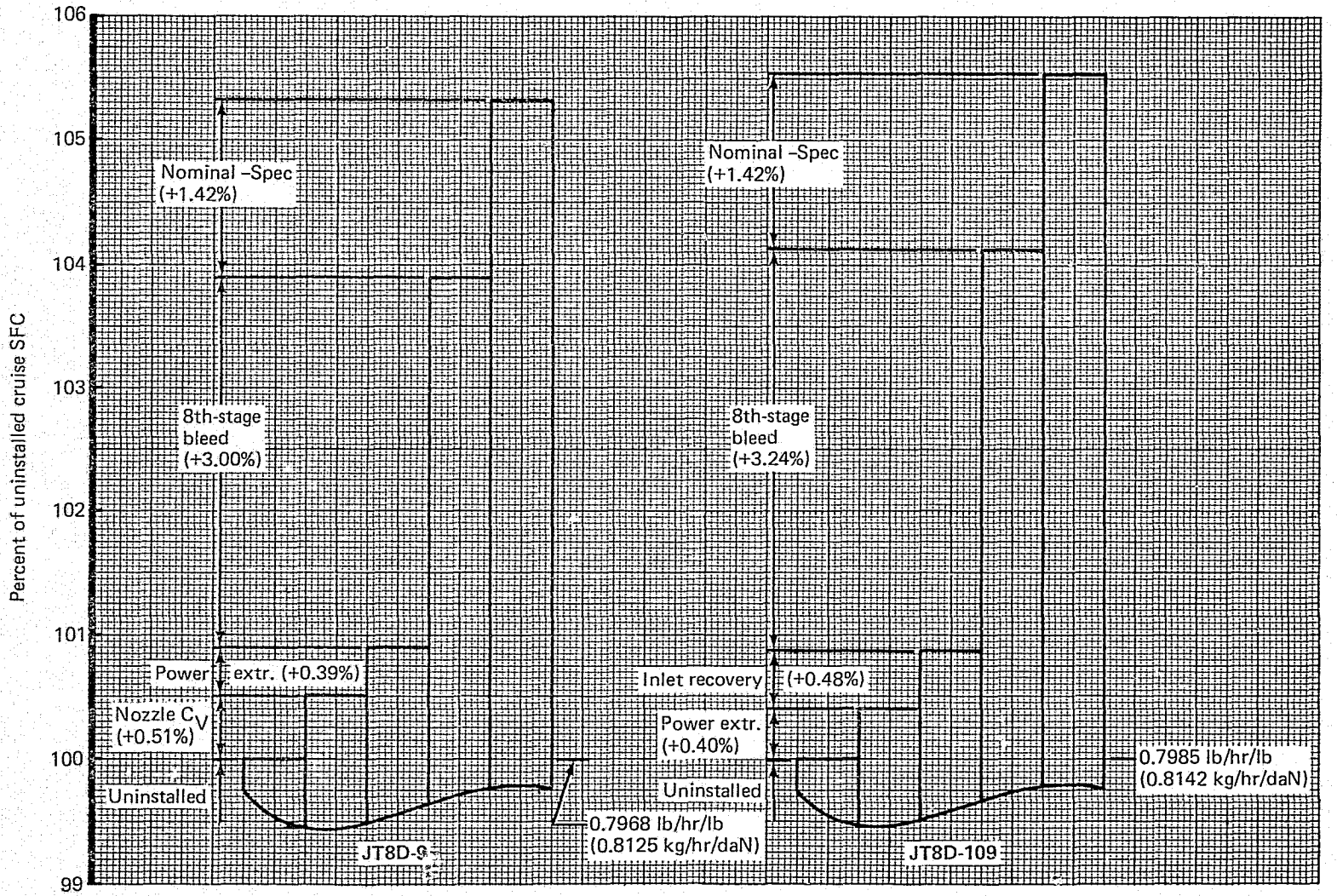

Figure 92.—JT8D-9 and -109 Side-Engine Cruise Sensitivity Comparison—Installation Effects—
M_∞ = 0.84 at 30 000 ft (9144 m), Standard Day, Net Thrust = 4050 lb (18 015 N)

loss on the JT8D-9 at cruise is assumed to be the same as for a low-loss bellmouth inlet (i.e., unity). The JT8D-109 nozzle velocity loss is zero as shown in section 3.3.4.

Figure 93 shows the JT8D-9 and -109 *center-engine* cruise sensitivities. Inlet and duct recovery is the predominant installation loss. No nozzle velocity loss is included for the JT8D-109 engine.

3.3.12 IDLE POWER SETTINGS

The idle power setting for the JT8D-9 on the 727-200 airplane influenced the design characteristics for many of the airplane subsystems such as brakes, cabin pressurization, and CSD capability. Installation of the JT8D-109 required analysis to determine if these subsystems designed for JT8D-9 idle characteristics could function properly at JT8D-109 idle power settings.

Evaluations of the JT8D-109 during Phase I trade studies indicated that the acceleration time of the engine would be slower than for the JT8D-9. Ground tests at P&WA and altitude testing conducted at NASA LeRC during Phase II confirmed the slower acceleration time, indicating a requirement for separate ground and flight idle power setting. The flight idle power setting is needed to meet an 8-sec acceleration requirement from idle to takeoff power at altitude in the event of a landing go-around.

3.3.12.1 Ground Idle

The JT8D-109 ground idle performance was established by P&WA during Phase II ground tests. The uninstalled thrust quoted by P&WA at ground idle conditions is 840 lb (3736 N) with a corresponding corrected high-pressure compressor speed ($N_2/\sqrt{\theta}_a$) of 6100 rpm (49.8% N_2).

General criteria that the ground idle power setting must meet (when the JT8D-109 is installed on the airplane) are to:

- Be sufficiently low so that brake overheating during taxiing will be prevented
- Provide sufficient compressor bleed air for generator cooling
- Keep the CSD above its lower limit trip speed so that electrical and mechanical power requirements will not be interrupted during ground operation

The idle trim setting for the side and center engines installed on the 727 refan was not dictated by brake requirements or generator cooling but by CSD operation. When the JT8D-109 with the ground idle power setting recommended by P&WA was analyzed on the 727 refan airplane, it was found that during cold day operation the N_2 rpm dropped below the CSD lower limit trip speed. To alleviate this problem, the uninstalled idle thrust was moved up to 975 lb (4336.8 N) and a corrected N_2 of 6450 rpm (52.7% N_2), the same speed as the JT8D-9 engine. Figure 94 shows the uninstalled and installed JT8D-109 idle N_2 speeds, as a function of ambient temperature, which were selected to meet the ground idle requirements. The uninstalled idle trim line is shown primarily for reference purposes.

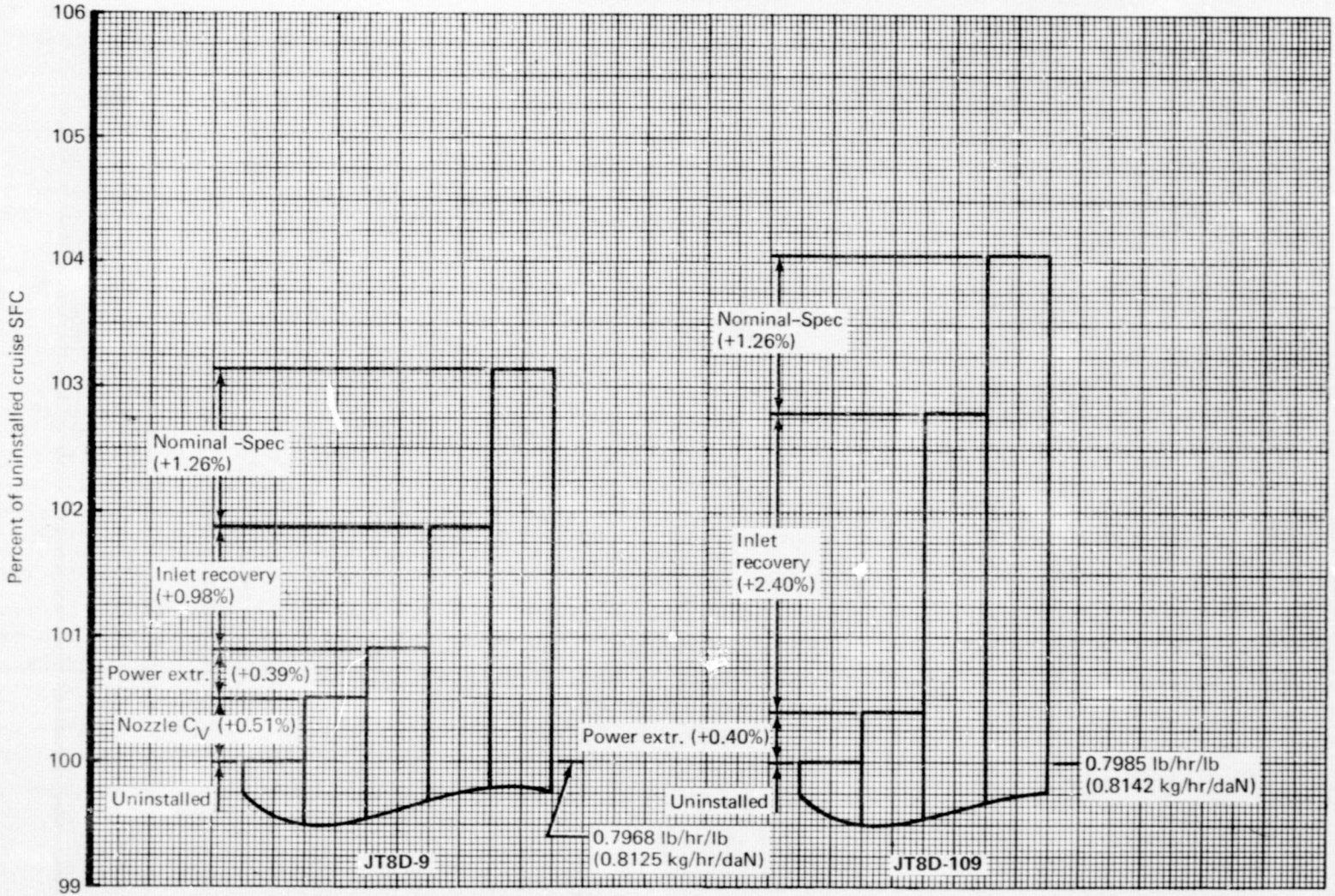

Figure 93.—JT8D-9 and -109 Center-Engine Cruise Sensitivity Comparison—Installation Effects—
M_∞ = 0.84 at 30 000 ft (9144 m), Standard Day, Net Thrust = 4050 lb (18 015 N)

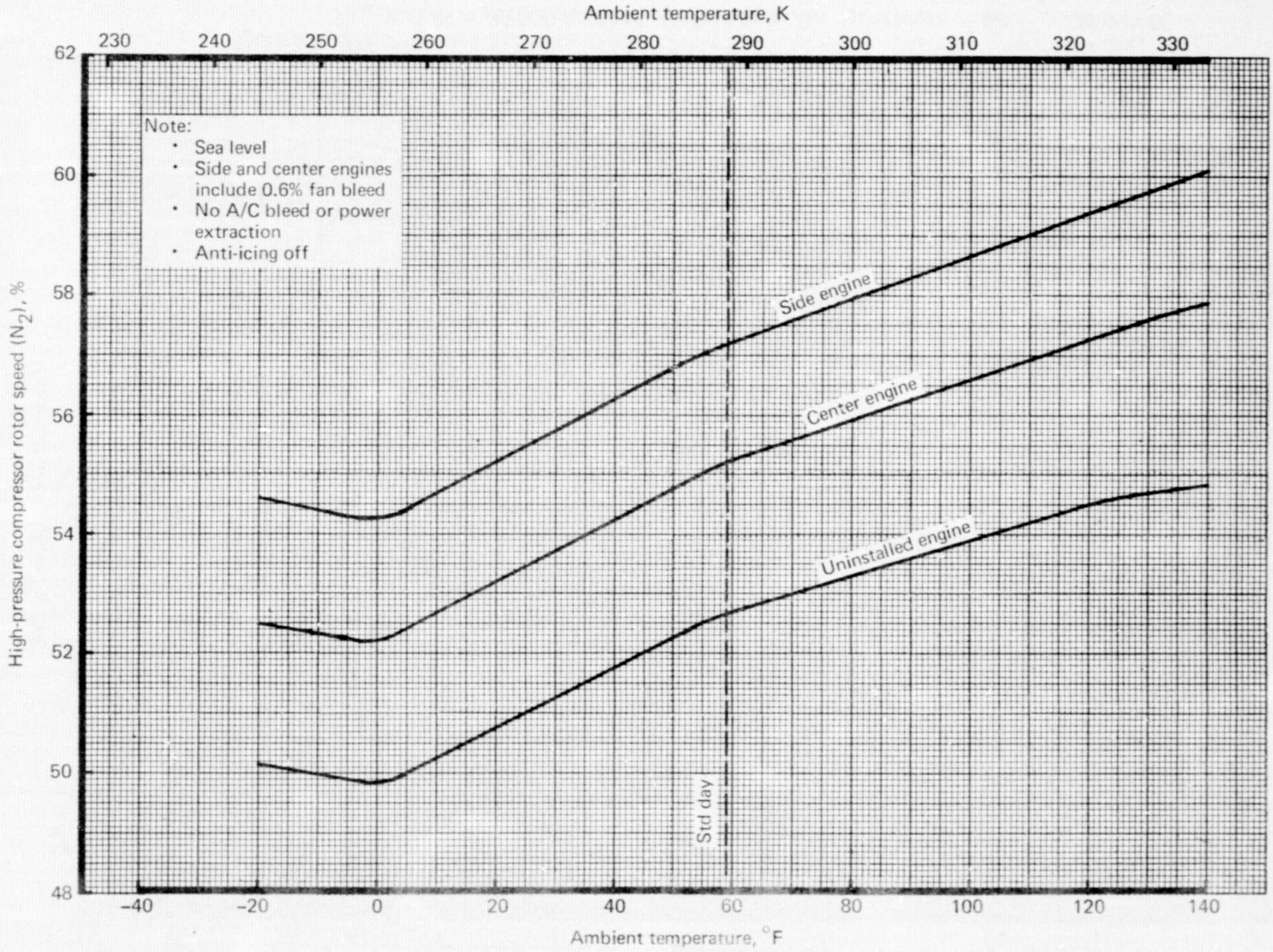

Figure 94.—JT8D-109 Ground Idle Trim Curve

To ensure trip-free CSD operation on the 727-200 side and center engines, it is standard JT8D-9 procedure to uptrim the engines on a standard day so that when the applicable airbleed is taken off the side engines and horsepower is extracted from both center and side engines, the corrected N_2 on all engines drops to no less than 53.7%, thus allowing for at least a 1% margin. In addition, the thrust drops back to approximately the same level as in the uninstalled case, 840 lb (3736 N). Therefore, the 727-200 side engines are trimmed to 57.2% N_2 and the center engine to 55.2% N_2 with 0.6% fan bleed for generator cooling, and no horsepower extraction, air-conditioning airbleed, or anti-icing bleed air.

The same procedure was used with the JT8D-109 engine. The 727 refan center and side engines were set on a standard day at 55.2% and 57.2% N_2, respectively, so that when applicable compressor bleed air and horsepower were extracted from the engines, the N_2 dropped to approximately 53.7%. The JT8D-109 installed idle thrust was then approximately 975 lb (4336.8 N). This trim procedure kept the JT8D-109 above the generator trip speed. The JT8D-109 N_2 reduction with decreasing ambient temperature was approximately the same as for the JT8D-9; therefore cold day CSD operation was also unchanged.

The JT8D-109 installed ground idle power settings therefore provide:

- Idle thrust slightly higher than for the JT8D-9 but below levels obtained from JT8D engines of higher ratings used on the 727-200 (This indicates that the 727-200 brake system is adequate for the 727 refan airplane.)
- The same capability for generator cooling as exists with the JT8D-9 engine
- CSD operation that will be essentially unchanged from that available with the JT8D-9 engine

3.3.12.2 Flight Idle

General installed engine idle characteristics that are required in flight include the following items:

- The engine must be capable of accelerating within 8 sec from idle to takeoff thrust for airplane go-around in the event of a refused landing.
- The idle thrust in flight shall enable the airplane to descend and land according to a given descent schedule.
- The idle power setting in flight shall be high enough so that the engine can provide sufficient compressor bleed air for cabin pressurization.
- Other engine and airplane requirements that must be satisfied include generator cooling, thermal anti-icing, and CSD operation.

The requirement for a higher flight idle power setting on the 727 refan engine is due to the fact that when the selected ground idle was evaluated at altitude, it was found that the

installed JT8D-109 engine would not accelerate to takeoff thrust in the 8-sec acceleration time which is an FAA requirement. P&WA evaluated the JT8D-109 acceleration characteristics through the use of computer simulations at flight conditions and from actual test data measured in the NASA LeRC altitude test facility.

The normal flight condition where the acceleration evaluation is conducted is at 10 000 ft (3048 m) and $M_\infty = 0.2$ on a standard day. The results of the analyses conducted at P&WA indicated that a corrected N_2 of 7750 rpm was required for flight idle in order to meet the acceleration requirement.

The flight idle power setting provided by P&WA was used to evaluate the idle descent requirements with respect to thrust available and compressor bleed air required for cabin pressurization. Figure 95 shows the 727-200 airplane low-speed descent schedule used to evaluate 727 refan descent capability. This descent schedule has been selected for comparison of 727 refan to 727-200 flight idle characteristics because it required the lowest thrust levels and resulted in minimum engine compressor bleed pressures and airflows available for cabin pressurization. Figure 96 shows the installed JT8D-109 side- and center-engine flight idle thrust that results from flying the low-speed descent schedule. These thrust characteristics were used to evaluate the 727 refan descent characteristics (section 3.1.7).

The 727 refan pressurization requirements for normal flight conditions are met with the flight idle power setting. Airflow requirements are always met at altitude conditions, but pressure requirements are sometimes difficult to satisfy. Figure 97 shows the engine bleed air pressure available for cabin pressurization. Throughout the normal 727-200 flight envelope up to an altitude of 36 200 ft (11 033 m) on an ISA + 40°F (22 K) day, the JT8D-109 meets or exceeds the pressure requirement for cabin pressurization. Above 36 200 ft (11 033 m) and up to 40 000-ft (12 192-m) altitude, the cabin pressure would be slightly off schedule.

Other engine and airplane requirements at idle power settings in flight, such as engine component cooling, CSD operation, etc., are met.

3.3.13 ENGINE STABILITY

Engine stability characteristics were investigated by P&WA (ref. 10) and the Contractor. P&WA tested the JT8D-109 engine, using screens to simulate typical side- and center-engine inlet duct pressure distortion reported in references 5 and 6. Using these screen pressure distortion patterns, P&WA demonstrated stable engine operation during steady-state operation as well as during accelerations to and decelerations from the engine red-line speed. This was accomplished with each of the following distortion screens installed: sea level static center-engine inlet; center-engine inlet with a 35-kn (18.0-m/s) crosswind; and side-engine inlet with a 30-kn (15.4-m/s) crosswind. This is not to say that there was no loss in low-pressure compressor (LPC) stall margin, but rather that the stall margin was adequate to maintain stable engine operation with the simulated 727 refan inlet distortion obtained from model test data.

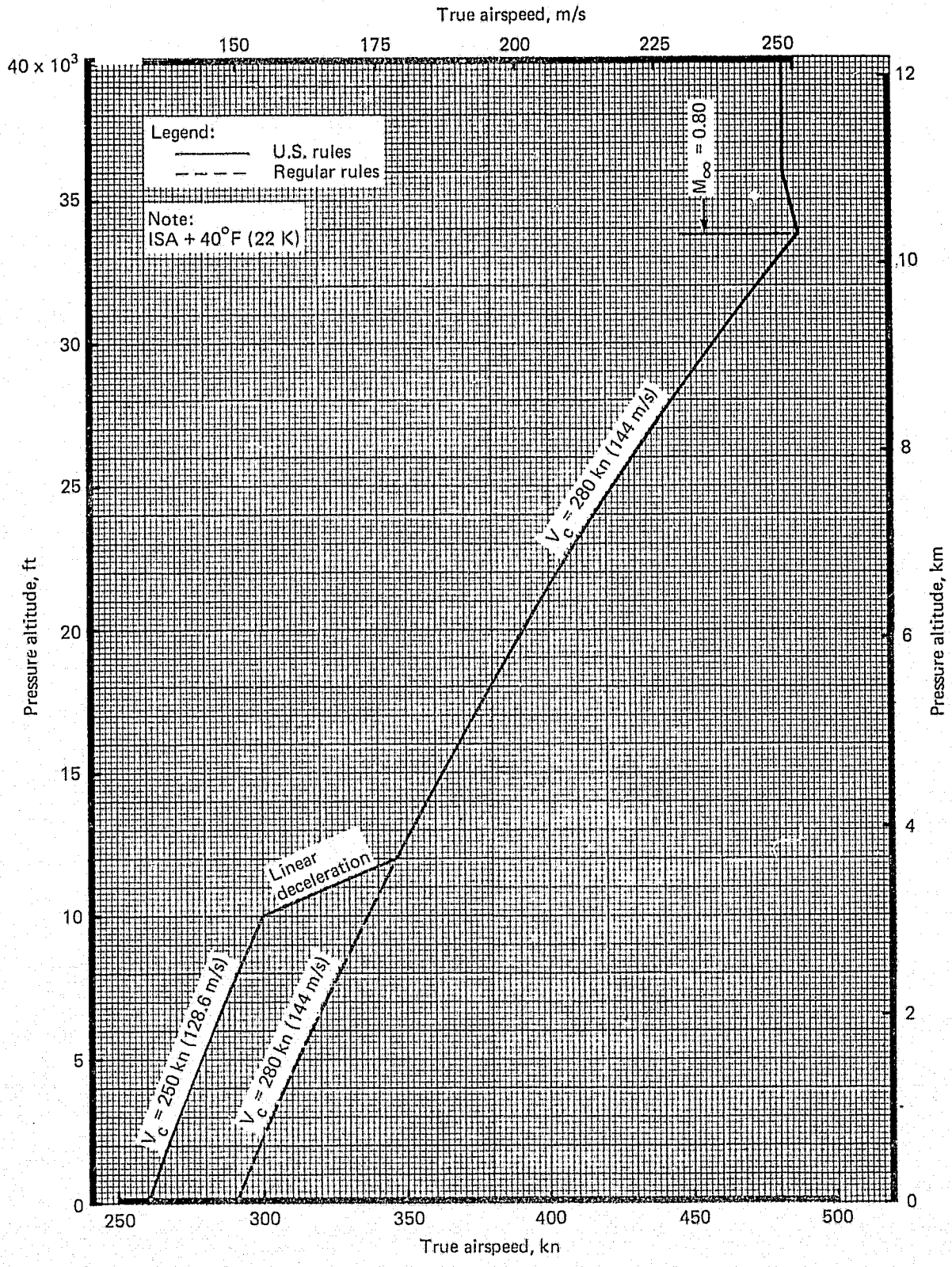

Figure 95.—727-200 Low-Speed Descent Schedule

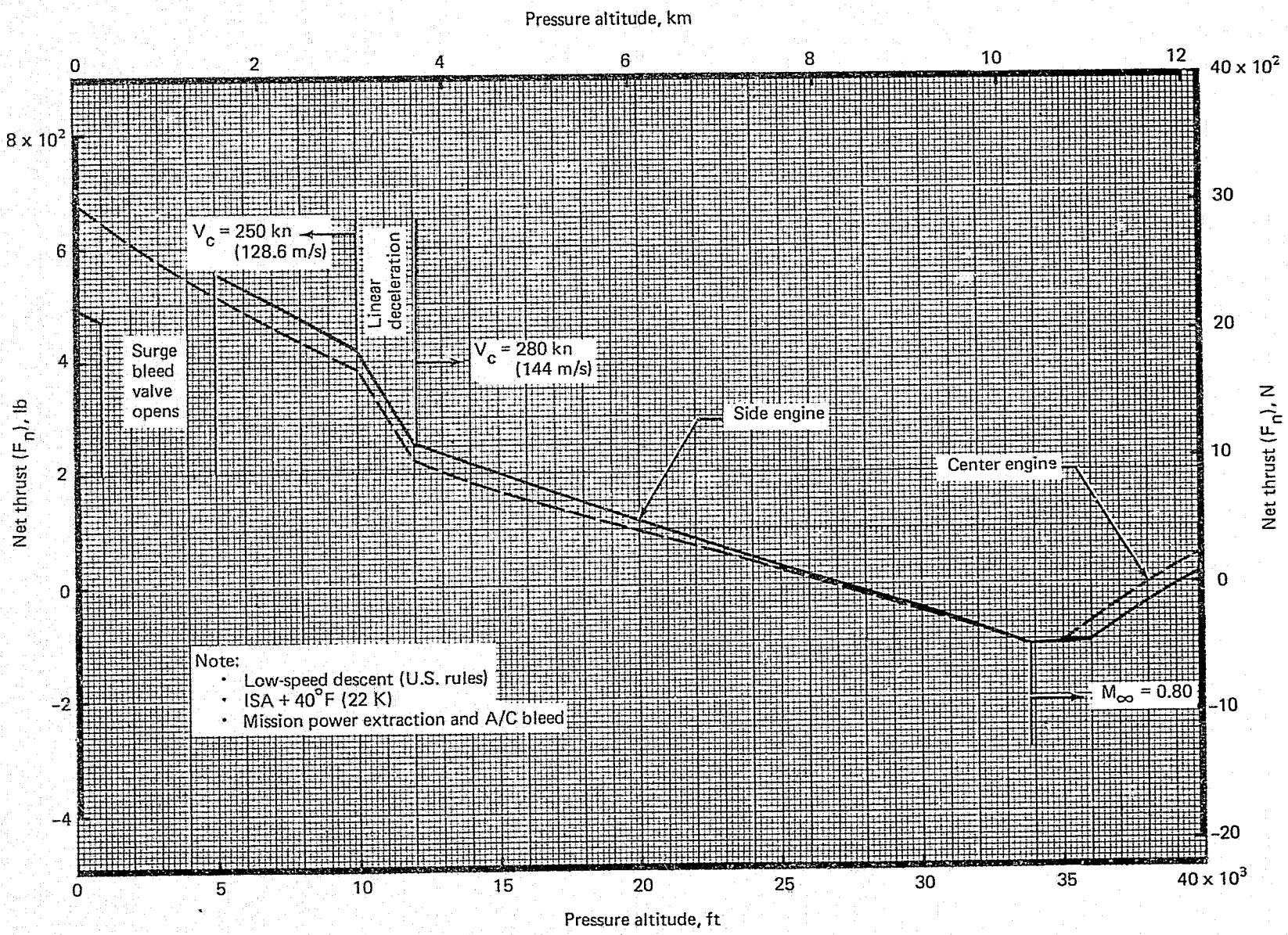

Figure 96.—Installed JT8D-109 Side- and Center-Engine Idle Descent Performance

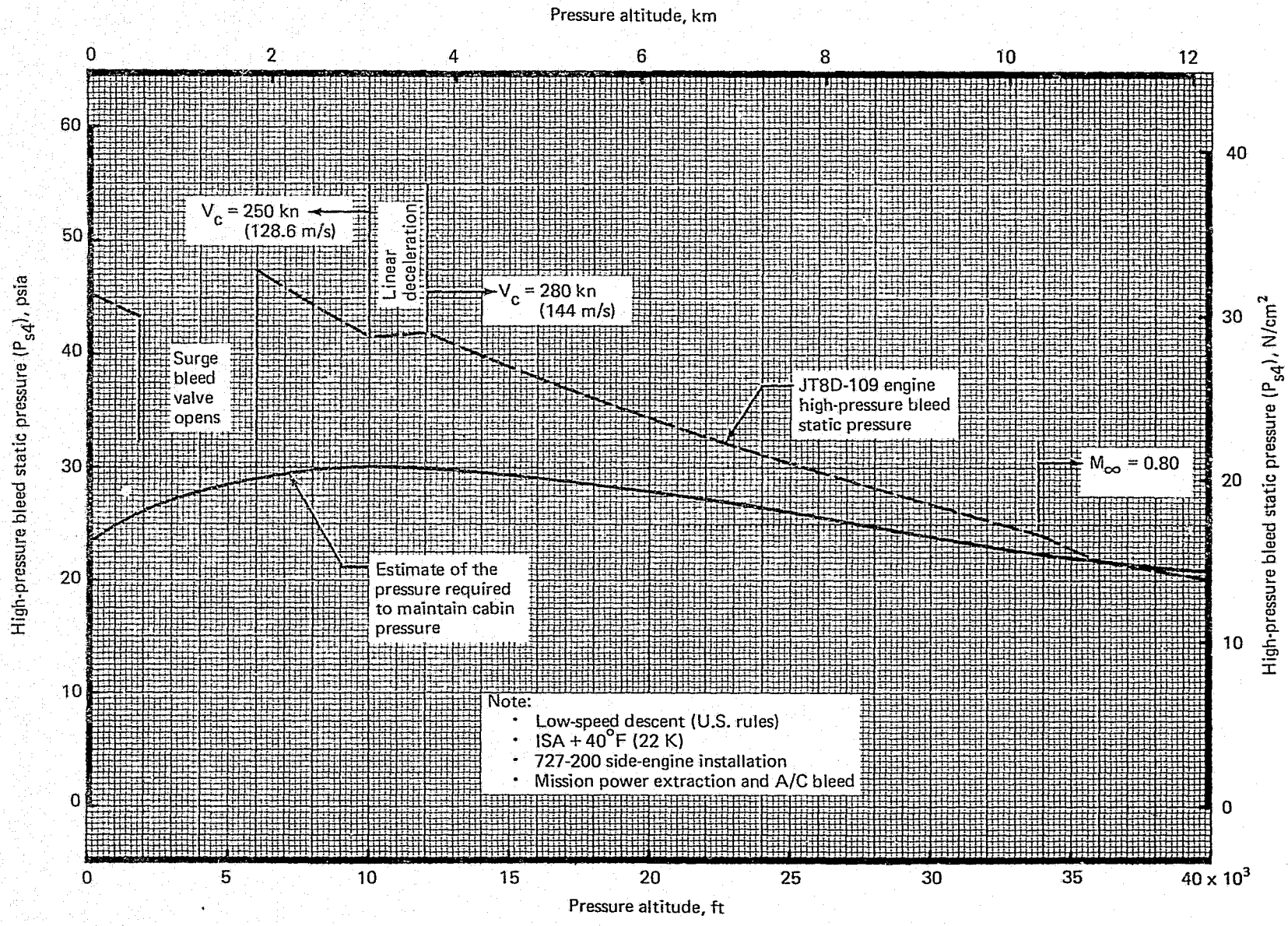

Figure 97.—Installed JT8D-109 Side-Engine Idle Descent High-Pressure Bleed Pressure

Similar LPC stall margin tests were conducted by the Contractor using the 727 refan center- and side-engine inlets in the refan engine ground test described in Volume III of this final report (ref. 3). These tests indicated that statically there was no loss in engine LPC stall margin for either the side- or center-engine inlet installations. With a 20-kn (10.3-m/s) crosswind, it was determined that the LPC stall margin was degraded by about 4%; nevertheless, stable engine operation was maintained. With these results and using the standard JT8D-9 takeoff power setting procedures, it is expected that the JT8D-109 inlets on the 727 refan airplane will meet operational engine stability requirements.

The JT8D-109 exhaust system and thrust reverser are also expected to present no engine stability problems. The JT8D-109 exhaust system was matched per P&WA requirements, as described in reference 3, and no engine instability was experienced during ground tests. The thrust reverser will not adversely affect engine match and stability, as reported in reference 8.

3.4 STRUCTURAL ANALYSIS

The structural analysis described in this section covers the structure designed (described in Volume II of this final report, ref. 4) and the modifications required to meet the program objectives to design certifiable structure.

In order to incorporate the JT8D refan engine and nacelle with minimum weight and airframe modification, advanced structural concepts were used.

Aluminum-brazed titanium acoustic honeycomb was used for the exhaust assembly and perforated aluminum backed by fiberglass honeycomb for the center-engine inlet duct. Heat-resistant epoxy fiberglass skins and phenolic honeycomb construction were proposed for the nacelle cowl panels of the side engines.

The major structural features of the titanium exhaust system were evaluated by detail tests which were reported in reference 11. Further test data were obtained from limited instrumentation on the center-engine inlet duct and fan/primary flow divider during the engine ground tests. These tests were reported in Volume III of this final report (ref. 3).

Extensive use was made of structural analysis computer programs to evaluate the load distribution in the major structural assemblies. Results obtained from these programs were used to derive the loads applied to components for the stress analysis.

Load conditions used for the 727-200 were also applicable to the 727 refan. The structural analysis was made for the JT8D-117 engine, since weight, thrust, and reverse thrust capability for that engine were greater than the -109 engine and thus critical to the structure. A dynamic landing analysis was used to verify that the new engine center of gravity and weights did not adversely affect the load factors. This is reported in section 3.4.12.

The Contractor's latest fatigue data were used to evaluate the fatigue durability of the structure to provide life of 70 000 flights.

The major breakout for each structural item discussed in this section includes the structural concept and analysis methods used to substantiate the structural adequacy. This analysis covers only major components.

3.4.1 SIDE-ENGINE INLET ASSEMBLY

3.4.1.1 Structural Concept

The side-engine inlet assembly would consist of the outer nose cowl, the acoustic inlet ring, and the nose dome (figs. 98 and 99).

The cowl design was similar to that used for the 727-200 nacelles, with the exception of modifications to the thermal anti-icing (TAI) distribution tube support brackets and additional ribs to support the inlet ring.

To increase service life, the existing TAI distribution tube support brackets would be replaced by leaf spring type supports, which allowed greater flexibility during thermal deflections of the spray ring. Three pairs of intercostal ribs were added to distribute loads from the inlet ring support struts into the cowl structure.

The inlet ring leading edge was designed using electro-formed nickel faired with acoustic honeycomb polyimide panels. It was supported concentrically in the inlet by three radial struts, which also distributed TAI air to the leading edge. This design concept was similar to that used in the FAA-sponsored Quiet Nacelle Program (ref. 12).

The nose dome design was similar to that used in the 727-200 nacelles. A formed aluminum cap was backed by a polyimide acoustic honeycomb body to which the attachment fittings for the bolts were mounted.

3.4.1.2 Analysis

Low-speed wind tunnel tests were conducted to determine the pressure distribution within the engine inlet nose cowl. From these tests, which are reported in reference 13, a more precise pressure distribution than had previously been available was obtained and used to derive loads in the inlet. A typical pressure distribution on the nose cowl for the nose down, flap 40° landing approach is shown in figure 100.

Engine asymmetric surge conditions were critical for the nose dome and inlet ring. Maximum design ultimate pressures were +4.65 psig (+32.06 kN/m^2) and -9.5 psig (-65.50 kN/m^2).

Loads from the inlet ring were distributed through the radial ribs into the cowl. Since only ground test hardware was to be built, the ring analysis was limited to comparing it with that designed for the Quiet Nacelle Program (ref. 12).

A summary of critical margins of safety and associated load conditions for the side-engine inlet assembly is shown in table 33.

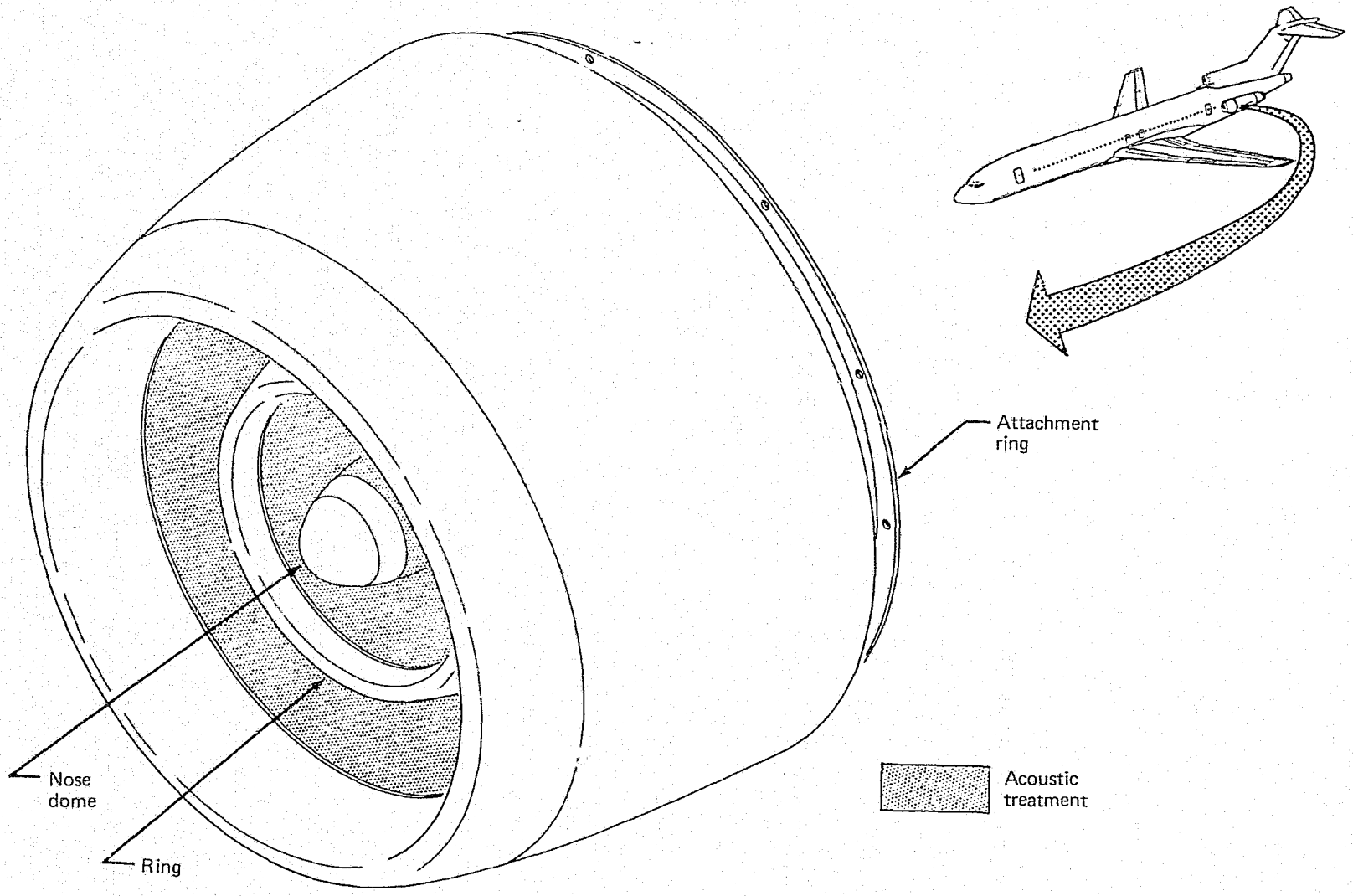

Figure 98.—JT8D Refan Side-Engine Inlet Assembly

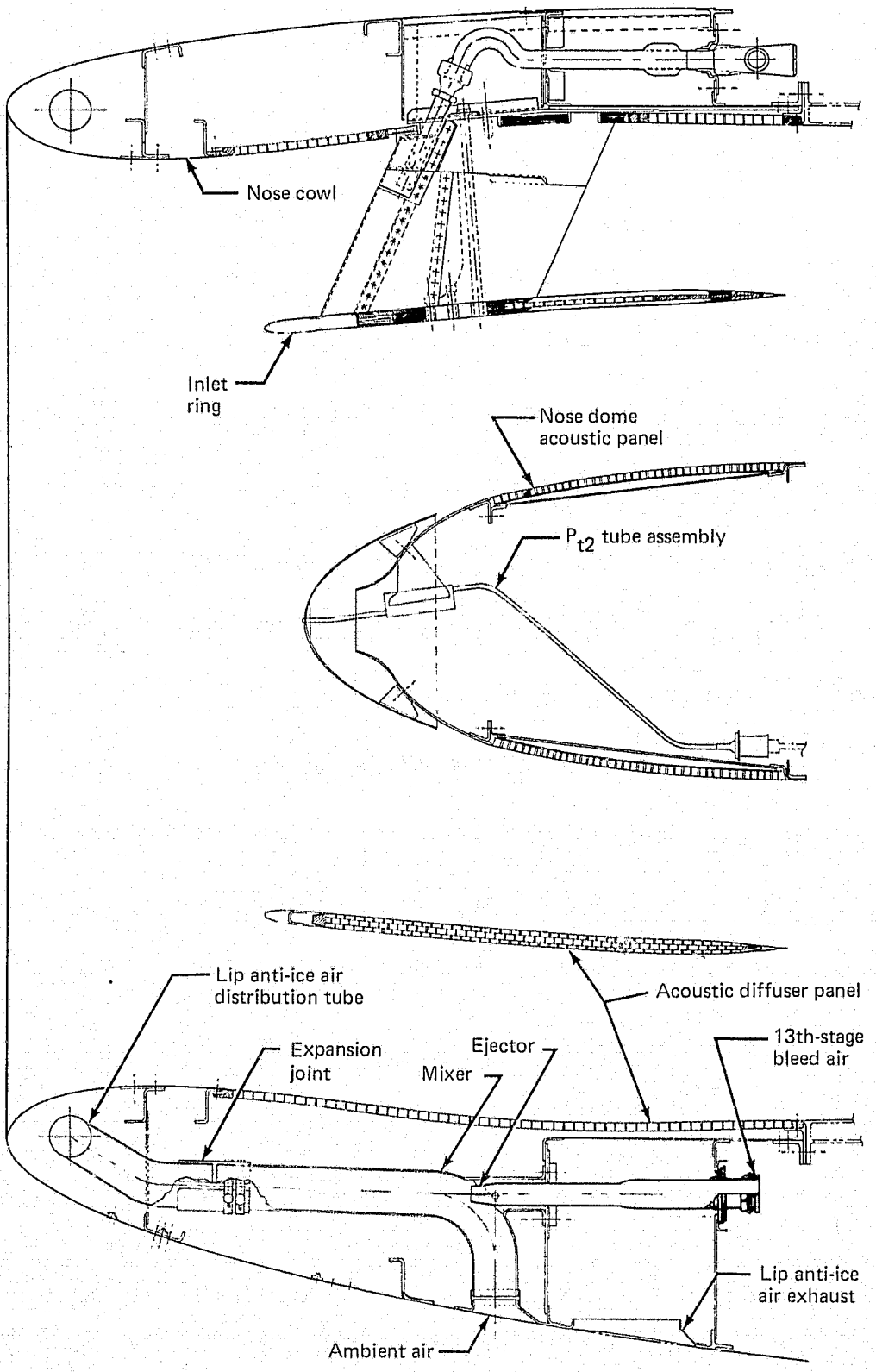

Figure 99.—JT8D Refan Side-Engine Inlet Construction

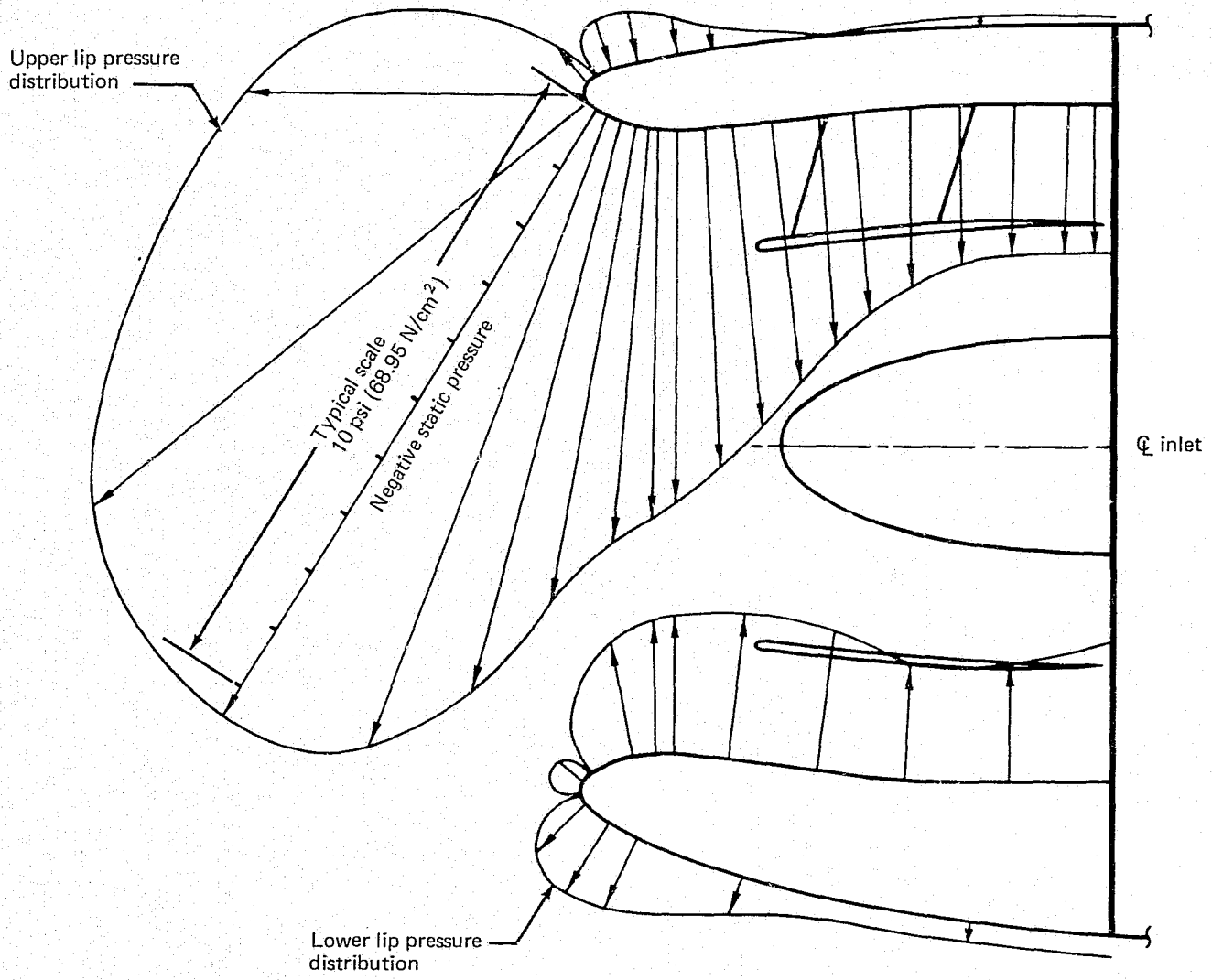

Figure 100.—JT8D Refan Side-Engine Inlet Pressure Distribution—Nose Down, 40° Flaps

Table 33.—JT8D Refan Side-Engine Inlet Cowl Margins of Safety Summary

Location	Condition	Margins of safety
Cowl attachment flange on engine[a]		
Vertical shear	Nose down approach	0.24
Axial load	Nose down approach	>2.0
Moment	Nose down approach	0.63
Flange bolt	Nose down approach	0.71
Nose dome attachment flange on engine[a]		
Vertical shear	Engine surge	0.03
Axial load	Engine surge	0.0
Moment	Engine surge	0.01
Flange bolt	Engine surge	0.10
Cowl outer skin station 57.35 in. (1.46 m)	Nose down approach	0.48
Thermal anti-icing ring	Failed valve 300°F (422 K)	0.51

[a] Based on P&WA engine allowables

3.4.2 SIDE-ENGINE COWL PANELS

3.4.2.1 Structural Concept

The cowl panels were designed in three sections: the inboard fixed cowl, which was attached to the engine frames, and two cowl doors, upper and lower, which formed the contour of the nacelle. These doors were locked together with seven latches, to produce a monocoque nacelle structure supported off the fixed cowl and the fore and aft engine bulkheads. Figure 101 shows the nacelle cowls hinged open about the fixed fairing hinge lines.

The fixed cowl would use conventional aluminum stiffener and skin construction similar to the existing 727 nacelle design. The movable cowl panels were designed to be made of fiberglass honeycomb construction, using heat-resistant two-ply fiberglass epoxy skins and 1-in. (2.54-cm)-thick phenolic core. A stainless steel wire mesh was inserted in the inner skin to provide flame resistance in the event of a nacelle fire.

The latch fittings were designed to be made of conventional cast aluminum, attached to suitably reinforced areas of the cowls.

3.4.2.2 Analysis

Wind tunnel tests determined the airload distribution on the cowls for low-speed, high angle-of-attack conditions. Results of these tests are reported in reference 13. The nacelle pressure distribution for the design ultimate, flaps down, high angle-of-attack condition is shown in figure 102.

The cowls are loaded by nacelle aerodynamic pressures, inertia loads, and also wind loads when open on the ground. A pressure relief door was provided in the upper cowl panel to withstand a design ultimate internal pressure of +3.36 psig (+23.166 kN/m^2) in the event of a high-pressure bleed duct failure. The structure was also designed to carry aerodynamic limit loads with any single latch or hinge failed or unlatched.

Nacelle loads were distributed to the fore and aft nacelle bulkheads and circumferentially to the fixed cowl hinges where they were carried into the engine casing.

Due to the omnidirectional strength characteristics of the honeycomb construction and multiple redundancies at the latches, hinges, and engine bulkheads, a finite element structural analysis was used to determine the internal load distribution, latch, hinge loads, and reactions. An initial analysis model was made of the doors only, and further development of the model added the fixed cowl with reactions to the engine and a simulation of the engine fore and aft bulkheads (fig. 103).

Analysis runs were made for both the design ultimate loads and internal pressure conditions, and simulated failed latch or hinge conditions.

A summary of cowl and latch margins of safety is given in table 34.

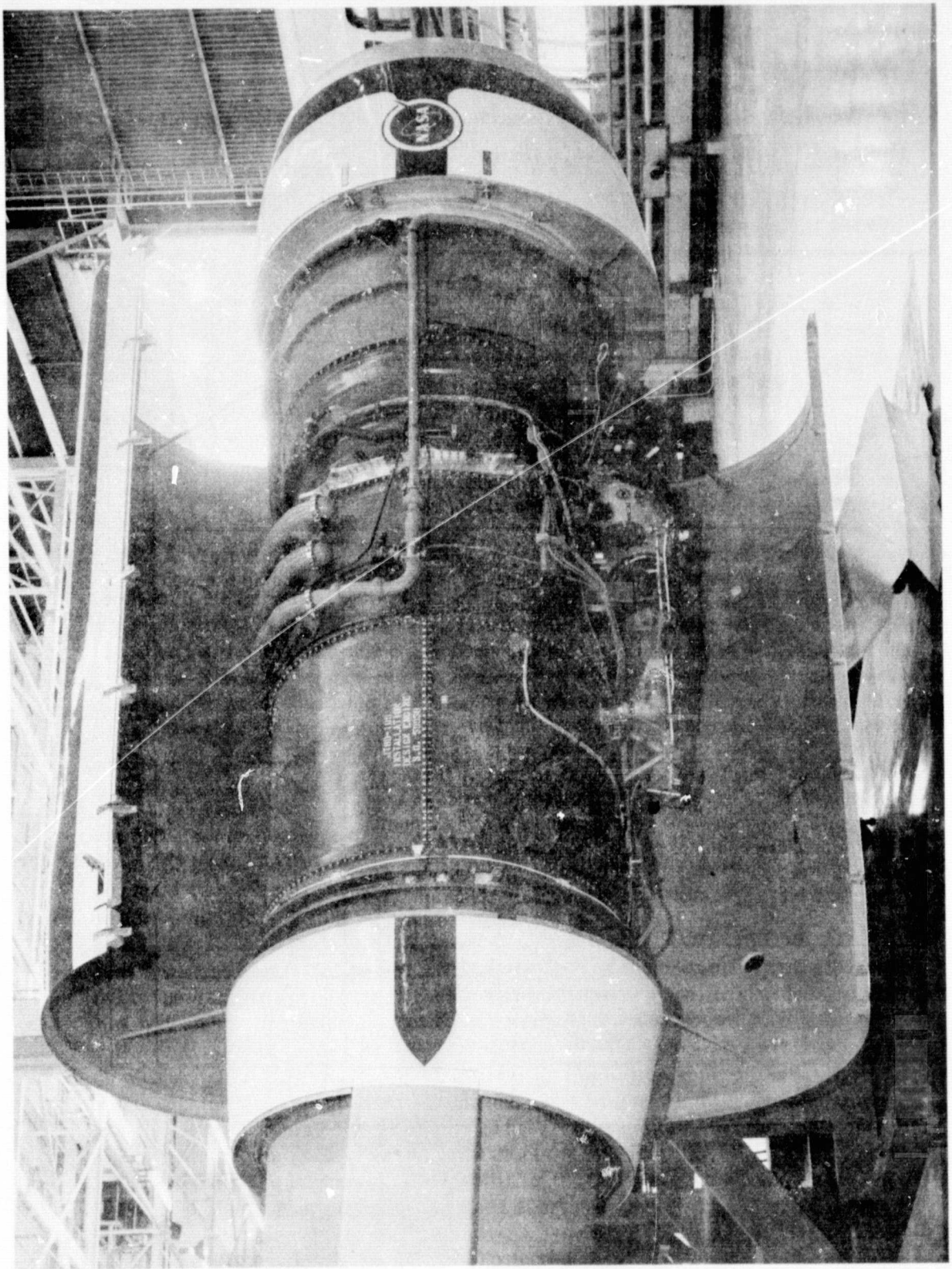

Figure 101.—JT8D Refan Mockup—Side-Engine Cowls

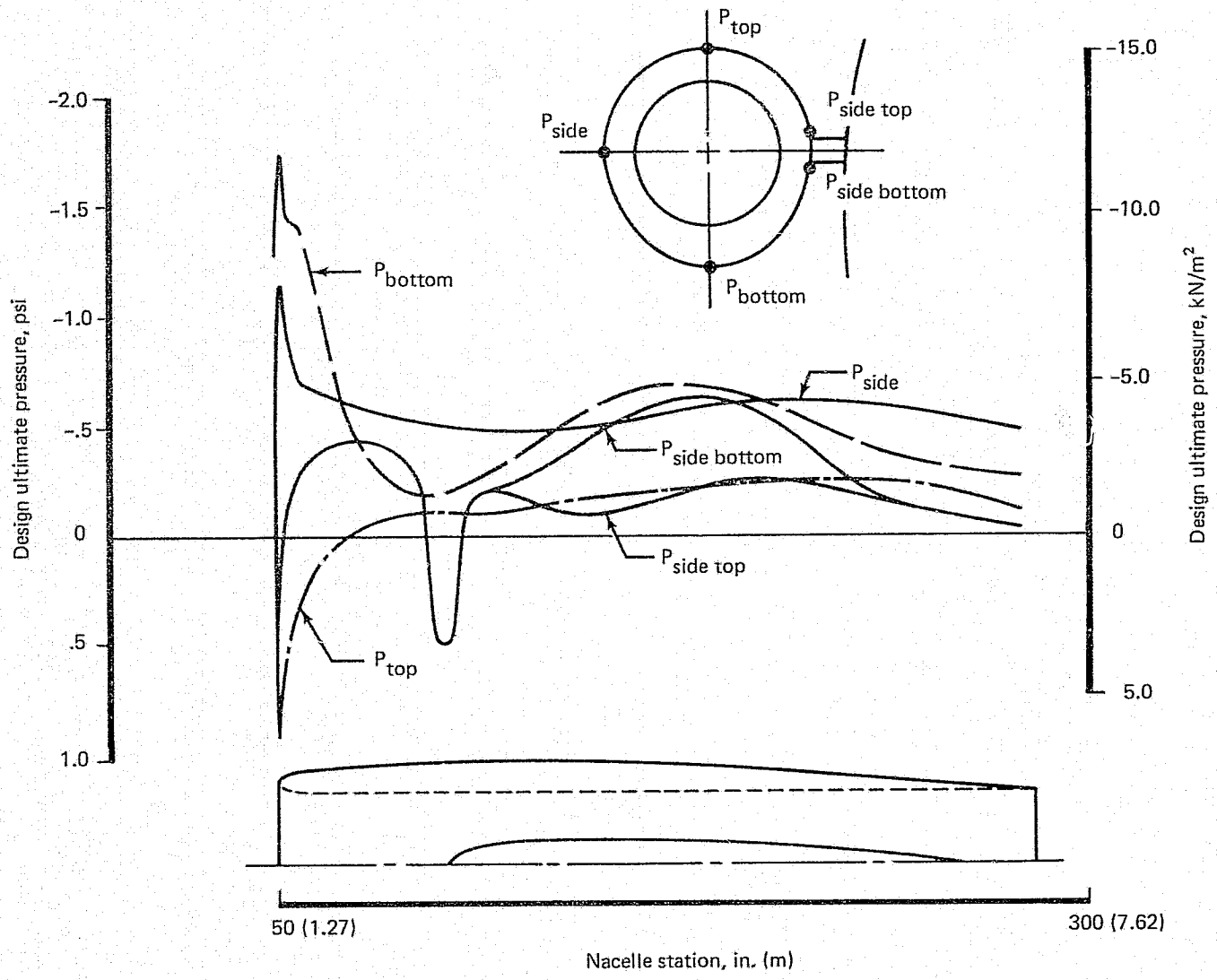

Figure 102.—JT8D Refan Side-Engine Nacelle Pressure Distribution—High Angle of Attack, 2.5-g Maneuver Condition

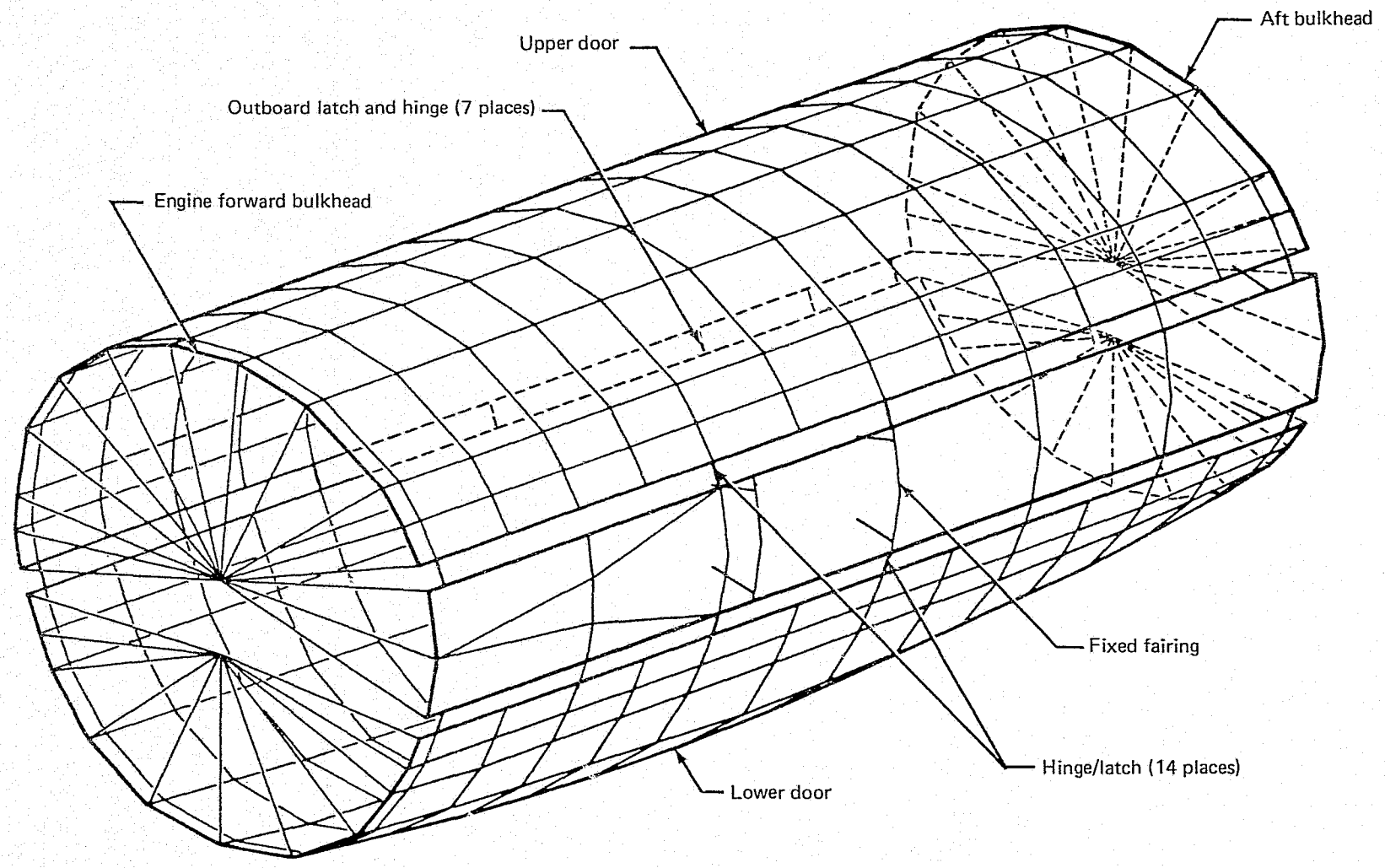

Figure 103.—JT8D Refan Side-Engine Nacelle Cowls—Finite Element Analysis Model

Table 34.—JT8D Refan Side-Engine Nacelle Cowl Margins of Safety Summary

Location	Condition	Margins of safety
Cowl frame 8 (local bending)	Duct failure at 240°F (389 K)	0.05
Latch casting frame 8 (casting factor = 1.5)	Duct failure at 240°F (389 K)	0.80
Latch casting frame 6	Failed latch 8	0.71

3.4.3 SIDE-ENGINE STRUT

3.4.3.1 Structural Concept

The side-engine strut design for the 727 refan airplane was structurally unchanged from that used on the 727-200 airplane, except for the vibration isolators and engine cone bolts which were changed to accommodate the heavier engine (fig. 104).

The forward support fitting would be made of steel and the aft support fitting of aluminum. Both fittings would be cantilevered off aft fuselage bulkheads and stabilized fore and aft by longitudinal members and the fairing skins, which together would form a torque box. The outer vertical longitudinal web would also form the firewall for the engine.

The aft fitting would react only the vertical and side load components; the forward fitting would react the thrust, drag, side, and torsional engine loads. These loads would be redistributed by the strut torque box and reacted into the aft fuselage structure.

3.4.3.2 Analysis

A finite element analysis was used to evaluate the load distribution in the strut. Results from the analysis were also used to define the engine flexibility matrix and cone bolt loads.

The strut outboard of the fuselage skin was simulated together with a simplified analysis model of the engine (fig. 105). The model checkout was made by comparing calculated deflections with deflections obtained in the 727 static test. When the analysis was found to be compatible with the test results, the model geometry was amended to represent the JT8D refan engine geometry and stiffness (table 35).

The 727-200 design load factors were used in the refan analysis. The vertical factors were subsequently shown to be conservative by the dynamic landing analysis results as reported in section 3.4.12. Nacelle weights and engine dynamic loads for the JT8D-117 which were applied to the model are shown in table 36.

Review of the load distribution in the structure showed the steel forward support fitting to be considerably more flexible than the aft one, and consequently it picked up less load than a simple geometric balance would suggest. In the case of a vertical load, the fore and aft component couple which was developed at the top and bottom forward cone bolts, respectively, was less than previously estimated and increased the aft fitting vertical load. This suggests that further analysis would yield a better design.

Cone bolt loads and the engine flexibility matrix, which was used in the dynamic landing analysis, were derived from the analysis results. A brief review was made of the strut structure to identify critical areas.

A summary of margins of safety is shown in table 37.

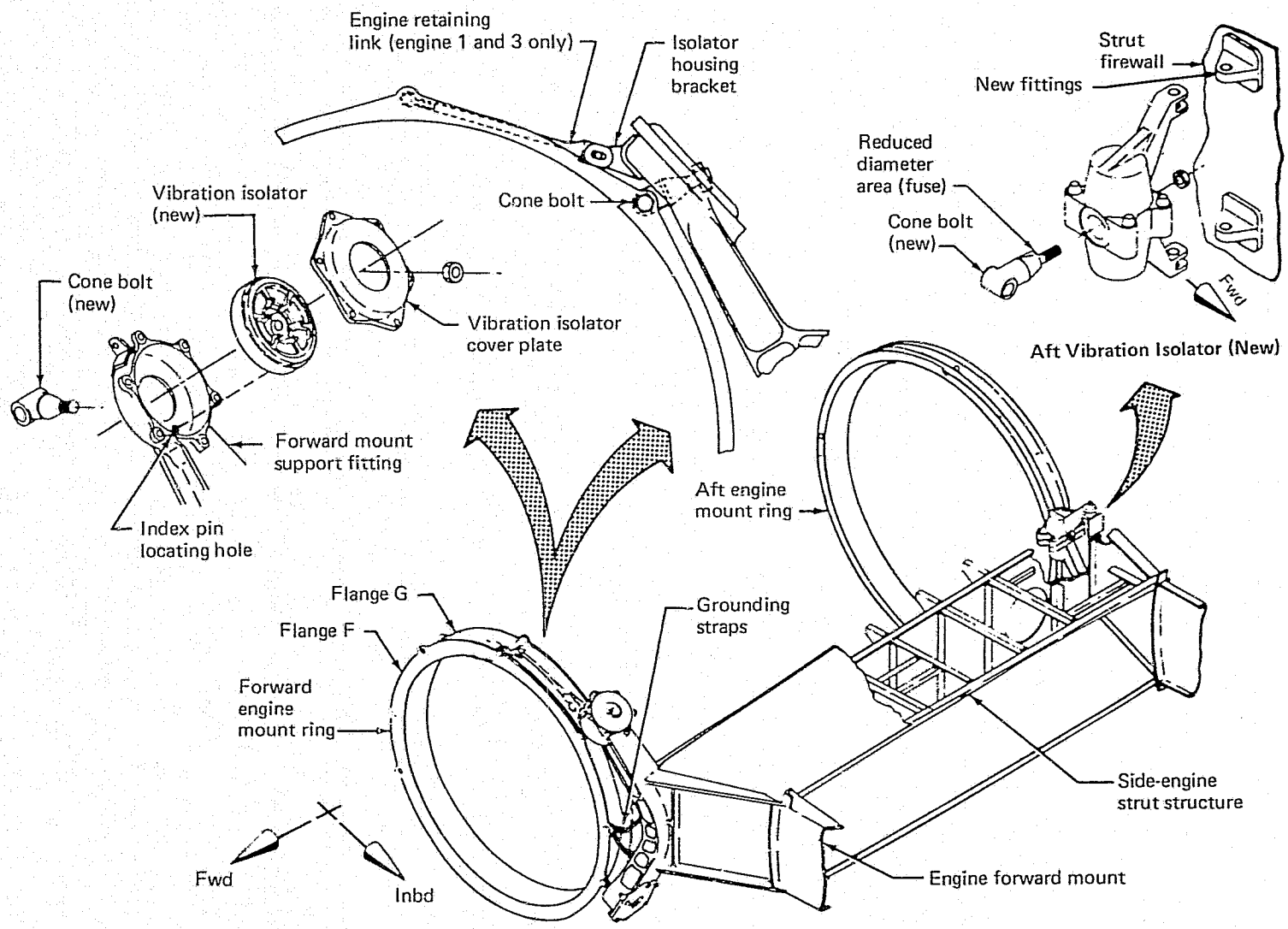

Figure 104.—JT8D Refan Side-Engine Strut and Mounts

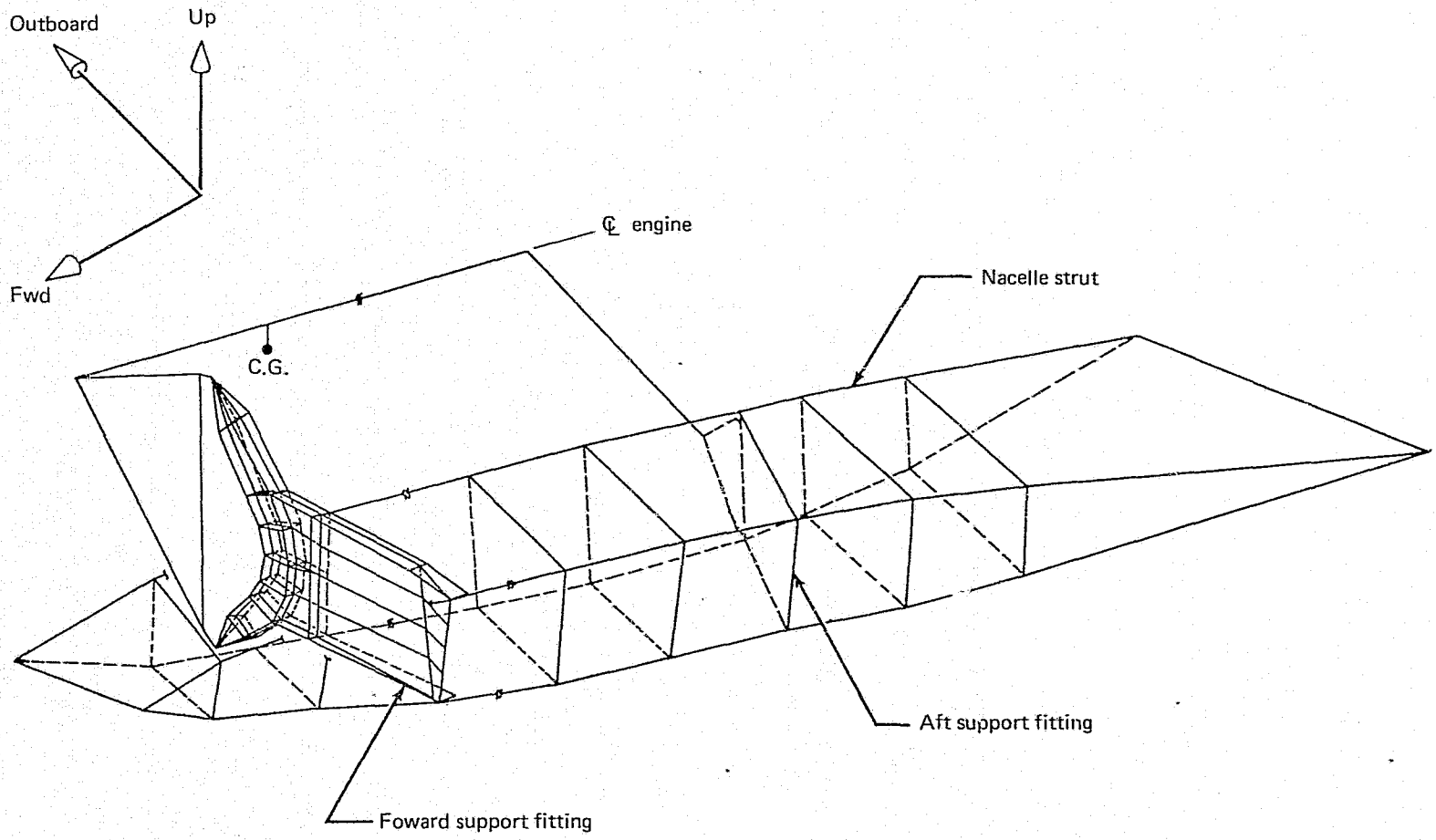

Figure 105.—Right-Hand JT8D Refan Side-Engine Strut—Finite Element Analysis Model

Table 35.—Comparison of 727 Static Test Results and Predicted Nacelle Vertical Deflections

Location	727		727 refan
	Test result, in. (mm)	Predicted, in. (mm)	Predicted, in. (mm)
Forward fitting engine ℄	0.478 (12.145)	0.461 (11.714)	0.637 (16.176)
Firewall	0.129 (3.267)	0.124 (3.144)	0.146 (3.699)
Aft fitting engine ℄	0.425 (10.789)	0.417 (10.604)	0.595 (15.106)
Firewall	0.039 (0.986)	0.041 (1.048)	0.042 (1.069)

Note: Vertical load applied at engine c.g. = 10 000 lb (44.48 kN)

Table 36.—JT8D-117 Side-Engine Nacelle Weights and Engine Dynamic Loads

Condition	Weights and loads
Engine weight	5 700 lb (2585.48 kg)
Thrust maximum	17 900 lb (79.623 kN)
Thrust cruise	14 450 lb (64.277 kN)
Thrust reverser	12 300 lb (54.713 kN)
Moment pitch (for 3-rad/sec yaw)	633 980 in-lb (71.630 m-kN)
Moment yaw (for 2.25-rad/sec pitch)	475 490 in-lb (53.723 m-kN)
Moment roll	422 250 in-lb (47.708 m-kN)

Table 37.—JT8D Refan Side-Engine Strut Margins of Safety Summary

Location	Condition	Margins of safety
Forward fitting		
Upper flange	12-g crash	0.16
Lower flange	12-g crash	0.06
Aft fitting		
Engine vibration isolator attachment	12-g crash	1.38

3.4.4 ENGINE EXHAUST SYSTEM

The engine exhaust system consisted of the wedge duct and exhaust nozzle, the fan/primary flow divider, engine exhaust plug, and wedge duct fairing (fig. 106). These assemblies are common to both side and center engines. The exhaust nozzle would be rotated relative to the wedge duct to accommodate the thrust-reverser exhaust pattern, which would be vertical on the side engines and to the sides on the center engine.

3.4.4.1 Exaust Duct Assembly (Wedge Duct and Nozzle)

Structural Concept.—The exhaust duct assembly would be attached to the engine fan case and would include a 3 ½° wedge section which deflects the exhaust nozzle up, relative to the engine axial centerline.

These assemblies would be made of aluminum-brazed titanium honeycomb, with welded perforated acoustic inner skins and solid outer skins to which machined joint flanges were welded. The nozzle section design also had two pairs of longitudinal machined rails welded into the outer skin to pick up the thrust-reverser support fittings and associated loads. Thrust-reverser loads would be distributed into the nozzle and would react at the engine fan case.

The flange and rail design concepts were subjected to static and fatigue testing (ref. 11). The purpose of the testing was to select the optimum design and to establish the static strength and fatigue durability of the flange and rail details.

Analysis.—The primary design loads on the exhaust nozzle are due to thrust-reverser operation and internal pressure. Refused takeoff (RTO), in-flight inadvertent deployment, and (for the fatigue analysis) normal landing deployment and restow were considered. Relevant side-nacelle and center-engine load factors were also considered where applicable.

The assembly was analyzed with the aid of a finite element analysis. The assembly was cut on the axis of symmetry and half of the structure modeled (fig. 107). The model was sufficiently detailed to reflect the thrust-reverser support fittings, rails, and flanges. Loads from the thrust-reverser door were applied to the model at the thrust-reverser support fittings (fig. 108). The analysis results were used to evaluate the effects of the thrust-reverser loads on the nozzle and to obtain the internal load distribution.

Critical stress levels in the nozzle would be due to the RTO condition and in-flight inadvertent deployment. A summary of typical margins of safety is shown in table 38.

3.4.4.2 Fan/Primary Flow Divider

Structural Concept.—The fan/primary flow divider would be attached to the engine primary case flange and due to the high engine primary gas temperature, would be made of Inconel 625 acoustic honeycomb on the primary flow side and aluminum-brazed titanium on the fan flow side where temperatures were significantly lower. Both items would be bolted together near the trailing edge of the Inconel brazement to complete the assembly. Flow side skins were designed to be perforated on both the Inconel and titanium for sound attenuation (fig. 109).

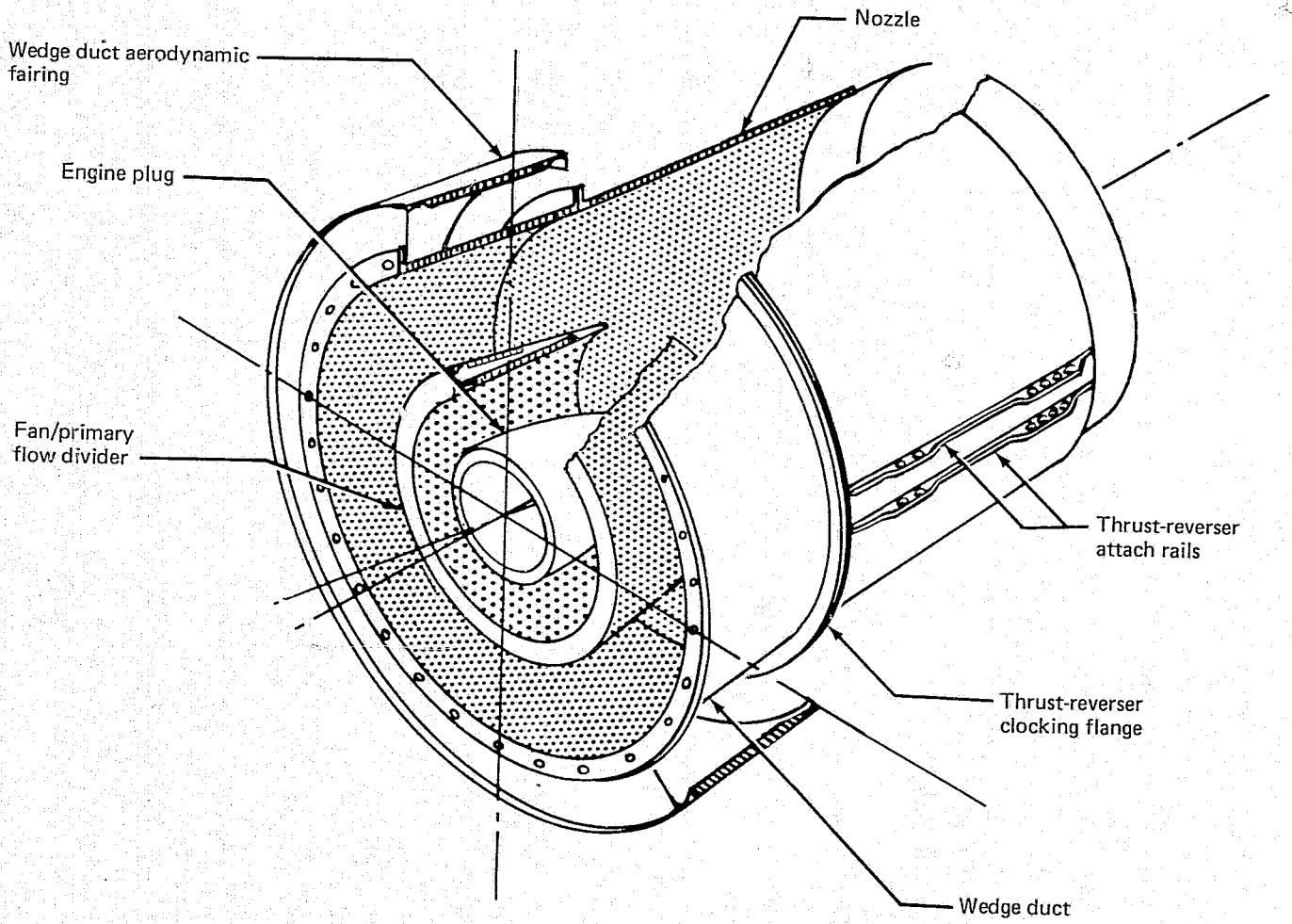

Figure 106.—JT8D Refan Exhaust System

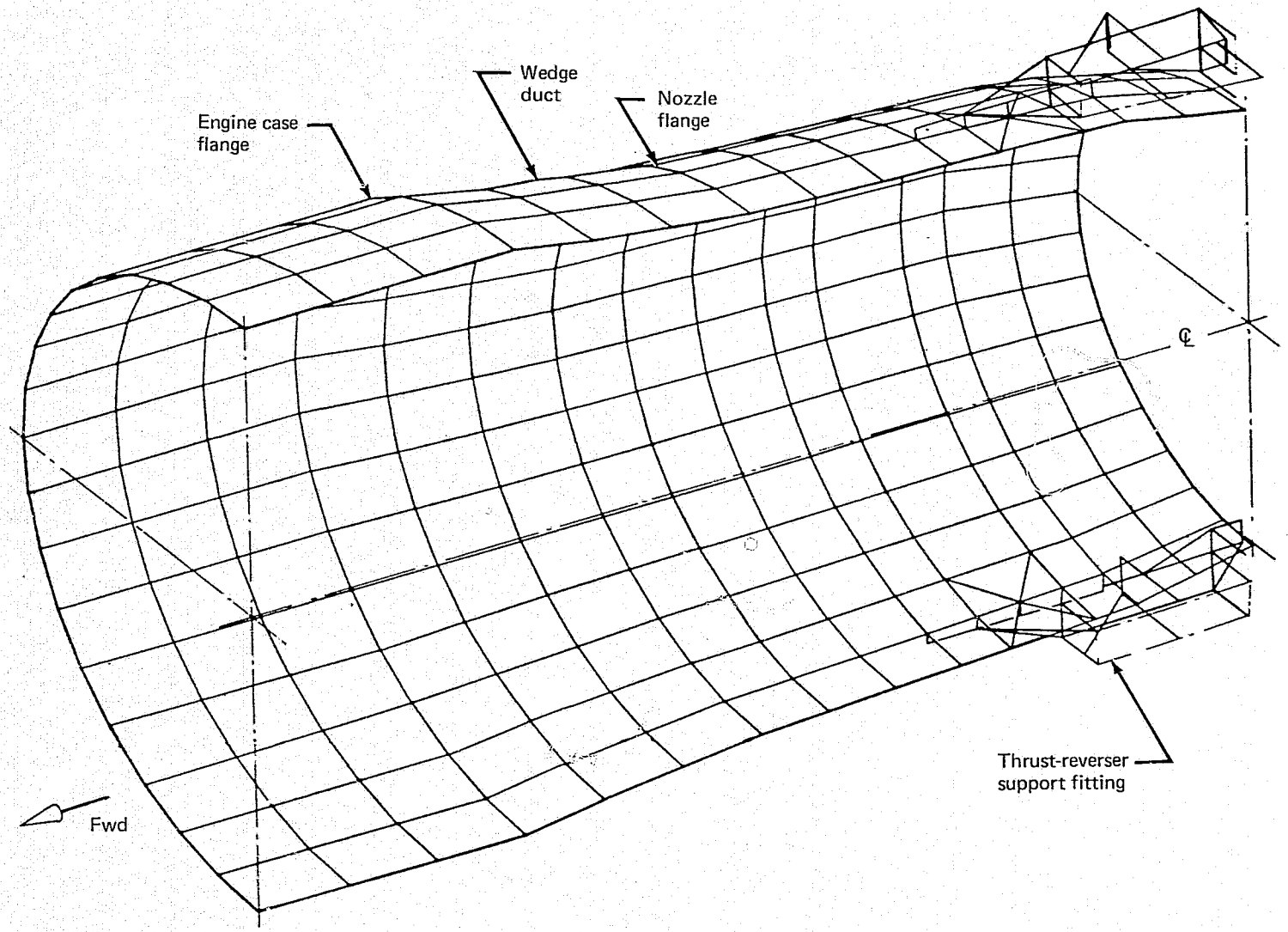

Figure 107.—JT8D Refan Wedge Duct and Exhaust Nozzle–Finite Element Analysis Model

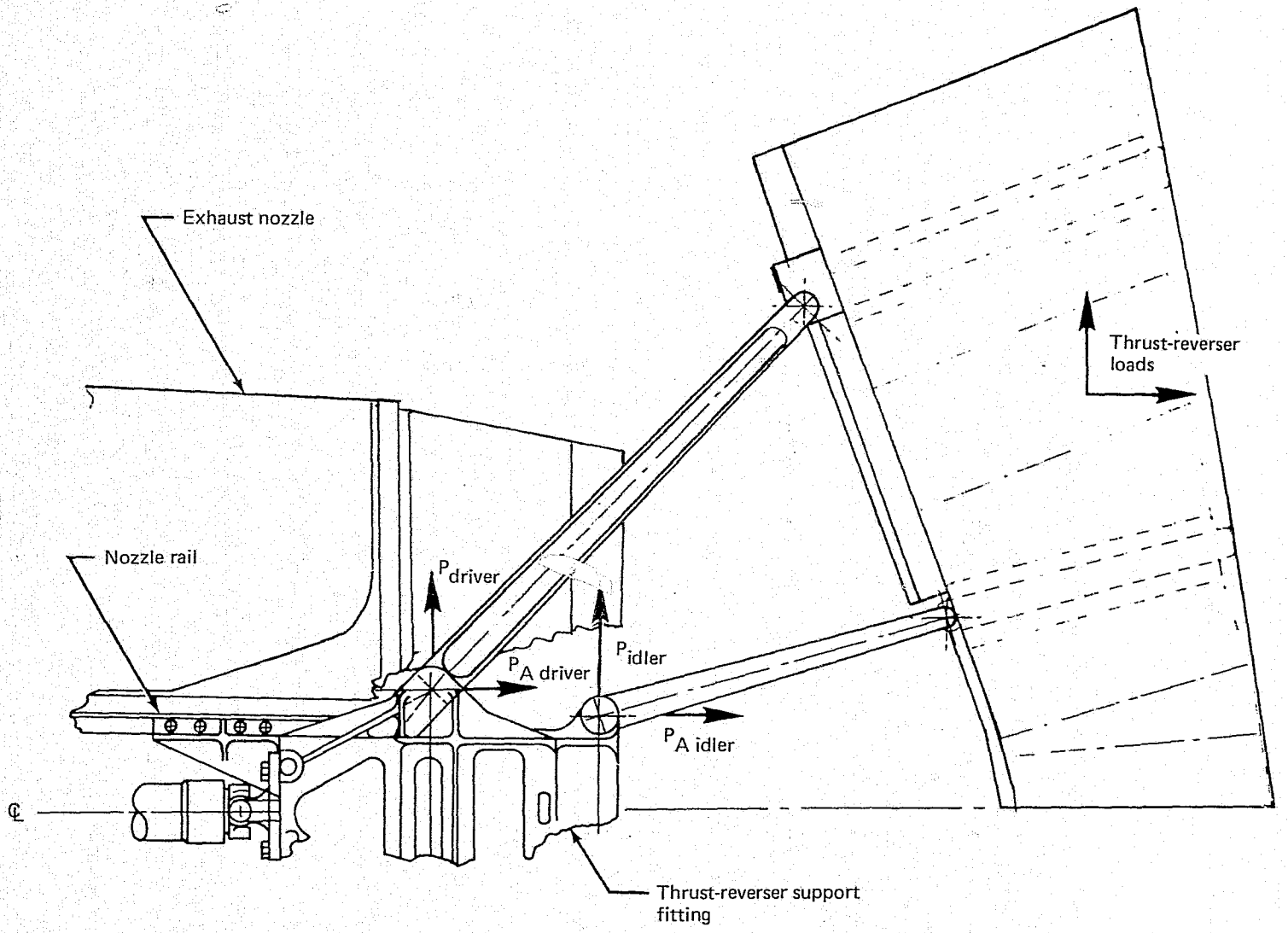

Figure 108.—JT8D Refan Exhaust Duct Assembly—Thrust Reverser Loads Applied to Support Fitting

Table 38.—JT8D Refan Exhaust System Margins of Safety Summary

Location	Condition	Margins of safety
Engine attachment flange[a]		
Vertical	In-flight inadvertent deployment	1.75
Axial		0.13
Moment		1.18
Bolt		0
Flange bending nozzle	RTO	0.28
Nozzle frame aft	RTO	0.33
Nozzle skin outer	RTO	0.10
Fatigue		
Flange bending perforated skin	Normal operation	0.31

[a]Based on P&WA allowables

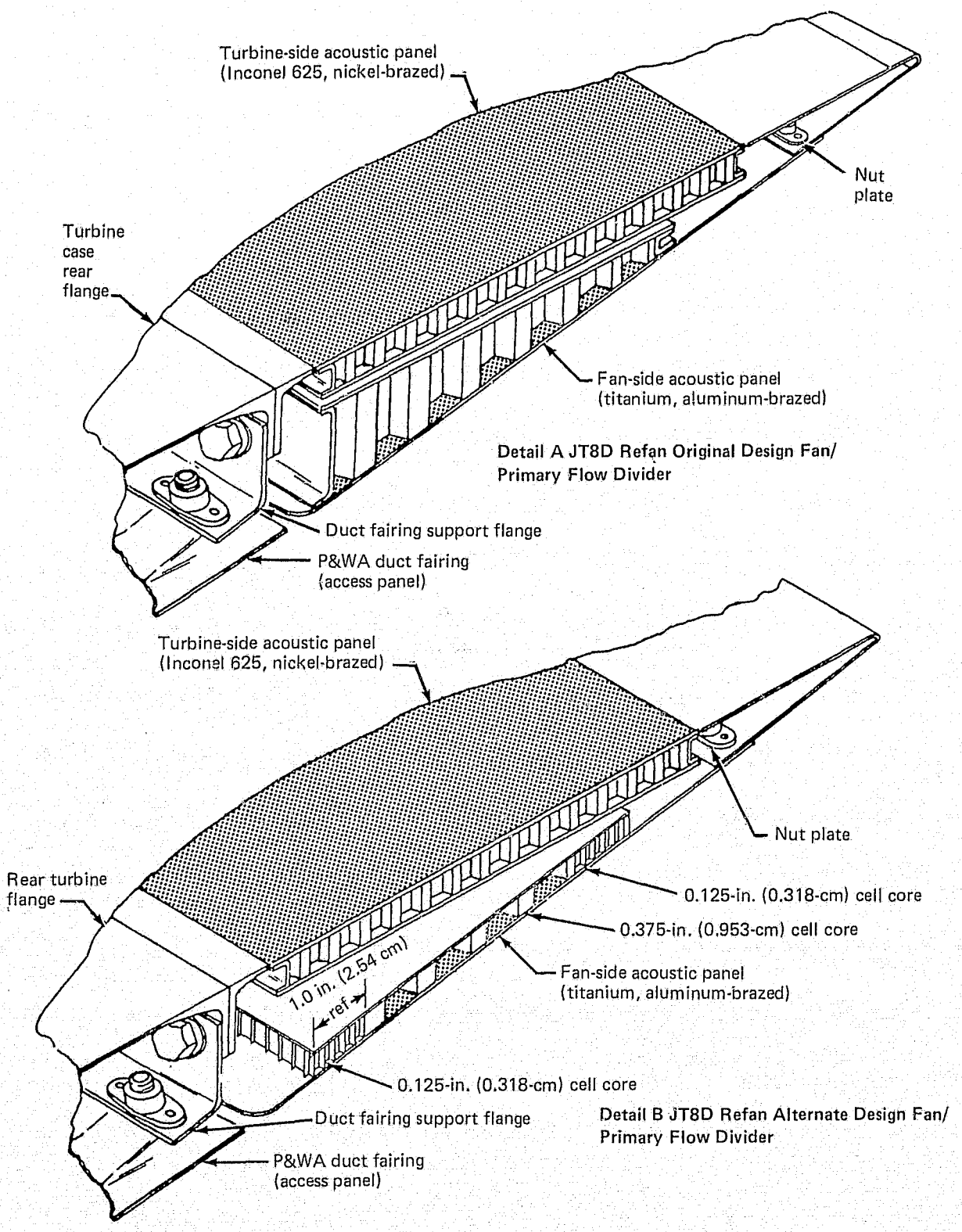

Figure 109.—JT8D Refan Fan/Primary Flow Divider—Original and Alternate Designs

The analysis was made for the original design (fig. 109, detail A). However, due to manufacturing considerations (scheduling and cost), the alternate design (fig. 109, detail B) was fabricated. A comparative analysis was made of the alternate and original designs to ensure equivalent strength.

Axial and lateral loads in the fan flow side of the divider assembly were designed to be carried through the trailing-edge joint to the inner Inconel skin of the primary flow side of the divider and reacted at the engine primary case flange. The pressure differential on the divider would be reacted internally as hoop stress; since the pressure loads would be small, the hoop stress would not be significant.

Analysis.—Maximum loading on the fan/primary flow divider would be due to induced internal thermal stresses caused by the temperature differential between the fan and primary gas streams during engine startup and maximum rpm transient to takeoff power. Maximum temperature on the Inconel was estimated to be 1200°F (922 K) and on the titanium assembly 600°F (589 K). The engine attachment flange design condition would be due to 60-g ultimate vibration loads which would result from an engine blade loss.

In order to investigate the thermal distribution through the divider, a heat transfer analysis model was constructed (fig. 110). Radiation, conduction, and convection coefficients for the gas flows, Inconel and titanium face sheets, and honeycomb assemblies and trapped air were simulated in the model. The analysis balanced the transient heat flow at incremental time intervals until stabilized temperature conditions were obtained. The computer thermal analysis program is described in the appendix under "Heat Transfer Program."

Engine operating conditions considered in the heat transfer analysis were (1) normal engine start to idle, (2) hot start to idle, and (3) maximum rpm transient from idle to takeoff power, hot day. A typical temperature distribution at takeoff power used for input to the structural analysis is shown in figure 111.

A finite element analysis was made of a 90° segment of the fan/primary flow divider to determine the load distribution resulting from the thermal environment (fig. 112).

Results from the structural analysis illustrate the high circumferential loads in the Inconel and titanium skins due to the temperature differential (fig. 113). The assembly bolt joint was located in the low-stress area to obtain maximum fatigue durability.

A summary of typical margins of safety is shown in table 39.

3.4.4.3 Engine Exhaust Plug

Structural Concept.—The exhaust plug was designed to be formed from Inconel 625 sheet and welded to a machined flange. Construction would be similar to existing designs.

Analysis.—Since the construction would be similar to existing designs, only the engine flange attachment loads were determined and local flange stresses checked. Loads on the plug would be due to the exhaust duct 3 ½° angle, internal pressure, and engine vibration which would result from blade loss.

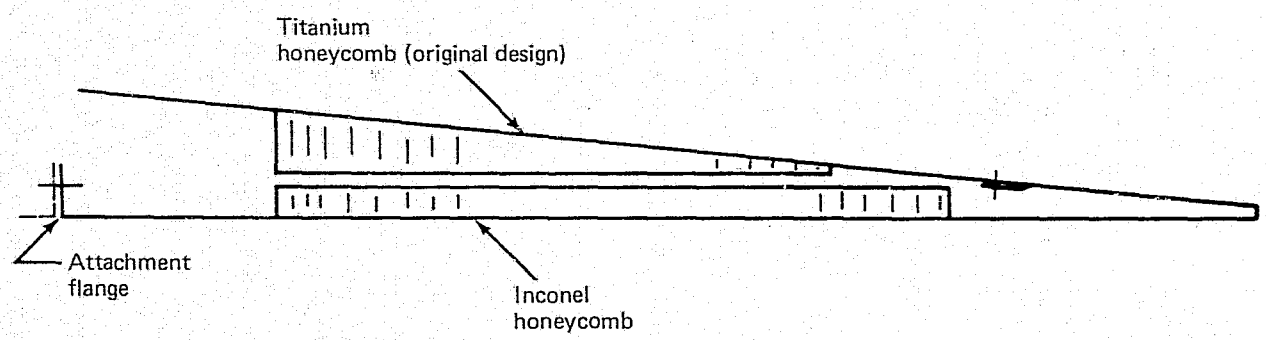

Section Through Fan/Primary Flow Divider

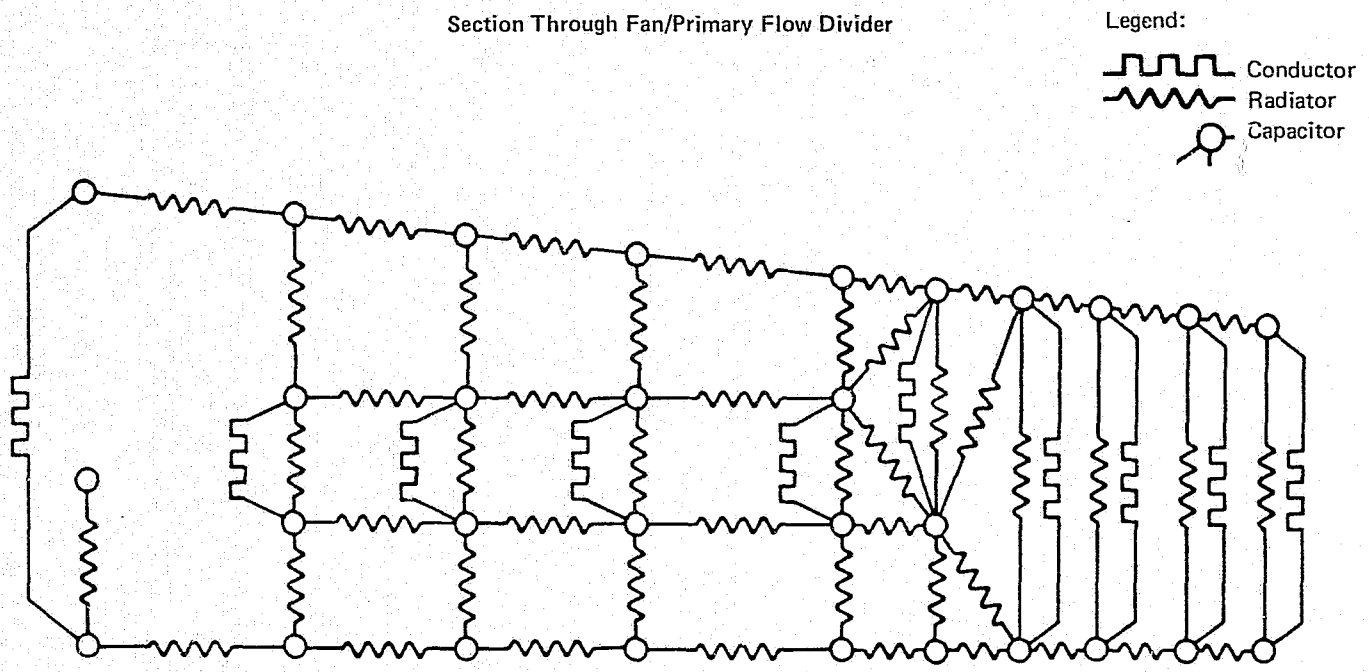

Figure 110.—JT8D Refan Fan/Primary Flow Divider—Thermal Analysis Model

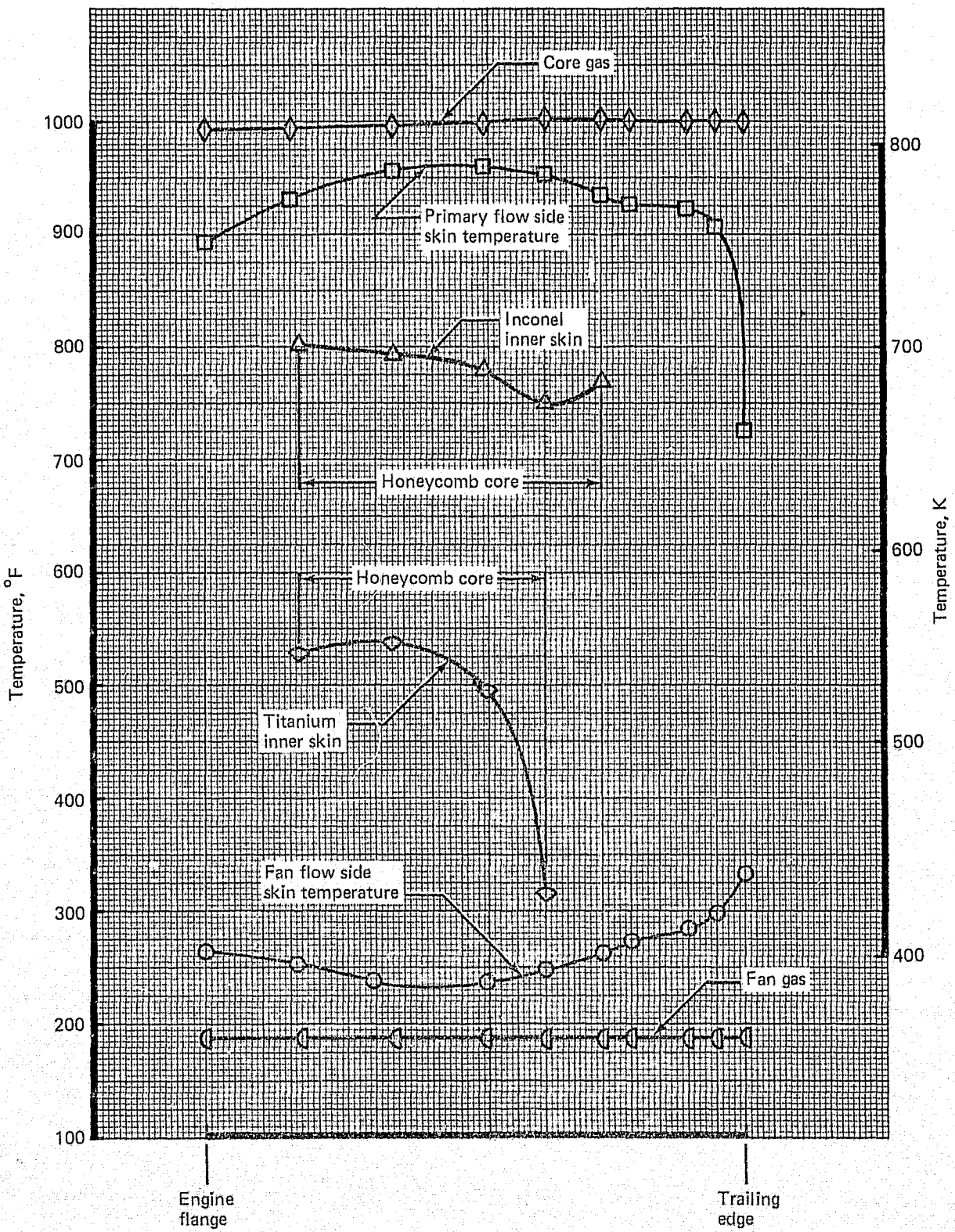

Figure 111.—JT8D Refan Fan/Primary Flow Divider Temperature Distribution—Stabilized Takeoff Power

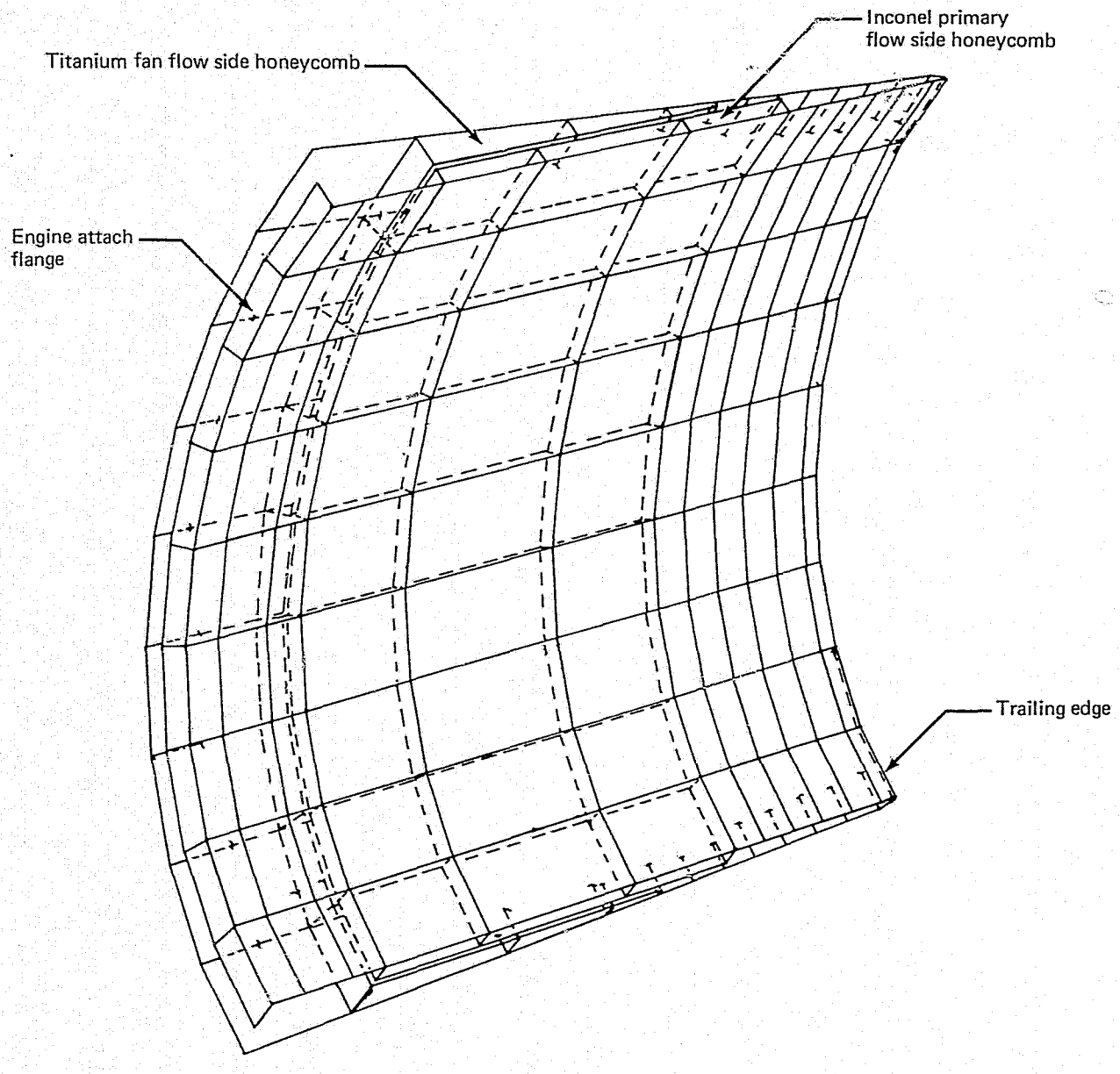

Figure 112.—JT8D Refan Fan/Primary Flow Divider—Finite Element Analysis Model

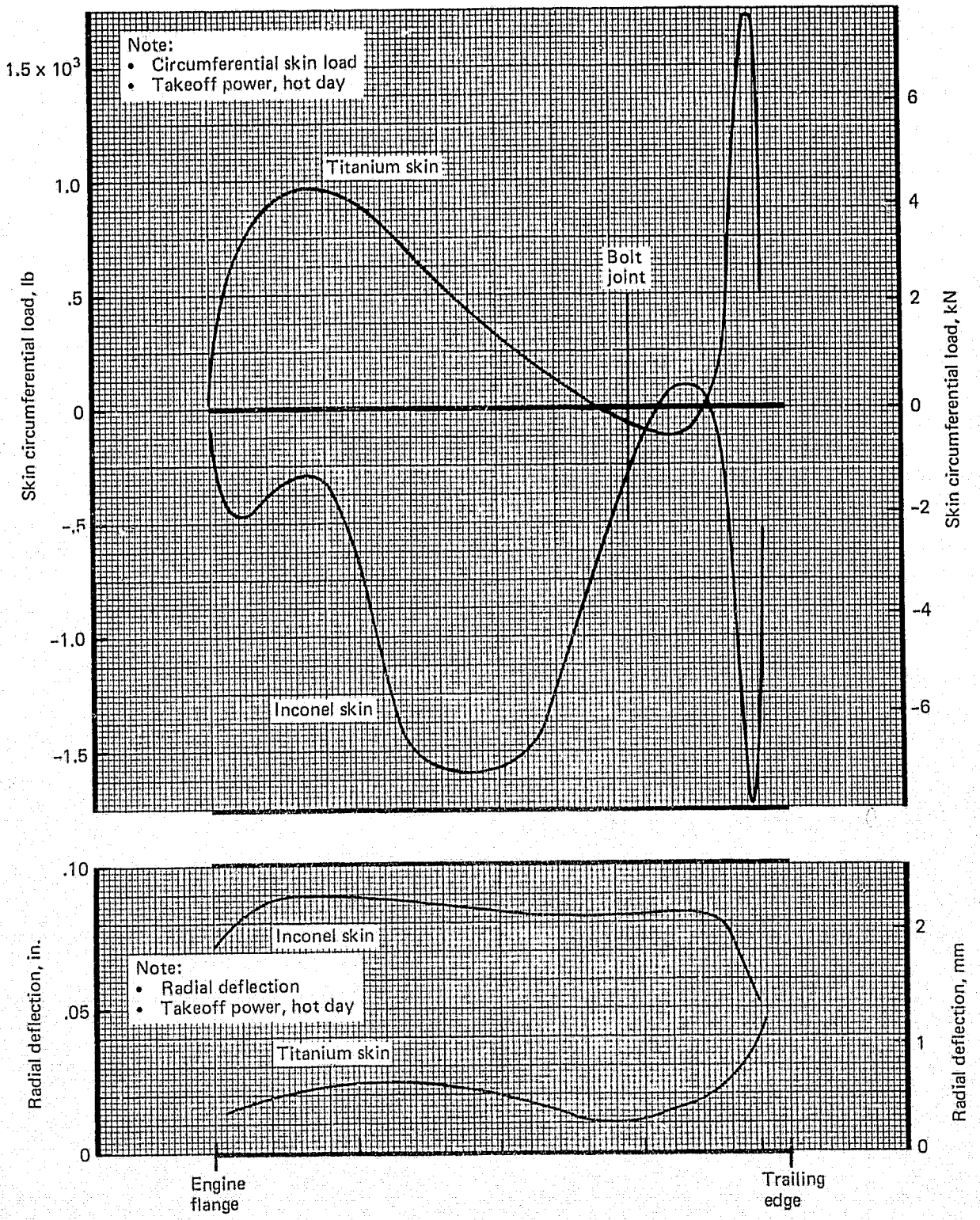

Figure 113.—JT8D Refan Fan/Primary Flow Divider Analysis Results—Circumferential Skin Load and Radial Deflection

Table 39.—JT8D Refan Fan/Primary Flow Divider Margins of Safety Summary

Location	Condition	Margins of safety
Attachment flange[a]		
Vertical	Design ultimate	0.02
Axial	Based on engine	0
Moment	Blade loss	0.05
Bolt	60-g vibration	0
Inconel skin	Takeoff hot day	1.31
Titanium skin	Takeoff hot day	>2.0
Flange	Normal operation	>2.0

[a] Based on P&WA engine flange allowables

Maximum engine flange loads would be due to the engine flange vibration and internal pressure-produced maximum flange bending in the plug.

A summary of margins of safety is shown in table 40.

3.4.4.4 Wedge-Duct External Fairing

Structural Concept.—The wedge-duct fairing would form the nacelle between the engine aft bulkhead and the stowed thrust-reverser doors (fig. 114). The fairing design consisted of four epoxy fiberglass phenolic honeycomb panels, joined along the axial edges by three bolts, to form a hoop. Aerodynamic loads would be reacted into the engine aft bulkhead and the closing frame. The engine aft bulkhead was designed to be braced fore and aft to the closing frame by four intercostal members to react nacelle internal pressure loads.

Analysis.—Critical loads on the fairing would be due to the nacelle high angle-of-attack condition and engine bleed duct rupture.

Predicted margins of safety were greater than 2.0 and none are tabulated here.

3.4.5 THRUST-REVERSER SYSTEM

3.4.5.1 Structural Concept

The thrust-reverser assembly would consist of support fittings, actuators, carriage and linkage, and target-type reverser doors (fig. 115).

The support fitting was designed to be made from a Ti-6Al-4V casting and reacted the reverser operating loads from both the actuator and door linkage system, which pivoted about lugs on the fitting. A separate titanium actuator carriage casting would be mounted on rails within the support fitting and would distribute the actuator loads through steel overcenter links to the driver links.

Both the driver and idler links were designed to be machined from Ti-6Al-4V annealed bar. The driver links would be subsequently heat treated to 150 000 psi (103 421 N/cm^2).

Rib and skin construction would be used for the thrust-reverser doors and the link attachment fittings machined from titanium. Moderate temperatures from the engine primary exhaust impingement on the doors would allow using titanium for the inner skin and ribs. Aluminum 2219-T62 would be used for the outer skin where temperatures were lower. The design of this combination of titanium inner skin and aluminum outer skin would minimize temperature-induced stresses and deflections.

3.4.5.2 Reverser Operation

During flight conditions, the stowed doors would be dually retained by the door lock and preload in the driver links with the retention induced by the actuator driving the carriage overcenter. The thrust reverser is shown stowed and locked in figure 116 and deployed in figure 117.

Table 40.—JT8D Refan Exhaust Plug Margins of Safety Summary

Location	Condition	Margins of safety
Attachment flange[a]		
Vertical	Design ultimate	0.25
Axial	Based on engine	0.08
Moment	Blade loss vibration	0.49
	60-g ultimate	
Bolt		>2.0
Flange bending	Internal pressure	0.41

[a]Based on P&WA engine flange allowables

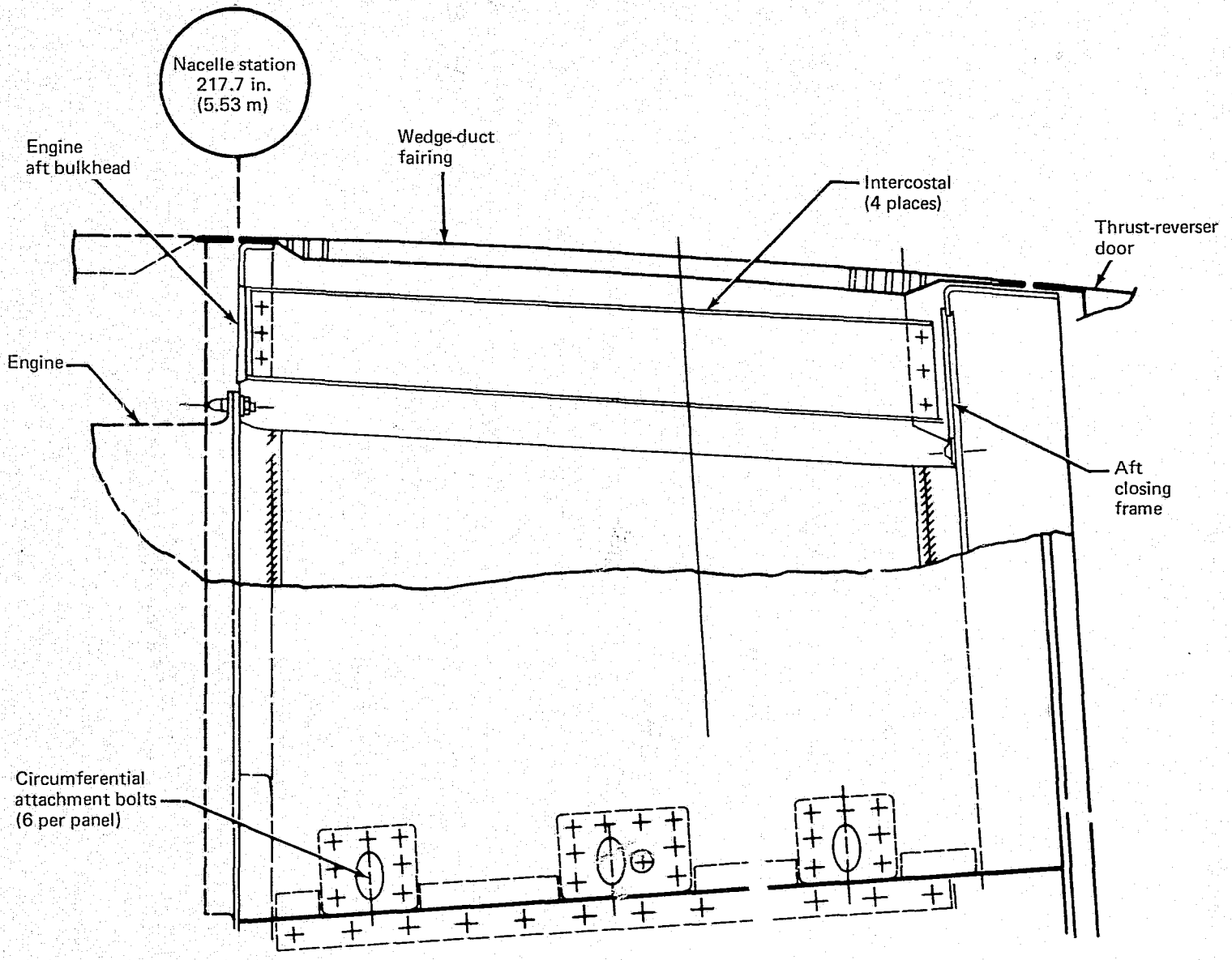

Figure 114.—JT8D Refan Wedge-Duct External Fairing

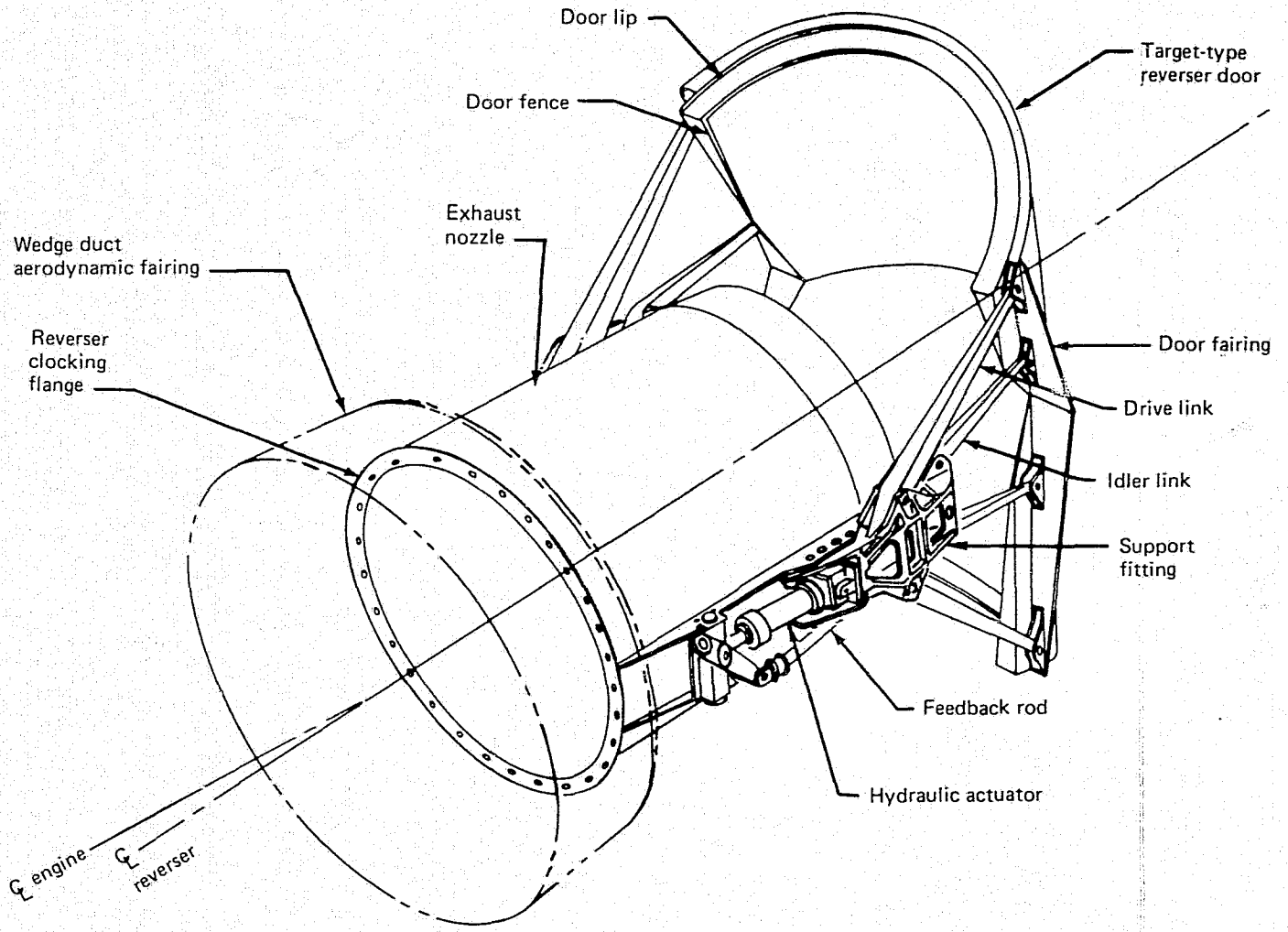

Figure 115.—JT8D Refan Thrust Reverser

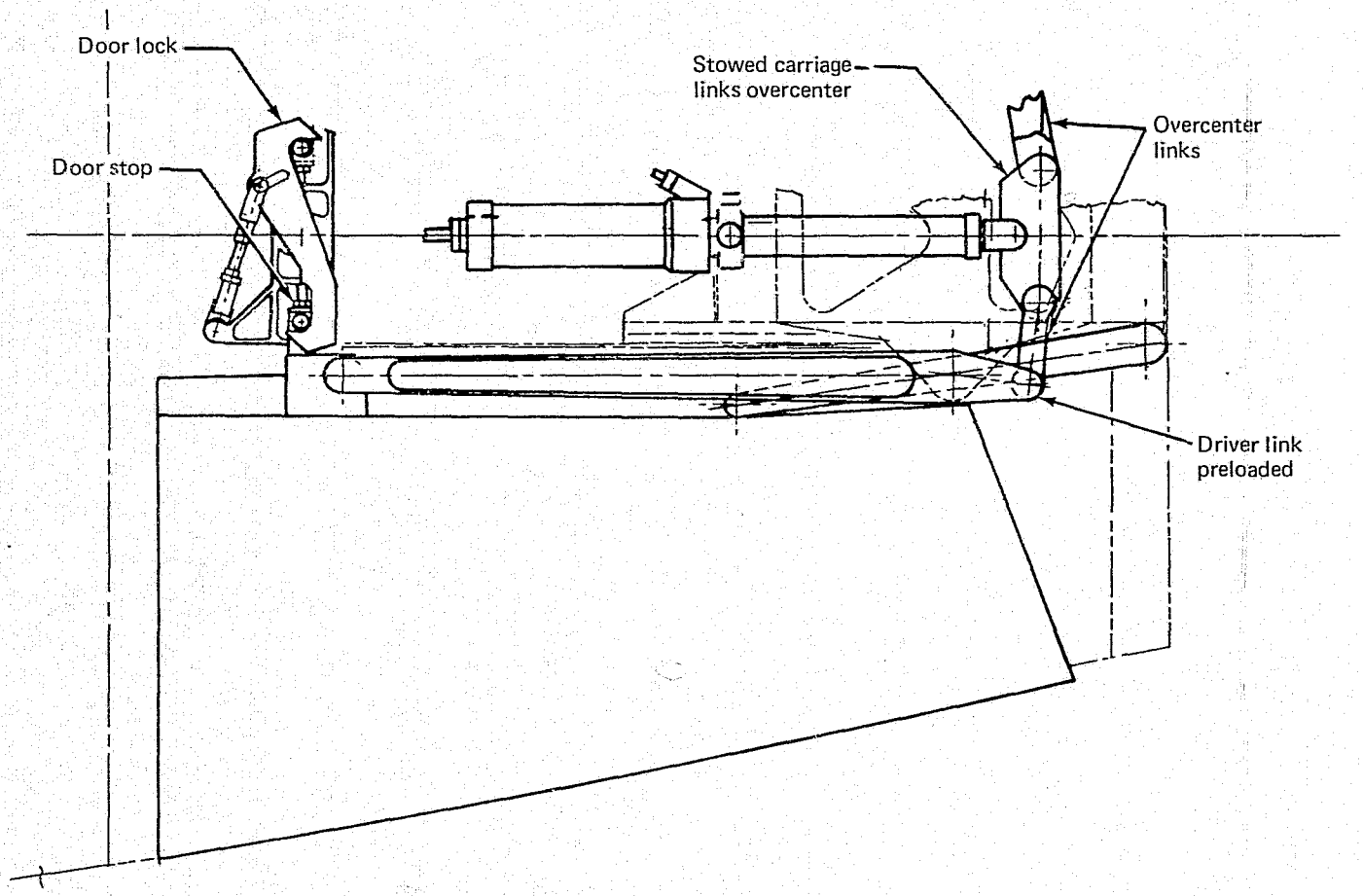

Figure 116.—JT8D Refan Thrust-Reverser System—Doors Stowed and Locked

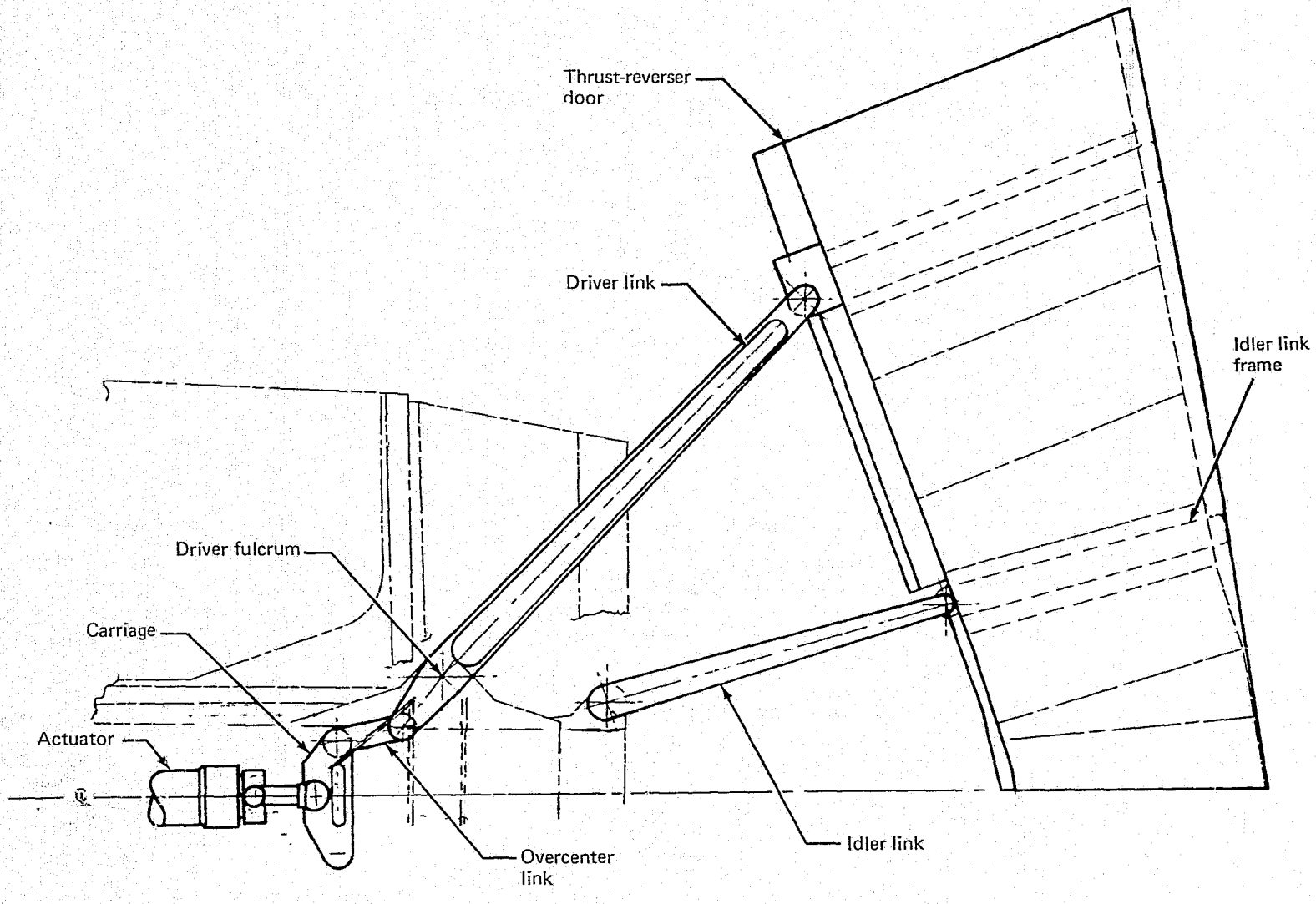

Figure 117.—JT8D Refan Thrust-Reverser System—Doors Deployed

The thrust-reverser operation sequence would be as follows. After reverse thrust selection, the door lock would be released and the actuator would overcome the overcenter preload which initiated deployment that would be completed by aerodynamic loads on the doors. The doors would be decelerated by hydraulic damping (snubbing) in the actuator and hydraulic system to prevent damage on contact at full travel. Actuator rod end pressure would retain the doors in the deployed position until restow is selected. Restow would be accomplished entirely by the actuator.

The actuator would control the reverser door operation through the overcenter and driver links. The idler links would carry only axial and side loads from the doors.

Link and actuator loads would react within the thrust-reverser support fitting, with only the net door loads being taken into the exhaust nozzle rails. At full deployment the axial, side, and inertia loads would react into the nozzle rails; all other forces would balance out between the reverser doors.

3.4.5.3 Analysis

Loads were derived for both ground and in-flight inadvertent thrust-reverser deployment conditions. Maximum load on the doors would be due to the high engine thrust during the refused takeoff condition. Aerodynamic pressure on the doors during in-flight deployment would result in the maximum loads in the linkage and actuator system. Loads in the actuation system would be limited by a snubbing device designed into the actuator. A fuse is also provided to protect the actuator system from overload in the event of high-speed in-flight deployment. Permanent deformation of the structure was acceptable for the inadvertent in-flight 380-kn (195-m/s) deployment condition.

The structure was also designed to withstand a lock malfunction or a mechanical jam in the linkage system with normal actuator power applied.

The thrust-reverser system fatigue durability objective was 20 years of service life with 95% reliability and 95% confidence, based on normal operating procedures; i.e., deployment at 110 kn (57 m/s) and restow at 70 kn (36 m/s). The thrust-reverser actuator and hydraulic system loads are discussed in section 3.7.1.

The principal thrust-reverser load conditions considered in the analysis are shown in table 41.

A finite element structural analysis method was used to determine the thrust-reverser door internal load distribution and linkage pivot reactions (fig. 118). Aerodynamic and engine exhaust thrust pressures were distributed on the door elements, together with internal and external skin temperature distributions. Deflections compatible with the exhaust nozzle were simulated at the link pivots in the support fitting. The analysis simulated the design conditions with the door stowed and deployed, and the fail-safe conditions with individual links failed.

The critical design condition for the doors was the RTO condition. Typical load distributions in the door driver and idler link ribs obtained from the analysis of the RTO condition are shown in figure 119.

Table 41.—JT8D Refan Thrust-Reverser Design Conditions

Condition	Load Factor	Door loads, lb (kN)
Ultimate design		
Refused takeoff 165 kn (85 m/s)	1.5	44 550 (198.17)
Inadvertent in-flight deployment at V_{mo} 270 kn (139 m/s)	1.5	40 130 (178.51)
In-flight restow; idle power 180 kn (93 m/s)	1.5	13 950 (62.05)
Fail-safe		
In-flight deployment 380 kn (195 m/s)	1.15	40 710 (181.09)
Normal operation; failed link deployed	1.0	20 180 (89.77)
Normal operation; lock malfunction	1.0	8 000 (35.59)
Normal operation; actuator malfunction or mechanical jam	1.0	16 700 (74.29)
Fatigue		
Normal operation deployment 110 kn (57 m/s)	1.0	20 180 (89.77)
Restow 70 kn (36 m/s) based on actuator capability	1.0	16 700 (74.29)

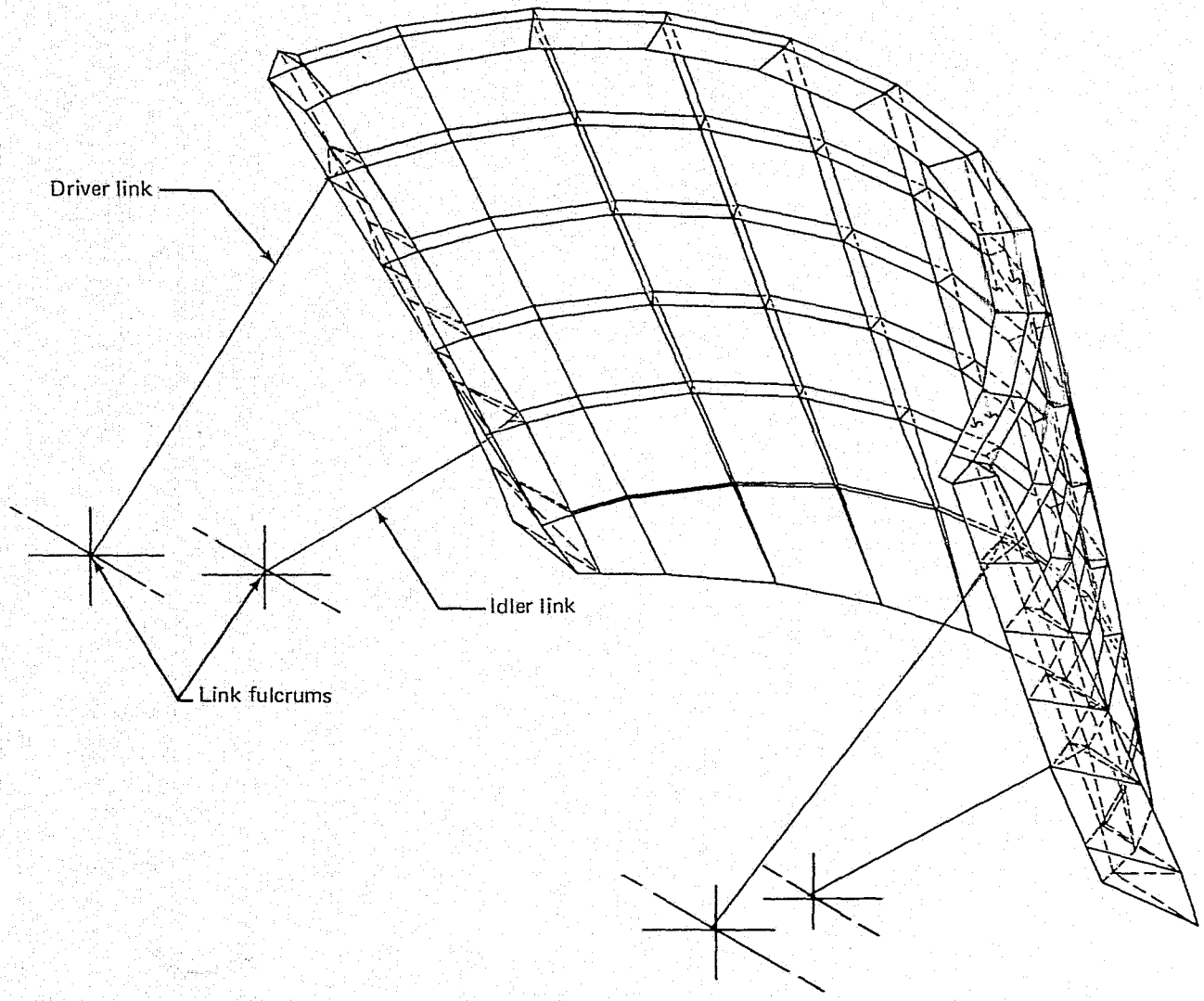

Figure 118.—JT8D Refan Side-Nacelle Thrust-Reverser Upper Door (Shown Deployed)—Finite Element Analysis Model

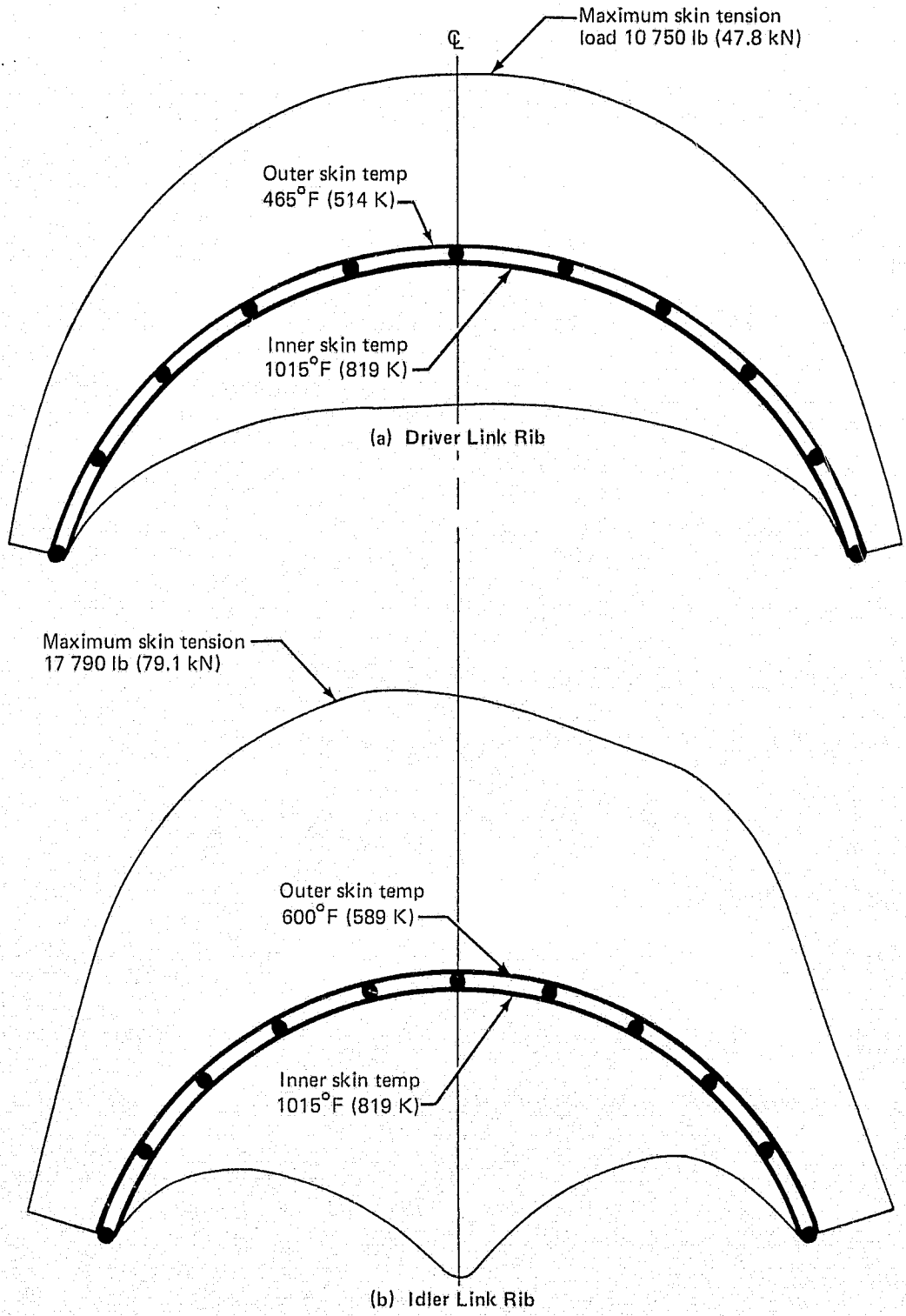

Figure 119.—JT8D Refan Thrust-Reverser Door Circumferential Load Distribution in Skins at Driver and Idler Link Ribs—Refused Takeoff Condition

The driver link door loads were combined with the actuator snubbing and door inertia loads to obtain the total loads on the thrust-reverser support fitting lugs (fig. 120). Maximum loads in the cast titanium support fitting are due to the RTO and inadvertent in-flight deployment at 270-kn (139-m/s) conditions.

Maximum loads on the driver links are due to the inadvertent in-flight deployment at 270-kn (139-m/s) conditions which necessitated heat treating the annealed titanium.

The fatigue load cycle in the driver link is due to the stress reversal during the stow and deploy locking and unlocking cycle. A further major fatigue cycle would result from the door loads during deployment and the actuator tension load following deployment. These cycles are shown in the driver link load-stroke curves for the RTO and in-flight restow conditions (fig. 121).

The design loads on the idler links are due to the RTO condition, and the fatigue load cycle was based on the thrust-reverser normal operation cycle.

Since the actuator was vendor supplied, no analysis for this item is shown herein. The actuator design loads and capability are shown in table 42, and typical actuator load-stroke curves for the RTO deploy and the in-flight restow conditions are shown in figure 122.

The stowed reverser doors are designed to be retained by preload in the driver links and also by a lock common to both doors. Lock loads are due to the nacelle aerodynamic pressures and, in the case of the lock not releasing, actuator stall load. Stress levels are low and not critical.

A summary of critical margins of safety in the thrust-reverser system is shown in tables 43 and 44.

3.4.6 CENTER-ENGINE INLET DUCT

3.4.6.1 Structural Concept

Air for the center engine would be ducted from the inlet above the fuselage, through the fin front-spar to the engine forward flange. The duct was designed to be an integrally stiffened shell, using solid and perforated aluminum inner skin backed by fiberglass phenolic honeycomb and epoxy fiberglass outer skin. A thermal anti-icing patch similar to that used in the production 727-200 duct was designed into the upper duct section forward of the fin front-spar. The duct varies from a circle at the nose cowl inlet to an ellipse where it passes through the fin front-spar fitting, and then back to a circle to match the engine fan case flange. The duct would terminate with a non-load-carrying flexible seal to the engine firewall bulkhead. At the forward end, the duct would be supported around its periphery by the center duct inlet fairing. A determinate system of links would support the duct at the fin front-spar and the aft fuselage structure forward of the engine seal, thus allowing the duct to deflect without introducing structural restraints and associated loads into the fuselage structure. The links forward of the fin front-spar fitting would allow deflections normal to the fitting, but restrain parallel and lateral deflections. The aft pair of links would restrain both vertical and lateral deflections normal to the duct axial centerline (figs 123 and 124).

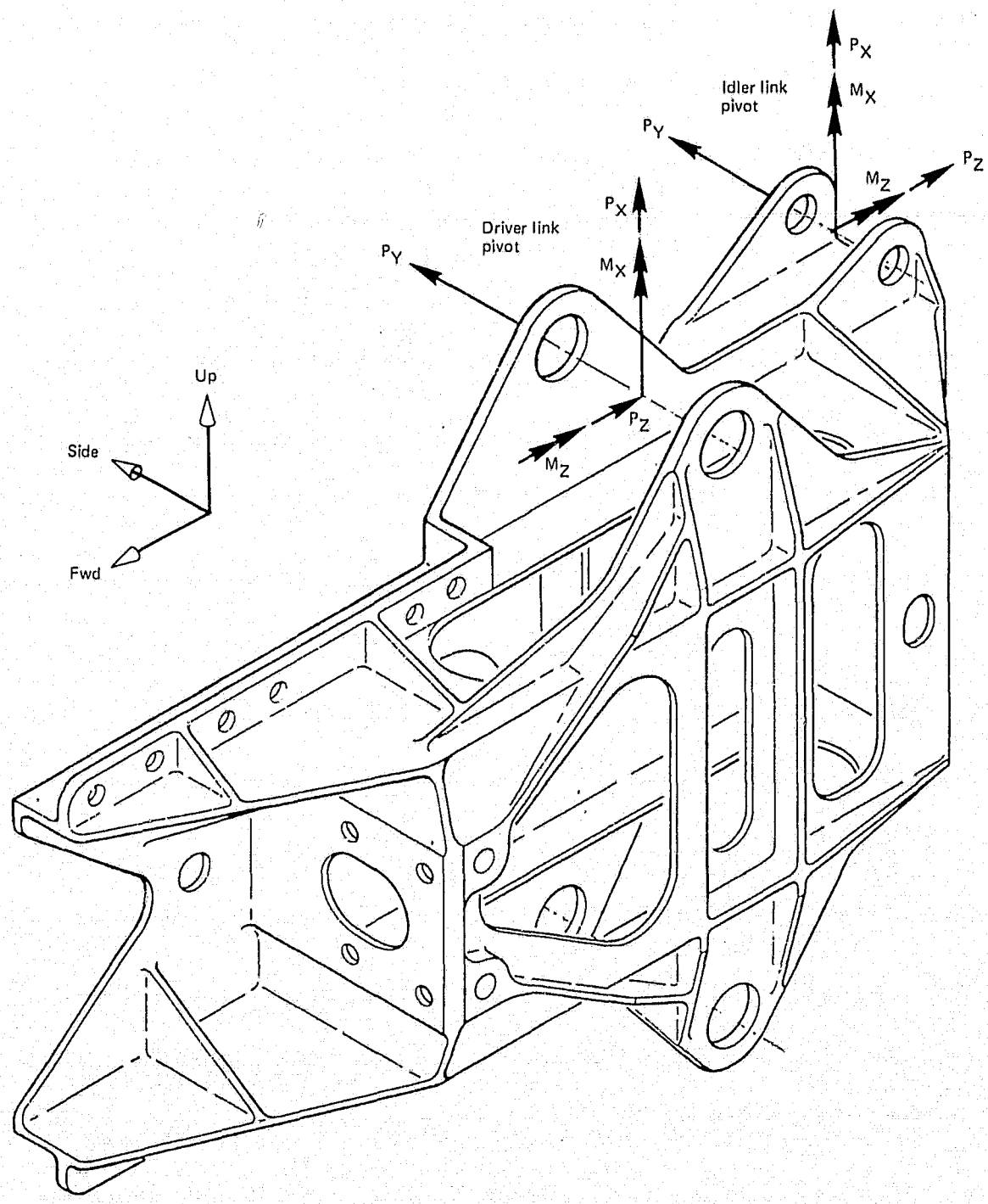

Figure 120.—JT8D Refan Thrust-Reverser Support Fitting Loads on Driver and Idler Link Pivots

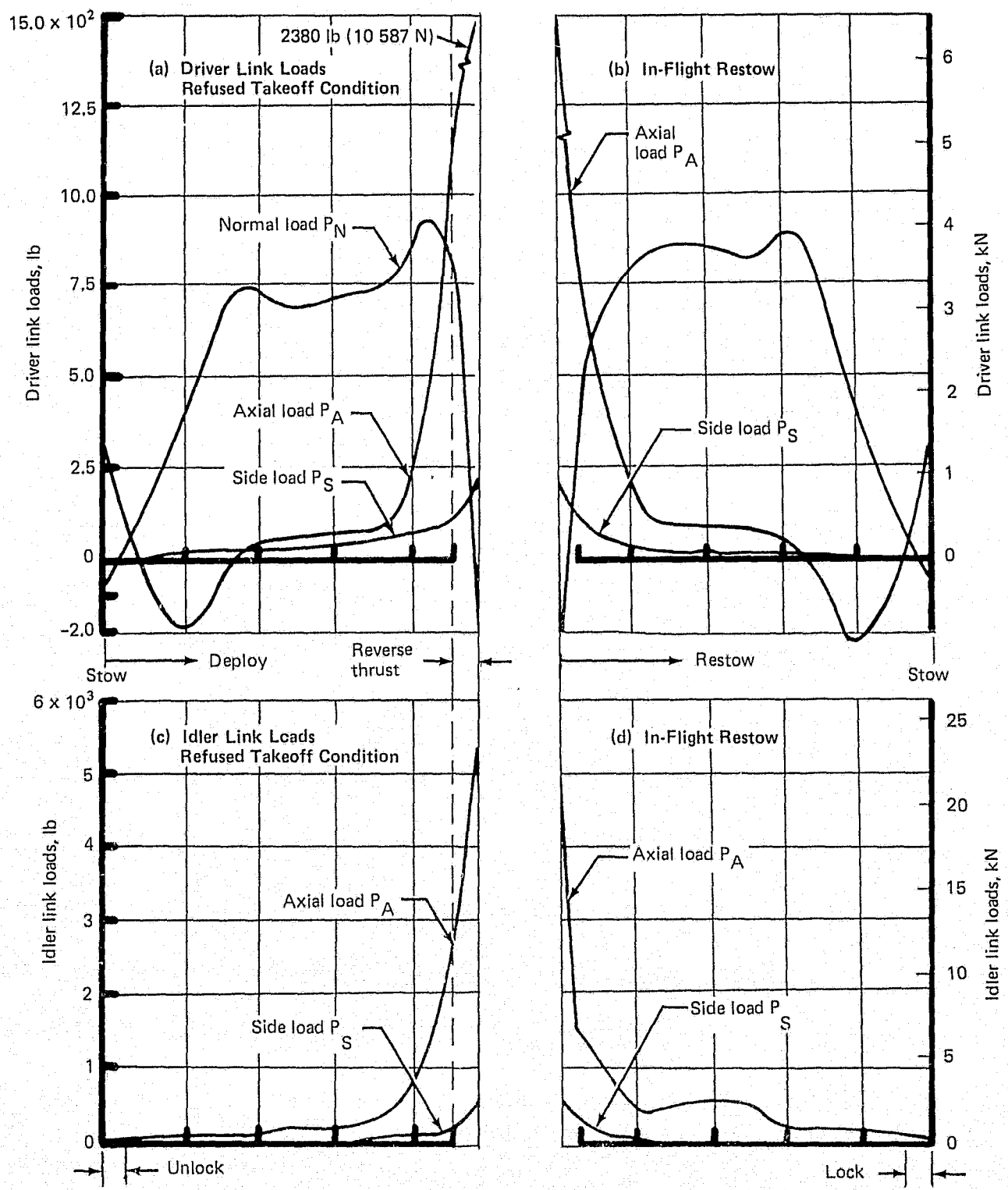

Figure 121.—JT8D Refan Thrust-Reverser Link Loads—Refused Takeoff and In-Flight Restow Conditions

Table 42.—JT8D Refan Thrust-Reverser Loads on the Actuator

Load condition	Actuator load (limit), lb (kN)	Actuator capability,[a] lb (kN)	Actuator function
Deployed RTO + 3 g	8 000 (35.59)	8 000 (35.59)	Maximum tension capability
RTO + snubbing	25 000 (111.21) 29 400 (130.78)	25 000 (111.21)	Snubbing runaround control, no snubbing
Restow at 180 KEAS (93 m/s)	14 000 (62.28)	16 700 (74.29)	Maximum compression capability
Inadvertent in-flight deployment 270 kN (139 m/s)	33 000 (146.79)	38 000 (169.03) 44 000 (195.72)	Actuation system fuse tolerance

[a] Actuator capability based on 3075-psi (21 200-kN/m^2) hydraulic pressure (maximum controller tolerance)

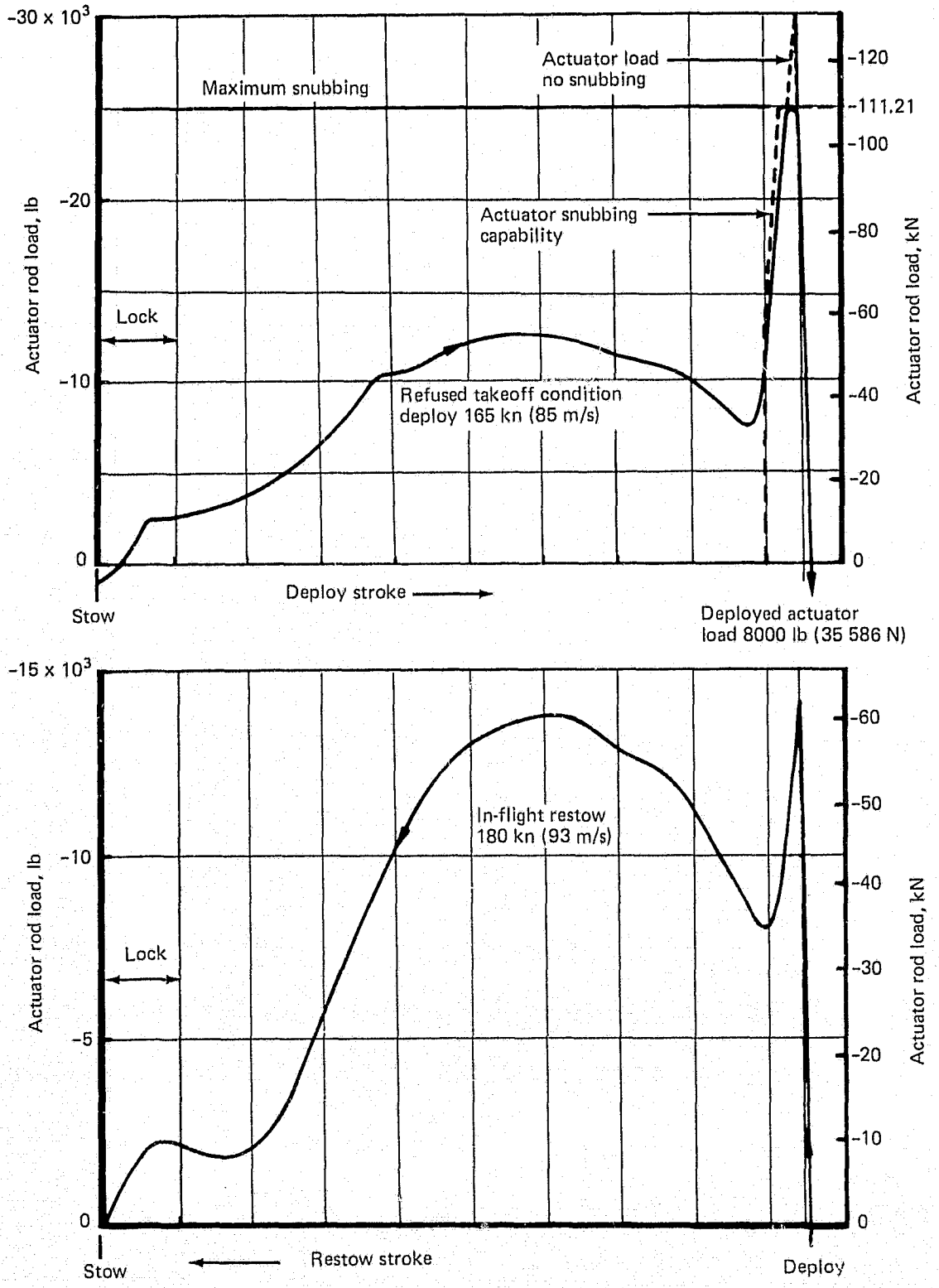

Figure 122.—JT8D Refan Thrust-Reverser System—Typical Actuator Load-Stroke Curves for Refused Takeoff and In-Flight Restow Conditions

Table 43.—JT8D Refan Thrust-Reverser Door and Link Margins of Safety Summary

Location	Condition	Margins of safety
Driver link		
Bending	RTO ultimate	0.40
	In-flight deployment	0.05
Fatigue	Normal operating	0.10
Door lug	In-flight deployment	0.0
Overcenter link lug	RTO ultimate	1.61
	In-flight deployment	0.13
Idler link		
Bending	RTO ultimate	0.12
Door lug	RTO ultimate	1.52
Fatigue	Normal operating	0.11
Thrust reverser door idler link frame		
Inner skin	RTO utlimate	0.07
Outer skin	RTO ultimate	0.80

Table 44.—JT8D Refan Thrust-Reverser Support Fitting Margins of Safety Summary

Location	Condition	Margins of safety
Driver link lug		
Strength	RTO ultimate	0.55
Strength	In-flight deployment	0.0
Fatigue	Normal operating	0.1
Idler link lug		
Strength	RTO ultimate	0.56
Strength	In-flight deployment	0.45
Fatigue	Normal operating	0.46
Actuator support lug		
Strength	RTO ultimate	0.08
Fatigue	Normal operating	0.30
Carriage actuator lug		
Strength	Maximum actuator capability	1.10
Fatigue	Normal operating	0.0
Bolt shear	Fail-safe	0.0

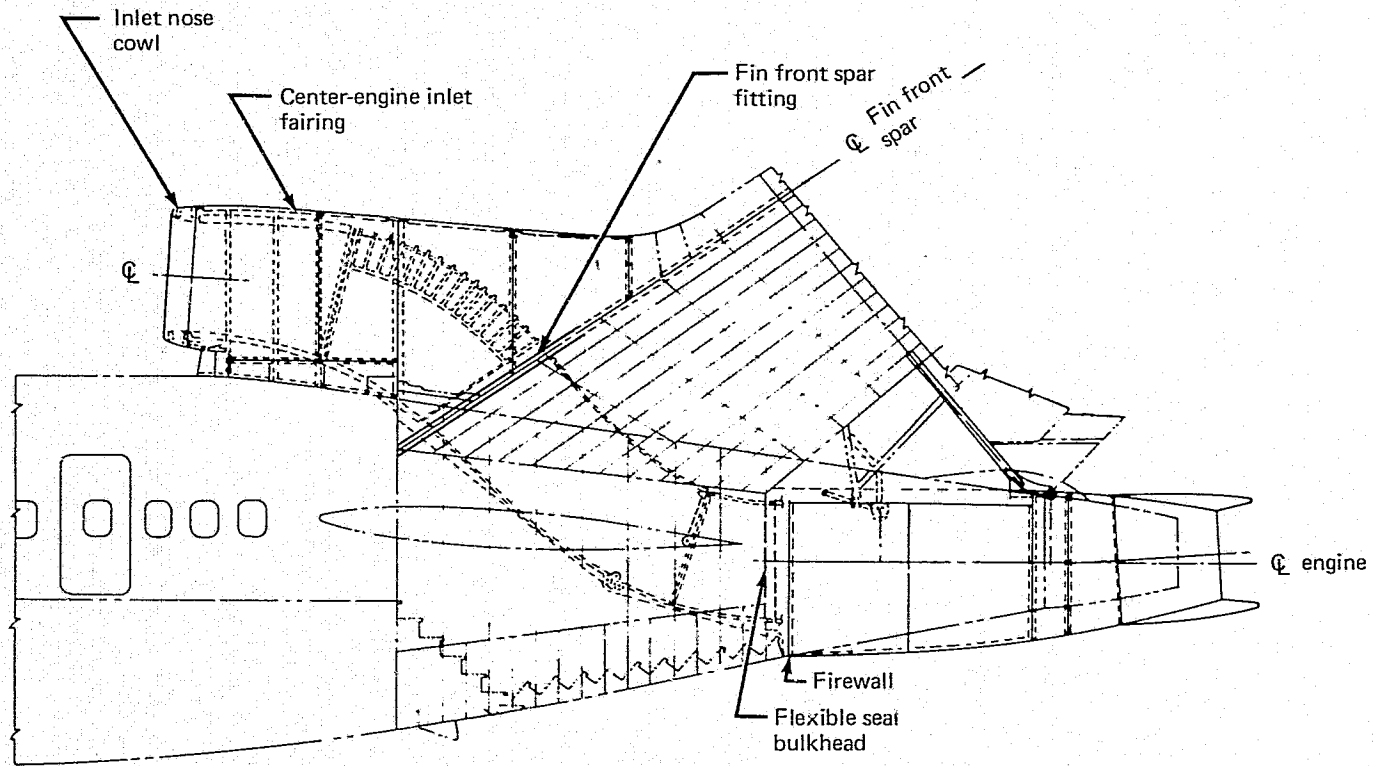

Figure 123.—JT8D Refan Center-Engine Inlet Duct, Fairing, and Aft Fuselage Structure

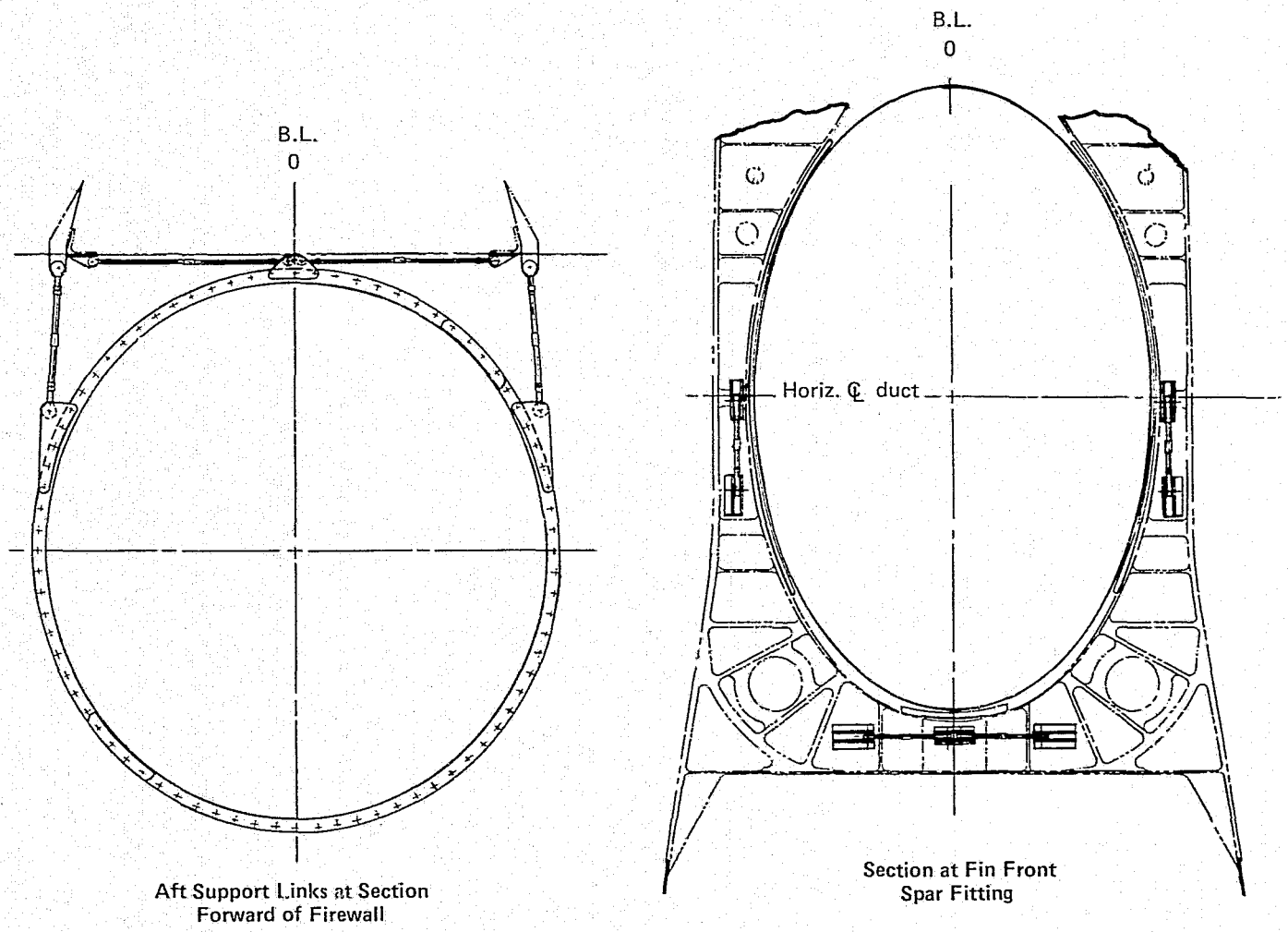

Figure 124.—JT8D Refan Center-Engine Inlet-Duct Support Links

The duct would be constructed in five sections which are rigidly connected at circumferential joints to form a single unit. The joint between the upper and aft sections would be made at the fin front-spar on final assembly in the aft fuselage. The duct was designed to have a nominal clearance with the front-spar fitting; however, during overpressure in the duct (e.g., surge), the fitting would provide support to the duct elliptical section. Rub strips attached to the fin front-spar fitting would distribute duct loads into the fitting and protect the structure from fretting due to the relative motion between the duct and the fixed structure.

In the airplane installation, the center-engine inlet duct support loads and fairing external pressure loads would be reacted by the fairing frames into the aft fuselage frames and fuselage skin.

3.4.6.2 Analysis

Due to the complex shape and redundant nature of the duct, a number of finite element analysis programs were used to develop the structural model used for the duct analysis. The areas of the structure these programs represented are shown in figure 125. The significant programs are outlined below.

Program DD01.—This model of a constant cross-section elliptical duct was used to evaluate the effect on deflections and circumferential bending moments of changing duct wall section properties. A comparison was made between the analysis predictions and the stress and deflection results obtained from the original 727-100 skin and frame duct tests. Results compared favorably and gave credence to the analysis technique being used.

This program was also used to locate skin panel joints at the minimum bending moment locations. A comparison of the circumferential bending moment for uniform and variable section ducts is shown in figure 126.

Program SD02.—This program represented a uniform thickness honeycomb structural model 168 in. (4.27 m) long that was used to investigate effects of changing the cross section from a circle to an ellipse.

Program SD03.—SD03 was a uniform thickness honeycomb structural model of the upper forward duct between the inlet and the fin front-spar. This program was used to evaluate various fixities at the fin front-spar and at the inlet nose cowl interface.

Program SD10.—Program SD03 was revised by modifying the honeycomb wall section constants to represent the manufactured duct.

Program SD05.—The center-engine inlet duct was represented by a simplified line model on the duct longitudinal axis. Loads obtained from program SD03 were applied to the model, and the distribution of loads into various duct support configurations was evaluated to obtain an optimum load distribution.

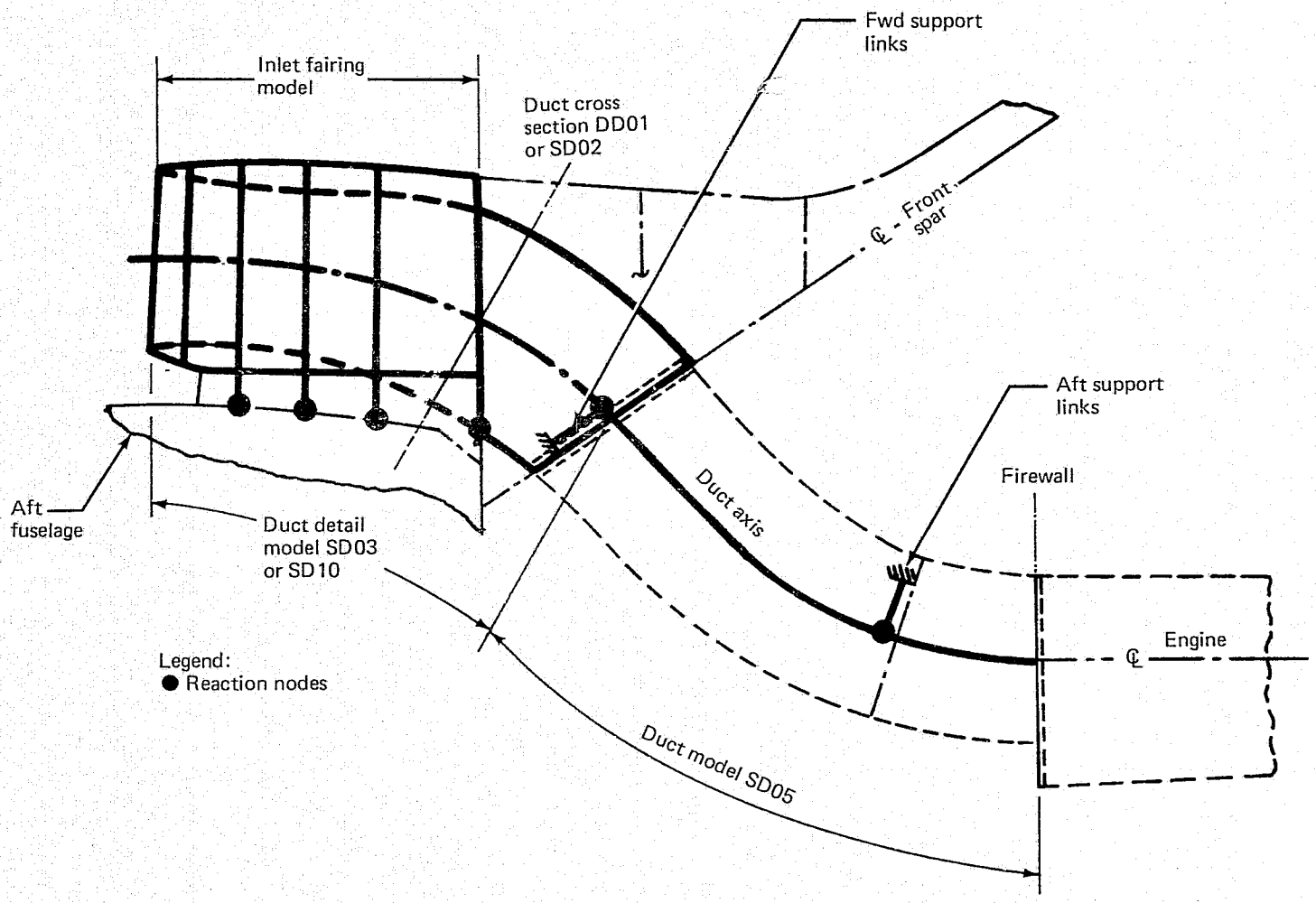

Note: Combination of inlet fairing model, model SD10, and model SD05 = model CD01

Figure 125.—JT8D Refan Center-Engine Inlet Duct Computer Analysis Model Diagram

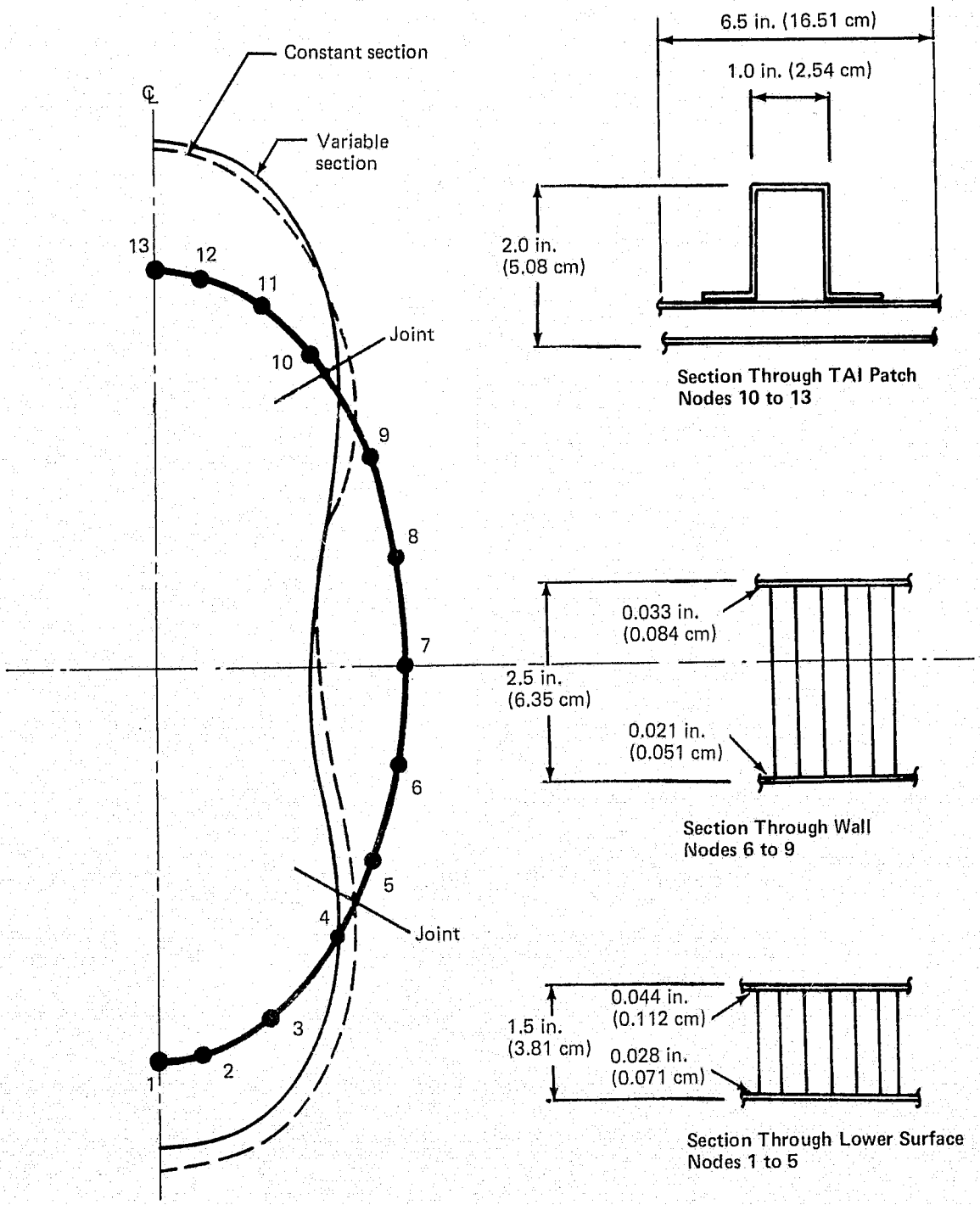

Figure 126.—JT8D Refan Center-Engine Inlet Duct—Comparison of Constant and Variable Section Bending Moment Distribution (Computer Program DD01)

Program CD01.—This program combined the center-engine duct and center-engine inlet fairing programs to form an integrated structure. The duct program consisted of the duct structure forward of the spar from program SD10 and line model program SD05 aft of the spar to the engine forward flange. Duct support links were provided at the fin front-spar and at the firewall (fig. 127).

Maximum loads on the duct result from positive and negative internal pressures associated with engine operating conditions. Pressures were derived from the center-engine duct model test (ref. 6). Only steady-state conditions were considered in the analysis (table 45).

The elliptical cross section at the fin front-spar fitting was unrestrained during internal negative pressure or positive pressure up to 1.10 psig (7.58 kN/m^2) when contact was made with the fitting. However, with increasing positive pressure, contact with the fitting restrained the duct cross section. Both of these conditions were analyzed using programs SD03 and SD10. Typical relationships of stress and pressure for the inner skin stresses due to both restraint conditions are shown in figure 128.

A summary of typical margins of safety for the center-engine inlet duct structure is shown in table 46.

Loads from the duct also react through the center-engine inlet duct fairing and are reported in section 3.4.7.

The manufactured duct was instrumented and tested during the refan engine performance evaluation (ref. 3). Test results indicated that the positive surge pressures were approximately 19% higher than the maximum pressures used in the analysis (table 47). However, adequate margins of safety existed and no structural changes would be required. Correlation of the analysis, predictions, and the stabilized pressure test results was good, thus giving confidence in the analysis methods used (fig. 129).

The surge test results revealed that the duct responded dynamically to the surge pressure, as seen by the nonlinear relationship of the stress and pressure test results (fig. 129). This had not been identified prior to analysis of the test results. A dynamic analysis of the duct and support structure would therefore be desirable to fully evaluate the effects of engine surge.

3.4.7 CENTER-ENGINE INLET FAIRING

3.4.7.1 Structural Concept

The center-engine inlet fairing would provide a pedestal structure off the aft fuselage structure to support the center-engine duct (fig. 130). Contoured fiberglass honeycomb skin panels would be supported by aluminum frames mounted with pinned fittings from the fuselage frames.

Lateral loads from the fairing and duct would react by the frames into the fuselage structure. Axial loads from the duct would be carried by the skin panels through the fixed pedestal shear panels and into the aft fuselage skin.

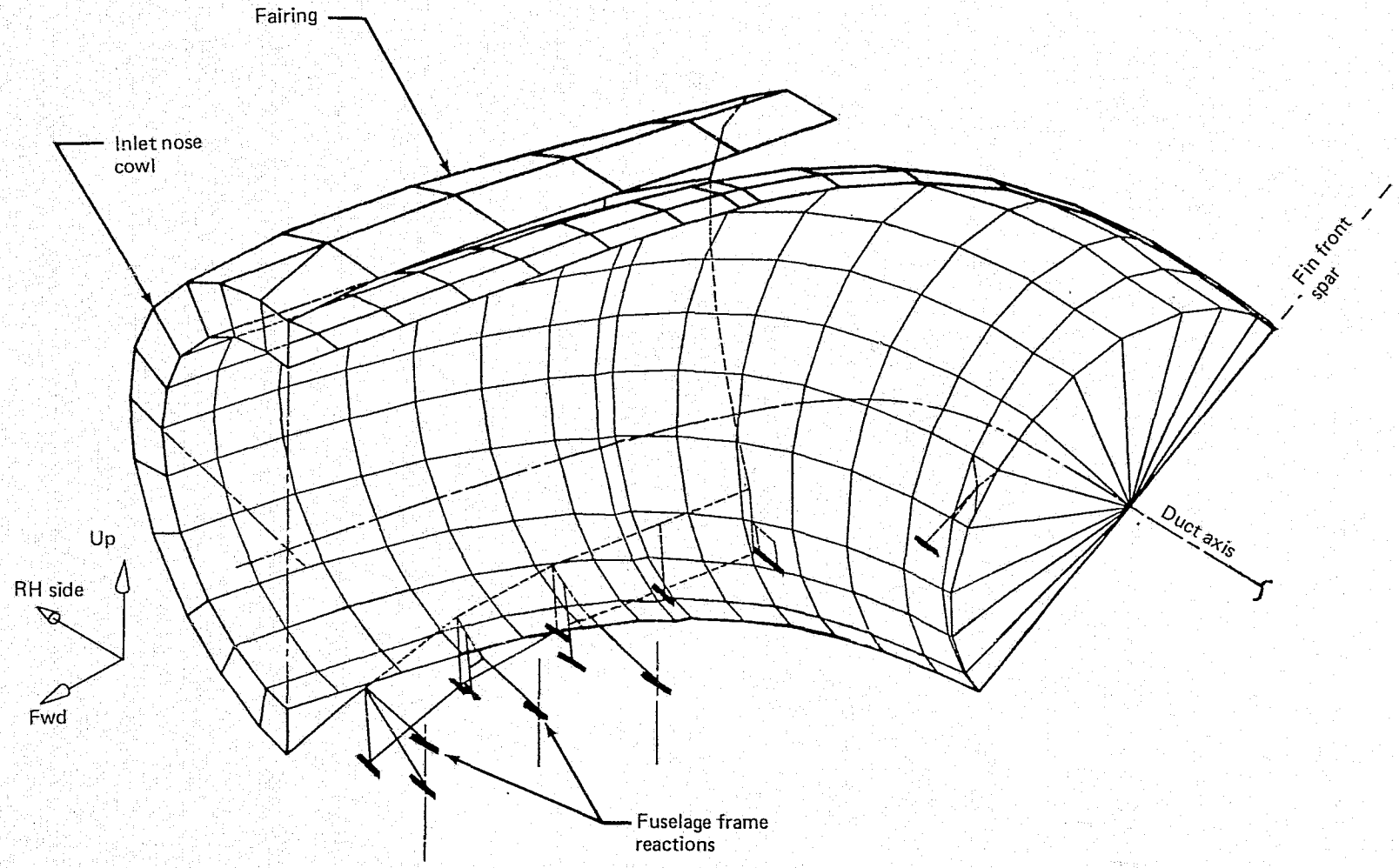

Figure 127.—JT8D Refan Center-Engine Inlet Duct and Fairing—Finite Element Analysis Model

Table 45.—JT8D Refan Center-Engine Inlet Duct Design Load Conditions

Condition	Ultimate loads
Engine surge at 10 000 ft (3048 m) Engine surge at sea level Side load	+15.75 psi (+108.59 kN/m^2) -7.5 psi (-51.71 kN/m^2) ±5.0 g
Fatigue loads Normal operating	 +2.25 psi (+15.51 kN/m^2) -3.0 psi (-20.68 kN/m^2)
Temperatures (maximum) Away from TAI patch Adjacent to TAI patch	 160°F (344 K) 330°F (439 K)
System failure Adjacent to TAI patch	 375°F (464 K)

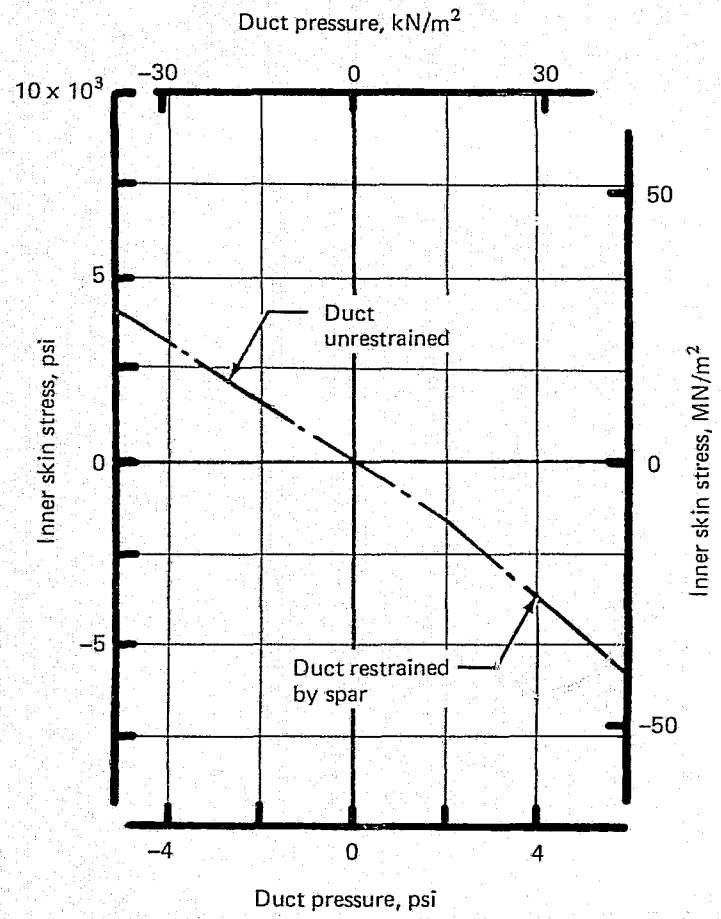

(a) Axial Stress Top Centerline

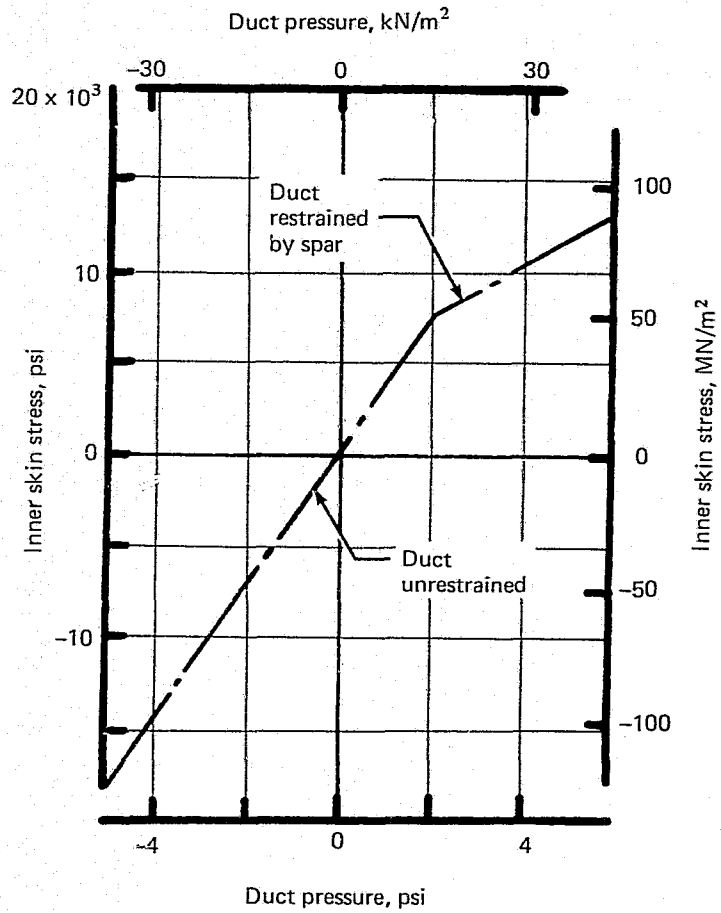

(b) Circumferential Stress, Duct Top Centerline

Figure 128.—JT8D Refan Center-Engine Inlet Duct Inner Skin Stress

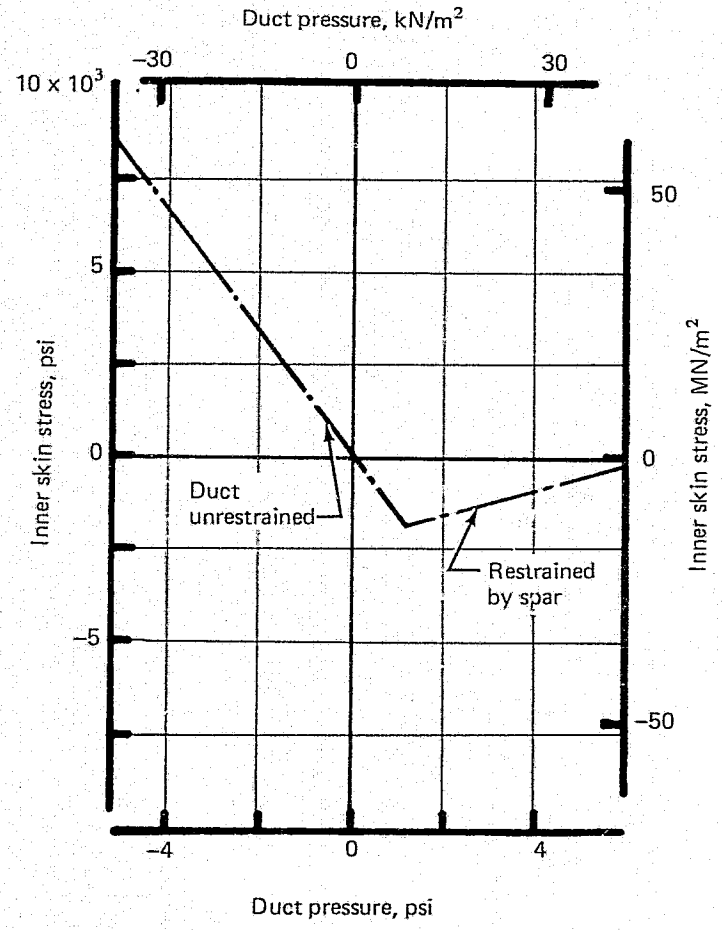

(c) Circumferential Stress Duct Sidewall

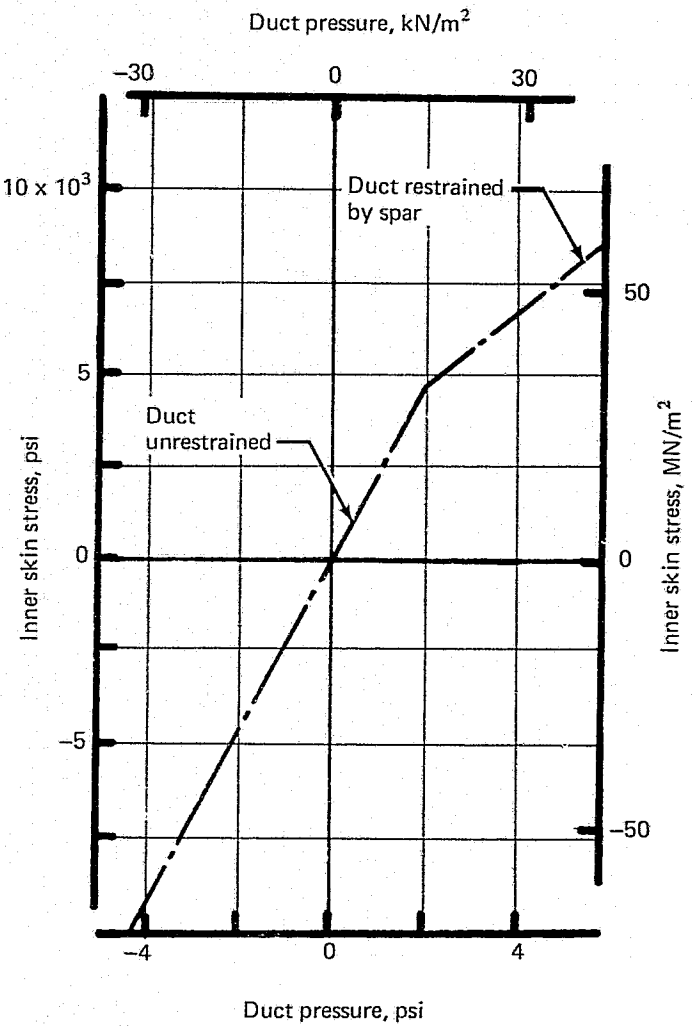

(d) Circumferential Stress Lower Centerline

Figure 128.–(Continued)

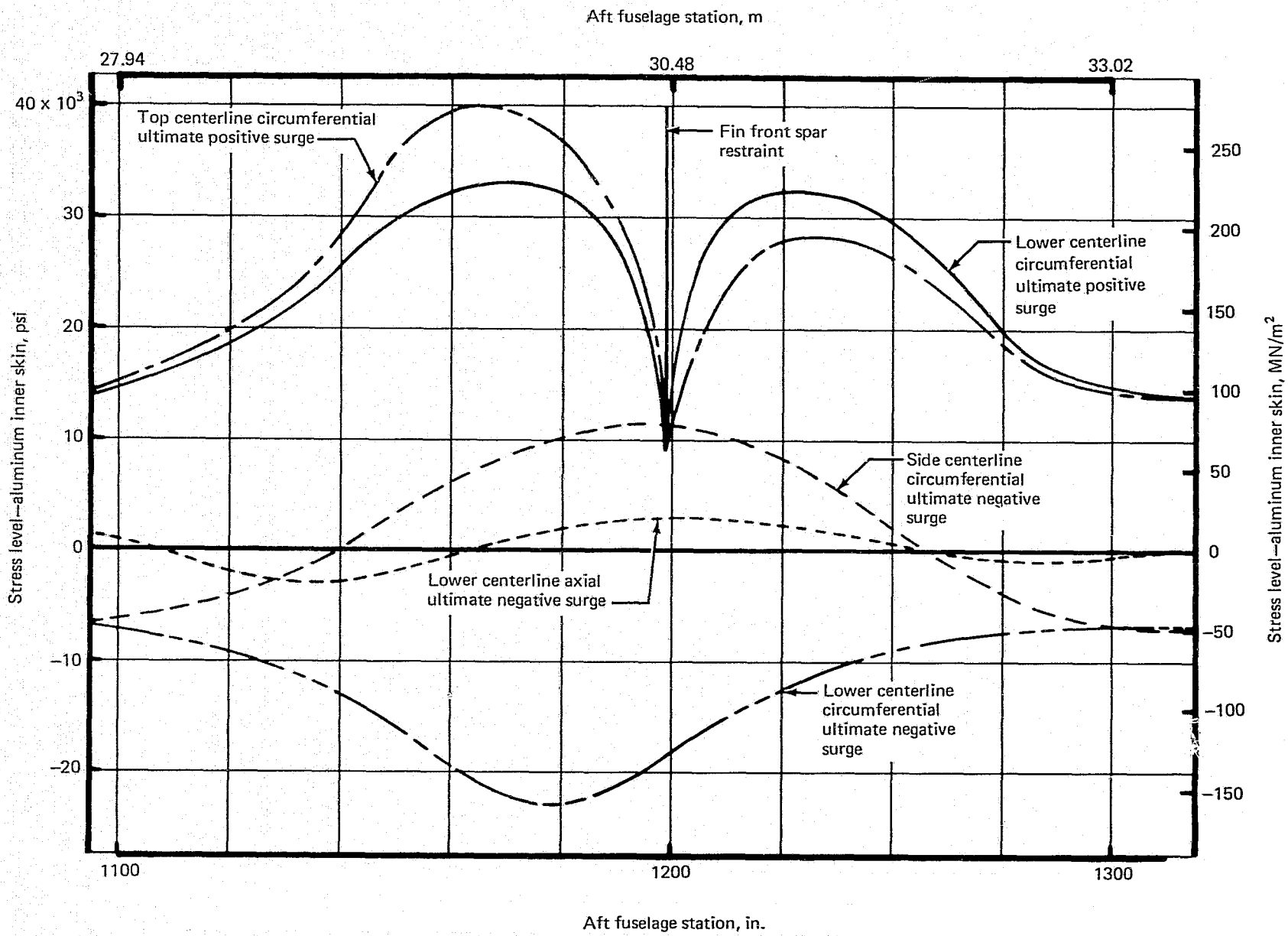

(e) Duct Design Ultimate Stress Levels

Figure 128.–(Concluded)

Table 46.—JT8D Refan Center-Engine Inlet Duct Margins of Safety Summary

Location	Margins of safety
B.S. 1180 in. (29.97 m) vertical centerline	
Aluminum inner skin[a]	0.28
Epoxy outer skin[a]	0.41
Fatigue (perforated aluminum skin)[b]	0.17
B.S. 1250 in. (31.75 m) vertical centerline	
Aluminum inner skin[a]	0.60
Epoxy outer skin[a]	>0.20
B.S. 1250 in. (31.75 m) horizontal centerline	
Aluminum inner skin[a]	>0.20
Epoxy outer skin[a]	0.24
Fatigue (perforated aluminum skin)[b]	0.37
Support link attachment	
Fin front spar[a]	0.01
Support link attachment aft[a]	0.48
Link[a]	0.21

[a] Condition: positive surge 15.75 psi (108.59 kN/m^2) ultimate

[b] Condition: cruise

Table 47.—JT8D Refan Center-Engine Inlet Duct—Comparison of Test, Predicted, and Duct Design Average Pressure

Condition	Test, psi (kN/m^2)	Predicted, psi (kN/m^2)	Design limit, psi (Kn/m^2)
Stabilized sea level	-2.81 (-19.374)	-2.90 (-19.995)	-3.00 (-20.684)
Surge (-) sea level	-4.40 (-30.337)	-5.00 (-34.474)	-5.00 (-34.474)
Surge (+) sea level	+4.94 (+34.060)		
Extrapolated to altitude	+12.50 (+86.185)	+10.50 (+72.395)	+12.00 (+82.737)

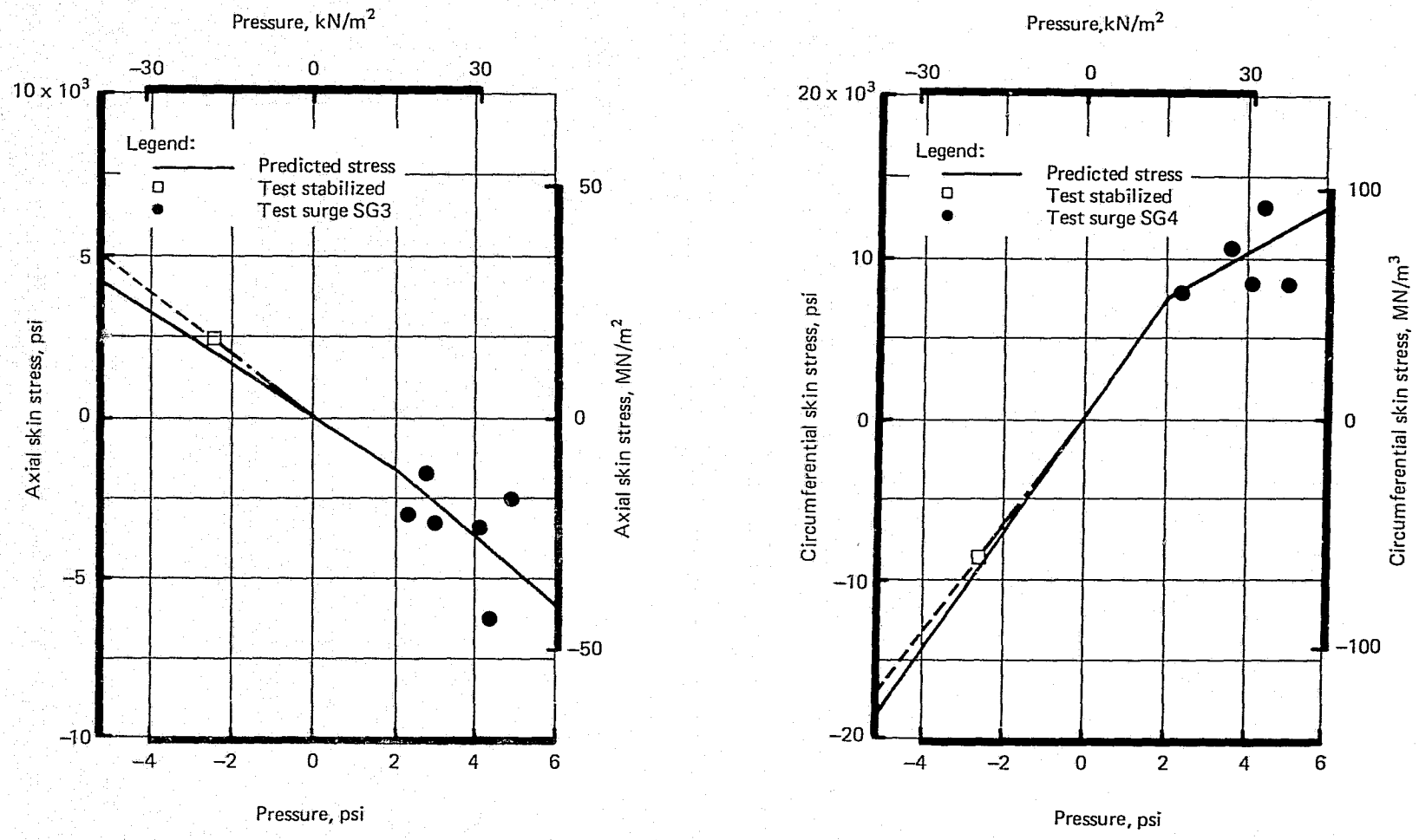

Figure 129.—JT8D Refan Center-Engine Inlet Duct—Comparison of Predicted Stresses and Test Strain Gage Stresses

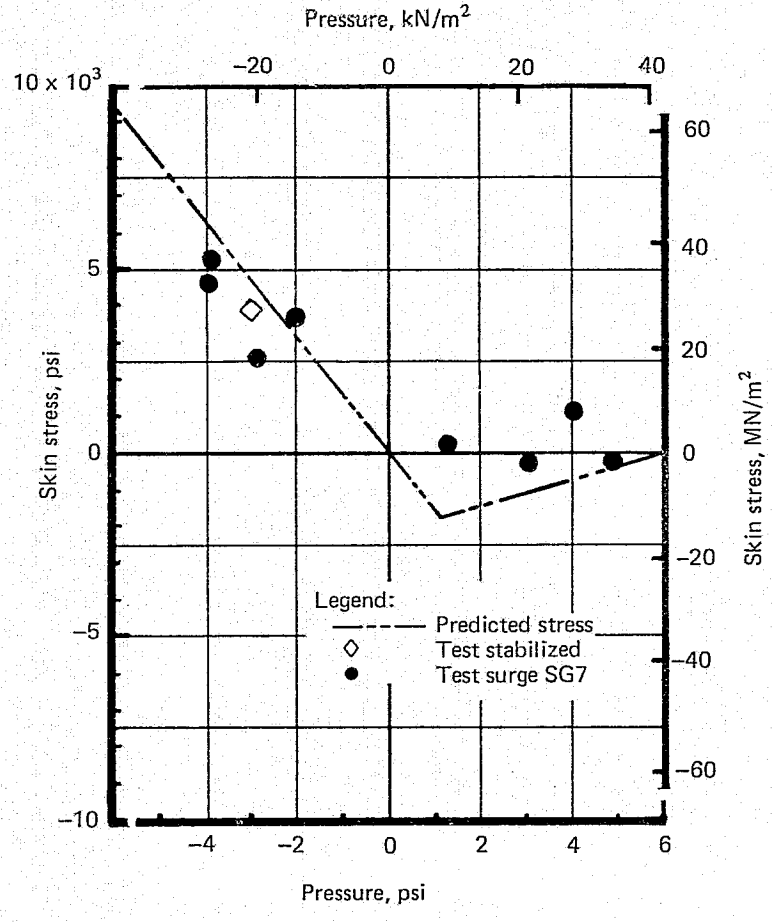

(c) Duct Sidewall Circumferential Stresses

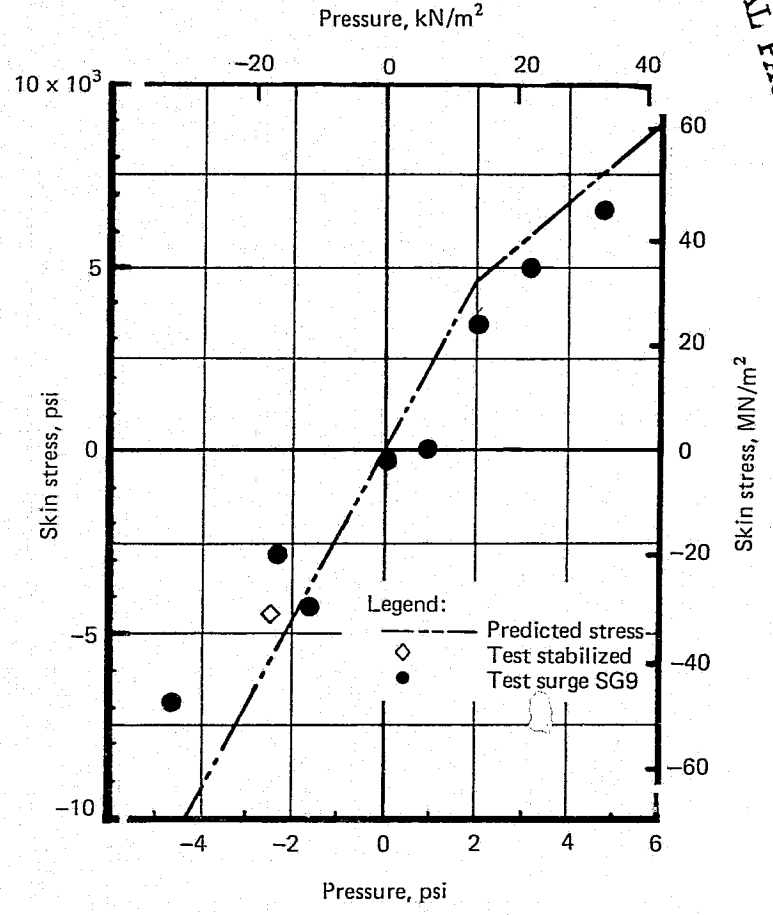

(d) Duct Lower Centerline Circumferential Stresses

Figure 129.—(Concluded)

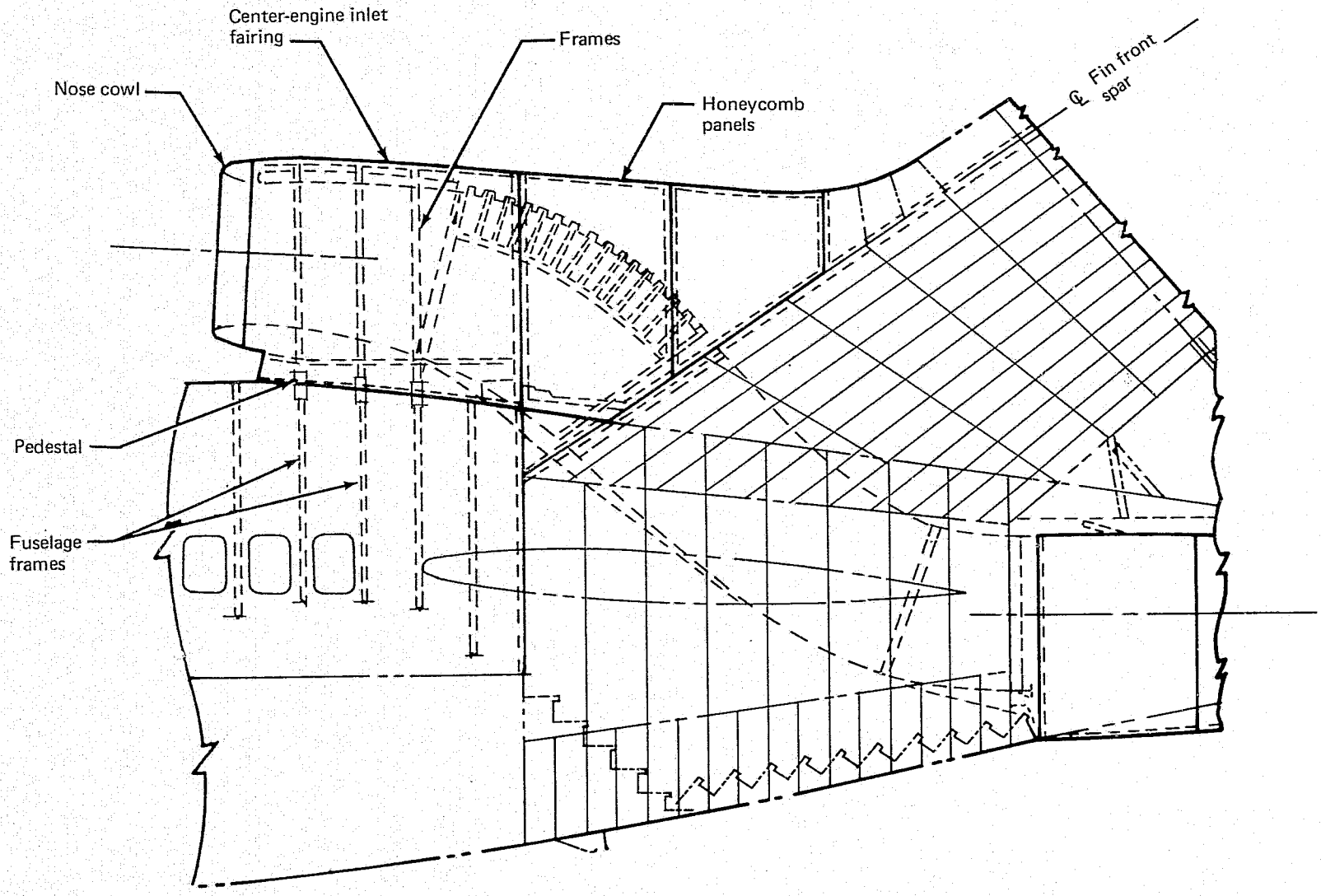

Figure 130.—JT8D Refan Center-Engine Inlet Fairing

3.4.7.2 Analysis

Aerodynamic pressures on the fairing for the symmetrical and yaw conditions were derived from the 727-200 data (figs. 131 and 132).

The center-engine structure was analyzed using a finite element analysis in which both the frames and skin panels were represented. Following initial development of the model, it was integrated with the center-engine inlet duct analysis model to complete the duct support structure as program CD01. This analysis was run with both symmetrical and antisymmetrical fairing load conditions and also with positive and negative duct pressures. (See section 3.4.6 for further analysis details.) Figure 133 shows a typical fairing frame idealization and cross section through the fairing.

Typical stress levels in the frames and skin panels were low and therefore no margins of safety are quoted.

3.4.8 CENTER-ENGINE SUPPORT STRUCTURE

3.4.8.1 Structural Concept

Relative to the engine in the 727-200, the center-engine supports would be moved 10.7 in. (27.2 cm) aft and the engine $\mathbb{Q}$ down 4.5 in. (11.4 cm), thus necessitating redesign of the engine attachment fittings and modification to the structure in the lower fin aft of the rear spar (fig. 134).

The aft support would be moved both up and aft and would require a new fitting to be cantilevered off the existing structure, with modifications also required to the closing ribs and side panels of the lower fin. The fairing above the firewall was redesigned to fair with the new lines, and new center-engine cowls would also be required.

Loads from the engine forward support fitting would be taken through the firewall into the modified diagonal members and into the fin rear spar. Forward components of the loads would be carried by the thrust links forward into the existing structure in a manner similar to that for the existing 727-200 design.

Only vertical and side loads would be reacted by the aft support fitting. Vertical loads would be carried primarily by the diagonal closing ribs to the fin rear spar and the side loads by the horizontal firewall beam.

3.4.8.2 Analysis

The original load factors used for the 727-200 analysis were also used for the 727 refan analysis. The dynamic landing analysis, reported in section 3.4.12, subsequently proved these factors to be conservative. The JT8D-117 center-engine data which were used in the analysis are shown in table 48.

The internal load distribution was determined by using a finite element structural analysis which represented the engine and structure aft of the fin rear spar (fig. 135).

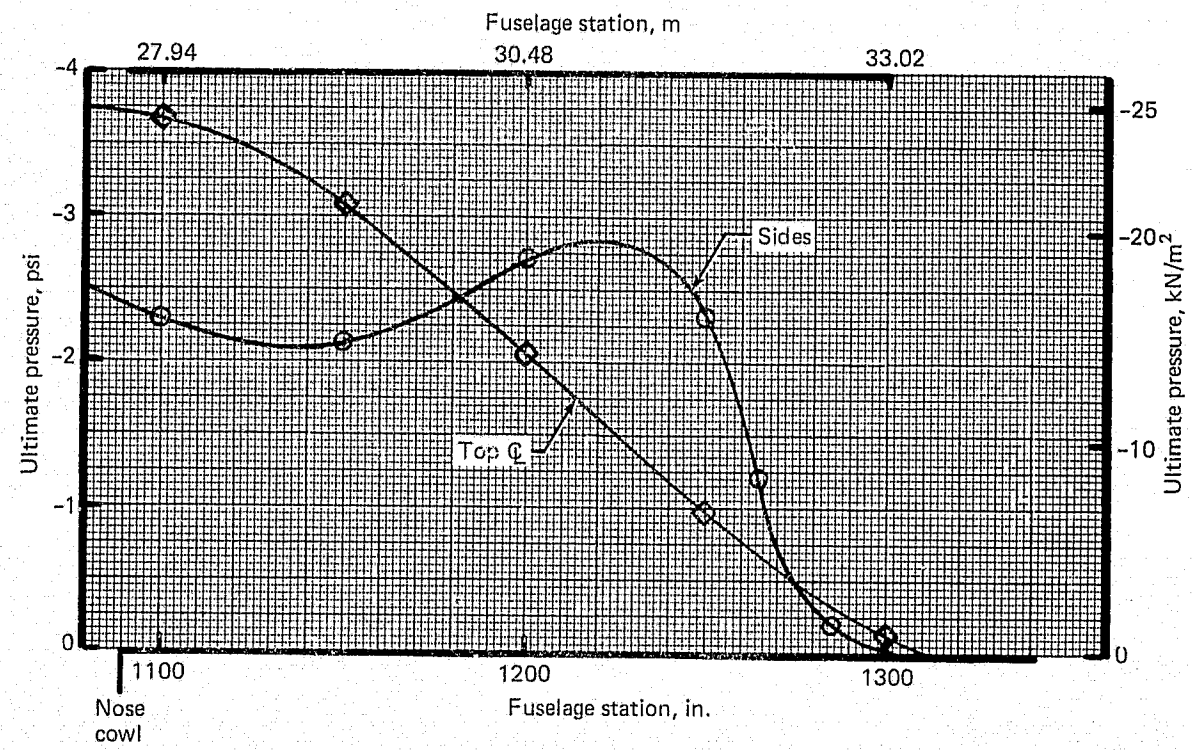

Figure 131.—JT8D Refan Center-Engine Inlet Fairing Pressure Distribution—Symmetrical Condition, 410 kn (211 m/s)

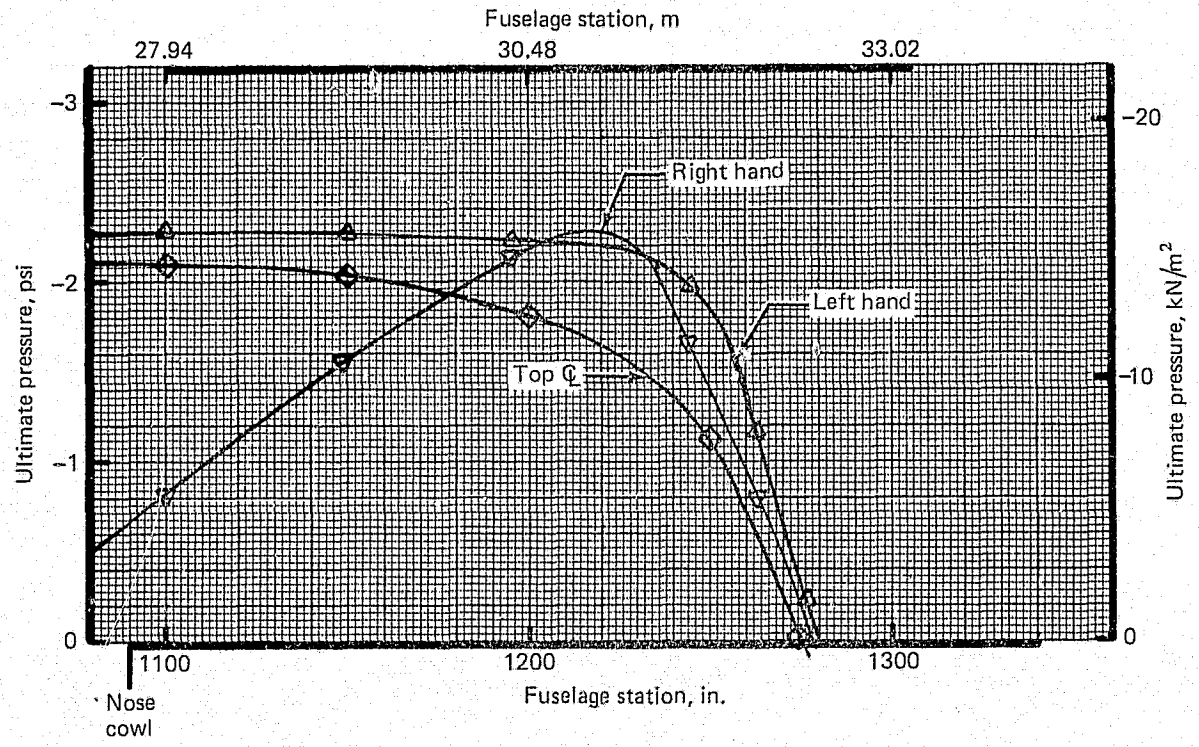

Figure 132.—JT8D Refan Center-Engine Inlet Fairing Pressure Distribution—Yaw Condition, 410 kn (211 m/s)

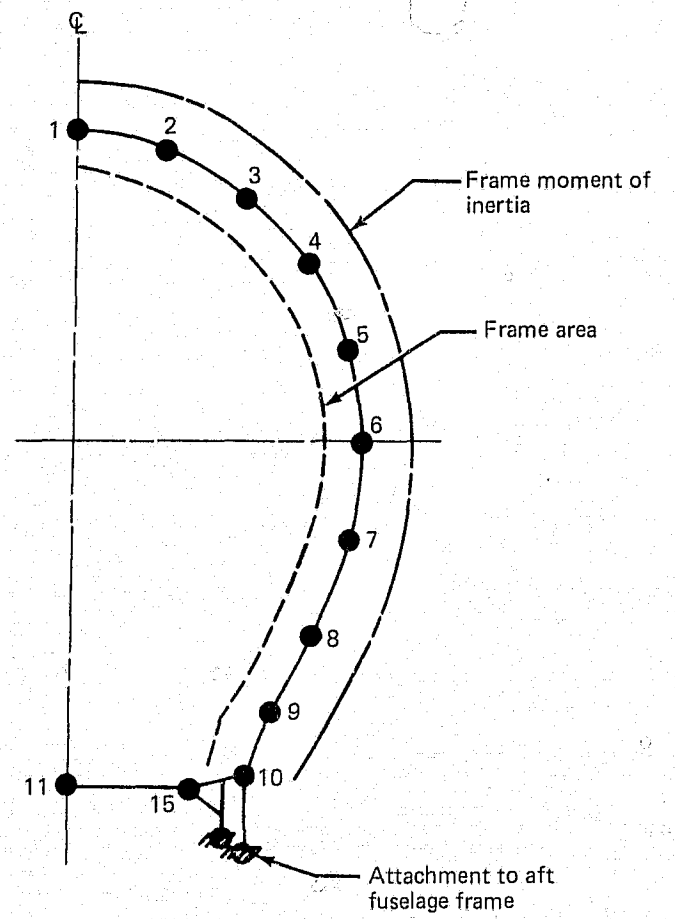

(a) Computer Idealization of Fairing Frame

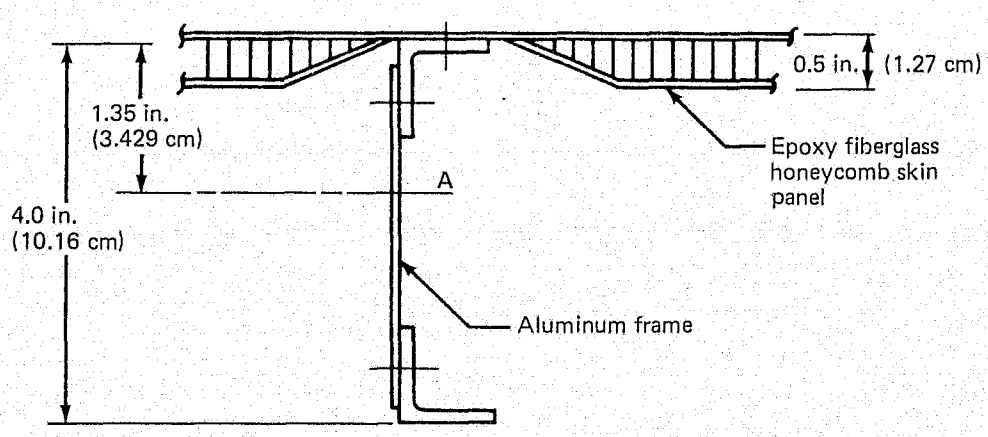

(b) Typical Section Through Frame

Figure 133.—JT8D Refan Center-Engine Inlet Fairing—Typical Section Through Frame and Computer Idealization of Frame

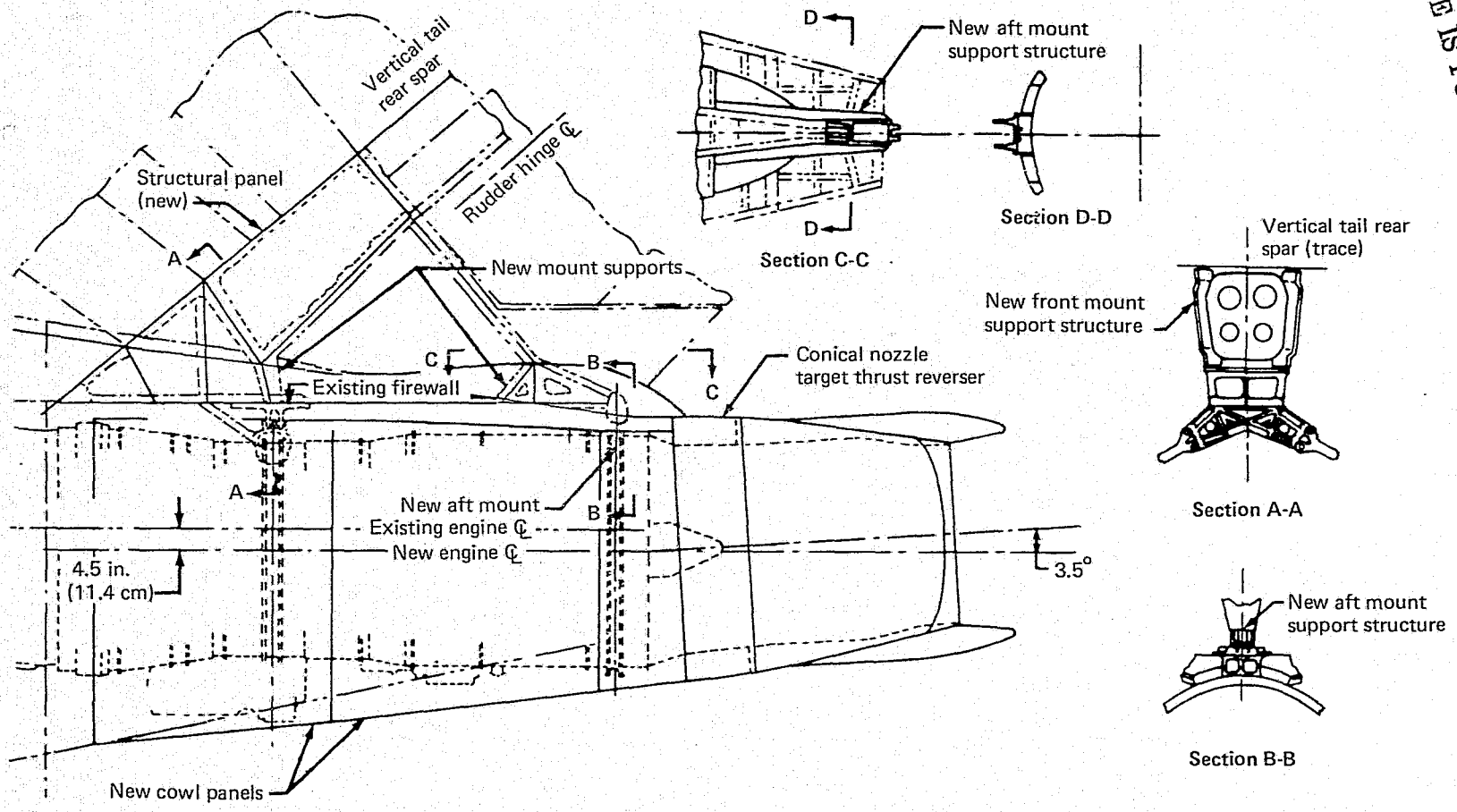

Figure 134.—727 Refan Center-Engine Installation

Table 48.—JT8D-117 Center-Engine Mount Loads

Condition	Weights and loads	
Engine weight	5 100 lb	(2313.321 kg)
Thrust maximum	17 900 lb	(79.623 kN)
Thrust cruise	14 470 lb	(64.366 kN)
Thrust reverse	12 300 lb	(54.713 kN)
Moment pitch (for 3-rad/sec yaw)	633 980 in-lb	(71.630 m-kN)
Moment yaw (for 2.225-rad/sec pitch)	475 490 in-lb	(53.723 m-kN)
Moment roll	422 250 in-lb	(47.708 m-kN)

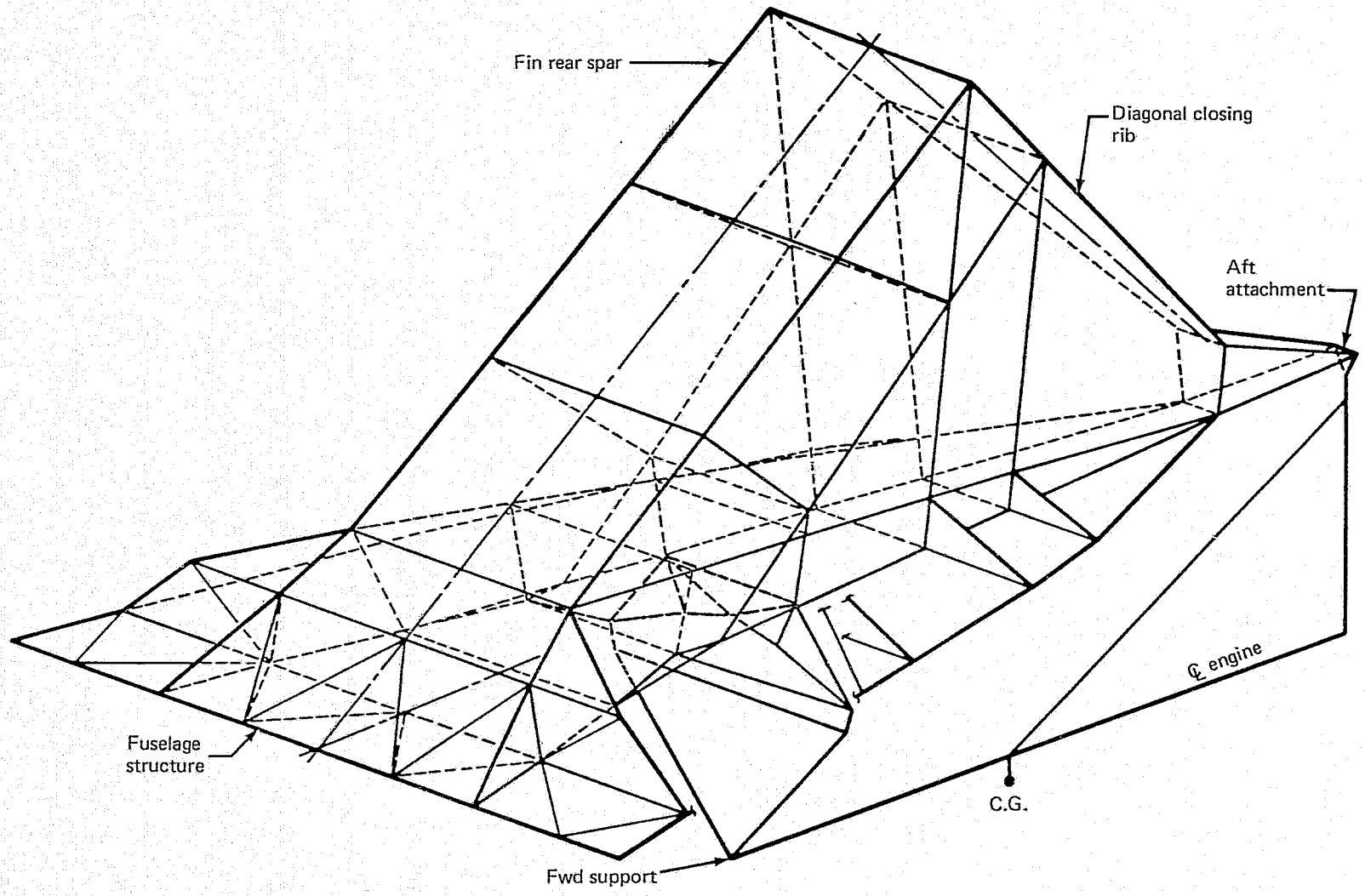

Figure 135.—JT8D Refan Center-Engine Support Structure—Finite Element Analysis Model

From the analysis results, the center-engine flexibility matrix used in the dynamic landing analysis was derived, and also the engine cone bolt loads.

Review of the internal load distribution indicated that 87% of the engine side loads were reacted as a couple by the fore-and-aft links of the forward support fitting; this significantly reduced the aft cone bolt side load.

Analysis of the structure was limited to determining the load distribution in the primary support structure.

The proposed modifications were reviewed for structural integrity and compatibility with the existing structure and were judged to be consistent with requirements.

Since the modifications to the center-engine support structure were not definitively sized, no significant margins of safety were calculated.

3.4.9 AFT FUSELAGE STRUCTURAL MODIFICATIONS

3.4.9.1 Fuselage Crown and Bulkheads

The modifications proposed for the fuselage crown at B.S. 1183 in. (30.048 m) and bulkheads at B.S. 1303 in. (33.096 m) and B.S. 1342 in. (34.087 m) were reviewed for structural feasibility and integrity only, with stress analysis for rough sizing based on loads from the existing 727-200 structural analysis.

3.4.9.2 Tail-Skid Support Structure

To prevent contact of the center engine with the ground during rotation on takeoff, the tail-skid compression range would be reduced by using a shorter, crushable cartridge together with a modified operating linkage geometry.

The 727 refan loads on the skid were calculated to be less than for the 727-200 and, therefore, the structure was judged to be acceptable for the refan installation.

The tail-skid energy absorption load-stroke curve is shown in figure 136.

3.4.9.3 Air Stairs

Modifications to the air stair power torque tube and uplock torque tube were reviewed for structural feasibility and compatibility with existing structure only. The modifications were judged to be acceptable.

3.4.10 MATERIAL MECHANICAL PROPERTIES

During the design phase, the static strength and fatigue durability of the materials used for the structural modifications and hardware for the JT8D refan installation were consistent with the Contractor's accepted manufacturing practices.

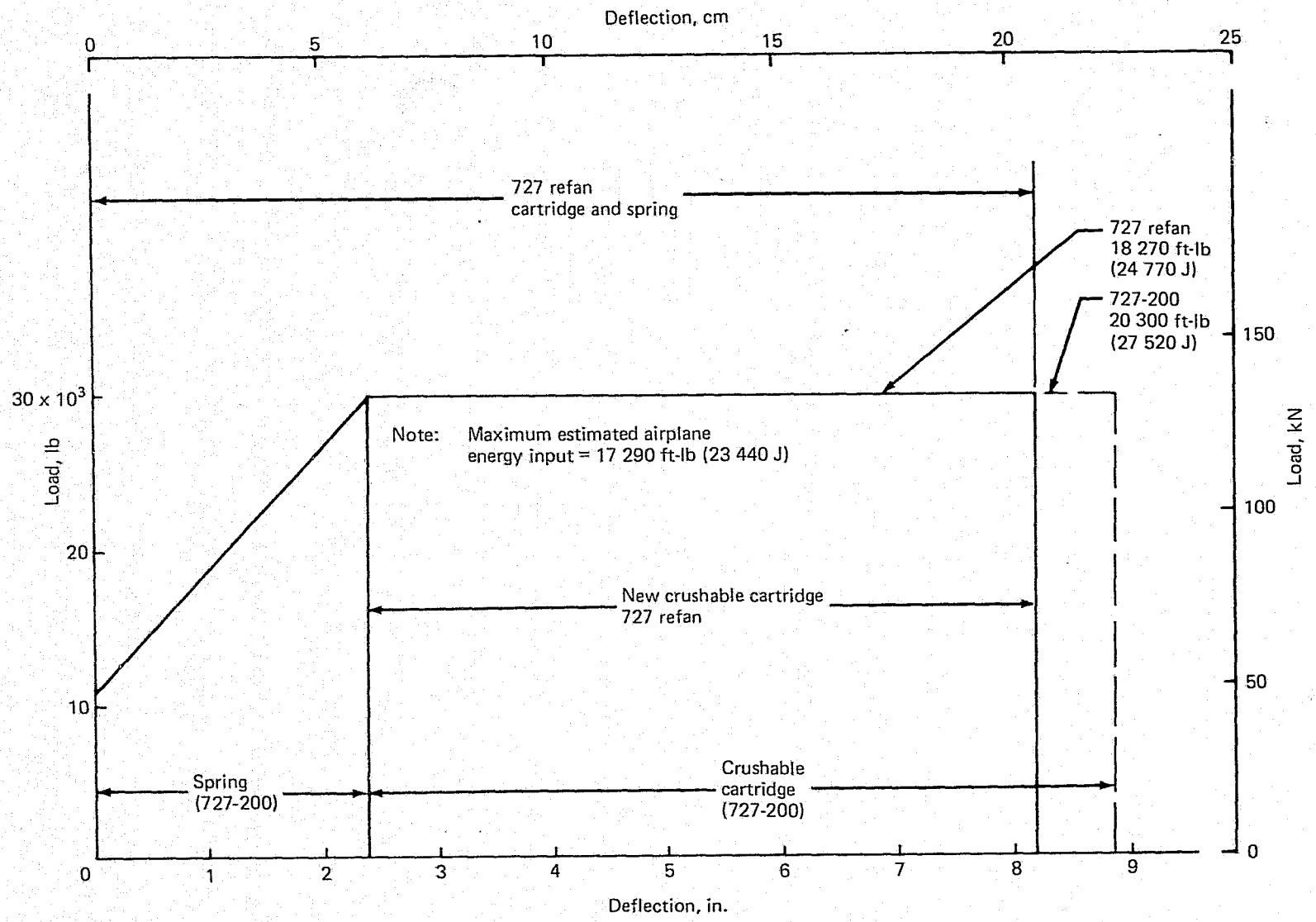

Figure 136.—727-200/727 Refan Energy Absorber Characteristics—Tail Skid

The hardware manufactured included many assemblies that were designed with advanced technology materials as summarized in table 49. These assemblies were manufactured in accordance with the Contractor's normal allowable strength criteria for commercial aircraft.

Allowables for aluminum-brazed titanium were those established in the Supersonic Transport (SST) Technology Follow-On Program (refs. 14, 15, and 16). Further tests were conducted to determine the static strength and fatigue durability of specific structural details of the JT8D refan exhaust-duct assembly (ref. 11). Fatigue data were obtained from Contractor proprietary fatigue design information, test results (ref. 11), and vendor data.

3.4.11 MATERIALS TECHNOLOGY

The advanced structural concepts used for the JT8D refan installation hardware structure were fabricated to Contractor manufacturing and process specifications. Material and process evaluation trade studies also were made prior to selection of materials and manufacturing techniques. Environmental and usage problems were also evaluated and solutions obtained.

3.4.11.1 Material Evaluation and Selection

The major decisions concerning material selection, process specification, and fabrication techniques are outlined in the following paragraphs.

Side-Nacelle Cowl and Nose Dome.—Trade studies were made, comparing various acoustic lining materials and fabrication methods. Major considerations were acoustic attentuation, weight, cost, and fabrication techniques. Typical materials and constructions are shown in table 50.

The single-layer acoustic polyimide, type 1, was selected for the cowl and nose dome. This material was used on the 727-200 and 737 nacelle inlets and therefore required no further development.

Side-Nacelle Cowls.—The nacelle cowls were to be fabricated from heat-resistant epoxy fiberglass face sheets with phenolic honeycomb core. This method reduced both manufacturing cost and number of parts when compared to the existing metal cowls.

The application of epoxy fiberglass and phenolic core in a fire zone necessitated that the cowls be able to resist flame penetration and remain functional and load carrying (ref. 17). Flame tests were conducted to select the optimum material combination fulfilling the requirements. A summary of test materials and results is shown in table 51. Panels 5, 6, and 7, which all had metal foil or wire mesh inserts, met the requirements. The wire mesh technique used for panel 7 was considered simplest to manufacture and was therefore selected for the JT8D refan nacelles.

Exhaust System.—The major criteria for the exhaust system material evaluation were acoustic attenuation, weight, strength, and environmental durability. Major materials evaluated in the trade studies are shown in table 52.

Table 49.—List of Major Assemblies Designed With Advanced Technology Materials

Assembly	Material
Side-nacelle inlet assembly	Acoustic polyimide fiberglass honeycomb liner
Side-nacelle cowls	Heat-resistant phenolic honeycomb and epoxy fiberglass skins
Center-engine inlet duct	Acoustic aluminum reinforced with phenolic honeycomb and epoxy fiberglass outer skin
Exhaust system fan/primary flow divider assembly	Acoustic nickel-brazed Inconel honeycomb
Exhaust system	Aluminum-brazed titanium honeycomb

Table 50.—JT8D Refan Inlets Acoustic Honeycomb Liner Selection

Type	Description face sheet	Core
1	Acoustic polyimide	Single layer
2	Acoustic polyimide	Double layer with septum
3	Porous epoxy	Single layer
4	Porous epoxy	Dougle layer with septum
5	Perforated aluminum	Single layer
6	Perforated aluminum	Double layer with septum
7	Type 347 stainless steel Brunscoustic	Single layer

Table 51.—Refan Side-Engine Cowl Fireproof Test Results

Specimen No.	Inner skin	Honeycomb	Outer skin	Test results
Panel 1	Two plies of glass-reinforced epoxy	Two layers of ½-in. (1.27-cm) glass-reinforced phenolic core with a one-ply glass-reinforced epoxy system	Two plies of glass-reinforced epoxy	Panel failed
Panel 2	Two plies of glass-reinforced epoxy with alumina + Metco 210 ceramic flame sprayed to outer surface	Two layers of ½-in. (1.27-cm) glass-reinforced phenolic core with a one-ply glass-reinforced epoxy system	Two plies of glass-reinforced epoxy with alumina + Metcoloy no. 2 stainless steel flame sprayed to outer surface	Panel failed
Panel 3	Two plies of glass-reinforced epoxy	1-in.(2.54-cm) thick glass-reinforced phenolic	Two plies of glass-reinforced epoxy alumina + Metco 405 nickel aluminide flame sprayed to outer surface	Panel failed
Panel 4	Two plies of glass-reinforced epoxy	1-in. (2.54-cm) thick glass-reinforced phenolic	Two plies of glass-reinforced epoxy	Panel failed
Panel 5	Two plies of glass-reinforced epoxy	Two layers of ½-in. (1.27-cm) thick glass-reinforced phenolic core with a Ti-3Al-2.5V titanium septum	Two plies of glass-reinforced epoxy	Panel acceptable
Panel 6	Two plies of glass-reinforced epoxy	1-in. (2.54-cm) thick glass-reinforced phenolic core	Two plies of glass-reinforced epoxy + Ti-3Al-2.5V titanium foil	Panel acceptable
Panel 7	Two plies of glass-reinforced epoxy with alumina + Metco 210 ceramic flame sprayed to outer surface	Two layers of ½-in. (1.27-cm) glass-reinforced phenolic core with a one-ply glass-reinforced epoxy system	Two plies of glass-reinforced epoxy with one layer of CP titanium wire mesh between	Panel acceptable
Panel 8	Two plies of glass-reinforced epoxy with alumina + Metco 210 ceramic flame sprayed to outer surface	1-in.(2.54-cm) thick glass-reinforced polyimide core	Two plies of glass-reinforced polyimide	Panel failed
Panel 9	Two plies of glass-reinforced polyimide	1-in. (2.54-cm) thick glass-reinforced phenolic core	Two plies of glass-reinforced polyimide	Panel failed
Panel 10	Two plies of glass-reinforced epoxy	1-in. (2.54-cm) thick glass-reinforced phenolic core	Two plies of glass-reinforced epoxy + alumina and Metco 405 nickel aluminide flame sprayed on PVA film bonded to panel	Panel failed

Table 52.—JT8D Refan Exhaust Nozzle Material Candidates

Specimen	Material	Honeycomb	Fabrication method
1	Inconel 625	Single layer	Nickel brazed
2	Inconel 625	Double layer with perforated septum	Nickel brazed
3	Inconel 625	Single layer	Welded
4	Inconel 625 Brunscoustic	Single layer	Welded
5	Titanium	Single layer	Aluminum brazed
6	Titanium	Single layer	Welded
7	Titanium	Double layer with perforated septum	Welded and brazed combination

Single-layer aluminum-brazed titanium honeycomb was selected for the exhaust nozzle assembly and for the fan flow side of the divider assembly. Because of the higher gas temperatures of the primary flow, single-layer nickel-brazed Inconel 625 honeycomb was selected for the primary flow side of the divider assembly.

Center-Engine Inlet Duct.—The major center-engine inlet duct criteria were weight, stiffness, acoustic attenuation, and ease of manufacturing. The materials evaluated are shown in table 50. An integrally stiffened shell was selected for the maximum stiffness-to-weight ratio. To meet the acoustic requirements, both single- and double-layer core with a septum were required in different areas of the duct. Perforated aluminum inner skin backed by phenolic core and epoxy fiberglass outer skin (types 5 and 6) was selected to meet the structural and acoustic requirements.

3.4.11.2 Material Process and Manufacturing Evaluation

Aluminum-Brazed Titanium Acoustic Honeycomb.—Fabrication methods and process specifications for controlling the manufacture of aluminum-brazed titanium were developed during the SST program (refs. 14, 15, and 16). Development was for basically flat structural panels. Feasibility of manufacturing acoustic exhaust duct type hardware was demonstrated. Further development of the detail design, manufacturing, and process specifications was required for the JT8D refan exhaust nozzle and fan divider assemblies. See reference 4 for specific details of the manufacturing.

The following principal areas required development and evaluation through analysis and test.

Detail Design: Panels representing the flange, rail, and honeycomb construction of the exhaust nozzle were tested to determine the static strength and fatigue durability, and also to qualify the design features and manufacturing processes used (ref. 11).

Exhaust Nozzle Usage:

- *Phosphate Ester Hydraulic Fluid Contamination.*—The constant presence of phosphate ester hydraulic fluid at elevated temperature was known to etch, pit, and embrittle titanium. Tests were conducted to establish the maximum temperature at which titanium could be used in a contaminated area, (i.e., exhaust nozzle, outer skin, and thrust-reverser support fitting adjacent to the actuators).

  Test results indicated that there would be no problem below 270°F (406 K). The maximum temperature recorded during the engine ground tests on the inner skin of the exhaust nozzle was 145°F (336 K). The exhaust nozzle outer skin and the titanium thrust-reverser support fitting would be below these temperatures and therefore not subject to contamination or intergranular attack.

- *Exhaust System Fire.*—A fire test was conducted to establish the exhaust duct skin temperature due to fire resulting from fuel puddling in the exhaust nozzle. The maximum temperature recorded was 800°F (700 K) which was below the structural allowable of 900°F (755 K).

Welding Technique and Tooling Concept: Semiautomated plasma arc fusion welding was used for the longitudinal skin joints and for attaching the machined rails and circumferential flanges to the skins. Welds were made in 0.025-in. (0.64-mm) thick material. The maximum allowable mismatch or bead on the faying surface with the core was 0.004-in. (0.1-mm) (required for the brazing process). Longitudinal welds met the specification requirements satisfactorily.

The circumferential welds were made using internal expanding tooling to align the skin and flange with external torch application. However, the thermal expansion of the skin during the welding operation caused misalignment, and further external clamping was required to keep the skin and flange aligned. Finally, the weld beads were roller planished to meet the specification requirements.

Further development of this welding technique would suggest the use of an external circumferential tool with an automated torch located inside the assembly. Thermal expansion of the part would then be restrained by the tool, and finer dimensional tolerances could be maintained.

Weld defects were reviewed for any potential problems which could have resulted from the repair, such as local distortion which could cause braze voids. No weld repairs could be made to the honeycomb structure following brazing due to the temperature and potential contamination. The gas tungsten arc process was used for any repairs prior to brazing, and for those in areas remote from the honeycomb, after brazing.

Fabrication: To obtain good quality brazing, close tolerance control was required as well as pressure between the skins and core. The exhaust nozzle skins and core were assembled on a specially sized stainless steel mandrel. During the braze cycle, the thermal expansion of the mandrel precisely hot-sized the skins and also applied pressure between the core and skins. This method resulted in uniform braze quality and close tolerances to the finished part.

Braze Alloy Flow: The braze process was developed using essentially flat panels. The circular exhaust-duct assemblies presented a unique problem in controlling the molten aluminum flow due to gravitational effects during the braze cycle. To neutralize these effects, the assemblies were slowly rotated in the furnace during the braze cycle. This technique provided excellent control of the braze alloy and resulted in uniform fillets throughout the honeycomb assemblies.

Prevention of Skin Perforation Plugging: Stop-off material was used to prevent the molten aluminum braze alloy from plugging the perforations.

This material was applied to the holes and resulted in minimal plugging (1% to 2%), which was well within the process requirements.

Since the perforated skin was adjacent to the braze mandrel, molten braze alloy could also flow between the skin and mandrel and result in the skin adhering to the tool. Adherence was prevented by using the stop-off material on the mandrel faying surface. Only minor attachment occurred during manufacture. However, the solid residue resulted in the inner skin being marked due to the pressure between the skins and tool during the brazing cycle.

The stop-off material binder was boiled off prior to reaching the braze cycle temperatures. This necessitated repeated purging of the retort to avoid contamination of the brazing alloy. While the results were satisfactory, further development would be required to reduce the solid residue content and binder boil-off from the stop-off material.

Nondestructive Inspection (NDI): All welds and weld repairs were radiographed prior to brazing the assemblies. The brazed assemblies were also radiographed and reviewed for quality control. Torn and crushed core, braze alloy puddling, and small fillets were identified by the radiography.

A small crack was identified in a longitudinal weld of the exhaust duct inner skin, following the braze cycle. An area of weld underfill had been identified at this location in the post-weld radiographic inspection. The crack length was noted and was kept under observation during the ground testing. Post-test inspection showed that no crack growth had taken place.

The basic NDI used on aluminum-brazed titanium structure was ultrasonic pulse echo C-scan using water immersion. This method could not be used on acoustic honeycomb because water leakage through the perforations caused erroneous signals. Determination of the fillet size using calibrated C-scan recording of eddy current signals was demonstrated on the SST Follow-On Technology Program (refs. 14, 15, and 16). This process was adapted for use on the exhaust system assemblies and gave excellent results.

The eddy current inspection was augmented with visual inspection of the fillets through the perforations. A special microscope having a "fish-eye" lens to view the inside of the cell and a fiber-optic light source for illumination were used. This system is illustrated schematically in figure 137. Figure 138 shows the honeycomb cell walls and braze fillets as seen through the microscope.

Nickel-Brazed Inconel 625.—The primary flow side of the divider assembly was fabricated using tooling principles similar to the titanium assemblies. The dimensional control was more critical than for the titanium brazing, due to the smaller differential between the coefficients of expansion of the Inconel 625 and corrosion-resistant steel mandrel.

To meet the test schedule, it was necessary to use the first assembly produced. The first part had two areas with marginal brazing; however, these areas were repaired with pins through the honeycomb welded to the skins. This part was then structurally acceptable for the ground tests.

This problem was the result of insufficient clamp-up during the braze cycle and would have been eliminated with further tool development.

3.4.11.3 Development of Titanium Thrust-Reverser Support Fitting Castings

Titanium castings were developed and produced for the JT8D refan thrust-reverser linkage support fitting and the reverser actuator slide carriage. Casting of the highly complex support fitting provided a significant cost saving compared to a welded construction (fig. 139). The large castings, 8 by 14 by 24 in. (0.2 by 0.36 by 0.61 m), weighed approximately 25 lb (11.34 kg) with the majority of web and flange thicknesses of approximately 0.2 in. (5 mm). The

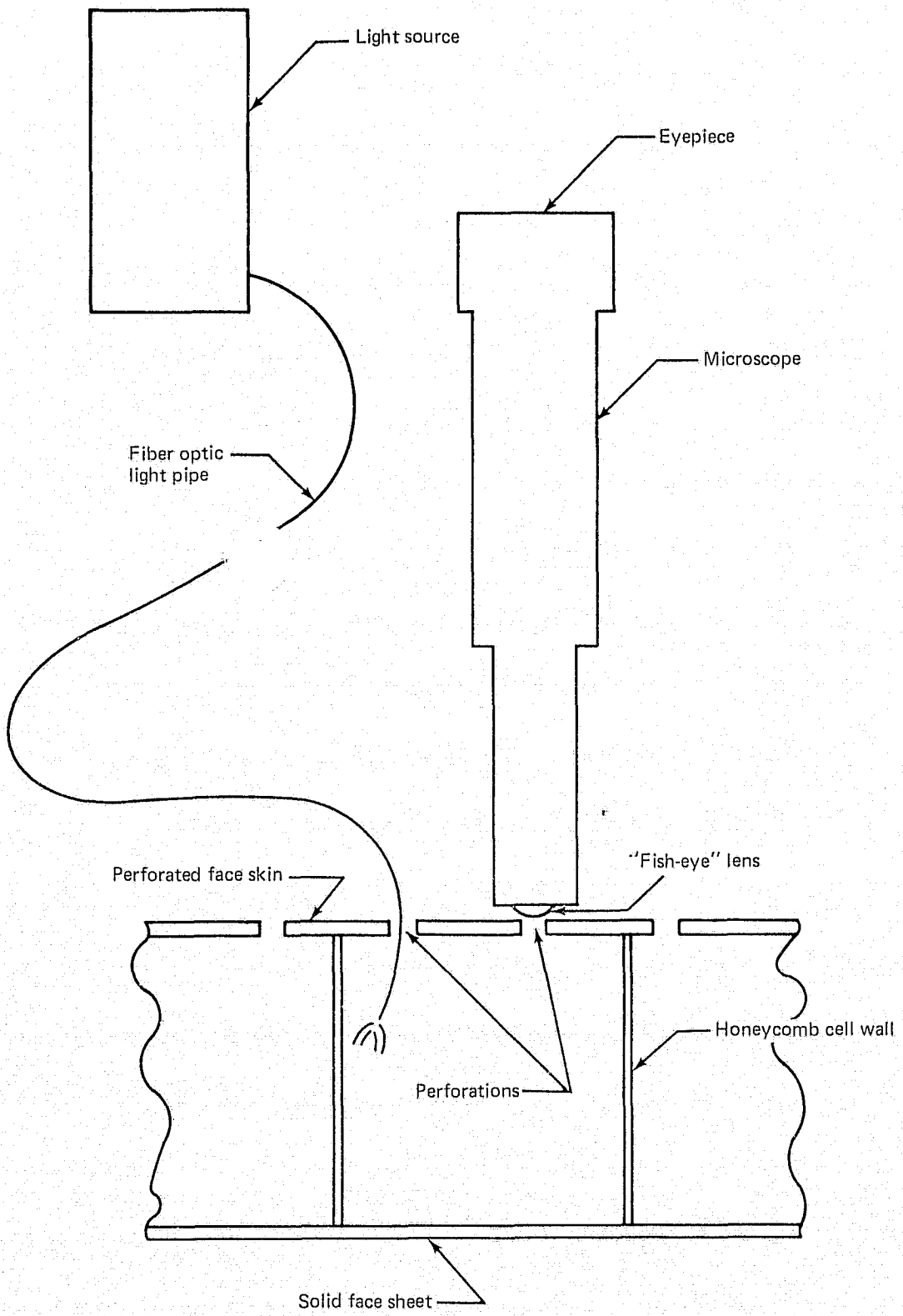

Figure 137.—Schematic Diagram of Fiber Optic/Fish-Eye Microscope Inspection Device

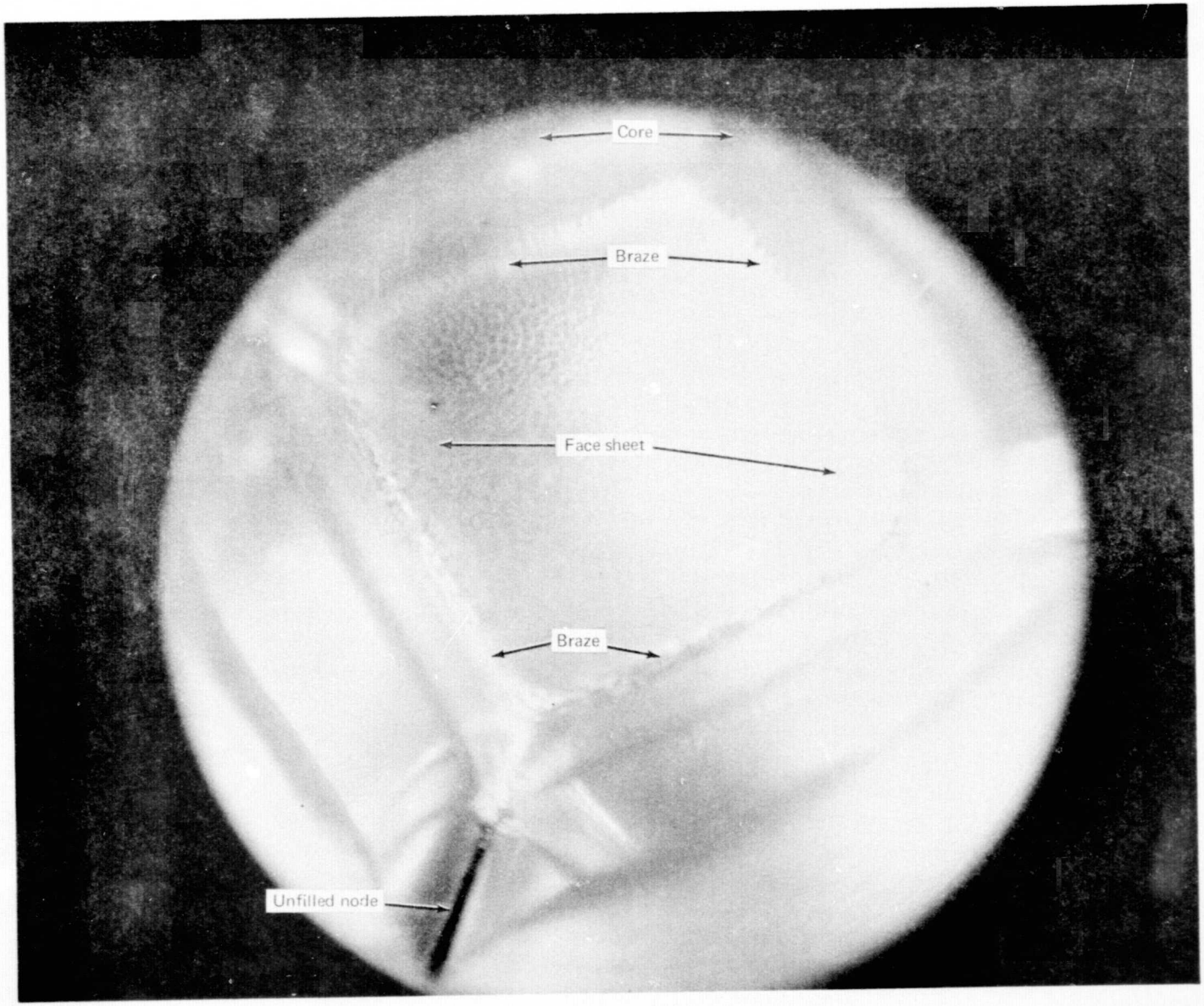

Figure 138.—Aluminum-Brazed Titanium—View Through Fish-Eye Microscope Showing Interior of Cell and Braze Fillets

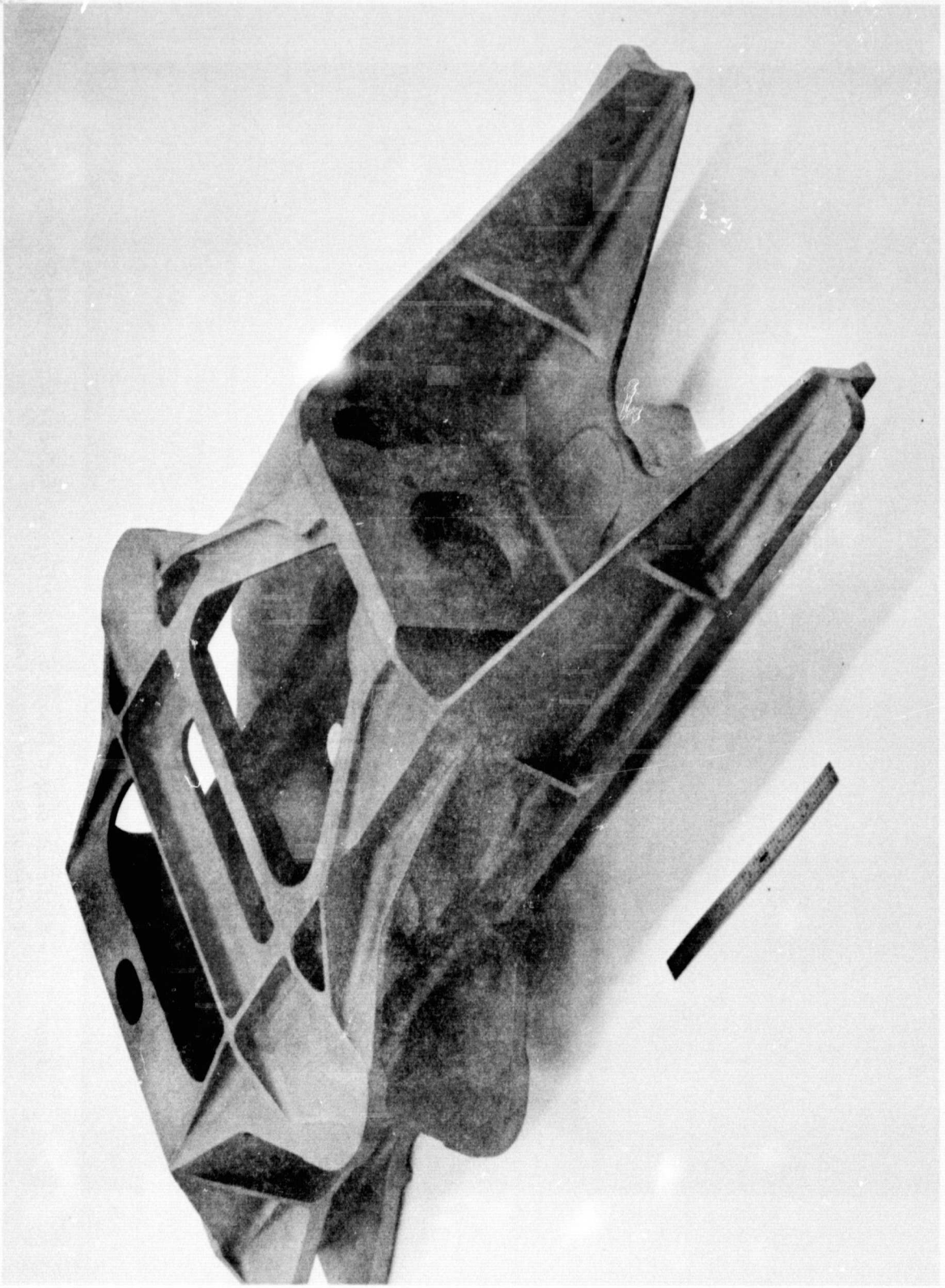

Figure 139.—JT8D Refan Thrust-Reverser Support Fitting Casting

castings were produced by the vendor using the rammed graphite process. Mechanical property requirements were equivalent to wrought Ti-6Al-4V bar. The inspection specification was MIL-C-6021F (ref. 18) with modifications to the radiographic defect levels to meet the specific application requirements.

The first castings were chemically milled to remove mold contamination. Defects or surface irregularities were ground out, and then the castings were blasted with heavy grit. After processing, the castings were inspected by visual, penetrant, and radiographic methods and were found to be acceptable. However, since both grinding and grit blasting were considered detrimental to fatigue properties, the castings were pickled an additional 0.015 in. (0.4 mm) to remove the ground and grit-blasted surfaces. Subsequent fluorescent dye penetrant inspection revealed three cracks, which were repaired by welding. The weld-repaired castings were stress relieved and resubmitted for radiographic inspection. The procured castings met the drawing requirements and successfully demonstrated production capability of large complex titanium parts.

3.4.11.4 Fabrication of Inlet Acoustic Honeycomb Liner

Center-Engine Inlet Duct.—The center-engine inlet duct was designed to provide acoustic treatment along the entire length of the duct. The configuration of the duct was perforated aluminum inner skin, fiberglass-reinforced phenolic honeycomb core, and heat-resistant epoxy fiberglass outer skin.

A reticulating epoxy adhesive was used for the aluminum skin-to-core bond. The process for application of the adhesive was developed by the Contractor. The process used an unsupported film adhesive which was reticulated on the honeycomb core using a bank of controlled infrared lights and a hot-air knife. This process provided a more uniform application of adhesive, which resulted in a more consistent adhesive fillet size than could be obtained by roller coating processes. The uniformity of adhesive application resulted in minimal acoustic skin hole blockage and more uniform bond strength within a part. The heat-resistant epoxy system was suitable for use in areas which were subjected to TAI temperatures.

The heat-resistant epoxy material used for the impervious outer skin was an existing Contractor production material and required no additional development work for the duct application.

Fabrication required the following multi-staging: (1) doubler-to-aluminum skin bonding, (2) honeycomb core-to-aluminum skin bonding, and (3) outer epoxy skin processing. Sections 1, 3, and 4 of the duct were fabricated as cylindrical sections on male mandrels, which were sectioned along molded-in cutting grooves for removal from the finished parts. This eliminated the need for longitudinal joints in these sections. Section 2, which contained the TAI patch, had acoustic treatment on only the lower half and was joined along a longitudinal splice.

Side-Nacelle Inlet.—The side-engine acoustic liner, inlet ring, and nose dome were fabricated using the Contractor's proprietary polyimide technology. This materials system was all-polyimide, including the acoustic and impervious skins, adhesive, and honeycomb core. The acoustic skin was fabricated from a carefully controlled fiberglass fabric which was preimpregnated with a polyimide resin. The skin layup and processing were controlled to produce

the required flow resistance. Acoustic skin material properties and processing requirements were controlled by proprietary specifications.

3.4.12 DYNAMIC LANDING ANALYSIS

The load factors used for certification of the existing 727-200 with JT8D-17 engines were used for the structural analysis of the 727 refan engine installation. In order to verify the adequacy of these factors, considering the increased engine weight and revised c.g. locations, a dynamic landing analysis was initiated to obtain the vertical load factors and also to investigate load factor sensitivity to variations in side-engine flexibility and weight.

The dynamic analysis was made using the dynamic analysis feature of the finite element structural analysis program described in the appendix under "Finite Element Structural Analysis Program". The total airplane structure and the center-engine and side-nacelle flexibilities were simulated in the model. From this analysis, the structural dynamic modes of the 727-200 and 727 refan were determined. The analysis considered the JT8D-109 and -117 engines, and also the JT8D-17, in order to obtain comparative results. The simulation of the structure in the mass model is shown in figure 140. The following airplane translation and dynamic components were considered in the analysis:

1. Symmetrical airplane and engine dynamics
2. Zero yaw
3. Rigid airplane pitch and translation
4. Aerodynamic lift and moment
5. Nonlinear landing gear characteristics
6. Landing gear spin-up and spring-back
7. Dynamic freedom in the following axes:
   a. Wings . . . . X, Z, Rx, Ry
   b. Fuselage and center engine . . . . X, Z, Ry
   c. Side-engine nacelle . . . . X, Y, Z, Rx, Ry, Rz
8. Fifteen flexible airplane and engine dynamic modes
9. Input of side- and center-engine flexibilities for nominal, 1.5 and 2.0 times nominal flexibility, as well as for rigid conditions

The critical landing condition at 10-ft/s (3.048-m/s) sink rate is shown in figure 141, together with the coordinate system orientation. Engine and nacelle weights and inertial characteristics are shown in table 53.

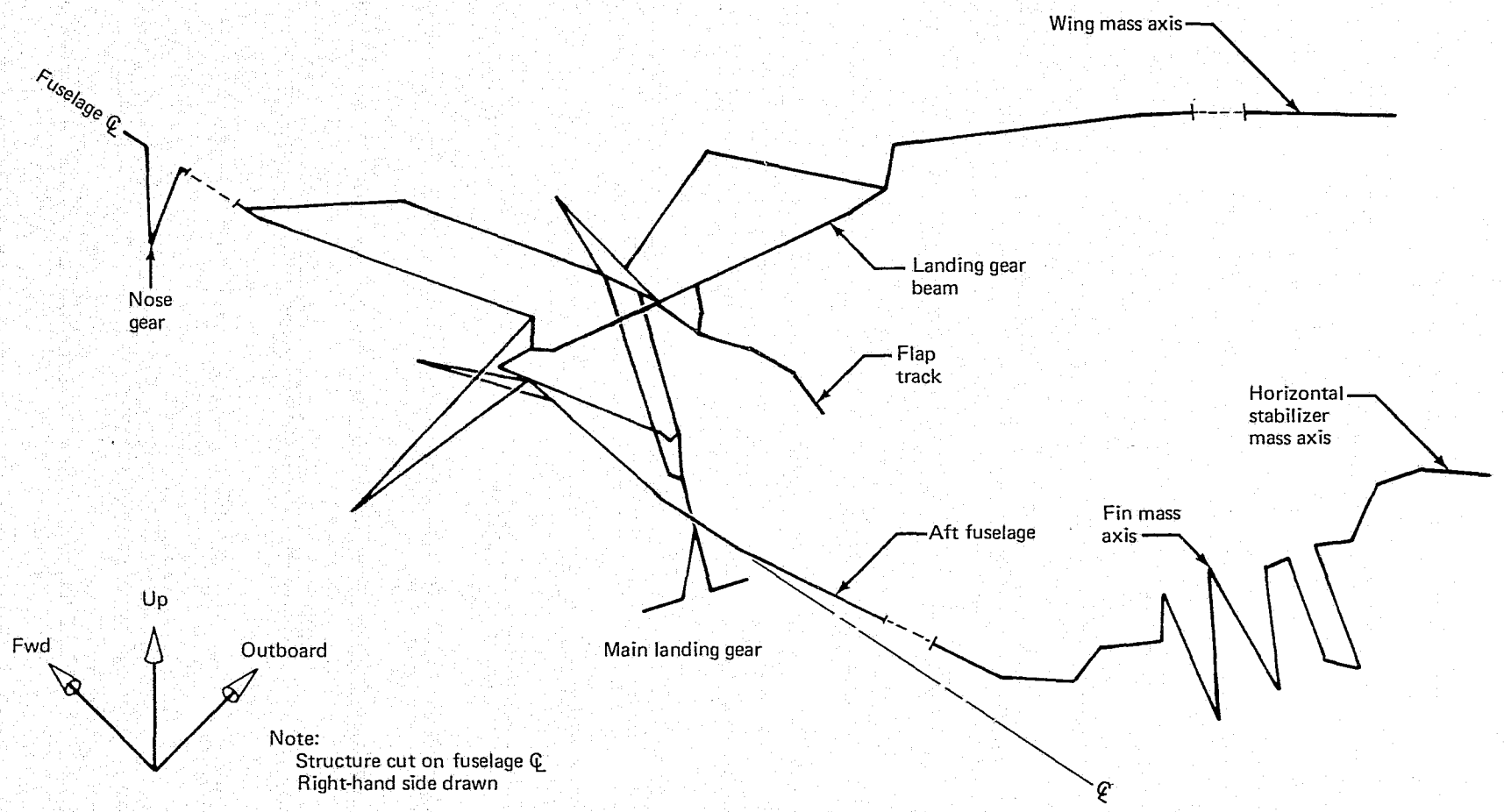

Figure 140.—727 Refan Dynamic Landing Analysis Structure Simulation Mass Model

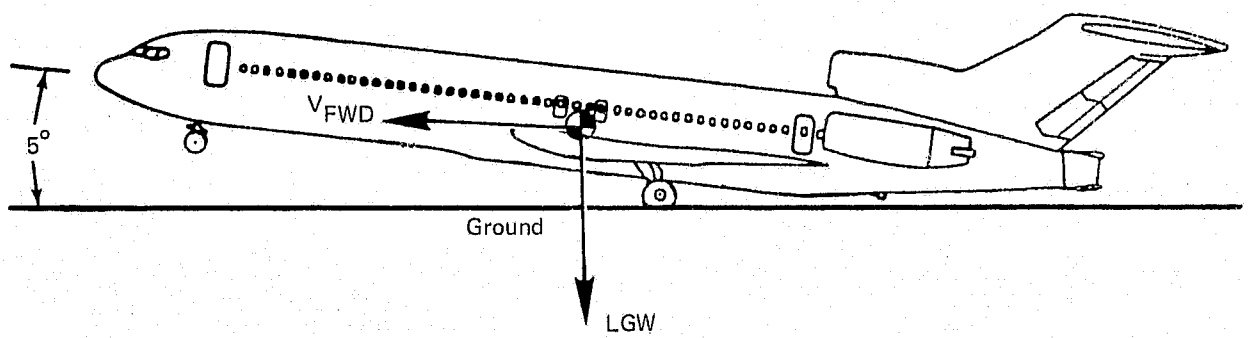

Sink = 10.0 ft/s
(3.048 m/s)

Coordinate System

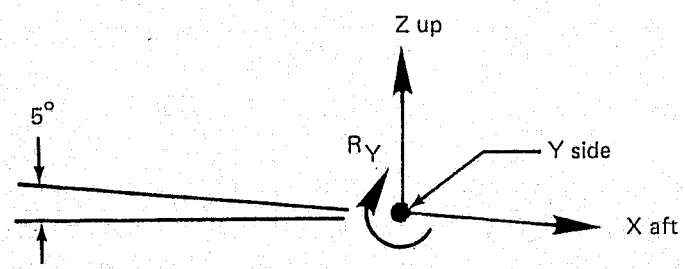

V_{FWD} = 120 kn (61.73 m/s)
LGW = 161 000 lb (73 028 kg)
c.g. at 11% MAC

Figure 141.—727 Refan Dynamic Landing Condition and Coordinate System

Table 53.—727 Refan Dynamic Landing Analysis—Side- and Center-Engine Weight

Characteristics	Side engine			Center engine		
	JT8D-17	JT8D-109	JT8D-117	JT8D-17	JT8D-109	JT8D-117
Weight[a], lb (kg)	5350 (2427)	5953 (2700)	6151 (2790)	4600 (2087)	4985 (2261)	5109 (2317)
Engine c.g. body coordinates, in. (m) X	1325.3 (33.663)	1321.2 (33.558)	1320.0 (33.528)	1532.0 (38.913)	1539.7 (39.108)	1539.7 (39.108)
Y	±105.4 (±2.677)	±115.3 (±2.929)	±115.3 (±2.929)	[b]0.0	[b]0.0	[b]0.0
Z	240.3 (6.104)	239.9 (6.093)	240.0 (6.096)	229.1 (5.819)	224.8 (5.710)	224.8 (5.710)
Moment of inertia about engine c.g., psi x 10^6 (kN/m^2) I_{xx}	1.69 (4.850)	2.66 (7.634)	2.76 (7.921)	1.14 (3.272)	1.75 (5.022)	1.82 (5.223)
I_{yy}	10.35 (29.703)	13.89 (39.862)	14.95 (42.904)	7.25 (20.806)	11.15 (31.998)	11.56 (33.175)
I_{zz}	10.45 (29.990)	14.14 (40.579)	15.19 (43.592)	6.93 (19.888)	10.64 (30.535)	11.04 (31.683)

a Side-engine weight included engine, nacelle, and strut

b Considered zero for analysis.

Engine flexibilities for the side nacelle and center engine were derived from the structural analyses as described in sections 3.4.3 and 3.4.8.

From the dynamic landing analysis results of the 727-200 with JT8D-17 engines, the side-engine first mode vertical frequency was 6.30 cps, which compared favorably with 6.17 cps obtained during the dynamic testing of the 727-200 airframe. The dynamic analysis results showed that the JT8D-117 load factors were higher than for the JT8D-17 (8.3% for the side engine and 7.8% for the center engine); however, the calculated values were less than the current design factors.

The calculated JT8D-17, -109, and -117 load factors are shown in table 54.

The engine c.g. dynamic response was the result of coupling between the airplane and engine mount dynamic modes. Variations in engine weight and mount structure flexibility changed the engine dynamic characteristics which, in turn, significantly influenced the airplane and engine mount coupling and the character of the dynamic response at the engine c.g.

Nacelle and engine dynamic response varied considerably with engine weight and engine flexibility, producing the wide range seen in the vertical load factor results. The dynamic response curves for the side- and center-engine c.g., which were plotted for the first 1/2 sec following runway landing impact, compare the 727 refan with the 727-200 airplane structure with JT8D-117 and -17 engines, respectively (figs. 142 and 143).

The significant results obtained from the dynamic landing analysis are summarized as follows:

1. The design load factors used for the refan structural analysis were adequate.

2. The dynamic landing analysis showed that the JT8D-117 load factors were higher than for the JT8D-17 engine, but still less than the current design factors.

3. Load factors were influenced by engine weight and flexibilities, as a result of the engine and airframe dynamic mode coupling.

3.5 AIRPLANE WEIGHT AND BALANCE

3.5.1 WEIGHT

Installation of the JT8D refan engine would result in a weight increase and an aft c.g. shift of approximately 6% MAC for a 727 refan airplane. This aft c.g. shift would be unacceptable; for the purposes of this study, nose radome ballast was used as a solution. An operating weight of 99 000 lb (44 906 kg) and BRGW of 172 500 lb (78 245 kg) were used as being representative of airplanes currently in service. A breakdown of the 727-200 airplane operating empty weight is shown in table 55. Table 56 lists and compares those items in the propulsion installation breakdown which would be modified by the installation of the JT8D refan engine.

Table 54.—727 Refan Side-Nacelle and Center-Engine Load Factors

Airplane configuration	Engine flexibility	Engine c.g. vertical ultimate load factor[a], g's	
		Side	Center
727-200 with JT8D-17 engines	Nominal	4.71	8.10
727-200 with JT8D-109 engines	Rigid	—	—
	Nominal	4.89	8.00
	1.5 x nominal	5.55	7.76
	2.0 x nominal	6.35	8.58
727-200 with JT8D-117 engines	Rigid	4.82	8.10
	Nominal	5.10	8.73
	1.5 x nominal	5.84	7.83
	2.0 x nominal	—	—
Refan design load factors		8.00	9.45

[a]Ultimate load factor = 1.5 x limit load

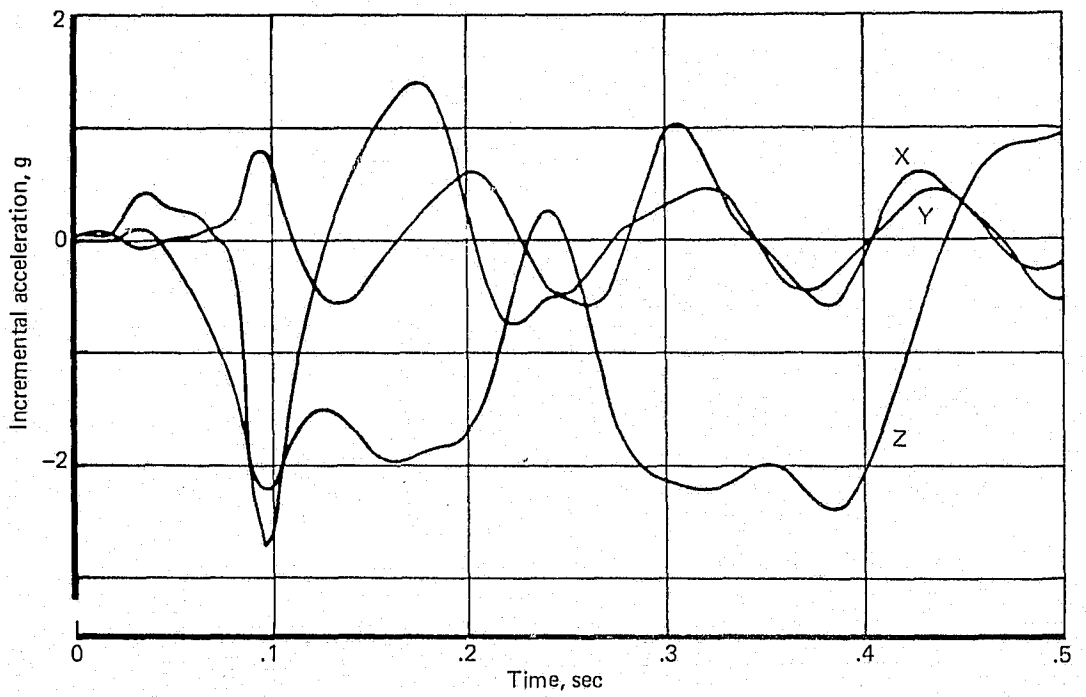

(a) JT8D-117

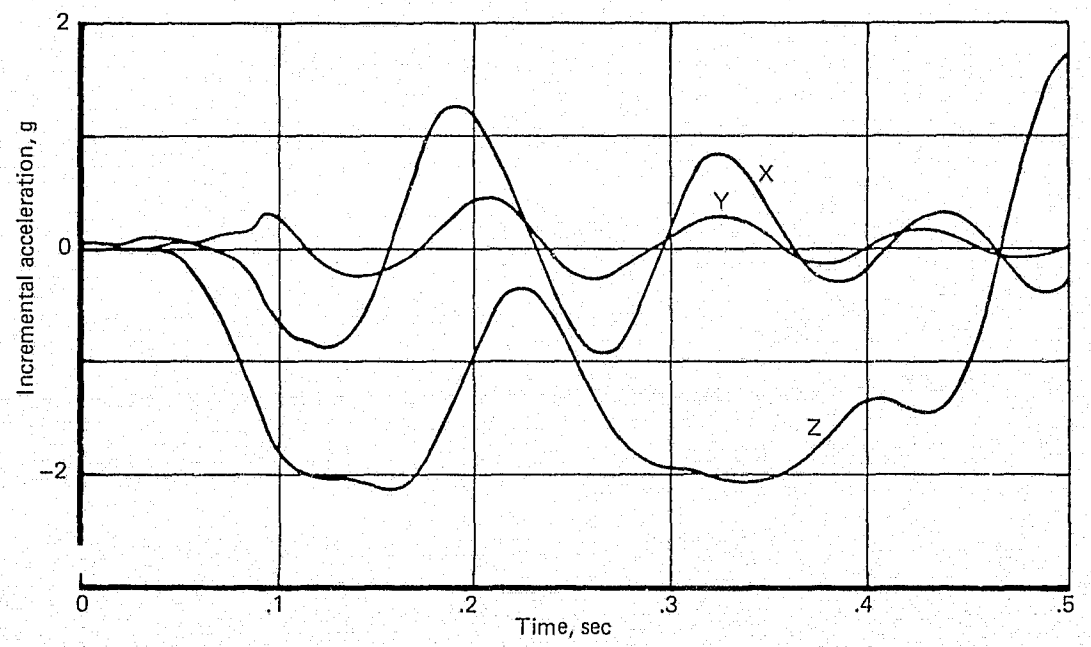

(b) JT8D-17

Figure 142.—Comparison of JT8D-17 and -117 Side-Engine C.G. Acceleration

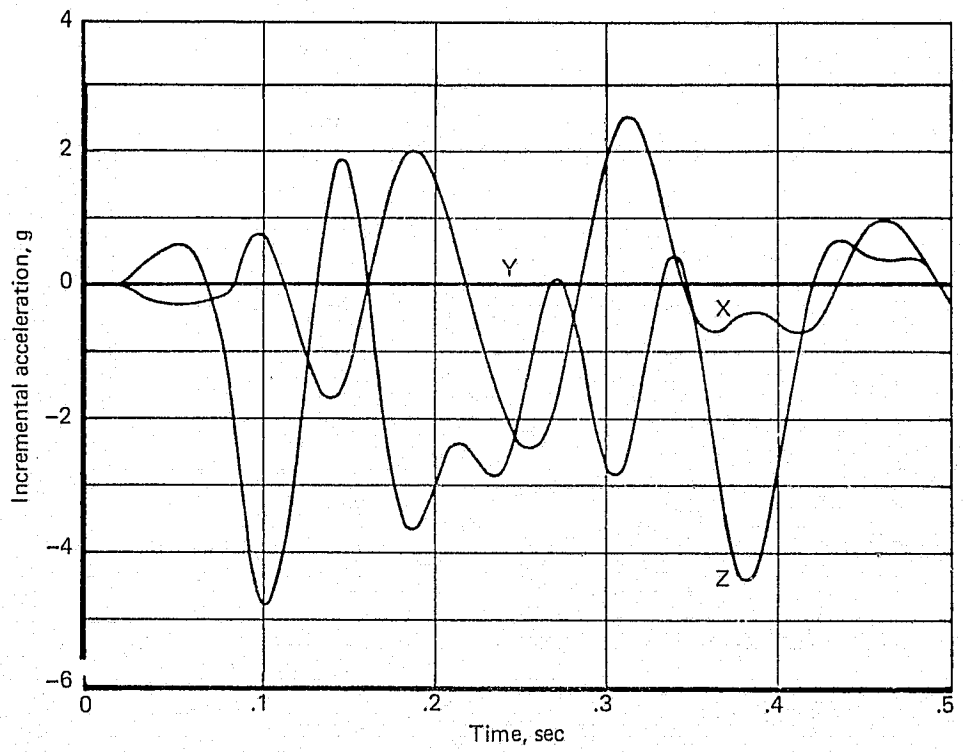

(a) JT8D-117

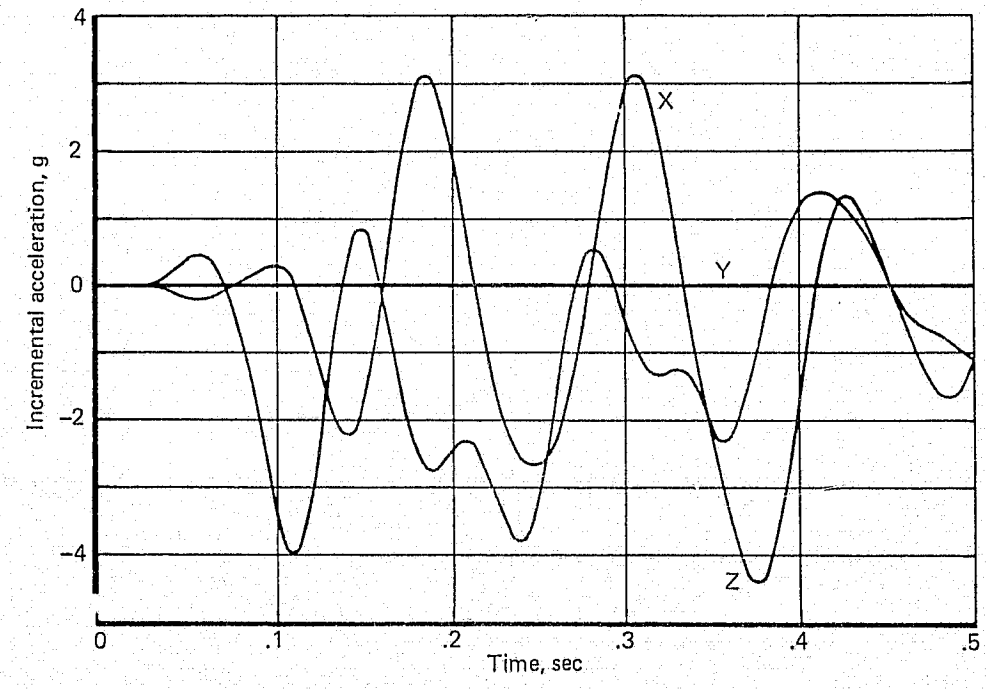

(b) JT9D-17

Figure 143.—Comparison of JT8D-17 and -117 Center-Engine C.G. Acceleration

Table 55.—727-200 Airplane Weight Breakdown

Item	Weight, lb (kg)
Wing	18 520 (8 401)
Horizontal tail	1 930 (875)
Vertical tail	2 220 (1 007)
Body	22 380 (10 152)
Main landing gear	6 520 (2 957)
Nose landing gear	1 140 (517)
Nacelle and strut	2 220 (1 007)
Total structure	54 930 (24 916)
Engine (JT8D-9)	9 680 (4 391)
Engine accessories	270 (122)
Engine controls	120 (54)
Starting system	150 (68)
Fuel system	1 210 (549)
Thrust reverser	1 580 (717)
Total propulsion group	13 010 (5 901)
Instruments	830 (376)
Surface controls	2 970 (1 347)
Hydraulics	1 430 (649)
Pneumatics	— —
Electrical	2 420 (1 098)
Electronics	1 830 (830)
Flight provisions	890 (404)
Passenger accommodations	8 820 (4 001)
Cargo handling	1 090 (494)
Emergency equipment	1 100 (499)
Air-conditioning	1 710 (776)
Anti-icing	490 (222)
Auxiliary power unit	850 (386)
Total fixed equipment	24 430 (11 081)
Exterior paint	100 (45)
Options	730 (331)
Manufacturer's empty weight	93 200 (42 276)
Standard and operational items	5 800 (2 631)
Operational empty weight	99 000 (44 906)

Table 56.—Airplane Weight Comparison—JT8D Refan Engine Installation

Item	727-200 weight, lb (kg)	727 refan weight, lb (kg)
Propulsion installation		
Side engine		
Engine	3 227 (1464)	3 797 (1722)
Inlet	120 (54)	256 (116)
Cowl	208 (94)	259 (117)
Exhaust system	524 (238)	598 (271)
Accessories	527 (239)	507 (230)
Engine mounts	131 (59)	131 (59)
Strut and contents	294 (133)	328 (149)
Total weight per side engine	5 031 (2282)	5 876 (2665)
Total side-engine weight	10 062 (4564)	11 752 (5331)
Center engine		
Engine	3 227 (1464)	3 797 (1722)
Center inlet duct	822 (373)	1 184 (537)
Cowl	232 (105)	275 (125)
Exhaust system	524 (238)	598 (271)
Accessories	527 (239)	521 (236)
Engine mounts	103 (47)	103 (47)
Engine support beam	264 (120)	305 (138)
Total center-engine weight	5 699 (2585)	6 783 (3077)
Total engine installed weight	15 761 (7149)	18 535 (8408)
Propulsion delta weight per airplane	Base	+2 774 (+1258)
Airplane modifications	0	+75 (+34)
Ballast	0	+990 (+449)
Total ΔOEW	Base	+3 839 (+1741)

The following brief explanation is listed for the weight differences.

- *Engine.*—The weight increase would be 570 lb (259 kg) per engine as provided by P&WA.

- *Nacelle.*—Weight increases would be due to revised nacelle geometry, increased engine weight, and acoustic treatment.

- *Body.*—The body weight increase would be due to:

  . Aft body structural changes in the center-duct area to accommodate the large center-engine inlet duct

  . Forward and aft body structural reinforcement, due to the increased body loads resulting from the JT8D refan powerplant package weight, geometry, and thrust

  . Center-engine support structural changes to accommodate new engine mount location and higher loads

- *Ballast.*—990 lb (449 kg) of ballast is assumed to be added to the nose radome bulkhead to counteract the aft c.g. shift caused by the powerplant and structural weight increases.

3.5.2 AIRPLANE BALANCE

The installation of the JT8D refan engine and all associated modifications would result in a 6% MAC aft shift in the "as-delivered fleet average" 727 airplane. This shift, if not compensated for, would violate two aft c.g. requirements: (1) an aft flight limit derived from a neutral stability flight consideration, and (2) a ground-handling limit derived from a tipping consideration. These situations are depicted in figure 144.

The OEW c.g. of the 727-200 airplane would be changed by the installation of the JT8D refan engine from 40% MAC to 46% MAC, 4% aft of the recommended 42% MAC required to keep within the aft flight limit. This could present some airline operators with loadability difficulties.

The severity of the loadability for each airline is a function of the OEW c.g.'s, passenger seating arrangements, and types of airline operations. Since these vary considerably from operator to operator, the magnitude of this difficulty will be different for each operator.

The solution of fixed ballast for the c.g. control/loadability difficulties for this study is based on the consensus of airline replies to a loadability survey. The survey, conducted during the contract, was submitted to nine domestic and four foreign airlines. The majority of replies indicated the most desirable solution to be the addition of fixed ballast to a forward bulkhead. The addition of 990 lb (449 kg) of lead ballast to the nose radome bulkhead will shift the "as-delivered fleet average" OEW c.g. forward to the recommended 42% MAC limit. There is, however, an economic penalty to payload/range due to carrying this extra dead weight on all flights.

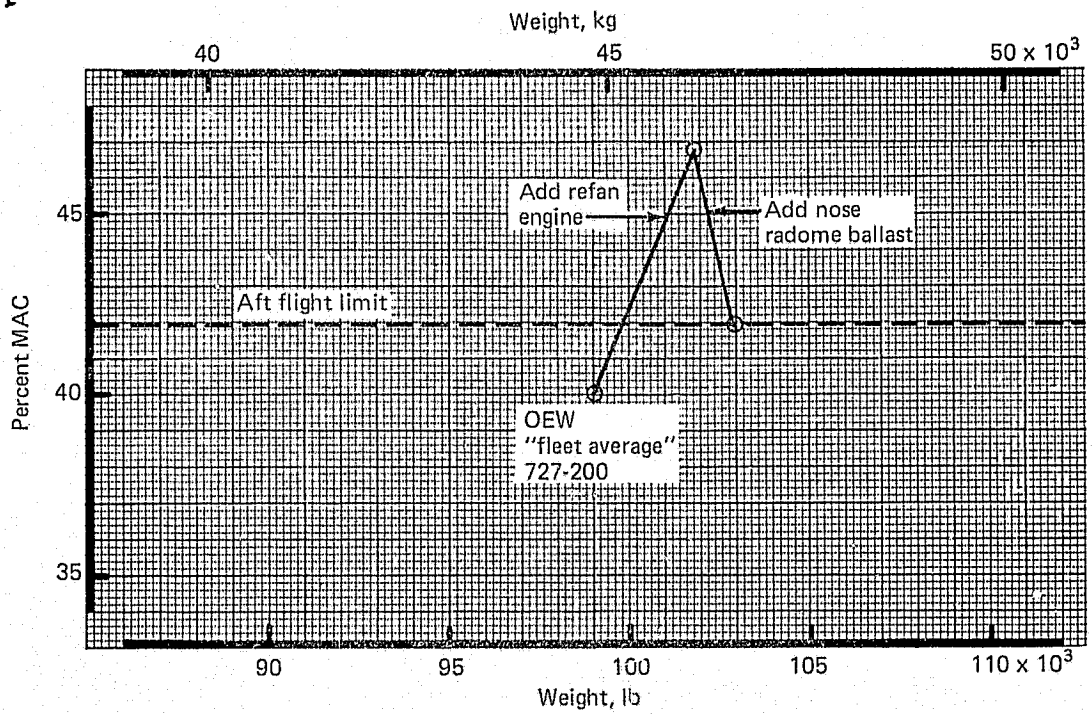

(a) OEW C.G. Travel

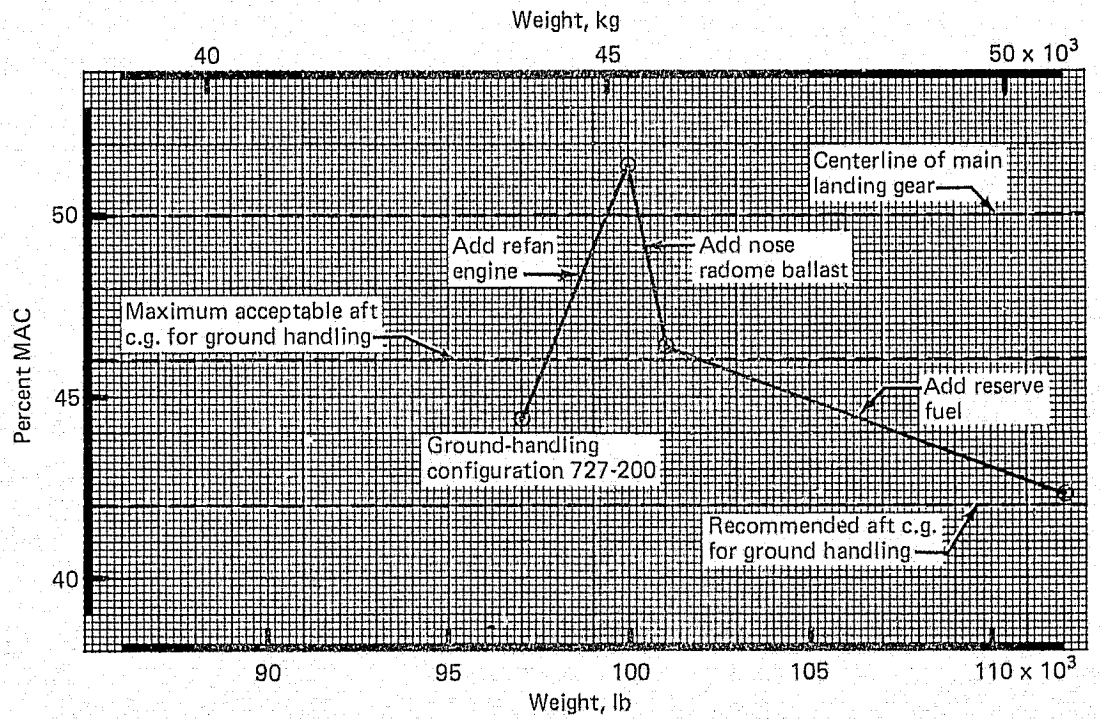

(b) Ground-Handling Configuration C.G. Travel

Figure 144.—727 Refan Airplane Balance Summary

In addition to airplane flight considerations, attention must be given to ensuring the airplane is stable with respect to nose gear steering and tipping for ground handling. The normal condition of the airplane during ground handling is with certain standard and operational items removed. The "ground-handling configuration" c.g. of the "as-delivered fleet average" airplane with JT8D refan engine and 990-lb (449-kg) radome ballast installed is at approximately 47% MAC. The maximum acceptable aft c.g. for ground handling to prevent tipping is 4% MAC forward of the main landing gear centerline or 46% MAC, and the recommended c.g. is 42% MAC. Therefore, reserve fuel or temporary ballast is recommended to bring the c.g. forward to 42% MAC.

Other possible but less desirable solutions were presented to the airlines. They were requested to consider the relative merits of each and their preference of the following possible solutions for their own particular operational needs.

- The forward cargo hold may be loaded with cargo or, if cargo is unavailable, with ballast to shift the c.g. forward.

- Passenger seating may be restricted to prevent passengers from sitting in the aft portion of the airplane until the forward seats are filled.

- Wing center-tank fuel may be carried as ballast to move the c.g. forward. However, fuel used for ballast is unavailable for use during flight.

- Airplane configuration changes can be made to shift the c.g. forward. For example, deletion of the aft air stair results in a 1% MAC shift, or moving an 800-lb (363-kg) galley from an aft position to a forward position results in a 4% MAC shift.

- Removable ballast may be carried in the nose wheel well.

Ballast represents the most practical technical solution to the airplane balance. However, airline concern was expressed regarding economics of operation. Additional studies would have to be conducted to firmly identify the most cost-effective solution for each airline operator.

3.5.3 TRADE STUDIES

Typical weight trade studies resulted in the selection of materials that were incorporated into the 727 refan airplane. The results of some of these studies follow.

- Titanium acoustic lining was selected for the exhaust duct rather than Inconel 625 acoustic lining. This would result in a weight saving of 279 lb (127 kg) per airplane. In addition, 178 lb (81 kg) of ballast would be saved by this change.

- Titanium was selected for the thrust-reverser doors rather than Inconel 625. This would result in a weight saving of 120 lb (54 kg) per airplane and reduce the nose radome ballast by an additional 76 lb (34 kg).

- An engine fan duct air-cooling system was selected for cooling the engine constant speed drive rather than using a ram air ejector. This change would result in a weight saving of 45 lb (20 kg) per airplane and an additional 20 lb (9 kg) of nose radome ballast.

The net saving of these three items was 444 lb (201 kg), plus 299 lb (136 kg) of nose radome ballast, per airplane.

3.6 AIRPLANE STABILITY AND CONTROL

Investigations into longitudinal stability, stall characteristics, directional stability, dutch roll, and reverse thrust effects on rudder effectiveness were conducted for the 727 refan airplane. The following subsections include the analyses and results.

3.6.1 LONGITUDINAL STABILITY AND CONTROL–HIGH-SPEED CHARACTERISTICS

The effect of the JT8D refan nacelles on high-speed longitudinal characteristics is small. The nacelles would cause a small nosedown pitching moment increment and a slight increase in stability. Two examples of high-speed wind tunnel test data are shown. Figures 145 and 146 show the effect of the refan nacelles on pitching moment for $M_\infty = 0.40$ and 0.85 respectively.

3.6.1.1 Speed Stability (Stick Force per Knot)

Although the JT8D refan nacelles did not degrade the high-speed pitch stability, the nosedown pitching moment increment would require a more noseup trim setting for level flight. Estimates of the effect on speed stability of this change in trim setting indicated a slight reduction in the control column force gradient (stick force is a function of stabilizer trim setting as well as airspeed). Figure 147 shows a comparison of the estimated control column force gradient for the 727 refan to the FAA certification flight test data for the 727-200 at the V_{mo} speed. The effect was considered negligible.

3.6.1.2 High-Speed Tuck

Figure 148 shows a comparison of the 727 refan and 727-200 tuck characteristics at gross weights of 130 000 lb (58 967 kg) and 160 000 lb (72 575 kg) for a constant trim setting. Estimates indicated a mild degradation for the 727 refan at 15 000-ft (4572-m) altitude near V_D for both gross weights. No significant differences existed at the other altitudes. The analysis did not include the effect of elevator downrig and, therefore, was considered somewhat conservative. Elevator downrig improves high-speed tuck characteristics because elevator effectiveness decreases with increasing M_∞ at a greater rate than stabilizer effectiveness. The resulting pitching moment from the horizontal tail becomes more noseup as speed increases, reducing the nosedown tuck effect.

3.6.1.3 Mistrim Dive Recovery

The FAA handling quality requirements include demonstration of airplane recovery capability at high speed with the airplane out of trim in the nosedown direction. The requirement is met by demonstrating a pullup capability of 1.5 g at the V_{DF}/M_{DF} placard following a 3-sec

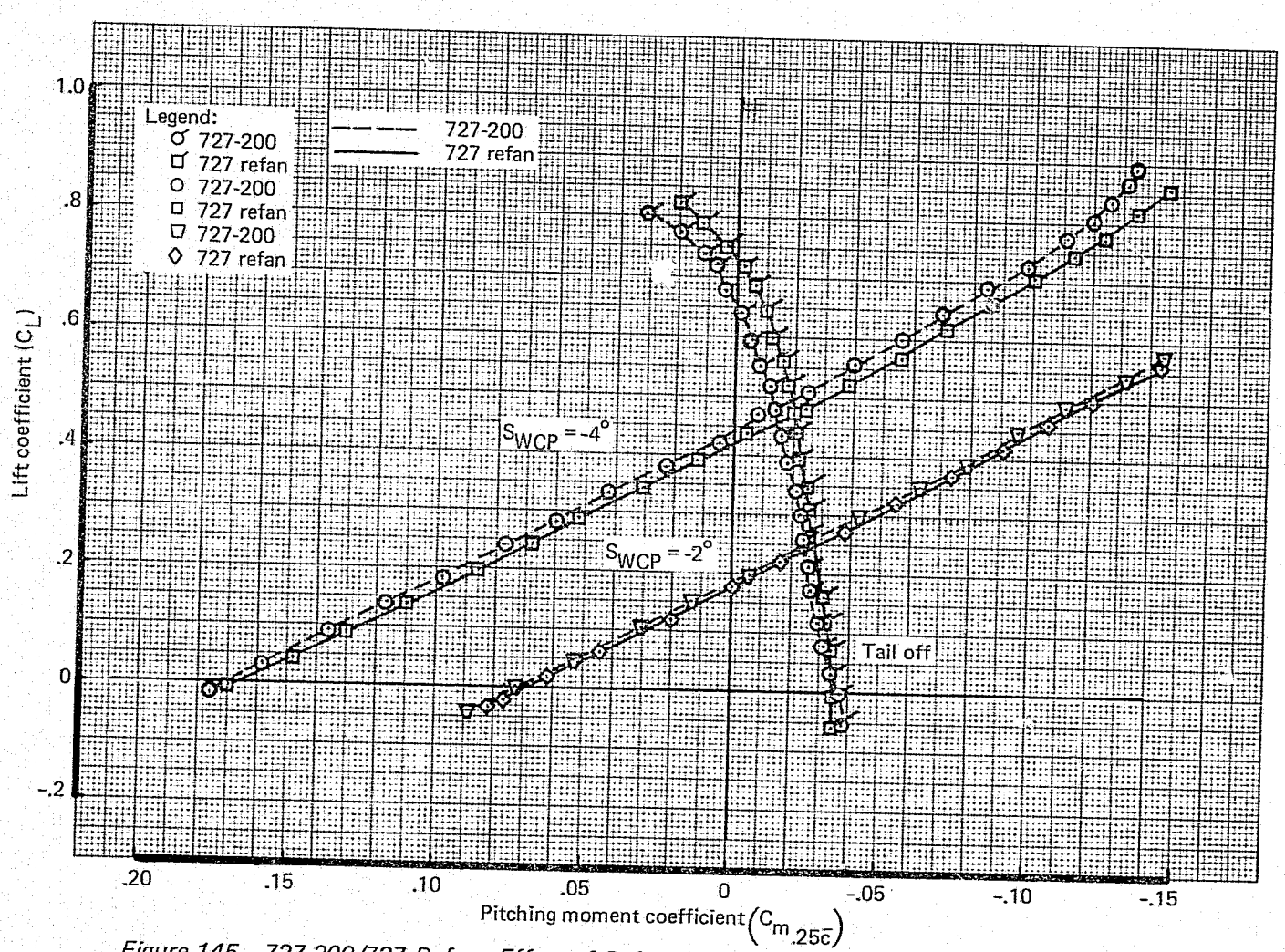

Figure 145.—727-200/727 Refan—Effect of Refan Configuration on Pitching Moment at $M_\infty = 0.40$

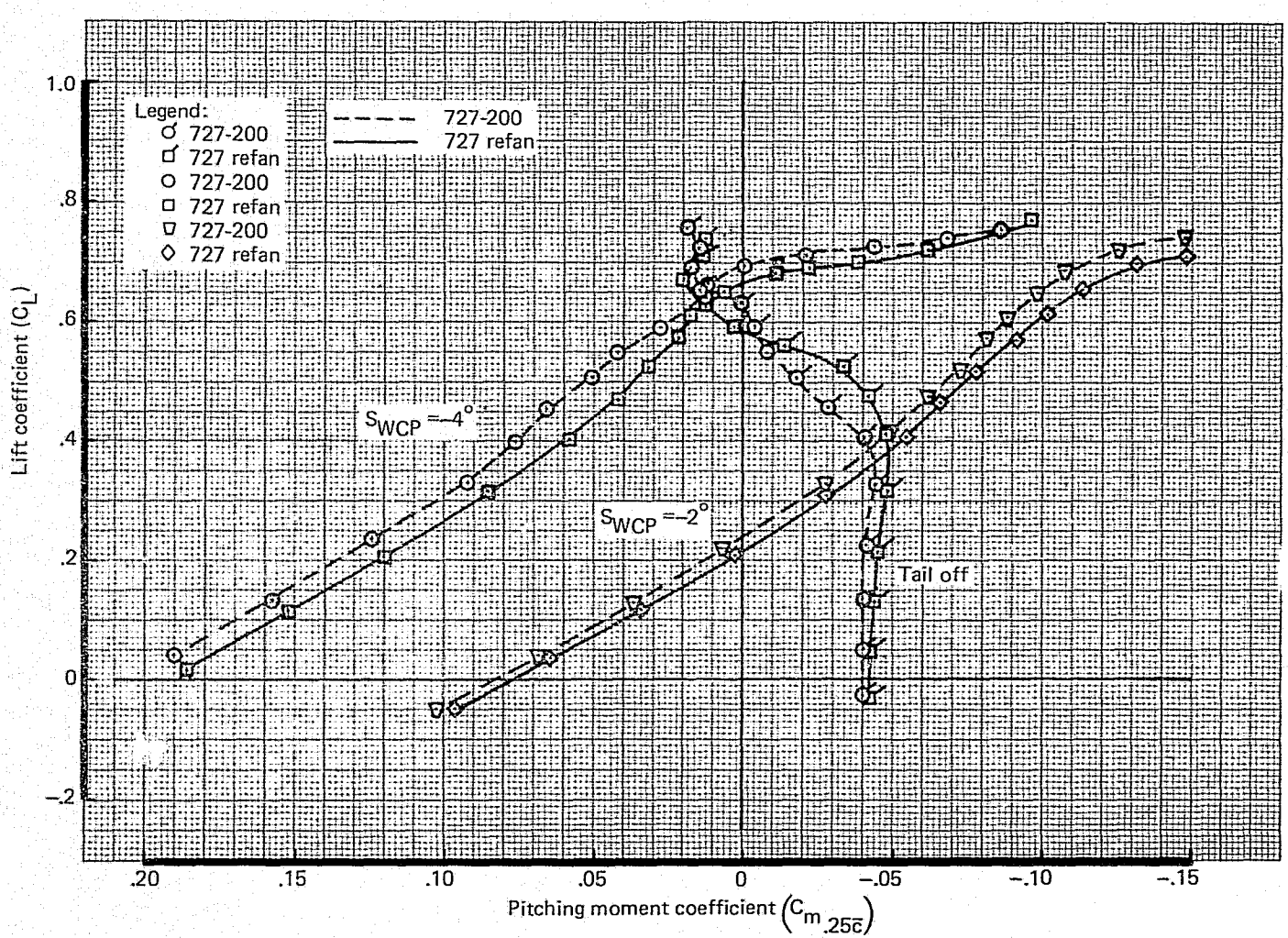

Figure 146.—727-200/727 Refan—Effect of Refan Configuration on Pitching Moment at M_∞ = 0.85

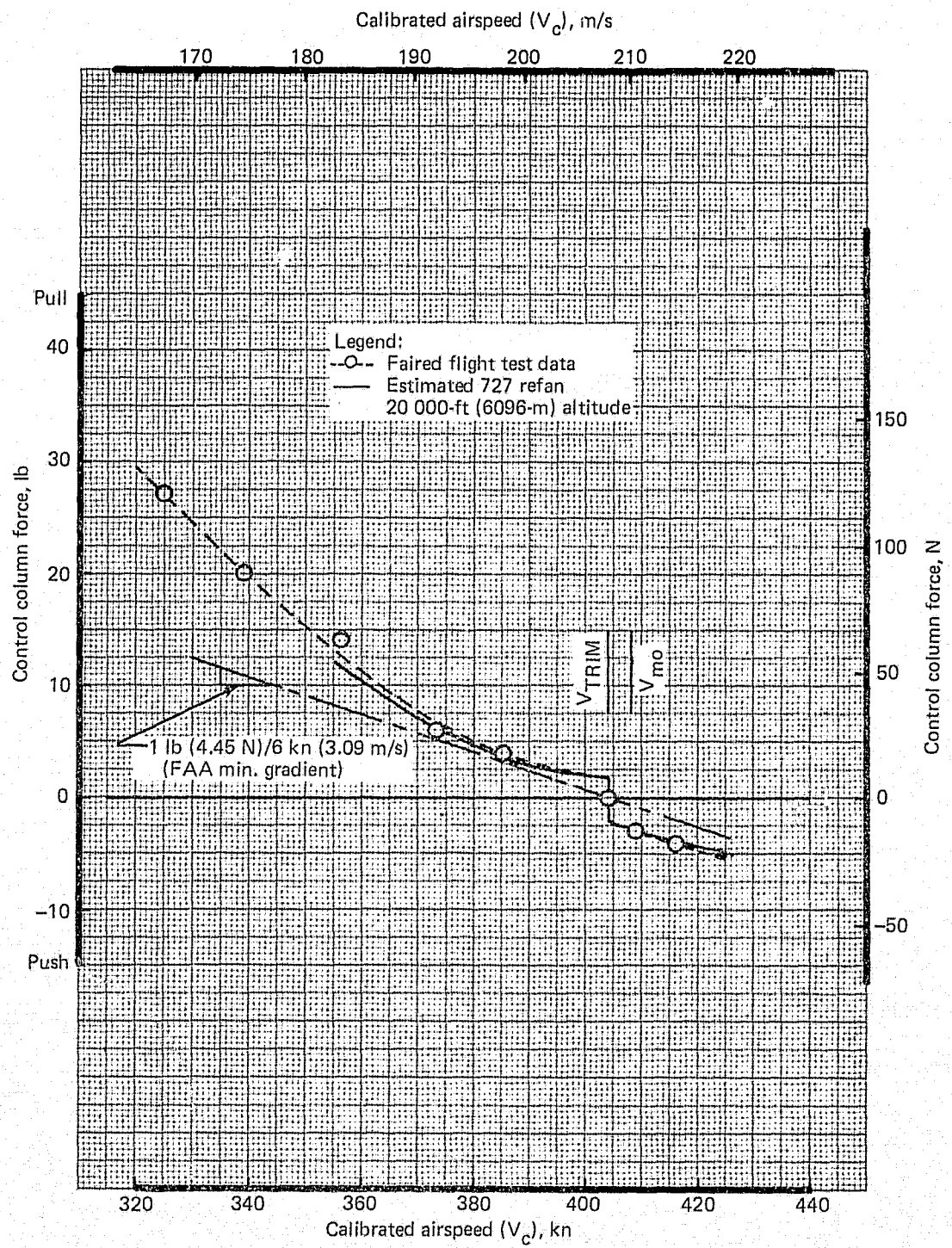

Figure 147.—727-200/727 Refan—Effect of Refan Nacelles on Speed Stability

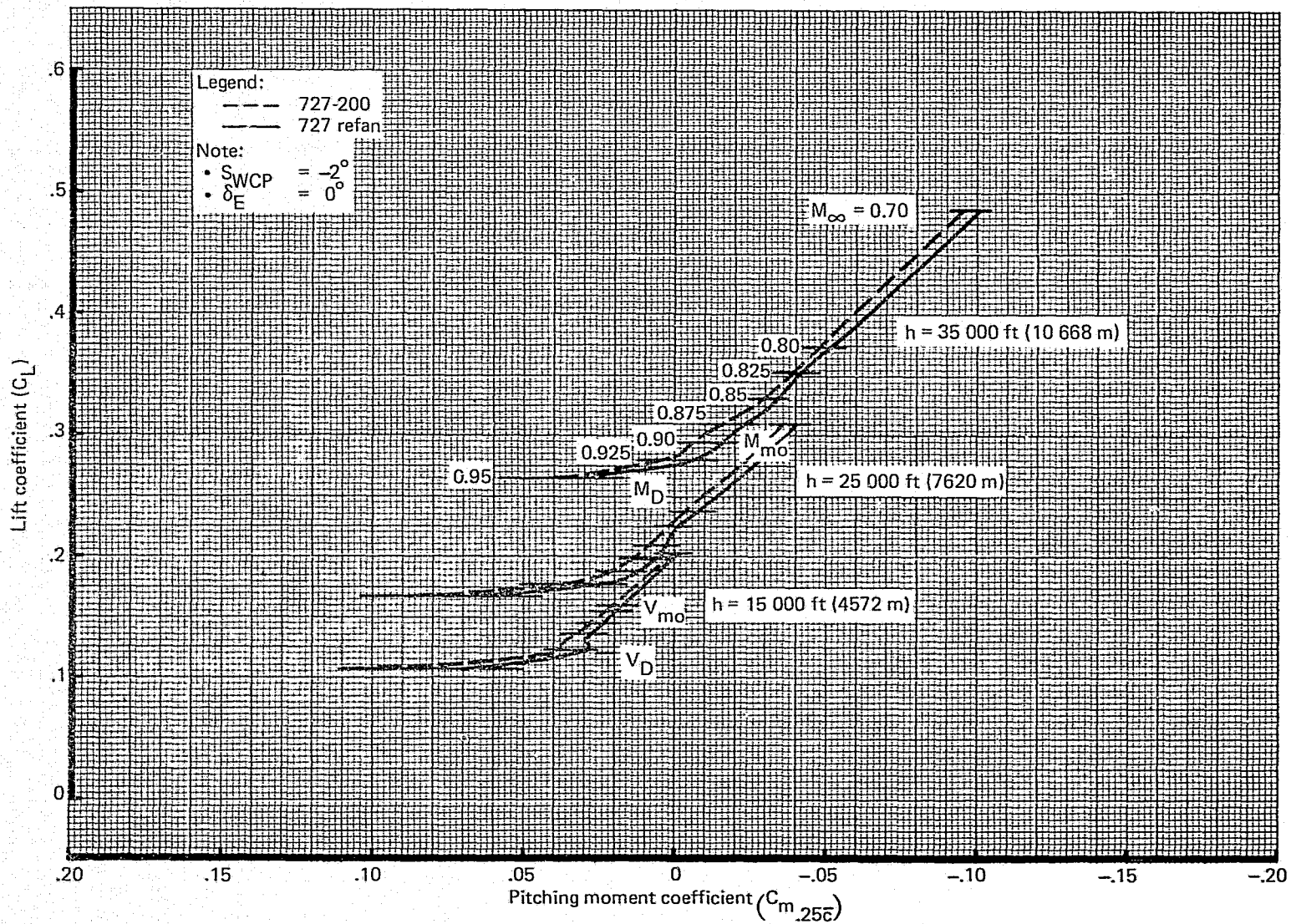

(a) Gross Weight = 130 000 lb (58 967 kg)

Figure 148.—727-200/727 Refan—Effect of Refan Configuration on Tuck Characteristics

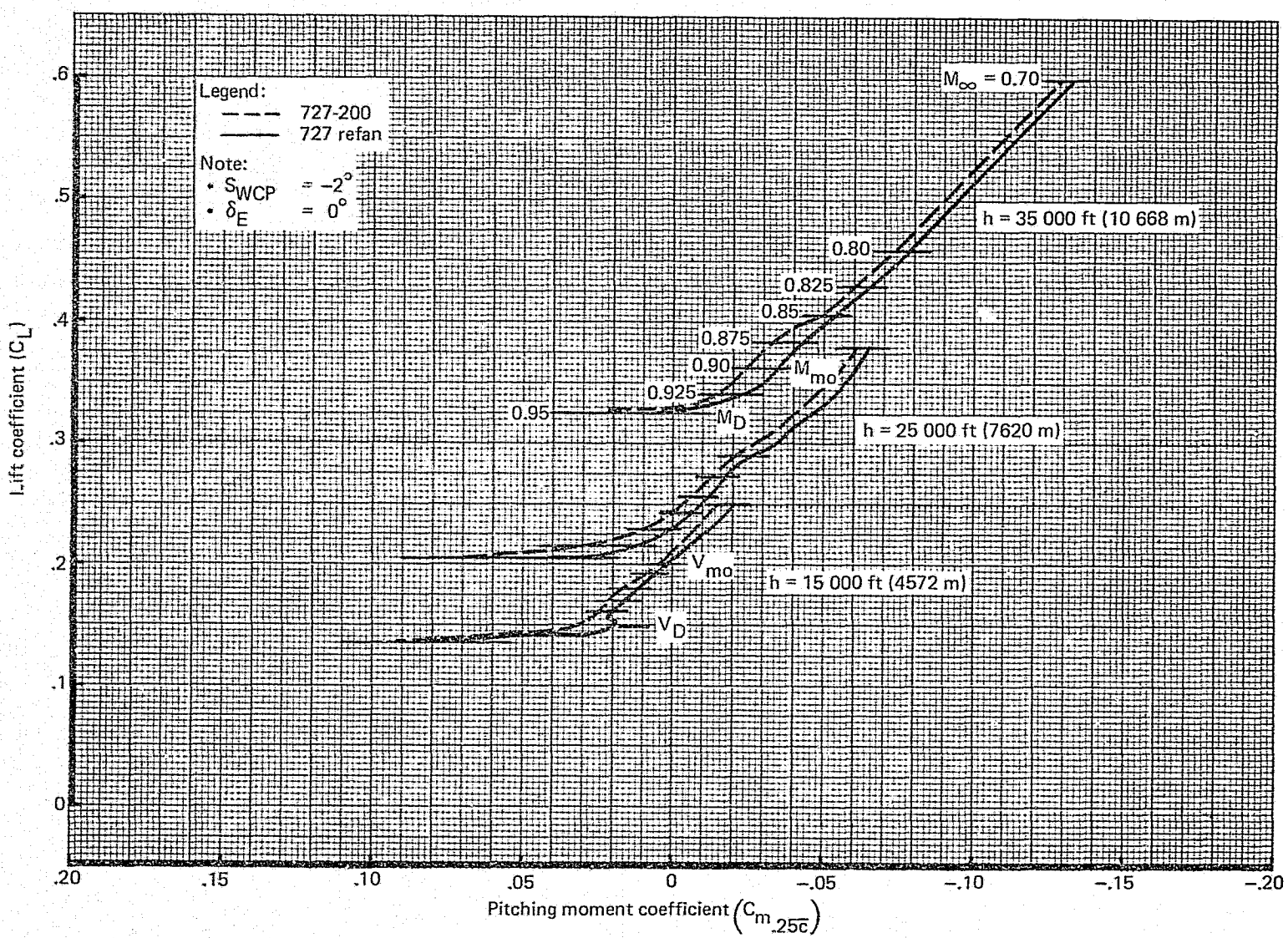

(b) Gross Weight = 160 000 lb (72 575 kg)

Figure 148.—(Concluded)

nosedown stabilizer mistrim from level flight trim at V_{mo}/M_{mo}. Retrimming of the stabilizer is allowed if required, when a minimum of 125 lb (56.7 kg) is applied to the column. Estimates of the mistrim dive recovery capability of the 727 refan indicate a slight degradation of the elevator-alone load factor capability over that of the 727-200. As indicated in figure 146, the 727 refan would require a slightly more airplane-noseup trim setting at high speed. This positions the stabilizer farther away from the existing electrical nosedown trim limit. Consequently a 3-sec stabilizer runaway (FAA condition) in the nosedown direction at V_{mo}/M_{mo} results in a larger mistrim and requires more elevator power for recovery.

Figure 149 shows the estimated elevator-alone load factor capability compared to flight test data for the 727-200 airplane. The 727 refan would exceed minimum FAA requirements below 27 000 ft (8230 m). Above this altitude, retrimming of the stabilizer would be required. (Adequate trim motor torque was available to retrim the stabilizer above 18 500-ft (5639-m) altitude.)

3.6.2 LONGITUDINAL STABILITY AND CONTROL—LOW-SPEED CHARACTERISTICS

3.6.2.1 Pitching Moment

Figure 150 shows the effect of the 727 refan nacelles on low-speed, 40° flaps pitching moment. The data show that the 727 refan produced a noseup pitching moment increment and an increase in stability of approximately 5% MAC.

3.6.2.2 Trim

The noseup stabilizer trim limit is determined by the forward c.g., landing flap, 1.3 V_s approach flight condition. The data, shown in figure 150, indicate a more noseup moment with the refan nacelles. This results in reduced (approximately ½° of stabilizer on approach) noseup trim requirements.

3.6.3 STALL CHARACTERISTICS

The 727-200 stall characteristics were not significantly altered by installation of the JT8D refan nacelles. The high angle-of-attack pitching moment characteristics of the 727 refan with maximum nosedown elevator and 40° flaps are compared in figure 151 to the 727-200. At initial wing stall ($\alpha_{WCP} = 15°$), the 727 refan exhibits a small, additional nosedown moment. At high angles of attack ($\alpha_{WCP} = 40°$), the refan nacelles cause a slight noseup pitching moment increment.

3.6.4 DIRECTIONAL STABILITY

3.6.4.1 High Speed

Installation of the JT8D refan nacelles increased high-speed directional stability ($C_{n\beta}$) up to 10%. The increase was attributed to the larger side area of the 727 refan center-engine inlet. Figure 152 presents wind tunnel data showing the effect of the refan nacelles. Vertical tail on and off data are shown plotted versus M_∞.

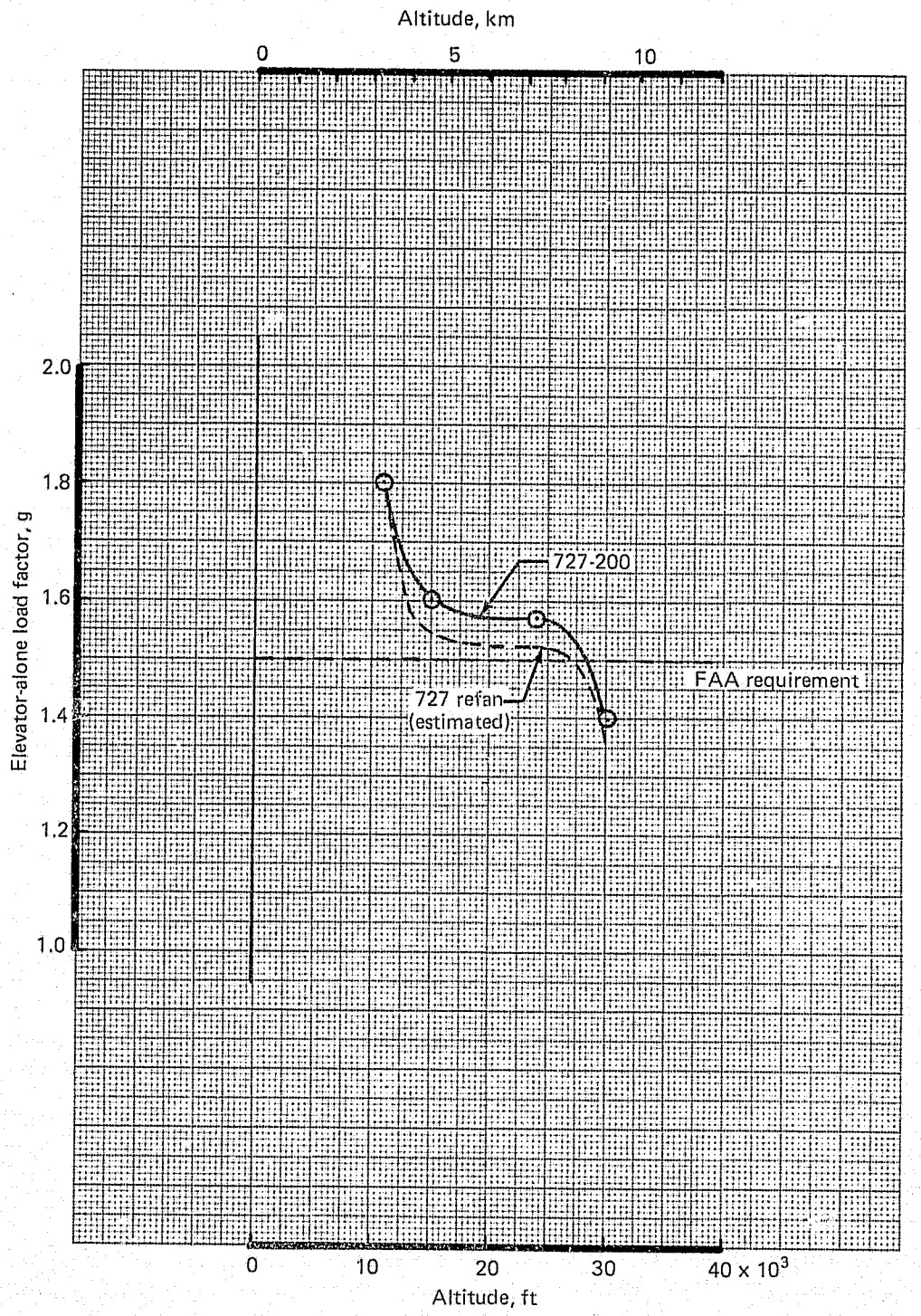

Figure 149.—727-200/727 Refan—Effect of Refan Nacelle on Elevator-Alone Load Factor Capability

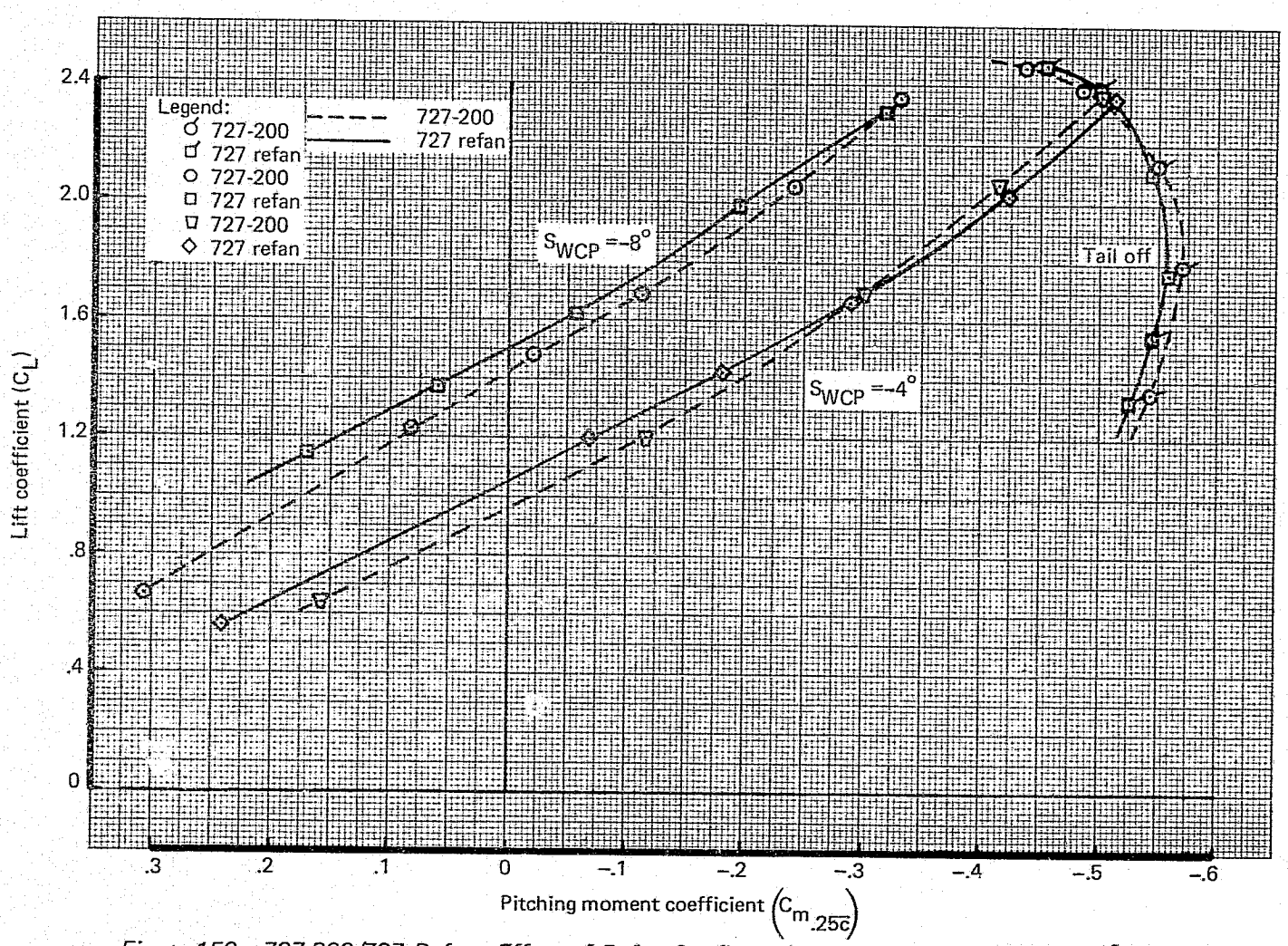

Figure 150.—727-200/727 Refan—Effect of Refan Configuration on Pitching Moment at 40° Flaps

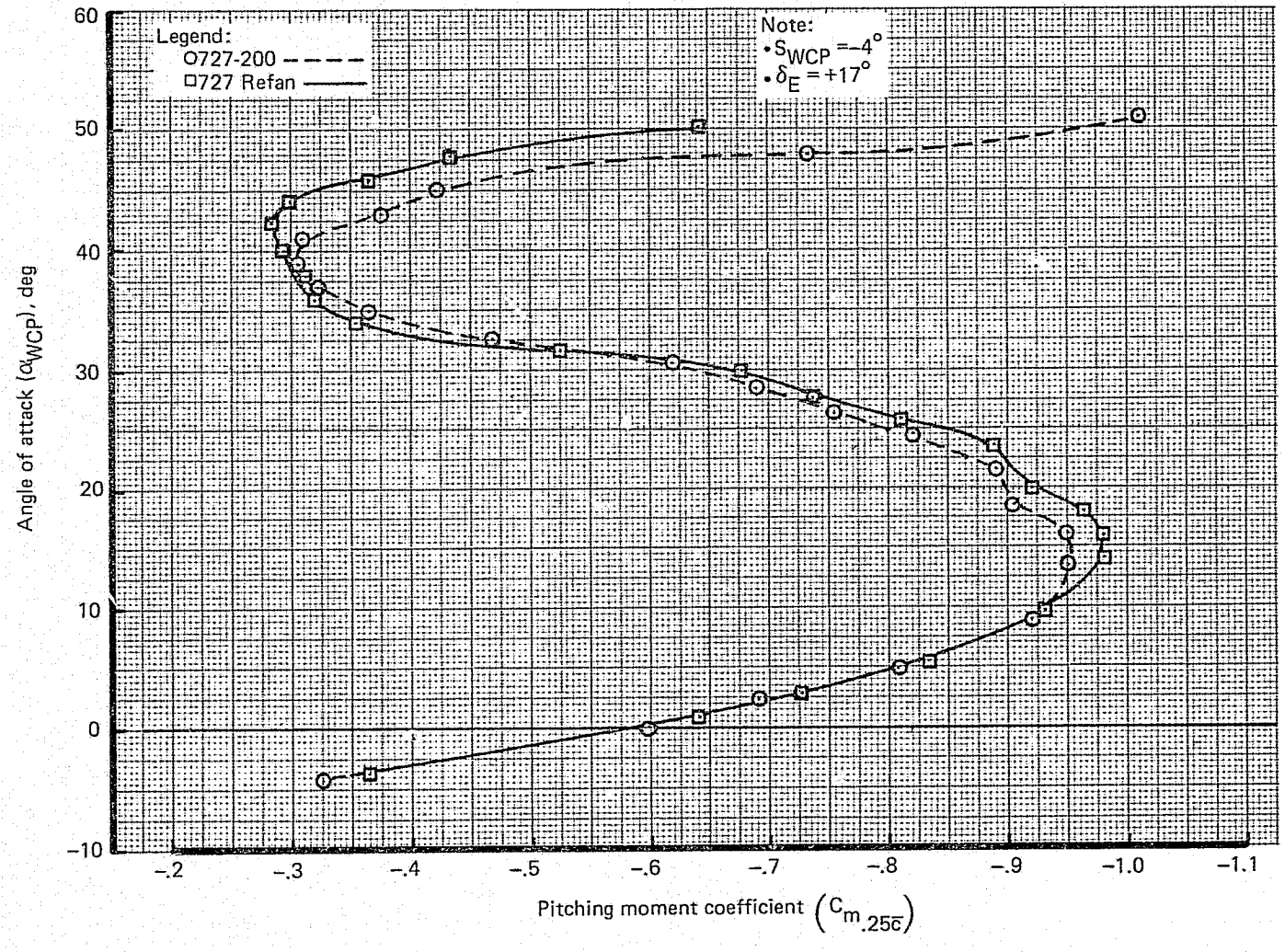

Figure 151.—727-200/727 Refan—Effect of Refan Configuration on Stall Characteristics at 40° Flaps With Gear Down

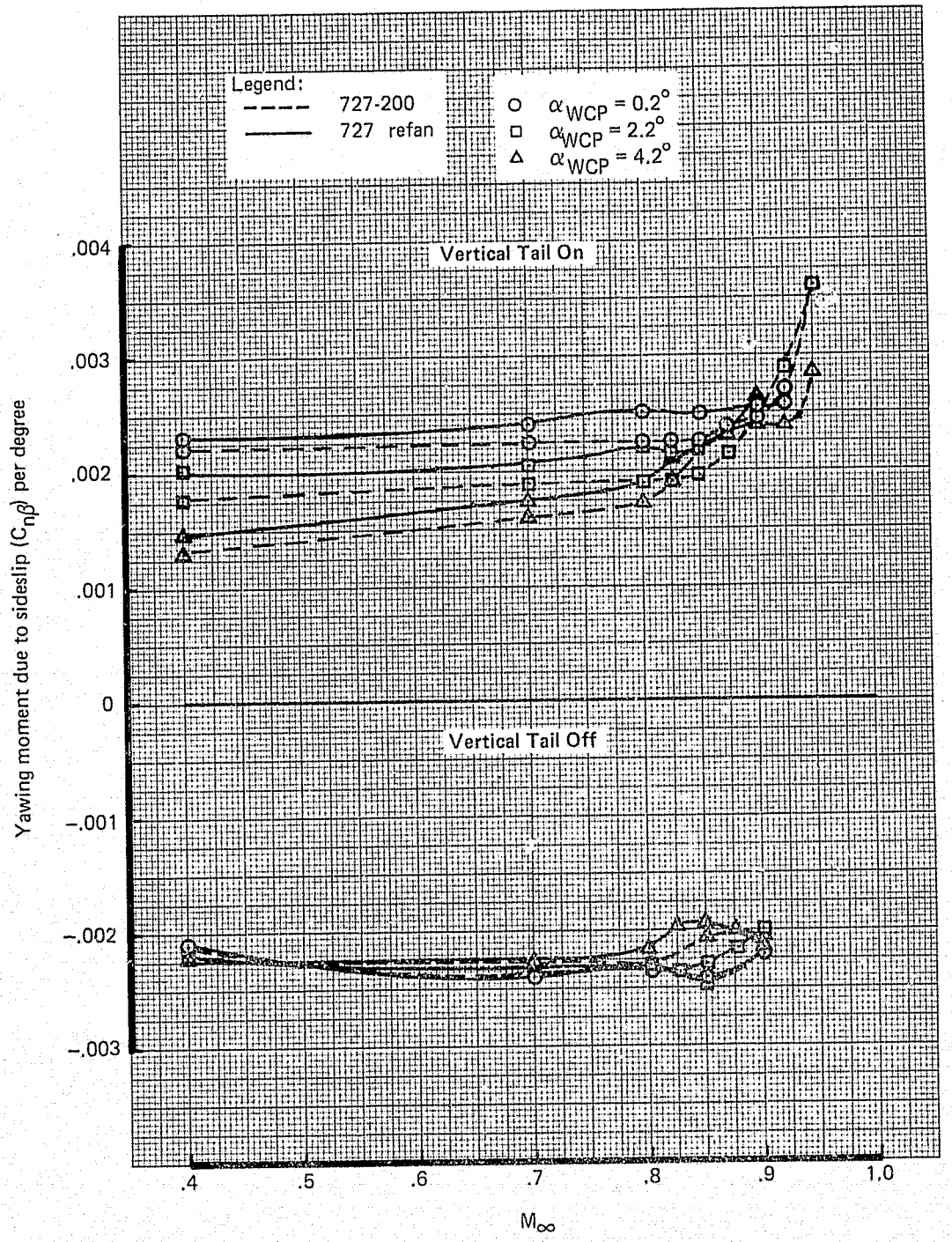

Figure 152.—727-200/727 Refan—Effect of Refan Configuration on Directional Stability With Flaps Up

3.6.4.2 Low Speed

Wind tunnel test data indicate no significant effect on JT8D refan nacelles on low speed, 40° flaps directional stability. Data are presented in figure 153 showing the directional stability characteristics of both the 727 refan and the 727-200 for zero and maximum rudder deflections.

3.6.5 DUTCH ROLL

Analysis of wind tunnel test data indicates the existing Dutch roll altitude placard was improved with the installation of the JT8D refan nacelles. This improvement was attributed to the increased directional stability of the refan configuration. The estimated Dutch roll altitude placard with yaw damper inoperative is shown in figure 154. The 727-200 FAA-certified Dutch roll altitude placard is also shown for comparison.

3.6.6 THRUST-REVERSER EFFECTS ON RUDDER EFFECTIVENESS

The 727 refan airplane equipped with target-type thrust reversers exhibits significantly better rudder effectiveness than the 727-200 with clamshell/deflector door reversers. Figure 155 presents rudder effectiveness ($C_{n\delta_R}$) versus velocity for different power (EPR) settings at sideslip angles of 0° and 15°. The plots compare the target-type reverser to the clamshell/deflector door reverser.

The effect of thrust-reverser clock angle on directional control was investigated. The clock angle is the angular rotation from vertical of the thrust-reverser doors on the side engines. Inboard clocking is defined as rotation of the top reverser door inboard. Outboard clocking is defined as the opposite rotation. The data showing the effect of clock angle are presented in figure 156. Inboard clocking reduces rudder effectiveness to essentially zero at speeds above 90 kn (46 m/s). At lower speeds the effect was small. Outboard clocking exhibits no significant effect on rudder effectiveness.

Propulsion reingestion tests, on the other hand, indicated unacceptably high reingestion speeds for +20° and 0° clocking. Only with -20° (i.e., inboard) clocking were reingestion speeds reduced to the point where an acceptable landing roll distance was obtained. (See section 3.3.5.) A compromise clocking angle between 0° and -20° will require further model testing as well as full-scale testing to demonstrate that both landing roll and flight control requirements are met.

3.7 ELECTRICAL AND MECHANICAL SYSTEMS

3.7.1 THRUST REVERSER

3.7.1.1 Design Criteria

The JT8D refan engine is designed with a hydraulically powered target-type thrust reverser similar to that used on the 737 airplane. The design criteria which determined actuator sizing and actuator control design are as follows:

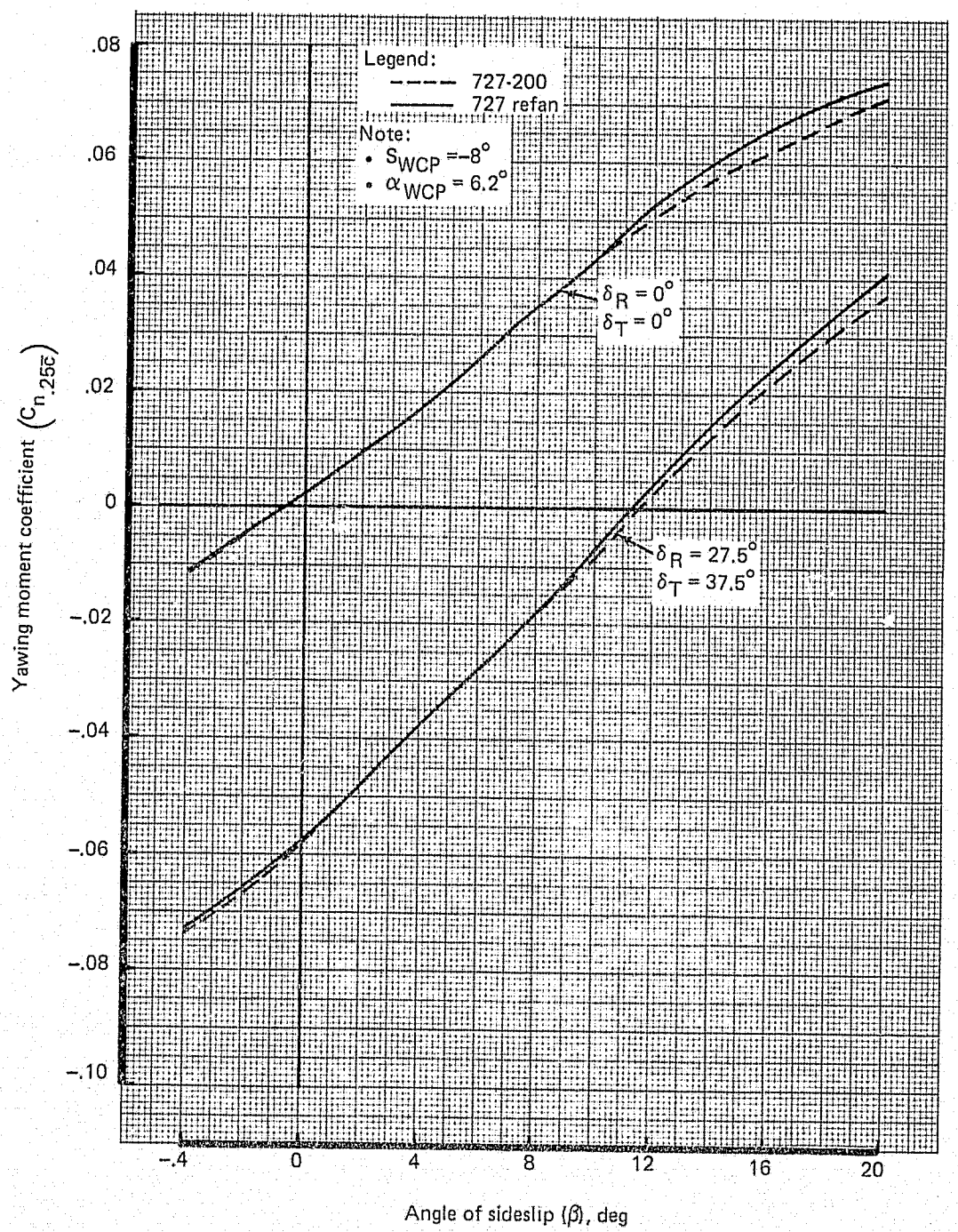

Figure 153.—727-200/727 Refan—Effect of Refan Configuration on Yawing Moment at 40° Flaps

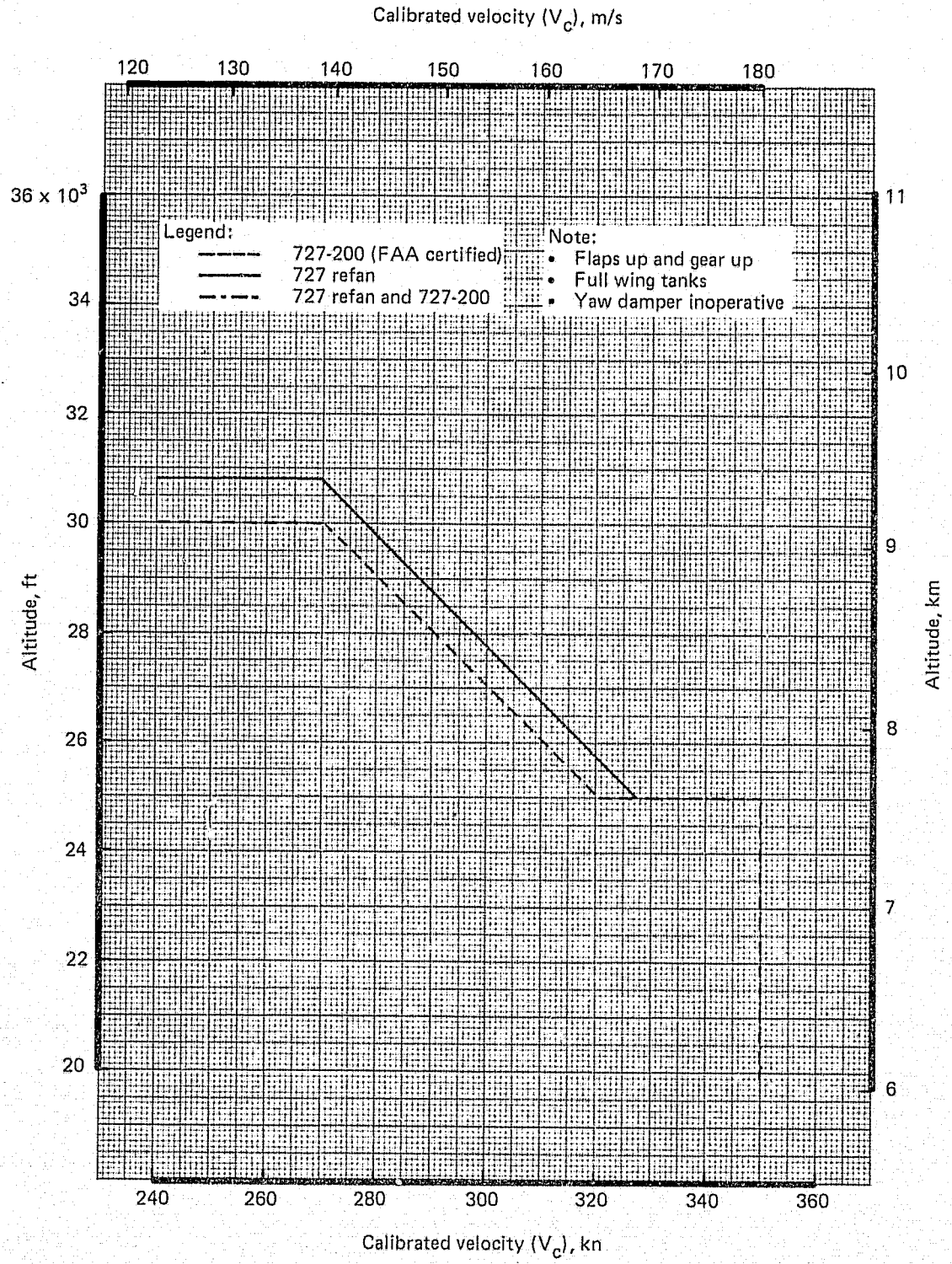

Figure 154.—727-200/727 Refan—Effect of Refan Configuration on Dutch Roll Altitude Placard

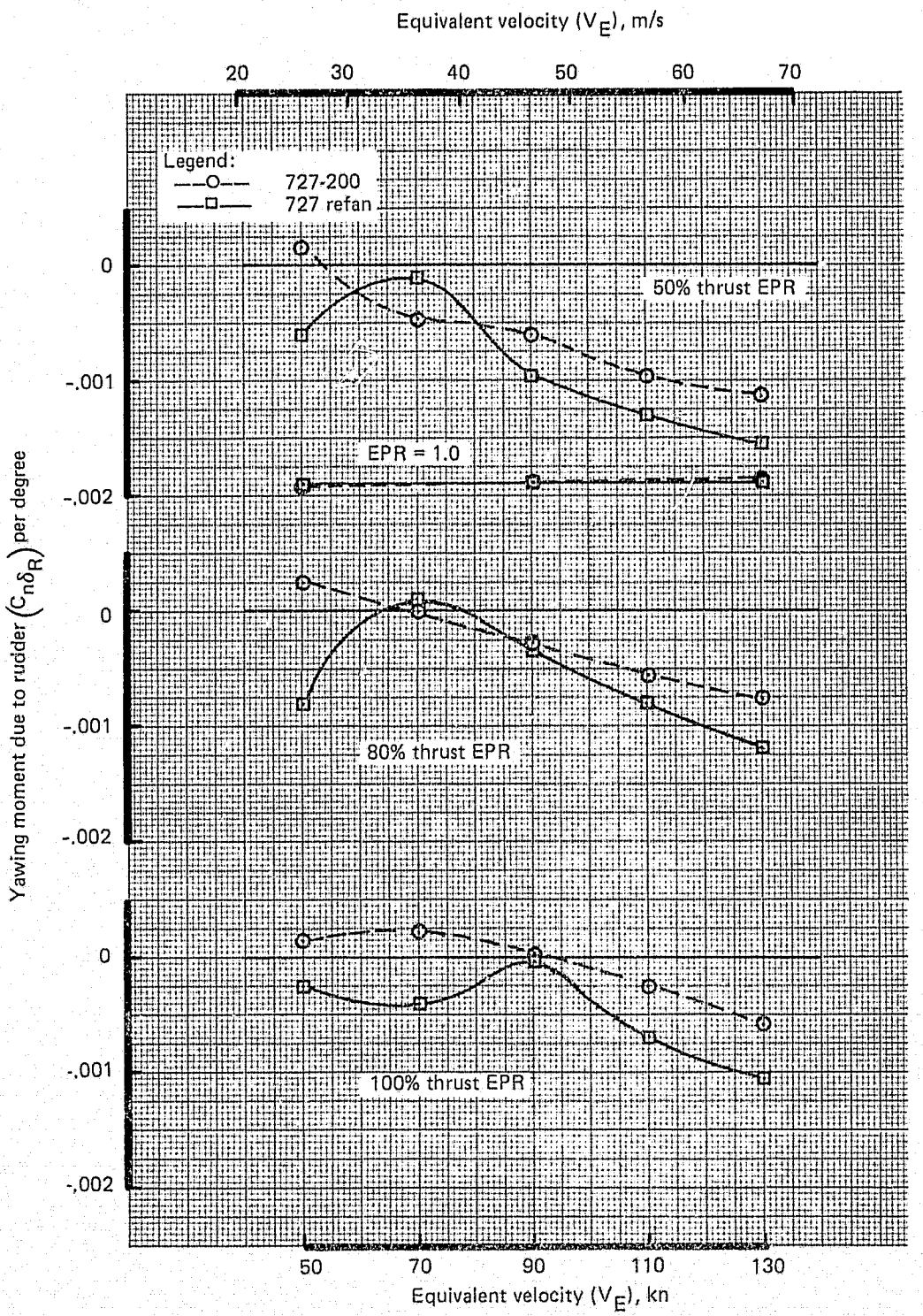

(a) Sideslip Angle (β) = 0°

Figure 155.—727-200/727 Refan—Effect of Refan Configuration on Rudder Effectiveness With Reverse Thrust

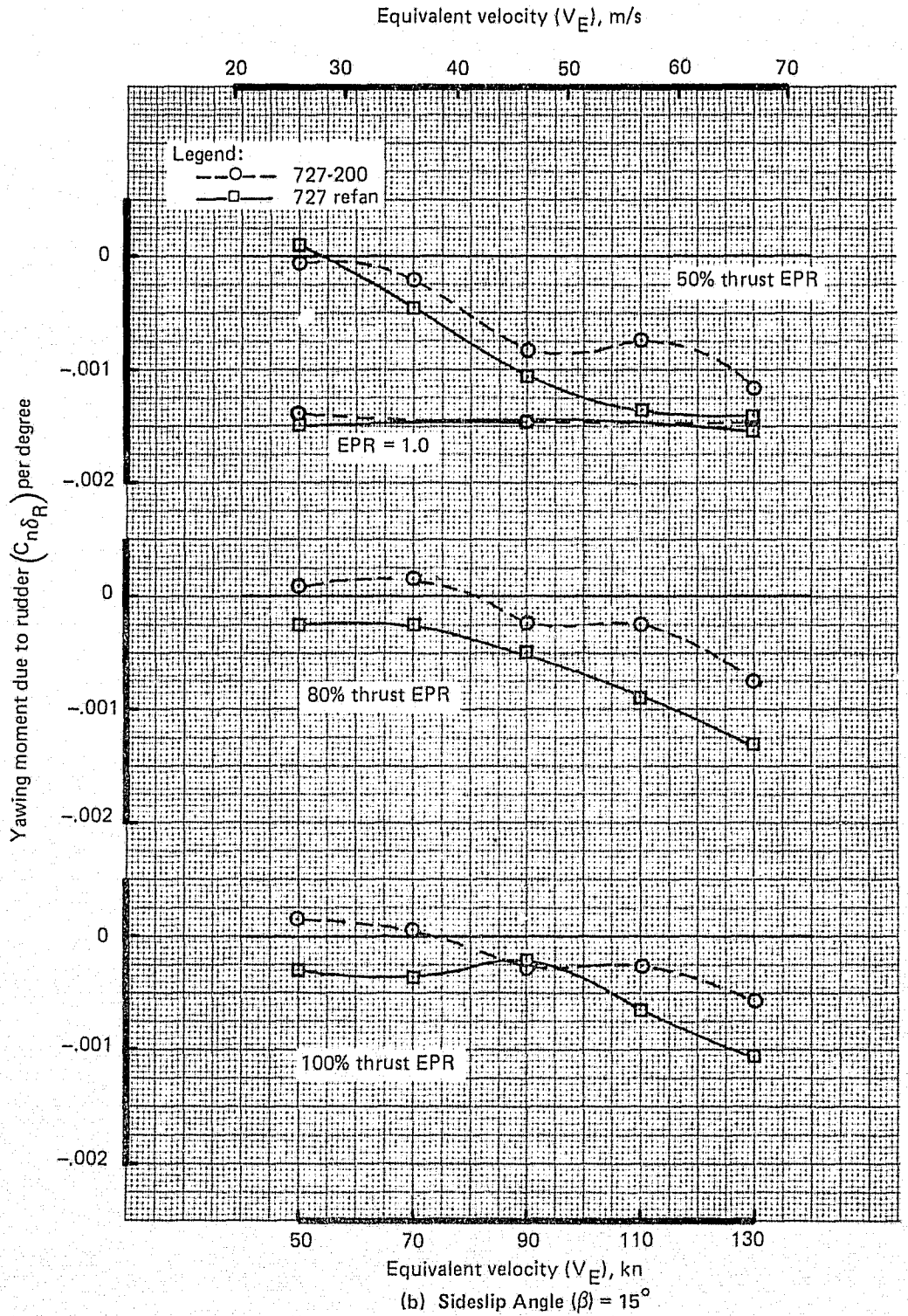

(b) Sideslip Angle (β) = 15°

Figure 155.—(Concluded)

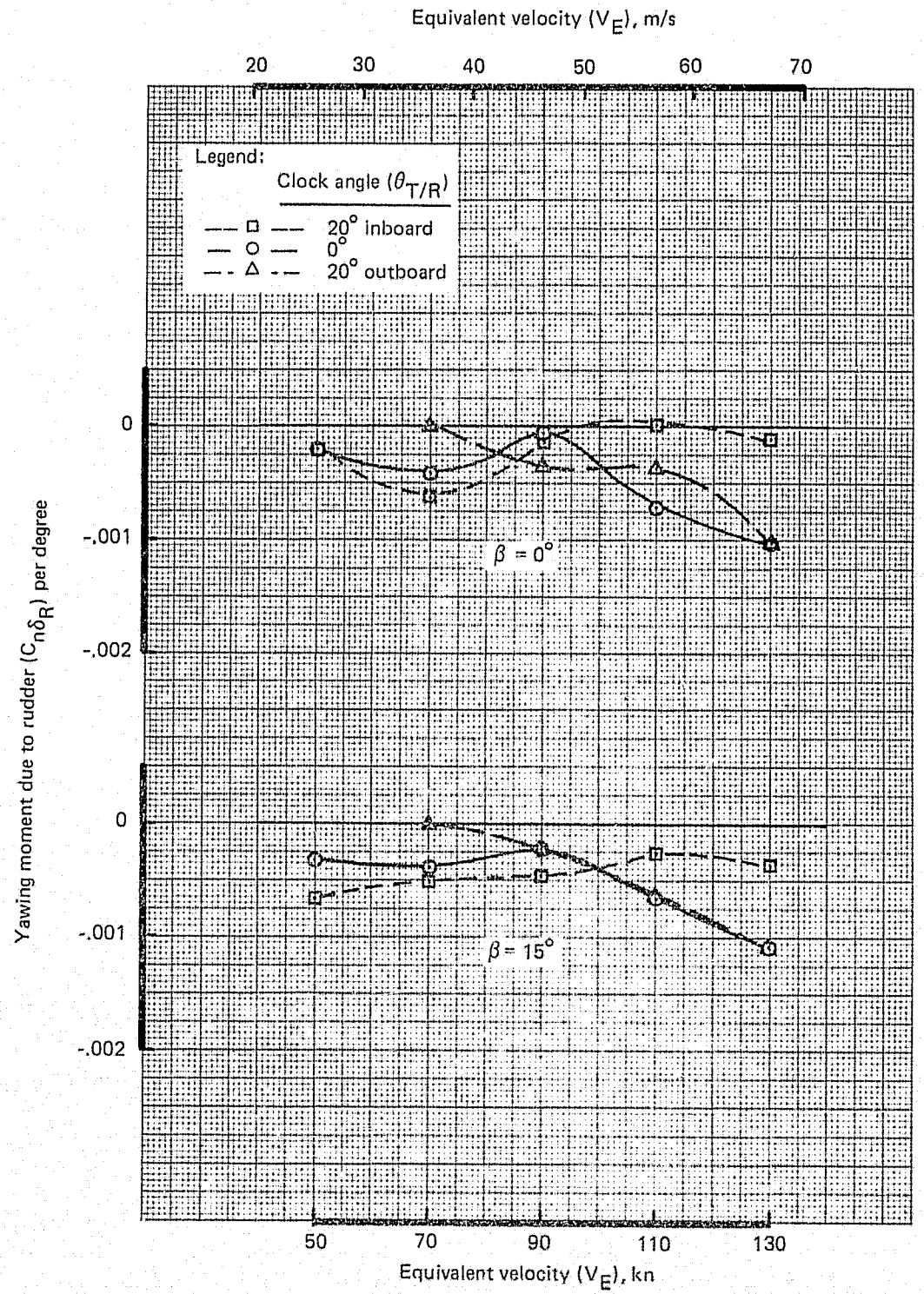

Figure 156.—Effect of 727 Refan Thrust-Reverser Clock Angle at 100% Thrust EPR

1. The reverser shall normally be in the stowed position during all airplane flight regimes. Reverse thrust mode shall be available only on the ground.

2. Deployment to reverse position from stowed position shall not take more than 1.5 sec from "reverser unlocked" to "reverser deployed" light illumination at engine ground idle, at sea level standard day and 120 KEAS (61.7 m/s).

3. The reverser shall withstand, without damage, RTO deployment at speeds up to 165 KEAS (84.9 m/s) at sea level. Thrust decay with elapsed time from 100% maximum forward thrust shall be assumed to follow the curve shown in figure 157.

4. The reverser shall not sustain damage that will prevent restoration of forward thrust in the case of an inadvertent deployment at 270 KEAS (138.9 m/s).

5. The reverser shall be capable of re-stowage at flight idle power setting and 180 KEAS (92.6 m/s) without sustaining structural failure or deformation.

6. The reverser shall be capable of sustaining inadvertent deployment to reverse thrust position without door separation from the airplane at speeds up to 380 KEAS (195.5 m/s) – V_{mo}.

7. The reverser actuation system shall be automatically depressurized in flight through use of an independent air/ground switch for each engine.

8. The door linkage system shall incorporate a mechanical redundant lock to preclude door movement from the stowed position by any force except that generated by actuator power.

9. Ground lockout means shall be provided at each engine that positively deactivates the power supply to the corresponding thrust-reverser actuation system. The lockout indication shall be easily visible from the ground.

3.7.1.2 Actuation and Control System Description

The JT8D refan thrust reverser would be actuated by two linear hydraulic actuators (on opposite sides of the engine) that each drive a four-bar linkage through an overcenter link. Each door would be held in the stowed position by the two overcenter links and a hydraulically sequenced redundant latch that holds down the forward edge of each door (fig. 158).

The primary power source for reverser actuation is the airplane engine-driven pump "A" hydraulic system. Hydraulic power (3000 psi (2068 N/cm^2)) is taken from the "A" system pressure manifold to a pair of hydraulic actuators through a shuttle valve, fuse manifold, isolation valve, manual control valve, and runaround module. The hydraulic/electrical control schematic typical for each engine is shown in figure 159.

Backup power to each reverser, in case of "A" hydraulic system loss, is provided by a 100-$in.^3$ (1639-cm^3) accumulator that is connected to the third port of the shuttle valve. The shuttle valve connects both "A" hydraulic power and backup power to the reverser circuits. An area

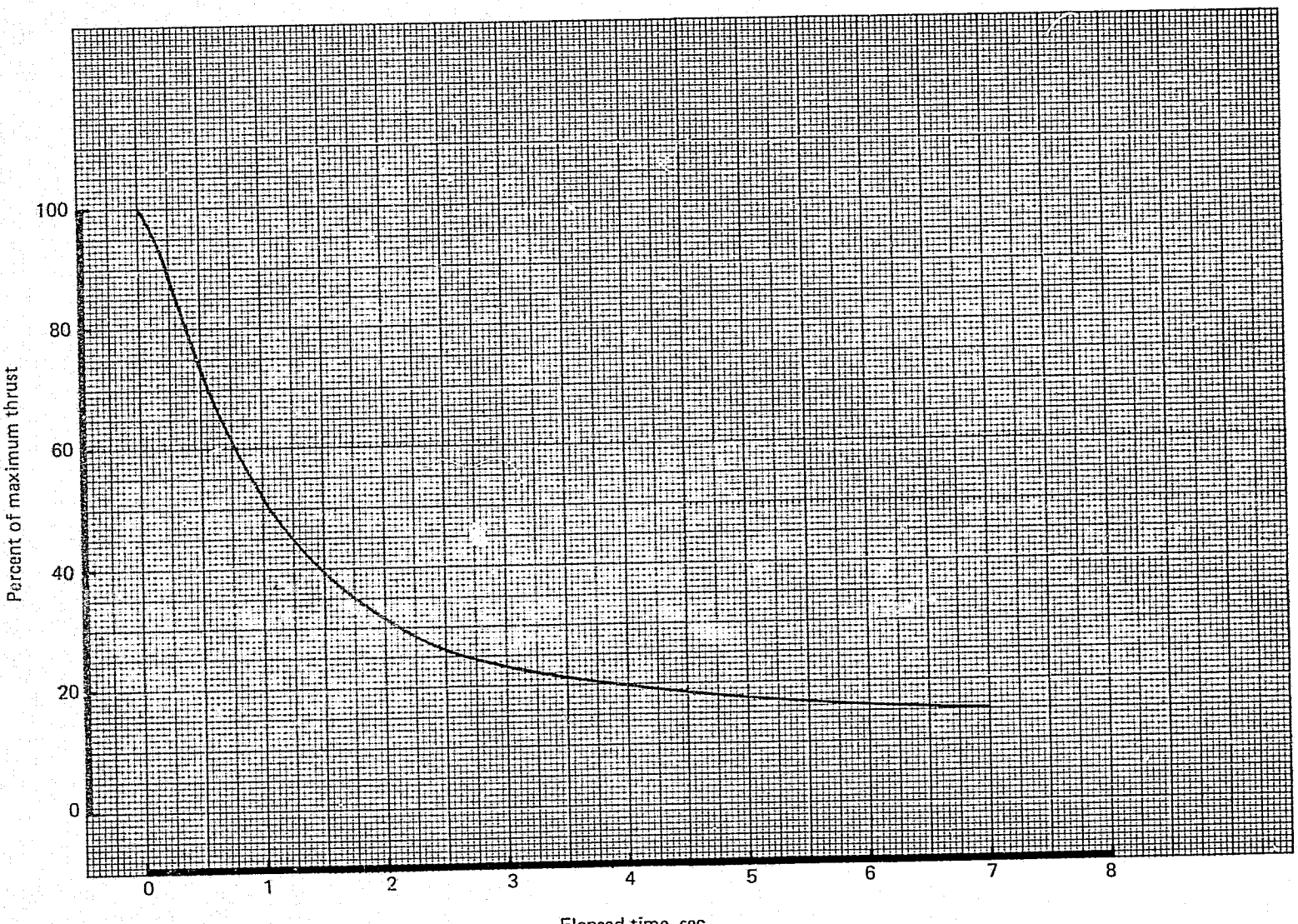

Figure 157.—JT8D-100 Series Engine Deceleration Characteristics

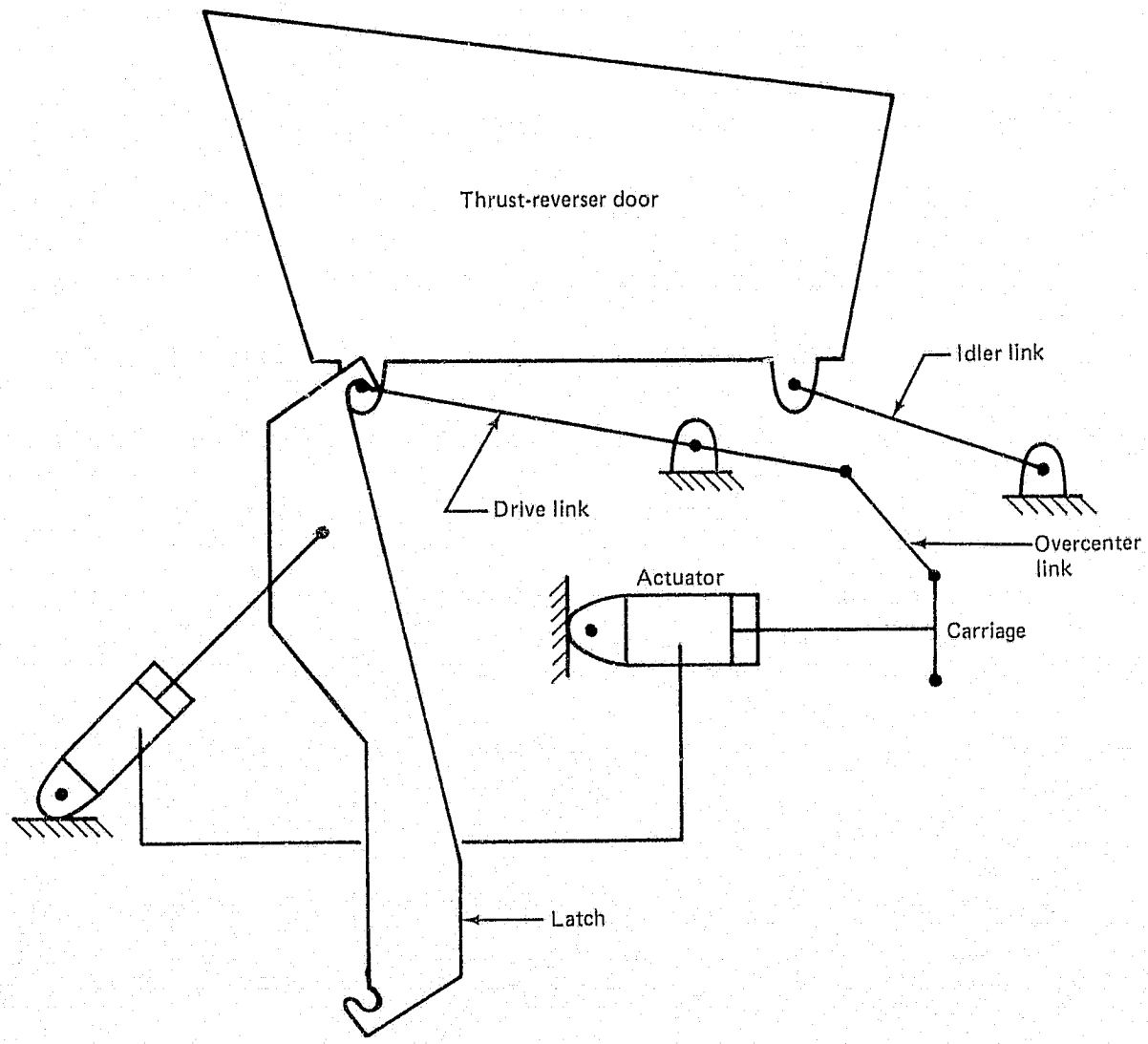

Figure 158.—JT8D Refan Thrust-Reverser Schematic Diagram

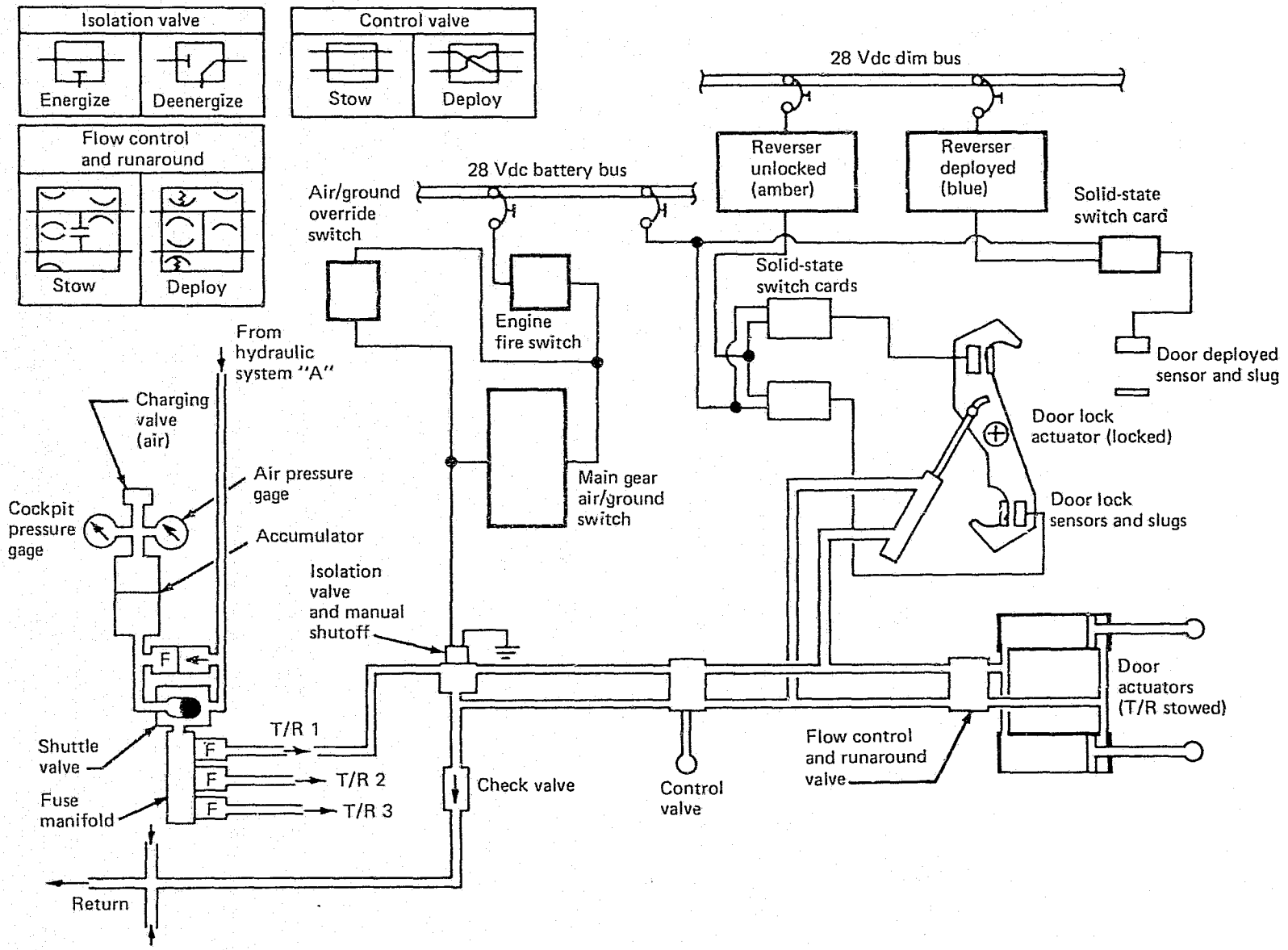

Figure 159.—JT8D Refan Thrust-Reverser Hydraulic/Electrical System Schematic Diagram

bias ports "A" system pressure to the reverser circuits under normal operation. In the case of "A" system loss, the shuttle valve then ports backup power to the reversers.

The fuse manifold, placed downstream of the shuttle valve, contains three Type I quantity measuring hydraulic fuses (one for each engine). Whenever a preset quantity of fluid passes through a given fuse, the fuse activates and blocks any further fluid from passing through. In this manner, the integrity of the airplane "A" hydraulic system and reverser backup power source is maintained in case of a hydraulic component failure downstream.

The isolation valves (one for each engine) would be mounted on the airplane-side of the engine firewall. These valves, electric solenoid-controlled, perform three functions:

1. Fire shutoff valve

2. In-flight reverser actuation power deactivation

3. Manual shutoff valve

The electric power to the isolation valves would be supplied from the 28-Vdc battery bus through the associated engine fire switch, and squat (air/ground-sensing) switch. An override switch is paralleled around the squat switches to allow application of reverser power in flight. Whenever a fire switch is activated during an engine fire, the isolation valve power will be removed, thus blocking hydraulic fluid flow to the engine.

The squat switches automatically deactivate each valve when the landing gear oleo extends, thus deactivating the reversers in flight.

The manual control valve downstream of each isolation valve is a four-port, two-position valve similar to the 737 design and is operated by cables from the cockpit reverser levers.

Because the reverser door airloads are in a "deploy aiding direction", use is made of this energy by allowing the rod end of the actuators to cavitate during high rate extensions. Head-end fluid is then ported through the runaround module back to the rod end to keep it full. In this way, over a portion of the stroke, the q-loads are extending the doors with hydraulic power (available instantaneously if the door should slow down for any reason). Incorporation of the runaround module, therefore, reduces the overall flow demand of reverser actuation on the hydraulic power systems.

The hydraulic actuators are of differential area design, using the rod-end area for deployment, and the larger, head-end area for stowing force. During the deploy cycle, the doors are decelerated into the fully deployed position by a variable orifice stroke-dependent snubbing gland in the head end of each actuator. The snubbing glands in the actuator operate over the last 2 in. (5.08 cm) of actuator stroke and limit actuator loads and decelerate doors to prevent damage at full deployment.

Design criteria required that the reverser be designed for inadvertent deploy at 270 KEAS (138.9 m/s) without failure and remain intact up to 380 KEAS (195.5 m/s). In order to limit head-end pressure and actuation link loads, each runaround module contains an atmospheric pressure biased relief valve (priority valve) that will limit actuator rod load.

3.7.1.3 Analysis Technique

Operational actuator axial loads used for actuator sizing were defined by scaling 737 thrust-reverser flight test data for door area, linkage mechanics, and engine thrust differences between the production JT8D-15 engine and the JT8D refan engines. The scaling factor was derived as follows:

$$F_{ACT_{REFAN}} = (f_{sc})\ F_{ACT_{737}}$$

assuming equal pressure distribution on the doors versus drive link angle for the JT8D-15 or JT8D refan engines. The axial actuator force was derived by summing moments about the four-bar instant center (I.C.).

Actuator axial force is then equal to the drive link moment divided by an effective moment arm which varies as a function of drive link rotation due to the linkage geometry as shown in figures 160 and 161. This results in the following scale factor expression:

$$f_{sc} = \frac{(A_{DOOR} \sin \gamma_{T/R})_{REFAN}}{(A_{DOOR} \sin \gamma_{T/R})_{737}} X \frac{\left[\frac{(C_{T/R})(R_{T/R})}{R_{T/R} + L_{T/R}}\right]_{REFAN}}{\left[\frac{(C_{T/R})(R_{T/R})}{R_{T/R} + L_{T/R}}\right]_{737}} X \frac{\left(\frac{r_{T/R}\cos\beta_{T/R}}{\cos\alpha_{T/R}}\right)_{737}}{\left(\frac{r_{T/R}\cos\beta_{T/R}}{\cos\alpha_{T/R}}\right)_{REFAN}}$$

f_{sc} versus drive link rotation angle (θ_{DL}) is shown in figure 162.

During reverser deployment, the reverser doors experience engine exhaust gas loading during the last 15° of drive link rotation. Since there exists a considerable difference between baseline and JT8D refan engine thrust, when the final load curves were developed, the door area ratio term in the scaling factor equation was replaced by the ratio of gross thrust for the two engines, or, for $115° \leqslant \theta \leqslant 140°$

$$f_{sc} = \frac{(F_g)_{REFAN}}{(F_g)_{737}} X \frac{\left[\frac{(C_{T/R})(R_{T/R})}{R_{T/R} + L_{T/R}}\right]_{REFAN}}{\left[\frac{(C_{T/R})(R_{T/R})}{R_{T/R} + L_{T/R}}\right]_{737}} X \frac{\left(\frac{r_{T/R}\cos\beta_{T/R}}{\cos\alpha_{T/R}}\right)_{737}}{\left(\frac{r_{T/R}\cos\beta_{T/R}}{\cos\alpha_{T/R}}\right)_{REFAN}}$$

Using the above technique and the actuator stroke versus drive link angle relationship, shown in figure 163, the following actuator rod load versus piston stroke data were developed to meet design criteria.

- JT8D refan actuator force during 40-KEAS (20.6-m/s) normal stow (fig. 164)
- JT8D refan actuator force during 110-KEAS (56.6-m/s) normal deploy (fig. 165)
- JT8D refan actuator force during 165-KEAS (84.9-m/s) RTO (fig. 166)
- JT8D refan actuator force for 180-KEAS (92.6-m/s) in-flight restow (fig. 167)

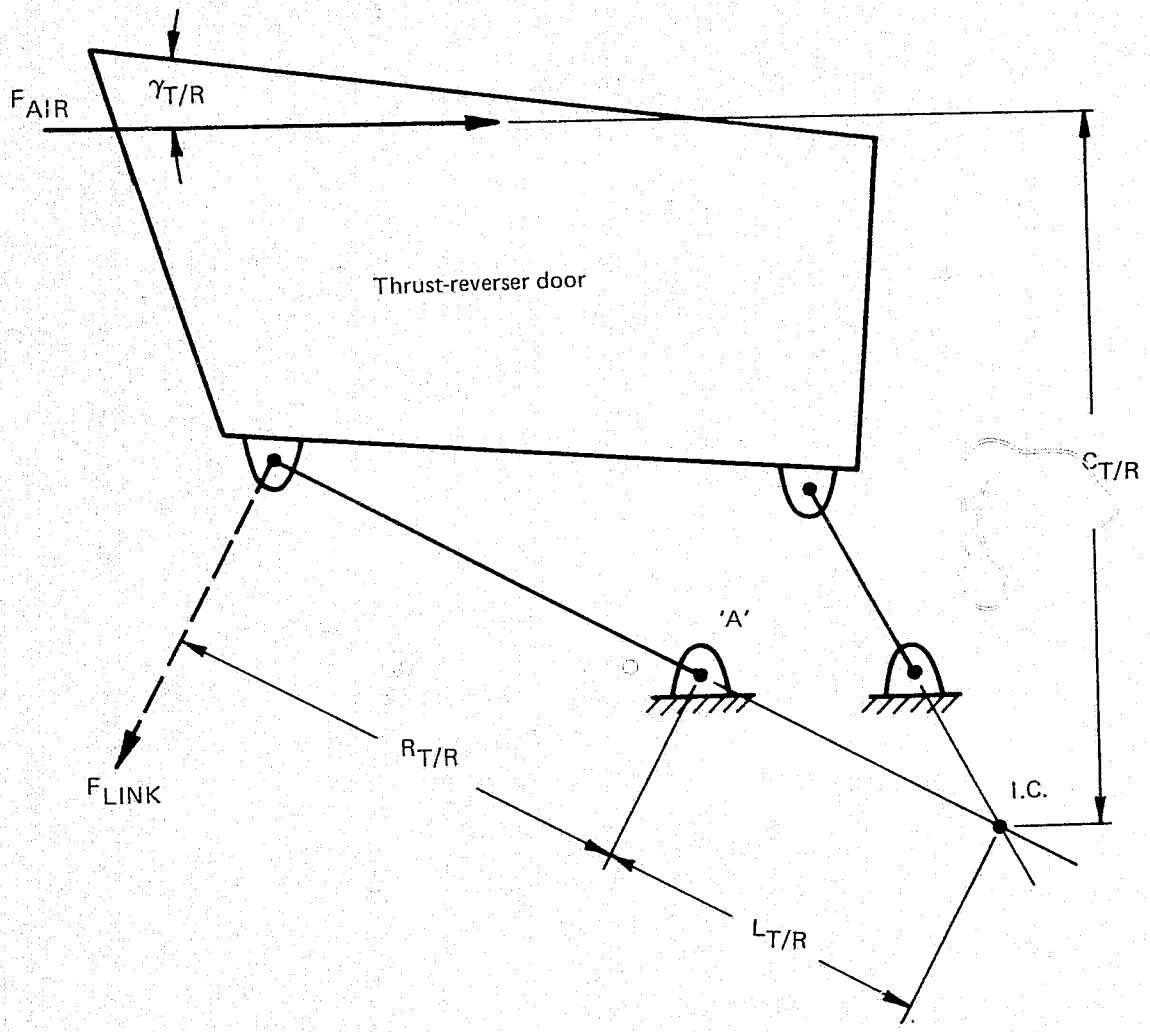

Figure 160.—JT8D Refan Thrust-Reverser Linkage Schematic Diagram

$$M_{ACT_{STOW}} = (P_H \times A_H - P_R \times A_R) \times \frac{r_{T/R} \times \cos \beta_{T/R}}{\cos \alpha_{T/R}}$$

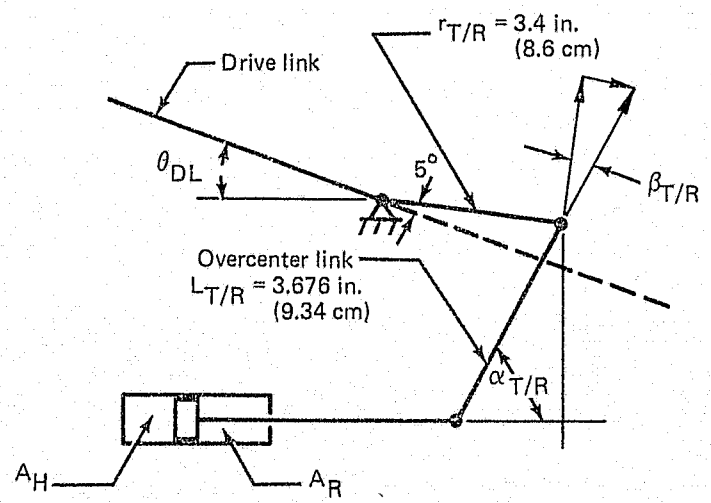

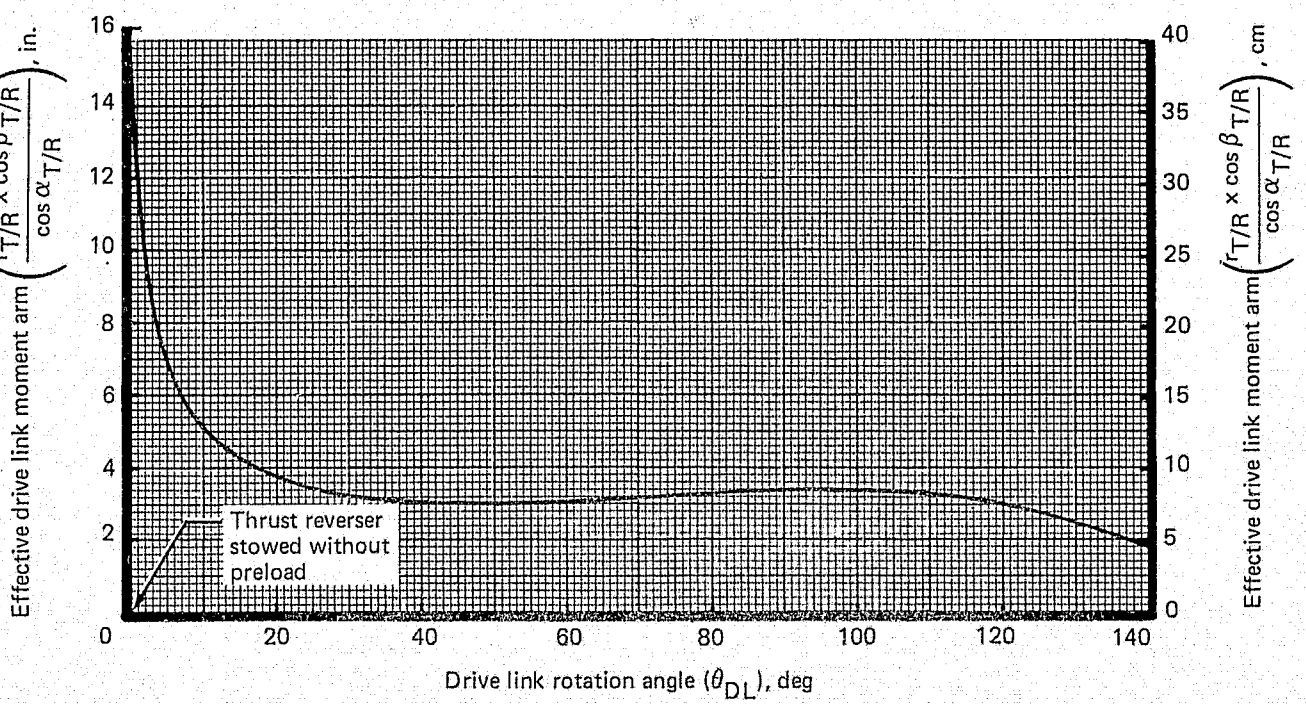

Figure 161.—JT8D Refan Thrust-Reverser Actuator Drive Link Moments

$$F_{ACT_{REFAN}} = f_{sc} \times F_{ACT_{737}}$$

$$f_{sc} = \frac{(A_{DOOR} \times \sin \gamma_{T/R})_{REFAN}}{(A_{DOOR} \times \sin \gamma_{T/R})_{737}} \times \frac{\left(\frac{C_{T/R} \times R_{T/R}}{R_{T/R} + L_{T/R}}\right)_{REFAN}}{\left(\frac{C_{T/R} \times R_{T/R}}{R_{T/R} + L_{T/R}}\right)_{737}} \times \frac{\left(\frac{r_{T/R} \times \cos \alpha_{T/R}}{\cos \alpha_{T/R}}\right)_{737}}{\left(\frac{r_{T/R} \times \cos \alpha_{T/R}}{\cos \alpha_{T/R}}\right)_{REFAN}}$$

$$A_{DOOR_{REFAN}} = 1.8 \times A_{DOOR_{737}}$$

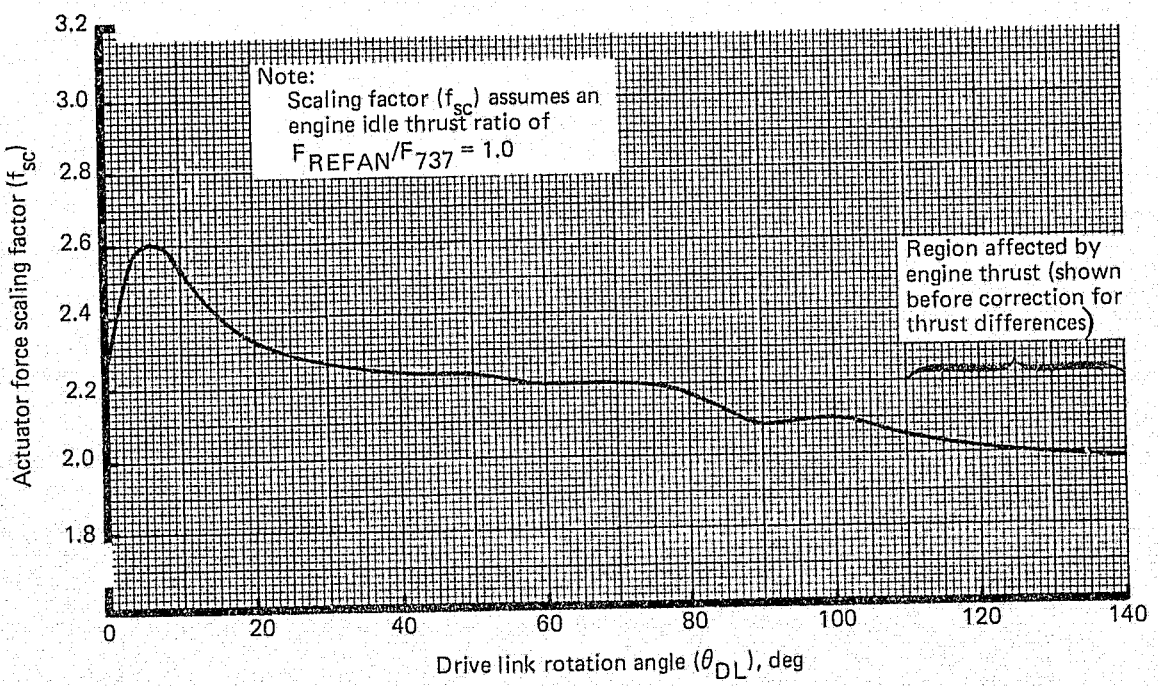

Figure 162.—JT8D Refan Thrust-Reverser Scaling Factor

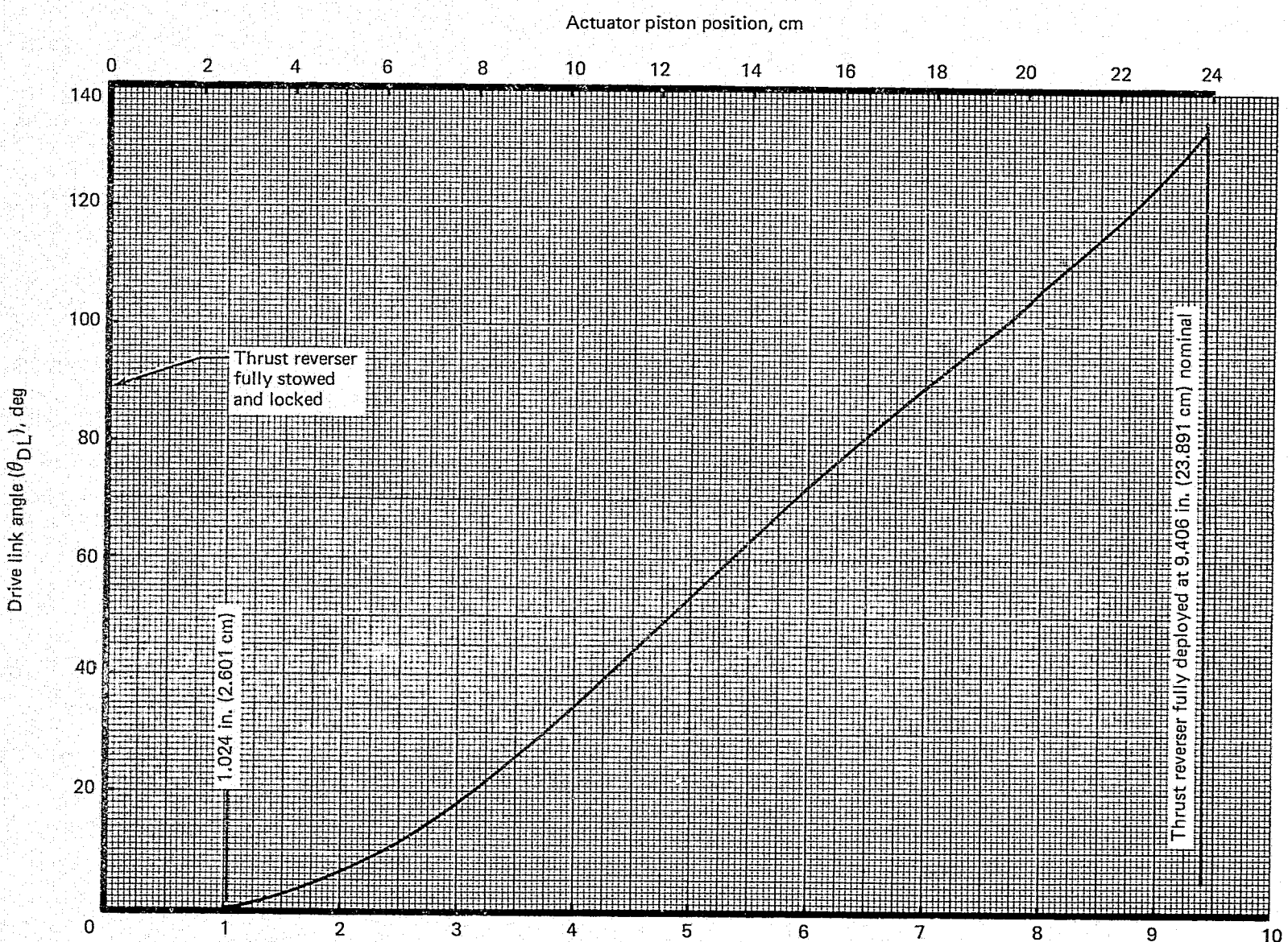

Figure 163.—JT8D Refan Thrust-Reverser Drive Link Angle Versus Piston Position

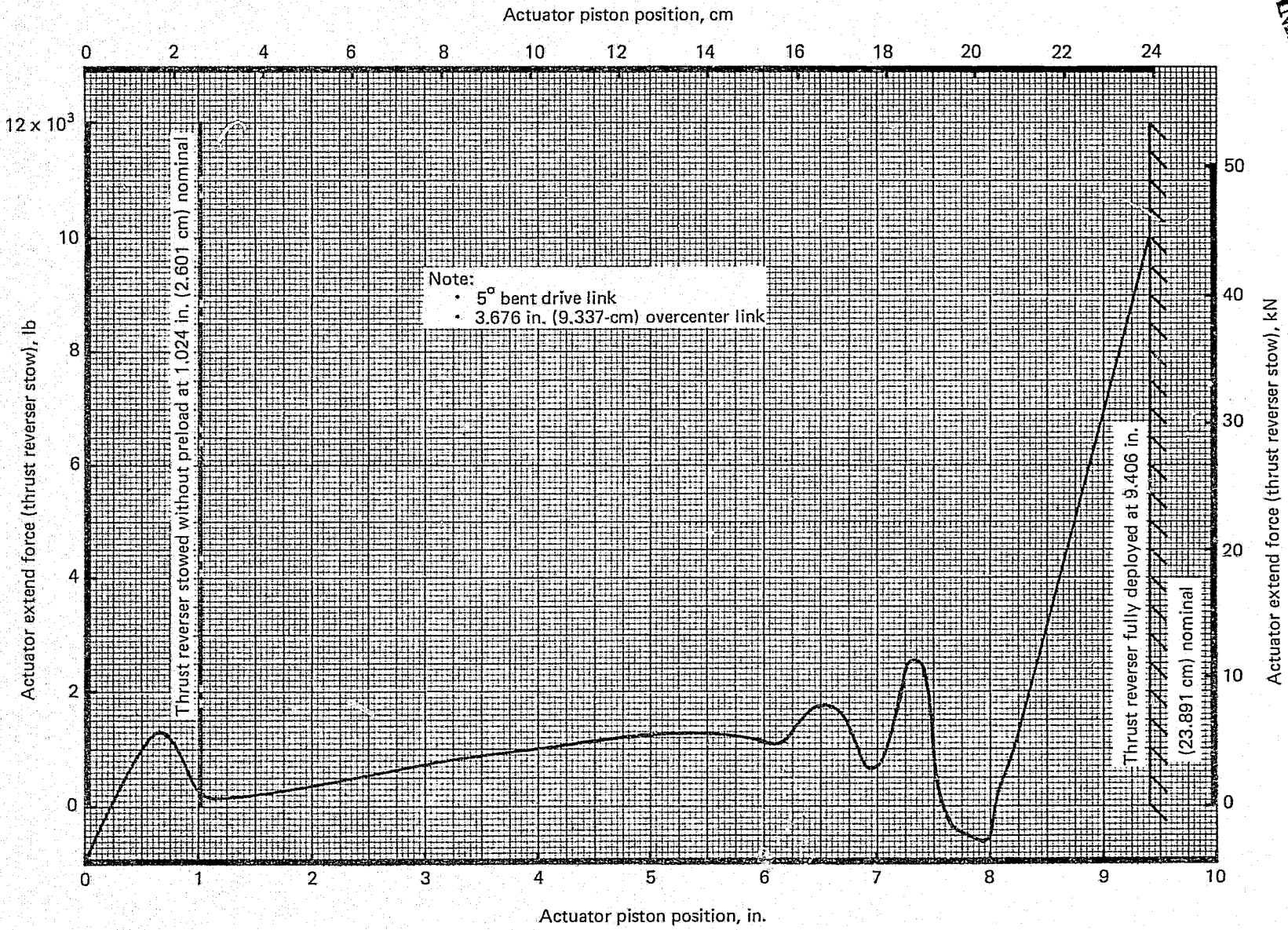

Figure 164.—JT8D Refan Thrust-Reverser Stow Actuator Force—Sea Level at 40 KEAS (20.6 m/s)

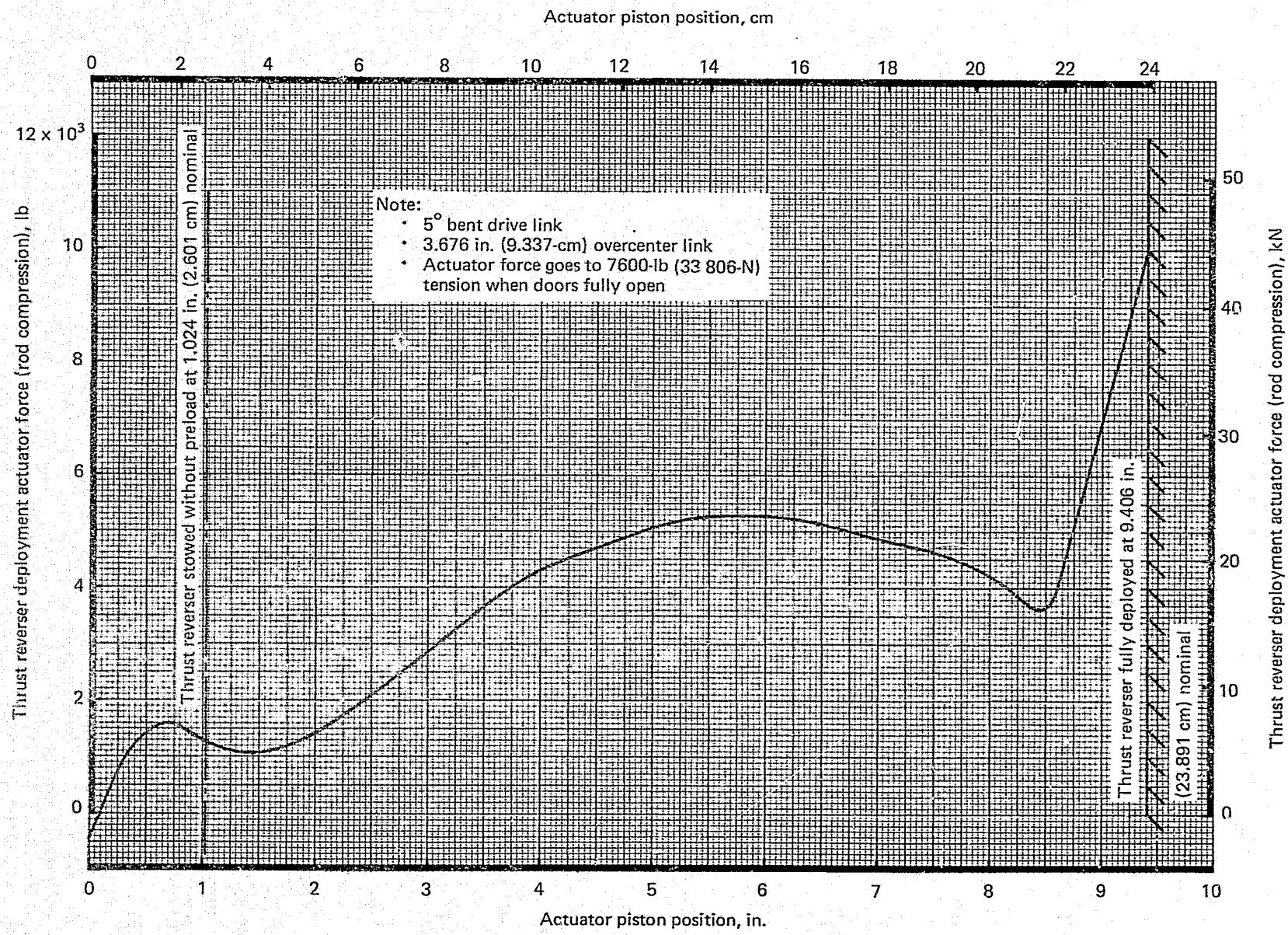

Figure 165.—JT8D Refan Thrust-Reverser Deployment Actuator Force—Sea Level at 110 KEAS (56.6 m/s)

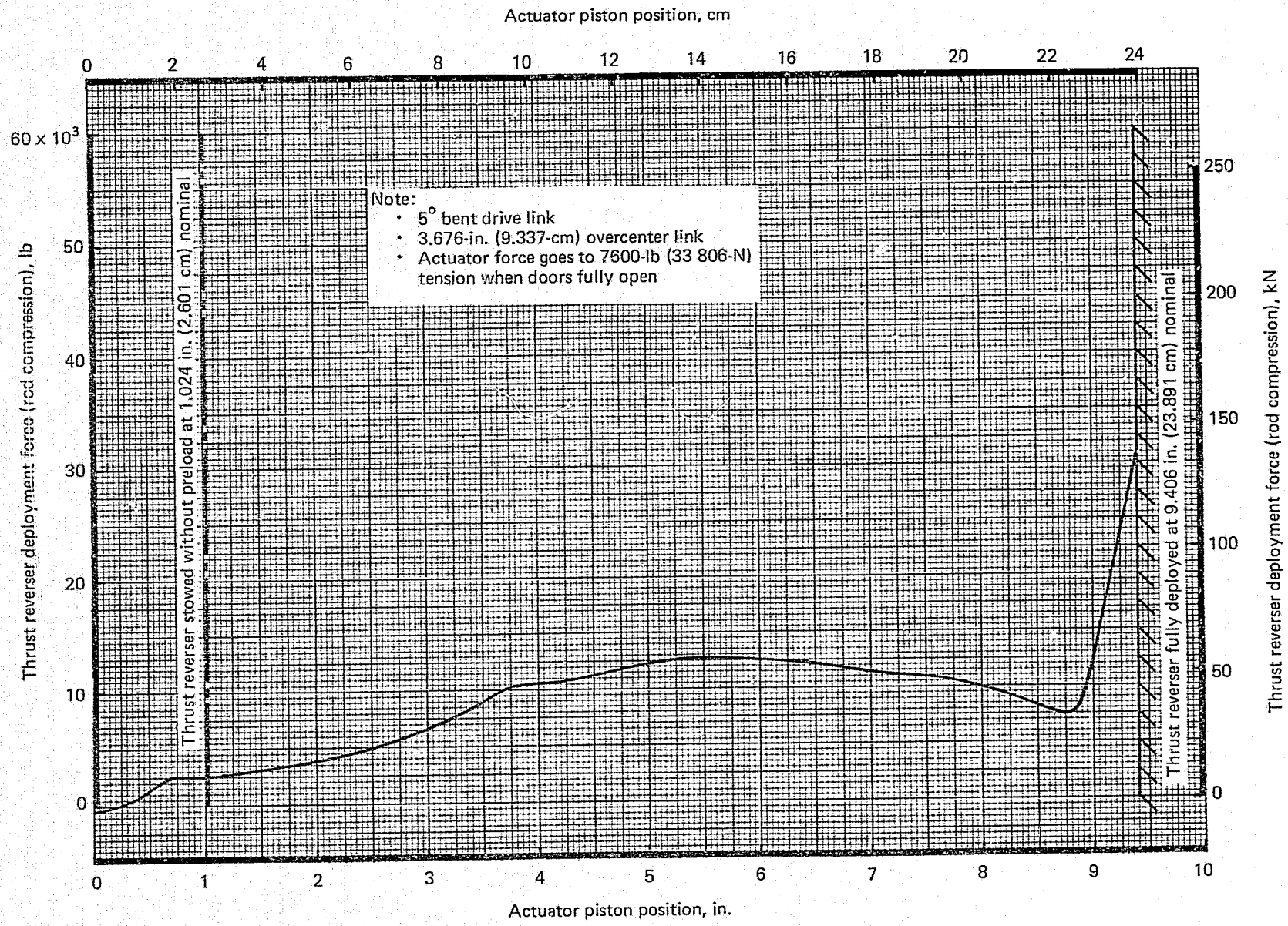

Figure 166.—JT8D Refan Thrust-Reverser Deployment Actuator Force—Sea Level at 165 KEAS (84.9 m/s)

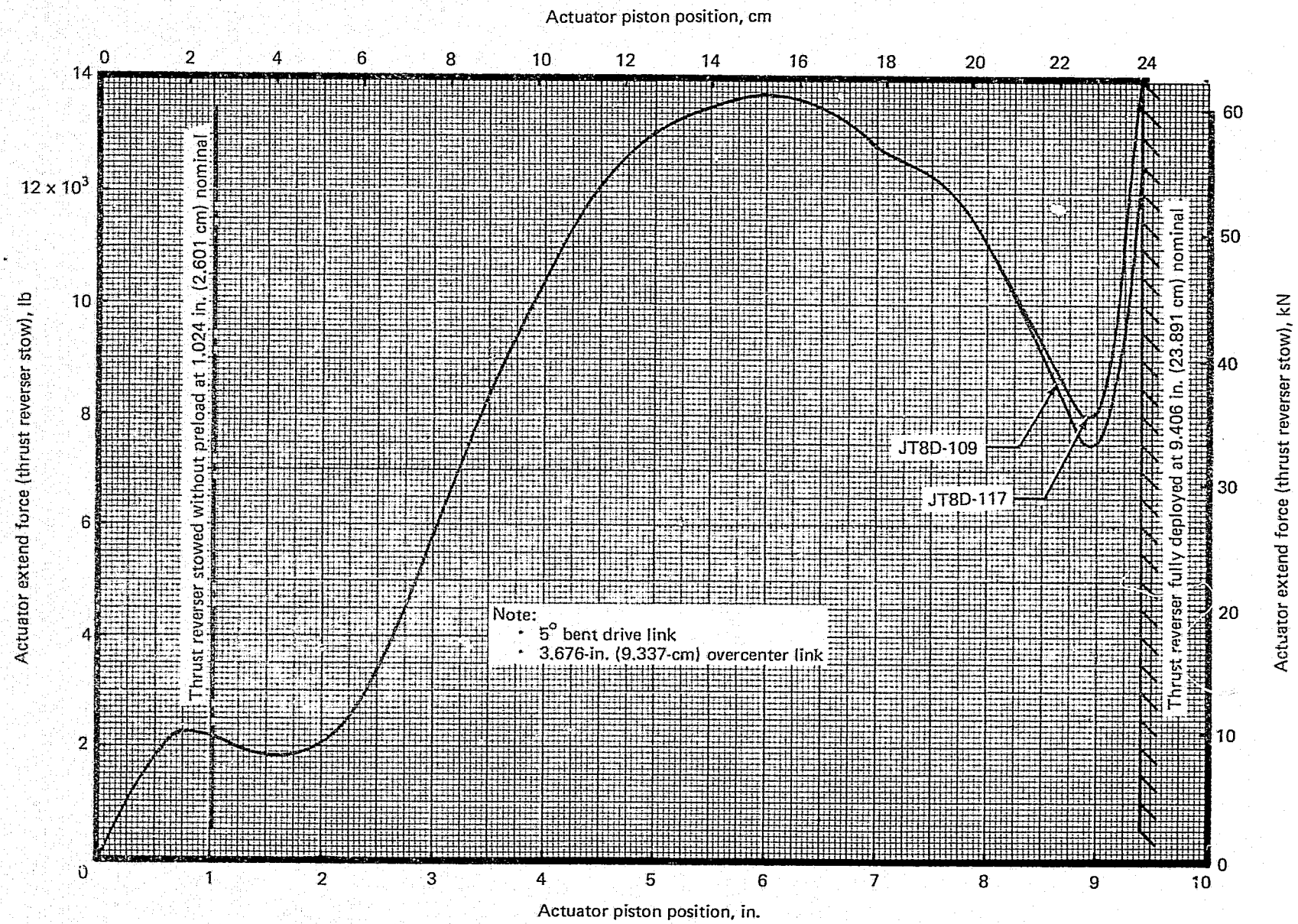

Figure 167.—JT8D Refan Thrust-Reverser Restow Actuator Force—12 000 ft (3658 m) at 180 KEAS (92.6 m/s)

- JT8D refan actuator force for 270-KEAS (138.9-m/s) inadvertent in-flight deploy (fig. 168)

3.7.1.4 Design Risk Areas

The technique used in determining actuator loads was judged to represent a design risk using scale factors for existing loads without the benefit of wind tunnel data. Actuator loads therefore should be examined further.

The control system concept, in particular the need for and the design of the runaround module, should also be examined further.

3.7.2 ICE PROTECTION–SIDE ENGINE

3.7.2.1 Cowl Leading Edges

The 727 refan cowl leading-edge TAI system is essentially the same as on the 727-200 system. The high-pressure compressor bleed air supply duct size was increased at the upstream end to accommodate the additional flow to the rings and struts. After the ring and strut flow is extracted from the common supply duct, the cowl supply air proceeds forward to an ejector as in the present system. The high-pressure primary nozzle of the ejector is only slightly larger than the present nozzle. The analysis showed that this larger nozzle would not provide as much high-pressure flow per unit length of the cowl lip as for the 727-200. An increase in total flow combined with a reduction in mixed air temperature would be required and would be obtained by increasing the control orifice sizes in the spray tube. The orifice change reduced the back pressure on the system, allowing a greater amount of secondary ambient air for a given amount of primary high-pressure air. Performance equivalent to that of the 727-200 was obtained with the increased total flow. This additional flow increased the heat transfer coefficients of the anti-icing air, which allowed the use of the lower temperature air. Figure 169 shows the JT8D refan bleed flow requirements for all ice protection systems.

3.7.2.2 Rings and Struts

The estimated TAI performance of the system provided for the JT8D refan inlet rings and struts was verified by analysis based on previous icing tunnel tests. In these Contractor-funded tests, high-temperature air from the high-pressure compressor was ducted through the struts and rings to protect leading-edge surfaces. The air exhausted from the aft portion of the ring leading edges provided heating to the aft portions of the rings by heating the boundary layer over the rings. Measurements of temperatures and pressures with various supply and exhaust configurations verified that desired flow distributions can be obtained within system pressure limitations. Figure 169 shows the JT8D refan bleed airflow requirements for rings and struts. High-pressure airflow requirements for the one-ring inlet are 78% of those for the cowl leading edge.

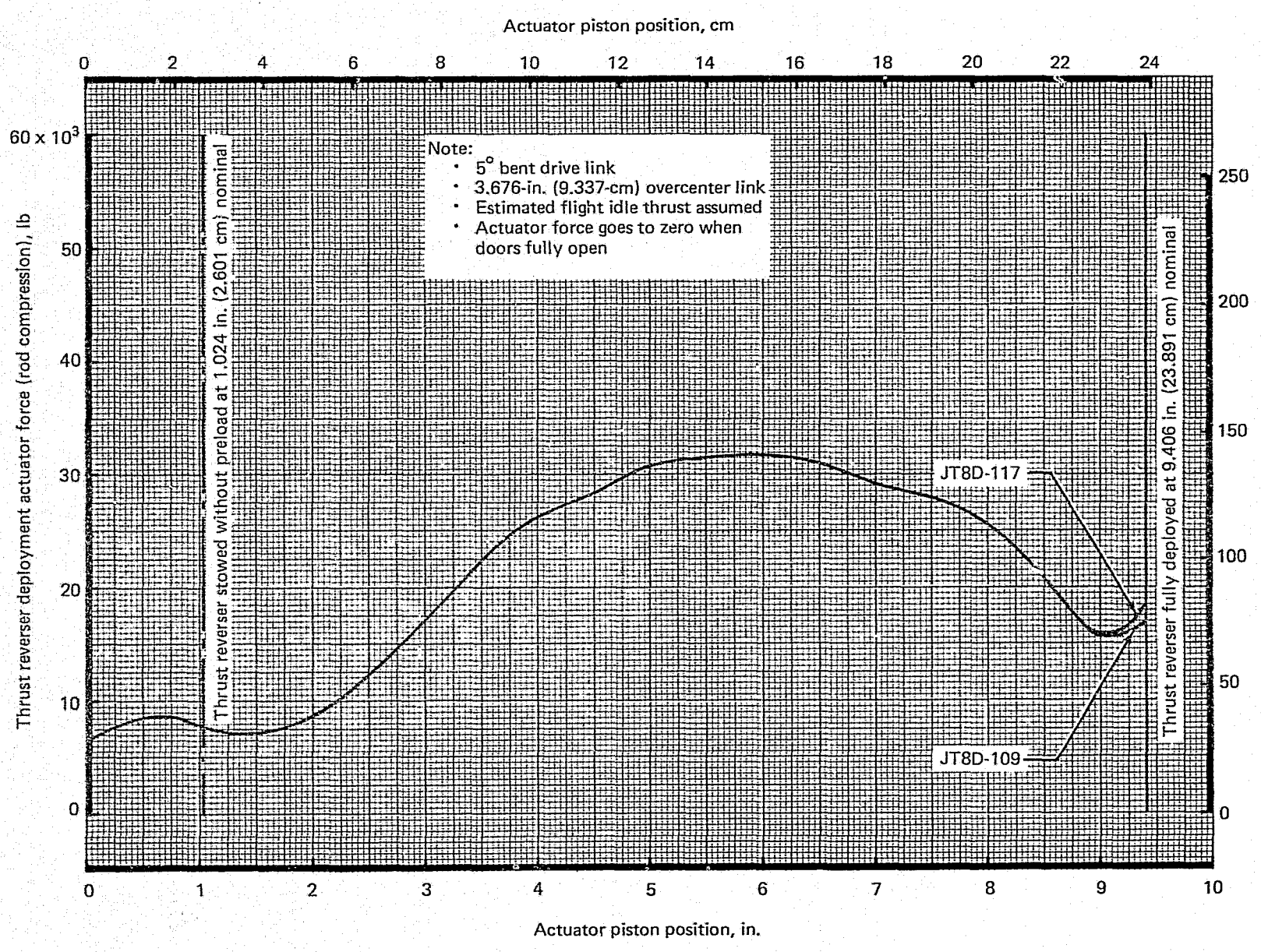

Figure 168.—JT8D Refan Thrust-Reverser Inadvertent Deploy Actuator Force—Sea Level at 270 KEAS (138.9 m/s)

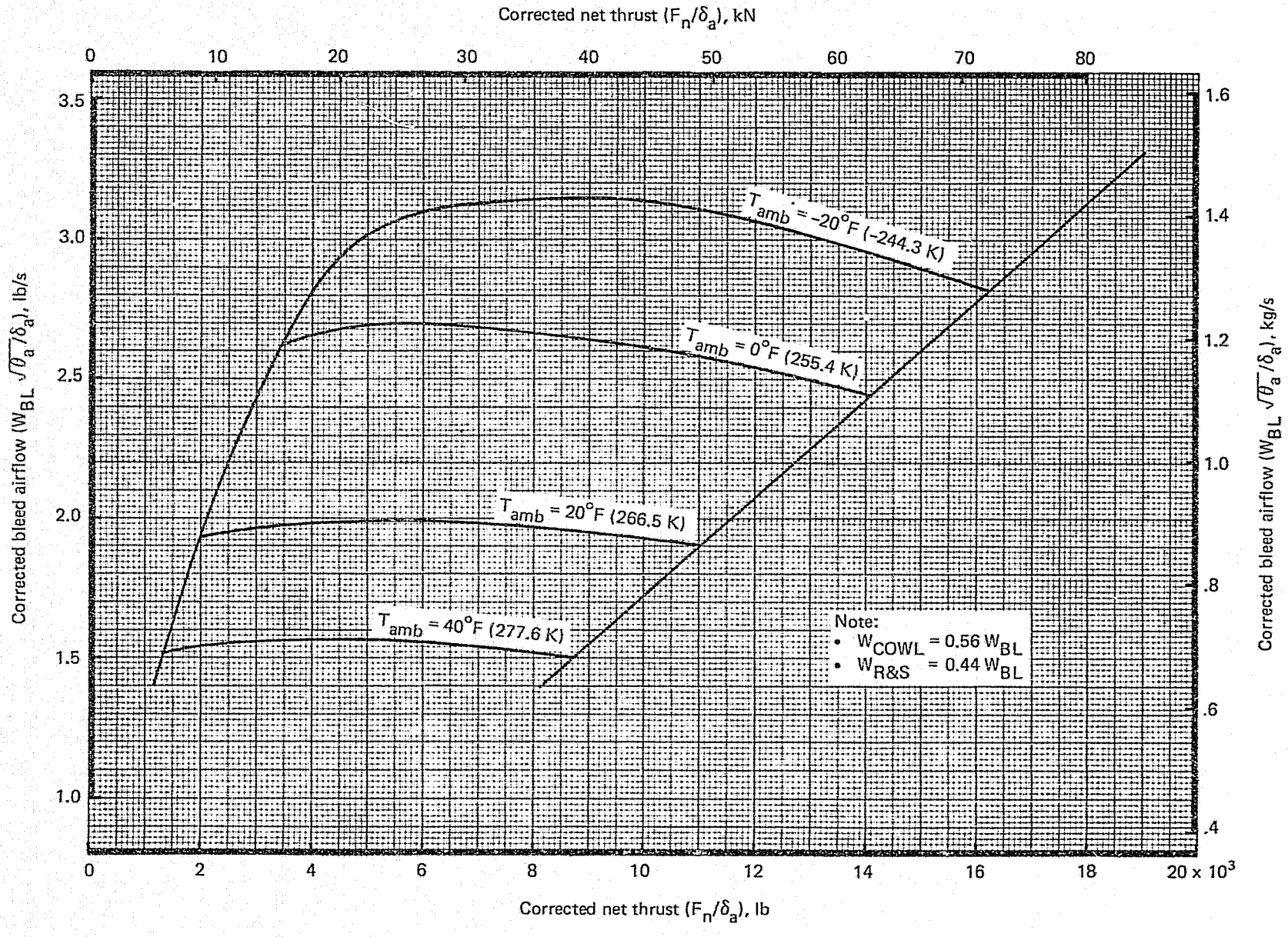

Figure 169.—JT8D Refan Engine Bleed Requirements for Ice Protection

3.7.2.3 Nose Dome

The nose dome of the JT8D refan engine is nearly identical to that of the 737 Quiet Nacelle. The internal configuration of the JT8D refan nose dome was modified as required to reduce internal pressures to within the limits specified for the refan engine. TAI performance was vertified by comparison to the 737 Quiet Nacelle nose dome, which was certificated on the basis of analysis, icing tunnel tests, and dry air ground tests on an installed engine.

3.7.3 ICE PROTECTION– CENTER ENGINE

3.7.3.1 Cowl Leading Edge

The 727 refan cowl leading-edge ice protection method is unchanged from the present 727-200 system except that additional airflow is provided in proportion to the differences in the cowl diameters.

3.7.3.2 Nose Dome

The side- and center-engine nose domes were designed to be interchangeable. Center-engine nose dome ice protection requirements were verified with analysis conducted on the side-engine nose dome.

3.7.3.3 Center-Engine Inlet Duct

The 727 refan center-engine inlet duct TAI patches, described in reference 4, are designed slightly different from those of the 727-200 system; however, the same airflows are provided. The primary concern in this study was to verify that acoustical panel temperatures would not exceed specified limits during TAI operation. System and acoustical panel temperatures were calculated for various system configurations and the final design was judged satisfactory.

3.7.4 AIR-CONDITIONING

3.7.4.1 Precooler

The 727-200 precooler performance was analyzed to determine its adequacy when matched with the JT8D refan engine. Specifically, the precooler cabin air discharge temperature must be under 450°F (505 K) during all flight conditions. The design point was maximum climb power, standard day temperature +40°F (22 K) $M_\infty = 0.78$, and altitude = 40 000 ft (12 192 m). Results indicated that lower fan stage pressures on the JT8D refan engine compared to the baseline engine will cause precooler cooling air to decrease, resulting in higher discharge temperatures. Although higher, JT8D refan engine precooler cabin air discharge temperature does comply with the 450°F (505 K) limit and is therefore acceptable.

3.7.4.2 Bleed System Crossover

The 727-200 engine bleed air system is designed to provide adequate engine 8th-stage compressor bleed pressure to the flow control valve to meet air-conditioning flow demands at airplane cruise conditions. These conditions are:

- 30 000-ft (9144-m) altitude, standard day temperature +20°F (11 K), maximum cabin pressure, $M_\infty = 0.75$, and an airplane gross weight of 140 000 lb (63 502 kg) at long-range cruise.

- 35 000-ft (10 668-m) altitude, standard day temperature, $M_\infty = 0.78$, maximum cabin pressure, and an airplane gross weight of 140 000 lb (63 502 kg) at long-range cruise.

When 8th-stage pressure is insufficient to meet air-conditioning flow demands, bleed system crossover to 13th-stage compressor bleed occurs.

Analysis shows that the JT8D refan engine would provide sufficient 8th-stage pressure to meet flow demands. The excess pressure provided is, in fact, equal to or slightly greater than the excess pressure provided by the baseline engine. Crossover to 13th stage will occur at cruise altitudes or temperatures approximately the same as for the 727-200 airplanes.

3.7.4.3 Pneumatic Duct Design Criteria

The engine bleed air ducts used to transport high-temperature and high-pressure engine bleed air were analyzed to determine if the JT8D refan engine bleed air conditions caused any problems with respect to the 727-200 bleed ducts or duct criteria. The maximum pressures and temperatures to which fan, 6th-, 8th- and 13th-stage bleed ducts would be subjected were estimated for the most extreme conditions, namely high airplane speed at sea level. The following three conditions were examined:

- Takeoff thrust rating at 170 KEAS (87.4 m/s), which was considered a normal condition

- The same condition with a compressor delivery pressure (CDP) limiter failure, with the engine accelerating to its maximum fuel flow capability (This case was used as the worst single malfunction condition.)

- Takeoff thrust setting with a failed CDP limiter at 380 KEAS (195.5 m/s), with the engine accelerating to its maximum fuel flow

Maximum temperatures and pressures within the JT8D refan engine would occur at sea level over a range of ambient temperatures from -65°F (219 K) to 120°F (322 K). The highest pressure temperature condition determined was at the 170-KEAS (87.4-m/s) sea level takeoff thrust condition with a CDP limiter failure. The JT8D refan temperatures and pressures were consistent with those found on the baseline engine at the same condition.

3.7.5 BRAKE SYSTEMS

The 727-200 brake capability was analyzed using the JT8D refan engine ground idle thrust characteristics. Since the JT8D refan engine ground idle thrust (section 3.3.12) is comparable to the JT8D engines currently in service on the 727-200, it was judged that the 727-200 brake system is adequate for ground operation procedures on the 727 refan airplane.

4.0 CONCLUSIONS

The Phase II Program on Ground Test of Refanned JT8D Turbofan Engines and Nacelles for the 727 Airplane was conducted to determine (through appropriate design, manufacturing, test, and analyses) the technical feasibility of retrofitting a 727-200 airplane with a modified version of the JT8D engine incorporating jet noise reduction features and improved performance. The credibility of such a retrofit concept was successfully demonstrated, and the principal results follow:

1. The analyses confirm that the 727 refan airplane would meet FAA airworthiness requirements (in existence at the time the 727-200 was certified).

2. The 172 500-lb (78 245-kg) BRGW 727 refan airplane would have noise levels, at FAR Part 36 conditions, of 6 to 8 EPNdB less than the baseline 727-200 airplane. The original program goals of 10-EPNdB lower noise levels were not achieved, with the following reasons involved: exhaust duct flow noise was not known to exist, and the significance of core noise was unknown at the start of the program. An exhaust mixer would have resulted in meeting the program goals at full-power takeoff and sideline.

3. The 727 refan airplane would meet the FAR Part 36 noise requirements with full-power takeoff.

4. The reduction in annoyance weighted footprint contour area for the 727 refan would be 68% to 83% when compared to the 727-200.

5. The 727 refan airplane would experience a 15% range loss when compared to the 727-200 airplane at equal gross weight, and the block fuel would increase by 1.5% to 3%. By making minor structural modifications to this particular model of 727-200, the range could be increased by 15% over the unmodified airplane.

APPENDIX

SYMBOLS AND ABBREVIATIONS

'A'	Pivot point
$A_{90\ EPNdB}$	90-EPNdB contour area
A/C	Air-conditioning
A_{DOOR}	Thrust-reverser door area
A_H	Actuator head-end area
A/I	Anti-icing
ALPA	Airline Pilots' Association
A_{pri}	Primary jet fully expanded flow area
A_R	Actuator rod-end area
A_{sec}	Secondary jet fully expanded flow area
ATA	Air Transport Association
B.L.	Buttock line
BRGW	Brake release gross weight
B.S.	Body station
Btu	British thermal unit
CAR	Civil Air Regulations
CDP	Compressor delivery pressure
CI	Community interface
c.g.	Center of gravity

$\mathbb{C}$	Centerline
C_L	Coefficient of lift
cm	Centimeters
C_m	Pitching moment coefficient
C_n	Yawing moment coefficient
$C_{n\beta}$	Yawing moment per degree of sideslip
$C_{n\delta_R}$	Yawing moment per degree of rudder
CORGE	Core noise correlation parameter
cps	Counts per second
CSD	Constant-speed drive
$C_{T/R}$	Distance from door center of pressure (on projected area) to 4-bar linkage instant center
C_v	Coefficient of velocity
daN	Dekanewton
dB	Decibel re 0.0002 μbar
dc	Direct current
deg	Degree
EPNdB	Effective perceived noise level in decibels
EPNL	Effective perceived noise level
EPR	Engine pressure ratio
extr.	Extraction
°F	Degrees Fahrenheit
FAA	Federal Aviation Administration
F_{ACT}	Actuator load

F_{AIR}	Dynamic airload
FAR	Federal Aviation Regulation
FC	First class
F_g	Gross thrust
Fig.	Figure
F_{LINK}	Drive link load
F_n	Net thrust
F_n/δ	Corrected net thrust
FPR	Fan pressure ratio including fan exit guide vane loss
freq	Frequency
f_{sc}	Scale factor
ft	Feet
fwd	Forward
g	Gravitational constant
gal	Gallon
h	Pressure altitude
hr	Hour
I.C.	Instant center
Inbd	Inboard
ISA	International Standard Atmosphere
J	Joule
K	Kelvin
KEAS	Knots equivalent airspeed
kg	Kilogram

km	Kilometer
kN	Kilonewton
knot, kn	Nautical miles per hour
KTAS	Knots true airspeed
lb	Pound
LGW	Landing gross weight
LPC	Low-pressure compressor
$L_{T/R}$	Distance from drive link pivot to linkage system instant center
m	Meter
M_∞	Freestream Mach number
MAC	Mean aerodynamic chord
M_{ACT}	Actuator moment
max	Maximum
M_D	Airplane maximum design Mach number
M_{DF}	Demonstrated flight diving Mach number
MFPOP	Modified full-power operational profile
min	Minute
min.	Minimum
mm	Millimeter
M_{mo}	Airplane maximum operating Mach number
N	Newton
N_1	Mechanical low-pressure compressor rotor speed
$N_1/\sqrt{\theta_{t2}}$	Corrected low-pressure compressor rotor speed
N_2	Mechanical high-pressure compressor rotor speed

NDI	Nondestructive inspection
nmi	Nautical mile
NTA	Noise-thrust-altitude
OEW	Operational empty weight
P&WA	Pratt & Whitney Aircraft
P_A	Axial load
P_a	Ambient pressure
P_{bottom}	Bottom pressure
P_H	Actuator head end hydraulic pressure
P_N	Normal load
PNdB	Perceived noise in decibels
PNL	Perceived noise level
PNLT	Tone-corrected perceived noise level
P_R	Actuator rod-end hydraulic pressure
P_S	Side load
P_{s4}	High-pressure compressor exit static pressure
psi	Pounds per square inch
psia	Pounds per square inch (absolute)
P_{side}	Side pressure
$P_{side\ bottom}$	Side bottom pressure
$P_{side\ top}$	Side top pressure
psig	Pounds per square inch (gage)
P_{top}	Top pressure
P_{t2}	Engine inlet total pressure

P_{t8e}	Primary stream total pressure at the engine exhaust mixing plane
q-load	Aerodynamic load due to flight velocity
°R	Degrees Rankine
rad	Radian
ref	Reference
RFNI	Relative footprint noise index
rpm	Revolutions per minute
RTO	refused takeoff
$R_{T/R}$	Drive link length from pivot point to door attach point
$r_{T/R}$	Distance from drive link pivot to overcenter link attach point
RTS	Relative fan tip Mach number (relative tip speed)
sec, s	Second
SFC	Specific fuel consumption
SI	Systeme Internationale
SL	Sea level
spec	Specification
SPL	Sound pressure level
SST	Supersonic Transport
std	Standard
S_{WCP}	Stabilizer incidence angle relative to wing chord plane
T_{amb}	Ambient temperature
TAI	Thermal anti-icing
TC	Tourist class
T/C	Thermocouple

T/O	Takeoff
T/R	Thrust reverser
TPR	Overall turbine pressure ratio
T_{t5}	Burner exit total temperature
T_{t8e}	Primary stream total temperature at the engine exhaust mixing plane
V	Volt
V_∞	Freestream velocity
V_2	Takeoff safety speed
V_c	Calibrated airspeed
V_D	Airplane maximum design speed
V_{DF}	Demonstrated flight diving speed
V_E	Equivalent airspeed
V_{FWD}	Airplane forward velocity
V_{mo}	Airplane maximum operating speed
V_{pri}	Primary jet fully expanded velocity
$V_{rel\ 4}$	Last stage turbine rotor tip relative velocity
V_s	Airplane stall speed
V_{sec}	Secondary jet fully expanded velocity
V_{son}	Last stage turbine rotor inlet sonic velocity
V_{TRIM}	Airplane trim speed
W_a	Airflow
W_{BL}	Bleed airflow
W_{COWL}	Engine cowl anti-icing airbleed
WHP	Turbine weight flow parameter corrected to station 5

W_{pri}	Primary jet weight flow
$W_{R\&S}$	Engine ring and strut anti-icing airbleed
W_{sec}	Secondary jet weight flow
wt	Weight
%	Percent
$\alpha_{T/R}$	Angle between overcenter link and plane parallel to actuator centerline
α_{WCP}	Wing angle of attack
β	Angle of sideslip
$\beta_{T/R}$	Angle from centerline of overcenter link to force component
γ	Flightpath gradient
$\gamma_{T/R}$	Side view angle of door top surface to horizontal
Δ	Delta (increment of change)
δ, δ_a	Relative ambient pressure
δ_E	Elevator angle
ΔP	Pressure differential
δ_R	Rudder angle
δ_T	Rudder tab angle
θ_a	Relative ambient temperature
θ_{DL}	Drive link rotation angle
$\theta_{T/R}$	Thrust reverser clock angle

DEFINITIONS

Accessories — Components required for engine operations and airplane systems components, which are mounted on the engine and strut.

Engine — The dry engine provided by P&WA.

Flight-type hardware — The Contractor's JT8D refan nacelle components.

Inlet assembly/ side-engine nose cowl — The portion of the nacelle forward of the fan case, including internal and external fairings and all components attached and normally removed with the inlet assembly/nose cowl.

JT8D — The P&WA JT8D parent engines used as the baseline in the evaluation of the refan concept included the JT8D-9, JT8D-15, and JT8D-17 untreated engines with hardwall nacelles.

- The JT8D-9 was selected for use as the baseline in the analysis of the 727 refan airplane because of its wide usage in the current airplane fleet.
- The JT8D-15 engine was selected for use as the baseline in the full-scale ground tests because of its availability from the Contractor's inventory at greatly reduced program costs compared to a JT8D-9 engine.
- The JT8D-17 was selected as the baseline in the structural analysis since the weight, thrust, and reverse thrust of the derivative JT8D-117 engine would be greater than the JT8D-109 and thus critical to the airplane structures.

For brevity in this final report, these parent engines will be referred to as the JT8D except when it is important to establish specific identification; then they will be referred as JT8D-9, JT8D-15, and JT8D-17.

JT8D refan — The refanned P&WA JT8D-100 series engines developed from JT8D parent engines during the Refan Program included the JT8D-109 and JT8D-115 engines and an analytical description of the JT8D-117 engine.

- The JT8D-109 side-engine installation is characterized by peripheral treatment in the engine fan duct and fan case; inlet diffuser wall, ring, and center-body treatment; exhaust duct and fan/primary flow divider (splitter) treatment. The center-engine installation had an acoustically treated inlet duct (without ring) with the same exhaust system treatment as the side engine. The JT8D-109 *(with hardwall nacelle)* has only the engine fan duct and fan case treatment.
- The JT8D-115 was selected for full-scale ground test because of the availability of the JT8D-15 parent engine.

- The JT8D-117 (derived through analysis) was used for the structural analysis since the weight, thrust, and reverse thrust capability would be greater than the JT8D-109 and thus critical to the airplane structures.

For brevity in this final report, these refanned engines will be referred to as JT8D refan except when it is important to establish specific identification; then they will be referred to as JT8D-109, JT8D-115, and JT8D-117.

Nacelle	As used in this document, the engine nacelle includes all components of an externally mounted propulsion package, including the engine plus all engine-mounted parts and accessories; the inlet, cowling, and thrust reverser (i.e., all components suspended from the engine mounts).
Reference hardware	The P&WA bellmouth inlet (inlet lip, diffuser, and nose dome) and exhaust system (exhaust duct, fan/primary flow divider, and plug) without acoustical treatment, which were used as a calibration reference during the full-scale ground tests.
Strut	A structure that separates and supports the nacelle external from the airframe, including primary and secondary structure and provisions for installation of airplane and engine systems components.
Thrust reverser	The structure and mechanisms required to reverse engine thrust.
727-200	The current production model 727-200 airplane, with a BRGW of 172 500 lb (78 245 kg), which was used as the baseline in the evaluation of the refan concept.
727 refan	The 727-200 airplane equipped with JT8D-109 (refan) engines and having a BRGW of 172 500 lb (78 245 kg). This airplane/engine combination was derived through analysis.

FINITE ELEMENT STRUCTURAL ANALYSIS PROGRAM

The structure was analyzed using the structural and vibration modules of a multipurpose finite element structural analysis program developed by the Contractor and using a high-speed digital computer system.

From the structural module, the redundant reaction forces, deflections, and internal beam loads were determined together with the mass and stiffness matrices used in the vibration module. The idealized structure computer models were also plotted using this module.

The vibration module was used to determine the airplane natural undamped mode shapes and structural frequencies which were then entered into the dynamic landing analysis program. The finite element structural model consisted of beams and plates oriented by nodes located in a three-dimensional global coordinate system, thus representing the airplane structure being analyzed.

Nodes were either free or fixed in space in the three axes of rotation and deflection. Beams were also either pinned or fixed at the ends and so had moment capability in the three local beam axes. Section constants and material properties were input for all types of elements, beams, and plates.

Point loads were input at nodes, and uniformly distributed loads could be applied on the beams or plates. Spring and temperature effects were also input to the analysis. Models could be split on the axis of symmetry and, by use of the nodal fixities, symmetrical or asymmetrical load conditions could be applied to the model.

The program printed out the reactions, moments, and forces for all fixed and spring nodes, plus the beam and plate element internal loads and also the rotation and deflection of all nodes in the structure.

DYNAMIC LANDING ANALYSIS

The Contractor's dynamic landing analysis was used to obtain the engine loads and response during landing. The complete airplane structure was simulated, including the side- and center-engine flexibilities and landing gear characteristics.

This analysis could simulate all forms of landing and taxi conditions, with either rigid body (six degrees of freedom), or symmetric and asymmetric flexible body normal modes. Aerodynamic lift and moment were included as were nonlinear landing gear characteristics and dynamics.

HEAT TRANSFER PROGRAM

The heat transfer program used in the analysis of the exhaust system fan/primary flow divider was an existing Contractor analysis program and was used to obtain both transient and steady-state thermal distribution in a structure.

A unit section through the structure was modeled in terms of the heat transfer capabilities of the structural elements and airgaps. The model included the relevant coefficients of radiation, conduction and convection, and dimensions of the structure. Known gas temperatures, pressures, flow, and time intervals to be considered were input. Thermal balances were derived at user-selected time intervals, until stabilized conditions were obtained.

REFERENCES

1. Anon: *Program on Ground Test of Modified Quiet, Clean, JT3D and JT8D Turbofan Engines in Their Respective Nacelles–Phase I Final Report.* BCAC D6-41244, Boeing Commercial Airplane Company, NASA CR-134553, September 1973.

2. Mechtly, E.A.: *The International System of Units–Physical Constants and Conversion Factors.* NASA SP-7012, (revised) 1969.

3. Anon: *Phase II Program on Ground Test of Refanned JT8D Turbofan Engines and Nacelles for the 727 Airplane–Final Report:* Volume III–Ground Tests. BCAC D6-42440-3, Boeing Commercial Airplane Company, NASA CR-134799, December 1975.

4. Anon: *Phase II Program on Ground Test of Refanned JT8D Turbofan Engines and Nacelles for the 727 Airplane–Final Report:* Volume II–Hardware Design and Manufacturing. BCAC D6-42440-2, Boeing Commercial Airplane Company, NASA CR-134798, December 1975.

5. Schuehle, A.L.: *727 Airplane Side Inlet Low-Speed Performance Confirmation Model Test for Refanned JT8D Engines.* BCAC D6-41521, Boeing Commercial Airplane Company, NASA CR-134609, March 1974.

6. Kaldschmidt, G.; Syltebo, B.E.; and Ting, C.T.: *727 Airplane Center Duct Inlet Low-Speed Performance Confirmation Model Test for Refanned JT8D Engines–Phase II.* BCAC D6-41513, Boeing Commercial Airplane Company, NASA CR-134534, November 1973.

7. Haugan, W.J. and Kern, P.R.A.: *727/JT8D-100 Series Engine Exhaust System Propulsion Performance Model Test.* BCAC D6-41805, Boeing Commercial Airplane Company, NASA CR-134617, May 1974.

8. Atkey, E.N. and Chow, C.T.P.: *727 Airplane Target Thrust Reverser Static Performance Model Test for Refanned JT8D Engines.* BCAC D6-41964, Boeing Commercial Airplane Company, NASA CR-134652, July 1974.

9. Hambly, D.: *Wind Tunnel Test of Model Target Thrust Reversers for the Pratt & Whitney Aircraft JT8D-100 Series Engines Installed on a 727-200 Airplane.* BCAC D6-41900, Boeing Commercial Airplane Company, NASA CR-134709, September 1974.

10. Sandberg, K.G.; et al.: *Summary and Analysis of Performance and Stability Characteristics of the Refan JT8D-109 Engine.* PWA-5284, United Technologies Corporation, Pratt & Whitney Aircraft Division, NASA CR-134874, September 1975.

11. Joynes, D. and Balut, J.P.: *Titanium Honeycomb Acoustic Lining Structural and Thermal Test Report.* BCAC D6-42352, Boeing Commercial Airplane Company, NASA CR-134783, December 1974.

12. Hiatt, D.L. and McKaig, M.B.; et al.: *727 Noise Retrofit Feasibility.* BCAC D6-60196. Boeing Commercial Airplane Company, Federal Aviation Administration, Final Report, FAA-RD-72-40, June 1973.

13. Bailey, R.W. and Vadset, H.J.: *727/JT8D Refan Side Nacelle Airloads.* BCAC D6-41527, Boeing Commercial Airplane Company, NASA CR-134547, March 1974.

14. Elrod, S.D. and Lovell, D.T.: *Development of Aluminum-Brazed Titanium Honeycomb Sandwich Structure.* BCAC D6-60203, Boeing Commercial Airplane Company, FAA-SS-72-03, July 1972.

15. Elrod, S.D. and Lovell, D.T.; et al.: *Development and Evaluation of the Aluminum-Brazed Titanium System:* Volumes I through VIII. BCAC D6-60277, Boeing Commercial Airplane Company, FAA-SS-73-5, May 1974.

16. Elrod, S.D. and Moji, Y.: *Creep and Corrosion Testing, Aluminum Brazed Titanium Honeycomb Sandwich.* BCAC D6-60214, Boeing Commercial Airplane Company, FAA-SS-72-14, July 1972.

17. Anon: Airworthiness Standards: Transport Category Airplanes, Paragraph 25.1191 Firewalls, *Federal Aviation Regulations,* Volume 3, Part 25, Federal Aviation Administration, June 1974.

18. Anon: *Military Specification, Castings, Classification and Inspection of.* MIL-C-6021F, 24 September 1962.